KU LEUVEN

ARENBERG DOCTORAL SCHOOL
Faculty of Engineering Science

Improved modeling of unit commitment decisions under uncertainty

Kenneth Bruninx

Supervisor:
Prof. dr. ir. W. D'haeseleer
Prof. dr. ir. E. Delarue, co-supervisor

Dissertation presented in partial fulfillment of the requirements for the degree of Doctor of Engineering Science (PhD): Mechanical Engineering

May 2016

Improved modeling of unit commitment decisions under uncertainty

Kenneth BRUNINX

Examination committee:
Prof. dr. ir. Patrick Wollants, chair
Prof. dr. ir. W. D'haeseleer, supervisor
Prof. dr. ir. E. Delarue, co-supervisor
Prof. dr. ir. R. Belmans
Prof. dr. ir. L. Helsen
Prof. dr. ir. D. S. Kirschen
(University of Washington, USA)
Prof. dr. A. Papavasiliou
(Université Catholique de Louvain, BE)

Dissertation presented in partial fulfillment of the requirements for the degree of Doctor in Engineering Science (PhD): Mechanical Engineering

May 2016

Uitgegeven in eigen beheer, Kenneth Bruninx, Celestijnenlaan 300 box 2421, B-3001 Heverlee (Belgium)

Dankwoord

Een doctoraat schrijven doe je niet alleen. Daarom wil ik vooreerst een aantal mensen in het bijzonder bedanken.

Een eerste woord van dank gaat naar mijn promotoren, William en Erik. William, bedankt voor alle mogelijkheden die u me bood tijdens dit doctoraat, voor alle conferenties en workshops die ik mocht bijwonen, om het verblijf in de VS mogelijk te maken, voor de vrijheid die ik kreeg in de onderzoeksprojecten die ik nastreefde. Erik, bedankt voor alle verhelderende discussies en uw eeuwig optimisme. Zonder uw bijdrage was dit werk niet geweest wat het vandaag is.

Secondly, I would like to thank all members of the jury, under the skillful guidance of the chairman, prof. Wollants. Lieve, Ronnie, Daniel and Anthony: your constructive feedback and thoughtful remarks have significantly improved the quality of this text. Any remaining errors, typo's and mistakes are mine and mine alone.

A special 'thank you' goes out to prof. Daniel Kirschen of the University of Washington, who was my host during a research visit in the fall of 2015. Daniel, I've learned a lot from you during my brief stay in Seattle. I would also like to thank Yury, Ricardo, Marcel, Tu, Rémy, ... who have made my stay in the US – also outside the office hours – much more enjoyable.

Ik wil ook graag mijn collega-doctoraatsstudenten in onze onderzoeksgroep en binnen het GOA project bedanken voor de fijne samenwerking, interessante discussies, mooie momenten tijdens conferenties en workshops,... Dieter, bedankt de fijne samenwerking in ons onderzoek naar vraagsturing. Alessia, thank you for pushing us to further pursue this line of research. Christina and Glenn, thank you for lending us your knowledge and expertise on building models. Kenneth VDB, merci voor de fijne samenwerking. Jeroen, bedankt om me te betrekken in je *power-to-gas* onderzoek. Juliana, thank you for introducing me to virtual power plant models.

Ook alle andere collega's op TME en binnen het GOA project hebben hun plaats in dit dankwoord meer dan verdiend. Bedankt voor vijf mooie jaren, met absurde discussies tijdens de middag, voetballen en *happy hours* op vrijdag en onvergetelijke droppings tijdens TME-weekends. Ook de mensen van ons secretariaat wil ik bedanken: Kathleen, Frieda, Marina en Valérie, merci voor alle hulp.

Tot slot wil ik ook mijn familie, schoonfamilie en vrienden bedanken voor alle steun tijdens mijn studies en doctoraat. Jullie – ongetwijfeld soms geveinsde – interesse en aanmoedigingen hebben ervoor gezorgd dat ik doorbeet wanneer het wat minder ging. In het bijzonder: Geert, Anne, Jeroen, Britte, Sien, Jan, Jort, Souz en Anke, merci voor de vele mooie avonden en nachten in Leuven en ver daarbuiten. Mama, Papa, Jolien en Anke, merci om er altijd te zijn. Zonder jullie was dit doctoraat niet mogelijk geweest.

Tot slot, Nikki, ik zou niet weten waar te beginnen om jou te bedanken. Daarom simpelweg: merci!

Kenneth
Leuven — 17 mei 2016

Abstract

The massive integration of variable and limitedly predictable electricity generation from renewable energy sources (RES) leads to so-called balancing costs (a.o. integration costs). Therefore, system operators are continuously seeking novel sources of operational flexibility and improved methods to size, procure and deploy the associated operational reserves.

With these challenges in mind, we develop an operational modeling framework to study the impact of stochastic RES-based generation, novel flexibility providers and demand response on day-to-day electricity generation system operation. This framework consists of a statistical characterization of the uncertainty, which provides input for the generation of scenarios and reserve sizing techniques, which in turn are representations of the uncertainty in so-called unit commitment (UC) models. Historically, these models were typically deterministic in nature, which may make them poorly suited to study and operate power systems with high shares of limitedly predictable RES-based generation. Therefore, the first objective set forth in this dissertation relates to the improvement of existing and the development of novel UC models considering imperfect RES-based electricity generation forecasts, with a focus on the cost-efficiency, reliability and computational effort associated with their solutions.

We study and improve the performance of three UC models found in the scientific literature: a deterministic UC model, a stochastic UC model and an improved interval UC model. A deterministic UC model tackles uncertainty by considering reserve constraints, which trigger – if properly designed – sufficient scheduled capacity to absorb forecast errors during real-time operation. The cost-efficiency of the deterministic model is improved by (1) the explicit consideration of energy storage-based reserve provision and (2) state-of-the-art probabilistic reserve sizing techniques, based on a novel distributional characterization of the uncertainty on RES-based generation forecasts. Stochastic models on the other hand employ a direct scenario-based representation of the uncertainty, which in theory leads to more cost-efficient UC schedules. The solution stability

and bias of the resulting UC schedules are drastically improved through the development of a dedicated scenario reduction technique. The improved interval UC model attempts to reduce the conservatism of the deterministic UC model by improving the realism of the ramping requirements imposed on the scheduled reserves. Nevertheless, the presented qualitative and quantitative analysis shows that the deterministic and improved interval models yield sub-optimal, overly conservative UC schedules, albeit at a low computational cost. We attribute this sub-optimal behavior to the inability of these models to account for the expected deployment cost of the scheduled reserves. In contrast, the stochastic UC model results in cost-optimal UC schedules if the selected scenarios are sufficiently representative of the uncertainty at hand, but at an extremely high computational cost.

In pursuit of a UC model that combines the cost-optimality of the stochastic model with the computational effort of the deterministic model, we develop two novel UC formulations: a hybrid deterministic-stochastic and a probabilistic UC model. Both formulations include, although through a different approach, an approximation of the expected deployment cost of the scheduled reserves. The hybrid UC model combines a probabilistic reserve requirement and a limited set of scenarios. This model allows approximating the stable solution of the stochastic UC model, but at a computational cost that is an order of magnitude lower than that of the original stochastic problem. The probabilistic model on the other hand is characterized by calculation times similar to that of the deterministic model, but allows for significant cost reductions through the internalization of the reserve sizing problem.

The second objective addressed in this dissertation relates to the study of the arbitrage and regulation services an activated demand side may offer. In particular, we study the system value of demand response with electric heating systems. To this end, an integrated model is proposed, which entails the inclusion of a physical demand side model, sufficient to represent the operational flexibility available in limitedly controllable residential electric heating systems, in a probabilistic UC model. In a numerical case study, inspired by the Belgian power system, demand response-based arbitrage and regulation services are shown to contribute significantly to the minimization of the balancing cost associated with imperfect RES-based generation forecasts.

The presented models and techniques can be used to assess the impact of uncertainty on reasonably large electric power systems, as illustrated in the last chapter of this dissertation. Independent system operators may use these models to optimize their UC decisions taking into account the uncertainty in their system. The integrated model may lead to adequate estimates of the system value of DR. In addition, demand aggregators may use the presented approach to optimize the scheduling and operation of DR-adherent loads.

Beknopte samenvatting

De grootschalige integratie van variabele en beperkt voorspelbare elektriciteitsproductie uit hernieuwbare energiebronnen (HEB) geeft aanleiding tot zogenaamde balanceringskosten (naast andere integratiekosten). Systeemoperatoren zijn daarom voortdurend op zoek naar nieuwe bronnen van operationele flexibiliteit en verbeterde methoden om de geassocieerde reserves te berekenen, te plannen en te activeren.

In het licht van deze uitdagingen ontwikkelen we een operationeel modelleerraamwerk om de impact van stochastische elektriciteitsproductie uit HEB, nieuwe bronnen van flexibiliteit en vraagsturing op de dagdagelijkse uitbating van het elektriciteitssysteem te bestuderen. Dit raamwerk bestaat uit een statistische karakteristatie van de onzekerheid, het startpunt voor scenariogeneratietechnieken en reserveberekeningsmethodes, die op hun beurt resulteren in voorstellingen van de onzekerheid in zogenaamde *unit commitment* (UC) modellen. In het verleden waren deze modellen typisch deterministisch, hetgeen deze modellen mogelijk niet geschikt maakt voor het bestuderen en uitbaten van elektriciteitssystemen met een groot aandeel beperkt voorspelbare elektriciteitsproductie uit HEB. Het eerste objectief in deze doctoraatsverhandeling relateert aan de verbetering van bestaande en de ontwikkeling van nieuwe UC modellen, rekening houdend met de imperfecte voorspellingen van elektriciteitsproductie uit HEB, focussend op de kostenefficiëntie, betrouwbaarheid en computationele inspanning geassocieerd met hun oplossingen.

We bestuderen en verbeteren de performantie van drie UC modellen uit de wetenschappelijke literatuur: een deterministisch model, een stochastisch model en een zogenaamd verbeterd interval UC model. Een deterministisch model brengt onzekerheid in rekening via reservebeperkingen, die – indien zorgvuldig bepaald – resulteren in voldoende geplande capaciteit om voorspellingsfouten te absorberen tijdens realtime uitbating. De kostenefficiëntie van het deterministisch model wordt verbeterd door (1) het expliciet beschouwen van energiestockage-gebaseerde flexibiliteit en (2) nieuwe probabilistische

reserveberekeningsmethoden, gebaseerd op een nieuwe distributionele karakterisatie van de onzekerheid op voorspellingen van elektriciteitsproductie uit HEB. Stochastische modellen hanteren daarentegen een directe, scenariogebaseerde voorstelling van de onzekerheid, hetgeen in theorie leidt tot meer kostenefficiënte UC planningen. De stabiliteit en bias van de resulterende UC planning worden verbeterd door de ontwikkeling van een gespecialiseerde scenarioreductietechniek. Het verbeterde interval UC model tracht het conservatisme van het deterministische model te verminderen via realistischere stijgsnelheidbeperkingen voor de geplande reserves. Desalniettemin toont de gepresenteerde kwalitatieve en kwantitatieve vergelijkende analyse aan dat het deterministische en verbeterde interval UC model resulteren in suboptimale, te conservatieve UC planningen, hetzij aan een lage computationele kost. We schrijven dit suboptimaal gedrag toe aan het onvermogen van deze modellen om de verwachte activatiekost van de geplande reserves in rekening te brengen. Het stochastische UC model daartegenover resulteert in kostenoptimale UC planningen indien de geselecteerde scenario's een voldoende representatieve voorstelling van de onzekerheid zijn, maar aan een extreem hoge computationele kost.

In de zoektocht naar een UC model dat de kostenoptimaliteit van het stochastische model en de computationele inspanning van het deterministische model combineert, ontwikkelen we twee nieuwe formuleringen van het UC probleem: een hybride deterministisch-stochastisch en een probabilistisch model. Beide formuleringen bevatten, zij het op een andere manier, een benadering van de verwachte activatiekost van de geplande reserves. Het hybride UC model combineert een probabilistische reservebeperking en een beperkte scenario set. Dit model laat toe om de stabiele oplossing van het stochastische model te benaderen, maar de geassocieerde computationele kost is een ordegrootte kleiner dan die van het originele stochastische probleem. Het probabilistische model daarentegen wordt gekarakteriseerd door rekentijden gelijkaardig aan die van het deterministische model, maar resulteert in significante operationele kostenreducties dankzij de internalisering van de reserveberekening.

Het tweede objectief in deze doctoraatsverhandeling relateert aan de studie van de mogelijke opportuniteiten inzake vraagsturingsgebaseerde arbitrage en balancering. In het bijzonder bestuderen we de systeemwaarde van vraagsturing met elektrische verwarmingssystemen. We stellen hiertoe een geïntegreerd model voor, hetgeen een probabilistisch UC model combineert met een fysisch vraagzijdemodel dat de operationele flexibiliteit van beperkt controleerbare residentiële elektrische verwarmingssystemen voorstelt. In een numerieke gevalstudie, geïnspireerd op het Belgische elektriciteitssysteem, tonen we aan dat vraagsturingsgebaseerde arbitrage en balancering toelaten om de balanceringskosten geassocieerd met imperfecte voorspellingen van

elektriciteitsproductie uit HEB significant te reduceren.

De gepresenteerde modellen en technieken kunnen gebruikt worden om de impact van onzekerheid te bestuderen in relatief grote elektriciteitssystemen, zoals geïllustreerd in het laatste hoofdstuk van deze doctoraatsverhandeling. Onafhankelijke systeemoperatoren kunnen deze modellen gebruiken om hun UC planning te optimaliseren, rekening houdend met de onzekerheid in hun systeem. Het geïntegreerde model kan leiden tot adequate inschattingen van de systeemwaarde van vraagsturing. Vraagaggregatoren kunnen de gepresenteerde aanpak hanteren om de planning en exploitatie van geactiveerde lasten te optimaliseren.

Abbreviations

AC	Alternating current
ACH	Air changes per hour
ADR	Active demand response
BOEC	Building owner energy cost
CCGT	Combined cycle gas turbine
cdf	Cumulative probability density function
CGB	Condensing gas boiler
CLT	Central limit theorem
DC	Direct current
DHW	Domestic hot water
DR	Demand response
DR	Design reliability (in the context of probabilistic reserve sizing)
DSM	Demand side management
DUC	Deterministic unit commitment
ED	Economic dispatch
ENS	Energy not served
ES	Energy storage
GCLT	Generalized central limit theorem
HP	Heat pump
HUC	Hybrid unit commitment
HV	High voltage
ICE	Internal combustion engine
iid	Independent and identically distributed
IUC	Interval unit commitment
IIUC	Improved interval unit commitment
IM	Integrated model
ISO	Independent system operator
IUC	Interval unit commitment

MC	Monte Carlo
MDT	Minimum down time
MILP	Mixed integer linear programming
MIQCP	Mixed integer quadratically constrained programming
MUT	Minimum up time
NP	Non-deterministic polynomial time
NRMSE	Normalized root mean square error
pdf	Probability density function
pp	Percentage point(s)
p.u.	Per unit
PHES	Pumped hydro energy storage
PTDF	Power transfer distribution factor
PUC	Probabilistic unit commitment
RES	Renewable energy sources
RUC	Robust unit commitment
SAA	Sample average approximation
SGT	Scenario generation technique
SH	Space heating
SO	System operator
SOCC	Second order conic constraint
SPFE	Solar power forecast error
SPP	Steam power plant
SRT	Scenario reduction technique
SUC	Stochastic unit commitment
TES	Thermal energy storage
TOC	Total operational cost
TSO	Transmission system operator
UC	Unit commitment
VGM	Virtual generator model
WPF	Wind power forecast
WPFE	Wind power forecast error
WS	Wind share
WUF	Wind utilization factor

Nomenclature

For sake of consistency and readability, we only list the sets, decision variables and parameters used in the (integrated) unit commitment models. All other symbols are defined throughout the text.

Sets and Indices

H	Set of buildings types, indexed by h.
I	Set of generators, indexed by i.
I^{FAST}	Subset of I, set of fast-starting generators, indexed by i.
J	Set of time intervals, indexed by j.
J^{O}	Subset of J, set of odd time intervals, indexed by j.
J^{E}	Subset of J, set of even time intervals, indexed by j.
L	Set of reserve levels, indexed by l.
M	Set of nodes in the transmission grid, indexed by m.
N	Set of lines in the transmission grid, indexed by n.
P	Set of states in the state-space model, indexed by p.
R	Set of PHES units, indexed by r.
S	Set of wind power scenarios, indexed by s.
s^{F}	Forecast scenario, element of set S.
S^{R}	Set of ramping scenarios, index by s^R.
$s_{\mathrm{e}}^{\mathrm{R}+}$	Upward ramping scenario, ending on even time intervals, element of set S^{R}.
$s_{\mathrm{o}}^{\mathrm{R}+}$	Upward ramping scenario, ending on odd time intervals, element of set S^{R}.
$s_{\mathrm{e}}^{\mathrm{R}-}$	Downward ramping scenario, ending on even time intervals, element of set S^{R}.
$s_{\mathrm{o}}^{\mathrm{R}-}$	Downward ramping scenario, ending on odd time intervals, element of set S^{R}.

Decision variables

Decision variables may appear with different indices in the various models. Below, we will list the most 'complete' notation, but the reader should be aware that in some models, these variables may be found with less indices. For example, the fuel cost $fc_{i,j,s}$ has indices i, j and s in the stochastic unit commitment model, but is only dependent on i and j in the deterministic model.

Binary decision variables

$p_{r,j,s}$	Pumping mode of PHES system r at time interval j under scenario s (1: pumping).
$t_{r,j,s}$	Turbining mode of PHES system r at time interval j under scenario s (1: turbining).
$v_{i,j}$	Start-up of power plant i at time interval j (1: start-up).
$v^*_{i,j,l}$	Start-up of fast-starting power plant i at time interval j in reserve level l (1: start-up).
$v^*_{i,j,s}$	Start-up of fast-starting power plant i at time interval j under scenario s (1: start-up).
$w_{i,j}$	Shut-down of power plant i at time interval j (1: shut-down).
$w^*_{i,j,l}$	Shut-down of fast-starting power plant i at time interval j in reserve level l (1: shut-down).
$w^*_{i,j,s}$	Shut-down of fast-starting power plant i at time interval j under scenario s (1: shut-down).
$y_{i,j,s}$	Non-spinning reserve scheduling of power plant i at time interval j under scenario s (1: scheduled).
$z_{i,j}$	Commitment status of power plant i at time interval j (1: online).
$z^*_{i,j,l}$	Commitment status of fast-starting power plant i at time interval j in reserve level l (1: online).
$z^*_{i,j,s}$	Commitment status of fast-starting power plant i at time interval j under scenario s (1: online).

Continuous decision variables

$\delta g^{\mathrm{T}}_{r,j,s}$	Auxiliary variable to enable feasibility of upward reserve provision of PHES system r at time interval j under scenario s, MW. Only used in the HUC model.
$\delta g^{\mathrm{P}}_{r,j,s}$	Auxiliary variable to enable feasibility of downward reserve provision of PHES system r at time interval j under scenario s, MW. Only used in the HUC model.

$\Delta g^{\mathrm{T}}_{r,j}$	Auxiliary variable to enable feasibility of upward reserve provision of PHES system r at time interval j, MW. Only used in the HUC model.
$\Delta g^{\mathrm{P}}_{r,j}$	Auxiliary variable to enable feasibility of downward reserve provision of PHES system r at time interval j, MW. Only used in the HUC model.
$\Delta^{+} g^{\mathrm{P}}_{r,j,s}$	Auxiliary variable to enable feasibility of upward reserve provision in the pumping mode of PHES r at time interval j under scenario s, MW. Only used in the IIUC model.
$\Delta^{-} g^{\mathrm{P}}_{r,j,s}$	Auxiliary variable to enable feasibility of downward reserve provision in the pumping mode of PHES r at time interval j under scenario s, MW. Only used in the IIUC model.
$\Delta^{+} g^{\mathrm{T}}_{r,j,s}$	Auxiliary variable to enable feasibility of upward reserve provision in the turbining mode of PHES r at time interval j under scenario s, MW. Only used in the IIUC model.
$\Delta^{-} g^{\mathrm{T}}_{r,j,s}$	Auxiliary variable to enable feasibility of downward reserve provision in the turbining mode of PHES r at time interval j under scenario s, MW. Only used in the IIUC model.
$\chi_{j,m,s}$	Curtailment of RES-based generation at time interval j on node m under scenario s, MW.
$\chi^{+,\mathrm{L}}_{j,l}$	Curtailment of RES-based generation as upward reserve provider at time interval j under scenario l, MW.
$\chi^{-,\mathrm{L}}_{j,l}$	Curtailment of RES-based generation as downward reserve provider at time interval j in reserve level l, MW.
$\phi_{j,m,s}$	Load shedding at time interval j on node m under scenario s, MW.
$\phi^{+,\mathrm{L}}_{j,l}$	Load shedding as upward reserve provider in time interval j in reserve level l, MW.
$acnsr^{+}_{i,j,l}$	Activation cost associated with non-spinning reserves provided by fast-starting power plant i at time interval j in reserve level l, €.
$acsr^{+}_{i,j,l}$	Activation cost associated with upward spinning reserves provided by power plant i at time interval j in reserve level l, €.
$acsr^{-}_{i,j,l}$	Activation cost associated with downward spinning reserves provided by power plant i at time interval j in reserve level l, €.
$c(g,z)$	Total operational cost as a function of generation g and commitment status z, €.
$co_2t_{i,j,s}$	CO_2-emission cost of conventional generator i at time interval j under scenario s, €.
d^{H}_{j}	Total electricity demand from electric heating systems at time interval j, MW.
$e_{r,j,s}$	State of charge of PHES system r at time interval j under scenario s, MWh.

$f_{j,n,s}$	Flow on line n at time interval j under scenario s, MW.
$fc_{i,j,s}$	Fuel cost of conventional generator i at time interval j under scenario s, €.
$g_{i,j,s}$	Output of conventional generator i at time interval j under scenario s, MW.
$g^{\mathrm{P}}_{r,j,s}$	Charging power (pumping mode) of PHES system r in the pumping mode at time interval j under scenario s, MW.
$g^{\mathrm{T}}_{r,j,s}$	Discharging power (turbining mode) of PHES system r in the turbining mode at time interval j under scenario s, MW.
$inj_{j,m,s}$	Injection of power at time interval j on node m under scenario s, MW.
$nsr^{+}_{i,j}$	Non-spinning reserves delivered by power plant i on time interval j, MW.
$nsr^{+}_{i,j,s}$	Output of fast-starting power plant i on time interval j under scenario s, MW.
$nsr^{+,L}_{i,j,l}$	Non-spinning reserves delivered by power plant i on time interval j in reserve level l„ MW.
$p^{\mathrm{A}}_{h,j}$	Electricity demand of the auxiliary heater in building type h at time interval j, W.
$p^{\mathrm{A,SH}}_{h,j}$	Electricity demand of the auxiliary heater for space heating in building type h at time interval j, W.
$p^{\mathrm{A,HW}}_{h,j}$	Electricity demand of the auxiliary heater for hot water production in building type h at time interval j, W.
$p^{\mathrm{HP}}_{h,j}$	Electricity demand of the heat pump in building type h at time interval j, W.
$p^{\mathrm{HP,SH}}_{h,j}$	Electricity demand of the heat pump for space heating in building type h at time interval j, W.
$p^{\mathrm{HP,HW}}_{h,j}$	Electricity demand of the heat pump for hot water production in building type h at time interval j, W.
$\dot{q}^{\mathrm{DZ,SH}}_{h,j}$	Thermal power provided by the heat pump to the day-zone of building type h at time interval j, W.
$\dot{q}^{\mathrm{NZ,SH}}_{h,j}$	Thermal power provided by the heat pump to the night-zone of building type h at time interval j, W.
$\dot{q}^{\mathrm{DZ,SH},+}_{h,j}$	Thermal power provided by the heat pump to the day-zone of building type h at time interval j if all upward reserves are deployed, W.
$\dot{q}^{\mathrm{NZ,SH},+}_{h,j}$	Thermal power provided by the heat pump to the night-zone of building type h at time interval j if all upward reserves are deployed, W.
$\dot{q}^{\mathrm{DZ,SH},-}_{h,j}$	Thermal power provided by the heat pump to the day-zone of building type h at time interval j if all downward reserves are deployed, W.

$\dot{q}_{h,j}^{\mathrm{NZ,SH},-}$	Thermal power provided by the heat pump to the night-zone of building type h at time interval j if all downward reserves are deployed, W.
$r_{i,j}^{+}$	Upward spinning reserve provided by generator i at time interval j, MW.
$r_{i,j}^{-}$	Downward reserve provided by generators i at time interval j, MW.
$r_{i,j,l}^{+,\mathrm{L}}$	Upward spinning reserve provided by generator i at time interval j in reserve level l, MW.
$r_{i,j,l}^{-,\mathrm{L}}$	Downward reserve provided by generators i at time interval j in reserve level l, MW.
$r_{h,j}^{\mathrm{A,SH},+}$	Upward reserve provided by the auxiliary heater in space heating mode in building type h at time interval j, W.
$r_{h,j}^{\mathrm{A,HW},+}$	Upward reserve provided by the auxiliary in hot water production mode in building type h at time interval j, W.
$r_{h,j}^{\mathrm{A,SH},-}$	Downward reserve provided by the auxiliary heater in space heating mode in building type h at time interval j, W.
$r_{h,j}^{\mathrm{A,HW},-}$	Downward reserve provided by the auxiliary in hot water production mode in building type h at time interval j, W.
$r_{h,j,l}^{\mathrm{H},+}$	Upward reserve provided by building type h at time interval j in reserve level l, W.
$r_{h,j,l}^{\mathrm{H},-}$	Downward reserve provided by building type h at time interval j in reserve level l, W.
$r_{h,j}^{\mathrm{HP,SH},+}$	Upward reserve provided by the heat pump in space heating mode in building type h at time interval j, W.
$r_{h,j}^{\mathrm{HP,HW},+}$	Upward reserve provided by the heat pump in hot water production mode in building type h at time interval j, W.
$r_{h,j}^{\mathrm{HP,SH},-}$	Downward reserve provided by the heat pump in space heating mode in building type h at time interval j, W.
$r_{h,j}^{\mathrm{HP,HW},-}$	Downward reserve provided by the heat pump in hot water production mode in building type h at time interval j, W.
$r_{r,j}^{\mathrm{P},+}$	Upward reserve provided by PHES system r in the pumping mode at time interval j, MW.
$r_{r,j}^{\mathrm{P},-}$	Downward reserve provided by PHES system r in the pumping mode at time interval j, MW.
$r_{j,l}^{\mathrm{P},+,\mathrm{L}}$	Upward reserve provided by PHES systems in the pumping mode at time interval j in reserve level l, MW.
$r_{j,l}^{\mathrm{P},-,\mathrm{L}}$	Downward reserve provided by PHES systems in the pumping mode at time interval j in reserve level l, MW.
$r_{r,j}^{\mathrm{T},+}$	Upward reserve provided by PHES system r in the turbining mode at time interval j, MW.

$r^{\mathrm{T},-}_{r,j}$	Downward reserve provided by PHES system r in the turbining mode at time interval j, MW.
$r^{\mathrm{T},+,\mathrm{L}}_{j,l}$	Upward reserve provided by PHES systems in the turbining mode at time interval j in reserve level l, MW.
$r^{\mathrm{T},-,\mathrm{L}}_{j,l}$	Downward reserve provided by PHES systems in the turbining mode at time interval j in reserve level l, MW.
$rc_{i,j,s}$	Ramping cost of conventional generator i at time interval j under scenario s, €.
s^{+}_{j}	Slack variable, violation of upward reserve requirement at time interval j, MW.
s^{-}_{j}	Slack variable, violation of upward reserve requirement at time interval j, MW.
$sc_{i,j}$	Start-up cost of conventional generator i at time interval j, €.
$t^{\mathrm{HW}}_{h,j}$	Temperature of the water in the hot water storage tank of building type h at time interval j, K.
$t^{\mathrm{SH}}_{h,p,j}$	Air temperature at state p of building type h at time interval j, K.
$t^{\mathrm{SH},+}_{h,p,j}$	Air temperature at state p of building type h at time interval j if all upward reserves are deployed, K.
$t^{\mathrm{SH},-}_{h,p,j}$	Air temperature at state p of building type h at time interval j if all downward reserves are deployed, K.

Parameters

ϵ_r	Round-trip efficiency of PHES system r.
$\overline{\Delta P^{-}_{i}}$	Maximum downward ramping rate of power plant i, MW/TP.
$\overline{\Delta P^{+}_{i}}$	Maximum upward ramping rate of power plant i, MW/TP.
$\overline{\Delta T^{\mathrm{SH}}_{h,p,j}}$	Upward violation of worst-case temperature constraint for building type h in state p at time interval j, K.
$\underline{\Delta T^{\mathrm{SH}}_{h,p,j}}$	Downward violation of worst-case temperature constraint for building type h in state p at time interval j, K.
$\overline{\Phi}$	Maximum allowed expected load shedding over the optimization period, MWh.
π_s	Probability of scenario s.
$A_{h,p}$	State-space model for building type h and state p.
B_i	CO_2-emission of power plant i when running at its minimum stable operating point, ton CO_2/h.
$B^{\mathrm{DZ}}_{h,p}$	State-space model for building type h and state p, K/W.
$B^{\mathrm{DZ}}_{h,p}$	State-space model for building type h and state p, K/W.

C_h	Thermal capacity of the hot water storage tank in building type h, K/W.
CAP_n	Transmission capacity of line n, MW.
COP_h^{SH}	Coefficient of performance of the heat pump in building type h when used for space heating.
COP_h^{HW}	Coefficient of performance of the heat pump in building type h when used for hot water production.
C_i	Fuel cost for running power plant i at its minimum stable operating point, €/h.
CO_2P	CO_2-emission price, €/ton CO_2.
$D_{j,m}$	Electricity demand at time interval j on node m, MW.
D_j^+	Upward reserve requirement at time interval j, MW.
D_j^-	Downward reserve requirement at time interval j, MW.
$E_{h,p,j}^{\mathrm{SH}}$	External disturbances in the state-space model for building type h and state p at time interval j, K.
$\overline{E_r}$	Maximum state of charge of PHES system r, MWh.
$\underline{E_r}$	Minimum state of charge of PHES system r, MWh.
$\overline{G_h}$	Thermal resistance of the hot water storage tank in building type h.
$G_{j,m,s}^{\mathrm{F}}$	Wind power scenario s at time interval j at node m, MW.
$G_{j,m}^{\mathrm{MR}}$	Output of must-run generation at time interval j on node m, MW.
$I_{m,i}^{\mathrm{G}}$	Location matrix, linking the power plant i with node m.
$I_{m,r}^{\mathrm{PHES}}$	Location matrix, linking the PHES system r with node m.
$K_{i,j}$	Constant, property of generator i at time interval j.
MA_i	Marginal increase in fuel cost for power plant i for generation above its minimum stable operating point, €/MWh.
MB_i	Marginal increase in CO_2-emissions of power plant i when running above minimum stable operating point, ton CO_2/MWh.
MUT_i	Minimum up time of power plant i, # TP.
MDT_i	Minimum down time of power plant i, # TP.
NB_h	Number of buildings of type h.
$NSRC_i$	Cost of scheduling power plant i as non-spinning reserve, €.
$\overline{P_i}$	Maximum stable operating point of power plant i, MW.
$\underline{P_i}$	Minimum stable operating point of power plant i, MW.
$\overline{P_r}$	Maximum power capacity of PHES system r, MW.
$P_{j,l}^+$	Probability of activation of reserves scheduled in upward reserve level l.
$P_{j,l}^-$	Probability of activation of reserves scheduled in downward reserve level l.
$\overline{P_h^{\mathrm{A}}}$	Maximum electric capacity of the auxiliary heater in building type h, W.

$\overline{P_h^{\mathrm{HP}}}$	Maximum electric capacity of the heat pump in building type h, W.
$PTDF_{n,m}$	Power transfer distribution factors, the effect of injections on node m on the flow on line n.
$\dot{Q}_{h,j}^{\mathrm{D}}$	Thermal demand due to hot water withdrawal in building type h at time interval j, W.
RCP_i	Ramping cost for power plant i, €/MW.
STC_i	Start-up cost for power plant i, €.
TP	Duration of the time interval j, h.
T	Optimization horizon, # TP.
T^{E}	Temperature of the environment, K.
$\overline{T_h^{\mathrm{HP}}}$	Maximum supply temperature of the heat pump in building type h, K.
$\underline{T_{h,j}^{\mathrm{HW}}}$	Minimum temperature of the water in the hot water storage tank of building type h at time interval j, K.
$\underline{T_{h,p,j}^{\mathrm{SH}}}$	Minimum air temperature at state p of building type h at time interval j, K.
$\overline{T_{h,p,j}^{\mathrm{SH}}}$	Maximum air temperature at state p of building type h at time interval j, K.
VOC	Value of curtailed RES-based generation, €/MWh.
$VOLL$	Value of lost load, €/MWh.
VOR	Value of shed reserves, €/MW.

Contents

Abstract iii

Abbreviations ix

Nomenclature xi

Contents xix

1 Introduction 1

1.1 Context 2

1.2 Motivation 3

1.3 Objectives 5

1.4 Terminology 8

1.5 Modeling framework 9

1.6 Scientific contributions 16

1.7 Outline 18

1.8 Conclusion 19

2 Operational electricity generation system models & uncertainty 21

2.1 Introduction 22

2.2 DUC 29

2.3 SUC 50
2.4 IIUC 67
2.5 HUC 81
2.6 PUC 91
2.7 Conclusion 102

3 Statistical analysis of the error on RES-based generation forecasts 107
3.1 Introduction: wind power forecast errors 109
3.2 The Lévy α-stable distribution 111
3.3 Methodology 114
3.4 Results & discussion 117
3.5 Applications 122
3.6 Conclusion 130

4 Scenario generation & reduction 133
4.1 Scenario generation & reduction: the basics 136
4.2 Scenario generation: theory 142
4.3 Scenario generation: results & discussion 155
4.4 Scenario reduction: theory 168
4.5 Scenario reduction: results & discussion 191
4.6 Comparision selected scenario generation & reduction techniques 213
4.7 Conclusion 218

5 Cross-comparison of selected unit commitment models 221
5.1 Introduction 222
5.2 The baseline: DUC 228
5.3 The benchmark: SUC 245
5.4 Increasing the cost-efficiency of the IIUC 258

5.5 Combining speed & optimality: HUC 273
5.6 Cost-effective, reliable & fast: PUC 287
5.7 Conclusion: cross-comparison 297

6 Limitedly controllable demand response as flexibility provider 305
6.1 Introduction 307
6.2 The modeling challenge: a literature review 310
6.3 Methodology 321
6.4 Results & Discussion 333
6.5 Conclusion 345

7 Applications 347
7.1 Balancing cost associated with wind power forecast errors . . . 348
7.2 Demand response with electric heating systems 358
7.3 Conclusion 373

8 Concluding remarks & suggestions for future research 375
8.1 Concluding remarks 376
8.2 Suggestions for future research 380

A Publications not included in this dissertation 383
A.1 Impact of the German nuclear phase-out on Europe's electricity generation 383
A.2 Bidding strategies for Virtual Power Plants considering CHPs and intermittent renewables 384
A.3 Effects of large-scale power to gas conversion on the power, gas and carbon sectors and their interactions 386

B Case study: data & assumptions 387

C Tight & compact UC formulations 391

C.1 DUC 391
C.2 SUC 396
C.3 IIUC 400
C.4 HUC 405
C.5 PUC 412

D The Lévy α-stable distribution **417**

E Chance constraints: analytical reformulation **423**

Bibliography **427**

Curriculum Vitae **459**

List of publications **461**

Chapter 1

Introduction

The electric power sector is currently undergoing unprecedented changes. The massive deployment of variable and limitedly predictable electricity generation from renewable energy sources (RES) requires power system operators to radically rethink the way power systems are studied, designed and operated. In light of this challenge, we propose a modeling framework to analyze the impact of stochastic RES-based electricity generation, novel operational flexibility providers and an activated demand side on day-to-day power system operation.

Section 1.1 provides some background to position this dissertation. The motivation for the presented research is summarized in Section 1.2. We define our research objectives in Section 1.3. We focus on some terminology in Section 1.4. The proposed framework to study the impact of intermittent RES-based generation on power systems is presented in Section 1.5. In addition, Section 1.5 lists the majority of publications that form the basis of this dissertation. The scientific contributions and relevance of the presented research are summarized in Section 1.6. The results and scientific contributions of some additional publications, which were not included in the main body of this dissertation as their content is not strictly in line with the objectives formulated in Section 1.3, are summarized in Appendix A. Before concluding this chapter (Section 1.8), we provide an outline of the remainder of this dissertation (Section 1.7).

1.1 Context

Present-day and future electric power systems are characterized by increasing shares of intermittent electricity generation from renewable energy sources (RES). Especially in Europe, wind and solar power capacities have steadily risen over the last years. The total wind power capacity in Europe now well exceeds 128 GW [1] and in 2013 alone over 10 GW of solar power capacity was connected to the grid [2]. This push for RES-based generation is in part the result of growing concerns on man-made climate change, which requires to decarbonize the power sector [3].

Some forms of RES-based electricity generation, in particular solar and wind power, have a stochastic character, i.e., they are variable and to some extent unpredictable. The limited predictability of RES-based generation requires that sufficient operational flexibility is available to the system operator to balance unexpected deviations from the forecasted RES-based generation profile in real time. Therefore, as forecast errors are made, reserves[1], i.e. controllable generation, energy storage or load must be procured ahead of time to ensure the system operator's ability to maintain the power system balance in real time. The associated operational costs are referred to as balancing costs [4, 5, 6, 7].

To minimize these balancing costs associated with RES-based electricity generation, researchers are actively pursuing the development of improved power system operation methods and novel sources of flexibility. First, novel power system operation methods and market designs are being investigated, in order to properly size and allocate operational reserves, ensuring a reliable and cost-efficient operation of the power system [4]. Second, system operators are continuously seeking novel means of flexibility, in addition to conventional sources of flexibility such as transmission, cycling of thermal power plants and curtailment of RES-based generation. Especially activating the demand side, via the introduction of local energy storage technologies and/or demand response (DR) programs, has received a lot of attention in the scientific literature. Demand response allows load to accommodate changes in the RES-based electricity generation profile, limiting the variability in the net load perceived by the electricity generation system [8]. A significant number of residential appliances, such as thermostatically controlled loads, contain some form of inherent 'energy storage', e.g. based on thermal inertia, which allows these loads to simultaneously be fully responsive and non-disruptive in terms of the perceived energy service [9]. This makes them excellent candidates for DR. Although industrial DR is currently exploited as a reserve provider in many power systems and residential demand-side technologies are sufficiently mature

[1] The concept 'reserves' requires a careful definition, which we will provide in Section 1.4.

to enable real-time control, the potential of residential DR remains to a large extent untapped [10, 11]. However, the adoption of residential DR is actively pursued, as illustrated by the successful deployment of residential DR programs in e.g. the PJM system [12] and demonstration projects such as e.g. LINEAR [11, 13].

1.2 Motivation

Despite a wide range of methodologies, considered power systems, input data and assumptions, most researchers agree that the integration cost of stochastic RES-based electricity generation such as wind and solar power is substantial [4, 5, 6, 7]. To study the aforementioned balancing costs, researchers typically turn to market data analysis and so-called **unit commitment (UC) and economic dispatch (ED)** models. These short-term operational models of a power system are used to determine the on/off states (i.e. the unit commitment status) of the power plants (UC) and the output of the scheduled and fast-starting power plants (ED), accounting for all relevant technical constraints of these units [14]. The system perspective adopted in these models corresponds to a vertically integrated environment, in which a regulated monopolist schedules the electricity power plant portfolio at minimum operational cost, or to an unbundled environment based on a centralized and controlled Electricity Pool model (e.g. the PJM market) [15]. Although the organization of the European electricity system is significantly different, these UC models are actively employed by European TSOs and researchers, e.g. for long-term energy policy implication and transmission grid expansion studies [16].

The operational UC models available in the scientific literature can be separated into two broad categories. In a deterministic paradigm, such a UC model considers some reserve requirements to ensure that modest deviations from the forecasted demand profile can be absorbed. However, with the large-scale integration of RES-based generation, the amount of variability and uncertainty on the residual load profile faced by the dispatchable units in the system may drastically increase. The question arises if such deterministic models capture all relevant costs and constraints to ensure a cost-effective and reliable power system operation. In light of this challenge, researchers have developed numerous alternative UC formulations, with varying success. One of the most prominent alternatives to reserve-constrained UC models is the so-called stochastic UC model. The uncertainty is represented via a set of discrete realizations of the uncertain parameter or variable, i.e. scenarios. By enforcing that the load must be met in each of those scenarios, the resulting UC schedule is hedged against all considered realizations of the uncertain parameter, e.g. the wind or solar

power forecast. Moreover, the operational cost associated with each of those scenarios is considered, allowing an optimal trade-off between reliability and operational cost. In theory, such an approach will yield optimal UC decisions under uncertainty. The precondition for such optimal UC decisions is that the considered set of scenarios is a sufficient representation of the uncertain variable. The high computational burden of the stochastic UC problem however puts an upper limit on the number of scenarios one can consider during optimization, which may reduce the cost-effectiveness of the resulting UC schedule. In addition, the computational cost of solving a stochastic UC problem considering a relatively small number of scenarios remains high, even for power systems of a modest size [17].

These different representations of the uncertainty and the associated reserve requirements in an operational electricity generation system model have a direct impact on the cost-effectiveness of the UC schedule, hence on the estimates of the balancing costs associated with intermittent RES-based electricity generation. In this dissertation, we will attempt to improve available UC models and to develop novel formulations, striving for the (theoretical) cost-optimality of a stochastic UC model at the computational cost of a deterministic UC model. We focus on a specific source of uncertainty, namely the error on wind power forecasts, and the impact of this forecast error on the power system. The relationship between wind forecasts and short-term operational planning of a power system is of such importance that some researchers include a state-of-the-art numerical weather prediction model within the same closed-loop optimization as the UC and ED model [18]. Despite our focus on wind power forecast uncertainty, which allows us to illustrate the methodological contributions developed in this dissertation, the presented techniques and models are more widely applicable.

Residential demand response (DR) is considered a possible game-changing technological break-through in the integration of intermittent RES-based generation. This optimism w.r.t. the possible benefits of DR is fed by numerous studies on the value of load shifting or arbitrage with DR-adherent loads. Nevertheless, real-life applications of residential DR remain rare [11], although residential DR has been implemented successfully in a.o. the PJM power system [12]. To some extent, the lack of adoption of residential DR stems from the inability to quantify the benefits for consumers and producers, as the models used to study the integration of RES-based electricity generation and novel flexibility providers such as DR may not capture all relevant effects. First, deterministic models may yield sub-optimal solutions in power systems facing a limitedly predictable demand and/or RES-based generation profile. Second, system-wide models typically include a simplified representation of the flexibility at the demand side. For example, in the context of DR, two typical representations are found in the literature: price-elasticity models [19]

and so-called virtual generator models [20]. Recently, some authors, including the author of this dissertation, have proposed so-called integrated models of both the supply of, and demand for, electric power [21]. Such integrated models allow accounting for the technical and comfort constraints of the demand side flexibility provider. For example, in the context of DR with electric heating systems, such integrated models allow providing estimates of the impact of DR on e.g. the perceived thermal comfort of the home owners providing demand side flexibility. Such metrics are, in addition to accurate system value estimates, of crucial importance in the assessment of the feasibility of DR. Third, the degree of controllability of residential DR technnologies is typically not questioned. However, research and field tests have shown that DR-adherent loads may exhibit a significant variability in their response to a control signal [22, 11].

In this dissertation, we aim to develop an integrated model, considering sufficient detail at the demand side and the supply side, to obtain realistic estimates of the system value of DR-based load shifting and reserve provision. This integrated model accounts for the variability and limited predictability of RES-based electricity generation and the limited controllability of DR-adherent loads. We focus on DR with residential electric heating systems. These systems could allow modifying their electric load pattern without affecting the quality of the final thermal energy service delivered, thanks to the inherent thermal inertia of the system (both in the building envelope [23] and in additional thermal energy storage tanks [24]). Small-scale electric heating systems can be installed in large numbers in the built environment and control access to these loads could be very inexpensive with the advent of communication platforms; so they are good candidates for DR [25, 9].

1.3 Objectives

In essence, we aim to develop a comprehensive framework to study the short-term operational impact of variable and limitedly predictable RES-based electricity generation on power systems with a high penetration of RES-based electricity generation and DR-based flexibility. To reach this goal, we must meet the following objectives. The first objective relates to the study and development of the aforementioned UC models:

(1) Improving existing and developing novel operational electricity generation system models considering high shares of limitedly predictable RES-based electricity generation, with a focus on the associated operational system cost, reliability and computational effort.

To this end, we will study the aforementioned UC problem, considering wind power forecasts as the only source of uncertainty. In reality, unplanned power plant and transmission system component outages, as well as erroneous load forecasts may increase the level of uncertainty in the power system. Limiting the considered sources of uncertainty to wind power forecasts however allows focusing on the methodological improvements required to adequately represent uncertainty in these UC models. The presented models and techniques can however be employed or extended to consider multiple sources of uncertainty. We will discuss some of these extensions by considering the uncertainty on wind and solar power forecasts simultaneously in Chapter 3 and Chapter 4. We define the following intermediate objectives:

(1.1) The development of a characterization of the stochastic process at hand, i.e. the wind power forecast error;

(1.2) The development of continuous and discrete representations of that stochastic process, suitable for consideration in a UC model;

(1.3) The study and improvement of existing UC formulations, in particular the deterministic and stochastic UC models found in the scientific literature. These improvements may relate to the inclusion of novel flexibility providers in deterministic formulations to improve the cost-effectiveness of the UC schedule or novel representations of the uncertain RES-based generation in a stochastic UC model to reduce the computational burden;

(1.4) The development of novel easy-to-solve, cost-optimal and reliable UC models, building on knowledge gained from the analysis of the UC formulations found in the scientific literature;

(1.5) Qualitative and quantitative comparison of the UC formulations, with a focus on the operational cost, reliability and computational burden.

Characterizing the stochastic process at hand (Objective (1.1)) is a prerequisite to the development of adequate reserve sizing algorithms and scenarios generation techniques (Objective (1.2)). The resulting scenarios and reserve requirements drive the performance of the studied UC formulations (Objectives (1.3) and (1.4)). The comparison of the performance of existing and to-be-developed UC models (Objective (1.5)) will be based on the following **three metrics**:

- The total **operational costs**, i.e. a measure for the cost-effectiveness of the resulting UC schedule, accounting for the wide range of possible realizations of the uncertain RES-based electricity generation;

- The **reliability** of the resulting UC schedule, i.e. the likelihood that the resulting UC schedule contains sufficient flexibility to avoid load shedding in real time. We will characterize the reliability of the UC schedule by calculating the expected load shedding or energy not served (ENS) volumes;
- The **computational tractability** of the UC model, characterized via the time required to compute the UC schedule.

To obtain statistically significant estimates of these metrics, we will perform Monte-Carlo ED simulations of the obtained UC schedules on a large set of scenarios (Section 1.5).

Our second objective relates to DR with electric heating systems:

(2) The inclusion of a physical demand side model, sufficient to represent the operational flexibility available in limitedly controllable residential electric heating systems, in operational electricity generation system models considering high shares of limitedly predictable RES-based electricity generation.

Objective (2) originates from the shortcomings found in models currently available in the scientific literature and is part of an attempt to obtain realistic estimates of the system value, i.e. the attainable operational cost reductions, associated with residential DR. We define the following sub-objectives:

(2.1) The inclusion of a validated, physical demand side model in state-of-the-art UC models, in order to obtain an estimate of the maximum attainable operational cost savings as a result of DR deployment;

(2.2) The development of novel techniques to account for the limited controllability of demand response providers.

The development of the demand side model is executed in close collaboration with D. Patteeuw, A. Arteconi and L. Helsen (Division of Applied Mechanics and Energy Conversion, Mechanical Engineering, KU Leuven) and C. Protopapadaki, G. Reynders and D. Saelens (Building Physics, Civil Engineering, KU Leuven). Our focus is on the integration of this model in state-of-the-art UC models, capturing all relevant constraints on the supply and demand side, accounting for the limited predictability of some forms of RES-based electricity generation (Objective (2.1)). We will take the perspective of a system operator and assume that we have control of all elements of the system, including the demand side flexibility providers (Section 1.5). This paradigm allows estimating an upper

bound to the attainable cost savings associated with a large-scale deployment of residential DR (Objective (2.1)). This upper bound however does not account for the limited controllability of residential DR providers. The envisioned methodology to meet Objective (2.2) addresses this shortcoming.

1.4 Terminology

Before introducing the proposed framework to study uncertainty in power systems, we want to focus the reader's attention on some terminology used throughout this dissertation.

Reserves We will use the term 'reserves' to refer to the total operational flexibility required in the power system at hand to maintain the system balance in real time. This is in line with the perspective of an ISO who has control over all assets in the system. The amount of reserve capacity depends on a trade-off between the socio-economic cost of load shedding and the cost of procuring and activating the reserves. Controllable load, energy storage systems and conventional electricity generation units may offer reserve capacity. If a dispatchable, conventional generation unit is scheduled as a reserve provider, it may be online ('spinning reserves') or off-line ('non-spinning reserves'). Non-spinning reserves, sometimes referred to as standing reserves [26], may only be offered by units that are able to start-up within 15 minutes (the time step in all simulations). Throughout the dissertation, the terms 'regulation services', 'reserves' and 'operational flexibility' are used interchangeably.

Reliability According to Luickx [27], reliability relates to the ability of the electricity generation system to deliver electricity to all users within acceptable standards and in the amounts desired. Reliability can be decomposed in adequacy and security. The adequacy of a power system is measured by its ability to meet the demand in all 'steady states' which may occur in that power system. It is typically related to the long-term reliability of the system [27]. The security (level) of a power system is defined by its ability to withstand sudden disturbances such as electric short circuits, unanticipated losses of system components, generation or load [27]. In this dissertation, we will focus on the security of a given power system, considering various operating regimes - i.e. different UC policies and reserve sizing procedures - and the availability of different flexibility providers (spinning, non-spinning, energy storage, DR). We will use the term 'reliability' to refer to the security of a power system and we

will use the expected volume of load shedding or energy not served (ENS) as a metric for the security level of a power system.

1.5 A framework to study power systems with high penetrations of limitedly predictable RES-based electricity generation

To meet the objectives outlined in Section 1.3, we introduce a modeling framework that allows studying and evaluating the impact of intermittent RES-based electricity generation on day-to-day power system operations. This framework starts from the characterization of the uncertainty, which provides input for scenario generation and reserve sizing techniques, which in turn are representations of the uncertainty in the UC problem. Throughout this dissertation, we take the perspective of a system operator, i.e. we assume that we have control and knowledge of all elements in the power system. By assuming perfect knowledge on (except on the uncertain variables) and control of the assets in the power system at hand, distorting influences, such as e.g. market inefficiencies, are removed from the equation. What is left, is the impact of intermittent RES-based electricity generation.

In the proposed framework, we will have to answer three questions with regard to the operational reserves. First, we need to solve the **reserve sizing** problem. In essence, we will try to answer the question how much flexibility is needed at each moment in time to mitigate the impact of forecast errors. In addition, one might also specify the technical properties that these reserves need to possess, such as ramping capabilities. The amount of required reserves depends on the required reliability level of the system, as well as on the cost a system operator is willing to incur to reach that reliability level. Once the required amount of reserves is determined, one needs to specify which sources of flexibility will provide these reserves. These flexibility sources are however not unlimited and typically need to be 'planned ahead' [28]. For example, if a system operator schedules an energy storage system as operational reserve, one needs to ensure that there is sufficient energy stored or available storage capacity to deploy this flexibility in real time. Similarly, if conventional power plants are used to provide up- and downward regulation, one needs to ensure that these units are online or available to ramp up/down and/or start-up/shut-down. This scheduling problem can be integrated in a UC problem. By solving this UC problem, we simultaneously (1) schedule generation and energy storage units to meet the demand and (2) decide upon the **reserve allocation or procurement**. This problem is referred to as a joint energy and reserve scheduling problem [29].

Such joint optimization ought to result in the most cost-efficient solutions of both scheduling problems [30, 31, 32], which resulted in the gradual evolution of some real (mostly US) markets such as PJM, ISO-NE, NYISO, CAISO and ERCOT from sequential to joint mechanisms (see [33, 34] and references therein). Last, once the units that will provide real-time flexibility are selected, one needs to activate these flexibility options in the most cost-effective way. This last step, referred to as the **reserve activation or deployment**, allows testing the adequacy and cost-efficiency of these reserves in mitigating the impact of the forecast error.

Throughout this scheduling problem, a system operator aims for reliability at the lowest possible operational cost. The operational cost associated with reserves, i.e. the **balancing cost**, can be decomposed in

- **allocation or procurement costs**, the operational cost that is associated with scheduling reserves. It is a combination of direct costs, resulting from additional start-ups and decreased power plant efficiency in part-load operation and an indirect opportunity cost, which is the result of the withholding of capacity from the scheduling procedure to meet the load;
- **activation or deployment costs**, which are the direct operational costs incurred when the reserves are activated or deployed.

Ideally, one takes into account both the procurement and deployment costs when sizing and allocating reserves. This requires simultaneously solving the reserve sizing, allocation and activation problem. For example, as we argue in Chapter 2, optimal reserve sizing is the result of a trade-off between the cost of reserve procurement and deployment and the socio-economic cost of load shedding and curtailment of available RES-based electricity generation. These costs are dependent on the operational 'state' of the power system at hand, which is typically unknown during ex-ante reserve sizing exercises. Moreover, the deployment costs are dependent on the flexibility providers scheduled and the realization of the unknown RES-based generation. In subsequent chapters we illustrate that not all UC models allow taking into account all these costs simultaneously.

To study the cost-effectiveness of different UC formulations and flexibility providers, we propose a framework which consists of four main steps, as illustrated in Fig. 1.1. First, the distribution of the stochastic variable –here the error on the wind power forecast– is analyzed and reduced to a conditional probability distribution of a certain error occurring given the forecast at each

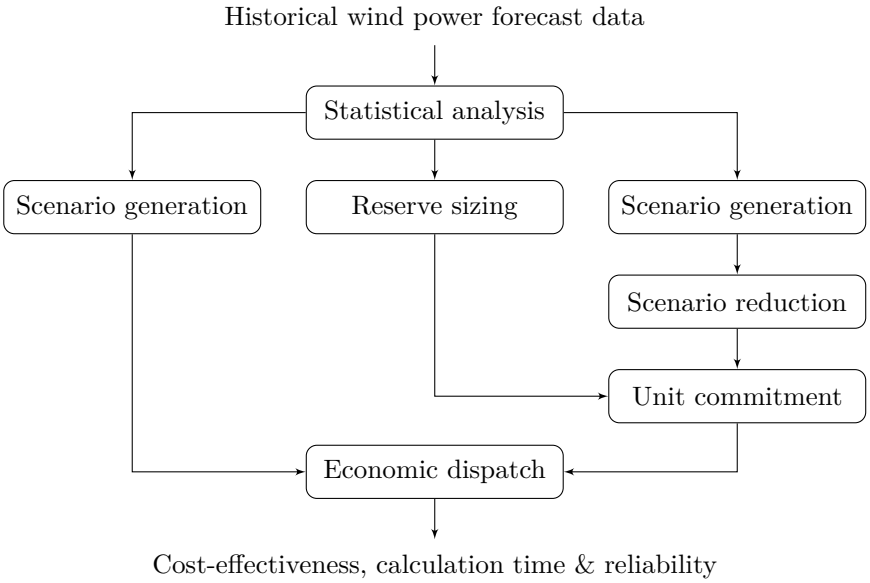

Figure 1.1: The proposed modeling framework to study short-term uncertainty in power systems. A statistical analysis of historical data facilitates scenario generation and reserve sizing algorithms. The resulting scenarios, if required after scenario reduction, and reserve requirements are representations of the (range of) possible realizations of the limitedly predictable RES-based electricity generation in a UC model. Monte-Carlo ED simulations allow testing the cost-effectiveness and reliability of the resulting UC schedule.

time step[2]. Second, this distribution will be used to generate a set of scenarios for each forecast that captures all relevant statistical properties of those forecast errors. In essence, we are representing the distribution of the forecast error as a set of discrete realizations with a probability of occurrence. Third, a UC model is used to solve the reserve allocation problem. The statistical information gathered in the first step may be used to obtain reserve requirements via reserve sizing algorithms. Last, the resulting solution – i.e. the UC schedule, including the scheduled reserves – is analyzed in a Monte-Carlo ED simulation. For a large set of scenarios an ED simulation is executed for each UC schedule in order to obtain a proxy for its expected performance in terms of operational

[2]Throughout this dissertation, we will use the concept of 'time step', 'time interval' and 'instance' interchangeably.

costs, curtailment of RES-based electricity generation and reliability (Section 1.3). The four steps in this framework are briefly discussed below.

Statistical analysis of the forecast error

As a first step, we develop a methodology to obtain a statistical description of the forecast error on RES-based electricity generation. Focusing on the uncertainty on wind power forecasts, we propose a so-called Lévy α-stable distribution as an improved description of the forecast error. The obtained distributions are essential in terms of input data for the rest of the methodology. In the proposed framework, they facilitate (probabilistic) reserve sizing techniques and scenario generation methods. An adequate description of the uncertainty at hand is of crucial importance for the performance and evaluation of any UC model.

Chapter 3 deals with the characterization of the error on RES-based electricity generation forecasts and contains elements from the following publications:

- K. Bruninx and E. Delarue, *A Statistical Description of the Error on Wind Power Forecasts for Probabilistic Reserve Sizing,* IEEE Trans. Sustain. Energy, vol. 5, no. 3, pp. 995–1002, 2014.
- K. Bruninx, E. Delarue, and W. D'haeseleer, *Statistical description of the error on wind power forecasts via a Lévy alpha-stable distribution,* in YEEES 2012, Young Energy Engineers & Economists Seminar 2012, December 7, 2012, Florence, Italy and EUI RSCAS Working Paper 2013/50, 2013.

Scenarios as a discrete representation of the forecast error

In the ideal case, one would optimize the UC schedule considering the full, continuous description of the forecast error. Computational limitations do however not allow this. Modelers therefore try to capture the distribution of a stochastic variable in predefined reserve requirements (reserve sizing) or a set of scenarios, i.e. a number of discrete realizations of the stochastic variable with a specific probability of occurrence. This set of scenarios can be used directly in a stochastic UC model (Chapter 2) and/or in ex-post Monte-Carlo ED simulations to evaluate the resulting UC schedule (see 'economic dispatch'). In some cases, it will prove to be necessary to reduce the number of scenarios considered in these stochastic UC models to maintain computational tractability. Therefore, researchers have developed algorithms to ex-ante select scenarios for consideration in a stochastic model, ideally without loss of solution quality

[35]. The process of identifying and selecting those scenarios that are critical to obtain reliable and cost-optimal UC schedules is referred to as 'scenario reduction'.

In Chapter 4, we provide an overview of available scenario generation and reduction techniques, each with its drawbacks and advantages. Although not exhaustive, this literature review allows identifying a suitable scenario generation technique, based on Pinson et al. [36]. In addition, we develop a scenario reduction algorithm, based on the so-called fast-forward selection scenario reduction technique, in which a probability-distance functional between the original and reduced set of scenarios is minimized [37, 38]. Chapter 4 is an extended version of the following publications:

- K. Bruninx and E. Delarue, *Scenario Reduction Techniques and Solution Stability for Stochastic Unit Commitment Problems,* ENERGYCON, April 4–8, 2016, Leuven, Belgium.
- K. Bruninx, E. Delarue and W. D'haeseleer, *A practical approach on scenario generation & reduction algorithms for wind power forecast error scenarios,* KU Leuven Energy Instititute WP EN2014–15, 2015.

Reserve allocation or procurement through unit commitment models

Although electricity systems and markets appear in many forms, some form of a day-ahead market clearing or scheduling mechanism is found in almost all of them [30]. Unit commitment-based scheduling is considered the most cost-efficient way to operate such day-ahead scheduling mechanisms [30, 31, 32]. In case reserves need to be procured, the integration of this reserve procurement problem in the UC problem is a logical step to ensure least-cost power system operation, while ensuring reliability and respecting the technical limitations of power plants, transmission systems, energy storage systems and activated loads. Five UC formulations are presented in Chapter 2, each of which deal with uncertainty differently:

- a deterministic unit commitment (DUC) model considering reserve constraints;
- a stochastic unit commitment (SUC) model considering a reduced set of scenarios instead of reserve constraints;
- an improved interval unit commitment (IIUC) model which characterizes the needed reserves via the ramping requirements they need to satisfy;

- a hybrid deterministic-stochastic unit commitment (HUC) model combining a small set of scenarios and reserve constraints;
- a probabilistic unit commitment (PUC) model with multiple reserve intervals, characterized by a probability of deployment.

Three of these UC models, i.e. the deterministic, stochastic and interval UC formulation, are available in the scientific literature. Improvements to the formulation of each of the aforementioned models are suggested. In addition, two novel UC formulations are presented: the probabilistic formulation and the hybrid deterministic-stochastic model. We focus on the way uncertainty is represented in these models, how reserves are procured and how the associated procurement and deployment costs are accounted for. Although all of the aforementioned formulations essentially describe the same problem, significant differences may be observed in their performance (Chapter 5).

These UC models form the backbone of this dissertation. The relevance of the other building blocks of our modeling framework can only be illustrated by understanding the way these models deal with uncertainty. In the second chapter of this dissertation, we therefore study the formulation of the aforementioned models. Chapter 2 is based on:

- K. Bruninx, Y. Dvorkin, E. Delarue, H. Pandžić, W. D'haeseleer, and D. S. Kirschen, *Coupling Pumped Hydro Energy Storage with Unit Commitment,* IEEE Trans. Sustain. Energy, vol. 7, no. 2, pp. 786–796, 2016.
- K. Bruninx and E. Delarue, *A probabilistic unit commitment model: cost-effective, reliable and fast,* Submitted to IEEE Trans. Power Syst., 2015.
- K. Bruninx, K. Van den Bergh, E. Delarue, and W. D'haeseleer, *Optimization and Allocation of Spinning Reserves in a Low-Carbon Framework,* IEEE Trans. Power Syst., vol. 31, no. 2, pp. 872–882, 2016.
- K. Van Den Bergh, K. Bruninx, E. Delarue, and W. D'haeseleer, *LUSYM: a unit commitment model formulated as a mixed-integer linear program,* KU Leuven Energy Institute Working Paper WP EN2014–07, 2015.

The models presented in Chapter 2 do not consider industrial or residential DR-based flexibility. However, as mentioned in the introduction of this chapter, activating the demand side may drastically reduce the cost of integrating variable and limitedly predictable RES-based electricity generation. Therefore, we extend the probabilistic UC model – which will prove to be a good compromise between computational complexity, cost-optimality and reliability – with a physical

demand side model. This demand side model is a detailed representation of (1) the technical constraints of residential electric heating systems, (2) the thermal behavior of the buildings and heat emission systems these heating systems are connected to, and (3) the residents' comfort constraints. The inclusion of such a demand side model in a UC formulation yields a so-called integrated model [21], which allows scheduling DR-based arbitrage and regulation services without loss of thermal comfort for the building owners providing these services. However, these distributed DR-based arbitrage and reserve providers may exhibit more variability in response to a control signal than large, centralized electricity generation and energy storage units [22]. Therefore, we will introduce so-called chance constraints to account for imperfectly controllable DR providers.

Demand response with residential electric heating systems is the topic at hand in Chapter 6, which contains elements of the following publications:

- K. Bruninx, D. Patteeuw, E. Delarue, L. Helsen, and W. D'haeseleer, *Short-term demand response of flexible electric heating systems : the need for integrated simulations,* in EEM13, 10$^{\text{th}}$ International conference on the European Energy Market, May 27–31, 2013, Stockholm, Sweden.
- D. Patteeuw, K. Bruninx, A. Arteconi, E. Delarue, W. D'haeseleer, and L. Helsen, *Integrated modeling of active demand response with electric heating systems coupled to thermal energy storage systems,* Applied Energy, vol. 151, pp. 306–319, 2015.

Reserve activation or deployment through economic dispatch simulations

To evaluate the performance of the day-ahead UC schedule, we study the results of the so-called economic dispatch (ED) problem for a large number of realizations or scenarios of the uncertain variable at hand. For each scenario, an ED optimization is performed given the (fixed) day-ahead UC schedule. This ED problem is formulated as a DUC model, without any reserve constraints, in which the UC schedule is fixed to the solution of the UC model at hand. To ensure these results are not biased towards the set of scenarios considered in the UC problem, we will perform this dispatch on a new set of scenarios (Fig. 1.1). Given a large enough set of scenarios, this Monte-Carlo approach allows calculating statistically relevant expected values as the probability-weighted averages of e.g. the objective value of the ED problem in every scenario, as well as standard deviations of these variables.

During dispatch, we will assume that we have perfect foresight over the full time horizon. This does not fully reflect the structure of the decision problem a system operator faces. In reality, information becomes available as time progresses, i.e.

during the dispatch in each time step. In the presented approach, the flexibility available during dispatch is thus overestimated, as the system operator can optimally dispatch the scheduled flexibility within the boundaries of the UC schedule[3].

1.6 Scientific contributions

The added value of the modeling framework proposed in this dissertation lies in the combination of a characterization of the uncertainty (Chapter 3), which allows generating statistically significant scenarios (Chapter 4), a scenario reduction technique that yields tractable UC problems and stable, unbiased UC schedules (Chapter 4) and state-of-the-art UC models to solve the reserve allocation problem (Chapter 2). In the scientific literature one seldom finds this combination. Researchers studying the performance of UC models will often assume that the uncertainty at hand follows a certain distribution. Although this approach is sufficient to compare the relative performance of UC models, this assumption does not allow calculating estimates of the balancing cost associated with e.g. limitedly predictable wind power. Likewise, the employed scenario generation and reduction techniques are often not validated for the specific case of limitedly predictable RES-based electricity generation in UC problems. At the other end of the spectrum we find detailed statistical analyses of the properties of limitedly predictable RES-based electricity generation, or in-depth studies of scenario generation and reduction techniques. Typically, this line of research has little attention for e.g. the operational models the resulting distributions or scenarios are used in. One example is the widespread use of the fast-forward scenario reduction technique [38, 37] in the power systems research community. Its simplicity, strong foundation in mathematical theory and availability makes it an appealing candidate to solve the scenario reduction problem in many stochastic programming problems. However, in Chapter 4 we will show that this technique may perform poorly in the context of stochastic UC models.

In addition, we will attempt to improve each of the building blocks in the proposed framework. A new distribution for the forecast error on wind power is proposed, which allows capturing the heavy-tailed and skewed character of wind power forecast errors. As these tails capture the probability of large forecast errors, which in turn drive the outcome of a reserve sizing problem, the impact

[3]The search for better ways to address these concerns is a topic of ongoing and future research. One current modeling trend that addresses this issue is the use of forward-rolling time horizons [39]. However, empirical testing has shown that for the particular power system studied in this dissertation, the impact of including a forward-rolling time horizon is negligible.

of such a refinement is not to be underestimated (Chapter 3). With current scenario reduction techniques, obtaining reliable and cost-effective (stochastic) UC schedules within reasonable calculation times appears to be a major challenge. We will illustrate why current techniques, such as the fast-forward scenario reduction technique [38, 37], may fail to capture those scenarios that are relevant in a UC problem. A new way of characterizing each scenario is introduced to alleviate the aforementioned problem, enhancing the cost-optimality of the resulting UC schedule. We improve existing UC models by introducing energy storage-based reserve provision (DUC, IIUC) and non-spinning reserves (IIUC). Last, we develop two novel representations of uncertainty in UC models, i.e. a hybrid model, considering reserve requirements and a small set of scenarios, and a probabilistic formulation, in which reserve requirements are split in various levels, each with a distinct probability of activation. The relevance of these improvements will be illustrated in Chapter 5, in which we compare various UC models in a case study, inspired by the Belgian power system, assuming a high wind power penetration.

Considering demand response modeling, our approach goes beyond the state-of-the-art by combining a detailed physical demand side model [40, 21], a probabilistic UC model which considers the full cost of reserve procurement and deployment [41] and an accurate, scalable representation of the variability in the response of DR-adherent loads using chance-constrained programming. The integrated model proposed in this dissertation allows optimally scheduling and activating DR-based arbitrage and reserves with explicit consideration of the thermal comfort requirements of the occupants. In addition, we consider the possibly limited controllability of demand response-based arbitrage and reserves using chance-constrained programming. Although Mathieu et al. show that DR-adherent loads can exhibit significant variability in their response to a control signal [22], which could have a profound effect on the value of DR for a system operator, this effect has – to the best of the author's knowledge – not yet been quantified. The proposed methodology allows (1) providing realistic estimates of the attainable operational cost savings with DR and (2) identifying the needed level of controllability that DR-programs should achieve to reach those operational cost savings.

Throughout this dissertation, we will highlight how we advance the current state-of-the-art. At the start of each chapter, we will indicate which publications provide the basis for that chapter and highlight the scientific contribution of the author of this dissertation.

1.7 Outline

Chapter 2 contains the formulation of the five selected UC models. As these models form the backbone of this dissertation and the necessity of other building blocks in our framework (Fig. 1.1) can only be understood in light of these UC formulations (Section 1.5), this dissertation starts with an extensive discussion of these operational models. We conclude Chapter 2 with a qualitative comparison of the selected UC models.

The statistical analysis of the forecast error on RES-based electricity generation is the topic at hand in Chapter 3. The resulting distributional description of the forecast error provides indispensable input for the scenario generation techniques discussed in Chapter 4. In a case study, focused on the wind power forecast error in the Belgian power system, we illustrate that the selected scenario generation technique allows obtaining an adequate discrete representation of this stochastic variable. Scenario reduction techniques, which are designed to select a sufficiently small set of scenarios for consideration in a stochastic UC model with a minimal impact on the quality of the solution, are also covered in Chapter 4. In a methodological and real-life case study, we illustrate that conventional scenario reduction techniques may not be well-suited to select scenarios for a stochastic UC problem. An alternative characterization of the forecast error is presented, which allows selecting those scenarios that yield stable, unbiased UC schedules in reasonable calculation times.

The models and tools developed in Chapters 2, 3 and 4 enable us to perform an extensive quantitative comparison of the selected UC models in Chapter 5. Considering a power system with a 30% wind energy penetration (annual, energy basis), inspired by the Belgian power system and with wind power forecasts as the only source of uncertainty, our focus is on the relative performance of the selected UC models. Specifically, we study the expected operational cost, the reliability of the obtained UC schedule and the calculation time needed to obtain a solution. The results provided in Chapter 5 allow illustrating the added value of the improved models and techniques developed in Chapters 2, 3 and 4. For example, we demonstrate the necessity of certain constraints developed in Chapter 2 on the reserves provided by energy storage units and the robustness of our observations to the availability of different flexibility providers.

Chapter 6 contains a discussion of the available demand side flexibility representations typically considered in UC models, the formulation of the proposed integrated model and an analysis of the attainable operational costs savings through DR-based arbitrage and regulation services with residential electric heating systems. In addition, a chance-constrained programming framework is introduced to account for the limited controllability of demand-

side flexibility providers. This allows us to illustrate how the system value of DR diminishes if these electric heating systems are not perfectly controllable. The focus is not on the characterization of the limited controllability, but on identifying the needed level of controllability that DR-programs should achieve to maintain their operational value for a system operator.

Before formulating a conclusion and some recommendations for future research (Chapter 8), we illustrate the scientific relevance of the methodological contributions developed within this dissertation in three case studies. Using results from Chapter 5 and [42], we calculate a balancing cost associated with wind power forecast errors. In the context of DR with electric heating systems, we employ the integrated model from Chapter 6 to calculate a so-called CO_2-abatement cost associated with DR-adherent electric heating systems [43] and study the impact of a varying market penetration of such DR-programs [44].

1.8 Conclusion

Increasing shares of variable and limitedly predictable RES-based electricity generation require system operators to actively pursue (i) improved methods to size and procure reserves and (ii) novel sources of operational flexibility. When dealing with short-term uncertainty and reserves in power systems, one seeks to minimize the impact on the power system's reliability at the lowest possible operational cost. In light of these challenges, we defined two objectives. Our first objective relates to the improvement of existing and the development of new UC models considering high shares of intermittent RES-based electricity generation. Second, we aim to develop an integrated model to study the operational cost reductions attainable with limitedly controllable demand response-programs.

To meet these goals, we have introduced a modeling framework, which consists of four main steps, each with a specific function, to study the impact of variable and limitedly predictable RES-based electricity generation on power systems:

- a statistical analysis of the uncertainty, which yields probability distributions of the forecast error, facilitating probabilistic reserve sizing and scenario generation techniques;
- a scenario generation (and reduction) technique, capable of representing the obtained distributions as discrete forecast error scenarios;
- a set of UC models to solve the reserve allocation problem, extended with a physical demand side model to account for the flexibility and constraints of DR-based flexibility;

- a Monte Carlo ED evaluation of the resulting UC schedules, in which the quality of the scheduled reserves is tested on a large set of scenarios (reserve activation).

The added value of this framework lies in the combination these building blocks, as well as in the improvements made to each of its individual components. Although the proposed framework is distinctly different from the way European markets and transmission system operators currently deal with uncertainty, it allows isolating the inherent operational cost associated with variable and limitedly predictable RES-based generation.

Chapter 2

Operational electricity generation system models & uncertainty

In this chapter, we study five unit commitment (UC) formulations. Each of these models is adapted or designed specifically to cope with stochastic RES-based electricity generation. After an introduction, we subsequently study

- a deterministic unit commitment (DUC) model considering reserve constraints (Section 2.2);
- a stochastic unit commitment (SUC) model considering a reduced set of scenarios instead of reserve constraints (Section 2.3);
- an improved interval unit commitment (IIUC) model which characterizes the needed reserves via the ramping requirements they need to satisfy (Section 2.4);
- a hybrid deterministic-stochastic unit commitment (HUC) model combining a small set of scenarios and reserve constraints (Section 2.5);
- a probabilistic unit commitment (PUC) model with multiple reserve intervals, characterized by a probability of deployment (Section 2.6).

For each of the aforementioned models, we focus on the way the stochastic RES-based electricity generation is represented and how reserves are scheduled. Only conventional generation, RES-based electricity generation and large-scale energy storage systems may provide reserves. We will turn our focus to DR-based reserve provision in Chapter 6. This chapter concludes with a preliminary comparison of the presented UC models (Section 2.7).

This chapter is based on the following papers:

- K. Bruninx, Y. Dvorkin, E. Delarue, H. Pandžić, W. D'haeseleer, and D. S. Kirschen, *Coupling Pumped Hydro Energy Storage with Unit Commitment,* IEEE Trans. Sustain. Energy, vol. 7, no. 2, pp. 786–796, 2016.
- K. Bruninx and E. Delarue, *A probabilistic unit commitment model: cost-effective , reliable and fast,* Submitted to IEEE Transactions on Power Systems, 2015.
- K. Bruninx, K. Van den Bergh, E. Delarue, and W. D'haeseleer, *Optimization and Allocation of Spinning Reserves in a Low-Carbon Framework,* IEEE Trans. Power Syst., vol. 31, no. 2, pp. 872–882, 2016.
- K. Van Den Bergh, K. Bruninx, E. Delarue, and W. D'haeseleer, *LUSYM: a unit commitment model formulated as a mixed-integer linear program,* KU Leuven Energy Institute Working Paper WP EN2014–07, 2015.

2.1 Introduction

The aim of any UC model is to schedule a set of power plants and energy storage systems in order to meet the demand for electric energy at all time steps in the considered time frame at the lowest (operational) cost possible without violating the technical constraints of the power plants and energy storage systems [31]. The demand and RES-based generation may be stochastic, i.e. they may be variable (not or only limitedly dispatchable) and to some extent unpredictable. Deviations from what is expected – e.g. forecast errors – need to be overcome with up- or downward regulation of dispatchable generation, load or storage. In this regard, novel power system operation methods will be needed to properly size and allocate operational reserves, in order to ensure a reliable and cost-efficient operation of the power system [45]. Under the assumption that RES-based generation is the only source of uncertainty (Chapter 1), optimal reserve scheduling is the result of a trade-off between (1) the socio-economic cost of load shedding and curtailment of RES-based generation and (2) the cost of reserve allocation or procurement – i.e. the operational short-term cost to have reserves available – and the cost of reserve activation or deployment – i.e. the cost of dispatching or activating these reserves [46].

Researchers have developed various UC formulations considering stochastic RES-based electricity generation. Thinking of the forecast error as a stochastic variable that follows a certain distribution, one would ideally solve a UC model that directly considers this continuous representation of the uncertainty. Unfortunately, computational limitations do not allow solving a UC model with a direct representation of e.g. the heavy-tailed, skewed wind power forecast error (Chapter 3). Modelers and power system operators therefore resort to simplified representations of the stochastic parameters in operational power system models [47, 48, 49, 50, 28, 51, 52, 53].

In general, one can distinguish two broad categories of UC models considering uncertainty. First, in a deterministic paradigm, one considers the expected value of the stochastic variable at each time step during UC scheduling. Explicit reserve requirements are imposed on the optimization problem, to ensure sufficient flexibility is available in real time to accommodate deviations from what is expected. These reserve requirements are typically determined ex-ante rather than endogenously, as advocated in [46, 54], which may lead to sub-optimal UC schedules. Moreover, the expected cost of deploying reserves is typically not accounted for during UC optimization [41]. Therefore, researchers have developed stochastic UC formulations.

Alternatively, in a scenario-based approach, one accounts for multiple forecast scenarios and minimizes the probability-weighted operational cost, which leads to lower expected operational costs and higher absorption rates of RES-based generation [45, 41]. Such two- or multi-stage stochastic UC models are typically computationally demanding and may become intractable for large scenario sets and/or large power systems [17]. A variant of the scenario-based stochastic UC formulation is the so-called robust UC model, in which one minimizes the worst-possible operational cost over a set of scenarios or uncertainty set, avoiding assumptions on the exact form of the distribution of the stochastic variable [55]. Although typically overly conservative, the computational burden of such models is low compared to their expected-value counterparts [56]. Alternatively, a group of UC formulations, referred to as chance-constrained UC models, attempts to optimize the UC schedule considering a continuous description of the forecast error [57, 58, 59, 60, 61][1]. Analytical reformulations of the problem and quadratically constrained programming techniques allow solving the UC problem with an exact representation of the continuous distribution [63]. However, such UC models currently may not guarantee the schedule to be sufficiently flexible to accommodate the variability of the stochastic variable and

[1] In some cases, the distribution of the stochastic variable is approximated by a (large) set of discrete scenarios [62], which yields a scenario-based chance-constrained UC model. Such a model can be considered a variant of the stochastic UC model. We will cover this type of models in our discussion on stochastic UC models (Section 2.3).

fail to monetize the value of downward flexibility (Section 2.6). Such formulations are closely related to the probabilistic UC formulation (Section 2.6) and we will return to this type of UC models in the discussion of Section 2.6. Within these broad categories, one can find many combinations and 'intermediate' formulations. For an overview, we refer the reader to [47, 48, 49, 50, 52].

Regardless of the representation of the stochastic variable, in each UC formulation, the modeler needs to consider[2]

- the operational *cost-efficiency*, i.e. the operational cost associated with meeting the demand and reserve requirements under all conditions must be minimized, which is typically dependent on the level of detail in the representation of the uncertainty and the available flexibility providers;
- the *computational effort* needed to obtain the UC schedule, which is dependent on the size, structure and level of detail of the representation of the power system and the uncertainty in the UC model;
- the *reliability* of the resulting UC schedule, which depends on the conservatism of the constraints imposed on the UC model and the available flexibility providers.

Typically, models excel in one or two of these categories. For example, a deterministic UC model simplifies the representation of the uncertainty to two reserve constraints, which results in an easy-to-solve model (small problem size, few variables). The reserve requirements must be met, and if they are adequate, the resulting UC schedule will allow for a very reliable dispatch. In contrast, a SUC model will prove to be difficult to solve, but yields – if the considered scenarios are an adequate representation of the underlying uncertainty – a cost-optimal trade-off between reliability and the operational cost of flexibility provision. Our goal is to develop operational models that combine the computational speed of DUC formulations with the cost-optimality of SUC models, using insight from both models.

In addition to moving to more sophisticated UC models, the cost performance of a UC schedule can also be improved by using additional sources of flexibility, such as energy storage (ES) [64] or DR (Chapter 6). However, potential investments in ES systems must be carefully weighed against their prospective operational efficiency gains [65],[66]. While battery ES systems and other prospective ES technologies remain expensive [66], system operators have gained significant experience in operating Pumped Hydro ES (PHES) systems, which is by far

[2]Recall that the elements in this trade-off correspond to the three metrics we defined in our research objectives (Section 1.3).

the most wide-spread ES technology and is available in many power systems worldwide [67]. Kalantari and Galiana [68] demonstrated that existing PHES systems can be used to provide critical flexibility to accommodate intermittent wind power generation. Additionally, PHES systems can be used for improving operational reliability when dealing with intermittent wind power generation [69]. A PHES system can also significantly increase the profits of a generating company in a market environment [70]. The common thread of the studies in [68, 69, 70] is that they employ a deterministic framework, which does not account for the possible activation of the regulation services offered by the PHES system. The PHES system may not be able to deliver the scheduled regulation services, resulting in wind energy spillage or load shedding. Alternatively, stochastic programming techniques can be used to assess the participation of PHES systems in regulation services ([64, 71] and references therein). As the PHES system is dispatched in each scenario considered in the UC formulation, the hydraulic constraints are satisfied in these scenarios. One must however check that these constraints remain satisfied during dispatch. For example, Jiang et al. [71] propose a robust UC model considering PHES systems and focus on the computational aspects of this model. Pozo et al. [64] study a SUC formulation including a generic, ideal storage. The SUC model yields cost-effective UC and PHES schedules, but is computationally intensive and the solution quality depends on the quality of the scenarios.

By their very nature, each of these models is non-linear and non-convex [15]. The non-convexity is caused by the binary nature of the on/off decision and non-linearities occur due to, amongst others, non-linear generation cost curves and non-linear transmission constraints. All this makes the UC problem a difficult problem to solve. Over the course of the last decades, different mathematical methods have been used to solve the UC problem. An overview can be found in [72, 73, 74, 75, 53]. The most important ones are Exhaustive Enumeration (i.e., listing all possible combinations of on/off-states and picking the most optimal one), Priority Listing (i.e., committing generation units in order of increasing operating cost until the electricity load is met), Dynamic Programming (i.e., optimization-based method that searches for the minimum cost solution by solving simpler sub problems), Lagrangian Relaxation (i.e., the Lagrangian of the optimization problem is solved), Mixed-Integer Programming (i.e., optimization-based method to solve a mixed-integer problem by means of the branch-and-bound method), Decommitment Method (i.e., starting with all units online and switching off units) and more recently metaheuristic methods such as Fuzzy Systems, Genetic Algorithms, Artificial Neural Networks, Evolutionary Programming, Tabu Search and Ant Colony Search Algorithms [15].

Mixed-integer programming (MIP), an operations research method, gained significant attention due to dramatic improvements in commercial, off-the-shelf

MIP solver performance [31]. The advantage of employing MIP to solve a UC problem is twofold: (1) the MIP solver returns a feasible solution (if feasible solutions exist and can be found), and (2) the level of optimality is known (the MIP solver returns the optimality gap between the MIP solution and the lower bound to the UC problem) [15]. Furthermore, in MIP formulations of a UC problem, one can add additional constraints to 'tighten' the formulation [28] and conditional inclusions of various constraints allow to improve the 'compactness' of the resulting model [15, 76, 77, 78, 79], further reducing the computational burden of the resulting UC problem. For an excellent discussion on the development and impact of tight and compact formulations of MIP UC problems, we refer the interested reader to [28]. For a discussion on the advantages and disadvantages of MIP UC formulations w.r.t its alternatives, we refer our readership to [28, 31, 14] and the references herein. Although solving a MIP problem has become 100 million times faster over the last 20 years [80, 81], solving a MIP UC formulation remains challenging compared to faster methods such as Priority Listing. Nevertheless, the increased accuracy and guaranteed optimality have persuaded many practitioners and researchers to develop and use MIP UC models. Well-known examples are the commercially available PLEXOS UC model, developed by Energy Exemplar [82] and the academic research-oriented WILMAR Joint Market Model [83]. Real-life applications of MIP UC-based scheduling can be found in PJM, one of the largest competitive wholesale electricity markets in the world, which switched from Lagrangian relaxation to MIP-based UC scheduling in 2004 [28, 84].

In the following sections, we present five selected UC formulations, each of which considers the stochastic RES-based electricity generation differently. We will focus on the UC models themselves. We present three UC formulations found in the literature and two novel UC formulations. First, we study a security-constrained deterministic UC formulation, the simplest and most common UC formulation [15, 14]. We improved the existing formulations found in the literature by introducing PHES-based reserves [85]. To the best of the authors' knowledge, no DUC model has been published that aims to account for the hydraulic constraints[3] of a PHES system, while allowing this PHES system to offer regulation services in order to approximate the solution of a SUC model at a significantly lower computational cost. Second, a stochastic equivalent is introduced. The direct representation of the uncertainty through a set of scenarios will allow for cost-optimal UC decisions, but will prove to be computationally burdensome [45]. Insights from the stochastic formulation were used to reduce the conservatism and improve the cost-optimality of the DUC formulation. This led to the development of the (improved) interval

[3]Hydraulic constraints are related the physical and technical limitations of the PHES system, such as the volumetric constraints on the amount of water that can be stored in the upper basin of the PHES system.

unit commitment model ((I)IUC) [86]. We improved the IIUC formulation found in [86] with the explicit consideration of non-spinning reserves and PHES-based reserves [85]. The fourth model is a hybrid deterministic-stochastic UC formulation, which combines reserve requirements with a scenario-based representation of the uncertainty [45]. Last, a probabilistic UC formulation is introduced [41], which considers various reserve levels with a distinct activation probability. The last two models were developed by the author of this dissertation, in close collaboration with K. Van Den Bergh, E. Delarue and W. D'haeseleer.

For each of these models, we present a basic mixed integer-linearized formulation. Additional constraints and conditional inclusions of constraints to improve the tightness and compactness of the formulation are omitted, but can be found in the full formulation presented in Appendix C. We will first present a formulation of each UC model in which only spinning units, i.e. units that are online and synchronized, can provide reserves. We will extensively discuss the way the allocation (procurement) and activation (deployment) costs of these reserves are considered during the scheduling process. Second, we will extend the presented formulation with non-spinning reserves, with specific attention for the way the associated operational costs are included in the objective function. Third, the participation of intermittent RES-based generation in the reserve requirements will be discussed. Last, we show how energy storage systems can provide reserves. We will focus on PHES systems, but the presented methodology is identical for other energy storage systems. We will end each section with a discussion of the UC model at hand and some relevant literature.

The aim of this chapter is to provide a thorough understanding of the selected UC models and their underlying assumptions. In order to facilitate the interpretation of the formulation and discussion in the following sections, as well as to highlight the need for, among others, advanced reserve sizing techniques (Chapter 3), scenario generation & reduction techniques (Chapter 4) and tested designs (Chapter 5), we will introduce a schematic illustration of the representation of the stochastic parameter, in this case the RES-based electricity generation forecast G^{F}, in each of the studied models (Fig. 2.1). For each model, we will illustrate how the distribution of possible realizations of the stochastic RES-based electricity generation at a particular time step $p(G^{\mathrm{F}})$ is converted to reserve requirements (DUC, PUC, HUC), scenarios (SUC, HUC) or ramping scenarios (IIUC).

Before proceeding to the DUC formulation (Section 2.2), we illustrate the output of such a UC model for a simple example: a DUC problem, in which only spinning reserves may be scheduled under a static reserve constraint. We study the Belgian power system, of which the characteristics may be found

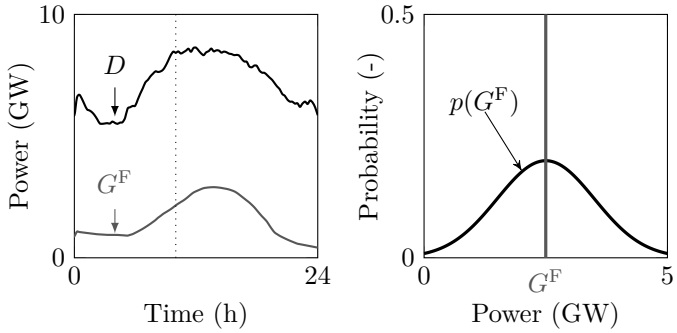

Figure 2.1: A schematic illustration of the representation of the stochastic RES-based generation in a UC formulation. Left: the demand D and the expected value of the forecasted RES-based generation G^{F} over time. Right: the distribution of the forecasted RES-based generation $p(G^{\mathrm{F}})$ at a particular time step, indicated by the dotted line in the left-handside figure. The forecast (left) corresponds to the expected value of the distribution (right) at each time step.

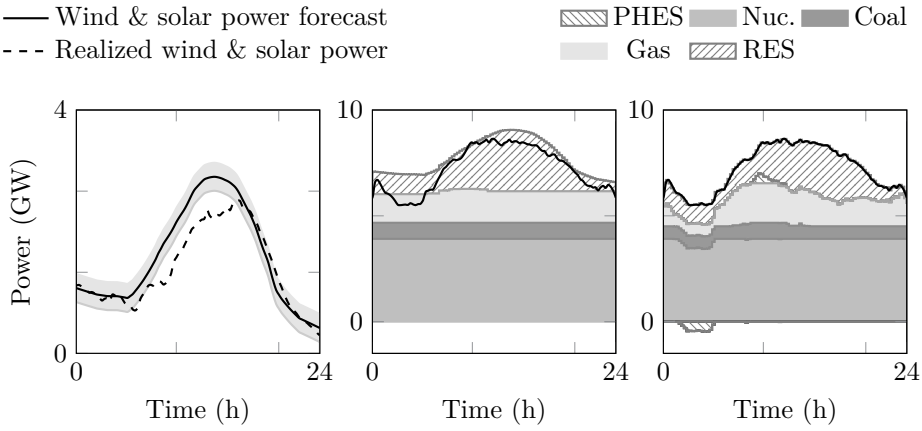

Figure 2.2: Left: The forecasted and measured solar and wind power generation in the Belgian power system on June 5, 2014, a windy and sunny spring day. The grey area illustrates the reserve requirements. Center: the solution of the UC model, visualized as the total committed capacity at each time step, seperated by fuel. Right: the result of the ED evaluation, i.e. the output of the scheduled units (UC), considering the measured wind and solar power output. The solid black line is the demand (center and right figure).

in Appendix B, on the 5th of June, 2014. Wind, solar and load data was taken from the Belgian TSO, Elia, [87]. During UC scheduling, we consider (1) the forecasted wind and solar power generation, (2) the measured load profile, corrected for must-run generation and the import-export balance on that particular day and (3) a static upward and downward reserve constraint equal to 5% of the installed wind and solar power capacity (4,597 MW) to absorb possible wind and solar power forecast errors. The forecasted and realized wind and solar power are visualized in Fig. 2.2, as well as the resulting UC schedule (the committed capacity) and the dispatch (the output of the scheduled power plants in real time). During UC optimization, units with low operational costs (nuclear, coal) are committed to meet the demand. The amount of committed gas-fired generation is limited. Note that more capacity is committed than strictly needed to meet the demand. This additional capacity is triggered by the reserve requirements. In the resulting dispatch (right-handside figure), mainly upward reserves are activated, as less wind and solar energy was generated than expected. During this dispatch, the UC schedule – i.e. the on/off state of the power plants – is fixed. Only units that were committed during the UC optimization can be dispatched to meet the demand. During dispatch, we here consider the measured wind and solar power output profile. To minimize the operational cost, the share of (expensive) gas-fired generation is minimized by running the cheaper units at maximum capacity as much as possible and by dispatching the PHES system. Note that the flexibility of the PHES system was not accounted for during the DUC optimization – an issue we will return to in Section 2.2.4.

2.2 A security-constrained deterministic unit commitment model[4]

In a security-constrained deterministic unit commitment model, from hereon referred to as a DUC model, the power plants are scheduled based on the forecasted RES-based electricity generation and demand profiles. To cover possible forecast errors on these stochastic variables, extra capacity, spinning and non-spinning, is added to the schedule to allow the power system to accommodate unexpected changes. This extra capacity, referred to as reserves, is triggered by the inclusion of reserve constraints (Eq. (2.10)-(2.11)). These reserve constraints are a simplified representation of (a part of) the domain of

[4]This section is based on K. Van Den Bergh, K. Bruninx, E. Delarue, and W. D'haeseleer, *LUSYM: a unit commitment model formulated as a mixed-integer linear program,* KU Leuven Energy Institute Working Paper WP EN2014–07, 2015 and K. Bruninx, K. Van den Bergh, E. Delarue, and W. D'haeseleer, *Optimization and Allocation of Spinning Reserves in a Low-Carbon Framework,* IEEE Trans. Power Syst., vol. 31, no. 2, pp. 872–882, 2016.

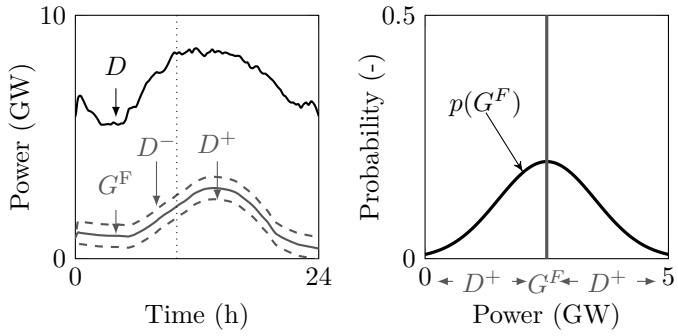

Figure 2.3: In a DUC model, the system operator has to decide upon the UC schedule based on the forecasted RES-based power (G^{F}) and needs to satisfy the upward (D^+) and downward reserve margins (D^-). These reserve requirements are a representation of (a part of) the range of possible realizations of the RES-based electricity generation, i.e. (a part of) the domain of the distribution of the stochastic RES-based electricity generation ($p(G^{\mathrm{F}})$).

the possible forecast error, as illustrated in Fig. 2.3. The inclusion of these constraints ensures that the resulting UC schedule is hedged against any possible realization of the forecast error in the interval $[G_j^{\mathrm{F}} - D_j^+, G_j^{\mathrm{F}} + D_j^-]$. We will argue below that such deterministic models are typically easy to solve, but may lead to sub-optimal results when the realization of the RES-based generation deviates significantly from its forecast.

In the description of the model below, we will focus on the representation of the reserves and the associated operational costs. The presented formulation, developed by Van den Bergh et al. [15] and detailed in Appendix C, is shown to be more tight and compact than that proposed by Carrion and Arroyo [88], based on the formulations proposed by Morales et al. [76], Ostrowski et al. [78] and Rajan and Takriti [79]. For a detailed discussion on the DUC formulation, see Van Den Bergh et al. [15]. For a discussion on the tightness and compactness of UC formulations and its impact on the computational performance of the UC formulation, the reader is referred to [28].

In a DUC model, the power plants are scheduled in such a way that the overall operational cost of generating the demanded electricity under forecast conditions over the simulated time period is minimized. This cost $c(g, z)$ consists of fuel costs $fc_{i,j}$, start-up costs $sc_{i,j}$, ramping costs $rc_{i,j}$ and CO_2-emission costs

$co_2t_{i,j}$. The objective function reads

$$min \quad c(g,z) = \sum_i \sum_j sc_{i,j} + fc_{i,j} + co_2t_{i,j} + rc_{i,j} \tag{2.1}$$

$$+ \sum_j \sum_m TP \cdot (VOLL \cdot \phi_{j,m} + VOC \cdot \chi_{j,m})$$

$$+ \sum_j VOR \cdot \left(s_j^+ + s_j^-\right)$$

in which I is the set of power plants present in the model (index i) and J is the set of time steps (index j, one time step is one hour). $VOLL$ is the value of lost load $\phi_{j,m}$ on node m and TP stands for the temporal resolution used in the optimization. To study the impact of e.g. feed-in tariffs or green certificates, a cost of curtailment ($\chi_{j,m}$: curtailment of forecasted RES-based electricity generation on node m in time step j; VOC: value of curtailment) can be added to the model. The last term in the objective function introduces two so-called *slack variables* s_j^+ and s_j^-. These slack variables allow the model to violate the reserve requirements (see below, Eq. (2.10)-(2.11)), albeit at a very high cost (VOR, value of not-scheduled reserve). If the value of not-scheduled reserves is lower than the value of lost load, the model will first curtail reserves before load is shed to satisfy the power balance (Eq. (2.8))[5].

The fuel cost ($fc_{i,j}$) is determined by the fuel price and the efficiency of the power plant:

$$\forall i, \forall j: \quad fc_{i,j} = TP \cdot \left(C_i \cdot z_{i,j} + MA_i \cdot \left(g_{i,j} - \underline{P_i} \cdot z_{i,j}\right)\right) \tag{2.2}$$

with C_i the fuel cost associated with running the plant at its minimum power level $\underline{P_i}$. The binary variable $z_{i,j}$ represents the commitment status of plant i. MA_i is the marginal cost for the additional generation above its minimum power level ($g_{i,j} - \underline{P_i} \cdot z_{i,j}$). This is a linear approximation of the quadratic cost curve of a power plant [14][6]. The CO_2-emission cost $co_2t_{i,j}$ is based on the emissions, the load level and a fixed CO_2-price per ton of emitted CO_2 (CO_2P):

$$\forall i, \forall j: \quad co_2t_{i,j} = CO_2P \cdot TP \cdot \left[B_i \cdot z_{i,j} + MB_i \cdot \left(g_{i,j} - \underline{P_i} \cdot z_{i,j}\right)\right] \tag{2.3}$$

[5]Note that VOR is expressed in €/MW and $VOLL$ in €/MWh. To ensure that reserves are shed before load shedding occurs, the following inequality must thus hold: $VOR < TP \cdot VOLL$.

[6]One could split the operational range of a power plant in multiple intervals, in which one could approximate the cost curve of that power plant by a linear relationship [89, 90]. As such, one obtains a piece-wise approximation of the cost curve of a power plant, which allows diminishing the error of the approximation. For details, see [15, 14, 89, 90]. For sake of simplicity, we will not use this piece-wise approximation. Empirical tests have shown that the impact of this simplification is limited.

Similar to the fuel costs, the CO_2-emission cost consists of a fixed part (the emissions when a plant is running at its minimum power level B_i) and a term accounting for the marginal emissions at different generation levels (MB_i). The start-up cost $sc_{i,j}$ is calculated as

$$\forall i, \forall j: \quad sc_{i,j} = STC_i \cdot v_{i,j} \tag{2.4}$$

with a fixed start-up cost, different per power plant and fuel, STC_i. The binary variable $v_{i,j}$ is equal to 1 at time step j if the plant starts up at that time step. In this model, we have not differentiated between hot and cold start-ups, nor did we include shut-down costs [15, 77][7]. Finally, the ramping costs $rc_{i,j}$ are determined via the following equations:

$$\forall i, \forall j: \quad rc_{i,j} \geq RCP_i \cdot \left(g_{i,j} - g_{i,j-1} - \underline{P_i} \cdot v_{i,j}\right) \tag{2.5}$$

$$\forall i, \forall j: \quad rc_{i,j} \geq RCP_i \cdot \left(g_{i,j-1} - g_{i,j} - \underline{P_i} \cdot w_{i,j}\right) \tag{2.6}$$

$$\forall i, \forall j: \quad rc_{i,j} \geq 0 \tag{2.7}$$

with binary variable $w_{i,j}$ indicating a shut-down of power plant i on time step j and RCP_i a cycling cost for power plant i.

This optimization is subject to a number of constraints. First, the supply and demand for electricity must be equal at all time steps j on each node m. The so-called market clearing condition or power balance reads:

$$\forall j, \forall m: \quad D_{j,m} - \phi_{j,m} = \sum_i I^{\mathrm{G}}_{m,i} \cdot g_{i,j} + inj_{j,m} + G^{\mathrm{MR}}_{j,m} + G^{\mathrm{F}}_{j,m} - \chi_{j,m} \tag{2.8}$$

$$+ \sum_r I^{\mathrm{PHES}}_{m,r} \cdot \left(g^{\mathrm{T}}_{r,j} - g^{\mathrm{P}}_{r,j}\right)$$

The demand $D_{j,m}$ on each time step j and each node m is assumed to be known and fixed (parameter of the model). This demand must be met by

- Electricity generated from dispatchable power plants located at that node m, calculated as $\sum_i I^{\mathrm{G}}_{m,i} \cdot g_{i,j}$, with $I^{\mathrm{G}}_{m,i}$ the incidence or location matrix of the power plants;
- Injections from the grid $inj_{j,m}$ (see Eq. (2.25)–(2.27));

[7] Although a more accurate representation of the dynamics and operational costs associated with the dynamic operation of the power plants may improve the cost-efficiency of the resulting UC schedule, the computational performance of the UC model typically suffers [28]. We have therefore opted not to included more detailed representations of e.g. the fuel cost curve [89, 90] or start-up and shut-down trajectories and costs [77, 89].

- Generation from must-run systems (including electricity generation from some forms of RES), of which the output is assumed to be known $G^{\mathrm{MR}}_{j,m}$;
- The forecast of some uncertain RES-based electricity generation, $G^{\mathrm{F}}_{j,m}$, which can be curtailed ($\chi_{j,m}$):

$$\forall j, \forall m: \quad 0 \leq \chi_{j,m} \leq G^{\mathrm{F}}_{j,m} \tag{2.9}$$

- The net injection of power from PHES systems (index r), calculated as the difference between the injection of power $g^{\mathrm{T}}_{r,j}$ and the withdrawal of power $g^{\mathrm{P}}_{r,j}$. $I^{\mathrm{PHES}}_{m,r}$ is the incidence matrix of the PHES systems;
- The shedding of load $\phi_{j,m}$, penalized at the value of lost load in the objective function. In the context of the DUC model, load shedding must be understood as a slack variable, not as a source of 'flexibility'. This slack variable is introduced to maintain mathematical feasibility of the problem when the residual demand exceeds the available cumulative power plant capacity. The high value of lost load $VOLL$ – which is not to be compared to the cost of emergency flexibility measures system operators have at their disposal to maintain the system balance, such as interruptible contracts with large consumers – ensures that load shedding is the most expensive option to balance demand and generation.

In addition to the market clearing condition above, the resulting UC schedule needs to maintain a certain amount of reserves in the system. The demand for upward reserves D^{+}_{j} can be met via spinning reserves ($r^{+}_{i,j}$, i.e. headroom of running power plants), non-spinning reserves ($nsr^{+}_{i,j}$, see Section 2.2.2) and curtailed RES-based generation:

$$\forall j: \quad D^{+}_{j} = \sum_{i} r^{+}_{i,j} + \sum_{m} \chi_{j,m} + s^{+}_{j} \tag{2.10}$$

The slack variable s^{+}_{j} allows violating Eq. (2.10) at a high cost (VOR). However, recall that this positive slack variable ($s^{+}_{j} \geq 0$) is penalized at a lower cost than load shedding in the objective function. The model will thus, in case of shortages, first shed reserves before load is curtailed ($\phi_{i,j}$). Similarly, one can define a demand for downward flexibility D^{-}_{j}:

$$\forall j | \sum_{m} \chi_{j,m} = 0: \quad D^{-}_{j} = \sum_{i} r^{-}_{i,j} + s^{-}_{j} \tag{2.11}$$

The demand for downward flexibility must be met via the available downward flexibility of the online power plants ($r^{-}_{i,j}$). A positive slack variable ($s^{-}_{j} \geq 0$) allows violating this constraint at a high cost, similar to the case of upward

reserves. Furthermore, this demand for downward reserves is set to zero if curtailment of RES-based generation is scheduled ($\sum_m \chi_{j,m}$). This expresses the trade-off between the cost of providing downward flexibility with conventional power plants and curtailing additional, unexpected increases in RES-based production. If the cost of providing downward flexibility is higher than the cost of curtailing one MWh of RES-based generation and the possible increase in operational costs to cover the curtailed RES-based generation, no downward flexibility is scheduled in these moments. Implicitly, one assumes that all downward flexibility is provided by curtailment in these cases. Note that this is an approximation of the real trade-off, as we are comparing the cost of curtailing one MWh of RES-based generation with the allocation cost of the most expensive MW of downward flexibility[8]. Ideally, one provides downward flexibility up to the point that the cost of providing that level of downward flexibility equals the expected cost savings associated with absorbing an additional MWh of RES-based generation in real time. This would however require explicit knowledge of the full expected operational cost of the scheduled downward reserves – information which is typically not available in a DUC formulation (Section 2.2.1) – and the expected cost saving that results from absorbing more RES-based generation during dispatch. We will discuss this issue in detail in Section 2.2.3.

Second, the power plants have several technical constraints, different per fuel and technology. The following constraints must hold

$$\forall i, \forall j: \quad g_{i,j} + r^{+}_{i,j} \leq \overline{P_i} \cdot z_{i,j} \tag{2.12}$$

$$\forall i, \forall j: \quad g_{i,j} - r^{-}_{i,j} \geq \underline{P_i} \cdot z_{i,j} \tag{2.13}$$

$$\forall i, \forall j: \quad g_{i,j},\ r^{+}_{i,j},\ r^{-}_{i,j} \geq 0 \tag{2.14}$$

in which the binary variable $z_{i,j}$ indicates the on-off status of power plant i at time step j. The scheduled output of each power plant is limited to its maximum ($\overline{P_i}$) and minimum stable operating level ($\underline{P_i}$). The amount of spinning reserve is limited to available headroom ($r^{+}_{i,j}$) and the output above the minimum operating point ($r^{-}_{i,j}$). At start-up or shut-down, it is assumed that 'slow' units, i.e. units with a minimum uptime (MUT) of at least two time steps, run at their minimum operating point for one time step:

$$\forall i | \{MUT_i \geq 2\}, \forall j: \quad g_{i,j} + r^{+}_{i,j} \leq \overline{P_i} \cdot z_{i,j} - \left(\overline{P_i} - \underline{P_i}\right) \cdot (v_{i,j} + w_{i,j+1}) \tag{2.15}$$

[8]This approximation will yield more cost-optimal UC schedules when the explicit cost of curtailment (VOC) is very low or zero, as it avoids scheduling downward flexibility (and incurring the associated costs) to absorb an uncertain increase in RES-based generation. If the cost of curtailment is significant, scheduling downward reserves may be more cost-optimal.

Alternatively, one can impose specific start-up and shut-down ramp-rates [15, 77]. The ramp-up and ramp-down rates of the power plants have been included as follows:

$$\forall i \notin I^{\text{FAST}}, \forall j: \quad g_{i,j} + r^{+}_{i,j} \leq g_{i,j-1} + \overline{\Delta P^{+}_{i}} \cdot (z_{i,j} - v_{i,j}) + \underline{P_i} \cdot v_{i,j} \tag{2.16}$$

$$\forall i \notin I^{\text{FAST}}, \forall j: \quad g_{i,j} - r^{-}_{i,j} \geq g_{i,j-1} - \overline{\Delta P^{-}_{i}} \cdot z_{i,j} - \underline{P_i} \cdot w_{i,j} \tag{2.17}$$

The $\overline{\Delta P^{+}_{i}}$ (maximum upward ramping rate (MW/TP)) and $\overline{\Delta P^{-}_{i}}$ (maximum downward ramping rate (MW/TP)) values are derived from the maximum ramping rates of the power plants (Appendix B). The binaries $v_{i,j}$ and $w_{i,j}$ indicate a start-up, respectively a shut down of a power plant i (see below). The equations above express the dynamic constraints of the power plants when they are online. These ramping constraints are only enforced for slow generators ($i \notin I^{\text{FAST}}$). I^{FAST} is a subset of the set of power plants I which contains those generators with a MUT (minimum up time) and MDT (minimum down time) of one time period and maximum ramp rates which allow ramping up to a level above their minimum operating point within one time period ($\overline{\Delta P^{+}_{i}} > \underline{P_i}$) . For the fast-starting generators, the equations above simplify to:

$$\forall i \in I^{\text{FAST}}, \forall j: \; g_{i,j} + r^{+}_{i,j} \leq g_{i,j-1} + \overline{\Delta P^{+}_{i}} \cdot z_{i,j} \tag{2.18}$$

$$\forall i \in I^{\text{FAST}}, \forall j: \; g_{i,j} - r^{-}_{i,j} \geq g_{i,j-1} - \overline{\Delta P^{-}_{i}} \cdot (z_{i,j} + w_{i,j}) \tag{2.19}$$

The inclusion of the reserve capacity $r^{+}_{i,j}$ and $r^{-}_{i,j}$ in the ramping constraints (2.16)-(2.19) limits the scheduled upward reserve capacity to the net available ramping capacity of each power plant i. Note that these constraints imply that the resulting schedule will be able to absorb any forecast error that imposes a ramp of at most $G^{\text{F}}_{j} \rightarrow G^{\text{F}}_{j+1} + D^{+}_{j+1}$ (upward reserve activation) or $G^{\text{F}}_{j} \rightarrow G^{\text{F}}_{j+1} - D^{-}_{j+1}$ on the system. In other words, the scheduled units will be able to ramp (1) up from their output under forecast conditions (G^{F}_{j}) to their output at full deployment of all scheduled upward reserves within one time step ($G^{\text{F}}_{j+1} + D^{+}_{j+1}$) or (2) down from their output under forecast conditions (G^{F}_{j}) to their output at full deployment of all scheduled downward reserves within one time step ($G^{\text{F}}_{j+1} - D^{-}_{j+1}$). These constraints furthermore restrict a slow power plant ($i \notin I^{\text{FAST}}$) from delivering reserves if it is running at its minimum operating point $\underline{P_i}$ due to a start-up or shut-down.

The minimum up- and down-times have been included in the model as proposed by Rajan and Takriti [79]. If the power plant i is started up in time step j, it must remain on for the next $MUT - 1$ time periods (and similarly when shut down). For every time step j that a power plant i starts up, respectively shuts

down, the following constraints must hold:

$$\forall i \notin I^{\text{FAST}}, \forall j: \quad \sum_{k=1}^{MUT-1} v_{i,j-k} \leq z_{i,j} \tag{2.20}$$

$$\forall i \notin I^{\text{FAST}}, \forall j: \quad \sum_{k=1}^{MDT-1} w_{i,j-k} \leq 1 - z_{i,j} \tag{2.21}$$

in which the binary variable $w_{i,j}$ equals 1 if the plant i is shut down at time step j[9]. These constraints are only enforced for 'slow' generators. The binary on-off status $z_{i,j}$ of each power plant is linked to the start-up and shut-down variables as follows:

$$\forall i, \forall j: \quad z_{i,j} - z_{i,j-1} - v_{i,j} + w_{i,j} = 0 \tag{2.22}$$

$$\forall i, \forall j: \quad z_{i,j},\ v_{i,j},\ w_{i,j} \in \{0,1\} \tag{2.23}$$

With the logic constraint below, simultaneous start-ups and shut-downs are excluded:

$$\forall i, \forall j: \quad v_{i,j} + w_{i,j} \leq 1 \tag{2.24}$$

If one differentiates between hot, warm and cold start-ups, one can tighten the formulation as proposed by Morales-España et al. [77].

Third, network constraints are taken into account through a DC–load flow approximation[10]. Via the so-called Power Transfer Distribution Factors (PTDF) the flows in the network are calculated as follows [15, 91, 92]:

$$\forall j, \forall n: \quad f_{j,n} = \sum_{m} PTDF_{n,m} \cdot inj_{j,m} \tag{2.25}$$

The flows ($f_{j,n}$) over the transmission lines (index n, set N) should respect the maximal capacity (CAP_n) of these lines:

$$\forall j, \forall n: \quad -CAP_n \leq f_{j,n} \leq CAP_n \tag{2.26}$$

Furthermore, the sum of the injections $inj_{j,m}$ on each time step j should be zero as electricity can not be stored in the grid itself:

$$\forall j: \quad \sum_{m} inj_{j,m} = 0 \tag{2.27}$$

[9] Although this formulation requires three binary variables per generator, it is considerably easier to solve than its one-binary equivalent [14]. This goes against a persevering myth that the calculation time needed to solve a MIP problem is positively correlated with the number of binary variables. This observation is confirmed by Morales-España et al. [76, 28].

[10] For details on the approximation error a DC power flow representation of an AC network entails, see [91, 92] and the references therein.

Note that we only account for the AC-network via this DC-load flow approximation. HVDC-grids, as well as active grid elements such as phase shifting transformers, can be included similarly. For the sake of readability, these are not discussed in this dissertation. The interested reader is referred to Van Den Bergh et al. [91].

Last, the pumped hydro energy storage (PHES) systems (index r) are included in the model formulation. For each power plant, the energy content of the reservoir $e_{r,j}$ for each PHES system r, accounting for the round trip efficiency of the PHES system ϵ_r, can be calculated as

$$\forall r, \forall j: \quad e_{r,j} = TP \cdot \left(g^{\mathrm{P}}_{r,j} \cdot \sqrt{\epsilon_r} - \frac{g^{\mathrm{T}}_{r,j}}{\sqrt{\epsilon_r}} \right) + e_{r,j-1} \tag{2.28}$$

The energy storage level of each PHES system is limited to a minimum and maximum level $\underline{E_r}$ and $\overline{E_r}$ respectively:

$$\forall r, \forall j: \quad \underline{E_r} \leq e_{r,j} \leq \overline{E_r} \tag{2.29}$$

Furthermore, the power output (or withdrawal) of the PHES system is limited to the capacity of the system $\overline{P_r}$. To ensure that the PHES system is not scheduled to pump and turbine at the same time, two binary variables $p_{r,j}$ and $t_{r,j}$ are introduced:

$$\forall r, \forall j: \quad 0 \leq g^{\mathrm{T}}_{r,j} \leq \overline{P_r} \cdot t_{r,j} \tag{2.30}$$

$$\forall r, \forall j: \quad 0 \leq g^{\mathrm{P}}_{r,j} \leq \overline{P_r} \cdot p_{r,j} \tag{2.31}$$

$$\forall r, \forall j: \quad p_{r,j} + t_{r,j} \leq 1 \tag{2.32}$$

Note that the introduction of the binary variables $p_{r,j}$ and $t_{r,j}$, as well as Eq. (2.32), is not strictly necessary. Indeed, although this will prevent the PHES system from turbining and pumping at the same time, this combination would only occur if excess RES-based generation is available. As such, it is an equivalent solution to the curtailment of RES-based generation. Due to the efficiency loss in the PHES unit, part of the absorbed electrical energy is lost as heat to the environment. Only if curtailment corresponds to a certain cost in the objective function (Eq. (2.1)), this solution is 'meaningful'. Indeed, allowing simultaneous pumping and turbining avoids some curtailment, thus operational costs. In all other cases ($VOC = 0$), simultaneous pumping and turbining is equivalent to curtailing the excess RES-based generation. However, for the sake of clarity, we explicitly prevent simultaneous pumping and turbining in each individual PHES system r. Note however that simultaneous pumping and turbining in different PHES systems is not excluded, as such behavior might

be triggered to avoid the violation of other operational constraints, such as network congestion.

In what remains of this section, we first argue that the allocation and activation costs of spinning reserves are not fully accounted for in the presented formulation. Second, we expand the proposed model with non-spinning and PHES-based reserves. Third, we discuss the participation of intermittent RES-based generation in the reserve requirements. We conclude this section with a comparison of the proposed model with formulations found in the literature.

2.2.1 Allocation & activation costs of spinning reserves

In the formulation above, we only (implicitly) include the allocation cost of spinning reserves. Indeed, the only operational cost the system operator incurs when scheduling spinning reserves is caused by (1) less efficient part-load behavior and (2) a possible increase in start-up costs. The cost of activating or deploying these reserves however is not included in the model.

Activation costs of spinning reserves depend on the fuel, CO_2-emission and ramping costs associated with the power plant that delivers these reserves. As these units are online, start-up costs are not due when activating the scheduled reserves. Activating upward regulation results in a increase in costs, while downward regulation may decrease the overall operating cost e.g. due to fuel savings. More importantly, these costs are probabilistic in nature: they are by definition 'expected' costs. These costs are a function of the probability that the reserves are activated and this probability is dependent on the power plant providing these reserves, changing from time step to time step. This information is however not included in a DUC model, which makes it impossible to accurately represent the expected activation cost of spinning reserves.

Neglecting the activation probability has several consequences. First, it requires ex-ante reserve sizing: before solving the model, a system planner must decide upon the amount and type of reserves that should be procured. During this reserve sizing process, a system operator ideally makes a trade-off between the expected socio-economic cost of load shedding or curtailment of RES-based generation and the expected cost of reserve procurement and activation [93, 46]. As both expected costs are not known in the DUC formulation, the reserve sizing procedure cannot be internalized in the UC model. Moreover, during the ex-ante reserve sizing procedure, the system operator has insufficient knowledge on the full cost of reserve provision, as this cost is dependent on the operational 'state' of the system, i.e. the UC decisions impact the cost of reserve provision. Second, for upward reserves, one may face a sub-optimal allocation of reserves. Reserves that are unlikely to be activated, can be provided cost-efficiently by

highly flexible, but expensive-to-run units, while efficient power plants, such as CCGTs, may be cost-optimal for the provision of frequently activated reserves. As the probability of activation is unknown, this trade-off between upfront allocation and real-time activation costs is impossible. Third, one neglects the possible benefits of downward regulation. By only accounting for the allocation cost of downward regulation, curtailment will in most cases be the most cost-efficient option[11]. Indeed, the decrease in operational costs by absorbing more RES-based power (here assumed to be zero-marginal cost) is not accounted for in the objective function, thus the model has no incentive to schedule downward reserves other than curtailment.

These insights will be crucial in understanding why stochastic formulations of the UC problem outperform the DUC model (Section 2.3 and Chapter 5) and the development of the probabilistic UC formulation (Section 2.6).

2.2.2 Allocation & activation costs of non-spinning reserves

Up to this point, non-spinning reserves have not been included in the DUC formulation. However, the availability of non-spinning reserves may have a significant impact on the operational cost and reliability of the UC schedule. Non-spinning reserves typically add flexibility to the UC schedule, lowering costs while maintaining the reliability of the schedule.

To incorporate non-spinning reserves, one should make the following changes to the presented model. First, we introduce an allocation or procurement cost for non-spinning reserves ($NSRC_j$), which should be accounted for in the objective function:

$$\begin{aligned} min \quad c(g,z) = & \sum_i \sum_j sc_{i,j} + fc_{i,j} + co_2t_{i,j} + rc_{i,j} \\ & + \sum_j \sum_m TP \cdot (VOLL \cdot \phi_{j,m} + VOC \cdot \chi_{j,m}) \\ & + \sum_i \sum_j NSRC_i \cdot y_{i,j} + \sum_j VOR \cdot \left(s_j^+ + s_j^-\right) \end{aligned} \tag{2.33}$$

with binary variable $y_{i,j}$ indicating the procurement of non-spinning reserves at time step j, provided by power plant i. The variable $nsr_{i,j}^+$ represents the

[11] Note that the UC schedule inherently contains some downward flexibility, as power plants running above their minimum stable operating point have 'downward flexibility' – i.e., their output can be decreased if needed. Bringing additional units online or switching between technologies to schedule additional downward flexibility is however unlikely.

non-spinning reserves provided by power plant i on time step j. When a power plant is providing non-spinning reserves, it must be off:

$$\forall i \in I^{\text{FAST}}, \forall j: \quad \underline{P_i} \cdot y_{i,j} \leq nsr^{+}_{i,j} \leq \overline{P_i} \cdot y_{i,j} \tag{2.34}$$

$$\forall i \in I^{\text{FAST}}, \forall j: \quad y_{i,j} + z_{i,j} \leq 1 \tag{2.35}$$

$$\forall i \in I^{\text{FAST}}, \forall j: \quad y_{i,j} \in \{0,1\} \tag{2.36}$$

$$\forall i \notin I^{\text{FAST}}, \forall j: \quad y_{i,j} = 0 \tag{2.37}$$

$$\forall i \notin I^{\text{FAST}}, \forall j: \quad nsr^{+}_{i,j} = 0 \tag{2.38}$$

I^{FAST} is a subset of the set of power plants I which contains those generators with a MUT (minimum up time) and MDT (minimum down time) of one time period and maximum ramping rates which allow them to ramp up to a level above their minimum operating point within one time period. Only power plants that belong to the subset I^{FAST} are allowed to offer non-spinning reserves[12]. A power plant in subset I^{FAST} may offer any capacity between its minimum and its maximum stable operating point as non-spinning reserve. The demand for upward reserves can now be satisfied by scheduled curtailment of RES-based generation, spinning and non-spinning reserves:

$$\forall j: \quad D^{+}_{j} = \sum_{i} \left(r^{+}_{i,j} + nsr^{+}_{i,j}\right) + \sum_{m} \chi_{j,m} + s^{+}_{j} \tag{2.39}$$

Alternatively, the upward reserve requirement can be split up in a demand for spinning and non-spinning reserves [94]. In this dissertation, we will not opt for a division between spinning and non-spinning reserve requirements.

The model will make a trade-off between the opportunity cost of not being able to schedule such a fast-starting power plant to meet the demand, the allocation or procurement costs associated with scheduling that power plant as non-spinning reserve ($NSRC_i$) and the operational cost savings of not incurring any operational cost for other spinning units providing that reserve capacity. The opportunity cost of fast-starting units will typically be zero, as these are expensive units that are rarely scheduled, unless the demand is high. Spinning reserves result in operational allocation costs due to e.g. increased part-load operation, which are to be compared against the allocation costs of the non-spinning reserves. This allocation cost should reflect the operational cost to keep this unit available (e.g. maintenance costs). Such costs are however difficult

[12]Ramping and minimum up-/downtime constraints are therefore omitted. If these assumptions would not hold, these constraints can be introduced analogously to Eq. (2.16)-(2.19) and (2.20)-(2.24).

to quantify. Moreover, these costs are typically rather low compared to the allocation costs incurred by scheduling spinning reserves[13]. As a result, all available fast-starting units will typically be scheduled as non-spinning reserves.

Such an approach may yield a sub-optimal UC schedule. This is the result of neglecting the expected activation cost of both non-spinning and spinning reserves (the *expected* cost of dispatching these reserves). To calculate the full, expected cost associated with non-spinning reserves, one should ex-ante predict the cost associated with (1) excluding these power plants from the UC schedule, i.e. an opportunity cost, (2) the explicit procurement cost of non-spinning reserves ($NSRC_i$) and (3) the operational cost of activating these reserves. Similar to the activation costs of spinning reserves (see above), the cost of activation is an *expected* cost, dependent on the fuel and efficiency of the power plant providing non-spinning reserves and the probability that this power plant will be activated. As this information is not accounted for in a DUC formulation, the expected activation cost of non-spinning reserves is typically unknown. The result is a trade-off based on incomplete information – only allocation costs are considered – which will typically result in over-procurement of non-spinning reserves. Upon activation, the system operator may however incur high operational costs if the realization of RES-based generation deviates significantly from its expected value, as these fast-starting units are typically expensive to operate.

To account for expected activation costs of non-spinning reserves in other UC formulations, we will follow a similar strategy as for the spinning reserves. We will return to this issue in Section 2.6.

2.2.3 Participation of intermittent RES-based generation in the reserve requirements

Before proceeding to the discussion on the participation of intermittent generation in the reserve requirements, we focus the reader's attention on two important assumptions w.r.t. RES-based generation and the reserve requirements:

- The forecast error on RES-based electricity generation is the only source of uncertainty, which allows us to define the reserve requirements relative to the forecasted RES-based electricity generation profile;
- It is assumed that all RES-based electricity generation can be curtailed.

[13] In this dissertation, we will typically set the allocation cost of non-spinning reserves ($NSRC_i$) to zero.

Note that in reality, several other sources of uncertainty, such as load forecasts, forced outages of conventional power plants and elements in the transmission system, affect the reserve requirements. Furthermore, some forms of RES-based electricity generation may not be curtailable due to technical or regulatory limitations. The simplifications above however allow focusing on how the different models deal with uncertainty and how this affects the resulting UC schedules.

Curtailment of forecasted RES-based generation ($\chi_{j,m}$) is directly accounted for in the demand for upward reserves (Eq. (2.10)). RES-based generation which is scheduled to be curtailed, can be 'used' to cover unexpected negative forecast errors in real time. This reflects a system in which we anticipated more RES-based generation, but were not willing to accept this. In real time, we observe less RES-based generation than expected, but this does not affect the dispatch of the power system at hand as we were unwilling to accept the forecasted level of RES-based generation from the start. Similarly, when the cost of allocating more reserves outweighs the cost of scheduling a MW of conventional generation to meet the demand, the model may schedule some forecasted RES-based generation as upward regulation power. This allocation cost may be caused by additional start-ups, increased fuel costs due to reduced efficiency in part-load operation, but also due to a switch to more flexible, but more expensive-to-run technologies due to the technical constraints of the various power plant technologies. Third, if the reserve requirements are very stringent, one may be forced to commit so much capacity that curtailment becomes unavoidable due to the (cumulative sum of the) minimum operating points of the committed power plants. Also in these cases, we will account for this curtailment as upward reserves, to avoid even more curtailment due to the scheduling of reserve capacity. Last, technical constraints on the operation of the power plants or the grid may require curtailment. In all cases above, curtailment will be accounted for in the upward reserve requirement. Note however that allowing intermittent RES-based power to satisfy the demand for reserves may reduce system reliability, as the actual realization of wind power during dispatch is uncertain. The participation of RES-based generation in upward reserve requirements is mainly important in power systems with high RES-penetrations and/or stringent operational constraints.

Figure 2.4 illustrates this approach. Compared to the example of Fig. 2.3, we scaled the RES-based electricity generation by a factor four. At noon, the forecasted RES-based generation (G_j^{F}) now exceeds the demand (D_j). To maintain the power system balance, curtailment (χ_j) is scheduled. This curtailment may be accounted for in the demand for upward reserves, as the upward reserve requirement is defined relative to the forecasted RES-based generation profile. Realizations of RES-based electricity generation in the

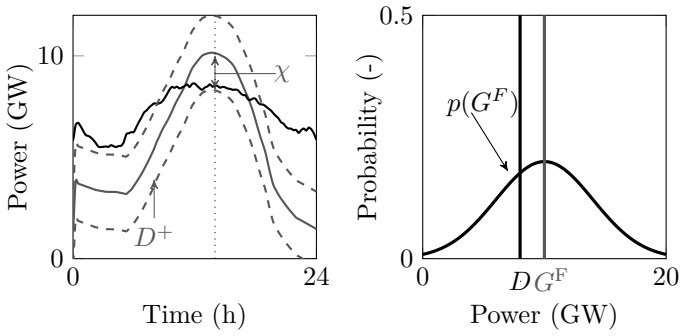

Figure 2.4: At noon (dotted line), the forecasted RES-based generation G^{F} exceeds the demand D. Curtailment χ is scheduled, which may be accounted for in the demand for upward reserves (D^+).

interval $[G_j^{\mathrm{F}} - \chi_j, G_j^{\mathrm{F}}]$ can be absorbed by the system without scheduling additional upward reserves. Not accounting for curtailment of excess RES-based electricity generation in the demand for upward reserves may lead to over-procurement of upward reserves, hence sub-optimal UC schedules.

The discussion is somewhat more complicated for downward reserves. One could argue that a system operator should include a demand for downward flexibility to absorb increases in RES-based generation. However, this could lead to somewhat adverse effects. For example, such a downward reserve constraint could trigger additional curtailment due to the (cumulative sum of the) minimum operating points of the power plants needed to provide these downward reserves. This would result in the curtailment of 'certain' forecasted RES-based generation to absorb an 'uncertain', possible increase in RES-based generation – a counter-intuitive approach[14]. Therefore, one could use the correction as proposed in Eq. (2.11). When VOC equals zero, and we typically will assume it does in the paradigm of the independent system operator, the model will typically schedule some curtailment to avoid scheduling more expensive, flexible power plants to provide downward reserve. The cost of switching technologies typically exceeds the cost of curtailing one MWh of RES-based generation and compensating for this unit of energy by producing one additional MWh with

[14]If all RES-based generation can be curtailed, it is reasonable to assume that all downward flexibility can be delivered by curtailment – i.e., all positive RES-based generation forecast errors are curtailed. Alternatively, if the RES-based generation cannot be curtailed (e.g. some types of residential photovoltaic systems), a fixed lower bound on the procured downward flexibility may be imposed on the optimization.

cheap, conventional generation. If the VOC is non-zero and compensates the difference in operational costs, more flexible power plants may be scheduled to provide downward flexibility. Note that the trade-off suggested above is incomplete, as already mentioned in the discussion of Eq. (2.11). In Eq. (2.11), we are comparing the operational cost of curtailing of one MWh of RES-based generation with the allocation cost of the most expensive MW of downward flexibility (see above). For a cost-optimal trade-off, one should be able to compare the benefit associated with scheduling downward reserves, i.e. expected operational cost savings associated with the ability of absorbing more RES-based generation, with the upfront allocation cost of scheduling downward reserves. The first term in this trade-off is typically not known in a DUC model, as it is dependent on the probability of activation of the downward reserve providers. If the cost of curtailment is significant, the expected benefits associated with scheduling downward reserves increase. Including a fixed downward reserve requirement may lead to more cost-optimal UC schedules in these cases. In other UC models, such as the stochastic UC model, the trade-off between the expected cost savings due to an increased absorption of RES-based generation and the upfront cost of allocating downward reserves is made explicit (see Section 2.3). This leads to more cost-efficient UC schedules.

In the example of Fig. 2.4, the correction suggested in Eq. (2.11) would relax the downward reserve requirement between 10 a.m. and 2 p.m. Recall that the resulting UC schedule may contain some downward flexibility in these hours. However, it will not be the result of an explicit downward reserve requirement.

2.2.4 Participation of pumped hydro energy storage systems in the reserve requirement[15]

In the formulation proposed above, PHES systems may not be scheduled to satisfy the demand for reserves. As the availability of the PHES system is dependent on the water level in the reservoir, which is in turn dependent on the actual dispatch of the PHES system, dependent on the realization of the uncertain RES-based generation, the availability of scheduled reserves would not be guaranteed. Indeed, as the PHES system does not present any allocation cost, the DUC model would continuously schedule PHES-based generation as upward reserves. However, upon activation, the amount of energy stored in the PHES system may be insufficient to provide both the arbitrage and regulation services it was scheduled to. This would lead to dispatching expensive, fast-starting units and load shedding in real time.

[15]This section is based on K. Bruninx, Y. Dvorkin, E. Delarue, H. Pandžić, W. D'haeseleer, and D. S. Kirschen, *Coupling Pumped Hydro Energy Storage with Unit Commitment,* IEEE Trans. Sustain. Energy, vol. 7, no. 2, pp. 786–796, 2016.

To allow the participation of PHES systems, or energy storage in general, in the reserve requirements, we will define four new variables and impose new constraints on the energy content of the PHES systems, in addition to Eq. (2.28) - (2.32). We define the following variables:

- $r_{r,j}^{\mathrm{P},+}$, the upward reserves provided by the PHES system in pumping mode – i.e., providing upward flexibility by reducing its pumping power;
- $r_{r,j}^{\mathrm{P},-}$, the downward reserves provided by the PHES system in pumping mode – i.e., downward flexibility by increasing its pumping power;
- $r_{r,j}^{\mathrm{T},+}$, the upward reserves provided by the PHES system in turbining mode – i.e., upward flexibility by increasing its output;
- $r_{r,j}^{\mathrm{T},-}$, the downward reserves provided by the PHES system in turbining mode – i.e., downward flexibility by reducing its output.

The reserve constraints read:

$$\forall j: \quad D_j^+ = \sum_i \left(r_{i,j}^+ + nsr_{i,j}^+\right) + \sum_m \chi_{j,m} + \sum_r \left(r_{r,j}^{\mathrm{P},+} + r_{r,j}^{\mathrm{T},+}\right) + s_j^+ \tag{2.40}$$

$$\forall j | \sum_m \chi_{j,m} = 0: \quad D_j^- = \sum_i r_{i,j}^- + \sum_r \left(r_{r,j}^{\mathrm{P},-} + r_{r,j}^{\mathrm{T},-}\right) + s_j^- \tag{2.41}$$

These reserves provided by the PHES systems are constrained to the capacity of each PHES unit and the scheduled output of those PHES systems:

$$\forall r, \forall j: \quad 0 \leq r_{r,j}^{\mathrm{P},+} \leq g_{r,j}^{\mathrm{P}} \tag{2.42}$$

$$\forall r, \forall j: \quad 0 \leq g_{r,j}^{\mathrm{P}} + r_{r,j}^{\mathrm{P},-} \leq \overline{P_r} \cdot p_{r,j} \tag{2.43}$$

$$\forall r, \forall j: \quad 0 \leq g_{r,j}^{\mathrm{T}} + r_{r,j}^{\mathrm{T},+} \leq \overline{P_r} \cdot t_{r,j} \tag{2.44}$$

$$\forall r, \forall j: \quad 0 \leq r_{r,j}^{\mathrm{T},-} \leq g_{r,j}^{\mathrm{T}} \tag{2.45}$$

$$\forall r, \forall j: \quad r_{r,j}^{\mathrm{P},-},\ r_{r,j}^{\mathrm{T},+} \geq 0 \tag{2.46}$$

This formulation is insufficient to allow the PHES systems to offer regulation services in the DUC formulation. Indeed, when scheduling PHES-based reserves, one should ensure that sufficient energy is stored in the upper basin of the PHES system (upward reserves) or that one can store the absorbed energy in the upper basin of the PHES unit (downward reserves). A system operator should not only take into account the storage level at each time step under forecast

conditions – which is a reflection of the 'expected' use of the PHES system – but also the impact of possible activation of up- and downward reserves. The limits on the energy content of the PHES system should be respected at each time step, in the worst-case scenario (activation of all reserves in one direction):

$$\forall r, \forall j: \quad e_{r,j} + TP \cdot \sum_{1}^{j} \left(\frac{r_{r,j}^{\mathrm{T},-}}{\sqrt{\epsilon_r}} + r_{r,j}^{\mathrm{P},-} \cdot \sqrt{\epsilon_r} \right) \leq \overline{E_r} \tag{2.47}$$

$$\forall r, \forall j: \quad e_{r,j} - TP \cdot \sum_{1}^{j} \left(\frac{r_{r,j}^{\mathrm{T},+}}{\sqrt{\epsilon_r}} + r_{r,j}^{\mathrm{P},+} \cdot \sqrt{\epsilon_r} \right) \geq \underline{E_r} \tag{2.48}$$

The inclusion of these last two constraints ensures that the hydraulic constraints of the PHES system are respected when the reserves are activated. This enables PHES systems to provide energy arbitrage and regulation services taking into account hydraulic and power system constraints. Although constraints (2.47)–(2.48) in most cases will be too conservative – the probability of continuously dispatching all upward or downward PHES-based reserves might be low – it allows scheduling PHES-based reserves, resulting in significant cost reductions, without affecting the reliability of the power system (Chapter 5).

Constraints (2.47)–(2.48) do not only affect the energy storage level of the PHES system under worst-case conditions, but also under forecast conditions during UC scheduling. For example, consider a case in which a SO desires to schedule upward PHES-based reserves. Equation (2.48) requires that the energy storage level must be increased to ensure the feasibility of deploying the scheduled reserves. This effectively increases the demand under forecast conditions at some time preceding the moment at which those upward reserves are scheduled. As a result, the total operational cost *under forecast conditions* may increase at that moment that the PHES system is charged. Alternatively, one can think of situations in which the PHES system is sufficiently charged to provide upward reserves. By scheduling the PHES system as upward reserves, part of the stored energy is virtually 'reserved' for regulation purposes. The full storage capacity of the PHES system can no longer be used to optimize the UC schedule under forecast conditions (arbitrage), which entails an opportunity cost. The combination of this operational cost increase and/or opportunity cost can be interpreted as an allocation cost of PHES-based reserves[16]. An equivalent deployment cost of the PHES unit is more difficult to quantify and is not accounted for in the DUC model. Similar reasoning applies to scheduling downward PHES-based reserves.

[16]Note that the total operational cost under forecast conditions, i.e. the objective of the DUC problem, can not increase with the introduction of PHES-based reserves. If scheduling PHES-based reserves would result in a total operational cost increase, the DUC model will not schedule the PHES system as a reserve provider.

Note that the trade-off with other flexibility providers is ill-informed. We compare an energy-based cost, e.g. the cost of increased charging in the case of upward PHES-based reserves, with capacity-based allocation costs of conventional flexibility providers, excluding the expected activation costs. As a result of this poor trade-off, and due to the conservatism imposed on the PHES-based reserves by Eq. (2.47)–(2.48), PHES-based flexibility will typically remain under-utilized in the DUC model. Nevertheless, including PHES-based reserve provision enhances the cost-efficiency of the DUC schedule significantly (Chapter 5).

We will extensively study the necessity of constraints (2.47)-(2.48) and the added value of PHES-based regulation services in Chapter 5. The impact of neglecting the activation cost of conventional flexibility providers on the use of PHES-based reserves is also explored in Chapter 5.

2.2.5 Discussion

The DUC model is historically the most-used UC model, mainly due to its simplicity and speed, while it allows representing most of the technical constraints of power plants, energy storage systems and transmission grids with sufficient detail (Chapter 1)[17]. However, with the rising shares of intermittent RES-based generation in power systems, day-to-day power system scheduling problems have become riddled with uncertainty. Moreover, the level of uncertainty now fluctuates strongly throughout time, depending on weather conditions and forecast quality. The ex-ante reserve sizing, a condicio sine qua non for the DUC model, becomes increasingly complex and important to ensure a cost-effective and reliable power supply. In addition, including flexibility offered by non-spinning units and PHES systems requires adaptations of the traditional DUC formulation. Required parameters, such as e.g. the reservation cost of non-spinning reserves, are difficult to estimate but may have a significant impact on the resulting UC schedules.

At the root of this possibly sub-optimal UC scheduling lies (1) the absence of the expected activation cost of the scheduled reserves and (2) overly conservative constraints on e.g. the reserves offered by energy storage-like flexibility providers or the ramping requirements imposed on the reserves offered by conventional

[17]The historical tenancy towards DUC models is also a reflection of the computationally limits of the day, as the first SUC models (see further) were already developed in the 1970s [95]. It wasn't until the 1990s that the SUC models reappeared due to the ability of computers to handle larger problems, together with the first notions of computational parallelization and decomposition frameworks [96, 97]. However, the tractability of stochastic programs remains an issue, as calculation times strongly increase with the problem size (Section 2.3 and Chapters 4-5).

power plants. Not including the expected activation cost has a number of consequences. First, and foremost, it requires ex-ante reserve sizing techniques to estimate the cost-optimal reserve margin that needs to be maintained throughout the planning period. Recall that optimal reserve sizing is the result of a trade-off between (1) the socio-economic cost of load shedding and curtailment of RES-based generation and (2) the expected cost of reserve allocation and activation [46]. As the probability of forecast errors, thus the probability of activation of the reserves, is not considered in the DUC model, the expected activation cost is unknown and internalization of an optimal reserve sizing procedure is impossible. Although this approach to uncertainty in a DUC model is straightforward, the amount of reserves required and the constraints imposed on the reserve providers may have a significant impact on the performance of such models, in particular on the operational costs and the reliability, because generators and energy storage resources are dispatched in a less economic manner [98, 93]. 'Over-sizing' the reserves will result in too much scheduled capacity, resulting in curtailment and inefficient part-load operation of power plants, which yields higher operational costs. In contrast, insufficient online capacity triggers load shedding, as too little capacity will be available to meet the demand. Reliability, and therefore operational costs, are affected by such 'under-sizing'. Although the cost performance of these reserve policies can be improved by means of parametric [99] or non-parametric [100] statistical analyses (see below), the exogenous nature of these requirements inhibits the co-optimization of the amount of reserve capacity with the UC decisions.

Second, only considering allocation costs results in sub-optimal trade-offs between conventional flexibility providers, curtailment of RES-based generation and energy storage-based flexibility providers. For example, the choice between conventional, spinning reserves with high allocation costs, but low activation costs and their non-spinning counterparts with low allocation costs, but high activation costs will be based solely on their allocation cost. For frequently activated reserves, this might be an ill-informed decision. Especially when considering non-spinning reserves, which typically are characterized by extremely low allocation costs and high activation costs, the ratio between spinning and non-spinning flexibility may be sub-optimal. Similarly, the value of downward flexibility is not considered: the possible operational cost savings (the activation 'cost' of downward flexibility) are not monetized in a DUC formulation. In real time, the system may not be able to absorb unexpected increases in RES-based generation, which may be sub-optimal. Last, this results in an incomplete comparison of the expected operational cost of PHES-based reserves and conventional reserves (Section 2.2.4).

Third, the imposed reserve requirements are typically too conservative, in order to avoid load shedding in real time. For example, we required that all upward

and downward reserves are available within one time step, i.e. they are limited to the available ramping capacity of each unit. The probability of activating all reserves in one direction, which would correspond to the occurrence of a zero forecast error followed by a forecast error equal to the reserve requirement, may however be extremely low. Similarly, the worst-case feasibility requirement imposed on the PHES-based reserves strongly limits the amount of reserves offered by PHES systems.

Last, not dispatching the scheduled reserves may result in the scheduling of reserves that cannot be activated in real time. For example, grid constraints may prevent reserves, scheduled via a DUC model, to be activated [94]. Indeed, the feasibility of the flows on the network is only guaranteed under forecast conditions (Eq. (2.25)-(2.27)). Congestion may prevent scheduled reserves to be activated, causing load shedding or curtailment in real time. To account for the impact of reserve activation on the flows on the network, one could enforce feasibility in a worst-case scenario for the network, similar to the constraints imposed on the PHES-based reserves. Determining such a worst-case scenario for the flows in the network may however be a non-trivial task and is out of the scope of this PhD dissertation.

To reduce the conservatism of DUC models, researchers continuously strive to improve reserve sizing procedures. Instead of static rule-of-tumb reserve sizing procedures, dynamic optimal reserve sizing techniques [93, 46] or probabilistic reserve sizing procedures [99, 100] are proposed. A recent overview can be found in [26]. Probabilistic reserve sizing techniques employ detailed, statistical representations of the uncertainty at hand to determine the amount of reserves needed based on the probability that a forecast error of a certain size occurs. Probabilistic reserve requirements have gained attention over the last years [101, 99, 100]. For example, Wang et al. [101] show that a probabilistic reserve requirement (based on a so-called quantile forecast) outperforms other reserve rules in a DUC model when dealing with uncertainty on wind power forecasts. Botterud and Zhou [102] demonstrate that a dynamic, probabilistic reserve requirement in a DUC model even (slightly) outperforms a SUC solution in terms of operational costs in some specific cases. However, one typically still has to specify the threshold as of which a forecast error becomes so improbable that maintaining reserves to cover that forecast error becomes economically unjustifiable. Alternatively, optimal reserve sizing techniques employ estimates of the expected cost of reserve provision, knowledge of the power system at hand and statistical descriptions of the uncertainty to decide upon the amount of reserves [93, 46]. In addition, some researchers include a fixed cost for reserve provision and deployment, different per technology and fuel, in a DUC formulation in order to ensure a 'logical' reserve procurement [26]. These penalties can be thought of as approximations of the deployment cost associated

with spinning reserves, but typically are not 'expected' costs. At best, a fixed probability of activation is included, constant across the flexibility providers and reserve requirements [103, 26]. We will come back to the issue of reserve sizing in Chapter 3. The impact of proper reserve sizing on the cost-effectiveness and reliability of the resulting UC schedule is studied in Chapter 5.

Although the DUC formulation thus has its merits, we will move to more advanced scheduling models, such as the stochastic UC model. Due to its complexity, this model will be more difficult to solve. However, if used correctly, the resulting UC schedules will be superior in terms of operational cost, uptake of RES-based generation and reliability. Insights gained from the analysis of the formulation and performance of these models allow improving existing UC models and developing new UC models.

2.3 A state-of-the-art stochastic unit commitment model[18]

In this section we present a state-of-the-art stochastic unit commitment (SUC) model. The full formulation can be found in Appendix C. In a SUC model, one seeks a UC schedule that minimizes the *expected* cost of providing the demanded electricity over the simulated period. To calculate the expected value, the model considers a set of scenarios that represents the uncertainty on wind and/or solar power forecasts (Fig. 2.5)[19]. Each scenario is a possible realization of the RES-based generation and has a specific probability of occurrence. The problem is typically formulated as a two-stage recourse problem [35]. The model ensures that the resulting UC schedule allows a dispatch in each of the considered scenarios. As such, the need for reserve requirements is abolished: the reserve sizing problem is internalized in the stochastic UC problem via the scenarios of the stochastic variable (Section 2.3.1). When a modeler is capable of capturing all relevant effects in the set of considered scenarios and the stochastic formulation is an accurate representation of the decision problem, one should, in theory, obtain an optimal UC schedule under uncertainty. The UC variables are the so-called *here-and-now* variables [35]. They are common to all scenarios. All other optimization variables, such as the output of the

[18]This section contains elements from K. Bruninx, K. Van den Bergh, E. Delarue, and W. D'haeseleer, *Optimization and Allocation of Spinning Reserves in a Low-Carbon Framework,* IEEE Trans. Power Syst., vol. 31, no. 2, pp. 872–882, 2016.

[19]In the scientific literature, this approximation of the objective function of the 'true' stochastic problem, considering the continuous description of the uncertain variable, as a weighted average over a number of discrete scenarios or samples is referred to as a Sample Average Approximation (SAA) [104].

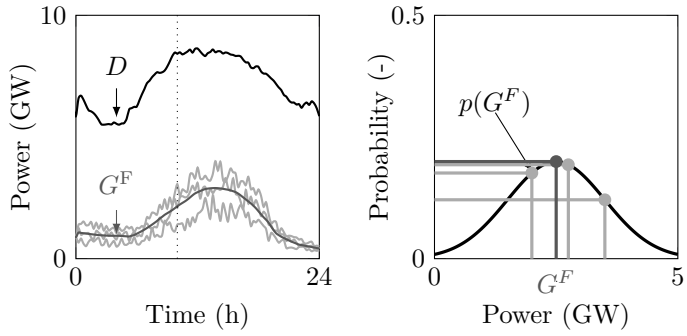

Figure 2.5: In the SUC paradigm, the SO has to decide on the UC schedule, taking into account a number of RES-based electricity generation scenarios, each with its probability of occurence. This set of scenarios, each of which is a possible realization of the RES-based electricity generation (left), form a discrete representation of the distribution of the stochastic RES-based electricity generation at each time step (right). The indicated scenarios are illustrative.

power plants, the curtailment of RES-based generation and the output of PHES systems, are the so-called *wait-and-see* or *recourse* decision variables: they are dependent on the scenarios [35].

The power plants are scheduled and dispatched in such a way that the overall expected cost of generating the demanded electricity over the simulated time period is minimized (Eq. (2.49)). This cost $c(g, z)$ consists of fuel costs $fc_{i,j,s}$, start-up costs $sc_{i,j}$, ramping costs $rc_{i,j,s}$ and CO_2-emission costs $co_2t_{i,j,s}$. The objective function reads

$$\min c(g,z) = \sum_i \sum_j \left[sc_{i,j} + \sum_s \pi_s \cdot (fc_{i,j,s} + co_2t_{i,j,s} + rc_{i,j,s}) \right] \tag{2.49}$$

$$+ \sum_j \sum_m \sum_s \pi_s \cdot TP \cdot (VOLL \cdot \phi_{j,m,s} + VOC \cdot \chi_{j,m,s})$$

where π_s is the probability of a scenario s (set S). Note that we no longer need slack variables for the reserve requirements, as these constraints are no longer enforced.

The fuel cost ($fc_{i,j,s}$) is now dependent on the scenario s, as the output of the power plant is scenario dependent[20]:

$$\forall i, \forall j, \forall s: \; fc_{i,j,s} \geq TP \cdot \left(C_i \cdot z_{i,j} + MA_i \cdot \left(g_{i,j,s} - \underline{P_i} \cdot z_{i,j}\right)\right) \tag{2.50}$$

Note that the binary variable $z_{i,j}$, representing the commitment status of plant i, is independent of the scenarios s. Similarly, the CO_2-emission cost $co_2t_{i,j,s}$ and ramping costs are now scenario dependent:

$$\forall i, \forall j, \forall s: \; co_2t_{i,j,s} \geq CO_2P \cdot TP \cdot \left(B_i \cdot z_{i,j} + MB_i \cdot \left(g_{i,j,s} - \underline{P_i} \cdot z_{i,j}\right)\right) \tag{2.51}$$

$$\forall i, \forall j, \forall s: \; rc_{i,j,s} \geq RCP_i \cdot \left(g_{i,j,s} - g_{i,j-1,s} - \underline{P_i} \cdot v_{i,j}\right) \tag{2.52}$$

$$\forall i, \forall j, \forall s: \; rc_{i,j,s} \geq RCP_i \cdot \left(g_{i,j-1,s} - g_{i,j,s} - \underline{P_i} \cdot w_{i,j}\right) \tag{2.53}$$

$$\forall i, \forall j, \forall s: \; rc_{i,j,s} \geq 0 \tag{2.54}$$

The start-up cost $SC_{i,j}$ is calculated via Eq. (2.4) and remains scenario independent.

This optimization is subject to a number of constraints, similar to the constraints in the DUC formulation. First, the supply and demand for electricity must be equal at all time steps j on each node m in each scenario s. The market clearing condition or power balance reads:

$$\forall j, \forall m, \forall s: \; D_{j,m} - \phi_{j,m,s} = \sum_i I^{\mathrm{G}}_{m,i} \cdot g_{i,j,s} + inj_{j,m,s} + G^{\mathrm{MR}}_{j,m} \tag{2.55}$$

$$+ G^{\mathrm{F}}_{j,m,s} - \chi_{j,m,s} + \sum_r I^{\mathrm{PHES}}_{m,r} \cdot \left(g^{\mathrm{T}}_{r,j,s} - g^{\mathrm{P}}_{r,j,s}\right)$$

The demand $D_{j,m}$ on each time step j and each node m is still assumed to be known and fixed (parameter of the model). This demand must be met on each node, in each scenario by

- electricity generated from dispatchable power plants $g_{i,j,s}$;
- injections from the grid $inj_{j,m,s}$ (see Eq. (2.63)–(2.65));
- generation from must-run systems with a known output $G^{\mathrm{MR}}_{j,m}$;

[20] Note the inequality sign in the definition of the fuel costs $fc_{i,j,s}$, start-up costs $sc_{i,j}$, ramping costs $rc_{i,j,s}$ and CO_2-emission costs $co_2t_{i,j,s}$. If only spinning reserves are allowed to be scheduled, this inequality sign can be replaced by an equality sign, as in the DUC formulation. To include non-spinning reserves, which we will mimic by allowing scenario-dependent UC variables for specific power plants, we however need to define the operational costs via inequalities to account for the operational cost associated with dispatching these reserves (see Section 2.3.2).

- the output of some uncertain RES-based electricity generation, $G^{\mathrm{F}}_{j,m,s}$, which can be curtailed ($\chi_{j,m,s}$)

$$\forall j, \forall m, \forall s: \quad 0 \leq \chi_{j,m,s} \leq G^{\mathrm{F}}_{j,m,s} \tag{2.56}$$

- the net injection of power from the PHES systems $\sum_r I^{\mathrm{PHES}}_{m,r} \cdot \left(g^{\mathrm{T}}_{r,j,s} - g^{\mathrm{P}}_{r,j,s}\right)$;
- the shedding of load $\phi_{j,m,s}$.

Second, the power plants have the same technical constraints as in the DUC model. The output of each power plant is limited to its maximum ($\overline{P_i}$) and minimum stable operating point ($\underline{P_i}$):

$$\forall i, \forall j, \forall s: \quad \underline{P_i} \cdot z_{i,j} \leq g_{i,j,s} \leq \overline{P_i} \cdot z_{i,j} \tag{2.57}$$

$$\forall i | \{MUT_i \geq 2\}, \forall j, \forall s: \quad g_{i,j,s} \leq \overline{P_i} \cdot z_{i,j} - \left(\overline{P_i} - \underline{P_i}\right) \cdot (v_{i,j} + w_{i,j+1}) \tag{2.58}$$

Note that for units with a MUT of at least two time steps, we impose a start-up and shut-down rate equal to their minimum stable operating point (Eq. (2.58)). The ramp-up and ramp-down rates of the power plants have been included as follows:

$$\forall i \notin I^{\mathrm{FAST}}, \forall j, \forall s: \; g_{i,j,s} \leq g_{i,j-1,s} + \overline{\Delta P^{+}_i} \cdot (z_{i,j} - v_{i,j}) + \underline{P_i} \cdot v_{i,j} \tag{2.59}$$

$$\forall i \notin I^{\mathrm{FAST}}, \forall j, \forall s: \; g_{i,j,s} \geq g_{i,j-1,s} - \overline{\Delta P^{-}_i} \cdot z_{i,j} - \underline{P_i} \cdot w_{i,j} \tag{2.60}$$

$$\forall i \in I^{\mathrm{FAST}}, \forall j, \forall s: \; g_{i,j,s} \leq g_{i,j-1,s} + \overline{\Delta P^{+}_i} \cdot z_{i,j} \tag{2.61}$$

$$\forall i \in I^{\mathrm{FAST}}, \forall j, \forall s: \; g_{i,j,s} \geq g_{i,j-1,s} - \overline{\Delta P^{-}_i} \cdot (z_{i,j} + w_{i,j}) \tag{2.62}$$

As the on/off status of the power plants is independent of the scenarios, the constraints that ensure that the MUT and MDT of each power plant are respected (Eq. (2.20)-(2.24)) are unchanged.

Third, the network constraints are taken into account through a DC–load flow representation. The flows on the network are now scenario dependent:

$$\forall j, \forall n, \forall s: \quad f_{j,n,s} = \sum_m PTDF_{n,m} \cdot inj_{j,m,s} \tag{2.63}$$

$$\forall j, \forall n, \forall s: \quad -CAP_n \leq f_{j,n,s} \leq CAP_n \tag{2.64}$$

$$\forall j, \forall s: \quad \sum_m inj_{j,m,s} = 0 \tag{2.65}$$

Last, the PHES systems (index r) are included in the model formulation. Again, the output of the PHES systems becomes dependent on the scenario s:

$$\forall r, \forall j, \forall s: \quad e_{r,j,s} = TP \cdot \left(g^{\mathrm{P}}_{r,j,s} \cdot \sqrt{\epsilon_r} - \frac{g^{\mathrm{T}}_{r,j,s}}{\sqrt{\epsilon_r}} \right) + e_{r,j-1,s} \tag{2.66}$$

$$\forall r, \forall j, \forall s: \quad \underline{E_r} \leq e_{r,j,s} \leq \overline{E_r} \tag{2.67}$$

$$\forall r, \forall j, \forall s: \quad 0 \leq g^{\mathrm{T}}_{r,j,s} \leq \overline{P_r} \cdot t_{r,j,s} \tag{2.68}$$

$$\forall r, \forall j, \forall s: \quad 0 \leq g^{\mathrm{P}}_{r,j,s} \leq \overline{P_r} \cdot p_{r,j,s} \tag{2.69}$$

$$\forall r, \forall j, \forall s: \quad p_{r,j,s} + t_{r,j,s} \leq 1 \tag{2.70}$$

$$\forall r, \forall j, \forall s: \quad p_{r,j,s},\ t_{r,j,s} \in \{0, 1\} \tag{2.71}$$

Note that in this formulation, PHES systems are per definition allowed to offer 'reserves'. Indeed, as their output differs per scenario, this can be seen as their output as if they were scheduled (and activated) as reserves. We will return to the implications of Eq. (2.66)-(2.71) in Section 2.3.4.

2.3.1 Allocation & activation costs of spinning reserves

The constraint of a UC schedule common to all scenarios ensures that sufficient capacity is available to meet the demand under each considered realization of the stochastic RES-based electricity generation. This will trigger e.g. increased start-up costs and impacts the dispatch under forecast conditions, as in the DUC model. Allocation costs are thus considered. By 'dispatching' the scheduled units in each of the considered scenarios, one also obtains an estimate of the expected activation or deployment cost of the scheduled reserves. Indeed, the changes in fuel, emission and ramping costs associated with changes in output of each of the scheduled units, triggered by forecast errors and represented via the set of scenarios, are explicitly modeled. Using the probability of each scenario as a weighting factor, these operational cost changes can be accounted for in the objective function.

The explicit consideration of the full expected second-stage cost has a significant impact on the way flexibility is procured. First, reserve constraints are no longer needed: the reserve sizing procedure is effectively internalized in the UC optimization. Load shedding (upward flexibility) and curtailment of RES-based generation (downward flexibility) are considered as flexibility options and their respective socio-economic cost is accounted for in the objective

function, as advocated by Bouffard et al. [105]. This allows the model to make the trade-off between the full cost of flexibility provision (i.e. the expected activation and allocation cost) and the expected socio-economic cost of load shedding and curtailment of RES-based generation. Recall that this trade-off was impossible in the DUC model, which led to the need for ex-ante reserve sizing techniques. Second, one will obtain a cost-optimal mix of reserve providers. Reserves that are unlikely to be activated, are provided cost-efficiently by highly flexible, but expensive-to-run units, while e.g. efficient CCGT units are cost-optimal for the provision of frequently activated reserves. Third, the operational cost savings that may result from the provision of downward flexibility are explicitly monetized. Scenarios with a higher-than-expected RES-based output are characterized by a lower operational cost, which is accounted for in the objective function as a measure of the value of downward flexibility.

2.3.2 Allocation & activation costs of non-spinning reserves

In the formulation above one does not consider non-spinning reserves. The model looks for a common UC schedule that will allow a feasible dispatch in each considered scenario. As such, all scheduled flexibility, upward and downward, is per definition of the 'spinning' type. In the literature, one often encounters this approach. During the dispatch, i.e. the evaluation of the resulting UC schedule, fast-cycling units are allowed to start-up if the load cannot be met and/or this load is simply shed [17, 106, 86]. In both cases, the possibility of scheduling non-spinning reserves was not taken into account during the UC optimization procedure, which may yield sub-optimal UC schedules.

Non-spinning reserves may however explicitly be included in a stochastic UC model as follows. We will again make the assumption that only fast-starting units may provide non-spinning reserves (subset I^{FAST}). In addition to the variables and model equations discussed above, we introduce a new binary variable $z^*_{i,j,s}$, indicating the scenario-specific commitment status of fast-cycling power plants ($i \in I^{\text{FAST}}$) in each scenario s. A fast-cycling unit may then be scheduled as spinning or non-spinning if it belongs to the subset of power plants I^{FAST}:

$$\forall i \in I^{\text{FAST}}, \forall j, \forall s: \quad z_{i,j} + z^*_{i,j,s} \leq 1 \tag{2.72}$$

$$\forall i \notin I^{\text{FAST}}, \forall j, \forall s: \quad z^*_{i,j,s} = 0 \tag{2.73}$$

The output of the non-spinning reserves in all scenarios is constrained to their maximum ($\overline{P_i}$) and minimum stable output level ($\underline{P_i}$):

$$\forall i \in I^{\text{FAST}}, \forall j, \forall s: \quad \underline{P_i} \cdot z^*_{i,j,s} \leq nsr^+_{i,j,s} \leq \overline{P_i} \cdot z^*_{i,j,s} \tag{2.74}$$

The units in the subset I^{FAST} per definition have a MUT of one time period, thus a scenario-dependent equivalent of Eq. (2.20)-(2.24) is not required for these units. The binary variables $z^*_{i,j,s}$ (on/off status non-spinning reserves), $v^*_{i,j,s}$ (start-up non-spinning reserves), $w^*_{i,j,s}$ (shut-down non-spinning reserves) are linked as follows:

$$\forall i, \forall j, \forall s : z^*_{i,j,s} - z^*_{i,j-1,s} - v^*_{i,j,s} + w^*_{i,j,s} = 0; \tag{2.75}$$

$$\forall i, \forall j, \forall s : v^*_{i,j,s} + w^*_{i,j,s} \leq 1 \tag{2.76}$$

These units may be subjected to ramping constraints:

$$\forall i \in I^{\mathrm{FAST}}, \forall j, \forall s : \quad nsr^+_{i,j,s} \leq nsr^+_{i,j-1,s} + \overline{\Delta P^+_i} \cdot z^*_{i,j,s} \tag{2.77}$$

$$\forall i \in I^{\mathrm{FAST}}, \forall j, \forall s : \quad nsr^+_{i,j,s} \geq nsr^+_{i,j-1,s} - \overline{\Delta P^-_i} \cdot (z^*_{i,j,s} + w^*_{i,j,s}) \tag{2.78}$$

As these units have a MUT of one time period, one cannot enforce any tighter constraints. Note furthermore that we assume for power plants in subset I^{FAST} that $\overline{\Delta P^+_i}$ and $\overline{\Delta P^-_i}$ exceed the minimum operating point $\underline{P_i}$. Start-up and shut-down rates (Eq. (2.59)-(2.62)) are thus not enforced. The output of the non-spinning reserves shows up in the market clearing condition as follows[21]:

$$\begin{aligned} \forall j, \forall m, \forall s : \quad D_{j,m} - \phi_{j,m,s} = &\sum_i I^{\mathrm{G}}_{m,i} \cdot \left(g_{i,j,s} + nsr^+_{i,j,s}\right) + G^{\mathrm{MR}}_{j,m} \\ &+ G^{\mathrm{F}}_{j,m,s} - \chi_{j,m,s} + inj_{j,m,s} \\ &+ \sum_r I^{\mathrm{PHES}}_{m,r} \cdot \left(g^{\mathrm{T}}_{r,j,s} - g^{\mathrm{P}}_{r,j,s}\right) \end{aligned} \tag{2.79}$$

The operational costs of these non-spinning units can be calculated analogously to Eq. (2.50)-(2.54):

$$\forall i, \forall j, \forall s : \ fc_{i,j,s} \geq TP \cdot \left(C_i \cdot z^*_{i,j,s} + MA_i \cdot \left(nsr^+_{i,j,s} - \underline{P_i} \cdot z^*_{i,j,s}\right)\right) \tag{2.80}$$

$$\begin{aligned} \forall i, \forall j, \forall s : \ co_2t_{i,j,s} \geq &CO_2P \cdot TP \cdot \left(B_i \cdot z^*_{i,j,s}\right. \\ &\left. + MB_i \cdot \left(nsr^+_{i,j,s} - \underline{P_i} \cdot z^*_{i,j,s}\right)\right) \end{aligned} \tag{2.81}$$

[21] In [45], we required that the demand in the forecast scenario s^{F} was met by spinning units ($z^*_{i,j,s^{\mathrm{F}}} = 0$). This constraint is not enforced in the formulation presented in this section, as in some cases it might be more cost-optimal to schedule flexible, non-spinning capacity under forecast conditions, effectively providing downward reserves by shutting down in some scenarios. In [45], this constraint facilitated the comparison between the hybrid and the stochastic UC formulation (see Section 2.5).

$$\forall i, \forall j: \; sc_{i,j} \geq \sum_{s} \pi_s \cdot STC_i \cdot v^*_{i,j,s} \tag{2.82}$$

$$\forall i, \forall j, \forall s: \; rc_{i,j,s} \geq RCP_i \cdot \left(nsr^+_{i,j,s} - nsr^+_{i,j-1,s} - \overline{\Delta P^+_i} \cdot v^*_{i,j,s}\right) \tag{2.83}$$

$$\forall i, \forall j, \forall s: \; rc_{i,j,s} \geq RCP_i \cdot \left(nsr^+_{i,j-1,s} - nsr^+_{i,j,s} - \overline{\Delta P^-_i} \cdot w^*_{i,j,s}\right) \tag{2.84}$$

$$\forall i, \forall j, \forall s: \; rc_{i,j,s} \geq 0 \tag{2.85}$$

Note that the start-up costs for non-spinning units are calculated as probability-weighted average of the start-up costs in each scenario. Including these operational costs associated with the dispatch of non-spinning reserves in the objective function and explicitly accounting for a procurement cost for non-spinning reserves ensures that the full expected cost of scheduling and dispatching non-spinning reserves is considered during UC optimization:

$$\begin{aligned} \min c(g,z) = & \sum_i \sum_j \left[sc_{i,j} + \sum_s \pi_s \cdot (fc_{i,j,s} + co_2 t_{i,j,s} + rc_{i,j,s}) \right] \\ & + \sum_j \sum_m \sum_s \pi_s \cdot TP \cdot (VOLL \cdot \phi_{j,m,s} + VOC \cdot \chi_{j,m,s}) \\ & + \sum_i \sum_j NSRC_i \cdot y_{i,j} \end{aligned} \tag{2.86}$$

with

$$\forall i, \forall j, \forall s: \; y_{i,j} \geq z^*_{i,j,s} \tag{2.87}$$

$$\forall i, \forall j: \; y_{i,j} \in \{0,1\} \tag{2.88}$$

With these additions, the model allows calculating an optimal trade-off between spinning flexibility (cheap, but online in all scenarios, leading to a less 'compressible' power system) and non-spinning flexibility (highly flexible, allowing a higher absorption of intermittent generation, but typically high activation costs). Recall that such a trade-off was not possible in the DUC model (Section 2.2.2). However, note the absence of any so-called bundle constraints [105] on the non-spinning reserve providers. If two identical units are available, of which only one is needed to cover the demand at the same time step in two different scenarios, the presented formulation may schedule a different unit in each scenario. If the allocation cost of the non-spinning reserve providers $NSRC_i$ equals zero, both options (i.e. scheduling one or both units) represent the same operational cost, thus the formulation is indifferent to which solution is retained. This may lead to over-procurement of non-spinning reserves, but this may easily be checked and corrected ex-post.

2.3.3 Participation of intermittent RES-based generation in the reserve requirements

Curtailment of RES-based electricity generation is scenario-dependent in a stochastic UC formulation, which ensures the participation of RES-based generation in the implicit upward and downward reserve requirements. In scenarios characterized by a lower-than-expected RES-based electricity generation curtailment may occur if it leads to a more cost-optimal dispatch in that scenario, or if it is required to respect the operational constraints of the power plants, grid elements or energy storage systems. This is the equivalent of accounting for curtailment of forecasted RES-based generation in the upward reserve requirement in the DUC formulation. Note however that the decision of curtailing RES-based generation is made on a scenario-by-scenario basis, whereas in the DUC model this is a one-shot decision.

In scenarios with a higher-than-expected RES-based output, which trigger the activation of downward reserves, the operational cost savings associated with absorbing more RES-based generation are monetized. Whereas the DUC model provides little incentive to schedule downward flexibility (Section 2.2.3), the value of such flexibility is explicitly calculated in the SUC model. The scenario-dependent curtailment decision variable allows to assess the level up to which downward reserves can be provided cost-effectively. Downward flexibility will be scheduled to the extent that the procurement costs of this flexibility are not longer outweighed by the expected operational cost savings of absorbing more RES-based generation (i.e. the expected deployment cost savings of the scheduled downward flexibility and expected cost savings due to less curtailment, penalized at VOC in the objective). Curtailment is scheduled in those scenarios that require more downward flexibility.

2.3.4 Participation of pumped hydro energy storage systems in the reserve requirements

The scenario-dependent dispatch of the PHES systems ensures (1) an optimal trade-off between conventional and PHES-based flexibility and (2) the feasibility of the scheduled PHES output. It allows the PHES system to perform energy arbitrage in each scenario and the demand may be met more closely – i.e. with less scheduled capacity – in each scenario. The PHES systems may exploit variability in the RES-based output in each scenario to charge/discharge and provide upward/downward flexibility in later time steps, which is a more realistic (compared to the DUC formulation) representation of the operation of a PHES system. Moreover, the inclusion of the full expected cost of flexibility provision

with conventional power plants and the energy balance constraint of the PHES system in each scenario ensures a correct trade-off between both flexibility providers. Recall that such a trade-off was not possible in the DUC model.

Constraints (2.66)-(2.71) are enforced in each scenario, ensuring the feasibility of the output of the PHES systems in each of the considered scenarios. This is a less conservative approach than the one taken in the DUC model. The worst-case evaluation (Section 2.2.4) would correspond with the occurrence of a scenario in which the RES-based generation is continuously at the highest (Eq. (2.47)), respectively lowest possible level (Eq. 2.48)[22]. The probability of occurrence of these scenarios may be extremely low. In contrast, the scenarios considered in the SUC model should all have a finite probability.

Nevertheless, the scenario-based approach to the PHES-scheduling problem has a considerable disadvantage. In absence of so-called bundle constraints, linking the output or energy storage levels in the different scenarios, the PHES schedule will be optimized toward the *considered* scenarios. Other possible realizations of the uncertain RES-based generation may contain events that are not captured by the scenario set considered during the UC optimization. Load shedding, dispatching expensive fast-starting units or curtailment of RES-based electricity generation in real time may be the result. For example, Pozo et al. [64] study a SUC model including a generic, ideal storage. The SUC models yields cost-effective UC and PHES schedules, but is computationally intensive and the solution quality depends on the quality of the scenarios. These observations can be understood via the following example. Consider two scenarios, with an identical negative forecast error at time step t (scenario A) and t+1 (scenario B). In both scenarios, the PHES unit may be scheduled to turbine at those time steps to meet the demand. If during dispatch a scenario C would be considered with an identical, negative forecast error on time step t *and* t+1, insufficient energy may be stored in the upper basin to cover the demand in those two subsequent time steps. The minimum energy content constraint was respected in scenario A and B, but we did not consider the occurrence of scenario C during the optimization of the UC schedule. Similar reasoning does not apply to the scheduling of spinning and non-spinning capacity, as the supply of fuel (i.e. the equivalent of the stored water or energy in the PHES system) is unlimited on the short term. Nevertheless, if a modeler succeeds in identifying all events relevant for the scheduling of conventional and PHES-based capacity, a SUC model should yield optimal UC decisions in light of uncertain RES-based generation.

[22] To be precise, these extreme scenarios would correspond to scenarios in which the RES-based generation would follow the profile given by $\sum_m G^{\mathrm{F}}_{j,m,s^{\mathrm{F}}} + D^-_j$ and $\sum_m G^{\mathrm{F}}_{j,m,s^{\mathrm{F}}} - D^+_j$ respectively.

2.3.5 Discussion

In theory, a SUC formulation has two distinct advantages over a DUC formulation. First, ex-ante reserve sizing is no longer needed: the inclusion of scenarios and the requirement of a UC schedule common to those scenarios ensures the internalization of the reserve sizing calculation. By accounting for the operational cost associated with dispatching these reserves in the considered scenarios, the model will yield an optimal trade-off between the cost of load shedding or reliability and the cost of allocation and activation of flexibility. The consideration of the full, expected cost of reserve provision allows an optimal trade-off between different flexibility providers. Especially when considering reserve providers with large differences between the associated procurement and deployment costs (e.g. non-spinning and spinning reserves), this is a major advantage of the SUC formulation.

Second, dispatching these reserves in the considered scenarios ensures the technical feasibility of these reserves. For example, grid constraints may prevent reserves, scheduled via a DUC model, to be activated (Section 2.2.5). Reserve scheduling through a SUC model will ensure that these grid constraints are respected in all considered scenarios, effectively ensuring the technical feasibility of the activation of the scheduled reserves. Similarly, PHES systems are accounted for in the demand for flexibility without any adaptations to the model. Via the dispatch in each of the scenarios, the feasibility of the PHES schedule is ensured (Section 2.3.4).

In conclusion, the direct representation of the uncertainty via a set of scenarios in the UC model leads to an optimal trade-off between reliability and operational system cost [107, 39, 102, 17, 45]. For example, Papavasiliou et al. [17] study the performance of a two-stage SUC model on the California power system, consisting of 122 generators, considering uncertain wind power production. The model is solved for eight representative days of the year, considering 11 wind power scenarios. The UC schedule is evaluated on 250 wind power scenarios. Papavasiliou et al. [17] observe an improvement, compared to a DUC formulation considering the (3+5) reserve policy [108], in overall operational costs of 0.39% (7.1% wind energy in the annual energy mix) to 1.33% (14% wind energy) on the CAISO test system. The average calculation time for the SUC formulation is 5,685 seconds – significantly higher than those expected for a DUC formulation on a similar system. Papavasiliou and Oren employ the same SUC model in combination with a novel importance sampling-based scenario reduction technique in [109]. In a similar case study, daily operational costs savings range between 145,000 $ and 244,000 $ compared to the best available DUC schedule and between 5,000 $ and 52,000 $ compared to an alternative

SUC policy[23]. Employing 20 machines and a parallel implementation, based on Lagrangian relaxation, Papavasiliou and Oren report average calculation times of approximately 24,000 seconds for the SUC problem, considering 42 wind power scenarios, 130 generators, 225 buses and 375 transmission lines.

However, these SUC models are not devoid of disadvantages. First, the computational cost of solving such a SUC model is high and strongly increases with the number of scenarios one considers. The SUC model applied to a real-life power system can take tens of hours to be solved, even with a large optimality gap and a small number of scenarios [110, 106]. Moreover, one might lose the so-called 'tractability' of the problem as the number of scenarios increases – i.e., one might not be able to solve the problem with the traditional MILP solvers. This is partly due to the large problem size and the relatively flat objective function, which is difficult to explore via classical branch-and-bound MILP solution methods. Solution stability[24] requirements however impose a lower limit on the number of scenarios one can use to ensure a meaningful solution of the SUC model. Second, Dvorkin et al. [106] also reveal that lowering the optimality gap and increasing the number of scenarios does not necessarily improve the accuracy of the SUC approach, leading to a less economic schedule. This can be explained by the dependence of the SUC schedule on the quality of the scenario generation and reduction techniques used to produce a representative set of scenarios, as illustrated by Lowery and O'Malley [113]. Capturing a continuous stochastic variable, such as e.g. the forecast error, in a (limited) set of discrete scenarios with sufficient accuracy requires a detailed description of the uncertainty at hand (Chapter 3) and advanced scenario generation and reduction techniques (Chapter 4). A common flaw of these techniques is that wind power generation is assumed to follow a probability distribution which does not precisely fit empirical data [114, 99, 100, 115] or scenario reduction techniques that fail to identify critical scenarios [116]. In real-life power systems, one needs to consider multiple sources of uncertainty and multiple regions, drastically increasing the complexity of the problem at hand. We will return to this issue in Chapter 4. Similarly, the value of lost load ($VOLL$) has a direct impact on the resulting solution, as it represents the 'budget' available to schedule reserves in order to avoid the last MWh of load shedding. As such, one could argue that we have shifted the ex-ante reserve sizing-problem to the problem of (1) the representation of the uncertainty in a set of discrete

[23] This operational cost difference is the result of the use of a different scenario reduction technique. We will return to this issue in Chapter 4.

[24] *Solution stability* means that the objective value – obtained by solving the SUC problem – does not change (too much) when the set of scenarios considered enlarges and that this value is close to the true objective function – obtained by solving the SUC problem on the 'full' set of scenarios with fixed first stage optimization variables [111]. We will extensively discuss this concept and its implications for SUC models in Chapter 4. The notion of solution stability should not be confused with power system stability [112].

scenarios and the probability of those scenarios and (2) the quantification of the value of lost load $VOLL$. Similar reasoning applies to downward reserves, curtailment and the value of curtailed RES-based generation VOC. However, if one succeeds in capturing the underlying stochasticity in a sufficiently small set of scenarios, resulting in a tractable SUC problem, this approach yields the optimal decision under uncertainty.

To limit the computational burden, modelers often resort to other UC formulations or they try to speed up the convergence of the SUC model. In the latter category, one can distinguish multiple approaches, such as, but not limited to, improved model formulations [117], decomposition techniques to exploit the structure of the problem [97, 118, 117, 119, 120, 121], advanced scenario reduction methods [37, 122, 102, 106, 116], relaxations of the problem [123] and the addition of reserve constraints in SUC model [107, 39, 102]. In this dissertation, we will not explore decomposition methods or relaxations of the SUC model. The impact of the addition of a reserve requirement to a SUC model will be discussed in Section 2.5 and quantified in Chapter 5. Scenario reduction is one of the topics tackled in Chapter 4.

Alternative formulations of the UC problem circumvent the sensitivity of the UC solution to the exact form of the distribution or scenario set describing the stochastic variable and the value of lost load. One of the best-known distribution-insensitive UC formulations is the so-called **robust unit commmitment (RUC)** model [56]. In a RUC formulation, one models potential realizations of RES-based generation as an interval around the central forecast, and thus avoids assumptions regarding individual scenarios [55]. A scenario-based RUC formulation may look very similar to a SUC model. Typically one will try to find a UC schedule which yields a feasible dispatch in all scenarios considered in the model. The only distinct difference lies in the objective function of the model: instead of minimizing the expected operational cost, using the probability of each scenario as a weighting factor, we will now optimize the cost of generating electricity in the worst possible outcome of the uncertain variable:

$$\begin{aligned}\min \quad & \sum_i \sum_j sc_{i,j} + \sum_i \sum_j NSRC_i \cdot y_{i,j} \\ & + \max_s \Big[\sum_i \sum_j \left(fc_{i,j,s} + co_2 t_{i,j,s} + rc_{i,j,s} \right) \\ & + \sum_j \sum_m TP \cdot (VOLL \cdot \phi_{j,m,s} + VOC \cdot \chi_{j,m,s}) \Big]\end{aligned} \tag{2.89}$$

All other constraints of the SUC model, Eq. (2.50)-(2.71), are enforced in a RUC model. Similar to the SUC model, the UC variables ($z_{i,j}$, $v_{i,j}$, $w_{i,j}$ and

$y_{i,j}$) are the first-stage variables, while all others, such as the output of the power plants, are second-stage variables and are thus scenario-dependent.

Such a RUC formulation has a number of specific properties. First, the resulting solution can be independent from the underlying, assumed distribution of the uncertain variable. Although this limits the risk of e.g. underestimating the probability of a very demanding scenario occurring, one by definition excludes available information. The calculation of the expected cost of reserve provision is impossible. The trade-off between e.g. load shedding and upward flexibility provision is thus not possible in a RUC model, which results in very conservative and possibly sub-optimal UC schedules. Similarly, non-spinning reserves may be included in the model formulation, but the scheduled 'non-spinning reserves' will be meaningless. Indeed, assume that a unit can be scheduled as 'non-spinning'. In the 'worst-case' scenario, which drives the objective function above, this unit may appear as spinning or non-spinning. If it has the same output, it will trigger the same cost in the objective function (worst-case scenario)[25]. The status of that unit in other scenarios, i.e. spinning or non-spinning, is irrelevant in determining the objective function. Last, calculation times are typically drastically lower for a RUC model, albeit still higher than a DUC formulation. As in the SUC model, calculation times increase with the number of scenarios, but at a lower pace. Intelligent solution techniques exist, which exploit the structure of the problem, similar to the decomposition techniques for the SUC problem. Under mild assumptions, the worst-case realization of the uncertain RES-based electricity generation may be identified ex-ante, effectively reducing the RUC model to a DUC model [28].

Although both the SUC and RUC formulations typically yield more cost-efficient UC schedules than the DUC model, these formulations differ in their computational and cost performance [124]. The RUC model can be solved faster than the SUC formulation because, unlike the SUC formulation, it models potential realizations of wind power generation as an interval around the central forecast, and thus avoids assumptions regarding individual scenarios [55]. However, as the RUC model hedges the system against any realization within a given uncertainty set but does not account for the probability of its occurrence, it may produce overly conservative schedules. To reduce the conservatism of a RUC formulation, some researchers allow that certain constraints, typically the power balance, are violated with a certain (low) probability. Small and unlikely violations of the constraints are tolerated, effectively relaxing the problem, while guaranteeing a solution with a certain reliability (e.g. an upper limit on the loss

[25] To be precise, this requires reformulating the calculation of the start-up cost of fast-starting units (Eq. (2.82)). Instead of a probability-weighted average, one should calculate the start-up cost as the maximum of the start-up cost of that unit over the considered scenarios: $\forall i, \forall j, \forall s: \; sc_{i,j} \geq STC_i \cdot (v^*_{i,j,s} + v_{i,j})$.

of load probability (LOLP)). In the context of a RUC model, the so-called budget of uncertainty can be used to alleviate the conservatism of the RUC formulation [125, 86]. Simulations on the ISO New England system have shown that a RUC model is more cost-effective than an equivalent DUC formulation [56], if the budget of uncertainty is chosen appropriately. The budget of uncertainty is a crucial mechanism to achieve a good trade-off between the operational cost and robustness of the RUC solution [125]. To the best of the author's knowledge, there is no systematic way to optimize the value of the budget of uncertainty a priori. Setting the budget of uncertainty, which drives the performance of the RUC model, ex-ante entails a trade-off between the full cost of providing reserves, which is unknown before solving the RUC problem, and the cost of load shedding. This lack of transparency may impede the application of the RUC model in real-life power systems. Alternatively, the conservatism of the RUC model can be partially alleviated by constructing uncertainty sets that take into account the temporal and spatial correlations of wind power generation [55, 126]. However, these uncertainty sets may worsen the computational performance of the RUC model [127]. In the remainder of this dissertation, we will not focus on the RUC model. For a comparison of the performance of the RUC and the SUC formulation, see a.o. [86].

Similarly, one can avoid the dependency on the cost of load shedding by moving to chance-constrained unit commitment models [59, 58, 60, 61, 57]. In such a chance-constrained UC formulation, we allow, similar to the budget of uncertainty, that certain constraints, are violated with a certain (low) probability. In the context of the UC problem one could e.g. introduce a chance constraint on the load shedding volume **ENS**[26]:

$$Pr\left(\mathbf{ENS} \leq \overline{\Phi}\right) \leq 1 - \epsilon \tag{2.90}$$

This constraint states that the load shedding volume in each scenario should be below $\overline{\Phi}$ with a probability of at least $1 - \epsilon$. Using a scenario-based approximate representation of the uncertain RES-based electricity generation forecast[27], this

[26] Sometimes the power balance is directly formulated as a chance constraint. Here we choose the load shedding volume for sake of clarity, but both formulations would be equivalent.

[27] Alternatively, for some distributions, one can analytically reformulate chance constraint (2.90) as a so-called second order conic constraint. Using Mixed Integer Quadratically Constrained Programming (MIQCP), one can solve a UC problem constrained by Eq. (2.90) exactly. As such a model is closely related to the probabilistic UC model, we will return to these models in the discussion of Section 2.6.

can be reformulated as

$$\forall s: \quad \sum_{j}\sum_{m} TP \cdot \phi_{j,m,s} \leq \overline{\Phi} + M \cdot (1 - \alpha_s) \tag{2.91}$$

$$\sum_{s} \pi_s \cdot (1 - \alpha_s) \leq 1 - \epsilon \tag{2.92}$$

in which M is a sufficiently large number (parameter of the model) and α_s a binary variable indicating whether the load shedding constraint is violated in scenario s.

Finally, remove the load shedding penalization from the objective function

$$\begin{aligned} \min c(g,z) = \sum_{i}\sum_{j}\left[sc_{i,j} + \sum_{s}\pi_s \cdot (fc_{i,j,s} + co_2t_{i,j,s} + rc_{i,j,s})\right] \\ + \sum_{j}\sum_{m}\sum_{s}\pi_s \cdot TP \cdot VOC \cdot \chi_{j,m,s} + \sum_{i}\sum_{j} NSRC_i \cdot y_{i,j} \end{aligned} \tag{2.93}$$

to obtain a chance-constrained UC model. This chance-constrained model allows scheduling some load shedding volume $\overline{\Phi}$ in each scenario, effectively relaxing the power balance, without penalization in the objective function. In addition, load shedding volumes may exceed $\overline{\Phi}$ in a fraction ϵ of the scenarios. The resulting UC schedule will be independent of the value of lost load $VOLL$, but will be driven by the choice of $\overline{\Phi}$ and ϵ. Again, these values should follow from a trade-off between the cost of providing additional (upward) flexibility - unknown before solving the model - and the (true) socio-economic cost of load shedding. In a scenario-based representation of the uncertainty, one will need a large number of scenarios to obtain meaningful solutions for small values of ϵ, which may drastically increase the computational burden of solving a chance-constrained UC model. For example, assuming equiprobable scenarios and $\epsilon = 0.01$, one needs at least 100 scenarios for the uncertain variable to obtain a meaningful solution. The quality of the resulting UC schedule is highly dependent on the quality and number of the considered scenarios. In light of these challenges and recent advancements in chance-constrained programming considering exact distributional representations of uncertain variables (see [128, 63] and the discussion in Section 2.6), we will not further discuss scenario-based chance-constrained UC models.

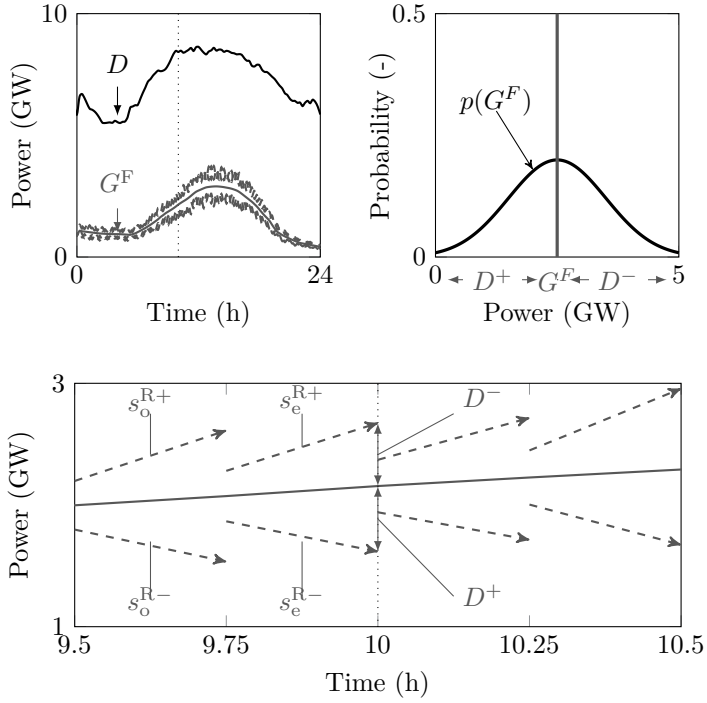

Figure 2.6: In the IIUC model, the system planner has to decide on the UC schedule using the RES-based power forecast and some upward and downward ramping scenarios. These scenarios, of which a detail around hour 10 is shown in the bottom figure, express the maximum possible upward and downward ramp of the RES-based generation. Note that these scenarios may not be interpreted as possible realizations of the RES-based generation. By shifting the end of each ramp to the maximum possible positive and negative realization respectively, we ensure that the required reserve capacity is identical to that required in the DUC model (Fig. 2.3). The upward and downward ramping scenarios are decoupled in two scenarios with ramps ending on odd and even time steps respectively, resulting in four scenarios ($s_{\mathrm{o}}^{\mathrm{R}+}$, $s_{\mathrm{e}}^{\mathrm{R}+}$, $s_{\mathrm{o}}^{\mathrm{R}-}$, $s_{\mathrm{e}}^{\mathrm{R}-}$) in total. The visualized scenarios are illustrative.

2.4 An improved interval unit commitment model[28]

Third, we study a so-called improved interval unit commitment (IIUC) model, as introduced by Pandžić et al. [86]. In such a model, a system operator will schedule the power plants such that costs are minimized under forecast conditions, while considering a small number of so-called ramping scenarios to trigger sufficient flexibility in the schedule to overcome forecast errors (Fig. 2.6). The objective function will therefore look very similar to the objective function of a DUC model (Eq. (2.1)):

$$min \quad c(g,z) = \sum_i \sum_j sc_{i,j} + fc_{i,j,s^{\mathrm{F}}} + co_2 t_{i,j,s^{\mathrm{F}}} + rc_{i,j,s^{\mathrm{F}}} \tag{2.94}$$

$$+ \sum_j \sum_m TP \cdot \left(VOLL \cdot \phi_{j,m,s^{\mathrm{F}}} + VOC \cdot \chi_{j,m,s^{\mathrm{F}}} \right)$$

In the forecast scenario s^{F}, the model is fully equivalent to the SUC formulation (Eq. (2.50)-(2.71)). To ensure that sufficient capacity is online to cover possible forecast errors on the RES-based generation, we will consider, in addition to the forecast scenario, four additional 'ramping' scenarios (set S^{R}) [86]. As explained in [86], these ramping scenarios reduce the conservatism of the original IUC formulation [129, 65, 101] by relaxing unnecessarily conservative inter-hour ramping requirements, as illustrated in Fig. 2.6. In line with [86], which argues that 'the required inter-hour rampable capacity should be no more than the maximum up and down ramps observed', in this work the ramping scenarios are obtained by calculating the maximum and minimum possible difference between the RES-based power output in two adjacent time steps. This information can be based on a large set of scenarios, statistical descriptions of the RES-based power output or historical data. Although the slope of these ramping scenarios is lower than in the original IUC formulation, these scenarios ensure the same (reserve) capacity requirements by shifting the end point of each ramp to the upper and lower bound of the interval formed by all possible realizations of the forecast error at each time step. We define the following four ramping scenarios:

- $s_{\mathrm{e}}^{\mathrm{R}+}$: the maximum upward ramp of a forecast error ending on even time steps;
- $s_{\mathrm{o}}^{\mathrm{R}+}$: the maximum upward ramp of a forecast error ending on odd time steps;

[28] This section contains elements from K. Bruninx, Y. Dvorkin, E. Delarue, H. Pandžić, W. D'haeseleer, and D. S. Kirschen, *Coupling Pumped Hydro Energy Storage with Unit Commitment,* IEEE Trans. Sustain. Energy, vol. 7, no. 2, pp. 786–796, 2016.

- $s_{\mathrm{e}}^{\mathrm{R}-}$: the maximum downward ramp of a forecast error ending on even time steps;
- $s_{\mathrm{o}}^{\mathrm{R}-}$: the maximum downward ramp of a forecast error ending on odd time steps.

We will clarify the procedure to calculate these ramping scenarios in more detail with an example at the end of this section. By considering these scenarios as constraints in the optimization – i.e., the UC schedule, common to all scenarios, must be as such that the demand can be met in each of these ramping scenarios – we ensure that sufficient capacity is online and that this capacity is flexible enough to cover the forecast errors. Note that the upward and downward ramping scenarios are decoupled in two scenarios for odd and even operating intervals (Fig. 2.6). This decoupling is used to ensure the mathematical feasibility of the IIUC model. Without this decoupling, there would be two operating points at each time period, which would be infeasible [86].

For the ramping scenarios, some additional constraints are needed to ensure the feasibility of the resulting UC schedule. First, as these scenarios do not appear in the objective function, one needs to constrain the amount of load shedding in these scenarios:

$$\forall j, \forall m, \forall s: \quad \phi_{j,m,s} = 0 \tag{2.95}$$

Indeed, without this condition, the model would be able to avoid bringing additional units online by scheduling load shedding in the ramping scenarios. Start-up costs would be avoided, while the costs associated with load shedding are not accounted for in the objective function. If the optimization problem constrained by Eq. (2.95) does not yield a feasible UC schedule, the power balance can be relaxed for the ramping scenarios by using slack variables penalized in the objective function, as explained in [86]. In other words, one should in this case allow 'load shedding' in the ramping scenarios, penalized in the objective function at the value of lost load $VOLL$ or the value of shed reserves VOR. This is the equivalent of the introduction of the slack variables in the reserve requirements in the DUC model (Section 2.2). Curtailment of excess wind power is allowed in all scenarios.

Second, the ramping constraints (Eq. (2.59)-(2.62)) only hold for the forecast scenario s^{F}. The ramping constraints for the ramping scenarios need to be adapted, as these ramping scenarios are 'engineered'. Indeed, some transitions between subsequent time steps have no meaning and should not be considered in the constraints, as explained above. The ramp-up and -down rates of the

various power plants are constricted in the ramping scenarios as follows:

$$\forall i \notin I^{\text{FAST}}, \forall j \in J^{\text{E}}: \; g_{i,j,s_e^{\text{R}+}} \leq g_{i,j-1,s_e^{\text{R}+}} + \overline{\Delta P_i^+} \cdot (z_{i,j} - v_{i,j}) + \underline{P_i} \cdot v_{i,j} \tag{2.96}$$

$$\forall i \in I^{\text{FAST}}, \forall j \in J^{\text{E}}: \; g_{i,j,s_e^{\text{R}+}} \leq g_{i,j-1,s_e^{\text{R}+}} + \overline{\Delta P_i^+} \cdot z_{i,j} \tag{2.97}$$

$$\forall i \notin I^{\text{FAST}}, \forall j \in J^{\text{O}}: \; g_{i,j,s_o^{\text{R}+}} \leq g_{i,j-1,s_o^{\text{R}+}} + \overline{\Delta P_i^+} \cdot (z_{i,j} - v_{i,j}) + \underline{P_i} \cdot v_{i,j} \tag{2.98}$$

$$\forall i \in I^{\text{FAST}}, \forall j \in J^{\text{O}}: \; g_{i,j,s_o^{\text{R}+}} \leq g_{i,j-1,s_o^{\text{R}+}} + \overline{\Delta P_i^+} \cdot z_{i,j} \tag{2.99}$$

$$\forall i \notin I^{\text{FAST}}, \forall j \in J^{\text{E}}: \; g_{i,j,s_e^{\text{R}-}} \geq g_{i,j-1,s_e^{\text{R}-}} - \overline{\Delta P_i^-} \cdot z_{i,j} - \underline{P_i} \cdot w_{i,j} \tag{2.100}$$

$$\forall i \in I^{\text{FAST}}, \forall j \in J^{\text{E}}: \; g_{i,j,s_e^{\text{R}-}} \geq g_{i,j-1,s_e^{\text{R}-}} - \overline{\Delta P_i^-} \cdot (z_{i,j} + w_{i,j}) \tag{2.101}$$

$$\forall i \notin I^{\text{FAST}}, \forall j \in J^{\text{O}}: \; g_{i,j,s_o^{\text{R}-}} \geq g_{i,j-1,s_o^{\text{R}-}} - \overline{\Delta P_i^-} \cdot z_{i,j} - \underline{P_i} \cdot w_{i,j} \tag{2.102}$$

$$\forall i \in I^{\text{FAST}}, \forall j \in J^{\text{O}}: \; g_{i,j,s_o^{\text{R}-}} \geq g_{i,j-1,s_o^{\text{R}-}} - \overline{\Delta P_i^-} \cdot (z_{i,j} + w_{i,j}) \tag{2.103}$$

in which J^{O} is the subset of J containing all odd time steps and J^{E} the subset of J containing all even time steps. Note that one can not further tighten these ramping constraints, as this would require that one enforces ramping constraints considering more than one time step. However, in the 'engineered' ramping scenarios, only certain transitions are meaningful. All other constraints, such as the minimum and maximum output of a power plant and the minimum up- and down-times, are enforced as in the SUC model. For the full formulation, see Appendix C.

Calculating the improved interval scenarios – an example[29]

Assume that a large set of scenarios, representative of the amplitude and variability of the forecast error, is available, as illustrated in Fig. 2.7[30]. For

[29] The procedure to calculate the ramping scenarios is taken from Pandžić et al. [86].

[30] In Chapter 5, we will compare the performance of the presented UC models. To avoid performance differences between the selected models because of mismatches in information available to set up the model, the starting point for each of those models will be the same, large set of wind power scenarios. Therefore, we will here illustrate how the ramping scenarios can be calculated from such a set of scenarios. The procedure is however identical for calculations based on e.g. historical data or distributions of the forecast error and its variability.

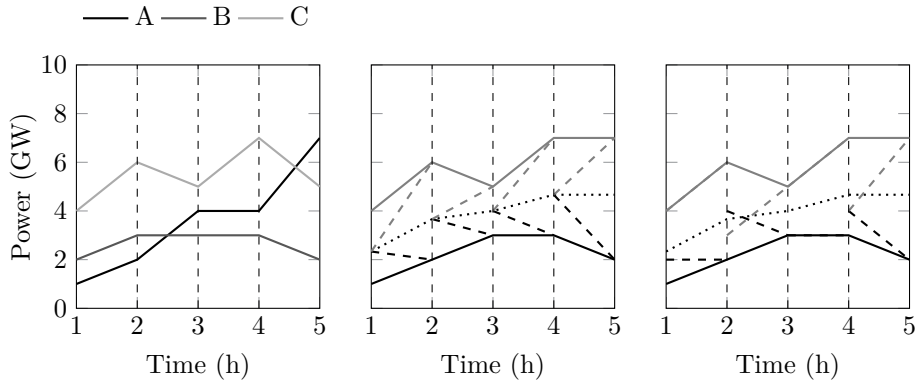

Figure 2.7: A set of scenarios, as one would consider in a SUC problem, (left) can be reduced to some reserve requirements for a DUC model (center) or ramping scenarios for an equivalent IIUC model (right). The solid lines indicate the enforced reserve capacity constraints. The dashed lines correspond to the ramping requirements imposed on the scheduled reserves. The dotted line corresponds to the expected value (forecast) of the RES-based generation.

sake of simplicity, we will here assume that three scenarios, which are equally likely to occur, are sufficient to represent the range of possible realizations of the RES-based generation.

The set of scenarios in Fig. 2.7 (left) can be reduced to equivalent reserve requirements for a DUC model (Fig. 2.7, center, solid lines) by selecting the maximum and minimum RES-based generation at each time step and calculating the difference with the RES-based generation forecast. The RES-based generation forecast is here calculated as the expected value of the three scenarios (dotted line, center and right figure). Scenario C sets the downward reserve requirement in hours one to four. In hour 5, the highest RES-based generation is observed in scenario A. Likewise, the combination of scenario A and B determines the upward reserve requirement.

Alternatively, one calculates (1) the maximum and minimum RES-based generation at each time step and (2) the maximum upward and downward ramp observed in the scenarios to obtain the ramping scenarios considered in an IIUC formulation. For example, in hour three, the highest RES-based generation is observed in scenario C: 5 GW (left, Fig. 2.7). The maximum upward ramp between hour two and three however occurs in scenario A and amounts to 2 GW/h. Combining this information allows calculating the trajectory of the upward ramping scenario ending on hour three ($s_{\mathrm{o}}^{\mathrm{R}+}$): from 3 GW at hour two

to 5 GW at hour three. Similarly, the downward ramping scenarios can be calculated. For example, between hour four and five, the largest downward ramp equals −2 GW/h (scenario A, left, Fig. 2.7). The lowest observed RES-based generation equals 2 GW (hour 5, scenario B). The downward ramping scenario ($s_{\mathrm{o}}^{\mathrm{R}-}$) between hour four and five starts at 4 GW and ends at 2 GW. Note that both trajectories do not occur in any of the scenarios considered in the SUC problem (left, Fig. 2.7).

For sake of comparison, we have also visualized (1) the ramping requirements imposed on the required reserves in the DUC formulation and (2) the equivalent reserve capacity requirement in the IIUC model. Several observations can be made. First, note that the reserve capacity requirement in the IIUC and DUC model is identical. Second, there is a large difference in required ramping capabilities of the scheduled reserves. As discussed in Section 2.2, we require the scheduled reserves to be available within one time step in the DUC solution. This effectively means that the equivalent 'ramping scenarios' in the DUC model start at the forecast and end at the maximum, respectively minimum possible RES-based generation level at each time step (dashed lines, center, Fig. 2.7). Compared to the IIUC formulation, in which the ramping requirements are based on the observed ramps in the scenarios, this may be overly conservative (e.g. hour one to two – Fig. 2.7) or not strict enough (e.g. hour two to three – Fig. 2.7).

In both models, the conservatism of the reserve requirements and ramping scenarios respectively may be reduced through advanced reserve sizing techniques (Chapter 3 and 5).

2.4.1 Allocation & activation costs of spinning reserves

Although the formulation of an IIUC problem resembles the formulation of a SUC problem, the representation of the uncertainty is fundamentally different. Whereas scenarios in a SUC model are a discrete representation of the distribution of the uncertain variable, the ramping scenarios can be thought of as an intelligent way of representing reserve constraints, as in a DUC model. Indeed, the ramping scenarios appear as mere constraints in the IIUC model. They only affect the objective through the changes in UC decisions and output of the scheduled units under forecast conditions they cause, as load shedding is not allowed. In other words, only the allocation costs of the scheduled flexibility are considered – a simplification that has a number of implications.

First, the absence of the full expected cost of scheduled flexibility requires a modeler to ex-ante decide upon the conservatism imposed on the ramping scenarios. One has to decide on minimum and maximum error and the ramp

rate enforced in the ramping scenarios, similar to the reserve sizing problem in a DUC model. Again, one has to make this decision before solving the UC problem, thus without knowledge of the cost of flexibility provision. Second, a cost-optimal trade-off between technologies scheduled to meet the demand in the ramping scenarios is unlikely, as the second stage cost, i.e. the activation cost of the scheduled flexibility, is not accounted for in the objective function. Third, if curtailment of excess RES-based power is allowed in the upward ramping scenarios (positive forecast errors) and curtailment is not penalized, the model has no incentive to schedule downward flexibility[31]. Indeed, as only allocation costs are accounted for, and possible operational cost savings resulting from scheduling downward flexibility, which only appear in the second stage cost, are neglected, curtailment is by definition the most cost-efficient downward flexibility provider. We will return to the interaction between curtailment of RES-based generation and downward flexibility provision in Section 2.4.3. Last, if load shedding and/or curtailment in the ramping scenarios is allowed and penalized at $VOLL$ or VOC in the objective function, the trade-off between the allocation cost of reserve provision and load shedding or curtailment of RES-based generation is ill-informed: the probability of occurrence of load shedding or curtailment, and thus the associated socio-economic cost, is unknown. Note that these issues are identical to those we observed w.r.t. the slack variables in the reserve requirements of the DUC formulation.

Nevertheless, the IIUC model has its merits, which we will discuss in Section 2.4.5.

2.4.2 Allocation & activation costs of non-spinning reserves

Including non-spinning reserves in an IIUC model requires the introduction of a 'reservation cost' $NSRC_i$ in the objective function:

$$min \quad c(g,z) = \sum_i \sum_j sc_{i,j} + fc_{i,j,s^F} + co_2 t_{i,j,s^F} + rc_{i,j,s^F} \tag{2.104}$$

$$+ \sum_j \sum_m TP \cdot \left(VOLL \cdot \phi_{j,m,s^F} + VOC \cdot \chi_{j,m,s^F}\right)$$

$$+ \sum_i \sum_j NSRC_i \cdot y_{i,j} \tag{2.105}$$

[31] The same remark as in Section 2.2.1 holds: the resulting UC schedule may contain some downward flexibility, but this will not be triggered by a trade-off between the possible cost savings that result from the ability to absorb more RES-based generation and the cost of scheduling more downward flexibility.

with $y_{i,j}$ a binary variable that equals one if power plant i is scheduled as non-spinning reserve at time step j. The output of these fast-starting units, scheduled as non-spinning reserves, appears in the power balance constraint in the ramping scenarios as in Eq. (2.79):

$$\forall j, \forall m, \forall s \in S^{\mathrm{R}}: \quad D_{j,m} - \phi_{j,m,s} = \sum_i I^{\mathrm{G}}_{m,i} \cdot \left(g_{i,j,s} + nsr^{+}_{i,j,s}\right) + G^{\mathrm{MR}}_{j,m} \tag{2.106}$$

$$+ G^{\mathrm{F}}_{j,m,s} - \chi_{j,m,s} + inj_{j,m,s}$$

$$+ \sum_r I^{\mathrm{PHES}}_{m,r} \cdot \left(g^{\mathrm{T}}_{r,j,s} - g^{\mathrm{P}}_{r,j,s}\right)$$

In the forecast scenario, the non-spinning reserves are not accounted for, effectively forcing their output to zero under forecast conditions. Note that the fast-starting units that may provide non-spinning reserves can be scheduled under forecast conditions. In this case, these units can of course not be scheduled as non-spinning reserves. The output of scheduled non-spinning reserves is constrained by their minimum and maximum stable operating point, ramping capacity and some binary logic (Eq. (2.74) - (2.88)). The ramping constraints (Eq. (2.77)-(2.78)) are adapted as follows, to account for the non-physical transitions between time steps in the ramping scenarios:

$$\forall i \in I^{\mathrm{FAST}}, \forall j \in J^{\mathrm{E}}: \; nsr^{+}_{i,j,s_e^{\mathrm{R}+}} \leq nsr^{+}_{i,j-1,s_e^{\mathrm{R}+}} + \overline{\Delta P^{+}_i} \cdot z^{*}_{i,j} \tag{2.107}$$

$$\forall i \in I^{\mathrm{FAST}}, \forall j \in J^{\mathrm{O}}: \; nsr^{+}_{i,j,s_o^{\mathrm{R}+}} \leq nsr^{+}_{i,j-1,s_o^{\mathrm{R}+}} + \overline{\Delta P^{+}_i} \cdot z^{*}_{i,j} \tag{2.108}$$

$$\forall i \in I^{\mathrm{FAST}}, \forall j \in J^{\mathrm{E}}: \; nsr^{+}_{i,j,s_e^{\mathrm{R}-}} \geq nsr^{+}_{i,j-1,s_e^{\mathrm{R}-}} - \overline{\Delta P^{-}_i} \cdot \left(z^{*}_{i,j} + w^{*}_{i,j}\right) \tag{2.109}$$

$$\forall i \in I^{\mathrm{FAST}}, \forall j \in J^{\mathrm{O}}: \; nsr^{+}_{i,j,s_o^{\mathrm{R}-}} \geq nsr^{+}_{i,j-1,s_o^{\mathrm{R}-}} - \overline{\Delta P^{-}_i} \cdot \left(z^{*}_{i,j} + w^{*}_{i,j}\right) \tag{2.110}$$

The operational costs associated with deploying non-spinning reserves are by definition not accounted for in the IIUC model, as (1) they only present non-zero operational costs in the ramping scenarios and (2) the operational cost in these scenarios does not appear in the objective function (2.104). By definition, they are therefore perceived as the cheapest flexibility provider given their low allocation costs $NSRC_i$, as in the DUC model (see Section 2.2). Considering non-spinning reserves will thus lower the effective upward reserve requirement imposed by scenarios $s_e^{\mathrm{R}-}$ and $s_o^{\mathrm{R}-}$. During real-time activation, this might lead to higher expected operational costs, as these units are typically more expensive to run.

2.4.3 Participation of intermittent RES-based generation in the reserve requirements

As in the DUC formulation, curtailed forecasted RES-based generation may be used to meet the demand for upward reserves in the IIUC model. Although not explicitly modeled, the scenario-specific decision variable reflecting curtailment effectively accounts for this effect. If curtailment is scheduled in the forecast scenario, less curtailment may be scheduled in the downward ramping scenarios, which ensures the SO does not commit excessive upward reserve capacity. Curtailment under forecast conditions may be caused by (1) the need to satisfy the power balance under forecast conditions or other operational constraints, (2) increasing upward reserve allocation costs or (3) the possibility of a more cost-efficient operation of the power system under forecast conditions (see Section 2.2.3).

With respect to downward reserves, curtailment is the de facto most cost-effective flexibility provider in the IIUC model due to the absence of an estimate of the expected operational cost savings that result from the activation of downward flexibility (Section 2.4.1). Note that a correction of a downward reserve requirement in case of curtailment under forecast conditions, as in the DUC formulation (Eq. (2.11)), is not necessary. Indeed, the scenario-specific curtailment decision decouples curtailment in the forecast scenario and the upward ramping scenarios.

2.4.4 The participation of pumped hydro energy storage systems in the reserve requirements[32]

In case one allows the participation of the PHES units in the power balance in the ramping scenarios (subset S^R) and does not further restrict the implicit reserve capacity these units may offer, the scheduled PHES-based 'reserves' may not be available in real time. During dispatch, it may occur that there is insufficient energy stored or insufficient energy can be stored in the upper basin to allow deploying the scheduled reserves. Therefore, similar to the constraints enforced on the PHES-based reserves in a DUC model, we will consider the following constraints on the scheduled output of the PHES units in an IIUC model.

First, we relate the energy content of the PHES system in the ramping scenarios to the energy content of the PHES unit under forecast conditions (scenario s^{F}).

[32]This section is based on K. Bruninx, Y. Dvorkin, E. Delarue, H. Pandžić, W. D'haeseleer, and D. S. Kirschen, *Coupling Pumped Hydro Energy Storage with Unit Commitment,* IEEE Trans. Sustain. Energy, vol. 7, no. 2, pp. 786–796, 2016.

The energy content of a PHES system r in the ramping scenarios $s \in S^{\mathrm{R}}$ is thus calculated as

$$\forall r, \forall j, \forall s \in S^{\mathrm{R}} : \; e_{r,j,s} = e_{r,j-1,s^{\mathrm{F}}} + TP \cdot \left(g^{\mathrm{P}}_{r,j,s} \cdot \sqrt{\epsilon_r} - \frac{g^{\mathrm{T}}_{r,j,s}}{\sqrt{\epsilon_r}} \right) \tag{2.111}$$

By linking the energy storage level in the forecast and ramping scenarios, anticipated changes in the energy storage levels are considered during the scheduling of the regulation services offered by the PHES systems. Neglecting to do so may lead to a severe underestimation of the regulation potential of the PHES unit in the ramping scenarios. Consider e.g. the situation in which the PHES system is empty at the start of the optimization period. Without Eq. (2.111), the PHES system would not be allowed to offer upward regulation services by increasing its output in the downward ramping scenarios, regardless of the evolution of the anticipated energy storage level. This equation replaces Eq. (2.66), i.e. the energy balance of the PHES system, in all ramping scenarios. Eq. (2.66) remains enforced in the forecast scenario.

Second, the output of the PHES unit is forced to zero at the beginning of a ramp, as the considered ramping scenarios are not real, possible realizations of the RES-based generation and may contain non-physical transitions between time steps:

$$\forall r, \forall j \in J^{O}, \forall s \in \{s^{\mathrm{R}+}_{\mathrm{e}}, s^{\mathrm{R}-}_{\mathrm{e}}\} : \; g^{\mathrm{P}}_{r,j,s}, \; g^{\mathrm{T}}_{r,j,s} = 0 \tag{2.112}$$

$$\forall r, \forall j \in J^{E}, \forall s \in \{s^{\mathrm{R}+}_{\mathrm{o}}, s^{\mathrm{R}-}_{\mathrm{o}}\} : \; g^{\mathrm{P}}_{r,j,s}, \; g^{\mathrm{T}}_{r,j,s} = 0 \tag{2.113}$$

Moreover, without these constraints non-zero PHES-based reserves at the start of a ramp may provide arbitrage opportunities, reducing the effective ramp enforced by the ramping scenario. For example, if a ramping event starts with a positive forecast error and ends with a negative forecast error, the PHES system might absorb the positive forecast error at the start of the ramp and release the stored energy at the end of the ramp, providing upward reserve. The latter action effectively reduces the ramping requirement enforced in the IIUC model and might lead to an underestimation of the flexibility needed, as the effective ramping requirement no longer reflects the worst-case realization of the forecast error.

Third, we enforce the feasibility of the output of the PHES systems in the worst-case realization of the uncertain RES-based generation (i.e., activation of

all reserves in one direction):

$$\forall r, \forall j, \forall s \in \{s_{\mathrm{e}}^{\mathrm{R}-}, s_{\mathrm{o}}^{\mathrm{R}-}\} : e_{r,j,s^{\mathrm{F}}} - \sum_{j^*=1}^{j} \sum_{s} TP \cdot \frac{\Delta^- g_{r,j,s}^{\mathrm{T}}}{\sqrt{\epsilon_r}} - \sum_{j^*=1}^{j} \sum_{s} TP \cdot \Delta^- g_{r,j,s}^{\mathrm{P}} \cdot \sqrt{\epsilon_r} \geq \underline{E_r} \tag{2.114}$$

$$\forall r, \forall j, \forall s \in \{s_{\mathrm{e}}^{\mathrm{R}+}, s_{\mathrm{o}}^{\mathrm{R}+}\} : e_{r,j,s^{\mathrm{F}}} + \sum_{j^*=1}^{j} \sum_{s} TP \cdot \frac{\Delta^+ g_{r,j,s}^{\mathrm{T}}}{\sqrt{\epsilon_r}} + \sum_{j^*=1}^{j} \sum_{s} TP \cdot \Delta^+ g_{r,j,s}^{\mathrm{P}} \cdot \sqrt{\epsilon_r} \leq \overline{E_r} \tag{2.115}$$

$\Delta^- g_{r,j,s}^{\mathrm{T}}$ represents the additional output of the PHES unit above the output under forecast conditions. Similarly, $\Delta^+ g_{r,j,s}^{\mathrm{P}}$ represents the additional pumping power. $\Delta^- g_{r,j,s}^{\mathrm{P}}$ and $\Delta^+ g_{r,j,s}^{\mathrm{T}}$ are corrections of the output, thus the energy content of the PHES unit, if it is scheduled with a non-negative output or input at time step j in both the forecast scenario and the ramping scenario, but in opposite directions. For example, if the PHES system is scheduled to generate electricity in the forecast scenario s^{F}, but to pump in a ramping scenario, the energy content of the PHES system under worst-case conditions is affected by (i) the increase in pumping power ($\Delta^+ g_{r,j,s}^{\mathrm{P}}$ in Eq. (2.115)) and (ii) the loss of output ($\Delta^+ g_{r,j,s}^{\mathrm{T}}$ in Eq. (2.115)). Mathematically, this can be summarized as follows:

$$\forall r, \forall j: \quad \Delta^+ g_{r,j}^{\mathrm{P}} \geq g_{r,j,s_o^{\mathrm{R}+}}^{\mathrm{P}} + g_{r,j,s_e^{\mathrm{R}+}}^{\mathrm{P}} - g_{r,j,s^{\mathrm{F}}}^{\mathrm{P}} \tag{2.116}$$

$$\forall r, \forall j: \quad \Delta^+ g_{r,j}^{\mathrm{T}} \geq g_{r,j,s^{\mathrm{F}}}^{\mathrm{T}} - g_{r,j,s_o^{\mathrm{R}+}}^{\mathrm{T}} - g_{r,j,s_e^{\mathrm{R}+}}^{\mathrm{T}} \tag{2.117}$$

$$\forall r, \forall j: \quad \Delta^- g_{r,j}^{\mathrm{P}} \geq g_{r,j,s^{\mathrm{F}}}^{\mathrm{P}} - g_{r,j,s_o^{\mathrm{R}-}}^{\mathrm{P}} - g_{r,j,s_e^{\mathrm{R}-}}^{\mathrm{P}} \tag{2.118}$$

$$\forall r, \forall j: \quad \Delta^- g_{r,j}^{\mathrm{T}} \geq g_{r,j,s_o^{\mathrm{R}-}}^{\mathrm{T}} + g_{r,j,s_e^{\mathrm{R}-}}^{\mathrm{T}} - g_{r,j,s^{\mathrm{F}}}^{\mathrm{T}} \tag{2.119}$$

$$\forall r, \forall j: \quad \Delta^+ g_{r,j}^{\mathrm{P}},\ \Delta^+ g_{r,j}^{\mathrm{T}},\ \Delta^- g_{r,j}^{\mathrm{T}},\ \Delta^- g_{r,j}^{\mathrm{P}} \geq 0 \tag{2.120}$$

To facilitate the interpretation of these constraints, we have listed the outcome of the worst-case correction variables $\Delta^+ g_{r,j}^{\mathrm{P}},\ \Delta^+ g_{r,j}^{\mathrm{T}},\ \Delta^- g_{r,j}^{\mathrm{T}},\ \Delta^- g_{r,j}^{\mathrm{P}}$ under different PHES system conditions in Table 2.1.

By enforcing Eq. (2.111)-(2.120), in addition to Eq. (2.66)-(2.71), we account for the technical constraints of the PHES systems, the evolution of the energy content of the PHES systems under forecast conditions and the impact of the activation of scheduled PHES-based reserves on that energy content, ensuring the feasibility of the activation of the scheduled PHES-based flexibility in real time. However, this formulation suffers from the same drawbacks we observed in the DUC formulation. Indeed, the ability to offer e.g. upward reserves – i.e. to meet the demand in the downward ramping scenarios – via the PHES systems, requires increasing the demand under forecast conditions to ensure sufficient energy is stored in the PHES system. This increase in demand increases the objective function, whereas the possible operational cost savings resulting from a more cost-effective flexibility provision via the PHES systems are not fully monetized in the objective function. Again, this is the result of the inability of this formulation to account for the expected activation cost of conventional flexibility providers (see above). In addition, constraints (2.111)-(2.120) are typically conservative estimates of the regulation potential of the PHES system, as the probability of deploying all scheduled reserves in the upward or downward direction may be extremely low. Nevertheless, the inclusion of PHES-based regulation services, constrained by Eq. (2.111)-(2.120), yields significant operational cost savings, with minimal impact on the computational cost of the IIUC model and without affecting the reliability of the UC schedule (Chapter 5).

Table 2.1: Worst-case PHES output correction variables used in the IIUC model. The first four columns list the combinations of the output of each PHES system in the forecast (s^{F}) and ramping scenarios (s^{R}) allowed by the constraints above. Each row corresponds to a certain 'state' of the PHES system in the forecast and ramping scenarios respectively. A variable is listed in the corresponding column if this variable has a non-zero value in this state. The last four columns show the corresponding value of the correction variables in Eq. (2.114)-(2.115). For sake of readability, we have ommitted indices referring to the PHES system (r), time (j) and odd/even (o, e). s^{R} refers to all ramping scenarios, s^{F} is the forecast scenario.

$g^{\mathrm{T}}_{s^{\mathrm{F}}}$	$g^{\mathrm{P}}_{s^{\mathrm{F}}}$	$g^{\mathrm{T}}_{s^{\mathrm{R}}}$	$g^{\mathrm{P}}_{s^{\mathrm{R}}}$	$\Delta^{+}g^{\mathrm{P}}$	$\Delta^{+}g^{\mathrm{T}}$	$\Delta^{-}g^{\mathrm{T}}$	$\Delta^{-}g^{\mathrm{P}}$
$g^{\mathrm{T}}_{s^{\mathrm{F}}}$	0	0	$g^{\mathrm{P}}_{s^{\mathrm{R}}}$	$g^{\mathrm{P}}_{s^{\mathrm{R}}}$	$g^{\mathrm{T}}_{s^{\mathrm{F}}}$	0	0
0	$g^{\mathrm{P}}_{s^{\mathrm{F}}}$	$g^{\mathrm{T}}_{s^{\mathrm{R}}}$	0	0	0	$g^{\mathrm{T}}_{s^{\mathrm{R}}}$	$g^{\mathrm{P}}_{s^{\mathrm{F}}}$
$g^{\mathrm{T}}_{s^{\mathrm{F}}}$	0	$g^{\mathrm{T}}_{s^{\mathrm{R}}} > g^{\mathrm{T}}_{s^{\mathrm{F}}}$	0	0	0	$g^{\mathrm{T}}_{s^{\mathrm{F}}} - g^{\mathrm{T}}_{s^{\mathrm{R}}}$	0
$g^{\mathrm{T}}_{s^{\mathrm{F}}}$	0	$g^{\mathrm{T}}_{s^{\mathrm{R}}} < g^{\mathrm{T}}_{s^{\mathrm{F}}}$	0	0	$g^{\mathrm{T}}_{s^{\mathrm{R}}} - g^{\mathrm{T}}_{s^{\mathrm{F}}}$	0	0
0	$g^{\mathrm{P}}_{s^{\mathrm{F}}}$	0	$g^{\mathrm{P}}_{s^{\mathrm{R}}} > g^{\mathrm{P}}_{s^{\mathrm{F}}}$	$g^{\mathrm{P}}_{s^{\mathrm{R}}} - g^{\mathrm{P}}_{s^{\mathrm{F}}}$	0	0	0
0	$g^{\mathrm{P}}_{s^{\mathrm{F}}}$	0	$g^{\mathrm{P}}_{s^{\mathrm{R}}} < g^{\mathrm{P}}_{s^{\mathrm{F}}}$	0	0	0	$g^{\mathrm{P}}_{s^{\mathrm{F}}} - g^{\mathrm{P}}_{s^{\mathrm{R}}}$

2.4.5 Discussion

In an IIUC formulation, one will only consider the costs associated with meeting the demand for electricity under forecast conditions. Although the scheduling of reserves is triggered via a different mechanism, the IIUC model suffers from the same issues as the DUC model: the cost of activating reserves is not taken into account during the scheduling process. As a result, a modeler needs to decide ex-ante upon (1) the minimum and maximum forecast error and (2) maximum upward and downward ramp rate imposed on the UC schedule via the ramping scenarios. Ideally, these requirements would represent a trade-off between the expected socio-economic cost of load shedding and curtailment and the operational cost of flexibility provision. Before solving the UC model, these expected costs are however unknown, and a modeler thus has to make this trade-off based on approximations of these costs or heuristic rules. One could argue that we have shifted the problem of 'reserve sizing' to the development of adequate ramping scenarios. As in the DUC model, a cost-optimal trade-off between flexibility providers is thus difficult to obtain (Section 2.4.1), downward flexibility is typically not scheduled (Section 2.4.3) and non-spinning reserves will be over-procured (Section 2.4.2). In addition, the structure of the IIUC formulation requires conservative estimates of the regulation services that can be offered by PHES systems (Section 2.4.4). Compared to a SUC model, the IIUC formulation typically yields sub-optimal, overly conservative UC schedules [129, 86].

However, the IIUC formulation has a number of distinct advantages over the DUC, IUC and SUC formulations. First, the computational effort to solve a IIUC problem is (1) significantly lower than that associated with a SUC problem and (2) comparable to that of a DUC problem [85, 86] (Section 5). Second, unlike in a SUC formulation, the UC schedule obtained via a DUC or IIUC formulation is insensitive to the exact form of the underlying distribution of the uncertain parameter [86]. Third, the IIUC formulation, as proposed by Pandžić et al. [86], improves the representation of the ramping requirements imposed on the scheduled reserves compared to the DUC and IUC formulation by limiting the ramping requirements to an observed maximum upward and downward ramp rate (as illustrated in the example at the start of this section). In the DUC formulation (Section 2.2), the scheduled reserves must be able to ramp up/down from zero (no forecast error) to their scheduled capacity, which corresponds to the occurrence of the largest forecast error covered by the reserve

requirement[33]. In the original IUC formulation, the ramping requirements are even stricter [129, 65, 101]: one requires the scheduled capacity to be able to facilitate up- and downward ramps equal to the difference between the maximum and minimum forecast error considered in the ramping scenarios, which might lead to very conservative UC schedules [86]. The ramping requirements in a DUC or IUC model are furthermore not linked to the observed ramp rates in the RES-based power output and might thus lead to overly conservative UC schedules (IUC, DUC) or the availability of too little ramping capacity (DUC). Last, the technical feasibility of dispatching the scheduled reserves is more likely to be guaranteed in an IIUC schedule than in a DUC solution. As the reserve requirements are modeled via the ramping scenarios, the scheduled reserves are virtually 'dispatched' in these scenarios. All constraints considered in the UC model, including the grid constraints, are thus enforced in a worst-case situation, i.e. the activation of all reserves in the upward or downward direction. In power systems in which grid congestion is common, this might drastically improve the performance of the IIUC model over the DUC formulation, which does not guarantee this worst-case feasibility [94]. Note however that the worst-case forecast error might not lead to highest level of congestion on the transmission grid, and that the feasibility of dispatching the scheduled reserves is thus not explicitly guaranteed in *all* possible realizations of the uncertain RES-based electricity generation.

Expansions of the IIUC formulation might improve its computational efficiency and cost-optimality. For example, a combination of a SUC and an IIUC model may improve the cost-efficiency of the IIUC formulation by considering a scenario-based representation of the uncertainty for the first hours of the scheduling period, which allows accounting for the full cost reserve provision, and an (I)IUC formulation for the last hours of the day, reducing the computational burden of a SUC problem, as proposed by Dvorkin et al. [130]. Furthermore, the inclusion of an approximation of the expected deployment cost of scheduled reserves may enable scheduling a cost-optimal mix of flexibility providers (e.g. spinning vs. non-spinning capacity) and the valorization of downward flexibility. Similarly, reducing the conservatism of constraints Eq. (2.111)-(2.120), i.e. the worst-case evaluation of the energy content of the PHES systems, may further improve the performance of the IIUC formulation.

[33]In a DUC formulation, one can impose specific ramping requirements on the reserves by defining additional reserve variables. However, empirical testing has shown that the impact of such an expansion does not affect the performance of the resulting UC model for the power system studied in this dissertation. If one considers power systems in which (1) extreme ramp rates are observed more often and/or (2) the power plants providing regulation services are characterized by stricter dynamic constraints, the improved representation of the reserve ramping requirement in the IIUC model may have a larger impact on the cost-efficiency of the resulting UC schedule.

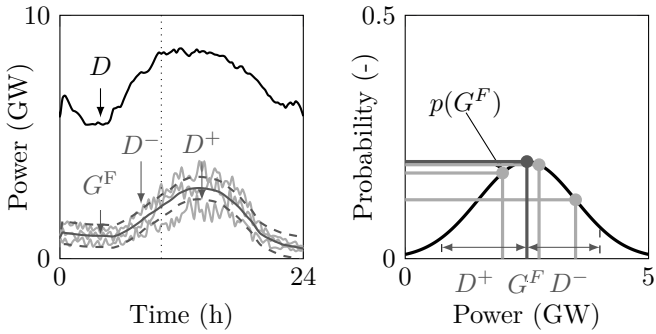

Figure 2.8: In the HUC model, the system operator has to decide on the UC schedule using the RES-based power forecast, a limited number of scenarios and some reserve requirements. The reserve requirements are typically less strict than those imposed on a DUC model, to avoid the conservatism associated with DUC formulations. The scenarios allow capturing more extreme, less likely events and ensure that the system operator accounts for the full, expected cost associated with reserve provision. The indicated scenarios and reserve requirements are illustrative.

2.5 A hybrid deterministic-stochastic unit commitment model[34]

To speed up the convergence of a SUC model towards a meaningful solution, one could consider the addition of reserve constraints to the SUC formulation as illustrated in Fig. 2.8. With the addition of these reserve constraints, one ensures a minimum level of upward (and downward, if needed) flexibility. By considering a small set of scenarios, one ensures that the scheduled reserves are optimally suited to absorb the forecast errors. These scenarios can in addition be used to consider extreme forecast errors. Moreover, the consideration of scenarios allows calculating the full expected operational cost of reserve provision. As we will show in Chapter 5, this approach allows us to approximate the stable solution of the equivalent stochastic problem, but at a fraction of the computational cost.

In a HUC model, like in a SUC model, the power plants are scheduled and

[34]This section in based on K. Bruninx, K. Van den Bergh, E. Delarue, and W. D'haeseleer, *Optimization and Allocation of Spinning Reserves in a Low-Carbon Framework,* IEEE Trans. Power Syst., vol. 31, no. 2, pp. 872–882, 2016.

dispatched in such a way that the overall expected cost of generating the demanded electricity over the simulated time period is minimized:

$$\min c(g,z) = \sum_i \sum_j \left[sc_{i,j} + \sum_s \pi_s \cdot (fc_{i,j,s} + co_2t_{i,j,s} + rc_{i,j,s}) \right] \tag{2.121}$$

$$+ \sum_j \sum_m \sum_s \pi_s \cdot TP \cdot (VOLL \cdot \phi_{j,m,s} + VOC \cdot \chi_{j,m,s})$$

$$+ \sum_j VOR \cdot \left(s_j^+ + s_j^-\right)$$

The fuel cost $fc_{i,j,s}$, the CO_2-emission cost $co_2t_{i,j,s}$ and ramping costs $rc_{i,j,s}$ are calculated through Eq. (2.50) - (2.54). The start-up cost $SC_{i,j}$ is calculated via Eq. (2.4). The addition of reserve requirements (see below) leads to the inclusion of slack variables s_j^+ and s_j^-, which allow relaxing the reserve requirements before scheduling load shedding under forecast conditions, e.g. to respect other operational constraints (Section 2.2). The power balance and all other technical constraints are enforced as in a SUC model (Eq. (2.50)-(2.71)).

To ensure a minimum level of upward and downward flexibility, two reserve requirements are added[35]:

$$\forall j: \quad D_j^+ = \sum_i r_{i,j}^+ + \sum_m \chi_{j,m,s^{\mathrm{F}}} + s_j^+ \tag{2.122}$$

$$\forall j | \sum_m \chi_{j,m,s^{\mathrm{F}}} = 0: \quad D_j^- = \sum_i r_{i,j}^- + s_j^- \tag{2.123}$$

Note that we only impose a demand for reserves with respect to the forecast scenario s^{F}. At each time step j, the demand for upward reserves must be met by headroom in online capacity (spinning reserves, $r_{i,j}^+$, see below) and scheduled curtailment of RES-based generation under forecast conditions χ_{j,m,s^F}, as in the DUC formulation (Section 2.2). If a shortage of supply occurs in the forecast scenario, the demand for reserves has to be relaxed before load shedding occurs. The introduction of a slack variable s_j^+, restricted to positive values and penalized at a high cost (VOR) in the objective function, allows this. Downward reserves may be provided by spinning units ($r_{i,j}^-$). If curtailment is scheduled in the forecast scenario, the downward reserve requirement is omitted, as in the DUC formulation (Section 2.2). A slack variable s_j^- allows violating constraint (2.123) at a cost VOR.

[35] In [45], we only enforce an upward reserve requirement. For sake of completeness, we include the downward reserve requirement here. The relevance of such a downward reserve constraint is discussed in Section 2.5.1.

To determine the spinning reserve capacity a scheduled power plant may provide, the following constraints are added to the model. A power plant is only allowed to be scheduled as spinning reserves if (1) it is online ($z_{i,j} = 1$) and (2) the sum of the output of that plant in the forecast scenario and the scheduled spinning reserve capacity does not violate the minimum/maximum stable operating point of the power plant. The following additional constraints must be satisfied:

$$\forall i, \forall j: \; g_{i,j,s^{\mathrm{F}}} + r^{+}_{i,j} \leq \overline{P_i} \cdot z_{i,j} \tag{2.124}$$

$$\forall i, \forall j: \; g_{i,j,s^{\mathrm{F}}} - r^{-}_{i,j} \geq \underline{P_i} \cdot z_{i,j} \tag{2.125}$$

$$\forall i | \{MUT_i \geq 2\}, \forall j: \; g_{i,j,s^{\mathrm{F}}} + r^{+}_{i,j} \leq \overline{P_i} \cdot z_{i,j} - \left(\overline{P_i} - \underline{P_i}\right) \cdot (v_{i,j} + w_{i,j+1}) \tag{2.126}$$

$$\forall i, \forall j: \; g_{i,j,s^{\mathrm{F}}}, \; r^{+}_{i,j}, \; r^{-}_{i,j} \geq 0 \tag{2.127}$$

Additionally, the scheduled reserves may not violate the ramp rate-limitations of the power plants if they are activated. Additional constraints considering the upward and downward ramp rates of the slow power plants ($i \notin I^{\mathrm{FAST}}$) have been included as follows:

$$\forall i \notin I^{\mathrm{FAST}}, \forall j: \; g_{i,j,s^{\mathrm{F}}} + r^{+}_{i,j} \leq g_{i,j-1,s^{\mathrm{F}}} + \overline{\Delta P^{+}_{i}} \cdot (z_{i,j} - v_{i,j}) + \underline{P_i} \cdot v_{i,j} \tag{2.128}$$

$$\forall i \notin I^{\mathrm{FAST}}, \forall j: \; g_{i,j,s^{\mathrm{F}}} - r^{-}_{i,j} \geq g_{i,j-1,s^{\mathrm{F}}} - \overline{\Delta P^{-}_{i}} \cdot z_{i,j} - \underline{P_i} \cdot w_{i,j} \tag{2.129}$$

$\overline{\Delta P^{+}_{i}}$ and $\overline{\Delta P^{-}_{i}}$ are the maximum ramp rates of the power plants. The binary variables $v_{i,j}$ and $w_{i,j}$ indicate a start-up, respectively a shut down of a power plant i at time step j. I^{FAST} is a subset of the set of power plants I which contains those generators with a MUT (minimum up time) and MDT (minimum down time) of one time period and maximum ramp rates which allow them to ramp up to a level above their minimum operating point within one time period. For the fast-starting generators ($i \in I^{\mathrm{FAST}}$), the equations above simplify to:

$$\forall i \in I^{\mathrm{FAST}}, \forall j: \; g_{i,j,s^{\mathrm{F}}} + r^{+}_{i,j} \leq g_{i,j-1,s^{\mathrm{F}}} + \overline{\Delta P^{+}_{i}} \cdot z_{i,j} \tag{2.130}$$

$$\forall i \in I^{\mathrm{FAST}}, \forall j: \; g_{i,j,s^{\mathrm{F}}} - r^{-}_{i,j} \geq g_{i,j-1,s^{\mathrm{F}}} - \overline{\Delta P^{-}_{i}} \cdot (z_{i,j} + w_{i,j}) \tag{2.131}$$

2.5.1 Allocation & activation costs of spinning reserves

The reserves, as scheduled with respect to the output of the power plants in the forecast scenario s^{F}, are not explicitly dispatched in the HUC model. However, the scheduled power plants are dispatched in the considered scenarios. The associated changes in operational cost are considered in the objective function, which allows scheduling a cost-optimal mix of technologies providing the reserves required to satisfy Eq. (2.122)-(2.123).

Nevertheless, the absence of the explicit consideration of the deployment cost of the scheduled reserves has a number of implications. First, load shedding and curtailment of RES-based generation can not be considered explicitly as flexibility measures to satisfy the reserve requirements. Indeed, without an explicit estimate of the *expected* socio-economic cost of not providing the required level of upward (i.e. allowing load shedding) or downward reserves (i.e. allowing curtailment), the modeler has to decide ex-ante, exogenously upon the amount and type of reserves that should be procured. Violating the reserve requirements is possible through the slack variables s_j^+ and s_j^-, but these violations are penalized at an arbitrary high cost VOR, which may not reflect the expected operational cost associated with not satisfying the reserve requirement. Second, the downward reserve requirement will in most cases be satisfied by curtailment, as the decrease in operational costs by absorbing more RES-based power (here assumed to have a zero-marginal cost) is not accounted for in the objective function, thus the model has no incentive to schedule downward reserves other than curtailment. Note however that, unlike in the DUC formulation, the operational cost savings due to downward flexibility are monetized in all other considered scenarios. Similarly, load shedding is a viable flexibility option in these scenarios, which allows for an optimal trade-off between (additional) upward flexibility and the risk of load shedding.

These observations explain why we will typically (1) only enforce an upward reserve requirement (as in [45]) and (2) use this requirement to ensure a minimum level of upward flexibility in the schedule. The effective reserve sizing – i.e. the trade-off between curtailment and downward flexibility, load shedding and upward flexibility – is internalized in the model by the consideration of a limited set of scenarios. If these scenarios are sufficient to approximate the tails of the distribution of the RES-based output (Fig. 2.8) and the full cost of flexibility provision in these scenarios is accounted for in the objective function, load shedding and curtailment can be allowed as explicit flexibility options in these scenarios.

As shown in Chapter 5, the combination of a probabilistic reserve sizing method (Chapter 3), a customized scenario reduction technique (Chapter 4 and 5)

and a limited set of scenarios allows the HUC formulation to approximate the cost-efficiency of a SUC model at a fraction of the operational cost.

2.5.2 Allocation & activation costs of non-spinning reserves

By introducing Eq. (2.72)-(2.88), a scenario-specific UC status is allowed for fast-starting units. They may be accounted for in the upward reserve requirement (1) if their output is equal to zero in the forecast scenario s^{F} and (2) if they are dispatched in at least one scenario:

$$\forall i \in I^{FAST}, \forall j, \forall s: \quad \underline{P_i} \cdot z^*_{i,j,s} \leq nsr^+_{i,j,s} \leq \overline{P_i} \cdot z^*_{i,j,s} \tag{2.132}$$

$$\forall i \in I^{FAST}, \forall j, \forall s: \quad z_{i,j} + z^*_{i,j,s} \leq 1 \tag{2.133}$$

$$\forall i \in I^{\mathrm{FAST}}, \forall j: \; nsr^+_{i,j,s^{\mathrm{F}}} \leq \overline{P_i} \cdot \sum_{s \in S/s^{\mathrm{F}}} z^*_{i,j,s} \tag{2.134}$$

$$\forall i \notin I^{\mathrm{FAST}}, \forall j, \forall s: \; nsr^+_{i,j,s} = 0 \tag{2.135}$$

The scheduled fast-cycling capacity is accounted for in the upward reserve requirement:

$$\forall j: \; D^+_j = \sum_i \left(sr^+_{i,j} + nsr^+_{i,j,s^{\mathrm{F}}} \right) + \sum_m \chi_{j,m,s^{\mathrm{F}}} + s^+_j \tag{2.136}$$

In the forecast scenario s^{F}, the output of the fast-cycling units, scheduled as reserves, should not be accounted for in the market clearing condition:

$$\begin{aligned} \forall j, \forall m, \forall s | \{s = s^F\}: \; D_{j,m} - \phi_{j,m,s} = & \sum_i I^{\mathrm{G}}_{m,i} \cdot (g_{i,j,s}) \\ & + G^{\mathrm{MR}}_{j,m} + G^{\mathrm{F}}_{j,m,s} - \chi_{j,m,s} + inj_{j,m,s} \\ & + \sum_r I^{\mathrm{PHES}}_{m,r} \cdot \left(g^{\mathrm{T}}_{r,j,s} - g^{\mathrm{P}}_{r,j,s} \right) \end{aligned} \tag{2.137}$$

$$\begin{aligned} \forall j, \forall m, \forall s | \{s \neq s^F\}: \; D_{j,m} - \phi_{j,m,s} = & \sum_i I^{\mathrm{G}}_{m,i} \cdot \left(g_{i,j,s} + nsr^+_{i,j,s} \right) \\ & + G^{\mathrm{MR}}_{j,m} + G^{\mathrm{F}}_{j,m,s} - \chi_{j,m,s} + inj_{j,m,s} \\ & + \sum_r I^{\mathrm{PHES}}_{m,r} \cdot \left(g^{\mathrm{T}}_{r,j,s} - g^{\mathrm{P}}_{r,j,s} \right) \end{aligned} \tag{2.138}$$

Similarly, the operational cost associated with dispatching the fast-cycling units (Eq. (2.80)-(2.85)) is accounted for in all scenarios except the forecast scenario s^{F}.

In addition to the consideration of an explicit procurement cost for non-spinning reserves in the objective (Eq. (2.86)), the introduction of a (limited) set of scenarios allows calculating an approximation of the activation cost of the non-spinning reserves. Indeed, Eq. (2.134) ensures that scheduled non-spinning reserves are dispatched in at least one scenario. The operational cost of these reserves is thus accounted for in the objective function. If the considered scenarios represent the uncertain RES-based generation with sufficient detail, this allows a near cost-optimal trade-off between spinning and non-spinning capacity to meet the reserve requirement. Compared to the DUC and IIUC formulation, accounting for the operational cost of these fast-starting units will prevent over-procurement of non-spinning reserves. The drawbacks associated with a scenario-based representation in a UC model w.r.t. scheduling non-spinning reserves however apply as well (Section 2.3.2).

2.5.3 Participation of intermittent RES-based generation in the reserve requirements

If intermittent RES-based generation is scheduled to be curtailed under forecast conditions, this is accounted for in the upward reserve requirement. This avoids scheduling additional upward reserves when the system is no longer able to accept RES-based power, as in the DUC formulation (see Section 2.2.3).

The downward reserve requirement, if considered, is only enforced when no curtailment of RES-based generation is scheduled under forecast conditions. As in the DUC formulation, this avoids scheduling more downward flexibility during periods when it is not cost-optimal or technically impossible to accept more RES-based generation. As a result, the downward reserve requirement will typically not trigger any additional downward reserves, i.e. downward flexibility that would not have been present in the UC schedule without the reserve requirement (see Section 2.2.3). However, in all other scenarios, curtailment is accounted for as a flexibility provider and the operational cost savings that may result from the absorption of more RES-based generation are accounted for in the objective function, which allows for an optimal trade-off between curtailment and downward flexibility provision if the considered scenarios adequately describe the forecast error distribution. In conclusion, compared to the DUC and IIUC formulation, the HUC formulation does provide an incentive to schedule downward flexibility through the operational cost savings associated

with dispatching power plants providing downward flexibility in the considered scenarios.

2.5.4 Participation of pumped hydro energy storage systems in the reserve requirements

In the HUC model, PHES systems are per definition allowed to offer 'reserves' in all scenarios but the forecast scenario. Indeed, as their output differs per scenario, this can be seen as their output as if they were scheduled as reserves. They are however excluded from the explicit reserve requirements with respect to the forecast scenario above. Below, we present an extension of the HUC model presented in [45] that allows accounting for the regulation services that PHES systems may offer w.r.t. their output under forecast conditions, while simultaneously guaranteeing the feasibility of dispatching those reserves in real time, based on [85].

We follow a similar approach as in the DUC formulation (Section 2.2.4). In addition to Eq. (2.66)-(2.71), we define the PHES-based reserve variables $r^{\mathrm{P},+}_{r,j}$, $r^{\mathrm{P},-}_{r,j}$, $r^{\mathrm{T},+}_{r,j}$ and $r^{\mathrm{T},-}_{r,j}$. The reserve requirements (2.122)-(2.123) are replaced by the following constraints:

$$\forall j : D^{+}_{j} = \sum_{i} \left(r^{+}_{i,j} + nsr^{+}_{i,j,s^{\mathrm{F}}} \right) + \sum_{m} \chi_{j,m,s^{\mathrm{F}}} + \sum_{r} \left(r^{\mathrm{P},+}_{r,j} + r^{\mathrm{T},+}_{r,j} \right) + s^{+}_{j} \tag{2.139}$$

$$\forall j | \sum_{m} \chi_{j,m,s^{\mathrm{F}}} = 0 : \; D^{-}_{j} = \sum_{i} r^{-}_{i,j} + \sum_{r} \left(r^{\mathrm{P},-}_{r,j} + r^{\mathrm{T},-}_{r,j} \right) + s^{-}_{j} \tag{2.140}$$

These reserves provided by the PHES systems are constrained to the capacity of each PHES system and the scheduled output of those PHES systems under forecast conditions:

$$\forall r, \forall j : \quad 0 \leq r^{\mathrm{P},+}_{r,j} \leq g^{\mathrm{P}}_{r,j,s^{\mathrm{F}}} \tag{2.141}$$

$$\forall r, \forall j : \quad 0 \leq g^{\mathrm{P}}_{r,j,s^{\mathrm{F}}} + r^{\mathrm{P},-}_{r,j} \leq \overline{P_r} \cdot p_{r,j,s^{\mathrm{F}}} \tag{2.142}$$

$$\forall r, \forall j : \quad 0 \leq g^{\mathrm{T}}_{r,j,s^{\mathrm{F}}} + r^{\mathrm{T},+}_{r,j} \leq \overline{P_r} \cdot t_{r,j,s^{\mathrm{F}}} \tag{2.143}$$

$$\forall r, \forall j : \quad 0 \leq r^{\mathrm{T},-}_{r,j} \leq g^{\mathrm{T}}_{r,j,s^{\mathrm{F}}} \tag{2.144}$$

$$\forall r, \forall j : \quad r^{\mathrm{P},-}_{r,j}, \; r^{\mathrm{T},+}_{r,j} \geq 0 \tag{2.145}$$

As in the DUC formulation, to schedule PHES-based reserves, the energy storage level must be sufficient to ensure feasibility of dispatching the scheduled reserves even under the most adverse conditions. The following constraints are enforced to ensure availability of the PHES-based reserves in the worst-case scenarios, i.e. the activation of all provided reserves in either direction, with respect to their output under forecast conditions *and* in the considered scenarios:

$$\forall r, \forall j: \quad e_{r,j,s^{\mathrm{F}}} + TP \cdot \sum_{1}^{j} \left(\Delta g^{\mathrm{P}}_{r,j} + \frac{r^{\mathrm{T},-}_{r,j}}{\sqrt{\epsilon_r}} + r^{\mathrm{P},-}_{r,j} \cdot \sqrt{\epsilon_r} \right) \leq \overline{E_r} \tag{2.146}$$

$$\forall r, \forall j: \quad e_{r,j,s^{\mathrm{F}}} - TP \cdot \sum_{1}^{j} \left(\Delta g^{\mathrm{T}}_{r,j} + \frac{r^{\mathrm{T},+}_{r,j}}{\sqrt{\epsilon_r}} + r^{\mathrm{P},+}_{r,j} \cdot \sqrt{\epsilon_r} \right) \geq \underline{E_r} \tag{2.147}$$

in which $\Delta g^{\mathrm{T}}_{r,j}$ and $\Delta g^{\mathrm{P}}_{r,j}$ are correction factors to account for charging or discharging rates of PHES system r in the considered scenarios that exceed the charging or discharging rate in the forecast scenario, augmented with the scheduled reserve capacity:

$$\forall r, \forall j, \forall s: \ \delta g^{\mathrm{T}}_{r,j,s} = \frac{g^{\mathrm{T}}_{r,j,s}}{\sqrt{\epsilon_r}} - \left(\frac{g^{\mathrm{T}}_{r,j,s^{\mathrm{F}}}}{\sqrt{\epsilon_r}} + \frac{r^{\mathrm{T},+}_{r,j}}{\sqrt{\epsilon_r}} + r^{\mathrm{P},+}_{r,j} \cdot \sqrt{\epsilon_r} \right) \tag{2.148}$$

$$\forall r, \forall j, \forall s: \ \Delta g^{\mathrm{T}}_{r,j} \geq \delta g^{\mathrm{T}}_{r,j,s} \tag{2.149}$$

$$\forall r, \forall j, \forall s: \ \delta g^{\mathrm{P}}_{r,j,s} = g^{\mathrm{P}}_{r,j,s} \cdot \sqrt{\epsilon_r} - \left(g^{\mathrm{P}}_{r,j,s^{\mathrm{F}}} \cdot \sqrt{\epsilon_r} + \frac{r^{\mathrm{T},-}_{r,j}}{\sqrt{\epsilon_r}} + r^{\mathrm{P},-}_{r,j} \cdot \sqrt{\epsilon_r} \right) \tag{2.150}$$

$$\forall r, \forall j, \forall s: \ \Delta g^{\mathrm{P}}_{r,j} \geq \delta g^{\mathrm{P}}_{r,j,s} \tag{2.151}$$

$$\forall r, \forall j, \forall s: \ \Delta g^{\mathrm{T}}_{r,j}, \ \delta g^{\mathrm{T}}_{r,j,s}, \ \Delta g^{\mathrm{P}}_{r,j}, \ \delta g^{\mathrm{P}}_{r,j,s} \geq 0 \tag{2.152}$$

Without the addition of a small set of scenarios, the trade-off with other flexibility providers is incomplete, as in the DUC formulation (Section 2.2.4). For example, in the case of upward reserves, we compare an energy-based allocation cost of the PHES system, i.e. the cost of increased charging under forecast conditions, with capacity-based allocation costs of other conventional flexibility providers, excluding the energy-based expected activation costs. The activation of the conventional flexibility providers in the scenarios however allows accounting for an approximation of the deployment cost of reserves, allowing a more cost-optimal trade-off between PHES-based and conventional reserve providers. Note that the ability of the PHES systems to provide flexibility w.r.t. their output under forecast conditions is still likely to be underestimated by imposing worst-case constraints (2.146)-(2.147). However, the output profile of

the PHES systems in scenarios other than the forecast scenario is not limited by constraints (2.146)-(2.147), allowing full exploitation of the flexibility the PHES systems may offer in those scenarios.

2.5.5 Discussion

Hybrid formulations combine a-priori reserve sizing rules and dedicated scenario reduction techniques with a SUC model in order to speed up the convergence of the SUC problem to a stable solution. As we will show in Chapter 5, the HUC model allows approximating the stable solution of the equivalent SUC problem at a fraction of the computational cost. Through the introduction of reserve requirements and customized scenario reduction techniques (Chapter 4 and Chapter 5), one can obtain approximately the same UC schedule by considering a small number of scenarios (compared to the number of scenarios needed to reach the stable solution of the SUC problem). As the number of scenarios drives the computational cost of stochastic models, calculation times are significantly lower for the HUC formulation. The HUC model outperforms the DUC and IIUC formulations in terms of cost-efficiency by taking into consideration more information than the aforementioned models: the (limited) set of scenarios allows for a coarse approximation of the full, expected cost of reserve provision and deployment. This allows (1) an optimal trade-off between flexibility providers scheduled to meet the reserve requirements and (2) internalizing the reserve sizing procedure in all but the forecast scenario. Moreover, by considering the reserve requirement, the solution of the HUC model is less sensitive to errors in the probability of the scenarios considered in the optimization. Compared to the DUC model, the HUC model typically requires less stringent reserve requirements, as extreme events are dealt with via the scenarios. As such, solutions of the DUC and HUC models are typically comparable in reliability, but the UC schedules obtained with the HUC formulation are typically more cost-optimal.

The addition of reserve constraints to a SUC model was first attempted by Ruiz et al. [107]. The addition of a static – i.e., constant over the time horizon of the optimization – reserve requirement to a SUC model considering 12 scenarios leads to lower expected costs compared to a DUC formulation when dealing with load and generation uncertainty in an IEEE reliability test system, consisting of 32 generators. The 12 scenarios considered in the stochastic optimization are not sufficient to capture the uncertainty in the system. Additional reserve constraints are added and the fast power plants are allowed to change their commitment status per scenario to ensure a reliable UC schedule. Ruiz et al. [131] use this model to study the impact of wind power on the Colorado power system. Six wind power scenarios are considered, which requires the addition

of reserve constraints. Operational cost reductions of 0.23% compared to the traditional reserve policy are obtained. Curtailment of wind power is drastically reduced, but the amount of lost load, albeit still limited, doubles. Tuohy et al. [39] employ the well-known WILMAR model, in which a reserve constraint based on the largest contingency (unplanned outage of the largest power plant in the system) and a fixed percentage of the forecasted wind power is added to the SUC model. Compared to a deterministic variant with a static reserve requirement, the SUC formulation can lead to operational cost savings up to 1%. Calculation times are however significantly higher: up to eight days for the SUC model, including reserve requirements, compared to three hours for the fastest deterministic variant. Abrell and Kunz [132] developed a model similar to the WILMAR model, but add a DC load flow representation of the transmission grid. The number of scenarios is reduced to three. This small set of scenarios requires the addition of reserve market models. From a one-week simulation of the German system, Abrell and Kunz note that the SUC formulation results in lower operational costs, although the difference is limited to 0.3%. Wang et al. [101] show that the addition of a reserve requirement equal to 5% of the load to a SUC model leads to decreased operational costs. Botterud and Zhou [102] demonstrate in a similar setting that a dynamic, probabilistic reserve requirement in a DUC model even (slightly) outperforms a SUC model without additional reserve constraints in terms of operational costs[36].

The added value of the model presented above compared to formulations found in the scientific literature is twofold. First, we present a new design of a HUC formulation (Chapter 5). A state-of-the-art reserve constraint and sizing methodology is combined with a SUC formulation (Chapter 3 and 5). This time-varying reserve requirement – in contrast to the static reserve requirements considered by e.g. Ruiz et al. [107, 131] – allows for more cost-efficient UC schedules. The reserve requirement will impose a lower limit on the scheduled reserves, while the considered scenarios will ensure that (1) additional reserves are scheduled if required; (2) the reserves are scheduled as cost efficiently as possible, considering the cost of allocation and activation; (3) the scheduled reserves are sufficiently flexible to overcome the highly variable forecast errors. This model allows explicitly considering spinning, non-spinning, RES-based and PHES-based reserves. In the scientific literature, only Tuohy et al. [39] consider all these reserve providers. PHES-based reserves are however restricted to the scheduled pumping power and worst-case feasibility constraints are not considered. The inclusion of a reserve requirement furthermore allows for a dedicated scenario reduction technique, which may yield more cost-effective UC schedules considering fewer scenarios (Chapter 5). This option has – to the best

[36]Note that this is only possible if the stable solution of the 'true' SUC problem was not reached. Solving the 'true' stochastic problem would yield a lower bound on the operational costs attainable.

of the author's knowledge – not been explored in the scientific literature. For example, Tuohy et al [39] and Abrell and Kunz [132] employ the well-known fast-forward scenario reduction technique [38], which does not leverage the description of the uncertainty at hand enclosed in the reserve requirement. We will return to this topic in Chapter 5. Second, the presented HUC model approximates the stable solution of the equivalent SUC model at a significantly lower computational cost, as shown in Chapter 5. This model can be used to assess the impact of uncertainty on reasonably large low-carbon electric power systems, for which SUC models would become computationally intractable.

However, a number of the disadvantages of the DUC and SUC formulations persist in the HUC model. First, although hybrid methods effectively internalize the reserve sizing problem and account for activation costs during the reserve allocation process, the limited number of scenarios considered may lead to over- or underestimations of the activation probability, thus the cost of the scheduled reserves. Errors in the representation of the scenarios (amplitude and/or probability of occurrence), may have an impact on the resulting UC schedule. The lower limit of scheduled reserve capacity, ensured by the reserve requirement, however limits the impact of the exact form of the (tails of the) distribution of the RES-based generation. At worst, load shedding is scheduled in all scenarios but the forecast scenario, or a less cost-efficient mix of reserve providers is scheduled. As in the SUC formulation, the gain in operational costs is dependent on the quality of the scenarios considered. Second, the reserve requirements still need to be decided upon ex-ante. Last, although the computational cost of solving a HUC problem is significantly lower than that of the equivalent SUC problem, it remains high compared to the calculation time of the equivalent DUC, IIUC and PUC problem (see below and Chapter 5).

2.6 A probabilistic unit commitment model[37]

In the DUC formulation, we only (implicitly) included the allocation cost of spinning reserves. Indeed, the only cost the SO incurs when scheduling spinning reserves is caused by (1) less efficient part-load behavior and (2) a possible increase in start-up costs. The cost of activating these reserves however is not included in the model. The expected activation costs can however be included in a DUC formulation if the probability of activation is known. Assuming that the probability distribution of the forecast error is known, one can include this probability as an activation probability. Below we present a novel probabilistic unit commitment model (PUC), in which we account for the probability of

[37] This section is based on K. Bruninx and E. Delarue, *A probabilistic unit commitment model: cost-effective, reliable and fast,* Submitted to IEEE Trans. Power Syst., 2015.

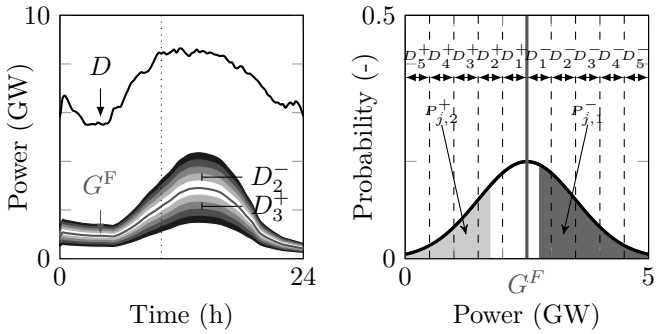

Figure 2.9: In the PUC model, the system operator has to decide on the UC schedule, taking into account the forecasted RES-based electricity generation and a discretized form of the probability density function of this RES-based electricity generation. The discretization gives rise to a number of individual reserve levels, each of which is associated with a probability of activation. This probability is calculated as the cumulative probability of a forecast error exceeding the sum of all preceding reserve levels and half the width of the reserve level. The calculation of the reserve levels and activation probabilities is discussed at the end of this section. The indicated distribution and reserve levels are illustrative.

activation of reserves based on the probability distribution of the forecast error. The PUC formulation is identical to the DUC formulation (Eq. (2.2)-(2.48)), but includes the reserve requirements (Eq. (2.10)-(2.11)) in a novel way and accounts for the expected cost of reserve deployment in the objective function (Eq. (2.1)).

The upward and downward reserve requirements (Eq. (2.10)-(2.11)) are split in L levels, each of which corresponds to a specific activation probability (upward $P^{+}_{j,l}$ or downward $P^{-}_{j,l}$). The calculation of the reserve levels and the corresponding activation probabilities is discussed at the end of this section. Assuming that the probability distribution of the uncertain wind power forecast is known, we will discretize the distribution in $2L$ (set L with cardinality L, index l) levels, as illustrated in Fig. 2.10. Equations (2.10)-(2.11) are replaced

by Eq. (2.153)-(2.154):

$$\forall j, \forall l: \; D^{+}_{j,l} = \sum_{i} r^{+,\mathrm{L}}_{i,j,l} + \chi^{+,\mathrm{L}}_{j,l} + \phi^{+,\mathrm{L}}_{j,l} \tag{2.153}$$

$$\forall j, \forall l: \; D^{-}_{j,l} = \sum_{i} r^{-,\mathrm{L}}_{i,j,l} + \chi^{-,\mathrm{L}}_{j,l} \tag{2.154}$$

Additional load shedding ($\phi^{+,\mathrm{L}}_{j,l}$) and curtailment of RES-based generation ($\chi^{-,\mathrm{L}}_{j,l}$ and $\chi^{+,\mathrm{L}}_{j,l}$) are explicitly considered as flexibility options. Assuming wind power is the only source of uncertainty, upward RES-based reserves are constrained to the 'scheduled' curtailment, i.e. curtailment of the forecasted wind power output, while downward RES-based reserves correspond to the additional curtailment of positive forecast errors:

$$\forall j: \sum_{l} \chi^{+,\mathrm{L}}_{j,l} \leq \sum_{m} \chi_{j,m} \tag{2.155}$$

$$\forall j, \forall l: \chi^{+,\mathrm{L}}_{j,l}, \chi^{-,\mathrm{L}}_{j,l} \geq 0 \tag{2.156}$$

Note that the explicit consideration of additional load shedding ($\phi^{+,\mathrm{L}}_{j,l}$) and curtailment ($\chi^{-,\mathrm{L}}_{j,l}$) abolishes the need for (1) slack variables in the reserve requirements and (2) corrections to the downward reserve requirement based on curtailment of RES-based generation under forecast conditions (Section 2.2). Conventional reserves ($r^{+}_{i,j}$ and $r^{-}_{i,j}$) are constrained to the ramping capacity and minimum/maximum stable load level of each power plant, as in the DUC model. They are allocated to at least one reserve level l ($r^{+,\mathrm{L}}_{i,j,l}$ and $r^{-,\mathrm{L}}_{i,j,l}$):

$$\forall i, \forall j: \quad \sum_{l} r^{+,\mathrm{L}}_{i,j,l} = r^{+}_{i,j} \tag{2.157}$$

$$\forall i, \forall j: \quad \sum_{l} r^{-,\mathrm{L}}_{i,j,l} = r^{-}_{i,j} \tag{2.158}$$

$$\forall i, \forall j, \forall l: \quad r^{+,\mathrm{L}}_{i,j,l}, \; r^{-,\mathrm{L}}_{i,j,l} \geq 0 \tag{2.159}$$

The cost of deploying or activating reserves ($acsr^{+}_{i,j,l}$, $acsr^{-}_{i,j,l}$, $TP \cdot VOLL \cdot \phi^{+,\mathrm{L}}_{j,l}$, $TP \cdot VOC \cdot \chi^{-,\mathrm{L}}_{j,l}$, $TP \cdot VOC \cdot \chi^{+,\mathrm{L}}_{j,l}$) can now be explicitly added to the objective

function. In the PUC model, Eq. (2.1) is replaced by

$$\begin{aligned} min \quad c(g,z) = & \sum_i \sum_j (fc_{i,j} + sc_{i,j} + co_2t_{i,j} + rc_{i,j}) \\ & + \sum_j TP \cdot VOC \cdot \chi_j + \sum_j TP \cdot VOLL \cdot \phi_j \\ & + \sum_i \sum_j \sum_l (P^+_{j,l} \cdot acsr^+_{i,j,l} - P^-_{j,l} \cdot acsr^-_{i,j,l}) \\ & + \sum_j \sum_l TP \cdot VOLL \cdot P^+_{j,l} \cdot \phi^{+,\mathrm{L}}_{j,l} \\ & + \sum_j \sum_l TP \cdot VOC \cdot (P^-_{j,l} \cdot \chi^{-,\mathrm{L}}_j - P^+_{j,l} \cdot \chi^{+,\mathrm{L}}_j) \end{aligned} \tag{2.160}$$

The operational cost under forecast conditions (first and second line in Eq. (2.160)) is complemented with the reserve activation costs (third, fourth and fifth line in Eq. (2.160)). These activation costs are dependent on the probability of activation of the reserve level (upward: $P^+_{j,l}$, downward: $P^-_{j,l}$) and the operational costs associated with each flexibility option (spinning reserves $acr^+_{i,j,l}$ and $acr^-_{i,j,l}$, curtailment $TP{\cdot}VOC{\cdot}\chi^{-,\mathrm{L}}_{j,l}$, $TP{\cdot}VOC{\cdot}\chi^{+,\mathrm{L}}_{j,l}$ or load-shedding $TP{\cdot}VOLL{\cdot}\phi^{+,\mathrm{L}}_{j,l}$) scheduled to provide the reserves in this level. Spinning reserves result in fuel and CO_2-emission costs:

$$\forall i, \forall j, \forall l: \quad acsr^+_{i,j,l} = r^{+,\mathrm{L}}_{i,j,l} \cdot TP \cdot (MA_i + CO_2P \cdot MB_i) \tag{2.161}$$

$$\forall i, \forall j, \forall l: \quad acsr^-_{i,j,l} = r^{-,\mathrm{L}}_{i,j,l} \cdot TP \cdot (MA_i + CO_2P \cdot MB_i) \tag{2.162}$$

As the ramp rate at which the reserves are activated is unknown, the associated ramping costs are not considered as reserve activation costs during the reserve allocation process. Activating upward reserves will always result in an operational cost increase ($acr^+_{i,j,l} \geq 0$). Downward reserves may however trigger cost reductions ($acr^-_{i,j,l}$), as fuel is saved if conventional generation is replaced by an increase in RES-based generation (w.r.t. the forecasted level of RES-based generation). Load shedding as upward flexibility ($\phi^{+,\mathrm{L}}_{j,l}$) is penalized at the value of lost load $VOLL$, corrected for the probability of activation ($P^+_{j,l}$). Similarly, curtailment of RES-based generation as downward flexibility ($\chi^{-,\mathrm{L}}_{j,l}$) is penalized at the value of curtailment VOC, corrected for the expected reduction of scheduled curtailment of RES-based generation, 'recycled' as upward flexibility ($\chi^{+,\mathrm{L}}_{j,l}$).

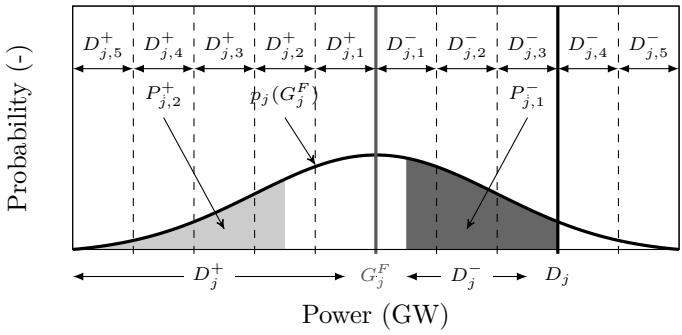

Figure 2.10: Assuming that the probability distribution of the forecast error ($p_j(G^F_j)$), the demand D_j and the forecasted wind power production G^F_j are known, one can calculate the probability of a positive (negative) forecast error occuring, thus the probability of activation of some predefined reserve levels. Assuming five reserve levels ($L = 5$), the probability of activation of reserves scheduled in $D^+_{j,2}$ is given by the light grey surface ($P^+_{j,2}$). Likewise, the probability of activation of $D^-_{j,1}$ ($P^-_{j,1}$) is calculated as the surface of the dark grey area. Note that interval on which the activation probability of downward reserves is calculated is limited by the demand D_j.

Reserve sizing and probability of activation

The probability that the scheduled reserves are activated, depends on the forecast of intermittent RES-based generation, changing from time step to time step. Assuming we have a full description of the probability density function (pdf) of the wind power forecast ($p_j(G^F_j)$), the different reserve levels and the associated probability of activation can be calculated as follows. First, we divide the domain of the probability density function $p_j(G^F_j)$ in a predefined number of intervals $2L$ (L intervals for positive forecast errors, L intervals for negative forecast errors) (Fig. 2.10). Each of the resulting intervals corresponds to a reserve level ($D^+_{j,l}$ and $D^-_{j,l}$). Second, the probability of activation of each of these intervals can be determined, assuming a uniform discretization and with ΔD the width of the reserve levels:

$$\forall j, \forall l: \quad P^+_{j,l} = \int_{-\infty}^{G^F_j - (l-\frac{1}{2})\cdot\Delta D} p_j(G^F_j) \tag{2.163}$$

$$\forall j, \forall l: \quad P^-_{j,l} = \int_{G^F_j + (l-\frac{1}{2})\cdot\Delta D}^{D_j} p_j(G^F_j) \tag{2.164}$$

The reserve requirements in the PUC model are limited to the 'useful' domain: only reserve levels that can avoid load shedding or curtailment are considered. For example, the demand for downward reserves is limited to the amount of additional RES-based generation that can be absorbed by the power system (no downward reserves above D_j, Fig. 2.10).

For the DUC model, we may quantify the upward D_j^+ and downward D_j^- reserves requirements at each time step as the smallest quantities that cover the full domain of the wind power forecast error at each time step (D_j^+ and D_j^-), limited to the useful range (see above). In this particular case, the total reserve requirement in the DUC and PUC problems is identical, as by definition $\sum_l D_{j,l}^- = D_j^-$ and $\sum_l D_{j,l}^+ = D_j^+$.

Note that we capture the dependency of the activation probabilities $P_{j,l}^+$ and $P_{j,l}^-$ on the power plant via the dependency on the reserve level l[38]. This activation probability expresses the probability that the scheduled reserves are called upon and can be calculated as illustrated in Fig. 2.10.

2.6.1 Allocation & activation costs of spinning reserves

The presented PUC model explicitly accounts for the probability and cost of activation of reserves during the allocation process, effectively allowing (1) internalizing the reserve sizing problem and (2) optimizing the allocation of reserves in a DUC model. The obtained UC schedule will be shown to be nearly as cost-effective as that obtained with a SUC formulation and significantly better than the DUC model, while the computational cost remains low (Chapter 5). The PUC formulation is a natural extension of the DUC model and allows chance-constrained optimization (see 'Discussion' – Section 2.6.5).

The internalization of the reserve sizing procedure is the result of including (1) the activation probability and operational cost of different reserve providers and (2) load shedding (upward) and curtailment of RES-based electricity generation (downward) as explicit reserve providers. This allows calculating the expected socio-economic cost of load shedding (curtailment) versus the expected cost of procuring and activating upward (downward) reserves. Effectively, we internalize the ex-ante reserve sizing procedure proposed by Ortega-Vazquez and Kirschen [93, 46] in a UC formulation.

Additionally, the consideration of the expected cost of deployment allows procuring a cost-optimal mix of flexibility providers to meet the reserve

[38]To be precise, one should interpret these probabilities as the probability that the scheduled reserves are *fully* activated, i.e. at the scheduled reserve capacity, on time step j.

requirements. This remark especially holds for the downward reserves, as the value of downward flexibility – i.e. possible operational cost savings associated with the ability to absorb more RES-based electricity generation – is explicitly monetized and accounted for in the objective function.

2.6.2 Allocation & activation costs of non-spinning reserves

Non-spinning reserves are added to the upward reserve constraint, Eq. (2.153):

$$\forall j, \forall l: \; D^{+}_{j,l} = \sum_{i} \left(r^{+,\mathrm{L}}_{i,j,l} + nsr^{+,\mathrm{L}}_{i,j,l} \right) + \chi^{+,\mathrm{L}}_{j,l} + \phi^{+,\mathrm{L}}_{j,l}$$

The non-spinning reserves $nsr^{+}_{i,j}$ are constrained to the ramping capacity and minimum and maximum stable load level of the fast-starting unit i (Eq. (2.34)-(2.39)), as in the DUC model. They are allocated to one reserve level l:

$$\forall i \in I^{\mathrm{FAST}}, \forall j: \quad \sum_{l} nsr^{+,\mathrm{L}}_{i,j,l} = nsr^{+}_{i,j} \tag{2.165}$$

$$\forall i \in I^{\mathrm{FAST}}, \forall j, \forall l: \quad \underline{P_i} \cdot z^{*}_{i,j,l} \leq nsr^{+}_{i,j,l} \leq \overline{P_i} \cdot z^{*}_{i,j,l} \tag{2.166}$$

$$\forall i \in I^{\mathrm{FAST}}, \forall j: \quad \sum_{l} z^{*}_{i,j,l} \leq 1 \tag{2.167}$$

$$\forall i \in I^{\mathrm{FAST}}, \forall j, \forall l: \quad z^{*}_{i,j,l} \leq y_{i,j} \tag{2.168}$$

$$\forall i \in I^{\mathrm{FAST}}, \forall j, \forall l: \quad z^{*}_{i,j,l} - z^{*}_{i,j-1,l} + v^{*}_{i,j,l} - w^{*}_{i,j,l} = 0 \tag{2.169}$$

$$\forall i \in I^{\mathrm{FAST}}, \forall j, \forall l: \quad z^{*}_{i,j,l},\; v^{*}_{i,j,l},\; w^{*}_{i,j,l} \in \{0,1\} \tag{2.170}$$

$$\forall i \notin I^{\mathrm{FAST}}, \forall j, \forall l: \quad z^{*}_{i,j,l},\; v^{*}_{i,j,l},\; w^{*}_{i,j,l},\; nsr^{+,\mathrm{L}}_{i,j,l} = 0 \tag{2.171}$$

In constraints (2.166) and (2.167), we implicitly assume that the width of a reserve level ΔD exceeds the capacity of the largest power plant providing non-spinning reserves. If ΔD is smaller than the capacity of the largest non-spinning reserve provider, that unit may still be scheduled as non-spinning reserve (if ΔD exceeds its minimum stable operating point), but not at its full capacity. A part of the capacity ($\overline{P_i} - \Delta D$) will not be accounted for as non-spinning reserve, e.g. in another reserve level. This may lead to over-procurement of non-spinning reserves, as more non-spinning reserve capacity may be scheduled than is accounted for in the reserve requirement. If required, constraints (2.166) and (2.167) can be reformulated to allow a fast-starting unit to provide non-spinning reserves in multiple reserve levels. However, in the case study presented in this

dissertation, only units with a capacity of 100 MW or less are non-spinning reserve providers. The width of the reserve levels exceeds 100 MW in almost all cases.

The allocation cost and the expected cost of activating non-spinning reserves ($acnsr^{+}_{i,j,l}$) can now be explicitly added to the objective function:

$$\begin{aligned} min \quad c(g,z) = & \sum_{i}\sum_{j}(fc_{i,j} + sc_{i,j} + co_2t_{i,j} + rc_{i,j}) \\ & + \sum_{j} TP \cdot VOC \cdot \chi_j + \sum_{j} TP \cdot VOLL \cdot \phi_j + \sum_{i}\sum_{j} NSRC_i \cdot y_{i,j} \\ & + \sum_{i}\sum_{j}\sum_{l}(P^{+}_{j,l} \cdot (acsr^{+}_{i,j,l} + acnsr^{+}_{i,j,l}) - P^{-}_{j,l} \cdot acsr^{-}_{i,j,l}) \\ & + \sum_{j}\sum_{l} P^{+}_{j,l} \cdot TP \cdot VOLL \cdot \phi^{+,\mathrm{L}}_{j,l} \\ & + \sum_{j}\sum_{l} TP \cdot VOC \cdot (P^{-}_{j,l} \cdot \chi^{-,\mathrm{L}}_{j} - P^{+}_{j,l} \cdot \chi^{+,\mathrm{L}}_{j}) \end{aligned} \tag{2.172}$$

Spinning reserves result in fuel and CO_2-emission costs (see above). The activation cost of non-spinning reserves ($acnsr^{+}_{i,j,l}$) consists of fuel, CO_2-emission and start-up costs:

$$\begin{aligned} \forall i, \forall j, \forall l: \quad acnsr^{+}_{i,j,l} = & STC_i \cdot v^{*}_{i,j,l} + TP \cdot (C_{i,j} + CO_2P \cdot D_{i,j}) \cdot z^{*}_{i,j,l} \\ & + TP \cdot (MA_i + CO_2P \cdot MB_i) \cdot (nsr^{+,\mathrm{L}}_{i,j,l} - \underline{P_i} \cdot z^{*}_{i,j,l}) \end{aligned} \tag{2.173}$$

As the ramp rate at which the reserves are activated is unknown, the associated ramping costs are not considered as reserve activation costs during reserve allocation. With the extension of the PUC model provided above, an optimal trade-off between spinning reserves (cheap, but online, leading to a less compressible power system) and non-spinning reserves (highly flexible, allowing a higher absorption of intermittent RES-based generation, but typically more expensive to run) becomes possible in a deterministic setting.

2.6.3 Participation of intermittent RES-based generation in the reserve requirements

The participation of intermittent generation in the upward reserve requirements is accounted for in a similar manner as in the DUC formulation. For the upward

reserves, the implementation may be different, but the behavior of the model with respect to curtailment as upward reserves is however very similar. In both formulations, curtailment of forecasted RES-based generation is accounted for in the upward reserve requirement. This reflects a situation in which we are – to a certain extent – not concerned with unexpected decreases in RES-based electricity generation, as the SO is unable or unwilling to absorb the forecasted RES-based generation. Negative forecast errors that exceed the scheduled curtailment should however be dealt with through conventional or PHES-based upward reserves.

With respect to the downward reserves however, the trade-off between scheduling downward flexibility provided by conventional generation and curtailing unexpected increases in intermittent RES-based generation is now made explicit. Indeed, by accounting for the expected operational cost savings associated with absorbing more RES-based generation than forecasted, an optimal trade-off between conventional downward flexibility and curtailment is sought. This approach is to be compared to the DUC model, in which, if curtailment of RES-based generation is scheduled under forecast conditions, the demand for downward reserves was explicitly forced to zero. As such, we avoided excessive procurement of downward regulation capacity. The DUC formulation thus provides an incentive to curtail forecasted RES-based generation in order to 'relax' the downward reserve requirement. In the PUC model, the model does not only take into account the operational costs associated with providing downward reserves, but also the expected benefits (decreases in expected operational cost). Combined with the inclusion of curtailment as a downward reserve provider, the model no longer has an incentive to schedule curtailment under forecast conditions to relax the downward reserve constraint. This results in a more realistic representation of the trade-off a system operator faces when scheduling downward reserves and leads to more cost-efficient UC schedules and higher RES-absorption rates, as shown in Chapter 5.

2.6.4 Participation of pumped hydro energy storage systems in the reserve requirements

To allow PHES systems to offer regulation services in the different, predefined reserve levels, we introduce four new variables: $r_{j,l}^{\mathrm{P},+,\mathrm{L}}$, $r_{j,l}^{\mathrm{P},-,\mathrm{L}}$, $r_{j,l}^{\mathrm{T},+,\mathrm{L}}$ and $r_{j,l}^{\mathrm{T},-,\mathrm{L}}$. We restrict the amount of reserves offered by the PHES systems in the different

levels to the scheduled reserves ($r^{\mathrm{P},+}_{r,j}$, $r^{\mathrm{P},-}_{r,j}$, $r^{\mathrm{T},+}_{r,j}$, $r^{\mathrm{T},-}_{r,j}$):

$$\forall j: \quad \sum_{l} r^{\mathrm{P},+,\mathrm{L}}_{j,l} = \sum_{r} r^{\mathrm{P},+}_{r,j} \tag{2.174}$$

$$\forall j: \quad \sum_{l} r^{\mathrm{P},-,\mathrm{L}}_{j,l} = \sum_{r} r^{\mathrm{P},-}_{r,j} \tag{2.175}$$

$$\forall j: \quad \sum_{l} r^{\mathrm{T},+,\mathrm{L}}_{j,l} = \sum_{r} r^{\mathrm{T},+}_{r,j} \tag{2.176}$$

$$\forall j: \quad \sum_{l} r^{\mathrm{T},-,\mathrm{L}}_{j,l} = \sum_{r} r^{\mathrm{T},-}_{r,j} \tag{2.177}$$

$$\forall j, \forall l: \quad r^{\mathrm{T},-,\mathrm{L}}_{j,l},\ r^{\mathrm{T},+,\mathrm{L}}_{j,l},\ r^{\mathrm{P},-,\mathrm{L}}_{j,l},\ r^{\mathrm{P},+,\mathrm{L}}_{j,l} \geq 0 \tag{2.178}$$

Note that these constraints are enforced in addition to Eq. (2.28) - (2.32) and (2.42)-(2.48). Eq. (2.153) and (2.154) are replaced by

$$\forall j, \forall l: \ D^{+}_{j,l} = \sum_{i} \left(r^{+,\mathrm{L}}_{i,j,l} + nsr^{+,\mathrm{L}}_{i,j,l} \right) + r^{\mathrm{P},+,\mathrm{L}}_{j,l} + r^{\mathrm{T},+,\mathrm{L}}_{j,l} + \chi^{+,\mathrm{L}}_{j,l} + \phi^{+,\mathrm{L}}_{j,l} \tag{2.179}$$

$$\forall j, \forall l: \ D^{-}_{j,l} = \sum_{i} r^{-,\mathrm{L}}_{i,j,l} + \chi^{-,\mathrm{L}}_{j,l} + r^{\mathrm{P},-,\mathrm{L}}_{j,l} + r^{\mathrm{T},-,\mathrm{L}}_{j,l} \tag{2.180}$$

PHES-based reserves do not present an explicit procurement or deployment cost. However, Eq. (2.42) - (2.48), which ensure the availability of the scheduled reserves in real time, do require changes to the PHES output profile under forecast conditions, which affects the operational cost under forecast conditions accordingly. These changes in the objective function are to be weighted against the expected operational cost of procuring and deploying conventional reserves, which are explicitly accounted for in the PUC formulation. Compared to a DUC model, the trade-off in the PUC formulation is a more accurate presentation of the real trade-off a system operator faces. However, constraints (2.42)-(2.48), which limit the amount of reserves that a PHES system can provide, are still more conservative than the constraints imposed on the PHES systems in the SUC formulation.

2.6.5 Discussion

In a DUC formulation, the expected activation cost of reserves is not taken into account. These activation costs are dependent on the probability that the scheduled reserves are activated, which in turn depends on the forecast

of intermittent RES-based generation, changing from time step to time step, and the variable cost structure of the power plant offering the reserves. Such information is typically not available in a DUC formulation. By defining distinct reserve levels, each with a probability of activation, one can account for the allocation and expected activation costs. The resulting PUC formulation yields significant improvements in the performance of the resulting UC schedule (Chapter 5).

The reason for these reductions in operational cost is threefold. First, the PUC model internalizes the reserve sizing problem in the UC optimization, which allows the consideration of inter-temporal constraints and 'trading' of risk – e.g. the risk of load shedding – over time. Second, the value of scheduling and activating downward flexibility will be explicitly monetized during the reserve scheduling process. Although curtailment can always provide downward reserves, not absorbing unexpected increases in RES-based generation may be sub-optimal, an effect which is represented in the PUC formulation. Third, activation probabilities allow upward reserves to be provided cost-effectively by a mix of (1) cheap, often activated running power plants (spinning reserves), (2) expensive, but rarely activated offline power plants (non-spinning reserves), (3) PHES-based flexiblity, which may impact the operational cost under forecast conditions and (4) RES-based generation which is scheduled to be curtailed under forecast conditions. Without considering the activation probabilities, this trade-off was not possible a DUC model.

Some of the drawbacks of the DUC formulation however persist. First, we still require the reserves to be sufficiently flexible to ramp up/down from zero to their full scheduled capacity within one time step, which may be an ill-informed approach resulting in too flexible or not flexible enough reserve capacity (Section 2.4). Second, the feasibility of deploying the scheduled reserves w.r.t. the grid constraints is not guaranteed: as the reserves are not 'dispatched', congestion may prevent real-time activation of the scheduled reserves. Third, the necessary worst-case feasibility constraints imposed on the PHES-based reserves are still conservative compared to the constraints imposed on the PHES systems in the SUC model. In addition, the approach above requires detailed knowledge of the probability of activation of each power plant offering reserves, at each time step. Ex-ante estimations of these probabilities may be difficult to come by and are prone to errors. Wrong estimates of these probabilities may have a significant impact on (1) the amount of reserves scheduled and (2) the technology mix providing the scheduled flexibility, which could result in sub-optimal UC schedules. This last point highlights the importance of a thorough statistical analysis of the uncertainty at hand, which is the topic of Chapter 3. Last, if one includes the full probability density function, discretized with sufficient precision, the activation probabilities of the extreme reserve levels will be very

low. The model is in this case able to make the explicit trade-off between providing these reserves and violating the reserve requirement at a very high cost, weighted by a very low probability. The cost of load shedding $VOLL$ is however critical in such a setting. One could additionally add constraints on the amount of 'reserve shedding' that is allowed, inspired by chance-constrained programming approaches [59, 58, 60, 61, 57]. If the probability density function is however represented with sufficient detail, such constraints are unnecessary and may lead to arbitrary and sub-optimal results. Similar constraints could be imposed on the amount of allowed curtailment, but show similar drawbacks and are not further explored in this dissertation.

In the scientific literature, two approaches can be found that are related to the presented PUC model. First, chance-constrained UC formulations[39] include similar (discretized) probability distributions[40] to introduce e.g. LOLP constraints on the optimization [59, 58, 60, 61, 57, 133]. However, during the reserve scheduling process, the reserve activation costs are typically not considered, which results in an ill-informed trade-off between (1) load shedding and upward reserve procurement and (2) curtailment and downward reserve procurement respectively. Second, Xiao et al. [134] present a PUC model similar to that discussed above, but simplify the representation of the power system. Ramping constraints, the minimum power output of power plants providing non-spinning reserves and their start-up cost, as well as energy storage systems and the regulation services they may offer, are neglected. The operational cost benefits associated with downward reserve provision is not monetized. In contrast, all these elements are considered in the PUC formulation presented above.

2.7 Conclusion: a preliminary comparison

The five formulations of the UC problem that we introduced in the previous sections all describe the same problem: the scheduling of a number of power plants to meet a certain demand for electricity at the lowest operational cost, considering stochastic RES-based electricity generation. Each of those

[39] Chance-constrained UC formulations [59, 58, 60, 61, 57] try to speed up the convergence of a SUC problem or to reduce the conservatism of a DUC model by imposing that certain constraints, typically the power balance, should be satisfied with a certain probability. Small and unlikely violations of the constraints are tolerated, effectively relaxing the problem, while guaranteeing a solution with a certain reliability (e.g. an upper limit on loss of load probability (LOLP)).

[40] Recently, a number of authors have introduced analytical reformulations of chance-constrained scheduling problems [63, 128]. These analytical reformulations allow accounting for the exact form of the distribution in the UC formulation. We will use the results of [63, 128] in Chapter 6 to study the impact of limitedly controllable demand response.

formulations utilizes a different description of that stochastic RES-based electricity generation (Table 2.2), which has a profound impact on the way the power plants, energy storage systems, curtailment and load shedding are scheduled.

In general, one can distinguish between two types of objective functions in a UC formulation. In its simplest form, the objective function of a UC problem consists of the minimization of the operational cost *under forecast conditions*, as is the case in the DUC and IIUC formulation. Alternatively, one can optimize the *expected operational cost to meet the demand in all (reasonable) realizations of the uncertain RES-based generation.* This objective is utilized in the SUC, HUC and PUC formulations, albeit the representation of the uncertainty, and thus the exact form of the objective function is different. Accounting for the expected operational cost rather than the cost under forecast conditions means that in addition to the cost of reserve procurement or allocation, one also takes into consideration the probability-weighted cost of reserve activation or deployment. If this is the case, the reserve sizing problem can be internalized in the UC formulation. Indeed, the modeler no longer has to make the trade-off between the socio-economic cost of not meeting the demand in some extreme, but unlikely realizations of the RES-based generation and the scheduling of (upward) reserves ex-ante, as this trade-off is now part of the objective of the UC problem. If this is the case, we will claim that we have *optimally internalized the reserve sizing problem.* Moreover, the procured reserves will consist of a cost-optimal mix of technologies, spinning and non-spinning, PHES- and RES-based flexibility providers, weighing the allocation and expected activation cost of each flexibility provider.

Also the technical constraints imposed on the required reserves differ per formulation (Table 2.2). First, the ramp rates that the reserves should be able to cover can be based on some heuristic rules, typically rather conservative (reserve requirements in the HUC, DUC and PUC formulations), or on the worst possible ramp observed in historical data or a set of scenarios (IIUC, HUC and SUC models). Conservative estimates of the ramp rates will lead to reliable UC schedules, but these schedules are typically less cost-optimal. Similar reasoning applies to the regulation services that may be provided by PHES systems. DUC, PUC, IIUC and, to a lesser extent, HUC models require conservative estimates of the regulation services available from the PHES system, as the probability of subsequent, continuous deployment of the scheduled reserves is unknown. Formulations in which the PHES system implicitly offers regulation services, represented by dispatching the PHES system in a set of scenarios, are typically less conservative, which leads to more cost-optimal UC schedules. However, when a modeler is inable to capture all relevant events in a set of scenarios of a reasonable size, this less conservative approach may lead to load shedding

or curtailment in real time. Third, the treatment of RES-based generation as a flexibility provider differs considerably between models, for upward and downward reserves. With respect to the downward reserves, only the PUC, HUC and SUC formulations allow estimating the value of downward flexibility. In absence of a (relatively large) value of VOC, the value of curtailed RES-based generation, curtailment will be the de facto downward flexibilty provider in the IIUC and DUC formulations. This approach may lead to sub-optimal UC schedules, as the inability to absorb additional RES-based generation may lead to higher operational costs. RES-based generation as an upward reserve provider, i.e. lowering the effective upward reserve requirements if RES-based generation is curtailed under forecast conditions or allowing scenario-specific curtailment variables, is allowed in all UC formulations. However, for all flexibility providers above, the economic trade-off between the available flexibility providers is incomplete in the DUC and IIUC formulation, as the deployment cost of conventional flexibility providers is not considered. Last, the technical feasibility of the real-time dispatch of the scheduled reserves is not guaranteed in all models. In the DUC and PUC models, the scheduled reserves are not 'dispatched', thus the feasibility of e.g. changes in the flows on the transmission grid resulting from the real-time activation of reserves is not guaranteed. In the SUC, IIUC and HUC solutions the feasibility of the real-time activation of the scheduled reserves is guaranteed if the RES-based generation is *identical* to the considered scenarios. In other realizations, the feasibility is not guaranteed. However, as the number of scenarios considered in the UC formulation increases, the likelihood of a feasible, least-cost real-time dispatch increases. A SUC formulation may thus be most likely to result in a UC schedule in which reserves can be dispatched without violating e.g. transmission grid constraints.

Regardless of the model chosen, adequately capturing the RES-based generation in a statistical distribution (DUC, PUC, IIUC, HUC) or a discrete set of scenarios (SUC, HUC) will be of critical importance for the performance of the model. Therefore, we will discuss the statistical description of the forecast errors on RES-based generation at length in Chapter 3, with a particular focus on the description of the tails of the distribution, which drive e.g. probabilistic reserve sizing procedures. Generating a balanced set of scenarios, as a discrete representation of the aforementioned distribution, and identifying the critical scenarios that drive the UC decisions, is the subject of Chapter 4. The tools developed in these chapters will allow us to quantify the relative performance of the presented models in a case study (Chapter 5).

Table 2.2: Qualitative comparison: the five selected UC models.

	DUC	SUC	IIUC	HUC	PUC
Representation uncertainty:	Reserve requirements	Set of discrete scenarios, incl. probability of occurrence	Four ramping scenarios, enforced as constraints	Set of discrete scenarios, incl. probability of occurrence and reserve requirements	Set of reserve levels or intervals, incl. probability of activation
Objective:	min. operational cost under forecast conditions	min. expected operational cost over set of scenarios	min. operational cost under forecast conditions	min. expected operational cost over set of scenarios	min. operational cost under forecast conditions and expected cost of activating reserves
includes:					
Allocation or procurement costs	Yes	Yes	Yes	Yes	Yes
Deployment or activation costs	No	Yes	No	Yes	Yes
allows:					
Optimal internal reserve sizing	No	Yes	No	Yes, but minimum level of reserves enforced	Yes
Optimal reserve procurement	No	Yes	No	Yes	Yes

Table 2.2: *(Cont'd)* Qualitative comparison: the five selected UC models.

	DUC	SUC	IIUC	HUC	PUC
Constraints:					
Ramp rate	Conservative	Realistic	Realistic	Conservative (reserve requirement), realistic (scenarios)	Conservative
PHES-based regulation	Conservative	Realistic	Conservative	Conservative (reserve requirement), realistic (scenarios)	Conservative
RES-based regulation	Sub-optimal, no incentive for downward reserve procurement	Optimal	Sub-optimal, no incentive for downward reserve procurement	Optimal (scenarios), sub-optimal (upward reserve requirement)	Optimal
Technical feasibility real-time dispatch	Not guaranteed	Guaranteed in most realizations	Guaranteed in worst-case realizations	Guaranteed in most realizations	Not guaranteed
Operational cost:	High	Low	Moderate	Low	Low to moderate
Reliability:	High	Varies	High	Usually high	High
CPU time:	Low	Very high	Low	Moderate	Low

Chapter 3

Statistical analysis of the error on RES-based generation forecasts

In this chapter, the focus is on the statistical, distribution-based description of the error on RES-based generation forecasts. Although non-parametrical approaches exist [100], the aim here is to capture the underlying stochastic processes that drive the forecast error in a statistical distribution. These distributions provide critical information on the accuracy of forecasts and facilitate proper reserve sizing and scenario generation techniques (Chapter 4). We developed the methodology below to study the wind power forecast error, in this chapter abbreviated as WPFE. The presented methodology is however more general and has been applied to e.g. solar power forecast errors (SPFE) [135]. We will briefly return to the error on solar power forecasts in Section 3.5.

First, we discuss some distributions proposed in the literature to describe wind power forecast errors and their relevance. We show that wind power forecast data is often assumed to follow a Gaussian or a so-called β-distribution, which might not be suited to fully describe the skewed and heavy-tailed character of WPFE data. The Lévy α-stable distribution is proposed as an improved description of the forecast error. Second, we introduce the methodology employed to obtain the distribution parameters from wind power forecast data. Third, based on recent historical wind power data, the feasibility of the Lévy α-stable distribution as a WPFE description is demonstrated. Last, we use the proposed methodology in three applications in Section 3.5. First, the added value of this improved

statistical model of the WPFE is illustrated in a state-of-the-art probabilistic reserve sizing method. Results show that this new statistical description of the WPFE can hold important information for short-term economic and operational (reliability) studies for power systems with a significant wind power penetration. Second, we analyze the difference in predictability of onshore and offshore wind power. Last, solar and wind power forecast errors are compared.

In the following sections, we present an analysis of real-life, day-ahead wind and solar power forecast data, in line with the proposed modeling framework to study short-term uncertainty in power systems (Chapter 1). In all applications, we study wind and solar power forecast and measurement data obtained from the Belgian TSO, Elia. Throughout the analysis presented in this chapter, a system perspective (aggregated wind farms in for example the control zone of a system operator or the portfolio of a power producer) has been adopted, albeit the analysis can be done for a single wind farm or turbine as well. The focus is on short-term forecasts[1] (here: 24 hours) with relatively long lead times (here: 13 hours (day-ahead forecasts) or 1 hour (intra-day forecasts))[2], in line with the modeling framework presented in Chapter 1. The analysis presented below is an updated version of that published in [99][3].

This chapter is based on the following papers:

- K. Bruninx and E. Delarue, *A Statistical Description of the Error on Wind Power Forecasts for Probabilistic Reserve Sizing*, IEEE Trans. Sustain. Energy, vol. 5, no. 3, pp. 995–1002, 2014.
- K. Bruninx, E. Delarue, and W. D'haeseleer, *Statistical description of the error on wind power forecasts via a Lévy alpha-stable distribution,* in YEEES 2012, Young Energy Engineers & Economists Seminar 2012, December 7, 2012, Florence, Italy and EUI RSCAS Working Paper 2013/50, 2013, pp. 1–8.

[1] The forecast horizon is the period over which a forecast is generated.

[2] The lead time of a forecast method is here defined as the time difference between the moment at which the forecast is made and the start of the forecast horizon. In the Belgian system, the lead time on the day-ahead wind and solar power forecast is 13 hours.

[3] In this dissertation, we only present an analysis of the wind power forecast error based on data from the Belgian power system, which will form the basis for our case studies in the following chapters. In [114], we perform a similar analysis for data obtained from 50Hertz, one of the four German TSOs. For sake of brevity, this analysis is not repeated here, as the qualitative conclusions are the same.

3.1 Introduction: wind power forecast errors

Various forecasting methods are being used and developed, ranging from basic persistence methods to complex statistical and physical models based on weather predictions [136]. None of these forecasting methods can generate a perfect wind power forecast (WPF). The error on a WPF has various sources: errors on the prediction of wind speed and direction, local effects due to the terrain, non-uniformity of the wind in a wind park, non-linearity in the dynamics of wind turbines, unplanned outages etc. [137, 138].

The operational and economical impact of the uncertainty on WPFs on the planning and operation of electricity generation systems has been studied extensively (e.g. [103, 139, 140, 141, 142, 143, 144, 145, 146, 147, 148, 149]). Makarov et al. [139] study the load-following capabilities of conventional power plants when faced with erroneous wind power and load forecasts in California. The wind power forecast error (WPFE) is modeled as a truncated normal distribution and fitted to measured wind power data. Doherty and O'Malley [140] present a probabilistic method to quantify the demand for reserves in power systems with a significant wind power capacity. The WPFE is modeled as a Gaussian variable with a zero mean and a certain standard deviation. Bouffard and Galiana [141] formulate a short-term electricity market-clearing problem in which the demand for reserves can be (partly) covered by wind power. The WPFE is modeled as Gaussian variable with a zero mean and non-zero variance. Bouffard and Galiana justify this assumption via a Central Limit Theorem (CLT) argument. Methaprayoon et al. [142] incorporate WPF uncertainty in a UC model via confidence intervals, based on the assumption that the WPFE follows a normal distribution. Ummels et al. [143] investigate the benefits of an optimal UC schedule for a thermal power plant in light of uncertain wind power forecasts. To characterize the WPFE, a Gaussian distribution is assumed. Delarue et al. [144, 145] investigate the effect of WPFEs on the economic dispatch problem, given a day-ahead UC schedule. A random normally distributed forecast error (zero mean, predefined standard deviation) is imposed on the wind power forecasts. Bludszuweit et al. [146, 147] employ the β-distribution to investigate the impact of WPFEs on optimal power ratings of energy storage systems. De Vos et al. [103] reviewed the Belgian support system to reduce imbalance costs for offshore wind power generators. Empirical statistical models of the forecast error are used to analyze the imbalance settlements. Bathurst et al. [148] assess the effect of imbalance prices and uncertain wind generation on the market behavior of a generator. Wind power forecast uncertainty is represented via so-called Markov chains. Fabbri et al. [149] quantify the operational cost associated with WPFEs. In their analysis, they employ a β-distribution to describe the WPFE.

A key element in all these studies is the probability density function (pdf) that is assumed to describe the wind power forecast error (WPFE). As the shape of the WPFE pdf is dependent on the forecast horizon and method, a proper definition for this pdf is hard to find. Up to today, mainly the Gaussian distribution [138, 140] and the so-called β-distribution (see Section 3.3) [146, 149] have been employed to describe the WPFE. Other distributions have been examined as well, such as the Cauchy distribution [150], the γ-distribution [151] and the Weibull distribution [152]. The analysis presented by Bludszuweit et al. [146] shows that the Gaussian distribution cannot describe the heavy-tailed character of the WPFE, an observation confirmed by Hodge et al. [150]. Bludszuweit et al. note that in some cases, the β-distribution is not sufficiently heavy-tailed to model the leptokurtosis[4] of the WPFE data, leading to an underestimation of the frequency of the largest errors. Obviously, these tails hold important information in reliability studies, as illustrated below. A number of approaches have been proposed to circumvent these shortcomings. Lange explores the idea to transform the well-behaved Gaussian distributions of the wind speed prediction errors into non-Gaussian distributions of the WPFE via Taylor expansions of the power curve of the wind farm in [153, 138]. However, this approach only accounts for the effect of the (equivalent) power curve of the wind turbine (park), neglecting all other effects. Pinson et al. [154, 155, 156, 36, 157] focus on the description of the WPFE from an operational vantage point. The WPFE is characterized via a non-parametric method. These characteristics are then employed to estimate and evaluate prediction intervals. Pinson et al. demonstrate the non-Gaussian character of the WPFE extensively. These results are further employed in the evaluation and design of ensemble prediction methods. However, one should treat the conclusions in this work with caution as the wind farms under consideration are relatively small (max. 21 MW) and therefore may not represent all effects found in present-day, large (aggregations of) wind farms. Tewari et al. [158] propose a mixed distribution function based on the Laplace distribution to model the WPFE at the level of a single wind farm. The distribution of the WPFE proposed by Tewari et al. is independent of the forecast.

In this chapter, the Lévy α-stable distribution is proposed as a novel, well-suited statistical model to describe the heavy-tailed character of the WPFE data. The rationale behind the choice for this distribution stems from the similarities that can be found between WPFE data and some financial data, such as the price of a stock (see Appendix D). Many of the concepts developed in finance (and WPFE analysis) rest upon the assumption that asset returns

[4]The kurtosis is a measure for the peakedness or tail weight of a distribution. It is the fourth standardized moment. Excess kurtosis is the fouth standardized moment minus the kurtosis of the Guassian distribution (3). Leptokurtic distributions are heavy-tailed compared to the Gaussian distribution (kurtosis > 3, excess kurtosis > 0).

follow a normal distribution. The strongest statistical argument for this choice is the central limit theorem. However, the empirical observations exhibit fat tails (financial data: [159, 160, 161, 162, 163], WPFE: [146, 150, 164]) – a characteristic that cannot be described through a normal distribution. Although various distributions could be used as heavy-tailed alternatives for the Gaussian distribution, the *generalized central limit theorem* (GCLT, see Appendix D) is invoked to motivate the use of stable distributions. In the GCLT the stable distributions are postulated as the only possible non-trivial limit distribution of normalized sums of independent and identically distributed random variables, such as the various sources driving the evolution of a stock price or the WPFE.

In the following sections, we present an approach similar to that of Bludszuweit et al. [146], which permits the quantification of the probability of a certain error ϵ given a certain wind power forecast G^{F}. The improved performance of the Lévy α-stable distribution compared to that of the Gaussian and β-distribution is demonstrated in a case study (Section 3.4.1). The Cauchy (a special case of the Lévy α-stable distribution), the γ-distribution (not general enough to capture the range of skewness and kurtosis values in WPFE data) and the Weibull-distribution (often used to describe wind speed data) are not further studied. The effect of the temporal (e.g. the forecast horizon or lead time [165]) and spatial resolution of the forecast data (e.g. spatial smoothing [166, 138]) is not explicitly discussed in this chapter. In [114], we analyze the adequacy of the Lévy α-stable distribution as a description of wind power forecast errors with varying lead times and forecast horizons. In line with the approach of Bludszuweit et al. [146], forecast scenarios were generated through the persistence approach[5]. Results show that the Lévy α-stable distribution outperforms the β- and Gaussian distribution as a description of the forecast error, except for very short prediction intervals and lead times (i.e., less than 2 hours). We will briefly return to spatial smoothing in Section 3.5 in the comparison of onshore and offshore wind power predictions.

3.2 The Lévy α-stable distribution

This section gives a brief overview of basic properties of the Lévy α-stable distribution. The effect of the various parameters of the distribution is illustrated (Fig. 3.1). It is not the goal to provide a full overview of the properties of the

[5]The persistence method is a very simple method to generate forecasts based on historical data. It is often used as a benchmark to compare forecasting methods [136]. In [114] it is employed to generate wind power forecast scenarios of different quality from a given wind power time series. The persistence method estimates the wind power generation on a certain interval $[t+k, t+k+T]$ as the average of a previous interval $[t-T, t]$ with the same length T [136]. T is the forecast horizon, k the lead time, t the moment at which the forecast is made.

stable distributions. For quick reference, a short discussion on the theoretical foundations of the Lévy α-stable distribution is provided in Appendix D. For a more complete discussion, the reader is referred to the specialized literature, such as (amongst others) Nolan [167, 168, 169], Zolotarev [170], Uchaikin and Zolotarev [171] and Samoradnitsky and Taqqu [172]. For the implementation of the stable distribution probability density function in MATLAB®, see Nolan [167].

The probability density function (pdf) and cumulative probability density function (cdf) of a Lévy α-stable distribution cannot be expressed in analytical form. The characteristic function $\phi(u)$ of a random stable variable X with cumulative distribution function F(x) can be parametrized and is most often written as in Samorodnitsky and Taqqu [172, 169] :

$$\phi(u) = E\left[\exp(iuX)\right] = \int_{-\infty}^{\infty} \exp(iux) dF(x) \tag{3.1}$$

$$= \begin{cases} \exp\left(-\gamma^{\alpha}|u|^{\alpha}[1 - i\beta - \tan(\frac{\pi\alpha}{2}) \cdot \text{sign}(u)] + i\delta u\right) & \leftrightarrow \alpha \neq 1 \\ \exp\left(-\gamma|u|[1 + i\beta - \frac{2}{\pi} \cdot \text{sign}(u) \cdot \ln|u|] + i\delta u\right) & \leftrightarrow \alpha = 1 \end{cases}$$

The parameters of this family of distributions $\text{S}(\alpha, \beta, \gamma, \delta)$ are:

- α, an index of stability $(0 < \alpha \leq 2)$;
- β, a skewness parameter $(-1 \leq \beta \leq 1)$;
- γ, a scale parameter $(\gamma > 0)$;
- δ, a location parameter $(\delta \in \Re)$.

The effect of the various parameters is visualized in Fig. 3.1[6]. The index of stability α determines the total probability contained in the tails, thus the kurtosis, of the distribution. The probability mass contained in the tails is inversely proportional to α. A positive skewness parameter β yields a distribution skewed to the right. The degree of skewness is larger as β increases. Similar reasoning applies to negative β-values. The third parameter γ defines the scale of the distribution and is linked to the variance σ^2 for $\alpha = 2$. The location parameter δ coincides with the mean of the distribution for $\alpha \geq 1$. For $\alpha < 1$, the mean of the distribution is not defined[7].

[6]The domain of the Lévy α-stable distribution is limited to $-10 \leq x \leq 10$ for Fig. 3.1 or $-G_j^{\text{F}} \leq \epsilon \leq 1 - G_j^{\text{F}}$ for the WPFE, with G_j^{F} the wind power forecast. The pdf is normalized as such that the integral of the pdf equals 1 on the supported domain.

[7]This can be generalized as follows: the p^{th} moment of a stable random variable is finite if and only if $p \leq \alpha$ [173]. Thus, for $\alpha < 1$, the first moment (mean) is not finite. For $1 \leq \alpha < 2$ the mean is finite, but the second moment (variance) is infinite. The variance is finite if and only if $\alpha = 2$.

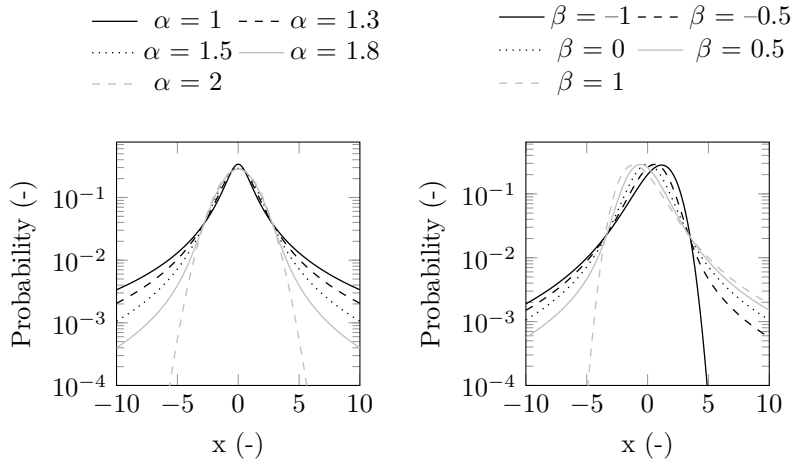

(a) $S(\alpha, 0, 1, 0)$

(b) $S(1.5, \beta, 1, 0)$

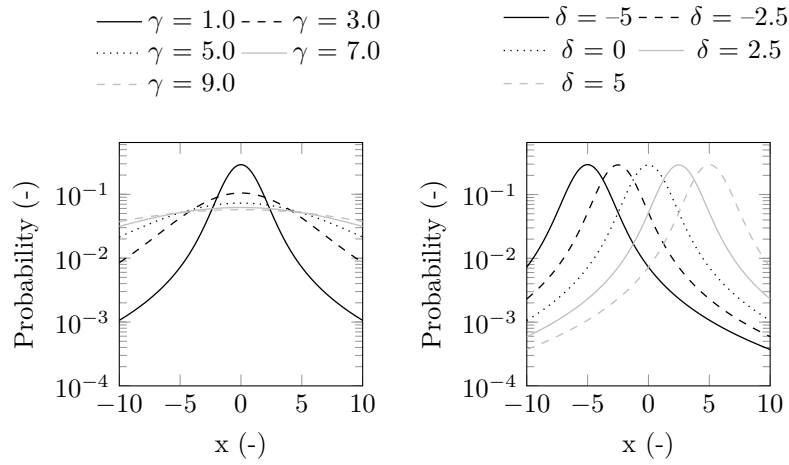

(c) $S(1.5, 0, \gamma, 0)$

(d) $S(1.5, 0, 1, \delta)$

Figure 3.1: The effect of the four parameters in the Lévy α-stable distribution. In each figure, one parameter is varied, while the others are kept constant. From left to right, top to bottom: the effect of α, β, γ and δ in the stable distribution.

The Gaussian ($\mathrm{N}(\mu, \sigma^2) \rightarrow \mathrm{S}(2, \beta, 2^{-0.5} \cdot \sigma, \mu)$), the Cauchy (scale γ and location δ: $\mathrm{C}(\delta, \gamma) \rightarrow \mathrm{S}(1, 0, \gamma, \delta)$) and the Lévy distribution (scale γ and location δ: $\mathrm{L}(\delta, \gamma) \rightarrow \mathrm{S}(0.5, 1, \gamma, \delta)$) are all stable distributions that can be described via the parametrization above. Only in these cases, the probability density function can be expressed analytically.

This lack of closed-form density functions complicates statistical inference for stable distributions, such as parameter estimation. Multiple methods have been developed [173]. The sample quantile method by McCulloch [174][8], a robust approach for $\alpha \geq 0.6$, has been used in this chapter (Section 3.3).

3.3 Methodology

As the behavior of the WPFE is highly dependent on the forecast, we focus on the joint distribution of the WPFE ϵ and the forecast G^{F}, further denoted by $f(\epsilon, G^{\mathrm{F}})$[9]. This joint distribution can be studied indirectly by focusing on the conditional (here: the observations of the forecast error ϵ given the forecasts $f(\epsilon|G^{\mathrm{F}})$) and the marginal (here: $f(G^{\mathrm{F}})$) distributions of $f(\epsilon, G^{\mathrm{F}})$. The distribution of the WPFE can hereby be approximated as $f(\epsilon, G^{\mathrm{F}}) \approx f(G^{\mathrm{F}}) \cdot f(\epsilon|G^{\mathrm{F}})$. This approach is known as the Murphy-Winkler verification framework [176].

The methodology employed in this chapter consists of four main steps. First, the conditional WPFE is calculated. In a second step, the parameters of the conditional distributions $f(\epsilon|G^{\mathrm{F}})$ are obtained. Third, the fit of the distribution is optimized. Last, the unconditional WPFE pdf $f(\epsilon)$ is assembled.

Step 1: calculating the conditional error

To obtain an empirical distribution for the WPFE, a similar methodology as in [146] is employed. Assume wind power forecast and measurement data are available, normalized w.r.t. the installed wind power capacity. First, the measured and forecasted wind power time series are sorted into power classes

[8] As shown by Weron [175], large datasets ($O(10^6)$ samples) are needed to adequately estimate the tail index, especially when the actual tail index is close to 2. Some estimators, such as the log-log regression method or the Hill estimator, may lead to gross over-estimations of the tail index. The McCulloch approach [163] is more robust and will not yield values greater than 2. Results should however still be regarded as estimates and interpreted with caution.

[9] Other dependencies of the forecast error, such as the inter-temporal dependencies between forecast errors and the dependency of the forecast error on the lead time of the forecast, are not studied. They may however be studied via the method presented in this section.

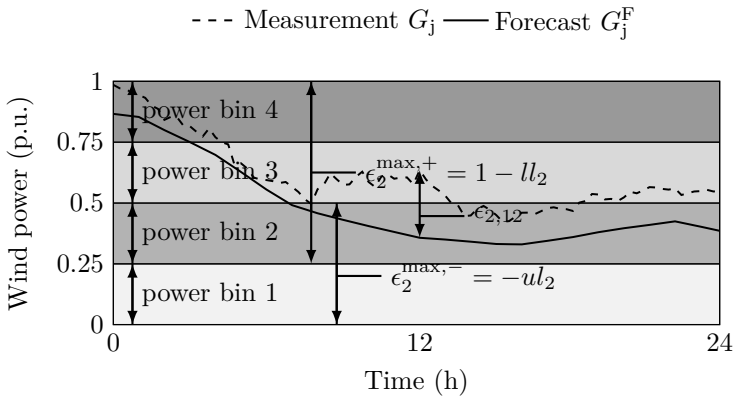

Figure 3.2: Conceptual illustration of the calculation of the conditional error. If the chosen power bin width W is 0.25 p.u., the data will be sorted in four power bins, based on the value of the forecast G_j^F. This is illustrated for the 12^{th} time step: as the forecasted wind power G_{12}^F lies within the second power bin, the error $\epsilon_{2,12}$ is sorted in this power bin. $\epsilon_2^{max,+}$ is the maximum positive forecast error that can be sorted in power bin 2, $\epsilon_2^{max,-}$ the largest negative forecast error, constrained by the lower ll_b and upper limit ul_b of the corresponding power bin.

or bins (index b, set B) with a certain width W according to the corresponding forecast G_j^F at time step j. The normalized conditional prediction error $\epsilon_{b,j}$ is defined as the difference between the measured G_j and the forecasted wind power G_j^F on each time step j and is assigned to a power bin b:

$$\epsilon_{b,j} = G_j - G_j^F \quad \leftrightarrow \quad ll_b \leq G_j^F < ul_b \tag{3.2}$$

In this equation, G_j^F is the wind power forecast that belongs to power bin b (lower limit ll_b and upper limit ul_b) on time step j and similarly, G_j is the measured wind power. With these WPFE data series (one per power bin), the empirical histogram of the error $\epsilon_{b,j}$ can be obtained for each forecast bin b. The resolution of this histogram (width of the intervals) is chosen equal to that of the WPF. This approach is conceptually illustrated in Fig. 3.2.

Step 2: obtaining estimates of the parameters of the distributions

The Gaussian, β and Lévy α-stable distributions are used to describe the WPFE. The parameters of the distributions, which will serve as starting values for the

optimization in Step 3, are estimated as follows:

The Gaussian distribution $N(\mu_\mathrm{b}, \sigma_\mathrm{b}^2)$ The mean μ_b and the standard deviation σ_b are calculated directly from the data sample for each power bin b.

The β-distribution $B(a_\mathrm{b}, b_\mathrm{b}, p_\mathrm{b}, q_\mathrm{b})$ The β-distribution according to Johnson [177] is characterized by four parameters. This distribution yields non-zero values on the interval $[a_\mathrm{b}, b_\mathrm{b}]$, here fixed on $[-ul_\mathrm{b}, 1 - ll_\mathrm{b}]$ (Fig. 3.2). The parameters p_b and q_b are restricted to positive values. The mean μ_b and the variance σ_b^2 of the data are related to the p_b and q_b-shape parameters of the β-distribution via the method-of-moments [177]:

$$p_\mathrm{b} = \frac{(1-\mu_\mathrm{b}) \cdot \mu_\mathrm{b}^2}{\sigma_\mathrm{b}^2} - \mu_\mathrm{b} \qquad\qquad q_\mathrm{b} = \frac{1-\mu_\mathrm{b}}{\mu_\mathrm{b}} \cdot p_\mathrm{b} \tag{3.3}$$

The Lévy α-stable distribution $\mathrm{S}(\alpha_\mathrm{b}, \beta_\mathrm{b}, \gamma_\mathrm{b}, \delta_\mathrm{b})$ The parameters of the stable distribution are estimated via the quantile approach by McCulloch[10] [174], the equivalent Gaussian and Cauchy distribution. In the latter case, γ_b has been chosen arbitrarily equal to one and the location parameter δ_b has been set to the position of the maximum in the empirical histogram.

Step 3: least-squares fit

The estimates of the parameters of all distributions are refined for each power bin via a least-squares fitting method, applied to the pdf. The supported domain of each distribution is limited to the possible range of non-zero error values $[-ul_\mathrm{b}, 1-ll_\mathrm{b}]$ (Fig. 3.2). The pdf is normalized such that the integral of the pdf equals 1 on the supported domain. Note that this least-squares fit is not strictly necessary. However, the estimates of the parameters of the distributions are of varying quality. To ensure a fair comparison between the different distributions, we optimize the parameters of the distributions, considering the same objective function.

Step 4: assembling the probability density function

To obtain an unconditional pdf for the WPFE, the pdfs of each bin $f_\mathrm{b}(\epsilon_\mathrm{b})$ are combined via the empirical probability that a wind power forecast will be an

[10] This approach is only robust for $\alpha \geq 0.6$. As will be shown in Section 3.4.2, the values of α_b are in this case well above this treshold.

element of that bin $f_{\mathrm{b}}(G^{\mathrm{F}})$:

$$f(\epsilon|a^1,\ldots,a^{\mathrm{N_P}}) = \sum_{\mathrm{b}=1}^{\mathrm{N_b}} f_{\mathrm{b}}(G^{\mathrm{F}}_{\mathrm{j}}) \cdot f_{\mathrm{b}}(\epsilon|a^1_{\mathrm{b}},\ldots,a^{\mathrm{N_P}}_{\mathrm{b}}) \tag{3.4}$$

where N_{b} is the number of bins defined, N_{p} is the number of parameters $(a^1,\ldots,a^{\mathrm{N_P}})$ in the chosen distribution $f_{\mathrm{b}}(\epsilon_{\mathrm{b}})$ and $f_{\mathrm{b}}(G^{\mathrm{F}})$ the empirical distribution of the forecasts over the power bins.

3.4 Results & discussion

Wind power data for 2012–2014, 102,031 data points in total, was taken from the Belgian TSO Elia N.V. [178, 179][11]. Based on these time series, we constructed the historical, normalized WPFE. This data is used to demonstrate the higher accuracy of the WPFE description based on the stable distribution, especially in capturing the tail behavior, compared to descriptions based on the Gaussian and the β-distribution. In the analysis below, the power bin width has been chosen equal to 0.025 p.u., resulting in 40 power bins[12].

3.4.1 Statistical analysis of the WPFE data

Table 3.1 summarizes the results of our statistical analysis. For each power bin, we list the lower ll_{b} and upper limit ul_{b} of that power bin, the percentage of forecasts that belongs to that bin $f_{\mathrm{b}}(G^{\mathrm{F}})$, the bias μ_{b}, the standard deviation σ_{b}, the skewness γ^1_{b} and kurtosis γ^2_{b} of the data in that power bin. In addition, we report the optimized parameters of the fitted Lévy α-stable distribution in each power bin. We will discuss these values in Section 3.4.2. No values are reported for power bins 38 to 40, as these contain less than 0.07% of the wind power data (70 data points in total).

The Normalized Root Mean Square Error (NRMSE) of the wind power forecast varies between 0.0421 and 0.0996 p.u. The high values for the NRMSE in

[11]The Belgian TSO Elia publishes day-ahead forecasted and measured wind power production profiles with a temporal resolution of 15 minutes as of January 2012. The forecasts are generated via a hybrid model, combining statistical algorithms, numerical weather prediction models and physical models of the wind turbines. The forecasts are published at 11 a.m. for the next day. The installed, monitored capacity varies from 930.65 MW (January 2012) to 1,835 MW (December 2014).

[12]This power bin width is a compromise between the level of detail needed to describe the distribution adequately within a power bin – pushing for a small power bin width – and the amount of data needed in each power bin to perform a meaningful statistical analysis, yielding a lower limit on the number of elements in a power bin, thus the power bin width.

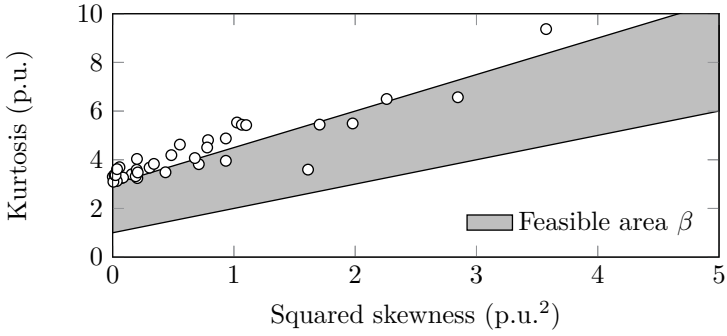

Figure 3.3: The majority of the observed values of (squared) skewness and kurtosis in the WPFE data are situated outside the feasible area of the Gaussian (kurtosis 3, skewness 0) and β-distribution (grey area).

certain power bins should be interpreted with caution, as these power bins may contain few data points – a remark that holds for the remainder of this case study. In general, the NRMSE in a power bin b rises as the probability that a forecast belongs to that power bin $f_{\mathrm{b}}(G^{\mathrm{F}})$ decreases. The bias varies from -0.0696 to 0.0270 p.u. over the power bins. The average[13] bias amounts to -0.008 p.u. Note that the non-zero bias implies that the zero-bias assumption in, among others, [141, 140, 139, 143] thus does not hold. The average standard deviation equals 0.081 p.u. and varies between 0.0322 and 0.0982 p.u. The skewness, as a measure for the asymmetry of the data, exhibits positive values in the lower power bins and negative values in the higher power bins, in line with our expectations. The skewness varies between -3.159 and 0.966. The kurtosis, as a measure of the peakedness of the distribution, varies here between 3.09 and 17.76. The average kurtosis amounts to 4.86. These values are in line with the literature [146, 150] and confirm the reported leptokurtic character of WPFE data. From Fig. 3.3, showing the possible values for the kurtosis and skewness of the β-distribution and the observed values in the WPFE time series for each power bin b, it is clear that the Gaussian and β-distribution do not allow capturing the asymmetry and peakedness of the WPFE data. The majority of the power bins are characterized by kurtosis values outside the feasible range of the β-distribution (grey area in Fig. 3.3).

[13]The reported averages are arithmetic averages and should thus not be interpreted as measure of the performance of the forecasting method at hand. A probability-weighted average of the bias, accounting for the probability of occurrence of a certain forecast, amounts to 0.0055 p.u.

Table 3.1: Based on wind power data for 2012-2014 obtained from the Belgian TSO Elia, we calculated the percentage of forecasts that belongs to power bin b ($f_{\mathrm{b}}(G^{\mathrm{F}})$), the bias μ_{b}, the standard deviation σ_{b}, the skewness γ_{b}^1 and kurtosis γ_{b}^2 of the data in that power bin. The last four columns contain the optimized parameters of the fitted Lévy α-stable distribution in each power bin.

b	ll_{b}	ul_{b}	$f_{\mathrm{b}}(G^{\mathrm{F}})$	μ_{b}	σ_{b}	γ_{b}^1	γ_{b}^2	α_{b}	β_{b}	γ_{b}	δ_{b}
(-)	(p.u.)	(p.u.)	(%)	(p.u.)	(p.u.)	(p.u.)	(p.u.)	(-)	(-)	(-)	(-)
1	0	0.025	9.99	0.027	0.032	0.966	3.956	1.454	0.999	0.023	0.040
2	0.025	0.05	7.56	0.025	0.038	0.843	3.819	1.856	1.000	0.027	0.022
3	0.05	0.075	6.45	0.025	0.049	0.966	4.875	1.621	0.861	0.033	0.030
4	0.075	0.1	5.63	0.026	0.059	0.887	4.806	1.888	1.000	0.040	0.021
5	0.1	0.125	5.33	0.022	0.066	1.013	5.530	1.616	0.867	0.042	0.031
6	0.125	0.15	4.48	0.018	0.067	0.744	4.624	1.866	1.000	0.044	0.018
7	0.15	0.175	4.17	0.012	0.072	0.552	3.676	1.870	1.000	0.048	0.011
8	0.175	0.2	4.07	0.011	0.081	0.660	3.485	1.642	0.876	0.051	0.020
9	0.2	0.225	3.86	0.006	0.078	0.451	3.247	1.883	1.000	0.053	0.004
10	0.225	0.25	3.78	0.004	0.082	0.396	3.402	1.902	1.000	0.056	0.003
11	0.25	0.275	3.05	-0.001	0.093	0.270	3.248	1.821	0.352	0.063	0.000
12	0.275	0.3	3.17	-0.001	0.093	0.445	3.588	1.857	0.995	0.063	-0.001
13	0.3	0.325	2.72	0.001	0.093	0.293	3.270	2.000	0.000	0.065	-0.005
14	0.325	0.35	2.88	-0.001	0.096	0.185	3.126	2.000	1.000	0.068	-0.004
15	0.35	0.375	2.66	-0.008	0.091	0.036	3.302	1.980	-0.230	0.064	-0.008
16	0.375	0.4	2.46	-0.013	0.093	-0.078	3.096	2.000	0.000	0.066	-0.012
17	0.4	0.425	2.31	-0.012	0.096	-0.237	3.693	1.629	-0.618	0.063	-0.028
18	0.425	0.45	2.32	-0.009	0.093	-0.436	3.321	1.584	-0.890	0.062	-0.033
19	0.45	0.475	2.09	-0.016	0.089	-0.126	3.385	2.000	0.000	0.062	-0.013
20	0.475	0.5	1.96	-0.014	0.093	-0.155	3.369	1.915	-0.054	0.063	-0.013
21	0.5	0.525	1.82	-0.012	0.098	-0.190	3.614	1.885	-0.407	0.066	-0.013
22	0.525	0.55	1.61	-0.013	0.091	-0.448	4.033	1.910	-0.969	0.061	-0.013
23	0.55	0.575	1.55	-0.008	0.092	-0.455	3.478	1.843	-0.999	0.062	-0.011
24	0.575	0.6	1.52	-0.009	0.087	-0.583	3.830	1.657	-0.999	0.057	-0.025
25	0.6	0.625	1.39	-0.012	0.085	-0.696	4.190	1.412	-0.233	0.053	-0.016
26	0.625	0.65	1.13	-0.015	0.088	-0.883	4.504	1.617	-0.126	0.052	-0.006
27	0.65	0.675	1.01	-0.021	0.096	-0.823	4.070	1.854	-0.869	0.060	-0.016
28	0.675	0.7	1.06	-0.020	0.091	-1.032	5.438	1.776	-1.000	0.058	-0.023
29	0.7	0.725	1.13	-0.026	0.089	-1.049	5.423	1.584	-0.946	0.055	-0.044
30	0.725	0.75	1.03	-0.026	0.096	-1.407	5.492	1.414	-0.944	0.048	-0.051
31	0.75	0.775	0.93	-0.019	0.093	-1.687	6.568	1.219	-0.794	0.041	-0.077
32	0.775	0.8	0.94	-0.022	0.086	-1.503	6.496	1.550	-0.984	0.043	-0.030
33	0.8	0.825	0.93	-0.024	0.083	-1.891	9.369	1.679	-1.000	0.042	-0.028
34	0.825	0.85	0.81	-0.024	0.069	-1.306	5.444	1.667	-1.000	0.040	-0.023
35	0.85	0.875	0.77	-0.033	0.072	-2.156	11.804	1.382	-0.918	0.034	-0.052
36	0.875	0.9	0.85	-0.040	0.074	-3.159	17.764	1.268	-0.998	0.029	-0.079
37	0.9	0.925	0.52	-0.070	0.071	-1.269	3.595	1.100	-0.942	0.027	-0.191

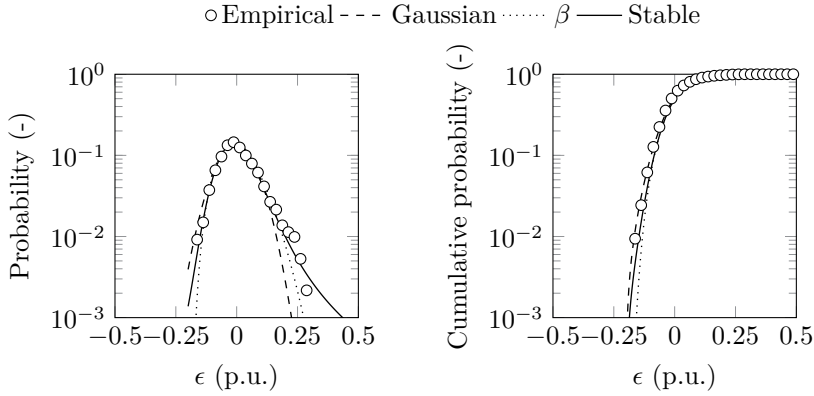

(a) pdf **(b)** cdf

Figure 3.4: The empirical histogram, the fitted pdf and cdf for the 8$^{\text{th}}$ power bin. The β– and Gaussian distribution exhibit a comparable performance. The stable distribution allows for the best fit. Note the asymmetry of the data: as the 8$^{\text{th}}$ power bin contains forecasts between 0.175 and 0.2 p.u., the error must fall in the interval [−0.2 p.u., 0.825 p.u.].

3.4.2 Description of the WPFE via a stable distribution

The adequacy of the stable distribution as a WPFE description is compared against the performance of the normal and the β-distribution. An example of the fitted distributions is displayed in Fig. 3.4 for the 8$^{\text{th}}$ power bin. The data in this power bin is asymmetric (skewness: 0.66) and leptokurtic (kurtosis: 3.485) (Table 3.1). The Gaussian and β-distribution do not allow capturing this behavior, the stable distribution does (Fig. 3.4).

With similar results in the other power bins, the overall pdf and cdf can be constructed (Fig. 3.5). Note that only the stable distribution captures the heavy-tailed character of the WPFE data. This is most evident for the left tail of the distribution. The Gaussian and β-distribution underestimate the probability of large negative errors. The pp-plot and qq-plot confirm this observation. The qq-plot, a plot of the empirical percentiles of the WPFE data versus the percentiles of the proposed distribution, shows that the tails of the distributions, i.e. the low and high percentiles, are not adequately captured by the Gaussian and β-distribution. In all but the 99$^{\text{th}}$ percentile, the stable distribution captures the behavior of the WPFE data, as the theoretical and empirical quantiles are in line.

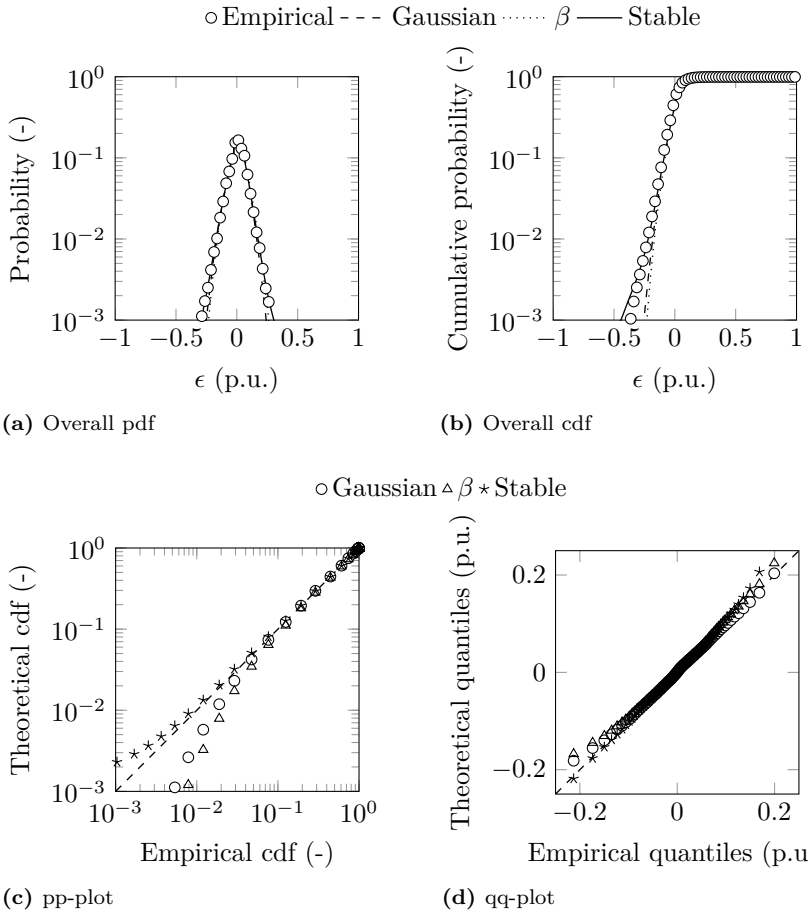

(a) Overall pdf **(b)** Overall cdf

(c) pp-plot **(d)** qq-plot

Figure 3.5: The stable distribution allows for a notably better fit of the WPFE data compared to the Gaussian and β-distribution. (a) Overall empirical histogram and fitted distributions (pdf). (b) Overall empirical cumulative histogram and fitted distributions (cdf). Note that the left tail of the empirical distribution is only captured by the stable distribution. (c) Overall pp-plot, showing the proposed ('theoretical') cdf as a function of the empirical cdf. (d) Overall qq-plot, plotting the theoretical quanitles (percentiles) of the fitted distributions as a function of the empirical quantiles.

The optimized tail index α_b varies between 1.09 and 2, with an average value of 1.708 (heavy tailed data) (Table 3.1). The confidence intervals of the estimated tail index, estimated based on Englezos and Kalogerakis [180], are on average 0.2 wide (+0.1,−0.1), confirming the heavy-tailed character of the underlying distributions. The trend of decreasing skewness values with rising power bin numbers observed in the data can also be found in the values of the optimized skewness parameter β_b. The location parameter δ_b exhibits the same behavior as the bias of the WPFE data: low power bin numbers show a positive bias, while higher power bin numbers are characterized by a negative bias. The scale parameter (γ_b) is situated between 0.023 - 0.068 and has an average value of 0.051. The stable distribution tends towards a normal distribution ($\alpha_b \to 2$, $\gamma_b \to 2^{-0.5} \cdot \sigma_b$, $\delta_b \to \mu_b$) in 4 power bins. The kurtosis and skewness values of the data in these power bins are comparable to the skewness (0) and kurtosis (3) of the normal distribution, explaining these results.

In conclusion, the stable distribution provides us with an adequate statistical description of the WPFE data, for each power bin and for the overall pdf/cdf. It is capable of capturing the heavy tails of the WPFE data, which can hold important information for short-term power system reliability studies, as illustrated in a probabilistic reserve sizing method in the next section.

3.5 Applications

The relevance of the proposed methodology and an adequate statistical description of the forecast error is illustrated in three applications. First, we study a probabilistic reserve sizing method [151, 165, 102, 181], for which a detailed description of the tails of the WPFE data is essential. These state-of-the-art reserve sizing strategies show substantial potential for reserve capacity and operational cost reductions compared to the current static reserve strategies, as they are dependent on the level of uncertainty present in the power system [165]. Transmission system operators (TSOs) are currently studying the implementation of such probabilistic reserve calculation methods [165, 182, 4]. For a detailed discussion on the sizing and allocation of operational reserves in light of increasing wind power penetration levels, see [26]. Results indicate that only the stable distribution is capable of capturing the tails of the distribution, ensuring adequate reserve sizing. Second, we analyze the difference in predictability of onshore and offshore wind power in the Belgian power system. Third, the error on solar power forecasts is compared to the error on wind power forecasts, again using data from the Belgian TSO, Elia. The results presented in this section are dependent on the data and power system studied and are not to be generalized.

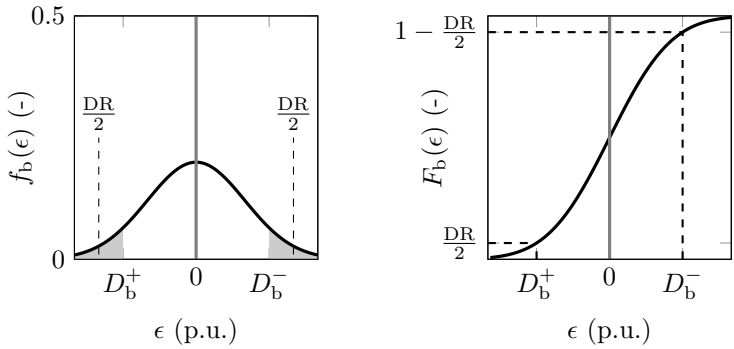

Figure 3.6: Conceptual example of the calculation of the required reserves for a power bin b. Given the design reliability DR and the cdf or pdf of the WPFE in power bin b, the upward D_{b}^{+} and downward reserve requirements D_{b}^{-} can be calculated.

3.5.1 Probabilistic reserve sizing & reliability

Upward and downward reserves are calculated per forecast power bin, based on the fitted probability density function. The reserves are sized to cover a certain percentage – i.e. a certain cumulative probability – of the WPFE. This percentage will be referred to as the *design reliability* or DR of the reserve requirement. The cumulative probability of forecast errors that are not covered by the reserves is equally distributed over the upward and downward reserves. For each forecast power bin b, upward D_{b}^{+} and downward D_{b}^{-} reserves are thus determined as the smallest amounts of reserves that satisfy the following inequalities

$$F_{\mathrm{b}}(D_{\mathrm{b}}^{+}) \leq \frac{DR}{2} \tag{3.5}$$

$$F_{\mathrm{b}}(D_{\mathrm{b}}^{-}) \geq 1 - \frac{DR}{2} \tag{3.6}$$

with $F_{\mathrm{b}}(\epsilon)$ the cdf of the forecast error ϵ for power bin b (Fig. 3.6). Alternatively, the reserves can be calculated directly from the pdf of the forecast error, as illustrated in Fig. 3.6. Based on the fitted distributions and Eq. (3.5) and (3.6), we can calculate the required amount of upward and downward reserves to ensure a certain design reliability level (DR) per power bin. For the stable

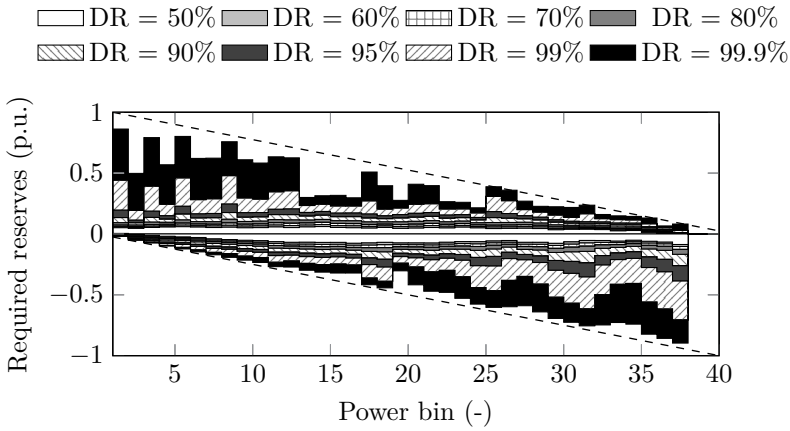

Figure 3.7: Upward (negative values) and downward (positive values) reserve requirements per power bin for DR levels between 50% and 99.9%. The dotted lines indicate the required reserves for a reliability level of 100%. Higher reliability levels require more reserves, but high reliability levels could be attained without scheduling reserves for the full wind power capacity.

distribution and DR levels ranging from 50% to 99.9%, the result of this calculation for each power bin b is shown in Fig. 3.7. As expected, higher reliability levels require more reserves. Note that high reliability levels could be attained without scheduling reserves for the full wind power capacity[14] (dotted lines in Fig 3.7). Furthermore, there are large differences between the required reserves for forecasts in the different power bins, especially for high reliability levels. This can partially be explained by the non-linearity of the wind power curve [137], which can cause small errors on the forecasted wind speed to result in large errors on the forecasted wind power. For example, the high levels of upward reserves for high forecast levels (power bins 27 and higher) may result from wind speed forecasts close to the cut-out speed[15] of the wind turbines. If the actual wind speed is slightly higher than the cut-out speed of certain wind turbines, this results in a large, negative WPFE. To be able to mediate these large WPFE errors, high levels of upward reserves are required. Recall however that the results visualized in Fig. 3.7 are a reflection of the distribution of the observed day-ahead wind power forecast error in the Belgian power system, and

[14]This is the reserve capacity that covers the full range of wind power forecast errors that could occur, given the forecast G^{F}: $[-G^{\mathrm{F}}, 1 - G^{\mathrm{F}}]$ (Fig. 3.2).

[15]The cut-out wind speed of a wind turbine is the maximal wind speed at which a turbine can produce power. At higher wind speeds, the turbine is forced to a standstill to avoid damage to the rotor.

is hence dependent on the employed wind power forecasting methodology. The observations above should thus not be generalized.

The proposed reserves should ensure the theoretical reliability level they are calculated for. In Table 3.2 the design reliability DR is compared with the actual reliability that the reserves, as calculated from the proposed distributions, would yield. To calculate the actual reliability, we use the forecasted and measured wind power production from Elia N.V. [179]. Given the forecast, the required reserves are determined for each time step. The actual reliability is then calculated as the ratio of the number of time steps that sufficient capacity would have been procured under the form of reserves to cover the observed wind power forecast error versus the total number of samples in the time series, in this case 102,031. As is evident from Table 3.2, the design reliability levels DR are only reached for low reliability levels if the reserves were calculated from the Gaussian and the β-distribution (70% and 80%). For higher reliability levels, only the stable distribution yields reserves that ensure the design reliability. The reason behind this result is simple: as reliability levels increase, the tails of the WPFE data become increasingly important in the determination of the reserve requirements. As only the stable distribution captures this behavior, only this distribution yields reserve requirements adequate to reach the design reliability DR.

Note that we here postulate a design reliability, equal for each power bin, without regard for the cost of ensuring that reliability. A reserve calculation method should balance the cost of providing these reserves and the pursued reliability [26]. Ideally, the chosen design reliability is the result of a trade-off between the cost of reserve procurement and deployment and the associated expected benefit, i.e. the avoided volumes of load shedding and wind power curtailment [93, 46]. For sake of simplicity, we have postulated a (range for the) design reliability, equal for each power bin, which allows us to illustrate the importance of an adequate representation of the tails of the WPFE distribution.

Furthermore, it is implicitly assumed that the only uncertainty in the system stems from wind power forecasts. In reality, reserves are designed to cope with various sources of uncertainty, such as imperfect demand forecasts, unplanned generator outages etc. However, the proposed methodology could easily be extended to incorporate multiple sources of uncertainty. One could, via the presented framework (Chapter 1), study the relevant sources of uncertainty and calculate the overall pdf through a convolution of the individual pdfs[16]. For example, in the context of imperfect solar and wind power forecast, we have studied the benefits of a coordinated approach to reserve allocation and

[16]This approach is valid if the sources of uncertainty are statistically independent. Note that the convolution should be performed on a per MW basis, not a p.u. basis.

Table 3.2: Design and actual reliability for reserve requirements based on the proposed distributions.

DR	Actual reliability		
	Gaussian	β	Lévy α-stable
50	49.1	48.8	48.9
60	59.8	59.6	**60.4**
70	**70.7**	**70.6**	**72.1**
80	**80.9**	**80.7**	**82.6**
90	89.6	89.7	**92.0**
95	93.5	93.9	**96.3**
99	97.4	97.7	**99.5**
99.9	98.9	99.2	**99.9**

activation in [94]. In this paper, the wind and solar power forecast errors were characterized via conditional pdfs, obtained with the approach above. To calculate the reserve requirement, these pdfs were combined via a convolution of the relevant pdfs at each time step[17]. Alternatively, one could apply the presented methodology to the net-load forecast error.

3.5.2 Predictability of onshore and offshore wind power in the Belgian power system

Wind power data for 2012-2014 was taken from the Belgian TSO Elia N.V. The total monitored capacity varies from 930.65 MW to 1,835 MW. The onshore wind power capacity varies between 736 MW and 1,123 MW. The offshore wind power capacity increased from 195 MW in 2012 to 712 MW at the end of 2014. Based on these time series, we constructed the historical, normalized WPFE time series (day-ahead forecasts and real-time measurements) for onshore and offshore wind power in the Belgian power system. Again, the power bin width has been chosen equal to 0.025 p.u., resulting in 40 power bins. Based on the methodology presented above, we constructed the overall pdf of the forecast error on onshore and offshore wind (Fig. 3.8).

Our analysis shows that in the period 2012-2014, offshore wind power was less predictable than onshore wind power in the Belgian power system. The NRMSE

[17]For wind and solar power forecast errors in the Belgian power system, the required assumption of statistical independence holds: in the period 2012-2014, the Belgian wind and solar power forecast error exhibit a correlation coefficient of less than 0.01 (p-value: 0.14, with a null-hypothesis 'existence of a correlation').

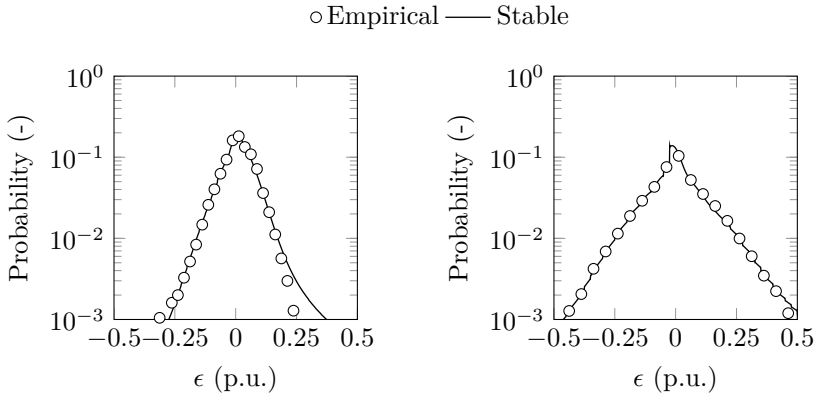

(a) Onshore WPFE **(b)** Offshore WPFE

Figure 3.8: The probability density function of the day-ahead wind power forecast error for onshore and offshore wind. In the period 2012–2014, offshore wind in the Belgian power system was less predictable: the probability of large errors is higher for offshore wind power forecasts than for onshore forecasts.

varies between 0.031 and 0.126 p.u. over the power bins for onshore wind power, with an average value of 0.084 p.u. These values are to be compared to a NRMSE between 0.039 and 0.1972 p.u. (average: 0.155 p.u.) for offshore wind power. Comparing the bias, standard deviation, skewness and kurtosis of the two time series, the high standard deviation of the offshore wind power forecast error is striking. The standard deviation varies between 0.037 p.u. and 0.19 p.u. for offshore wind power, compared to a standard deviation between 0.015 p.u. and 0.115 p.u. for onshore wind power. The bias of the errors on onshore and offshore wind power forecasts is comparable. On average, the bias equals -0.0125 p.u. (onshore) and -0.006 p.u. (offshore) respectively. Both time series are skewed and heavy-tailed. These metrics follow the trends discussed in Section 3.4.1. For offshore wind, these trends are somewhat more pronounced. The resulting empirical and fitted stable distribution is shown in Fig. 3.8. In both cases, the stable distribution is an adequate representation of the WPFE.

This difference in predictability may have various reasons. First, onshore wind turbines are spread out over a larger geographical area, which may smooth out the forecast error. Positive and negative forecast errors may cancel out. Likewise, errors in the timeliness of the forecast may be smoothed. In contrast, the Belgian offshore wind power capacity is concentrated on a relatively small geographical area. This increase in predictability with the size of the geographical area is referred to as spatial smoothing [166, 138]. Second, a specific support mechanism for offshore wind is currently in place in Belgium, which obliges the TSO to settle

a significant part of the imbalances, caused by erroneous forecasts of offshore wind power production, at beneficial rates [103]. This support mechanism may provide insufficient incentives for offshore wind power producers to improve their forecast models.

3.5.3 The equivalence of solar and wind power forecast errors

Solar power data for 2013-2014 was taken from the Belgian TSO Elia [183][18]. Elia reports day-ahead and intra-day forecasts. The day-ahead forecasts are published at 11 a.m. for the next day, simultaneously with the wind power forecasts. At the same time, the intra-day forecast is published, i.e. the forecast for the rest of that day (11 a.m. to 11 a.m. the next day). The total monitored capacity varies from 2,211 MW (January 2013) to 2,915 MW (December 2014). Based on these time series, we constructed the historical, normalized SPFE (solar power forecast error) time series for the Belgian power system. Only data in hours between sunrise and sunset have been considered. Again, the power bin width has been chosen equal to 0.025 p.u., resulting in 40 power bins. Based on the methodology presented above, we constructed the overall pdf of the day-ahead and intra-day solar power forecast error. We performed a statistical analysis on both time series, similar to the analysis we did for the wind power forecast error. For sake of brevity, we will not discuss any details of this analysis, but present an overview of the results. We will focus on (i) the differences and similarities between solar and wind power forecast errors and (ii) the improvement in forecast accuracy moving from day-ahead to intra-day forecasts.

The equivalence of day-ahead solar and wind power forecast errors

Obviously, solar and wind power forecasts are fundamentally different. Whereas solar power follows a clear diurnal pattern, wind power forecasts introduce uncertainty throughout the day. However, looking at the day-ahead forecast error as a function of the forecast itself, i.e. $f(\epsilon, G^{\mathrm{F}})$, remarkable similarities are to be noted.

First, the accuracy of both forecasts is comparable. The NRMSE varies between 0.012 p.u. and 0.12 p.u. for the day-ahead solar power forecast, compared to 0.042 p.u. to 0.10 p.u. for the day-ahead wind power forecast. On average, the NRMSE equals 0.087 p.u. (solar) and 0.085 p.u. (wind). Solar power forecasts are more accurate in the lower power bins (low solar power forecasts). The

[18] Prior to November 14, 2012, no solar power forecast data was reported by Elia.

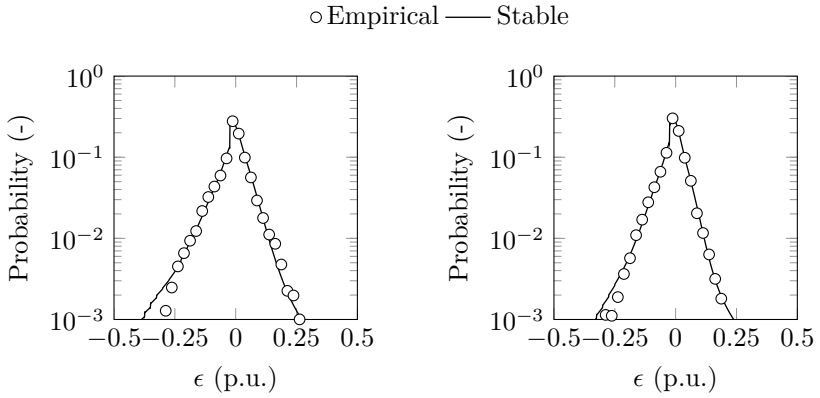

(a) Day-ahead SPFE **(b)** Intra-day SPFE

Figure 3.9: The histogram and the fitted stable pdf for the day-ahead and intraday solar power forecast error (SPFE).

same trend of rising inaccuracy with the power bin number (thus forecast) as for the day-ahead wind power forecast can be observed. Second, the bias and standard deviation of the day-ahead forecast error are similar for solar and wind power. Not only their average value, but also the range and trends observed in the bias and standard deviation of day-ahead wind power forecast errors are again observed in the solar power forecast error data. The bias of the solar (wind) power forecast error equals on average −0.026 p.u. (−0.008 p.u) and ranges from −0.065 p.u to 0.008 p.u. (−0.07 p.u. to 0.027 p.u.). Low forecast power bins are characterized by a positive bias, high forecast power bins exhibit negative values. The standard deviation rises with the power bin number, but levels off around power bin 10 (i.e. for forecasts exceeding 0.25 p.u.). For the solar power forecast error, standard deviations are found between 0.0124 p.u. and 0.109 p.u. (0.082 p.u. on average). Similar values are observed in the wind power forecast error data, with standard deviations between 0.032 p.u. and 0.0982 p.u. (0.082 p.u. on average). Also the skewness shows a similar evolution over the power bins for the solar and wind power forecast error. Excluding the extreme skewness values observed in the first and second solar power bin, the average skewness of the solar power forecast error equals 1.37 p.u, which is to be compared with 1.01 p.u. for wind. The kurtosis of the solar power forecast error ranges from 2.5 to 7.35, excluding the extreme values observed in the first and second power bin. On average, the kurtosis equals 4.33 p.u. (5.87 p.u. including the values of the first and second power bin), which is to be compared with 4.86 p.u. for the wind power forecast error. Again, the forecast error appears to be

heavy-tailed. Combined with the observations above, this may justify the use of a stable distribution to describe the day-ahead solar power forecast error.

Fig. 3.9 shows the fitted, stable solar power forecast error distribution and the empirical distribution, obtained from two years of solar power forecast data. The stable distribution captures the DA forecast error well, but slightly overestimates the probability of large, negative forecast errors (left tail).

Improving forecast accuracy through shorter lead times

As the lead time of a forecast decreases, its accuracy generally increases [165]. We will quantify this effect for the solar power forecast error by comparing the forecast error on the day-ahead and intra-day forecasts.

Reducing the lead time of the forecast reduces the NRMSE from 0.087 p.u. to 0.067 p.u (average values). The range of the NRMSE reduces from [0.012 p.u., 0.12 p.u.] to [0.009 p.u., 0.09 p.u.]. Similar reductions are observed in the bias and standard deviation, although the trends discussed above persist. The skewness of the solar power forecast error is unaffected. The average kurtosis increases from 4.33 p.u. to 4.68 p.u., excluding extreme kurtosis values (i.e. kurtosis values exceeding 10 p.u.).

Fig. 3.9 shows the empirical solar power forecast error and the fitted stable distribution for the day-ahead and intra-day solar forecast error. Although the accuracy of the forecast increases, the heavy-tailed character of the solar forecast error persists. The stable distribution captures this behavior. Note that the overestimation of the probability of large negative forecast errors (left tail of the distribution) subsides. Although the increase in forecast accuracy is notable, the probability of large negative and positive forecast errors remains significant.

3.6 Conclusion

Some forms of RES-based electricity generation, such as wind and solar power, are limitedly predictable. A correct description of the wind and solar power forecast error (WPFE and SPFE) holds important information for short-term economical and operational (reliability) studies, as illustrated in this chapter via a probabilistic reserve calculation method. The focus of this chapter is therefore on the development of a statistical, distribution-based description of the wind power forecast error. These distributions will provide crucial information to

generate adequate scenarios (Chapter 4) and to determine cost-efficient reserve requirements (Chapter 5).

Based on the relevant scientific literature and own calculations, we showed that WPFE data exhibits heavy tails. The Lévy α–stable distribution is proposed as an alternative description of the WPFE. This distribution allows modeling the skewness and kurtosis observed in the WPFE data – in contrast to the Gaussian and β-distributions currently proposed in the scientific literature.

The performance of the Lévy α–stable distribution is compared to that of the Gaussian and the β-distribution in a case study of the historical WPFE in the Belgian power system. The analysis has shown that the Lévy α–stable distribution adequately captures the heavy tails of the WPFE data, while the Gaussian and β-distribution fail to describe this characteristic. This improvement can be partially explained by the higher number of parameters used in the stable distribution. The relevance of this statistical description of WPFE data has been demonstrated via a probabilistic reserve sizing method. Reserves are calculated per forecast power bin based on the fitted probability density function. It was shown that only reserves calculated from the Lévy α–stable distribution yield reliability levels equal to or greater than the desired reliability level of the power system. In addition, we used the developed method to illustrate the differences and similarities between (i) wind and solar power forecast errors, (ii) errors on onshore and offshore wind power forecasts and (iii) day-ahead and intra-day solar power forecast errors.

The improved representation of the WPFE and SPFE allows researchers and practitioners to develop improved operational models that reflect the heavy-tailed nature of the WPFE. This can further facilitate the integration of wind power in the power system through advanced operational techniques, such as dynamic reserve levels and stochastic operational power system models.

This research may be further strengthened on the following ways. First, the procedure for the estimation and optimization of the parameters of the distributions may be improved, e.g. by employing a maximum likelihood estimation method. The objective function (min. squared residuals) utilized in this chapter has merely been chosen to demonstrate the superiority of the stable distributions in capturing the shape of the WPFE. If one aims to characterize specific shape characteristics of the WPFE (e.g. the tails or peaks), this criterion might not be suitable. Second, including the influence of inter-temporal dependencies and the lead time of the forecast in the analysis may further increase the accuracy of the resulting statistical description of the forecast error. Similarly, studying statistically dependent sources of uncertainty may lead to interesting insights. Third, the presented reliability levels are calculated from static comparisons of the historical wind power forecast errors

and the calculated reserves. Employing the calculated reserve requirements in a UC and ED model may yield better estimates of the attainable reliability levels. We will return to this issue in Chapter 5. Moreover, we have assumed that a certain reliability level should be reached, regardless of the associated costs. Further research may focus on more cost-effective reserve sizing (and allocation) methods, balancing the (expected) cost of load shedding, curtailment of power generated from renewable energy sources and the procurement and deployment cost of the reserves. We will address these issues at length in Chapter 5.

Chapter 4

Scenario generation & reduction

In this chapter, we introduce scenario generation and reduction techniques in the context of stochastic unit commitment (SUC) models[1]. As computational limitations currently do not allow solving a UC model with a continuous representation of a stochastic variable, researchers resort to *scenario generation techniques* (SGTs) to translate the continuous description of the stochastic variable at hand to a set of discrete realizations of that stochastic variable, i.e. scenarios. The 'true' SUC problem with a continuous description of the uncertainty is approximated by the so-called sample average approximation (SAA) of the SUC problem [184] (Chapter 2). As mentioned in Chapter 1, which introduced the proposed modeling framework, and studied by a.o. Dvorkin et al. [106], qualitative scenarios are essential in the SUC model and in the evaluation of the resulting UC schedule. Generating a set of scenarios that is an adequate discrete representation of the stochastic variable is the goal of any SGT.

[1]In SUC models, uncertainty is represented via a number of realizations of the uncertain variable at hand, i.e. scenarios. The problem is typically represented as a two-stage recourse problem. One tries to find a UC schedule, common to all scenarios, as such that a feasible dispatch is possible for all possible realizations (scenarios) of an uncertain variable at the lowest possible expected operational cost. A feasible dispatch here means that the demand for electricity in each time step is met in all of the considered scenarios, while all technical constraints of the power plants are respected (Chapter 2).

This chapter is based on the following papers:

- K. Bruninx and E. Delarue, *Scenario Reduction Techniques and Solution Stability for Stochastic Unit Commitment Problems,* ENERGYCON, April 4–8, 2016, Leuven, Belgium.
- K. Bruninx, E. Delarue and W. D'haeseleer, *A practical approach on scenario generation & reduction algorithms for wind power forecast error scenarios,* KU Leuven Energy Instititute WP EN2014–15, 2014.

Given a set of scenarios[2], researchers typically employ *scenario reduction techniques* (SRTs) to identify ex-ante those scenarios that drive the decision variables in a SUC model, essentially reducing the number of scenarios one needs to consider (Section 4.4). The necessity of these SRTs stems from the extremely high computational burden of solving a SUC model with a large number of scenarios, rendering the SUC model impractical for real-life purposes. For example, Papavasiliou et al. [110] show that a SUC model applied to a real-life power system can take tens of hours to be solved, even with a large duality gap and a small number of scenarios. To avoid so-called intractability, SRTs are used to limit the number of scenarios needed in the stochastic model. These algorithms are designed to select those scenarios that affect the value of the first-stage variables, and thus the objective function, of the stochastic problem. If designed and executed correctly, one can drastically reduce the computational burden of solving a SUC model with minimal loss in quality of the obtained solution. The challenge here lies in the *ex-ante* character of the selection: one needs to decide which scenarios will affect the solution of the problem, before solving the problem. Failing to identify critical scenarios during scenario reduction will have a significant impact on the quality of the resulting UC schedule, as it might trigger load shedding and/or curtailment of RES-based generation in real time.

Setting up the relevant set of scenarios with a manageable cardinality is one of the most difficult steps in developing a stochastic programming model. As will be illustrated below, the importance of the considered scenarios cannot be underestimated [187, 35, 111, 188, 106]. Scenario generation and reduction

[2]We assume that a discrete representation of the uncertainty at hand, i.e. a set of possible realizations with a probability of occurrence, is available to the system operator. This is typically the result of a scenario generation technique. However, some forecasting methods allow generating so-called ensemble forecasts [185]. Other characterizations of this uncertainty are possible, e.g. conditional kernel density estimation [186] or prediction interval (quantiles) estimations [115]. Regardless of the origin of a set of scenarios describing the uncertainty, in most cases scenario reduction techniques will be required to keep the resulting SUC problem tractable.

methods need to be adapted to the optimization problem at hand – no scenario reduction method will fit all purposes. They are a critical part of the model, not just a part of the input data.

In this chapter, we will therefore discuss scenario generation and reduction techniques in depth. In Section 4.1, we give an overview of some theoretical elements of scenario generation and reduction, as well as some requirements for what we believe to be a good scenario generation and reduction technique. The focus is on the practical application, not the theory, for which an interested reader is referred to specialized literature (e.g. [188, 187, 37]). Throughout this chapter, we will focus on SGTs and SRTs in the context of wind power forecasts, currently a very active field of research. Our results and recommendations can however easily be used to model other sources of uncertainty, which we will illustrate by applying the presented methodology to solar power forecasts. Section 4.2 presents an overview of SGTs found in the scientific literature. We describe the selected SGT that we believe to be adequate to generate wind power forecast scenarios in detail. In the subsequent section, we will show that the selected SGT leads to a relatively small set of scenarios that captures the stochastic behavior of the wind power forecast error in the Belgian power system. For this modeling exercise, we will start from the statistical description developed in Chapter 3. The correspondence of the resulting scenarios and the original distribution will be verified via standard statistical methods, as well as via an event-based verification framework, as advocated by Pinson and Girard [185]. Section 4.4 treats SRTs, with a special focus on the probability distance-based SRTs such as the *fast forward* algorithm [38], by far the most-used SRT in the scientific literature. Via a methodological example, we will illustrate why current SRTs are not well-suited to select critical wind power forecast scenarios and how their performance can be improved. To this end, we propose a new metric to characterize a scenario during scenario reduction, which allows identifying those scenarios that are critical to obtain a cost-optimal UC schedule. In Section 4.5, the added value of the proposed SRT will be illustrated in a solution stability analysis of a SUC model, considering a power system inspired by the Belgian power system with a high penetration of wind energy. Before formulating a conclusion and some suggestions for future work, we will compare the performance of the selected SGT and four selected SRTs in an extensive numerical analysis. We study the aforementioned power system during four representative weeks. Our results illustrate that the combination of the modified SGT and SRT proposed in this chapter may allow obtaining stable, unbiased UC schedules. The computational effort involved in solving a SUC problem however remains high and the presence of energy storage-based flexibility providers threatens the stability of the solution.

4.1 Scenario generation & reduction: the basics

We will first briefly discuss the concept of scenarios and the so-called scenario tree. The discussion will be general and not applied to the specific case of wind power forecast errors. It is however not the aim of this work to go into detail, but to provide some needed background to facilitate the interpretation of the rest of this chapter. Second, we will discuss the governing ideas behind scenario generation and reduction techniques. We will deal with scenario generation and reduction in detail in Section 4.2 and Section 4.4 respectively. Last, a list of requirements for a good SGT and SRT is given, to which we will hold the SGTs and SRTs discussed in Section 4.2 and Section 4.4.

Scenario trees: basic concepts

The structure of the optimization problem that the decision maker, i.e. the system operator in the UC problem, faces is conveniently visualized through a scenario tree. Visually, a scenario tree consists of nodes and leafs (Fig. 4.1). A node represents the state of a problem at a particular moment in time – i.e. the moment at which a decision is made – and is often referred to as a stage. The first node is the root node and indicates the beginning of the planning horizon: at this node or stage, the so-called *here-and-now*-decisions are taken. These variables, typically referred to as first-stage variables, are fixed before the realization of the stochastic process. The root node is connected via branches to the second-stage nodes, where the *wait-and-see* or second-stage variables are fixed after realization of the stochastic process. The branches or arcs – the paths from the root node to the leafs – are possible realizations of the random variables, i.e. scenarios. Each branch has a probability of occurrence. For a two-stage decision process – like the problem at hand – the second-stage nodes are equal to the scenarios [35]. The probability of a scenario is thus equal to the arc probability. In this case, the scenario tree is characterized by a fan-like structure [187].

Scenario generation & reduction

Before moving to scenario generation and reduction methods, we need to answer the question *'What is an adequate scenario tree in a SUC model?'*. Many SGTs and SRTs are found in the scientific literature, as there is no obvious way to pass from random variables (continuous) to an adequate (and what is adequate in this context) discrete description of those variables [188]. However, all scenario generation and reduction techniques have the same goal: minimizing the error on

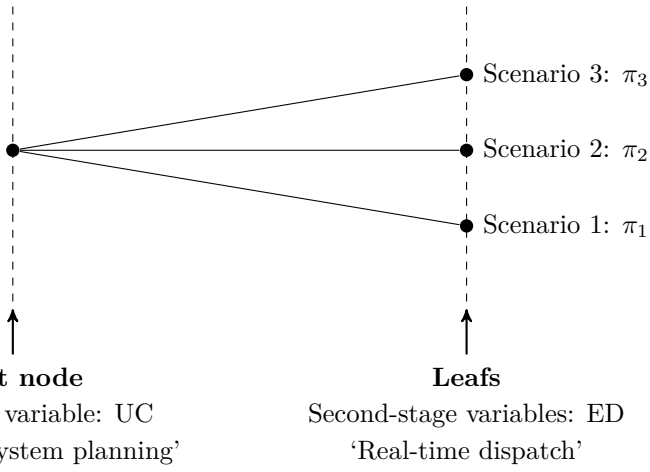

Figure 4.1: A scenario tree for a two-stage decision problem with tree scenarios with probability π_s. In the problem at hand, the system planner has to decide on the unit commitment schedule ('Day-ahead system planning') at the root node. In the second stage, the dispatch is executed ('Real-time dispatch').

the solution of the stochastic problem caused by the approximation of the true stochastic process $\tilde{\epsilon}$ with a scenario tree $\check{\epsilon}$ [111, 189, 188]. This approximation error or bias[3] is defined by Pflug [189] for a a two-stage stochastic programming model $\min_{x \in \mathbf{X}} \; G(x, \tilde{\epsilon})$ as follows:

$$\beta(\tilde{\epsilon}, \check{\epsilon}) = G\left(\operatorname{argmin}_{x \in \mathbf{X}} \; G(x, \check{\epsilon}), \tilde{\epsilon}\right) - \min_{x \in \mathbf{X}} \; G(x, \tilde{\epsilon}) \tag{4.1}$$

As the size of the scenario tree $\check{\epsilon}$ increases and the difference between $\check{\epsilon}$ and $\tilde{\epsilon}$ subsides, the approximation error $e_G(\tilde{\epsilon}, \check{\epsilon})$ approaches zero. Note that not the optimal values of the decision variable x, but the corresponding values of the objective function are compared. The objective function of a stochastic programming problem is typically flat, which leads to similar objective values for different scenario trees and different values of the first-stage decision variables. In other words, different scenario trees may lead to a different solution of similar quality.

[3] In [111, 188], the approximation error is also referred to as the 'optimality gap'. In order not to cause confusion with the optimality gap as a stopping criterion of a MILP solver, we will not use 'optimality gap' as a synonym of the bias or approximation error introduced by a scenario tree approximation of a stochastic process.

Requirements for an adequate scenario tree for stochastic unit commitment

According to Eq. (4.1), a good scenario tree yields the same solution of optimization problem as the stochastic problem if it could be solved with the full, continuous description of stochastic variables. Unfortunately, definition (4.1) is of little practical use, as it requires solving the stochastic problem considering the true stochastic process $\tilde{\epsilon}$. If this would be possible, no scenario trees would be needed. Moreover, $\breve{\epsilon}$ is typically too large to solve $\min_{x \in \mathbf{X}} \; G(x, \breve{\epsilon})$ directly. Scenario reduction techniques are employed to reduce $\breve{\epsilon}$ to $\overline{\epsilon}$ ($\overline{\epsilon} \subseteq \breve{\epsilon}$)[4], further complicating the evaluation of the approximation error (4.1). However, through certain approximations, one is able to test the quality of a scenario generation or reduction method [35, 111, 188, 190]. We will define the following criteria for SGTs and SRTs in the context of SUC problems:

1. The **number of stages** and the **number of nodes** in the scenario tree should directly reflect the decision process you are studying – in this case two stages is an obvious choice. We will study a UC problem with a 24 hour horizon and a 15 minute temporal resolution, so each scenario should contain 96 values, one for each time step;

2. The set of scenarios should **characterize the stochastic variable**. The set of scenarios needs to capture all events that affect the UC decisions and the probability with which they occur. For the case of wind power forecast errors, this means e.g. that the scenarios should respect the heavy-tailed character of the wind power forecast error and its variability. Mathematically, we require that $\breve{\epsilon} \sim \tilde{\epsilon}$;

3. The set of scenarios should be as **small** as possible to avoid computational intractability;

4. The resulting solution of the stochastic program should exhibit **in- and out-of-sample stability**, indicating that the addition of more scenarios to the optimization problem does not change the objective function of the stochastic program (Section 4.5). Kaut and Wallace [111, 188] argue that stability can be tested by solving the stochastic program with several different scenario trees, generated by the same method. If the objective value does not change (too much), we can claim **in-sample stability**. With $\min_{x \in \mathbf{X}} G(x, \overline{\epsilon})$ the stochastic problem at hand, and $\overline{\epsilon}$ the *reduced* scenario tree approximation of the stochastic process $\tilde{\epsilon}$, in-sample stability

[4] In this dissertation, a reduced scenario set $\overline{\epsilon}$ is selected from a large scenarios set $\breve{\epsilon}$: $\overline{\epsilon} \subseteq \breve{\epsilon}$. Other techniques may however construct new scenarios from the initial scenario set (see Section 4.4.1).

is claimed if

$$\forall i, \forall j: \quad G(\overline{x_i}, \overline{\epsilon_i}) \approx G(\overline{x_j}, \overline{\epsilon_j}) \tag{4.2}$$

with $\overline{x_i}$ the optimal value of the first-stage variables obtained on reduced scenario tree $\overline{\epsilon_i}$, i.e. $\overline{x_i} = \text{argmin}_{x \in \mathbf{X}} \; G(x, \overline{\epsilon_i})$. Scenario trees $\overline{\epsilon_j}$, $\overline{\epsilon_i}$ are different reduced scenario trees of increasing cardinality, generated by the same deterministic method or scenario trees of equal cardinality, generated by the same stochastic method[5]. The second requirement for stability is **out-of-sample stability**, which guarantees that the true objective function for fixed optimal first-stage decision variables, obtained from solving the stochastic program considering $\overline{\epsilon}$, does not change (too much) if the cardinality of the scenario tree increases (deterministic SGT/SRT) or if different scenario trees of the same cardinality are generated (stochastic SGT/SRT) [111, 188]. Mathematically, this can be expressed as follows:

$$\forall i, \forall j: \quad G(\overline{x_i}, \tilde{\epsilon}) \approx G(\overline{x_j}, \tilde{\epsilon}) \tag{4.3}$$

with $\overline{x_i} = \text{argmin}_{x \in \mathbf{X}} \; G(x, \overline{\epsilon_i})$. In the context of SUC problems, we will not evaluate $G(\overline{x_i}, \tilde{\epsilon})$, as it requires solving the second-stage dispatch problem considering the 'true' stochastic process $\tilde{\epsilon}$. We approximate $G(\overline{x_i}, \tilde{\epsilon})$ by solving $G(\overline{x_i}, \breve{\epsilon})$, with $\breve{\epsilon}$ a large scenario tree that satisfies $\breve{\epsilon} \sim \tilde{\epsilon}$ as such that $G(\overline{x_i}, \breve{\epsilon})$ is a good approximation of $G(\overline{x_i}, \tilde{\epsilon})$. The quality of this approximation will be tested via a minimum variance calculation [191] (Section 4.5). Calculating $G(\overline{x_i}, \breve{\epsilon})$ can easily be accomplished by fixing the first-stage decision variables – i.e. the UC schedule – to the solution of the SUC model and solving all second-stage problems – i.e. a set of economic dispatch problems – resulting from this large scenario tree $\breve{\epsilon}$. These stability requirements will set a lower bound on the cardinality of the reduced scenario set[6];

5. The solution obtained with the reduced scenario tree $\overline{\epsilon}$ should be **unbiased** with respect to the true solution obtained from a stochastic optimization employing a continuous description of the stochastic variable. The bias (Eq. (4.1)) is the difference between the value of the true objective function at the optimal solution of the original problem (with a continuous, full description of the stochastic variable) and the approximation of the problem (with a discrete representation of the stochastic variable – i.e.

[5] A stochastic SGT or SRT yields different scenario trees at every run of the algorithm. A deterministic SGT or SRT returns the same scenario tree, given the same input parameters, with every execution of the algorithm.

[6] This requirement opposes the process often encountered in the literature. Typically, one selects the number of scenarios that is 'computationally manageable', rather that the number of scenarios needed for high-quality solutions [192].

the scenario tree). A solution of a stochastic programming problem $\overline{x} = \text{argmin}_{x \in \mathbf{X}} \; G(x, \overline{\epsilon})$, obtained considering a reduced, discrete scenario tree $\overline{\epsilon}$, is said to be unbiased if the approximation error (Eq. 4.1) tends to zero. Following Kaut and Wallace [111], a stochastic upper bound to the bias $\beta(\overline{x})$ for a stable, optimal first-stage solution $\overline{x}$ is given by

$$\beta(\overline{x}) \lessapprox G(\overline{x}, \tilde{\epsilon}) - G(\overline{x}, \overline{\epsilon}) \approx G(\overline{x}, \breve{\epsilon}) - G(\overline{x}, \overline{\epsilon}) \tag{4.4}$$

with $G(\overline{x}, \breve{\epsilon})$ an approximation of $G(\overline{x}, \tilde{\epsilon})$. Equation (4.4) provides support for the intuitive idea that the first-stage $G(\overline{x}, \overline{\epsilon})$ and second-stage objective values $G(\overline{x}, \breve{\epsilon})$ for an optimal solution $\overline{x}$ should be approximately the same: the difference between those values is an upper bound to the approximation error. Note that an unstable solution by definition is biased, but a stable solution is not guaranteed to be unbiased: a SGT/SRT may yield scenario trees $\overline{\epsilon_i}$ that trigger an in-sample and out-of-sample stable solution $\overline{x}$ ($G(\overline{x}, \overline{\epsilon})$ and $G(\overline{x}, \breve{\epsilon})$ no longer change), but that are sub-optimal ($G(\overline{x}, \overline{\epsilon}) \neq G(\overline{x}, \breve{\epsilon})$).

In this dissertation, we will propose a two-step approach to obtain a meaningful scenario tree that captures the stochastic wind power forecast error and triggers a stable, unbiased UC schedule (Fig. 4.2). It is important to note that throughout the discussion we assume that a wind and/or solar power forecast is given, from historical data or calculated from wind speed and irradiation data, on which we will superimpose a (distribution of the) forecast error. First, a SGT will be employed to generate a limited set of scenarios $\breve{\epsilon}$ that forms a meaningful representation of e.g. the wind power forecast error (requirements (1), (2) and (3)). The aim of the SGT is to generate a relatively small set of scenarios (scenario tree $\breve{\epsilon}$) that is a good representation of the statistical properties of the uncertain variable $\tilde{\epsilon}$ and captures all events that will significantly affect (the objective function and optimization variables of) the UC problem. Assuming a description of the probability density function of the forecast error is given (Chapter 3), we generate scenario sets for the wind power forecast error using a method based on Pinson et al. [36], refined by Ma et al. [193] (Section 4.2.3). The quality of these scenario sets is verified by comparing the resulting distributions of the forecast error and its variability to historical data, as well as via an event-based verification framework [185] (Section 4.3). The second step consists of a modified probability distance-based SRT (Section 4.4.3). This technique allows selecting a set of scenarios (scenario tree $\overline{\epsilon}$) from the generated scenario tree $\breve{\epsilon}$ ($\overline{\epsilon} \subseteq \breve{\epsilon}$) that triggers stable and unbiased UC decisions (requirement (4) & (5)). The objective of the SRT is not to obtain a scenario tree which makes the discrete representation of the uncertainty as close to the original distribution (or original, large scenario tree) as possible, but to trigger a stable, unbiased SUC solution. To test the stability and bias of the

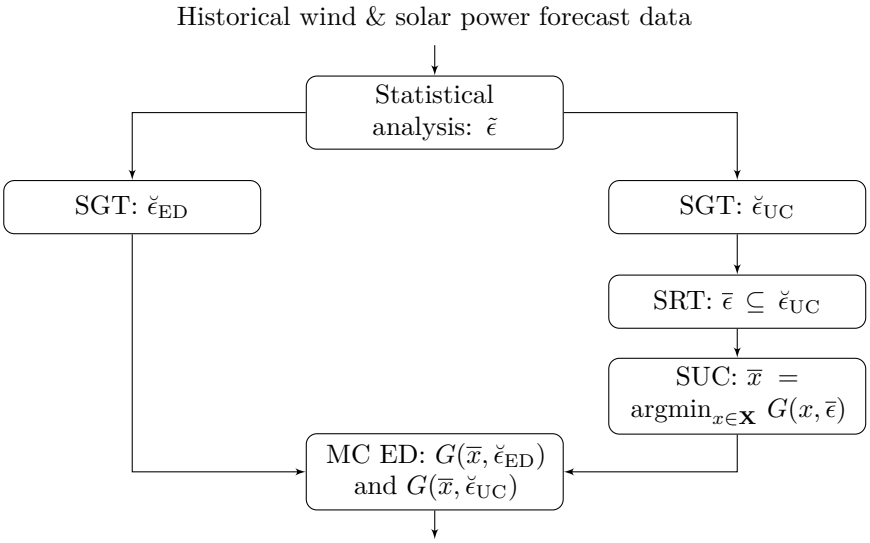

Figure 4.2: The relation between the proposed modeling framework, scenario generation, scenario reduction, solution stability and bias. A statistical analysis of historical data reveals the stochastic process $\tilde{\epsilon}$, which is approximated via a discrete scenario tree $\breve{\epsilon}$ that stems from a SGT. The SUC model is solved on a reduced version of that scenario tree $\overline{\epsilon}$, containing scenarios selected via a SRT. The resulting UC schedule $\overline{x}$ is evaluated via MC ED simulations on $\breve{\epsilon}_{\text{UC}}$, which allow isolating the bias introduced by the SRT, and on a new set of scenarios $\breve{\epsilon}_{\text{ED}}$, which allow testing the bias of the solution introduced by the SRT and SGT.

obtained solution introduced by the SRT, we evaluate the solution $\overline{x}$ on the set of scenarios $\breve{\epsilon}_{\text{UC}}$ from which we selected the reduced scenario tree $\overline{\epsilon}$, which allows estimating the bias introduced by the SRT:

$$\beta_{\text{SRT}}(\overline{x}) = G(\overline{x}, \breve{\epsilon}_{\text{UC}}) - G(\overline{x}, \overline{\epsilon}) = G(\overline{x}, \breve{\epsilon}_{\text{UC}}) - \min_{x \in \mathbf{X}} G(x, \overline{\epsilon}) \tag{4.5}$$

The bias introduced by the SRT can be calculated exactly if one assumes $\breve{\epsilon}_{\text{UC}}$ is an exhaustive description of the uncertainty at hand. However, this entails that the SUC model had perfect foresight on some of the realizations of the uncertain wind power forecast, which may lead to underestimations of the true bias of the SUC solution. Indeed, we did not account for the approximation error or bias introduced by the SGT. Therefore, we additionally evaluate the

solution $\overline{x}$ on a new set of scenarios $\breve{\epsilon}_{\text{ED}}$, as such that the scenarios considered during UC optimization are not contained within the scenario tree considered in the Monte Carlo ED simulations ($\overline{\epsilon} \not\subseteq \breve{\epsilon}_{\text{ED}}$). A stochastic upper bound to the bias introduced by the SRT *and* the SGT can be calculated as [188]

$$\beta_{\text{SGT\&SRT}}(\overline{x}) \lessapprox G(\overline{x}, \tilde{\epsilon}) - G(\overline{x}, \overline{\epsilon}) \approx G(\overline{x}, \breve{\epsilon}_{\text{ED}}) - G(\overline{x}, \overline{\epsilon}) \tag{4.6}$$

Recall that this upper bound is only meaningful if the solution $\overline{x}$ is stable [188].

4.2 Scenario generation: theory

With the requirements listed in Section 4.1 in mind, we now turn our focus to the so-called scenario generation techniques (SGTs). This section is organized as follows. First, we give a brief, non-exhaustive overview of SGTs available in the scientific literature. The overview below is based on Conejo et al. [35], Dupačová et al. [187] and our own review of the current scientific literature. We continue with a detailed description of the SGT we selected, based on Pinson et al. [36] and Ma et al. [193]. Before concluding this section, we illustrate the specifics of the selected SGT in a methodological example (Section 4.2.4).

Throughout the discussion, we will have to pay attention to some specific statistical properties of e.g. wind power forecast errors, as discussed in Chapter 3. First, the wind power forecast is heavy-tailed, i.e. the probability of severe forecast errors is higher than one would expect under the assumption of a normal distribution. Second, the variability of the error may have a significant impact on the optimal UC schedule. Last, the forecast error is auto-correlated: the error at a certain time step is dependent on the error in the previous and subsequent time steps. All of these properties will have to be reflected in the generated scenarios.

4.2.1 Scenario generation techniques

In the literature, one finds an abundance of SGTs. However, no widely accepted classification exists. In this chapter, we discuss four (broad) categories of SGTs, based on the classification proposed in [194, 187]:

- Sampling;
- Path-based methods;
- Property matching;

- Optimal scenario generation techniques based on probability metrics.

Note that we here define *scenario generation* as the process of passing from a continuous description to a discrete description of a stochastic variable. Some authors list scenario reduction as a method for scenario generation. In this dissertation, we will discuss scenario generation and scenario reduction techniques separately, as they have different objectives (Section 4.1). In what follows, we discuss the four categories of SGTs. The principles governing the SGT are discussed, as well as some advantages and disadvantages. Some examples and applications will be listed, with special attention for applications in the field of wind energy. For the readers' convenience, we summarize our discussion in Table 4.1.

In **sampling-based SGTs**, one 'picks' values from a time series or underlying distribution. Given the distribution, one can obtain the probability of the sampled value or scenario. Multiple variants of sampling exist, of which random or Monte Carlo (MC) sampling is the best-known and simplest form [184]. Alternatives include Quasi Monte Carlo (QMC) sampling (sampling is not random) [195], bootstrap sampling (sampling from a time series) [196], importance sampling (sampling with more emphasis on certain parts of the domain) [197], conditional sampling (accounts for e.g. inter-temporal relations within a scenario) [111, 187] and stratified sampling methods (MC sampling in predefined sub-domains, e.g. Latin hypercube sampling) [198]. These techniques exhibit perfect limit properties: as the cardinality of the scenario set grows, the associated discrete probability density function becomes a better representation of the underlying stochastic process. However, in all but the simplest cases, it will be very difficult to randomly sample the 'correct' scenarios: or the tree is too small to represent the underlying distribution (representation problem), or the tree is too large to yield a tractable optimization problem (numerical problem) [188]. Sampling random vectors (multivariate random variables) may strongly increase the complexity of the sampling procedure, but may be required to limit the size of the tree. Several expansions and corrections have been proposed to circumvent these drawbacks, mostly in combination with other techniques or by correcting the resulting scenario tree ex-post to preserve certain statistical properties of the original distribution. Sampling-based SGTs in the context of wind power have been proposed by Papaefthymiou and Pinson [199] (spatially dependent wind power forecasts) and Feng et al. [200] (load forecast scenarios, based on Rios et al. [201]). They have been applied to study uncertainty in power systems by Pappala et al. (wind power and demand forecasts) [202], Bouffard and Galiana (net load forecast) [203], Ortega-Vazquez and Kirschen (wind speed forecast error) [46] and Wang et al. (wind power forecasts) [198].

In contrast, **path-based methods** generate complete paths or scenarios by evaluating the stochastic process via econometric or time series models. Examples include amongst others the well-known auto-regressive moving average models (ARMA, ARIMA), generalized auto-regressive conditional heteroskedasticity models (GARCH) and (Bayesian) vector auto-regressive models (VAR, BVAR) [35]. The result is a set of scenarios, characterized by a fan-like structure in the scenario tree [35]. These methods generally require the assumption of a Gaussian stochastic variable, but can accommodate otherwise distributed stochastic variables through distribution transformations (e.g. Conejo et al. [35], Sharma et al. [204]). Statistically dependent random processes may be represented via these models. However, the resulting scenario set is not guaranteed to be an adequate representation of the underlying distribution. Capturing extreme events, i.e. the tails of the distributions, may require an extremely large set of scenarios. In the context of power systems, ample applications of auto-regressive moving-average models can be found, e.g. Sharma et al. [204], Sturt and Strbac [205], Plazas et al. [206], Nürnberg and Römisch [207], Ruiz et al. [107], Papavasiliou and Oren [17], the scenario tree tool included in the well-known WILMAR SUC model [39, 208], Morales et al. [209], de Mello et al. [210] and Sen et al. [211].

Property or moment matching techniques generate a discrete distribution (under the form of a set of scenarios) that satisfies a prefixed set of statistical properties (e.g. moments, correlation matrix, percentiles, ...) of the stochastic variable. These property-matching techniques may build on other SGTs, modified or constrained to ensure that the moments or properties of the original distribution are preserved [188]. King et al. [188] present a heuristic moment-matching SGT that ensures that the set of scenarios reflects the four marginal moments and the correlations that exist in the original distribution. Høyland and Wallace present a moment-matching SGT, formulated as a non-convex optimization problem [212], for which they propose a heuristic solution procedure in [213]. As only the (statistical) properties of the uncertain variable that are considered important by the modeler need to be known, this technique is especially useful when little information is available [187]. Other advantages of property matching techniques are the possibility to include inter-period statistical dependencies and the possibility to impose the inclusion of a worst-case scenario as a statistical property. However, these properties can typically be 'matched' with a relatively low number of scenarios. In practice, modelers will employ much more scenarios than strictly necessary to match e.g. the specified moments [111], but property matching techniques do not provide a quality metric or stopping criterion for (the number of) 'additional' scenarios. In addition, it is difficult to assess the importance of a statistical property in a stochastic programming problem ex-ante. Hochreiter and Pflug [214] illustrate that the moment-matching technique may lead to strange results,

as the difference between the moments of the distribution and the proposed approximation may never lead to a real 'probabilistic' distance or metric between the two. As these methods generally do not guarantee convergence, increasing the number of scenarios may not improve the fit between the original distribution and the scenario-based representation of that distribution. To the best of the author's knowledge, SGTs based on moment-matching techniques have not been applied in the context of power systems. In finance, a number of applications can be found, see e.g. Kaut [111, 188]. Moment-matching techniques have been applied as SRTs (Section 4.4).

Optimal SGTs employ probability metrics such as the Wasserstein or Kantorovich distance to express the difference between two distinct scenarios or scenario sets, or a scenario set and a continuous distribution. By minimizing these probability metrics, in theory optimal scenario trees (i.e. with the smallest possible approximation error for a specific cardinality of the scenario set) should be obtained. However, empirical evidence seems to contradict this (see a.o. [102, 116]). The method is typically complex and requires solving an optimization problem, directly or via dedicated heuristics. The structure of the tree is typically fixed, but can be optimized simultaneously by formulating the problem as a facility location problem [214]. As will be illustrated in Section 4.4, in which we employ a similar metric in a SRT, the major drawback of these methods lies in the calculation of the Kantorovich distance based on a norm of the difference between two scenarios. As a result, all inter-temporal information (i.e. the variability of a scenario) is lost, which might lead to sub-optimal UC schedules in light of uncertain wind power forecasts. A well-known example of these optimal SGTs is provided by Pflug et al. [189, 215]. However, to the best of the author's knowledge, SGTs based on probability metrics have not been applied in the context of power systems. They have been extensively applied as SRTs in the context of power system studies (Section 4.4).

Table 4.1: Scenario generation techniques. Governing principles, advantages, disadvantages, examples and applications.

Category	Principle	Advantages	Disadvantages	Examples	Applications
Sampling	'Picking' values from a time series or a known underlying distribution.	• perfect limit properties • conditional sampling for e.g. intertemporal relationships	• representation vs. tractability; • complex for multivariate variable.	• Papaefthymiou and Pinson [199]; • Feng et al. [200].	[202, 203, 46, 198]
Path-based	Generating scenarios by evaluating econometric or time series models.	• well-known and documented; • statistically dependent random variables.	• representation not guaranteed.	• ARIMA, GARCH, BVAR [35]	[204, 205, 206, 207, 107, 17, 39, 208, 209, 210, 211].
Property or moment matching	Match set of statistical properties of uncertain variable.	• statistical properties may be defined by modeler; • little information on stochastic variable needed.	• Increasing number of scenarios does not guarantee reduction stability or bias.	• King et al. [188, 213] • Høyland and Wallace [212, 213]	[111, 188]
Optimal SGTs based on probability metrics	Minimizing probability metrics (e.g. Kantorovich distance) between scenario set and original distribution.	• smallest possible approximation error for a specific cardinality of the scenario set.	• empirical evidence contradicts theoretical performance.	Pflug et al. [189, 215]	-

4.2.2 Discussion: selecting a scenario generation technique

To evaluate the adequacy of each of the discussed techniques as a way to obtain a discrete representation of the uncertainty on e.g. wind and solar power forecasts, we hold them against the criteria outlined in Section 4.1.

First, the structure of the resulting scenario tree should reflect the decision problem we are studying. The requirement can easily be met in all methods discussed above, as the scenario tree structure can be imposed on all of them.

Second, the resulting scenario set should be an adequate discrete characterization of the stochastic variable, capturing all events that are relevant to the UC problem. The perfect limit properties of sampling-based techniques are in this context interesting. Path-based methods and property-matching techniques typically do not guarantee a perfect match of the discrete, scenario-based distribution and the original, continuous distribution as the size of the tree grows. Property-matching methods suffer from the distinct disadvantage of the ex-ante selection of the relevant properties, typically the statistical moments of the distribution. As discussed above, a scenario set that is characterized by the same moments as the original distribution is not guaranteed to contain all relevant scenarios, nor to be an adequate representation of the uncertainty at hand [214]. For the specific case of wind and solar power forecast errors, the scenario generation technique should additionally be able to account for the auto-correlation, i.e. the correlation between forecast errors at different time steps, and the spatial correlation, i.e. the correlation between errors on wind or solar power forecasts for different locations. This adds complexity to the scenario generation problem, which may be problematic in optimal scenario generation problems. For sampling-based procedures, extensions have been proposed to account for inter-temporal [36, 193] and spatial correlations [199].

Third, the resulting scenario set should be as small as possible to avoid computational intractability or excessively complex scenario reduction methods. The sampling-based methods may be in the disadvantage w.r.t. the other SGTs, as the match between the discrete representation and the original distribution is only guaranteed in the limit, i.e. by generating an infinite number of scenarios. Optimal scenario generation algorithms have a clear advantage in this context, as these techniques should yield optimal scenario sets, i.e. the scenario set smallest possible approximation error for a specific cardinality or size of that scenario set. Due to the computational cost to solve the true optimal scenario generation problem, researchers resort to heuristic algorithms. These methods are fast, but reaching the optimal scenario set is however not guaranteed.

Additionally, we require the selected SGT to be easy-to-use and easy-to-solve, flexible and widely applicable. Property matching and probability metric-based

SGTs can in theory be used to generate scenarios from a continuous description of a stochastic variable, but in practice few examples are found[7]. Based on these observations, we propose a SGT based on conditional sampling techniques. This algorithm is based on Pinson et al. [36], extended by Ma et al. [193] and Papaefthymiou and Pinson [199]. It has been employed in the context of SUC models by e.g. Botterud et al. [102] and Wang et al. [181]. In essence, the scenarios are sampled from a multivariate normal distribution, which allows taking into account inter-temporal effects within a scenario, i.e. auto-correlation effects. Via a distribution transformation, one ensures that the sampled scenarios follow the original, non-Gaussian distribution of the wind power forecast error. A major advantage of this SGT is that it is much easier, compared to representing e.g. a multivariate non-Gaussian distribution directly, to sample the joint multivariate normal distribution. In addition, the computational complexity of the method remains acceptable, in contrast to e.g. optimal SGTs based on probability metrics. Combined with the perfect limit properties of sampling-based techniques, this provides sufficient arguments to have a closer look at the method proposed by Pinson et al. as a tool for wind power forecast error scenario generation (Section 4.2.3). Compared to the literature (and especially compared to Pinson et al. [36] and Ma et al. [193]), we will improve the methodology on two fronts. First, we introduce a correction factor for the covariance matrix that captures the more erratic behavior of the wind power forecast error at intermediate wind power forecast levels. Second, an ex-post evaluation of the resulting scenarios is performed in order to detect improbable scenarios. Removing these scenarios avoids overestimating of the impact of wind power forecast errors.

4.2.3 The proposed scenario generation technique

The proposed method consists of **three main steps** (Fig. 4.3). We will focus on the generation of wind power forecast errors, but the selected SGT can easily be applied to other stochastic processes. Throughout the discussion of the proposed SGT, we assume that a statistical analysis (Chapter 3) has been performed on available wind power forecast error data or any other uncertain variable at hand. The result of this statistical analysis is a description of the probability density function ($f(\epsilon_j|G_j^{\mathrm{F}})$, $f(\epsilon_j|\epsilon_{j-1})$) and the cumulative probability density function ($F(\epsilon_j|G_j^{\mathrm{F}})$, $F(\epsilon_j|\epsilon_{j-1})$) of the forecast error and its variability for a number of predefined forecast power bins or intervals (Chapter 3).

[7]Mostly, these techniques are used in combination with another SGT. A large set of individual scenarios is generated, which are aggregated to construct the scenario tree. We will discuss this type of use of property-matching and probability metric-based methods in Section 4.4.

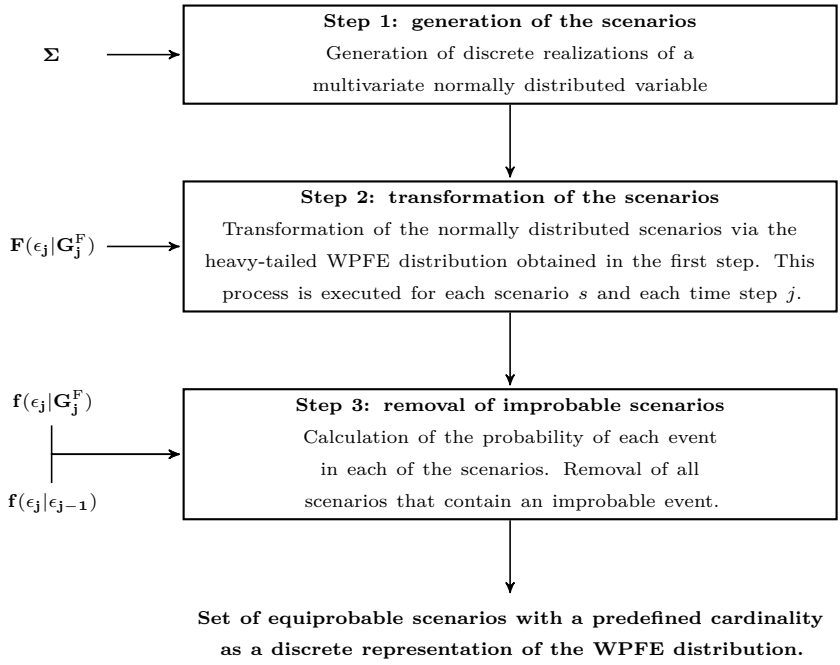

Figure 4.3: Visual representation of the proposed SGT. The required input of at each step of the SGT is indicated on the left. The distributions $F(\epsilon_j|G_j^{\mathrm{F}})$, $f(\epsilon_j|G_j^{\mathrm{F}})$ and $f(\epsilon_j|\epsilon_{j-1})$ are obtained from a statistical analysis of historical data as presented in Chapter 3.

Step 1: generate random realizations of a multivariate Gaussian distribution

First, a random number generator is used to **generate random realizations of a multivariate Gaussian distribution** $N(\mathbf{0}, \mathbf{\Sigma})$. The covariance matrix $\mathbf{\Sigma}$ represents the interdependence of the transformed, normally distributed forecast errors over the planning horizon T. Each element Σ_{j,j^*} of the covariance matrix $\mathbf{\Sigma}$ is estimated using an exponential covariance function [193]:

$$\Sigma_{j,j^*} = \exp\left(-\frac{|j^* - j|}{\delta\left(\bar{g}_j^F\right) \cdot \lambda}\right) \tag{4.7}$$

with λ a range parameter controlling the strength of the correlation between forecast errors at different lead-times, here set to 75, and $\delta\left(\bar{G}_j^F\right)$ a novel correction function, dependent on the average wind power forecast $\bar{G}^F$ over the planning horizon. This correction function allows, if necessary, accounting for

the difference in variability of the forecast error at different forecast levels. For example, due to the non-linear nature of the power curve of a wind turbine or farm, forecast errors tend to be larger and more erratic at intermediate forecast levels or close to the wind turbine's cut-out speed (Chapter 3). This correction function is optimized in order to minimize the approximation error of the resulting discrete probability density function and the original probability density function. At the end of the first step, we have obtained a set of equiprobable scenarios $\mathbf{Z}$ (scenarios Z_s, values $Z_{j,s}$) with a predefined cardinality that form a discrete representation of a multivariate Gaussian distribution $N(\mathbf{0}, \mathbf{\Sigma})$. These scenarios are inter-temporally consistent, i.e. their variability reflects the variability of the transformed wind power forecast error, as will be illustrated in Section 4.3.

Note that other methods to estimate the covariance matrix exist. For example, the covariance matrix can be estimated from forecast error data [36, 193]. However, in our case study, this problem tends to be ill-conditioned, which results in poor estimates of the covariance matrix. As we will show in Section 4.3, the exponential covariance function suffices to capture the variability and inter-temporal relations of wind power forecast errors.

Step 2: transform the normally distributed scenarios to wind power forecast error scenarios

In the **second step**, the scenarios, generated from a Gaussian distribution, are **transformed to wind power forecast error scenarios** using the cumulative probability distribution (cdf) functions of the forecast error. From statistics, it is known that the inverse transformation of any cdf yields a uniform distribution on the interval $[0, 1]$ [36, 193]. In addition, the cdf of the Gaussian distribution in Step 1 is a uniform distribution on the interval $[0, 1]$. Therefore, one can use the following transformation, as illustrated in Fig. 4.4, for each node (value $Z_{j,s}$) in each scenario s:

$$\epsilon_{j,s} = F^{-1}\left(\Phi\left(Z_{j,s}\right) | G_j^{\mathrm{F}}\right) \tag{4.8}$$

$$\Phi(Z_{j,s}) = \int_{-\infty}^{Z_{j,s}} \frac{1}{\sqrt{2\pi}} e^{-\frac{x^2}{2}}\, dx \tag{4.9}$$

F^{-1} is the inverse cumulative probability density function of the forecast error, which is dependent on the forecasted wind or solar power G_j^{F} at that time step j. In the particular case of the wind power forecast error in the Belgian power system, this is the Lévy α-stable distribution obtained in Chapter 3. $\Phi(Z_{j,s})$ is the cdf of the standard Gaussian distribution (random variable $Z_{j,s}$). This

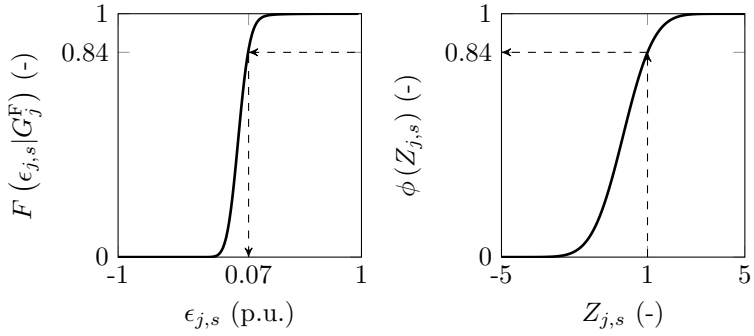

Figure 4.4: The generated realizations of the normally distributed variable $Z_{j,s}$ are transformed via the conditional cdf of the wind power forecast error $F_j\left(\epsilon_{j,s}|G_j^{\mathrm{F}}\right)$, dependent on the wind power forecast G_j^{F} at that time step j. The visualized distributions are illustrative.

transformation is performed on each value in all scenarios. The result is a set of equiprobable wind power forecast error scenarios.

Step 3: calculate probability of each event & remove improbable scenarios

Finally, the probability of each event in the scenarios is calculated via a Lévy α-stable distribution, fitted to the historical wind power forecast error data (Chapter 3), in order to **remove improbable scenarios**. As the SGT does not take into account all information on the variability of the error, some impossible transitions (e.g. too high variability) may occur in the generated scenarios. To avoid that the power system is exposed to these challenging, but unrealistic scenarios, these scenarios should be removed from the considered set. The probability of each event in each scenario $\pi_{j,s}$ is calculated, over the simulated planning horizon T, via

$$\forall j, \forall s: \quad \pi_{j,s} = f(\epsilon_{j,s}|\epsilon_{j-1,s}) \cdot f(\epsilon_{j,s}|G_{j,s}^{\mathrm{F}}) \tag{4.10}$$

in which $f(\epsilon_{j,s}|\epsilon_{j-1,s})$ is the conditional pdf of the occurrence of an error $\epsilon_{j,s}$ given the previous error $\epsilon_{j-1,s}$. Similarly, $f(\epsilon_{j,s}|G_{j,s}^{\mathrm{F}})$ is the conditional pdf of an error $\epsilon_{j,s}$ occurring given the wind power forecast $G_{j,s}^{\mathrm{F}}$. If a scenario s contains an improbable transition at a time step j ($\pi_{j,s} = 0$), that scenario is removed from the set. The retained scenarios are assumed to be equiprobable. The sum of the probability of occurrence of all retained scenarios is thus, by definition, set to unity.

Extension: multiple sources of uncertainty

In case multiple sources of uncertainty are present in the power system at hand, we suggest two possible approaches to extend the methodology above. Assuming that two sources of uncertainty, namely wind and solar power forecast errors, are considered, these approaches can be summarized as follows.

In the first method, the three-step process above is executed for the solar and wind power forecast error individually. For the solar power forecast errors, only day-time hours are considered. The result consists of two sets of equiprobable scenarios that represent the error on the wind (set S^{W}, index s^{W}) and solar (set S^{S}, index s^{S}) power forecast respectively. The set of scenarios that represents the uncertainty in the power system is given by each possible combination of the solar and wind power forecast error scenarios:

$$\forall j, \forall s^{\mathrm{W}}, \forall s^{\mathrm{S}}: \quad \epsilon_{s,j} = \epsilon^{\mathrm{W}}_{s^{\mathrm{W}},j} + \epsilon^{\mathrm{S}}_{s^{\mathrm{S}},j} \tag{4.11}$$

However, not all combinations of solar and wind power forecast errors are possible. Therefore, similar to the probability calculation in Eq. (4.10), the probability of occurrence of a combination of a solar $\epsilon^{\mathrm{S}}_{s^{\mathrm{S}},j}$ and wind $\epsilon^{\mathrm{W}}_{s^{\mathrm{W}},j}$ power forecast error is compared to the probability of occurrence of such a combination in historical data, which provides an empirical probability distribution $f(\epsilon^{\mathrm{W}}, \epsilon^{\mathrm{S}})$. Again, only combinations that occur with a non-zero probability are retained. The retained scenarios are assumed to be equiprobable and their probability of occurrence sums, by definition, to unity.

Equation (4.11) exposes the Achilles' heel of the selected SGT: depending on the number of scenarios needed to characterize the solar and wind power forecast error respectively, the number of possible combinations quickly explodes. For example, if 100 scenarios are required to capture the solar and wind power forecast error respectively, 10,000 possible combinations of forecast error scenarios emerge. This drastically increases the complexity of the scenario reduction problem and the computational burden of the Monte Carlo economic dispatch simulations (see further). Capturing uncertainty in a small scenario set (Requirement (3), Section 4.1) thus becomes increasingly important in light of multiple sources of uncertainty.

To circumvent the aforementioned combinatorial explosion, one could perform a convolution of the probability distributions of the wind and solar power forecast error and generate scenarios directly from the resulting distribution. Note that the convolution has to occur on a per MW-basis, not on the normalized p.u.-basis. As such, the installed capacity of solar and wind power plays a role. Changes in the installed capacity require re-generating the scenarios, which may impair cross-comparing results over time and models.

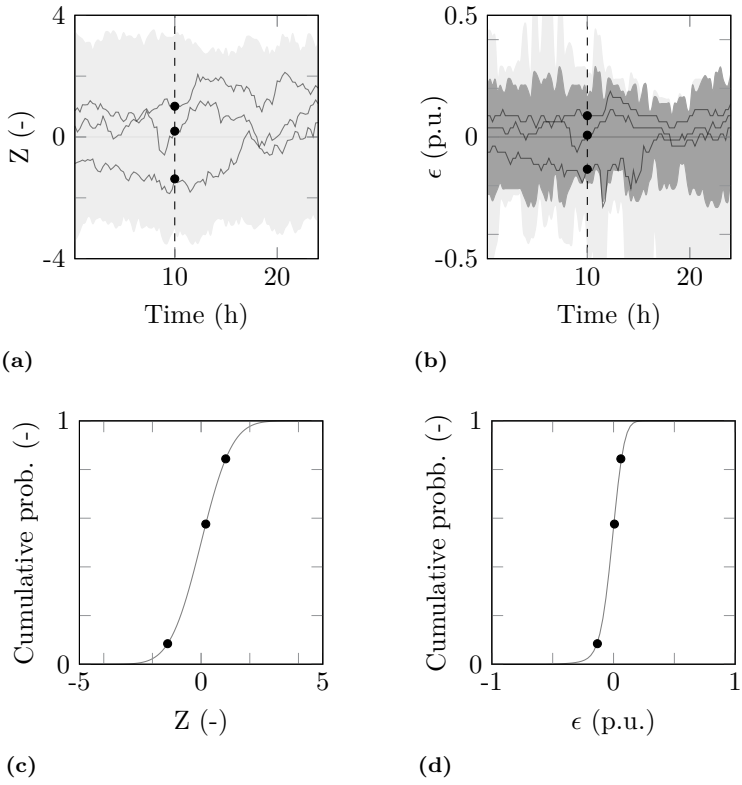

Figure 4.5: Illustration of the working principles of the scenario generation technique. The solid lines correspond to three different, randomly selected scenarios, the dots mark the corresponding values at hour 10, for which the distribution transformation is illustrated in Fig. 4.5c and 4.5d. In Fig. 4.5a and Fig. 4.5b, the light grey area corresponds to the range of values in the scenario set before the removal of those scenarios that contain improbable events. The dark grey area in Fig. 4.5b visualizes the same range after removal of those scenarios that contain improbable events.

Both approaches are only valid if the solar and wind power forecast error are weakly correlated. For wind and solar power forecast errors in the Belgian power system, this assumption seems to hold: in the period 2012-2014, the Belgian wind and solar power forecast error [178, 183] exhibit a correlation coefficient of less than 0.01 (p-value: 0.14, with a null-hypothesis 'existence of a correlation').

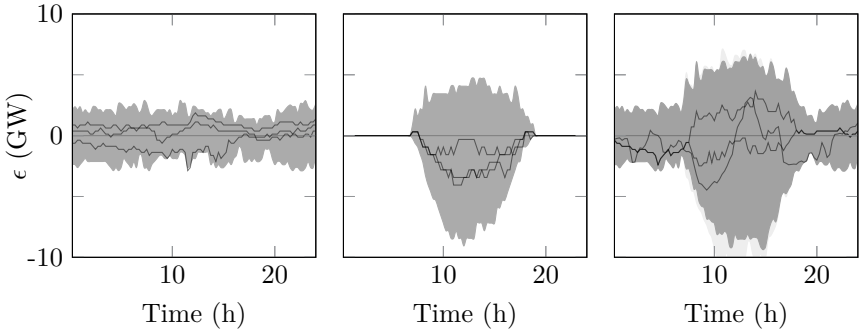

(a) Wind **(b)** Solar **(c)** Combination

Figure 4.6: Illustration of the working principles of the scenario generation technique: the combination of wind (Fig. 4.6a) and solar power forecast errors (Fig. 4.6b). The light grey area in Fig. 4.6c corresponds to the range of forecast errors in the scenario set before the removal of improbable combinations of solar and wind power forecast errors. The dark grey area visualizes the same range after removal of those improbable combinations.

4.2.4 A methodological illustration

We will use the first day of week 39 to illustrate the working principles of the scenario generation technique presented above. The same day will be used to illustrate the difference in performance of the various UC models (Chapter 5) and to execute an in-depth solution stability analysis (Section 4.5).

Figure 4.5 visualizes the proposed procedure for the **wind power forecast error** on this particular day. First, scenarios are generated as samples of a multivariate Gaussian distribution. In Fig. 4.5a, three specific scenarios (black, solid lines) and the range of scenarios (light grey area) are shown. The dots mark the values of these scenarios in hour 10, for which the cumulative distribution of the Gaussian distribution in shown in Fig. 4.5c. With the cumulative distribution of the wind power forecast error, which follows a Lévy α-stable distribution (Chapter 3), shown in Fig. 4.5d, we can transform the normally distributed samples to wind power forecast error samples. This procedure is repeated for every time step, until all samples are mapped from the Gaussian distribution (Fig. 4.5c) to the Lévy α-stable distribution of the wind power forecast error (Fig. 4.5d). The resulting scenarios are visualized in Fig. 4.5b. Last, the wind power forecast error scenarios are checked for 'improbable events'. We repeat this procedure until all scenarios that contain improbable events are

removed from the set. As a result, the range of forecast errors contained in the set of scenarios strongly decreases (Fig. 4.5b). The impact of the removal of these improbable scenarios on the match between (1) the original distribution of the forecast error and (2) the discrete representation of the distribution of the forecast error formed by the scenarios will be explicitly discussed in Section 4.3.

We repeat the methodology above for the **solar power forecast error** on the same day, which results in the scenarios shown in Fig. 4.6. So far, the installed capacity in wind or solar power did not play a role (all values are expressed in p.u., i.e. normalized). However, if we want to combine wind and solar power forecast error scenarios, one needs to scale these values with the installed capacity of each technology, as this recombination needs to occur on a per MW-basis. We may combine all scenarios one-on-one, as the solar and wind power forecast error are uncorrelated[8]. Assuming a 30% wind and solar power penetration (annual, energy basis), the resulting forecast error scenarios are shown in Fig. 4.6. Again, we compare the resulting combinations with observed combinations of solar and wind power forecast errors in historical data. Improbable combinations are removed, which reduces the range of possible realizations of the RES-based generation considerably, as illustrated in Fig. 4.6c.

4.3 Scenario generation: results & discussion

In this section, the performance of the proposed SGT is evaluated w.r.t. the proposed criteria for an adequate scenario tree (Section 4.1). The SGT is shown to yield an adequate representation of the historical wind and solar power forecast error in the Belgian power system. We will generate scenarios as a discrete representation of a fitted Lévy α-stable distribution, as discussed in Chapter 3. The discrete distribution formed by the scenarios is compared to the original, fitted distribution and an empirical distribution of the variability of the error. We explicitly discuss the impact of the removal of so-called 'improbable scenarios' (Section 4.2.3). The correspondence between the distribution of the historical forecast error data and the generated scenarios is studied via an event-based evaluation framework, as advocated by Pinson and Girard [185].

[8]Note that the correlation between the solar and wind power *forecast* is preserved, as we use historical wind and solar power forecast data, on which uncorrelated wind and solar power forecast error scenarios are imposed.

4.3.1 Scenario generation & the distribution of the wind power forecast error

First, we study the correspondence between the discrete distribution, represented through the scenario sets, and the original distribution of the wind power forecast error. In order to address this issue, we have generated 500 scenarios for each day in 2013[9], using historical wind power forecast data from the Belgian TSO Elia [179], the fitted Lévy α-stable distributions (Chapter 3) and the proposed SGT (Section 4.2.3). From these scenario sets, we calculated the empirical probability density functions (pdf) and cumulative probability density functions (cdf) for each so-called power bin. As described in Chapter 3, the forecast errors are sorted into different subsets according to the forecast at which they occurred. We calculate the empirical pdf for each of these subsets or power bins and compare these with the fitted, Lévy α-stable pdfs we obtained in Chapter 3. Likewise, the representation of the variability of the forecast error can be studied by investigating the probability of a forecast error of a certain amplitude, given the forecast error on the previous time step. The data is again sorted in subsets or power bins, according to the forecast error on the previous time step and the distribution for each of these subsets is calculated. By comparing these empirical distributions, as represented by the generated scenario sets, to distributions obtained from or fitted to historical data, we can assess the match between the distribution of the amplitude and variability of the wind power forecast error in the generated scenarios and the historical data.

The distribution of the forecast error

As the SGT employed in this dissertation directly employs the distribution of the error given the forecast, a perfect match between the original distribution and the distribution of the simulated scenarios should be obtained. The only precondition for this match is that one generates sufficient scenarios. As illustrated in Fig. 4.7 for the 10^{th} forecast power bin[10] – containing all forecast errors observed for forecasts between 0.225 and 0.25 p.u. – the distribution of the generated forecast error scenarios and the stable distribution (the input for the scenario generation method) is perfect. If the distributions of the

[9]The number of scenarios was chosen after a variance analysis [191], which provides an estimate of the number of scenarios needed to ensure that the probability-weighted average of the objective functions of the MC ED simulations are, within a certain confidence interval, representative of the objective of the 'true' ED problem. We will return to this issue in Section 4.5.

[10]We sort the wind power forecast error in 40 power bins (power bin width: 0.25 p.u.), as in Chapter 3. This allows a one-on-one comparison of the fitted and scenario-based distribution of the forecast error in each power bin.

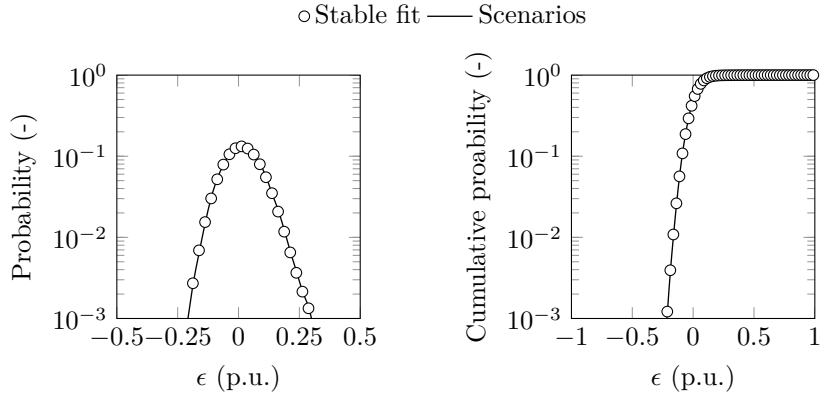

(a) pdf **(b)** cdf

Figure 4.7: The empirical ('Scenarios') and original distribution ('Stable fit') pdf and cdf of the wind power forecast error for the 10^{th} forecast power bin. Note the asymmetry of the data: as the 10^{th} power bin contains forecasts between 0.225 and 0.25 p.u., the error must fall in the interval [−0.25 p.u., 0.775 p.u.].

forecast error in the generated scenarios over the various forecast power bins are merged, using the probability that a forecast belongs to a certain power bin as a weighting factor, the distributions displayed in Fig. 4.8 are obtained. The probability density function and the cumulative distribution of the generated scenarios and stable distributions are almost identical, as expected. This is further illustrated in the so-called pp- and qq-plots in Fig. 4.8. The pp-plot shows the cumulative probability density function of the stable distribution as a function of the empirical cumulative probability density function as represented by the scenario sets. Similarly, the qq-plot visualizes the percentiles of the stable distribution versus the percentiles calculated from the generated scenarios. In both cases, all points lay on a straight line through the points $(10^{-3}, 10^{-3})$ and $(1, 1)$, respectively $(-0.25, -0.25)$ and $(0.25, 0.25)$, indicating a nearly perfect agreement between both data sets.

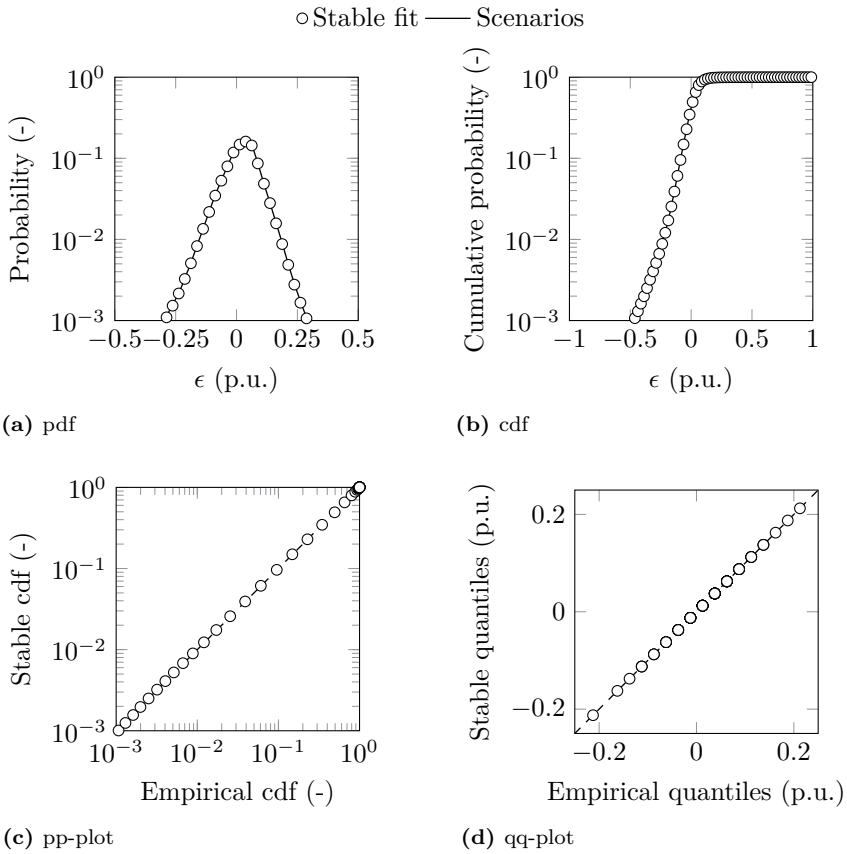

(a) pdf **(b)** cdf

(c) pp-plot **(d)** qq-plot

Figure 4.8: The overall distribution of the generated forecast errors ('Scenarios') and the original, stable distribution ('Stable') is in perfect agreement. Subfigure (a) shows the overall probability density function (pdf). Subfigure (b) displays the overall cumulative density function (cdf). Subfigure (c) contains the pp-plot, which shows the stable cdf as a function of the empirical cdf (scenarios). Subfigure (d) shows the qq-plot, plotting the empirical quantiles (percentiles) of the scenario-based distribution as a function of the quantiles of the stable distribution.

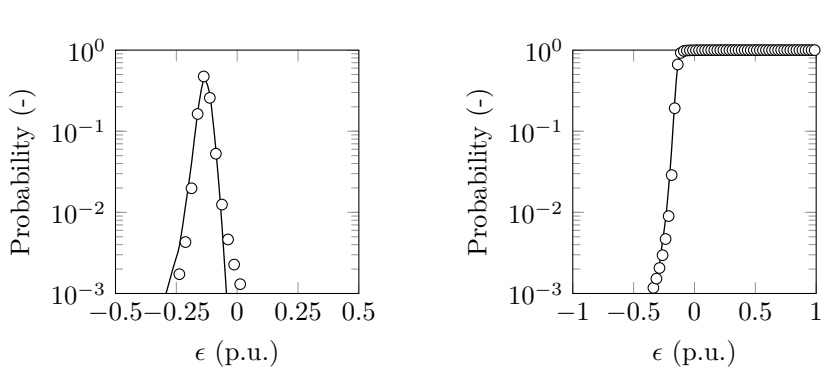

(a) pdf **(b)** cdf

Figure 4.9: The empirical ('Scenarios') and 'historical' pdf and cdf of the wind power forecast error for the 35$^{\text{th}}$ 'previous forecast error' power bin. This power bin contains forecast errors observed subsequent to a forecast error in the interval [−0.15 p.u., −0.125 p.u.].

The distribution of the variability of the forecast error

In contrast to the distribution of the amplitude of the forecast error in each forecast power bin, the correspondence of the distribution of the variability of the forecast error with historical data is not guaranteed. Indeed, the only temporal relation that exist between forecast errors within a scenario is described by the covariance matrix. This is a mere estimate of the 'true' covariance matrix, which does not guarantee an adequate representation of the variability of the forecast error. To validate the correspondence between the historically observed variability and the variability contained in the generated scenarios, we will discuss the conditional distribution of the error on time step j, given the error on the previous time step $j-1$. Similarly to the forecast power bins (Chapter 3), we have defined 'previous error power bins' with a width of 0.025 p.u., in which the forecast error is sorted based on the forecast error observed on the previous time step. This leads to 80 power bins, given the range of the forecast error ([−1 p.u., 1 p.u.]). For example, the 10$^{\text{th}}$ power bin contains (the distribution of) all forecast errors observed immediately preceded by a forecast error between −0.75 p.u. and −0.725 p.u. on the previous time step. In Fig. 4.9 and 4.10 we examine the correspondence between the distribution of the variability of the forecast error observed in historical data ('Historical') and the variability of the forecast error in the generated scenarios ('Empirical' or 'Scenarios'). In

Fig. 4.9, the distribution of the forecast error in the 35^{th} power bin (containing forecast errors observed after a forecast error between -0.15 p.u. and -0.125 p.u.) is shown. Although the agreement is not as good as for the errors in each forecast power bin, we assume that this set of scenarios represents this distribution with sufficient accuracy. Note that after a negative error, it is much more likely that this error persists than that this error will disappear or turn positive (Fig. 4.9). In Fig. 4.10, the overall distribution[11] of the variability of the generated scenarios is shown. Fig. 4.10 illustrates that the variability of the forecast error in the generated scenarios is an adequate representation of the observed variability in the wind power forecast error.

Impact of removal of improbable scenarios

As the only relation between forecast errors at different time steps considered during scenario generation is an estimation of the 'true' covariance matrix, the obtained scenarios may contain events – transitions from one forecast error to the next one – that in reality were not observed. Keeping these events in the scenario sets may lead to an over- or underestimation of the stress imposed on the power system by the wind power forecast errors. Therefore, we will remove those scenarios containing such an improbable event, as discussed in Section 4.2.3. In this case study, on average 10% and at most 23% of the generated scenarios contain an improbable event.

Removing these scenarios – assuming the remaining scenarios are equally probable – will distort the probability density functions of the forecast error as represented by the resulting scenario sets. The magnitude of this distortion is visualized in Fig. 4.11. In this figure, the qq-plots before and after removal of the improbable scenarios are shown for the overall pdf of the forecast error given the forecast and the overall pdf of the forecast error given the previous forecast error, as represented via the corresponding scenario sets. As shown in Fig. 4.11, the effect is most pronounced on the probability of a forecast error, given the forecast. The probability of large forecast errors is slightly underestimated. On the distribution of the variability of the forecast error, the effect is negligible.

This distortion of the resulting probability density functions may be minimized by optimally redistributing the probability of occurrence of the retained scenarios. This option was however not explored in this dissertation.

[11] The distributions in the various 'previous forecast error power bins' are merged as a probability-weighted sum, in which the weights indicate the probability that a forecast error belongs to such a 'previous forecast error power bin'.

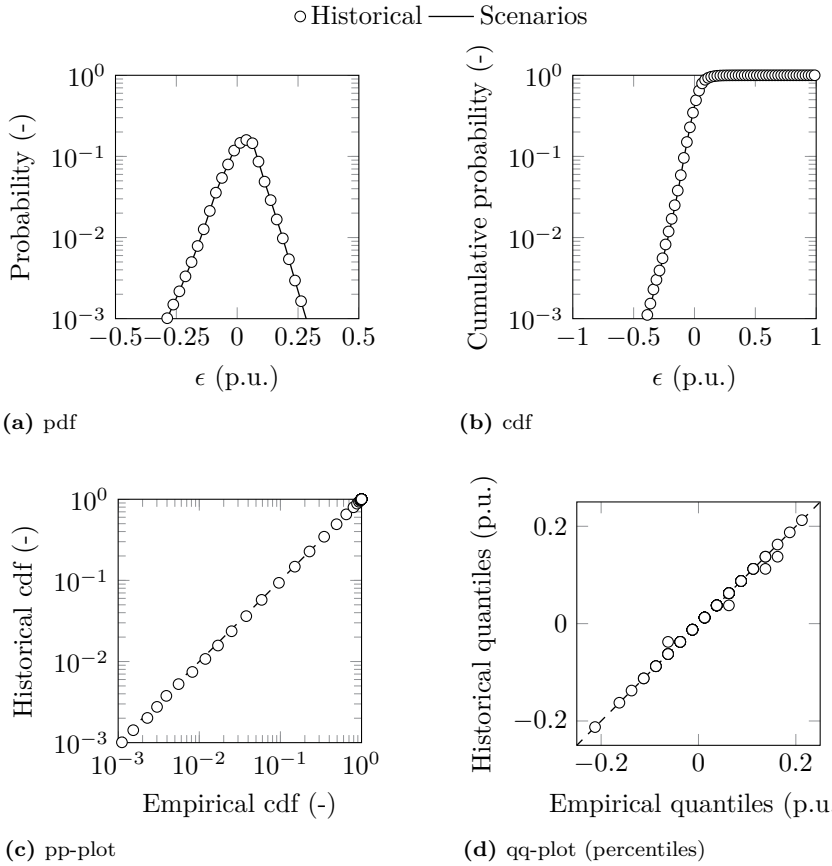

(a) pdf **(b)** cdf

(c) pp-plot **(d)** qq-plot (percentiles)

Figure 4.10: The overall distribution of the variability of the generated forecast error scenarios and the distribution of the variability observed in historical forecast data is in good agreement. Subfigure (a) shows the overall probability density function (pdf). Subfigure (b) displays the overall cumulative probability density function (cdf). Subfigure (c) contains the pp-plot, showing the proposed historical cdf versus the empirical cdf (scenarios). Subfigure (d) shows the qq-plot, plotting the empircal quanitles of the scenario-based distribution against the quantiles obtained from historical data.

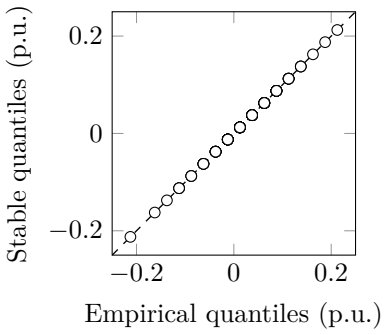

(a) Before removal improbable scenarios – probability of a forecast error, given the forecast

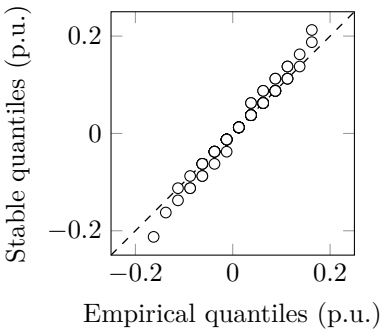

(b) After removal improbable scenarios – probability of a forecast error, given the forecast

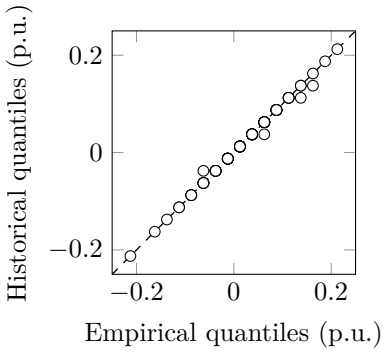

(c) Before removal improbable scenarios – probability of a forecast error, given the previous forecast error

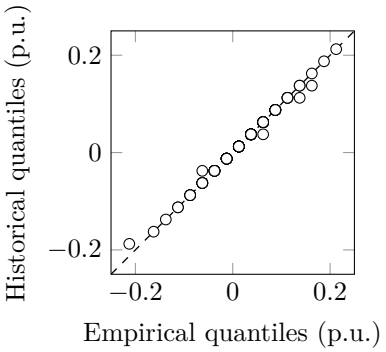

(d) After removal improbable scenarios – probability of a forecast error, given the previous forecast error

Figure 4.11: The effect of the removal of scenarios containing improbable events on the probability density functions of the wind power forecast error as represented by the different scenario sets.

Event-based verification

Up to this point, we have only focused on the distribution of the forecast error, given the forecast or the previous forecast error. However, some events, such as positive or negative forecast errors that persist over multiple time steps or prolonged negative or positive ramps in the forecast error, may be challenging for the power system at hand. Therefore, if these events occur in real life, these events and their probability of occurrence should be reflected in the generated scenarios. To evaluate how well a set of scenarios captures the probability of a certain event, Pinson and Girard developed a so-called event-based verification framework, based on Brier-scores [185][12].

In this dissertation, we have defined two types of events for which we will check the probability of occurrence in historical data and the generated scenario sets. The probability of these events is calculated via two so-called functionals, here indicated by g_1 and g_2, designed to detect prolonged forecast errors and prolonged ramps in the forecast error[13]. The first type of event is the occurrence of a wind power forecast error of at least magnitude ξ that persists over a certain time period h. The functional g_1, used to detect the occurrence of such an event, can mathematically be expressed as

$$g_1(\epsilon_{j,s}, k, h, \xi) = \prod_{j=k}^{j=k+h} \mathbf{1}\{\epsilon_{j,s} \geq \xi\}, \tag{4.12}$$

in which $\mathbf{1}\{\}$ is an indicator variable, which equals one if the expression between brackets is true and zero otherwise. $\epsilon_{j,s}$ is the wind power forecast error scenario to which this functional is applied, while k is an auxiliary variable to select the moment of interest in this scenario. The second event of interest relates to the variability of the forecast error. We will check the occurrence of a significant gradient ξ in the wind power forecast error over a certain period of time h, which is detected via functional g_2:

$$g_2(\epsilon_{j,s}, k, h, \xi) = \mathbf{1}\{\max_{j\in[k,k+h]}\epsilon_{j,s} - \min_{j\in[k,k+h]}\epsilon_{j,s} \geq \xi\}. \tag{4.13}$$

[12]In their paper, Pinson and Girard [185] discuss the need for and the added value of such an event-based evaluation framework in detail. They illustrate that while traditional statistical verification frameworks (such as the one presented above) have their merits, they should be complemented with event-based approaches to check if e.g. a SGT or forecasting method is capable of mimicking specific characteristics of the stochastic process at hand.

[13]Other events and functionals can be defined. The events mentioned above were chosen here as they may be - from an operational vantage point - particularly challenging for a power system (operator).

Table 4.2: The average Brier scores for prolonged forecast errors (functional $g_1(\epsilon_{j,s}, k, h, \xi) = \prod_{j=k}^{j=k+h} \mathbf{1}\{\epsilon_{j,s} \geq \xi\}$) shows that the generated scenarios include all relevant events of type g_1 and that these events occur with a reasonable probability. The value between brackets is the variance on the Brier score.

		h [h]						
		0.5	1	2	3	4	5	6
ξ [$p.u.$]	-0.5	0 (0)	0 (0)	0 (0)	0.0001 (0)	0 (0)	0.0001 (0)	0.0001 (0)
	-0.4	0.0001 (0.0001)	0.0002 (0.0002)	0.0003 (0.0003)	0.0006 (0.0004)	0.0009 (0.0005)	0.0013 (0.0006)	0.0017 (0.0007)
	-0.3	0.0040 (0.0018)	0.0050 (0.0024)	0.0062 (0.0033)	0.0072 (0.0041)	0.0081 (0.0047)	0.0090 (0.0053)	0.0099 (0.0059)
	-0.2	0.0146 (0.0065)	0.0182 (0.0076)	0.0219 (0.0092)	0.0253 (0.0107)	0.0282 (0.0122)	0.0311 (0.0140)	0.0339 (0.0159)
	-0.1	0.0539 (0.0150)	0.0693 (0.0175)	0.0833 (0.0205)	0.0951 (0.0231)	0.1050 (0.0252)	0.1139 (0.0274)	0.1220 (0.0297)
	0	0.1877 (0.0090)	0.2007 (0.0061)	0.2055 (0.0045)	0.2059 (0.0042)	0.2046 (0.0046)	0.2022 (0.0057)	0.1986 (0.0072)
	0.1	0.1049 (0.0152)	0.0719 (0.0126)	0.0484 (0.0096)	0.0338 (0.0072)	0.0243 (0.0054)	0.0178 (0.0039)	0.0125 (0.0028)
	0.2	0.0120 (0.0015)	0.0059 (0.0006)	0.00265 (0.0003)	0.0010 (0.0001)	0.0004 (0)	0.0001 (0)	0 (0)
	0.3	0.0012 (0.0001)	0.0005 (0)	0.0002 (0)	0.0001 (0)	0 (0)	0 (0)	0 (0)
	0.4	0.0001 (0)	0 (0)	0 (0)	0 (0)	0 (0)	0 (0)	0 (0)
	0.5	0 (0)	0 (0)	0 (0)	0 (0)	0 (0)	0 (0)	0 (0)

Table 4.3: The average Brier scores for gradients in the forecast errors (functional $g_2(\epsilon_{j,s}, k, h, \xi) = \mathbf{1}\{\max_{j\in[k,k+h]}\epsilon_{j,s} - \min_{j\in[k,k+h]}\epsilon_{j,s} \geq \xi\}$) shows that the generated scenarios include all relevant events of type g_2 and that these events occur with a reasonable probability. The value between brackets is the variance on the Brier score.

		h $[h]$						
		0.5	1	2	3	4	5	6
ξ $[p.u.]$	0.1	0.0023 (0.0001)	0.0372 (0.0033)	0.1197 (0.0173)	0.1869 (0.0279)	0.21.85 (0.0267)	0.2245 (0.0200)	0.2173 (0.0136)
	0.2	0.0001 (0)	0.0031 (0.0001)	0.0114 (0.0012)	0.0256 (0.0042)	0.0441 (0.0092)	0.0646 (0.0167)	0.0861 (0.0257)
	0.3	0.0001 (0)	0.0003 (0)	0.0016 (0.0001)	0.0038 (0.0003)	0.0066 (0.0008)	0.0107 (0.0019)	0.0159 (0.0040)
	0.4	0.0001 (0)	0.0002 (0)	0.0004 (0)	0.0010 (0.0001)	0.0020 (0.0002)	0.0031 (0.0005)	0.0042 (0.0009)
	0.5	0.0001 (0)	0.0001 (0)	0.0003 (0)	0.0006 (0.0001)	0.0009 (0.0001)	0.0013 (0.0003)	0.0016 (0.0005)

The functionals g_1 and g_2 are applied to each time step j of each scenario $\epsilon_{j,s}$ in scenario set $\mathbf{S}$ to obtain so-called 'probability forecasts' $P_j\left[g(\mathbf{S}, k, h, \xi)\right]$ as follows:

$$P_j\left[g(\mathbf{S}, k, h, \xi)\right] = \frac{1}{N}\sum_{s=1}^{N} g(\epsilon_{j,s}, k, h, \xi), \tag{4.14}$$

in which P_j should be understood as the probability of the event described by functional g at time step j, as predicted by the set of scenarios $\mathbf{S}$ (containing N scenarios). Using this probability forecast, Brier scores Bs [185] can be obtained for each event by calculating the quadratic distance between the probability forecast, obtained from the set of scenarios, and the value of the functional applied to the historical wind power forecast errors at the same time step j:

$$Bs = \frac{1}{T-h}\sum_{j=1}^{T-h}\left(P_j\left[g(\mathbf{S}, k, h, \xi)\right] - g(\mathbf{WPFE}, k, h, \xi)\right)^2, \tag{4.15}$$

with T the length of the scenarios considered, $\mathbf{S}$ the set of forecast error scenarios and $\mathbf{WPFE}$ the historical wind power forecast error data. This Brier score Bs varies between 0 and 1, with a Brier score equal to 0 indicating a perfect

correspondence between the probability of occurrence of a certain event in the set of scenarios and the observations.

In Table 4.2 and 4.3, we have summarized the Brier scores that describe the correspondence between the generated scenarios and the historical wind power forecast error observed in the Belgian power system. The values displayed are average Brier scores: we calculated the Brier score for each set of scenarios, which were generated to represent the forecast error for a specific day, and averaged the resulting Brier scores over the year. The numbers between parentheses indicate the variance on the obtained Brier scores. The Brier scores for events described by functional g_1 are all below an acceptable 21%, with the largest Bs values for events with ξ equal to zero. Similarly, for the gradient-type events (functional g_2), Brier scores are below 23%, with the highest Brier scores for small gradients over a long period of time. In both cases, the variance on these values is small, which allows us to conclude that the presented, average Brier scores are a good representation of the Brier score for each set of scenarios. As these Brier scores are low, we conclude that the set of scenarios captures the probability of occurrence of the investigated events adequately.

4.3.2 Scenario generation & the distribution of the solar power forecast errors

An identical analysis has been performed for the solar power forecast error. Again, 500 scenarios per day were generated for each day of the year 2013, based on a fitted Lévy α-stable distribution (Chapter 3). The resulting discrete representations of the distribution of the solar power forecast error and the variability of the solar power forecast error were compared to the solar power forecast error observed in the Belgian power system in the same year. For sake of brevity, the results of the analysis are summarized in Fig. 4.12. Before the removal of those scenarios that contain 'improbable' events, the correspondence of the quantiles of the solar forecast error scenarios and the historical data is nearly perfect, as expected (Fig. 4.12a and Fig. 4.12c). Removing improbable scenarios from the scenario sets (on average 15% of the generated scenarios) leads to minor differences between the original distributions and the scenario-based distributions (Fig. 4.12b and Fig. 4.12d). The likelihood of a large positive or negative forecast error is slightly underestimated, similar as for the wind power forecast errors. Again, the distribution of the variability of the solar power forecast error is nearly unaffected. The Brier scores for prolonged solar power forecast errors and gradients in the solar power forecast error confirm the adequate representation of the solar power forecast error. As the Brier scores for the solar power forecast error show the same trends as those obtained for the wind power forecast error, they are not repeated here.

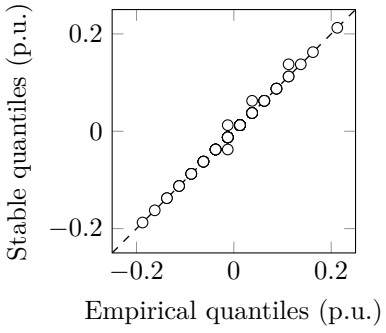

(a) Before removal improbable scenarios – probability of a forecast error, given the forecast

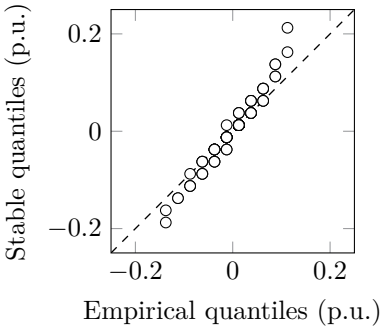

(b) After removal improbable scenarios – probability of a forecast error, given the forecast

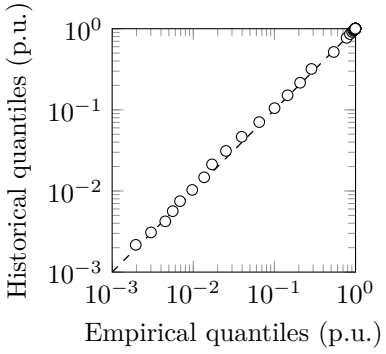

(c) Before removal improbable scenarios – probability of a forecast error, given the previous forecast error

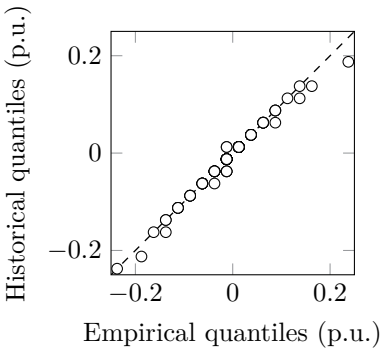

(d) After removal improbable scenarios – probability of a forecast error, given the previous forecast error

Figure 4.12: The historical or fitted ('stable') solar power forecast error distribution and the distribution of the generated solar power forecast scenarios, before and after removal of scenarios that contain improbable events, are in good agreement. All figures are so-called qq-plots, showing the quantiles of the original distributions as a function of the empirical quantiles as calculated from the scenario sets.

4.3.3 Conclusion: scenario generation

We have shown that the technique proposed above allows capturing the behavior of the wind and solar power forecast error with a reasonable number of scenarios. Not only the amplitude of the forecast error, but also its variability is represented in these scenarios. An event-based evaluation framework showed that the resulting scenarios include those events (prolonged errors, large gradients over time) that are deemed challenging for the power system and that these events occur with a realistic probability.

The proposed scenario generation technique may be improved on two fronts. First, better estimates of the covariance matrix, which governs the intertemporal relations in a scenario, may lead to a more accurate representation of the variability of the forecast error. Second, the removal of scenarios that contain improbable events results in a mismatch of the scenario-based and original distribution of the forecast error. Optimally redistributing the probability of occurrence of the retained scenarios may allow minimizing this distortion. These improvements are however not pursued in this dissertation.

4.4 Scenario reduction: theory

In this section, scenario reduction techniques (SRTs) are introduced. The focus is on those methods that have been or could be applied to scenario trees representing uncertain RES-based generation in SUC models. In our discussion, we will assume that a large set of scenarios is given, characterizing the statistical variable at hand[14]. However, considering this large set directly in a SUC model will typically render the optimization problem at hand intractable, or will yield high computing times. Regaining tractability of the problem with minimal loss in solution quality is the objective of any SRT. In other words, a SRT aims to reduce the considered set of scenarios, while minimizing the resulting difference in objective function of the optimization problem solved on the reduced set of scenario and on the full set of scenarios[15]. To trigger optimal decisions in the stochastic program, one does not necessarily need to capture the full distribution, but only those elements or events that affect the decision process.

[14]Note that some authors combine scenario tree generation and reduction in a one-step approach. However, scenario generation and reduction methods typically have different objectives. Scenario generation methods will seek to characterize the stochastic variable at hand via a set of discrete realizations. Scenario reduction methods try to reduce the computational effort needed to solve a stochastic problem without loss of solution quality.

[15]Recall that we related this objective to the concepts of stability and bias in Section 4.1. We will use these metrics in Section 4.5 to assess the performance of selected SRTs. For now, it suffices to keep the aforementioned objective in mind.

For example, if the stochastic program at hand yields a stable, unbiased optimal solution by considering an 'average' and a 'worst-case' scenario, a SRT should be able to select those scenarios. However, one can hardly argue that the resulting set is an adequate discrete representation of the uncertain variable.

Scenario reduction techniques can act on two fronts. First, they can aim to reduce the number of individual scenarios through the selection or removal of scenarios from an original, large set (scenario reduction). Second, they can reduce fan-like scenario trees by grouping equal or similar values in all but the last node, without reducing the number of scenarios present (scenario aggregation). In the context of wind power, not only the amplitude, but also the auto-correlation between wind power forecast errors in a scenario is of importance. By merging (parts of) scenarios, this information will be lost. Therefore, in this chapter, we will only focus on the first category of SRTs.

The remainder of this section is organized as follows. First, we will present a non-exhaustive overview of current SRTs. For each technique, we will list some advantages and disadvantages. Some examples will be listed, with special attention for applications in the field of wind and solar energy. For the readers' convenience, we summarize our findings in Table 4.4. Second, we discuss an improved SRT, inspired by the work of Dupačová et al. [38] and Heitsch and Römish [216], in Section 4.4.3. For sake of comparison, we will briefly discuss the SRTs proposed by Morales et al. [122] and Papavasiliou and Oren [109]. Before moving to a quantitative analysis of the added value of this novel SRT (Section 4.5), we will illustrate its working principles in a methodological example (Section 4.4.4).

4.4.1 Scenario reduction techniques

The following classification is inspired by Heitsch and Römisch [217], Dupačová et al. [187] and our own review of the current scientific literature. We will distinguish between the following categories of SRTs:

- Importance sampling-based techniques;
- Moment matching-based techniques;
- Clustering techniques;
- Optimal approximation methods based on probability metrics.

No widely accepted classification exists and we do not aim to be exhaustive. In addition to the SRTs listed above, heuristic scenario reduction methods are

found in the scientific literature [17, 205]. Although such heuristics typically are highly customizable and may yield good results, they have no theoretical foundation and no guaranteed performance. These 'purely heuristic' SRTs will not be discussed below, as most authors in the scientific literature acknowledge the need for a methodological, widely-applicable approach. However, note that SRTs often require solving optimization problems themselves. These problems are often characterized by many local maxima and minima and are thus difficult to solve exactly. In many cases, heuristics have to be employed to approximate the solution of the original scenario reduction problem in reasonable calculation times. We will classify these heuristics based on the original approach (thus optimization problem) they refer to. Note furthermore that combinations of the SRTs below are possible. In addition, all of these methods may be complemented with statistical approaches to check the solution quality during the optimization process. If the solution quality does not meet certain criteria, a larger scenario tree is used to solve the problem once more. These techniques are typically referred to as 'internal sampling' techniques [111, 35]. Given the high computational cost of solving a SUC model, even with a moderate number of scenarios [17], we will not further consider these iterative approaches.

In **importance sampling-based SRTs**, one will select scenarios from an initial set based on some sampling criteria that ideally reflect the 'importance' or impact of a scenario on the solution and objective of the stochastic program [109, 218, 219]. These techniques can be one-shot or sequential ('internal importance sampling'). Note that in its simplest form, i.e. when all scenarios are 'of equal importance', importance sampling is the same as Monte-Carlo sampling. The user has the freedom to define whatever sampling rule, but efficiency of the method depends heavily on the adopted sampling rule. If the sampling criterion is sufficiently representative of the impact of the scenario on the solution of the stochastic program, importance sampling techniques can yield stable solutions considering scenario sets of low cardinality [109]. Papavasiliou et al. [109, 110] present a one-shot, probabilistic importance sampling technique, based on the operational cost of a wind power forecast scenario obtained from an equivalent single-scenario ED problem, considering the best available deterministic UC policy. A set of scenarios with a predefined cardinality is selected based on the ratio between the operational cost associated with each scenario and the average operational cost over all scenarios. Papavasiliou et al. employ this SRT to study the impact of transmission constraints in a multi-area SUC problem with a high wind energy penetration.

Scenario reduction techniques based on the **moment-matching principle** select scenarios in order to minimize a measure of distance, e.g. a norm, between the statistical properties of the distributions as represented by the constructed,

reduced scenario set and the original scenario set[16]. As this problem is often non-convex, heuristics have been developed to approximate the optimal solution [212]. The user can specify the statistical parameters that he or she deems important in the problem at hand and only those parameters must be specified, making these methods especially useful when little information is available on the underlying statistical process [187]. Hochreiter and Pflug [220] however illustrate that the difference between the moments of the distribution and the proposed approximation may never lead to a real (probabilistic) distance or metric between these two representations. These methods generally do not guarantee convergence, i.e. increasing the number of scenarios may not improve the solution stability or reduce the bias of the resulting solution of the stochastic problem [111, 188]. Furthermore, one can intuitively see that multiple combinations of scenarios can approximate the statistical moments of the distribution. The modeler has to select one of those scenario sets, but the moment-matching principle does not provide a basis for this decision. Moreover, modelers will typically employ more scenarios than strictly necessary to match the selected statistical properties, driven by solution stability requirements. Moment-matching techniques do not provide criteria to select those 'additional' scenarios. Recently, Li et al. [221] proposed a moment matching SRT in the context of wind power. The resulting NP hard optimization problem is solved via a fast heuristic search algorithm. Results show that the proposed algorithm leads to lower probability distances between the reduced and original scenario set compared to the backward probability distance-based SRT [38] and the particle swarm optimization algorithm proposed by Pappala et al. [202]. Papavasiliou et al. [17] study the SUC problem considering uncertain wind power forecasts. Scenarios are selected based on a set of heuristic rules, after which probabilities are assigned to the retained scenarios to match the first (average) and second (standard deviation) moment of the original distribution.

In so-called **clustering SRTs**, one tries to group a number of scenarios in a number of predefined bins or clusters, based on any index or metric that characterizes the scenario or its effect on the solution of the stochastic problem. This typically results in a NP-hard optimization problem, but the solution can be approximated by local-search algorithms [222, 223, 224, 225]. The user can freely define any metric to describe a scenario, but the quality of the clustering is highly dependent on the chosen metric. Typically, one still has to select one or more scenarios from each cluster and assign probabilities to these scenarios. Especially if one starts from a large set of scenarios or uses few clusters, this may be a non-trivial task. One merely reduces the size of the scenario reduction problem from the initial set of scenarios to the set of scenarios contained in the cluster. For this reason, clustering techniques are often used in combination

[16]Recall that these methods can also be used as a SGT, if one starts from continuous distributions instead of a discrete scenario tree (Section 4.2).

with other scenario reduction methods [222, 223, 224, 225]. A well-known and often-used clustering technique is the k-means method, which seeks to minimize the squared distance between points in the same cluster [226, 227], applied by Greenhall [228] in the context of SUC problems. Dvorkin et al. [106] however show that this improved k-means clustering algorithm is outperformed by probability distance-based SRTs. Recently, Feng and Ryan [223, 224, 225] propose the so-called 'fast forward in recourse clusters' (FSRC) and 'fast forward in wait-and-see clusters' (FSWC) algorithms. Scenarios are clustered using the k-means algorithm based on user-defined 'solution sensitivity indexes'. These solution sensitivity indexes are e.g. the total operational cost, the amount of curtailed RES-based generation or the total load shedding volume obtained from a single-scenario equivalent UC problem (FSWC) or an economic dispatch problem solved on a UC schedule calculated via a DUC problem considering the expected value of the uncertain variable (FSRC)[17]. After clusters are obtained, one scenario is selected from each cluster using the fast forward algorithm (a probability distance-based method, see below). Feng and Ryan apply their FSWC algorithm in the context of generation expansion planning models [222] and FSRC in SUC problems [225, 223]. A similar method is developed by Y. Wang [229], in which scenarios are clustered according to the value of key first-stage decision variables, obtained from solving a deterministic equivalent of the stochastic program.

As already briefly noted in our discussion on SGTs, **optimal SRTs based on probability metrics** build on the notion of probability metrics such as the Kantorovich distance [37, 230, 216, 231, 38, 217]. The Kantorovich functional can be seen as a measure of the probabilistic distance between two scenario sets (as discrete descriptions of a probability density function) and can thus be used to determine the optimal reduced set of scenarios that minimizes the probabilistic difference between the original and the reduced set of scenarios [38]. This optimal scenario reduction problem however yields a non-differentiable non-convex combinatorial optimization problem that is often too large in scale to be practical in many applications [189, 38]. Therefore, researchers have developed heuristics to approximate the true solution of the aforementioned problem, of which the so-called 'backward' and 'fast forward' scenario reduction techniques are the best known [38][18]. The probability of the not-selected scenarios is redistributed optimally over the selected scenarios.

[17] Note the similarity between the FSWC and the importance sampling SRT as proposed by e.g. Papavasiliou et al. [110, 109] and between the FSRC with the probability-distance based algorithm proposed by Morales et al. [122] (see below).

[18] These algorithms are further refined by Gröwe-Kuska et al. [37] and Heitsch and Römisch [216, 217]. Some modifications are made based on stability results and via the inclusion of a filtration distance by Heitsch and Römisch [231, 230]. The backward and the forward reduction algorithms are included in the GAMS library SCENRED.

Table 4.4: Scenario reduction techniques. Governing principles, advantages, disadvantages, examples and applications.

Category	Principle	Advantages	Disadvantages	Examples	Applications
Importance sampling	'Picking' scenarios based on metric for impact on solution of SUC problem.	• free choice of sampling rule; • stable solutions possible.	• result strongly depends on sampling rule; • no theoretical foundation.	• Papavasiliou et al. [109, 110];	[109, 110]
Moment-matching	Minimize distance between statistical properties of reduced and original scenario set.	• statistical properties may be defined by modeler; • little information on stochastic variable needed.	• increasing number of scenarios does not guarantee reduction stability or bias.	• Høyland and Wallace [212]; • Li et al. [221]; • Papavasiliou et al. [17].	[17, 221]
Clustering	Group scenarios in clusters, based on metric that characterizes scenario or impact on SUC.	• free choice of clustering metric.	• still requires SRT to select scenario in cluster.	• k-means [226, 227]; • Feng and Ryan [223, 224, 225] • Y. Wang [229]	[222, 228, 222, 223, 224, 225, 106]
Optimal SRTs based on probability metrics	Minimize probability metric (e.g. Kantorovich distance) between reduced and original scenario set.	• smallest possible approximation error for a specific cardinality of the scenario set.	• complex optimization, heuristics required; • empirical evidence.	• Fast-forward and backward SRT [37, 38] • Morales et al. [122] • Pineda and Conejo [232]	[192, 233, 208, 234, 39, 235, 206, 236, 202, 198]

The original SRTs, if applied in every stage of the tree, may destroy the auto-correlation that exists between the nodes. This can however be avoided by applying the reduction algorithm for complete scenarios, by using dedicated methods [237] or characterizing scenarios via alternative, single-value metrics [122]. Papavasiliou et al. [17, 109, 110] argue that the algorithms proposed by Dupačová et al. [38] and Heitsch and Römish [231, 230] perform poorly in a SUC setting, which is attributed to two characteristics of these methods. First, they highlight that probability-based metrics are not guaranteed to preserve the moments of the underlying probability function, deemed essential for the performance of the SUC model. Second, these methods do not allow a modeler to directly specify scenarios that are considered critical. Feng and Ryan [223, 222, 224, 225] state that these probability-based SRT only consider the parameters of the scenarios (value and probability), not their impact on the solution of the stochastic problem, which may result in sub-optimal scenario sets and thus solutions of the stochastic problem. Morales et al. [122] therefore introduce a new metric to characterize a scenario, i.e. the objective value as obtained from an equivalent deterministic single-scenario problem for each scenario, in which the first-stage variables have been fixed to values obtained from an equivalent deterministic single-scenario problem considering the probability-weighted average of the original scenario set[19]. Similar modifications are proposed by Pineda and Conejo [232] to explicitly consider risk-averseness. De Oliveira et al. [237] apply the SRT proposed by Dupačová et al. to the values contained in the scenarios at each time step and modify the SRT to retain the auto-correlation between values in the scenarios in the reduced scenario set. Despite the shortcomings of these techniques, their use is widespread in the power system research community. The backward or forward SRT [38] is used in the well-known SUC model WILMAR [192, 233, 208, 234, 39], and by, amongst others, Wu et al. [235], Plazas et al. [206], Latorre et al. [236], Pappala et al. [202] and Wang et al. [198].

4.4.2 Discussion: selecting a scenario reduction technique

To select a SRT, suited for the SUC problem at hand, one must carefully weigh the advantages and disadvantages of each the discussed SRT. Little dedicated scientific literature has been published on the comparison of SRTs in the context of SUC problems to support the discussion above. Recently, Dvorkin et al. [106] compared four SRTs: (1) a clustering technique based on the *k-means* algorithm [226]; (2) the fast forward and (3) backward scenario reduction heuristic based on probability distance metrics [37, 38]; and (4) an importance

[19]The details of the scenario reduction technique as proposed by Morales et al. [122] are introduced in Section 4.4.3.

sampling technique [109]. Based on simulations performed for the 24-bus 1996 IEEE RTS (Reliability Test System) [238], Dvorkin et al. conclude that the fast-forward scenario reduction algorithm yields the most cost-optimal UC schedule and results in the lowest computational cost. Although extensive simulations were performed, little difference is to be observed in the solutions obtained on scenario sets selected with different SRTs. This can partially be explained by the assumption that fast-starting units can be committed and dispatched in real time, even if they were not committed during UC scheduling: more flexibility is available in real time, damping the impact of inadequate UC schedules. Papavasiliou and Oren [109] illustrate that their importance sampling-based technique yields better results than the probability distance-based approach of Dupačová et al. [38]. Moreover, Botterud et al. [102] show that fast-forward scenario selection and a clustering technique do not necessarily outperform a random selection of scenarios. Feng and Ryan [223, 224, 225] compare their FSRC algorithm with the fast-forward heuristic in the context of SUC problems. They show that the FSRC and fast forward algorithm yield similar performance in terms of operational system cost, but that the FSRC allows focusing on reliability. In the context of expansion planning, Feng and Ryan show [222] that the FSWC algorithm yields stable results with scenario sets up to five times smaller than the fast forward SRT, highlighting the importance of accounting for the impact of the scenarios on first-stage decisions during scenario reduction. Pineda and Conejo [232] compare the fast forward algorithm, the modified fast forward algorithm as proposed by Morales et al. [122] and their version of the fast forward algorithm, adapted to account for risk-averseness [232]. In the considered producer trading problems, the techniques as proposed by Morales et al. [122] and Pineda and Conejo [232] yield similar results. Both require a small set of scenarios to capture the so-called conditional value at risk. Only under the assumption of a very risk-averse system operator, the Pineda and Conejo-technique [232] outperforms the modification as proposed by Morales et al. [122].

Probability-based SRTs are fast, easy to implement and well-documented. Although these techniques are supported by a solid theoretical basis and are widely used by power system researchers, they have been criticized in the scientific literature. Some researchers observe that the proposed algorithms do not succeed in selecting those scenarios that trigger cost-effective UC decisions under uncertainty. As shown later in this dissertation, our own research confirms this observation. In the scientific literature, this poor performance is attributed to the fact that probability distance-based techniques (1) may not preserve the moments of the underlying distribution [17, 109, 110], (2) modelers are not allowed to specify critical scenarios [17, 109, 110], (3) the impact of the selected scenarios on the objective and first-stage decisions in the stochastic optimization problem are not taken into account during scenario reduction [223, 222, 224, 225].

Indeed, the approach by Dupačová et al. [38] yields the same set of scenarios regardless of the problem the scenarios are used in – a rather counter-intuitive approach. However, these drawbacks can be overcome by combining notions of importance sampling and probability-based SRTs (Section 4.4.3).

We will not opt for clustering, nor moment-matching techniques as a SRT. Although these techniques have their merits, clustering techniques typically require an additional scenario reduction method to select one or multiple scenarios within a cluster. For the problem at hand, we will use 500 scenarios to represent the wind or solar power forecast error (Section 4.3). The cardinality of this set does not require us to use clustering techniques to reduce the size of the scenario reduction problem. We will therefore try to improve the more direct SRTs and will not further discuss the algorithms proposed by Feng and Ryan [223, 224, 225]. However, the SRT outlined below can be applied in combination with clustering techniques. Moment-matching techniques will not be considered as they typically, by design, do not guarantee convergence towards the stable solution of the stochastic program at hand [111, 188]. In addition, multiple scenario sub-sets can be defined that capture the moments of underlying stochastic variable. The resulting set may thus be not-unique, but different sets that exhibit the same statistical moments may have a significantly different impact on the first-stage decisions and objective value of the stochastic problem at hand.

In the remainder of this section, we will discuss the fast-forward SRT [38] and the proposed modifications to boost the performance of the proposed algorithm. The focus is on the performance, i.e. the tractability of the SUC problem and the cost-efficiency of the resulting UC schedule, of probability-distance based scenario reduction techniques [38]. These are (i) by far the most-used and (ii) considered the best-in-class SRTs [106], although some empirical evidence seems to contradict this observation. We focus on the so-called 'cost function' used to characterize and distinguish between different scenarios. We propose a novel cost function, using notions from importance sampling [109, 110, 219], in addition to the original cost function and the one proposed by Morales et al. [122]. The importance sampling technique as proposed by Papavasiliou and Oren [109] and the fast-forward algorithm by Morales et al. [122] will be briefly summarized for sake of comparison. We conclude this section with a methodological example, illustrating the necessity of the proposed modifications to and the working principles of the fast forward SRT.

4.4.3 The proposed scenario reduction method: an improved fast-forward scenario reduction heuristic

In what follows, we will not discuss the theoretical background of the fast forward algorithm and importance sampling algorithm in detail. The interested reader is referred to specialized literature, e.g. [37, 230, 216, 231, 38, 217] (fast forward, probability distances) and [218, 219, 109, 110] (importance sampling).

Probability distance-based scenario reduction: the fast-forward algorithm

If one succeeds in defining some metric that describes the difference between two (sets of) scenarios or the difference in impact on the SUC solution of these scenarios, scenario reduction boils down to an optimization problem in which one tries to minimize a so-called *probability distance metric* between the original set of scenarios and a new, reduced set of scenarios with a predefined cardinality. In this line of thought, researchers have considered the *Monge-Kantorovich mass transport problem* as a description of the scenario reduction problem. Without going into details, one can think of this Monge-Kantorovich mass transport problem as an optimization problem that defines the optimal, in this case minimal, probability mass transportation that needs to occur to map one probability density function on another [239]. In the context of two (discrete) probability density functions formed by two sets of scenarios, the solution to this optimization problem represents the optimal redistribution of probability over a reduced set of scenarios that minimizes the statistical distance between the original and reduced set.

As shown in [38], the Monge-Kantorovich mass transport problem can be formulated as follows for two sets of discrete scenarios Ω (scenarios ω) and Ω_s (scenarios ω') with finite probability distributions Q and Q' [38, 122, 35][20]:

$$D_K(Q, Q') = \min \sum_{\omega,\, \omega'} c(\omega, \omega') \cdot \eta(\omega, \omega') \tag{4.16}$$

$$\text{subject to} \quad \forall \omega, \omega' : \quad \eta(\omega, \omega') \geq 0 \tag{4.17}$$

$$\forall \omega' : \quad \sum_{\omega} \eta(\omega, \omega') = \pi_{\omega'} \tag{4.18}$$

$$\forall \omega : \quad \sum_{\omega'} \eta(\omega, \omega') = \pi_{\omega} \tag{4.19}$$

[20] In line with the scientific literature on scenario reduction techniques, we will use index ω (set Ω) instead of index s (set S) (Chapter 2) to refer to a scenario in this section.

In this formulation $c(\omega, \omega')$ is referred to as the cost function, i.e. a measure to differentiate between two scenarios, such as a L2-norm. π_ω and $\pi_{\omega'}$ represent the probability of scenario ω, ω' in sets Ω and Ω_s respectively. $\eta(\omega, \omega')$ relates to the joint probability distributions defined on the domain $\Omega \times \Omega$. The Kantorovich distance is a measure of the probabilistic distance between two scenario sets and can thus be used to determine the optimal reduced set of scenarios that minimizes the probabilistic difference between the original Ω and the reduced set of scenarios Ω_s.

The Kantorovich distance (4.16) can, for two stage problems such as the SUC problem and under mild assumptions[21] [122], be simplified to

$$D_K(Q, Q') = \sum_{\omega \in \Omega \setminus \Omega_s} \pi_\omega \cdot \min_{\omega'} c(\omega, \omega') \tag{4.20}$$

Equation (4.20) describes a NP-hard set-covering problem that is too large in scale to be practical in many applications [37]. Researchers have developed several heuristics to solve this problem in reasonable time, of which the *fast forward* and *backward algorithm* developed by Dupačová et al. [38] are the best-known. In this dissertation, we will, similarly as in [122], focus on the *fast forward algorithm*. Although this heuristic does not guarantee to select the set of scenarios with the lowest possible Kantorovich distance to the original set of scenarios [122], the literature suggests that the solutions obtained on reduced sets of scenarios, selected via the *fast forward algorithm*, are more cost-optimal than solutions obtained on other scenario sets of the same cardinality [122, 106].

The iterative *fast forward* algorithm (see below and Fig. 4.13) will select a set of scenarios Ω_s with a predefined cardinality from an original set of scenarios Ω in order to minimize the Kantorovich distance $D_K(Q, Q')$ between the probability density distributions Q' and Q of the reduced and original set of scenarios respectively [38, 122]. Starting from an empty set, scenarios are selected one-by-one until the predefined number of scenarios or, in some cases, a certain Kantorovich distance is reached. A detailed description of the algorithm can be found in [38].

In the original scenario reduction technique proposed by Dupačová et al. [38], the cost function $c(\omega, \omega')$ is given by

$$c(\omega, \omega') = \max\{1,\ h(||\omega - \omega_0||),\ h(||\omega' - \omega_0||)\} \cdot ||\omega - \omega'|| \tag{4.21}$$

[21] This approximation is exact if (i) the stochasticity is pertained to the right-hand sides and (ii) set Ω_s is a subset Ω: $\Omega_s \subset \Omega$.

with ω_0 some fixed element in Ω and h a positive, continuous, non-decreasing function. Typically, the cost function $c(\omega, \omega')$ is simplified to [37, 38][22]:

$$c(\omega, \omega') = ||\omega - \omega'||_2 = \sqrt{\sum_j (\omega_j - \omega'_j)^2} \tag{4.22}$$

Cost function (4.22) only considers the amplitude of the wind power forecast to differentiate between the different scenarios[23]. As illustrated below, the original SRT is hence indifferent to the variability of the wind power scenario. However, this variability might have a significant impact on the objective function and optimal UC schedule for the problem at hand. For example, the possible absence of highly variable scenarios might lead to a UC schedule that is not able to facilitate strongly fluctuating injections of wind power due the ramping constraints of the scheduled units. In addition, cost function (4.22) does not account for the impact of a scenario on the first-stage decisions, i.e. the UC schedule, and on the objective function of the SUC problem [122]. Although the proposed cost function is generic, thus widely applicable, it fails to recognize that the SRT cannot be decoupled from the stochastic problem at hand.

We therefore propose a new cost function $c(\omega, \omega')$, inspired by [122]. The goal is to capture the effect of the addition of a certain scenario to the reduced set of scenarios on the objective function and first-stage decision variables of the SUC problem. The proposed cost function $c(\omega, \omega')$ is given by

$$c(\omega, \omega') = |z_\omega - z_{\omega'}| \tag{4.23}$$

in which z_ω represents the objective value of the deterministic single-scenario equivalent of the SUC problem at hand, in which the set of wind power forecast scenarios is replaced by the realization in scenario ω. Morales et al. [122] calculate the cost of the one-scenario equivalent problem with fixed first-stage decision variables, i.e. the UC schedule. The values of these first-stage decision variables are obtained from the expected value problem corresponding to the SUC problem, i.e. a DUC problem in which wind power forecast is replaced by the expected value over the set of wind power forecasts at each time step. By definition, this approach is risk-averse: during the calculation of the operational cost of the one-scenario equivalent failing to meet the demand will lead to load

[22]The use of higher order metrics may be considered to ensure the match of higher order moments of the distributions as represented by the original and reduced set of scenarios. This option has not been explored in this dissertation.

[23]Note that we characterize and select entire scenarios at once, rather than selecting the relevant wind power forecast values at each time step individually. As such, we preserve the variability and auto-correlation entailed in the wind power forecast scenarios. Neglecting to do so may lead to gross over- or underestimations of the required ramping capacity of the scheduled reserves.

shedding, which is penalized at a very high cost ($VOLL$). The cost function $c(\omega, \omega')$ is thus governed by differences in ENS-volumes (energy not served, load shedding) in the one-scenario equivalent problems, which results in a scenario set with predominantly lower-than-average wind power output scenarios.

In this dissertation, in contrast to the cost function proposed by Morales et al., the first-stage decision variables are not fixed in the one-scenario equivalent DUC problems. Cost function (4.23) allows us to capture the possible benefits of different UC decisions. Scenarios with a lower-than-average wind power output will be characterized by higher fuel costs and vice versa. Moreover, the variability of the wind power output will affect the resulting operational cost, which allows identifying particularly challenging wind power scenarios. In addition, the operational cost that corresponds to the realization of a particular forecast error scenario depends on the expected state of the power system at each time step.

With the objective function (Eq. (4.20)) and the cost function definition (Eq. (4.23)) in mind, we can now use the *fast forward algorithm* [38] to determine the scenarios in set Ω_s that minimize the Kantorivich distance between the original set Ω and the reduced set of scenarios Ω_s (Fig. 4.13). In the first step, the cost function $c(\omega, \omega')$ is calculated for each pair of scenarios. In the second step, one needs to select the first scenario that will form the basis of the reduced set of scenarios. In the *fast forward algorithm* the scenario that is most equidistant from the other scenarios in the set is chosen as the first scenario in the reduced set. This scenario can be obtained by solving

$$\omega_1 = \arg\{\min_{\omega' \in \Omega} \sum_{\omega \in \Omega} \pi_\omega c(\omega, \omega')\} \tag{4.24}$$

As of the third step, one will start iterating, adding a scenario to the reduced scenario set in each iteration until the chosen cardinality of the reduced scenario set N_s is reached. The selection of these scenarios is based on the following equation for each step i:

$$\omega_i = \arg\{\min_{\omega' \in \Omega \setminus \Omega_s^i} \sum_{\omega \in \Omega \setminus \Omega_s^i \setminus \omega'} \pi_\omega \min_{\omega'' \in \Omega_S^{i-1} \bigcup \omega} c(\omega, \omega'')\} \tag{4.25}$$

in which Ω_S^{i-1} is the set that contains the scenarios that are selected before iteration i. After repeating this step in the algorithm $N_s - 1$ times, the reduced set of scenarios Ω_s contains N_s scenarios. As a final step, the probability of not selected scenarios (set $\Omega \setminus \Omega_s$) is optimally redistributed over the retained

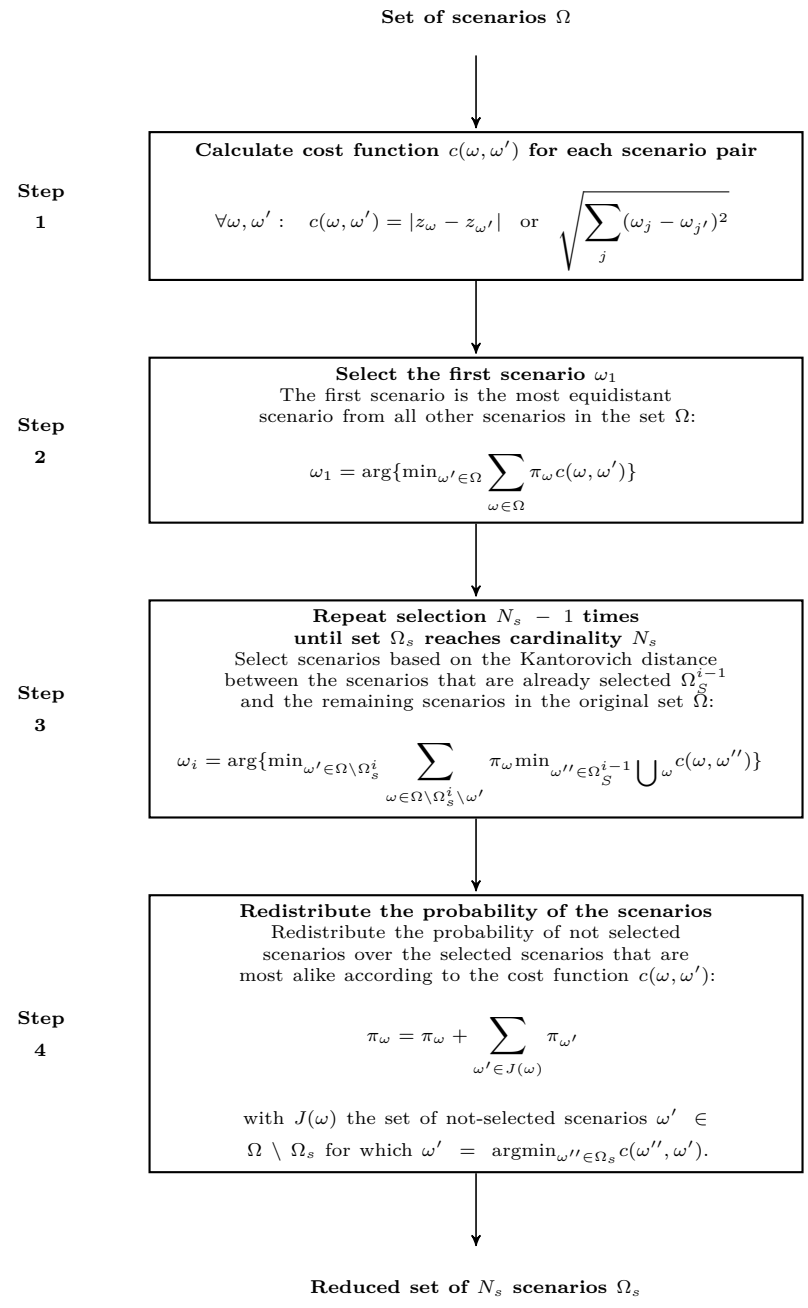

Figure 4.13: Illustration of the *fast forward scenario reduction algorithm* as developed by Dupačová et al. [38, 37].

scenarios (set Ω_s):

$$\pi_\omega = \pi_\omega + \sum_{\omega' \in J(\omega)} \pi_{\omega'} \tag{4.26}$$

with $J(\omega)$ the set of scenarios that (1) are not selected ($\omega' \in \Omega \setminus \Omega_s$) and (2) for which holds that $\omega = \text{argmin}_{\omega'' \in \Omega_s} c(\omega'', \omega')$. This means that the probability of a scenario that is not selected is added to the probability of the scenario that is most alike according to the cost function $c(\omega, \omega')$. As shown in the methodological illustration (Section 4.4.4) and the numerical analysis (Section 4.5), the objective values of the single scenario deterministic equivalent DUC problems are the best available proxies for the impact of the wind power forecast error scenarios on the objective function of the SUC model and thus the only relevant metric to decide on the inclusion or exclusion of a scenario in the stochastic optimization problem.

Importance sampling scenario reduction method

In an approach similar to the one described above, Papavasiliou et al. [109, 110] propose an importance sampling-based SRT in order to account for the impact of a scenario on the objective function of the SUC problem during scenario reduction.

The proposed technique requires the calculation of the operational cost z_ω of the equivalent single-scenario ED problem for each scenario in the original set Ω. The UC schedule of the slow power plants is set to the solution of the *best available* DUC policy, whereas the UC status of fast-responding power plants may change during dispatch. In this dissertation we will however, for sake of simplicity, calculate the operational cost from an equivalent deterministic UC problem per scenario, i.e. the best possible UC policy *per scenario*. Scenarios are subsequently selected one-by-one, in which the probability of picking a scenario p_ω[24] is given by

$$\forall \omega \in \Omega : p_\omega = \frac{z_\omega}{\overline{z_\omega} \cdot N} \tag{4.27}$$

with N the cardinality of the original scenario set Ω and $\overline{z_\omega}$ the average operational cost of a scenario, $\overline{z_\omega} = \sum_{\omega \in \Omega} z_\omega / N$. After N_s scenarios are chosen, each of them is assigned a probability π_ω according to the operational cost of the equivalent single-scenario problem in order to ensure an unbiased

[24]The probability of selecting a scenario p_ω should not be confused with the probability of occurrence of a scenario π_ω. Note furthermore that this is a stochastic technique, which will yield a different set of scenarios with each run of the algorithm.

UC schedule:

$$\forall \omega \in \Omega_s : \pi_\omega = z_\omega^{-1} \tag{4.28}$$

The probability of each scenario is normalized as such that they sum up to unity. This redistribution of the probability of occurrence of the scenarios assumes one starts from a scenario set in which each scenario is equiprobable [109, 110].

The computational cost of scenario reduction

Compared to the approach of Dupačová et al., the calculation of the cost function (4.23) may become computationally challenging. In the approach proposed by Morales et al., solving the one-scenario equivalent problems requires solving (i) one MILP problem, a DUC model considering the expected value of all wind power scenarios, and (ii) N LP problems (no non-spinning reserves) or N easy-to-solve MILP problems (non-spinning reserves), i.e. one dispatch for each scenario in the initial scenario set Ω. The dispatch problems can be solved in parallel and are not computationally demanding. Solving the MILP DUC problem requires $O(10s)$ to $O(100s)$, but needs only to be solved once per scenario set. In contrast, the approach suggested in this dissertation and the importance-sampling approach by Papavasiliou et al. [109, 110] would require solving N MILP UC problems[25]. Although these may be solved in parallel, the resulting computational burden may render the suggested approach impractical. Therefore, we will approximate the operational cost of each MILP UC problem via a simplified UC model (Section 4.5). This simplified MILP model considers the efficiency, minimal and maximal power output of the power plants, but neglects all other technical constraints. This model can be solved in $O(1s)$ to $O(10s)$. We will explicitly discuss the impact of this simplification on the stability and bias of the resulting UC schedule in Section 4.5.

4.4.4 A methodological illustration

Before concluding this section, we will consider a methodological, stylized version of a SUC problem. Although the example is engineered, it allows illustrating the shortcomings of current SRTs and the added value of our novel cost function. In Section 4.5 we show that these observations also hold for the full SUC problem solved for real-life power systems.

[25] To be precise, if one applies the SRT as original proposed by Papavasiliou et al. [109, 110], this would require solving (i) one MILP problem to obtain the best-available DUC policy and (ii) N easy-to-solve MILP problems, i.e. one dispatch for each scenario in the initial scenario set Ω in which the UC status of the fast-responding power plants may be changed w.r.t. the best-available DUC solution.

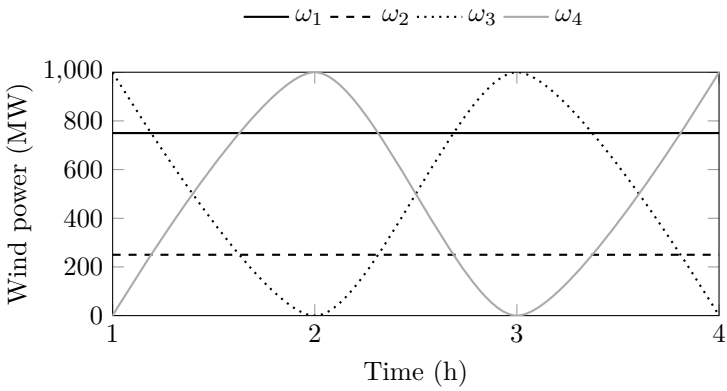

Figure 4.14: Four wind power scenarios are considered in this example. Scenario 1 (ω_1) corresponds to a stable output of 750 MW, scenario 2 (ω_2) to a stable output of 250 MW. In scenario 3 (ω_3) and scenario 4 (ω_4) the wind power forecast varies between 0 and 1000 MW.

A stylized stochastic unit commitment problem

Consider a power system with two generators, A and B, characterized by their start-up costs SC ($SC_A = 50{,}000$ €, $SC_B = 50{,}000$ €), direct fuel costs FC ($FC_A = 50$ €/MWh, $FC_B = 60$ €/MWh) and ramping costs RC related to changes in output ($RC_A = 10$ €/MW, $RC_B = 0$ €/MW). The optimization period is four hours long (index j, set J), which leads to the following objective function:

$$\min \quad SC_A \cdot z_A + SC_B \cdot z_B + \sum_{\omega} \pi_\omega \Big[\sum_{j=1}^{4} (FC_A \cdot g^A_{\omega,j} + FC_B \cdot g^B_{\omega,j}) \qquad (4.29)$$

$$+ \sum_{j=2}^{4} (RC_A \cdot |\Delta^{\omega,j}_{\omega,j-1} g^A| + RC_B \cdot |\Delta^{\omega,j}_{\omega,j-1} g^B|) \Big]$$

In this equation, index ω (set Ω) indicates the wind power forecast scenarios, each with a probability of occurrence π_ω. $g^{\mathrm{A}}_{\omega,j}$ is the output of power plant A on hour j in scenario ω. z is a binary variable indicating the on/off status of the power plant, independent of the scenario ω and time j. This optimization problem is subjected to two constraints. First, the demand for electric power, which is always equal to 1,000 MW, must be met in each hour by the output of

the generators $g^{\mathrm{A}}_{\omega,j}$ and $g^{\mathrm{B}}_{\omega,j}$ and some uncertain wind power forecast $G^{\mathrm{F}}_{\omega,j}$:

$$\forall j, \forall \omega: \quad g^{\mathrm{A}}_{\omega,j} + g^{\mathrm{B}}_{\omega,j} + G^{\mathrm{F}}_{\omega,j} = 1,000 \;\; MW \tag{4.30}$$

Second, a unit can only produce power if it is switched on for the duration of the studied period:

$$\forall j, \forall \omega: \quad 0 \leq g^{\mathrm{A}}_{\omega,j} \leq 1,000 \;\; MW \cdot z_A \tag{4.31}$$

$$\forall j, \forall \omega: \quad 0 \leq g^{\mathrm{B}}_{\omega,j} \leq 1,000 \;\; MW \cdot z_B \tag{4.32}$$

Now, consider four wind power forecast scenarios, as shown in Fig. 4.14. Scenario 1 corresponds to a stable output of 750 MW, scenario 2 to a stable output of 250 MW. In scenario 3, the output varies between 0 and 1,000 MW. Scenario 4 is the reverse of scenario 3. Each of these scenarios occurs with a probability of 0.25.

The optimal solution to the stylized stochastic unit commitment problem

The solution of the stochastic optimization problem described above can be determined at sight using Table 4.5. In this table, the operational cost is calculated for each value of the first-stage variables z^A and z^B. The expected operational cost, i.e. the objective value of the stylized SUC problem would be 187,500 € if generator A is switched on and 170,000 € if generator B is switched on. Switching both generators would reduce fuel costs and eliminate ramping costs, but the increased start-up costs would render this solution more expensive. The optimal solution for the first-stage variables thus equals $z_A = 0$ and $z_B = 1$, with an expected cost of 170,000 €.

Scenario reduction

The optimal solution above was obtained by considering all possible outcomes of the uncertain wind power. Imagine we would reduce the number of scenarios considered in this optimization. Which scenarios do we need to select to trigger the optimal first-stage decision? Scenarios 3 and 4 are the only scenarios that would result in the optimal decision $z_A = 0$ and $z_B = 1$. The SRT should be able to identify these scenarios without prior knowledge of the optimal solution of the stochastic problem at hand.

Fast-forward scenario reduction The cost function will determine which scenario is selected, as it determines the Kantorovich distance between the

Scenario →	ω_1		ω_2		ω_3		ω_4	
↓ Hour	$z_A = 1$	$z_B = 1$	$z_A = 1$	$z_B = 1$	$z_A = 1$	$z_B = 1$	$z_A = 1$	$z_B = 1$
1	12.5	15	37.5	45	0	0	50	60
2	12.5	15	37.5	45	75	60	25	0
3	12.5	15	37.5	45	25	0	75	60
4	12.5	15	37.5	45	75	60	25	0
FC+RC (k€)	50	60	150	180	175	120	175	120
SC (k€)	50	50	50	50	50	50	50	50
TOC (k€)	100	110	200	230	225	170	225	170

Table 4.5: Solution of the stylized SUC problem. Each row corresponds to the operational cost (fuel costs + ramping costs), expressed in k€, in a specific hour under a specific scenario. The last three rows list the total fuel and ramping cost ('FC+RC'), start-up cost ('SC') and total operational cost ('TOC') respectively. The situation in which the two power plants are simultaneously online has not been considered, as start-up costs would dominate the solution and yield a more expensive, hence sub-optimal solution.

reduced and original set of scenarios. In the first step of the scenario reduction algorithm, we calculate the cost function $c(\omega, \omega')$ for all combinations of individual scenarios. We distinguish $c_D(\omega, \omega')$, the cost function as proposed by Dupačová et al. [38, 37]; $c_M(\omega, \omega')$, the cost function as proposed by Morales et al. [122] and $c_B(\omega, \omega')$, the cost function proposed in this dissertation (Section 4.4.3):

$$c_D(\omega, \omega') = \begin{pmatrix} 0 & 2,000 & 2,000 & 2,000 \\ 2,000 & 0 & 2,000 & 2,000 \\ 2,000 & 2,000 & 0 & 4,000 \\ 2,000 & 2,000 & 4,000 & 0 \end{pmatrix} \tag{4.33}$$

$$\rightarrow \quad d_D(\omega) = c_D(\omega, \omega') \cdot \begin{pmatrix} 0.25 \\ 0.25 \\ 0.25 \\ 0.25 \end{pmatrix} = \begin{pmatrix} 1,500 \\ 1,500 \\ 2,000 \\ 2,000 \end{pmatrix}$$

$$c_M(\omega, \omega') = \begin{pmatrix} 0 & 100,000 & 125,000 & 125,000 \\ 100,000 & 0 & 25,000 & 25,000 \\ 125,000 & 25,000 & 0 & 0 \\ 125,000 & 25,000 & 0 & 0 \end{pmatrix} \tag{4.34}$$

$$\rightarrow \quad d_M(\omega) = c_M(\omega, \omega') \cdot \begin{pmatrix} 0.25 \\ 0.25 \\ 0.25 \\ 0.25 \end{pmatrix} = \begin{pmatrix} 87,500 \\ 37,500 \\ 37,500 \\ 37,500 \end{pmatrix}$$

$$c_B(\omega, \omega') = \begin{pmatrix} 0 & 100,000 & 70,000 & 70,000 \\ 100,000 & 0 & 30,000 & 30,000 \\ 70,000 & 30,000 & 0 & 0 \\ 70,000 & 30,000 & 0 & 0 \end{pmatrix} \tag{4.35}$$

$$\rightarrow \quad d_B(\omega) = c_B(\omega, \omega') \cdot \begin{pmatrix} 0.25 \\ 0.25 \\ 0.25 \\ 0.25 \end{pmatrix} = \begin{pmatrix} 60,000 \\ 40,000 \\ 25,000 \\ 25,000 \end{pmatrix}$$

The cost function $c_D(\omega, \omega')$ is easily calculated as the sum of the absolute difference between the wind power scenarios[26]. For example, $c_D(1,2)$ equals $4 \cdot (750 \text{ MW} - 250 \text{ MW}) = 2,000$ MW. Note that according to this cost function the distance between all scenario pairs but scenario 3 and 4 is equal. However, from our analysis above it is clear that scenario 3 and 4 are clearly distinct from scenario 1 and 2, and only those trigger the optimal first-stage decision $z_B = 1$. This cost function thus does not allow capturing the variability in scenario 3 and 4 and its impact on the objective function.

Calculating $c_M(\omega, \omega')$ requires knowledge of the first-stage solution, i.e. the value of z_A and z_B, in the one-scenario equivalent of the SUC problem in which the wind power scenarios are replaced by their expected value. One can easily verify that this expected value corresponds to a stable wind power output of 500 MW, which would yield a solution $z_A = 1$ and $z_B = 0$ and an operational cost of 150,000 €. $c_M(\omega, \omega')$ can thus be calculated via Table 4.5 as the absolute difference between operational costs corresponding to $z_A = 1$ for each scenario. For example, $c_M(2,3)$ equals $|200,000 \text{ €} - 225,000 \text{ €}| = 25,000$ €. The cost function $c_B(\omega, \omega')$ can be derived from Table 4.5 as well. It is calculated as the absolute difference between the objective value of each one-scenario equivalent of the SUC problem, i.e. the optimal solution for each scenario. For example, $c_B(2,3)$ equals $|200,000 \text{ €} - 170,000 \text{ €}| = 30,000$ €.

Based on these cost functions, one can calculate the Kantorovich distance $d(\omega)$ between the reduced set Ω_s that would contain one of the scenarios ω and the original set. For example, $d_B(\omega_1)$ should be interpreted as the Kantorovich

[26] In this simplified example, we use the L1-norm instead of the L2-norm in Eq. (4.22) for sake of simplicity. The reader can however easily verify that the statements below hold as well if the cost function is calculated with the L2-norm.

distance between $\Omega_s = \{\omega_1\}$ and set Ω. This Kantorovich distance now allows selecting a first scenario. For the cost function as proposed by Dupačová et al. [38] the resulting Kantorovich distance does not allow for any differentiation between the scenarios 1 and 2 or 3 and 4: the algorithm does not show a preference between these scenarios. Moreover, this approach would force you to (arbitrarily) select scenario 1 or 2. Both of these scenarios yield the sub-optimal soluton $z_A = 1$. Morales et al. [122] propose an alternative cost function, which yields a minimum Kantorovich distance if one selects scenario 2, 3 or 4. Although we have a good chance of selecting the 'correct' scenario, the algorithm does not succeed in recognizing the difference in impact of scenario 2, 3 and 4 on the solution of the stochastic program. The cost function as proposed by Morales et al. [122] focuses on the large deviations in operational cost from the expected-value solution. In this particular example, a low wind power production (scenario 2) and a highly variable wind power production (scenario 3 and 4) yield cost differences in the same order of magnitude. However, this difference in operational cost is artificially high, as the cost function $c_M(\omega, \omega')$ is calculated without accounting for possible operational cost reductions that stem from different first-stage decisions. As a result, scenario 2 is – wrongfully – indicated as 'equally important' as scenario 3 and 4. The cost function proposed in Section 4.4.3 does result in the selection of scenario 3 or 4: $\Omega_s^B = \{3\}$. By allowing the first-stage variables to change in the single-scenario deterministic equivalent problem, one finds a better proxy for the contribution of scenario 3 and 4 to the objective function of the stochastic problem with optimal first-stage decisions. Note that both $c_M(\omega, \omega')$ and $c_B(\omega, \omega')$ show similar differences between each of the scenarios, while the Kantorovich distances expresses different preferences towards the selection of each of the scenarios. Note furthermore that the cost functions $c_M(\omega, \omega')$ and $c_B(\omega, \omega')$ do not differentiate between scenario 3 and 4. Indeed, both have the same 'impact' on the SUC problem, and differentiation is here thus unnecessary.

The question now remains how we should judge the quality of these results. One can do this by solving the SUC model considering the scenarios in Ω_s. Ideally, one would like to obtain the same solution from this optimization as one would if one solves the SUC model considering all scenarios (Section 4.1). This is the case for $\Omega_s^B = \{3\}$, while $\Omega_s^M = \{2\}$ would yield $z_A = 1$ and $z_B = 0$. In addition, the objective value of the solution should be as close as possible to the objective value of the full stochastic problem (solution stability). In this case, the solution for $z_A = 1$ considering scenario 3 would yield an objective value of 170,000 €, which is close to the objective of the full stochastic problem (175,000 €). One could claim that we have reached the stable solution of the stochastic program with a bias of 5,000 €, if one employs the cost function proposed in this dissertation. This difference in performance stems from the method used to calculated the cost function. Morales et al. [122] base the

operational cost used to characterize each scenario on the evaluation of the resulting deterministic equivalent considering fixed first-stage decision variables. Although this allows capturing costs that depend on variability, such as the ramping costs in this simple problem, and thus to differentiate between scenarios with the same average value, one neglects the impact alternative first-stage decisions might have. If one would allow z_A and z_B to take on other values, as we did to calculate $c_B(\omega, \omega')$, one sees the opportunity to reduce costs in scenario 3 or scenario 4 by setting z_A to 1.

In the second step of the scenario reduction algorithm, one needs to update the cost matrix $c(\omega, \omega')$. We will illustrate this for $c_B(\omega, \omega')$, but the reasoning is the same for the other cost functions. Using Eq. (4.25), the values of all rows except the row corresponding to the selected scenarios are updated. Each value in the cost matrix is compared to the corresponding c_B value of the selected scenario. The minimum of these two values is retained:

$$c_B(\omega, \omega') = \begin{pmatrix} 0 & 70,000 & 70,000 & 70,000 \\ 30,000 & 0 & 30,000 & 30,000 \\ 70,000 & 30,000 & 0 & 0 \\ 0 & 0 & 0 & 0 \end{pmatrix}$$

For example, the new value $c_B(1,2)$ is obtained as $\min(c_B(1,2), c_B(1,3)) = \min(100000, 70000) = 70,000$. Note that the third row, corresponding to the selected third scenario, is unchanged. With this updated cost matrix the Kantorovich distance between set $\Omega_s = \{3\}$ and set $\Omega \setminus \Omega_s$ can be calculated as follows:

$$d_B(\omega \in \Omega) = \pi_{\omega \in \Omega \setminus \{w\}} \cdot c_B(\omega, \omega')^T$$

which yields

$$d_B(\omega \in \Omega) = \begin{pmatrix} d_1 \\ d_2 \\ d_4 \end{pmatrix} = \begin{pmatrix} \pi_2 \cdot c_B(2,1) + \pi_4 c_B(4,1) \\ \pi_1 \cdot c_B(1,2) + \pi_4 \cdot c_B(4,2) \\ \pi_1 \cdot c_B(1,4) + \pi_2 \cdot c_B(2,4) \end{pmatrix} = \begin{pmatrix} 7,500 \\ 17,500 \\ 7,500 \end{pmatrix}$$

for this particular instance. Hence, in the second step of this algorithm, we would select scenario 1 or 4: $\Omega_s = \{3, 1\}$.

In the final step of the scenario reduction algorithm, the probabilities are redistributed optimally based on the original cost matrix $c_B(\omega, \omega')$. Scenario 2 and 4 are closest to scenario 3, thus the probability of scenario 2 and 4 is added to scenario 3: $\pi_3 = 0.75$.

Importance sampling-based scenario reduction If one would apply an importance sampling SRT as described by Papavasiliou et al. [109, 110], one

would obtain the following procedure. First, the single-scenario equivalent problems are solved. The resulting operational costs are listed in Table 4.5 and correspond to the best possible solution for each scenario. The average operational cost $\overline{z_\omega}$ equals 110,000 €. By dividing the objective value of each single-scenario equivalent UC problem by the average cost and the number of scenarios in the original set, one obtains the probability p_ω of selecting a particular scenario ω:

$$p_\omega = \begin{pmatrix} \frac{z_1}{N \cdot \overline{z_\omega}} \\ \frac{z_2}{N \cdot \overline{z_\omega}} \\ \frac{z_3}{N \cdot \overline{z_\omega}} \\ \frac{z_4}{N \cdot \overline{z_\omega}} \end{pmatrix} = \begin{pmatrix} \frac{100{,}000}{4 \cdot 110{,}000} \\ \frac{200{,}000}{4 \cdot 110{,}000} \\ \frac{170{,}000}{4 \cdot 110{,}000} \\ \frac{170{,}000}{4 \cdot 110{,}000} \end{pmatrix} = \begin{pmatrix} 0.23 \\ 0.45 \\ 0.39 \\ 0.39 \end{pmatrix}$$

In this particular case, scenario 2 has the highest probability of being selected ($p_2 = 0.45$), due to the associated high operational cost. However, as discussed above, scenario 3 and 4 are the only scenarios that trigger the optimal first-stage decisions. As in the method proposed by Morales et al. [122], this SRT focuses on scenarios with a high operational cost impact, which not necessarily results in an optimal first-stage decision in the SUC problem. To avoid over-emphasizing these scenarios and thus being too risk-averse, the probability of occurrence assigned to each of the selected scenarios is inversely proportional to the operational cost obtained from the equivalent single-scenario problem in the importance sampling technique proposed by Papavasiliou et al. [109, 110]. In the remainder of this dissertation, we will not further explore this importance sampling-based SRT.

Relevance for stochastic unit commitment problems

Although the presented example is engineered, it allowed us to illustrate some of the features of the SRTs that drive their performance in SUC problems. Unit commitment problems are riddled with costs that depend on more than just the amplitude of a stochastic variable such as the wind power forecast. For example, the variability of wind power may lead to loss of load (with a very high cost) when insufficient flexible capacity has been committed. Scenario reduction techniques based on the absolute difference between the scenarios (Dupačová et al. [38]) fail to recognize the importance of these scenarios in reaching the optimal UC schedule. Likewise, SRTs based on the cost of each scenario obtained from a dispatch considering a fixed expected-value UC solution (Morales et al. [122]) will over-emphasize scenarios that trigger load shedding in this dispatch problem. As curtailment of RES-based generation typically is considered to be free, cost differences between scenarios that trigger various amounts of curtailment will not be as pronounced. This asymmetry in the impact of positive (curtailment)

and negative forecast errors (load shedding) yields an unbalanced sampling of the probability distribution of the wind power forecast (error), an effect which is illustrated in Section 4.5. This focus on worst-case outcomes of the uncertain variables leads to stable results obtained from optimization problems considering small scenario sets, but those solutions may be biased, hence sub-optimal due to this conservatism (Section 4.5 and 5.6.2). The SRT proposed in this dissertation employs the objective value of single-scenario UC problems as a characteristic of each scenario. This characteristic reflects the operational cost (benefit) of absorbing a certain wind power scenario, which allows (1) identifying critical scenarios, in terms of operational cost increases and reductions and (2) an adequate representation of the wind power forecast (error) distribution in a limited set of scenarios. We will verify these statements in a numerical case study in the following sections.

4.5 Scenario reduction: results & discussion

To illustrate the added value of the proposed SRT, we will study the so-called **stability** and **bias** of the solution of a SUC model (Section 4.1). The analysis is performed on a power system model inspired by the Belgian power system, for which recent wind and solar power forecast and measurement data is available from the Belgian TSO Elia NV [178, 183]. A wind power penetration of 30% is assumed (annual, energy basis). For sake of simplicity, wind power is assumed to be the only source of uncertainty in the system at hand (Chapter 1). Details on the data and assumptions in this case study – omitted here not to disturb the flow of the text – can be found in Section 5.1.1 and Appendix B. In a detailed analysis, we focus on one particular day (the first day of week 39 of the calendar year) based on 2013 data. On this particular day, the wind power forecast rises from 1,000 MW to 6,000 MW (Fig. 4.15). In Chapter 5, we will use the same day to illustrate the differences between the selected UC models in a qualitative analysis. In what follows, we extensively discuss the differences in performance between the four selected SRTs. In addition to the SRT proposed by Dupačová et al. (from hereon 'Dupačová') , Morales et al. ('Morales') and the method proposed in this chapter ('Bruninx'), we also consider a subset of randomly selected, equiprobable scenarios ('Random') as a benchmark, in line with the approach of Botterud et al. [102].

We will furthermore distinguish between four settings of the SUC model, based on the availability of non-spinning and PHES-based flexibility providers. In the first strategy ('SR') only online capacity may be used to meet the demand in all scenarios. The output profile of the PHES systems is common to all scenarios during the UC optimization. During dispatch, their output may be

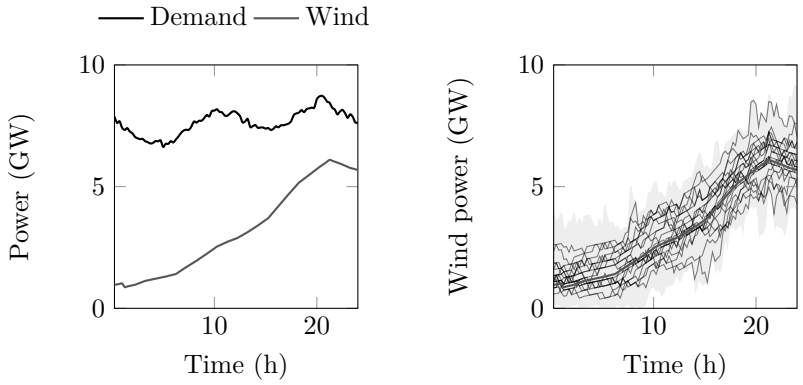

(a) Demand and wind power forecast. **(b)** Wind power scenarios.

Figure 4.15: The demand, forecasted wind power and the generated scenarios on the first day of week 39. On this day, the wind power forecast ramps up from 1,000 MW to 6,000 MW, capable of covering approximately 47% of the demand. For sake of legibility, only the first 20 scenarios are explicitly visualized. The grey area represents the range of the wind power forecast errror in the scenario set.

adapted freely. Second, non-spinning reserves are introduced by allowing a scenario-dependent UC status for fast-starting units ('SR, NSR'). These units can be started-up if required in the ED simulations. In the third strategy ('SR, PHES'), the non-anticipativity constraint on the output of the PHES system is dropped. Last, all flexibility providers are simultaneously available ('SR, PHES, NSR'). During the Monte-Carlo ED simulations, the output of all scheduled units, spinning and non-spinning, and the PHES system is optimized assuming perfect foresight of each wind power scenario. The ED simulations provide a proxy of the expected reliability and operational system cost of the calculated UC schedule. Note that start-ups or shut-downs of flexible units during dispatch are only allowed if they were *scheduled* as non-spinning reserves, regardless of the availability of other fast-starting units. Although this approach is conservative, it allows us to correctly evaluate the bias and stability of the obtained UC schedules.

As will be shown below, the original fast forward SRT does not yield a stable solution of the SUC model. The stable solution of the SUC model is however attainable with the SRT proposed in Section 4.4.3. For the specific day studied in this section, considering 7% of the scenarios is sufficient to obtain a first-stage and second-stage objective value within a 2% range of the stable solution of

the stochastic program. In Section 5.6.2, these conclusions are validated in a four-week analysis. Although the focus of our analysis is on wind power forecast errors, the conclusions below are more generally applicable. A similar analysis, albeit more limited, has been conducted in the context of solar power forecast errors [135]. For sake of brevity, and due to the computational burden of the stability analysis (see below), these results are not reproduced in this dissertation.

The remainder of this section is organized as follows. First, the impact of scenario reduction on the distribution of the forecast error is examined. Second, we will study the quality of the solution of the SUC model in a solution stability analysis and calculate the bias introduced by the SRTs. Third, the computational effort involved is discussed. We introduced a simplified model to calculate the cost function in order to reduce the computational cost of the proposed SRT. We provide an in-depth analysis of the performance of the selected SRTs, using results for one particular day (the first day of week 39) to facilitate the discussion.

4.5.1 Scenario reduction & distribution of the forecast error

To understand the solution of a SUC model on a reduced set of scenarios, one needs to understand how the scenarios considered in the optimization were selected and what this means for the distribution they are supposed to represent. Before moving to the results of the stability analysis, we will first discuss the ability of the SRTs to capture the underlying distribution of the stochastic variable, here the wind power forecast error, in a scenario set with a reduced cardinality. Recall that an exact representation of the original distribution is not a goal in itself for a SRT. The discussion below is intended is to facilitate a better understanding of the factors governing the performance of the SRTs.

Figure 4.16 shows the first 20 scenarios selected from an initial set of 500 scenarios using the four different SRT. Significant differences are apparent. As illustrated in the methodological example, the SRT proposed by Dupačová et al. [38] only considers the amplitude of the wind power forecast scenario itself, but not the impact of that scenario on the result of the stochastic program. More extreme scenarios, i.e. scenarios that are closer to the bounds of the possible wind power production, are not selected. The random SRT suffers from the same problem: extreme, unlikely scenarios have a low probability of being selected. The SRT proposed by Morales et al. [122] selects scenarios based on the operational cost upon realization of these scenarios, assuming first-stage variables are fixed to their values obtained from a DUC model considering the expected value of the wind power forecast scenarios. Consequently, scenarios

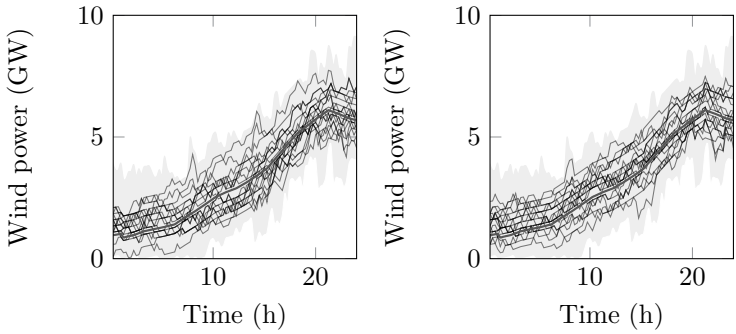

(a) Random **(b)** Dupačová

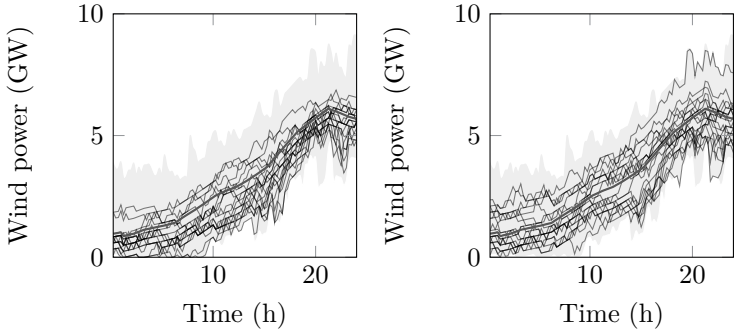

(c) Morales **(d)** Bruninx

Figure 4.16: Twenty scenarios for the wind power forecast selected with four different SRTs from an initial set of 500 wind power scenarios. The grey area indicates the range of the wind power forecast in the original set of scenarios.

with large negative forecast errors, which cause load shedding and hence high operational costs, will be over-emphasized. Few scenarios that contain positive forecast errors are selected. By selecting scenarios based on the operational cost of a single-scenario equivalent UC problem, as proposed in Section 4.4.3, one can obtain a more balanced mix of scenarios. Both scenarios which contain high positive and high negative forecast errors, characterized by operational cost decreases and increases w.r.t. the operational cost under forecast conditions respectively, are selected. This results in a mix of (i) likely, but not too extreme and (ii) less likely, but extreme scenarios.

The impact of these SRTs on the representation of the probability density

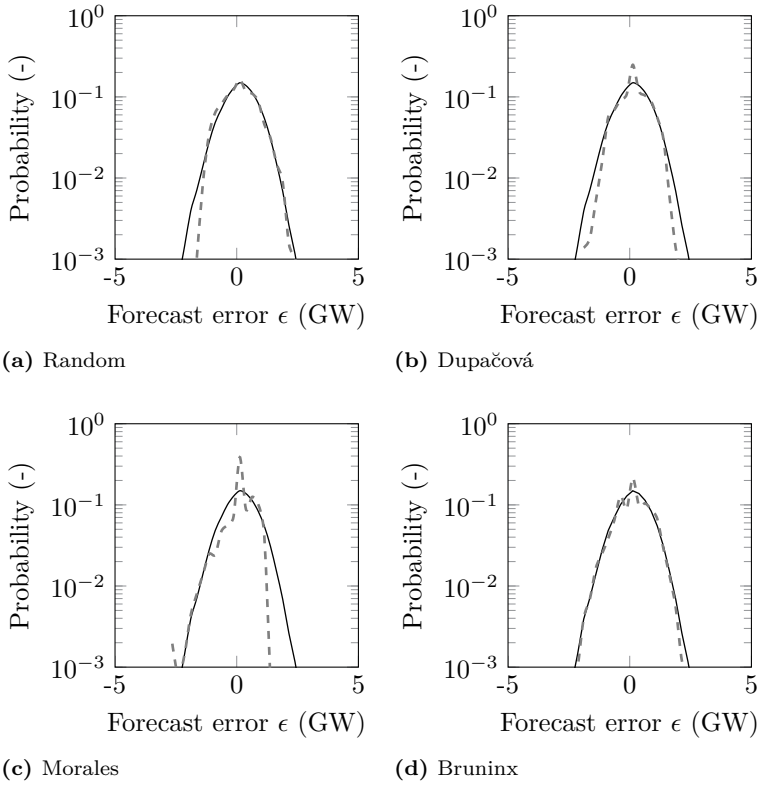

(a) Random **(b)** Dupačová

(c) Morales **(d)** Bruninx

Figure 4.17: The probability density function of the forecast error as represented with different reduced scenario sets for the first day of week 39. The solid, black line is corresponds to the empirical distribution obtained from the full scenario set. The dashed line corresponds to the forecast error distribution represented by 20 selected scenarios from this inital set.

function of the forecast error is shown in Fig. 4.17. As a reference, we visualize the distribution of the forecast error on this particular day as calculated from the initial set of scenarios (solid black line). The dashed lines represent the probability density function of the forecast error obtained from the reduced set of scenarios, accounting for the probability redistribution by the SRT at hand. Both the random SRT and the SRT by Dupačová et al. [38] do not select sufficient 'extreme' scenarios, thus cannot assign sufficient probability to these scenarios, to capture the tails of the distribution. Especially the left tail of the distribution has a significant impact on the UC schedule, as it contains those

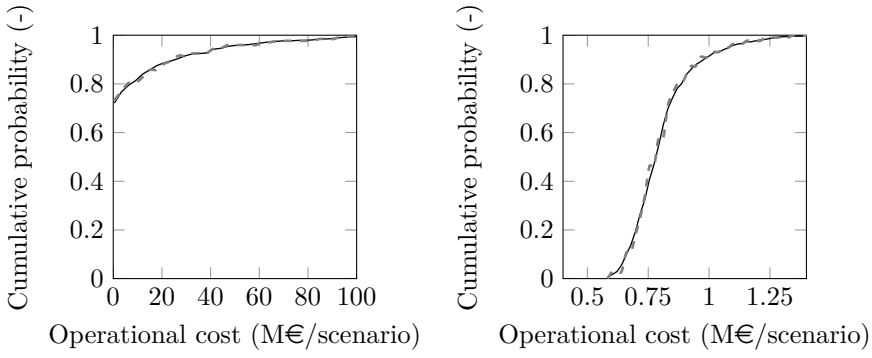

(a) Morales **(b)** Bruninx

Figure 4.18: The probability density function of the operational cost per scenario on the first day of week 39, used as a metric to characterize a scenario in the SRT proposed by Morales et al. (left) and in this dissertation (right). Note the difference in scale on the horizontal axis. The dashed line corresponds to the distribution of the operational cost per scenario represented by 20 selected scenarios from this initial set.

scenarios that trigger load shedding (and the associated high operational costs) during dispatch.

To understand the distribution of selected forecast error scenarios obtained using the methods proposed by Morales et al. [122] and in this chapter (Section 4.4.3), we study the distribution of the metric, i.e. the operational cost per scenario, these methods use to characterize scenarios (Fig. 4.18). The distribution used by Morales et al. [122] shows a clear concentration of probability mass at the lower end of the spectrum of the operational cost. This 'concentration' corresponds to those scenarios that represent close-to-forecast wind power conditions, and to those that represent positive forecast errors. In both cases, the operational cost in these scenarios will be similar to the operational cost under forecast conditions, given the low cost of wind power curtailment. The long right tail (high operational costs) is caused by scenarios with various volumes of load shedding, triggered by negative forecast errors. The SRT proposed by Morales et al. [122] hence cannot distinguish between scenarios that (1) represent the possibility of positive forecast errors; (2) are close to the forecast and/or (3) are characterized by low volumes of load shedding in the corresponding single-scenario equivalent dispatch solution. Scenarios that would trigger load shedding, i.e. scenarios that contain (large) negative forecast errors, are over-emphasized.

The difference in operational cost between the most extreme scenarios and cost under forecast conditions is too extreme to represent the possible impact of a scenario on the actual operational cost in the SUC model. These observations explain (1) the absence of the right tail and (2) the strong emphasis on negative forecast errors (left tail) in the reduced scenario set obtained with the SRT proposed by Morales et al. [122] (Fig. 4.17).

The distribution of the operational cost obtained from a single-scenario DUC problem, proposed in Section 4.4.3 to characterize a scenario, is a more balanced representation of the possible operational cost impact of a wind power forecast error scenario (Fig. 4.18). If a positive forecast error occurs, one expects some operational cost reductions (left tail) compared to the operational cost under forecast conditions (center of the distribution). Likewise, negative forecast errors are expected to result in operational cost increases (right tail). Because the (marginal) cost of electricity generation increases with the demand – i.e. peak power units are more expensive per MWh/h than nuclear power plants – the operational cost of scenarios with severe or prolonged negative forecast errors will typically be further from the operational cost associated with the forecast scenario than the operational cost associated with those scenarios characterized by positive forecast errors of the same size and duration. Consequently, this technique will have the tendency to select more scenarios that are 'costly', hence scenarios containing (large, prolonged) negative forecast errors, compared to the inexpensive scenarios, containing positive forecast errors. However, this effect can only be observed in very small scenario sets and can be considered reflective of the operational cost impact of these scenarios in the SUC problem. If one considers a sufficiently large number of scenarios, the proposed approach allows capturing both tails of the distribution of the forecast error (Fig. 4.17).

By comparing reduced scenarios sets of the same cardinality, it is clear that the proposed SRT succeeds better in methodologically selecting a balanced mix of scenarios, with a focus on those that are challenging for the power system (i.e. large negative forecast errors). The impact of these SRTs on the resulting UC schedules and the objective value of the SUC problem will be studied below in a so-called solution stability analysis.

4.5.2 Solution stability & bias

As introduced in Section 4.1, **in-sample stability** (i.e. stability of the first-stage objective function of the stochastic program) will be claimed if the objective value of the stochastic program does not change (too much) if more scenarios are considered in the optimization. **Out-of-sample stability** is reached if the objective value of the stochastic program considering the full set of scenarios,

with fixed first-stage variables, does not change (too much) if the cardinality of the reduced scenario set increases. This can easily be tested by fixing the first-stage decision variables, i.e. the UC schedule, to the solution of the SUC model and solving the second-stage problem on the original, full set of scenarios. In addition, as an indicator of the **bias** introduced by the SRT, we require this second-stage solution to be close to the first-stage solution. In summary, a solution of a SUC model is said to be stable and unbiased w.r.t. to the selected scenarios[27] if (1) the first-stage objective function and (2) the second-stage objective function no longer change with the addition of more scenarios in the SUC model and (3) the first-stage objective is a good representation of the second-stage objective.

First, we only address the simplest SUC model: scenario-dependent UC statuses are not allowed (no non-spinning reserves) and the output profile of the PHES systems is assumed to be common to all scenarios. This analysis allows estimating the minimum number of scenarios required to reach solution stability. As we discussed in Chapter 2, non-spinning and PHES-based flexibility allow following the demand more closely. Not considering a particular event, i.e. a particular scenario, during the optimization of the UC schedule may more easily trigger load shedding or curtailment of RES-based generation during dispatch, hence solution stability may be more difficult to reach. We will explore the impact of non-spinning and PHES-based reserves on the solution stability requirement at the end of this section.

Solution stability, bias & spinning reserves

Figure 4.19 summarizes the results of the stability analysis on the first day of week 39. As more scenarios are considered during UC scheduling, the total

[27] To be precise, we here claim a solution to be unbiased if the employed SRT does not introduce any bias in the resulting solution. In other words, following the terminology introduced in Section 4.1, we require the bias on the UC schedule resulting from the SRT at hand $\beta_{\text{SRT}}(\overline{x})$ to be small. For a stable solution of the SUC problem $\overline{x}$, $\beta_{\text{SRT}}(\overline{x})$ is calculated as

$$\beta_{\text{SRT}}(\overline{x}) = G(\overline{x}, \breve{\epsilon}_{\text{UC}}) - G(\overline{x}, \overline{\epsilon}) = G(\overline{x}, \breve{\epsilon}_{\text{UC}}) - \min_{x \in \mathbf{X}} G(x, \overline{\epsilon})$$

with $\breve{\epsilon}_{\text{UC}}$ the initial scenario set, $\min_{x \in \mathbf{X}} G(x, \epsilon)$ the stochastic optimization problem at hand and $\overline{\epsilon}$ the reduced scenario set ($\overline{\epsilon} \subseteq \breve{\epsilon}_{\text{UC}}$). To test the bias of the resulting UC schedule, we will perform the second-stage optimization, i.e. the Monte-Carlo economic dispatch simulations, on the original set of scenarios instead of a new set of scenarios. As such, we avoid small variations in the results due to (minor) mismatches in information between the scenario set considered for scenario reduction and the UC problem and the scenario set considered in the second-stage dispatch optimization (i.e. the bias introduced by the SGT). This allows focusing on the stability of the solution and the bias introduced by the SRT. In Section 5.6.2, we will study the bias introduced by the SGT via a Monte Carlo ED simulation over a new set of scenarios.

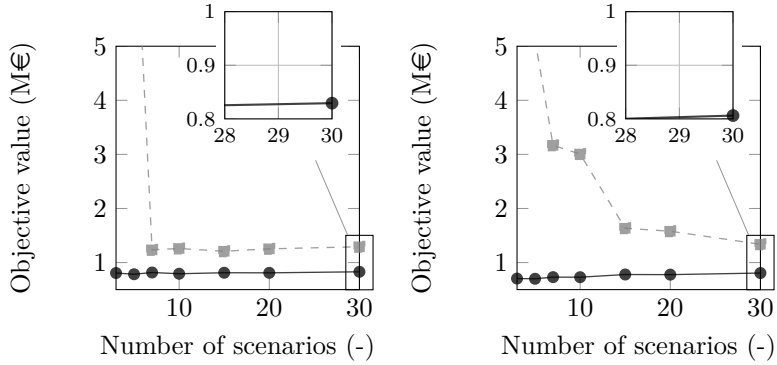

(a) Random **(b)** Dupačová

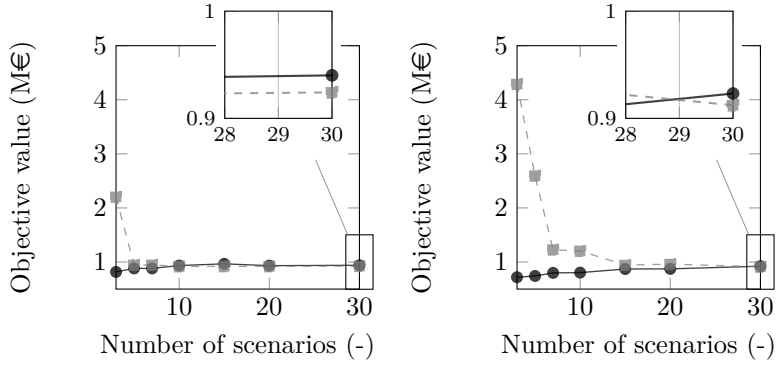

(c) Morales **(d)** Bruninx

Figure 4.19: Solution stability is reached considering 30 scenarios with the SRT proposed in Section 4.4.3. Randomly selecting scenarios and considering these scenarios to be equally probable outperforms the SRT as proposed by Dupačová et al. [38]. In both cases, a stable solution of the SUC is not reached. Although the modification by Morales et al. [122] does lead to a quick convergence to a relatively stable solution considering a low number of scenarios, the resulting UC schedule is overly conservative and sub-optimal. The solid line with circle markers corresponds to the first-stage objective (UC), the dashed line with square markers corresponds to the second-stage objective (ED). Non-spinning and PHES-based flexibility are not considered.

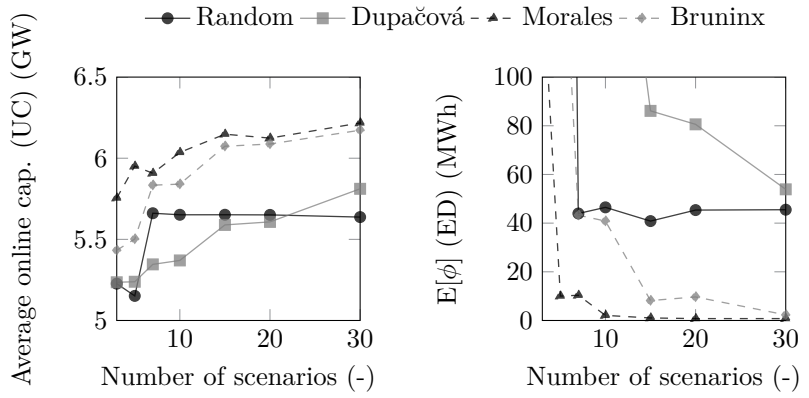

(a) Average committed capacity **(b)** Expected load shedding

Figure 4.20: The average scheduled capacity (UC) and expected load shedding (ED) level off as the solution of the SUC problem becomes stable.

first-stage operational cost increases as a UC schedule is calculated that hedges the system against more (extreme) wind power scenarios by committing more capacity (Fig. 4.20). Consequently, the total expected cost during ED decreases considerably (Fig. 4.19) as the volume of ENS during dispatch decreases (Fig. 4.20). Solution stability is reached if both values, i.e. the total operational cost during UC and the total expected operational cost during dispatch, are approximately the same and do not change considerably with the addition of more scenarios in the SUC problem [111, 188].

For this particular day, a stable, unbiased solution of the UC problem yields an expected operational cost of approximately 0.92 M€. Randomly selecting scenarios or using the SRT proposed by Dupačová et al. does not yield a stable solution. Although the first-stage solution is relatively stable (in-sample stability), the second-stage solution is still far from the first-stage solution (no out-of-sample stability and/or large bias). Note furthermore that a random selection of scenarios outperforms the method as proposed by Dupačová et al. [38], an observation that can also be made in the results presented by Botterud et al. [102]. Although results for this particular day cannot be generalized, it remains a peculiar observation, given the wide-spread use of the SRT proposed by Dupačová et al. [38]. Solving the first-stage problem considering 30 scenarios in the optimization leads to an underestimation of the expected operational cost of the stable solution by approximately 10.2% and 12.7% respectively. The second-stage objective exceeds the stable objective value by 41.6% to 46.7% due to high volumes of load shedding (Fig. 4.20, note the inverse relation between

the pattern of the second-stage objective value and the expected volume of load shedding).

Only when considering scenario sets obtained via the approaches suggested by Morales et al. and in this chapter, solution stability is reached if one considers 30 scenarios in the SUC problem. The risk-averse character of the method proposed by Morales et al. allows reaching stable solutions with small scenario sets (in this case, as of 10 scenarios), but leads to an overly conservative UC schedule. The total operational cost is (i) overestimated, i.e. the first-stage objective value exceeds the second-stage objective value, and (ii) sub-optimal compared to that obtained with the scenario reduction technique suggested in this chapter (Fig. 4.19). The overestimation of the second-stage operational cost (i.e. the bias) varies between 1.6% and 4.5% and shows no clear trend w.r.t. the number of considered scenarios[28]. This peculiar behavior is the result of the over-emphasis of unlikely, extreme scenarios in the SRT. These scenarios, which trigger disproportional load shedding volumes in the single-scenario operational cost metric used for scenario reduction, result in the scheduling of too much capacity and an overestimation of the activation or deployment probability, hence expected operational costs, of these units. Consequently, the expected operational cost in the first-stage optimization (Fig. 4.20) is overestimated. As shown in Fig. 4.19, solution stability is reached when one considers 30 scenarios, selected with the SRT suggested in Section 4.4.3. At this point, the difference in first and second-stage operational cost, i.e. the bias, drops to 1.2%. Expected load shedding volumes and curtailment of RES-based generation during UC and ED are nearly identical, indicating that the reduced scenario set adequately captures the magnitude and probability of occurrence of the wind power forecast error. The proposed method results in a clear evolution towards in- and out-of-sample stability and a low bias, a feature that is not found in the other SRTs studied.

So far, we only discussed the expected value of the objective function. System operators may however be risk-averse, and are thus concerned with the risk of high operational costs. In other words, not only the expected value, but also the distribution of the operational cost is of importance. Fig. 4.21 shows the distribution of the operational cost after MC ED simulations, considering the UC schedules obtained from a SUC problem solved considering reduced scenario sets selected with the four studied SRTs on this particular day. If one selects scenarios randomly or via the method by Dupačová [38], the peak in the probability density function occurs at operational cost values of approximately

[28]The solution stability analysis and the bias of the 'Morales'-results *alone* do not provide sufficient arguments to claim that these results are sub-optimal. This requires another stable solution of the same SUC problem, here provided by the results obtained on scenario sets selected with the SRT proposed in Section 4.4.3.

0.8 M€. However, as shown in Fig. 4.19, the expected value of the operational cost remains high. This is the result of the persistence of large load shedding volumes in a number of scenarios. Although these scenarios occur with a low probability, their high operational cost has a significant impact on the expected operational cost. When selecting scenarios via the technique by Morales et al. [122], the risk of high operational costs in unlikely scenarios is almost completely mitigated. The peak in the probability density function is situated near the expected value of the stable solution (approximately 0.92 M€). Similar results can be observed when one uses the SRT proposed in this chapter. When considering 30 scenarios in the SUC problem, the solution still contains a single scenario characterized by an increased load shedding volume. The peak in the probability density function occurs at operational cost values slightly lower than the expected operational cost of the stable solution.

The underlying causes of these differences in performance were already discussed above. The scenario sets obtained with the random SRT or the approach suggested by Dupačová et al. fail to capture the left tail of the forecast error distribution. As a result, load shedding occurs in some scenarios during dispatch, resulting in the peaks in the distribution at high operational cost levels in the operational cost distribution. The scenario set obtained with the approach proposed by Morales et al. overemphasizes the occurrence of negative forecast errors and drastically underestimates the probability of positive forecast errors. The resulting UC schedule is overly conservative, which leads to (i) a very low probability of load shedding (no scenarios with high operational costs), but (ii) an inability to profit from increases of wind power (low probability of low operational cost).

In what follows, we will gradually drop the assumption that the demand must be met in all scenarios by spinning units. First, the impact of non-spinning reserves on the solution stability and bias is investigated. Second, the PHES units are allowed to be scheduled with different output profiles in different scenarios. It is important to note that selected scenarios (see above) or their probability of occurrence do not change, regardless of the availability of PHES-based or non-spinning flexibility. Scenario reduction methods which do not yield a stable solution of the SUC problem in absence of these units will not yield stable solutions of the same SUC problem considering these flexibility providers, which allow meeting the demand more closely. Therefore, only the SRT according to Morales et al. [122] and the technique proposed in Section 4.4.3 are discussed.

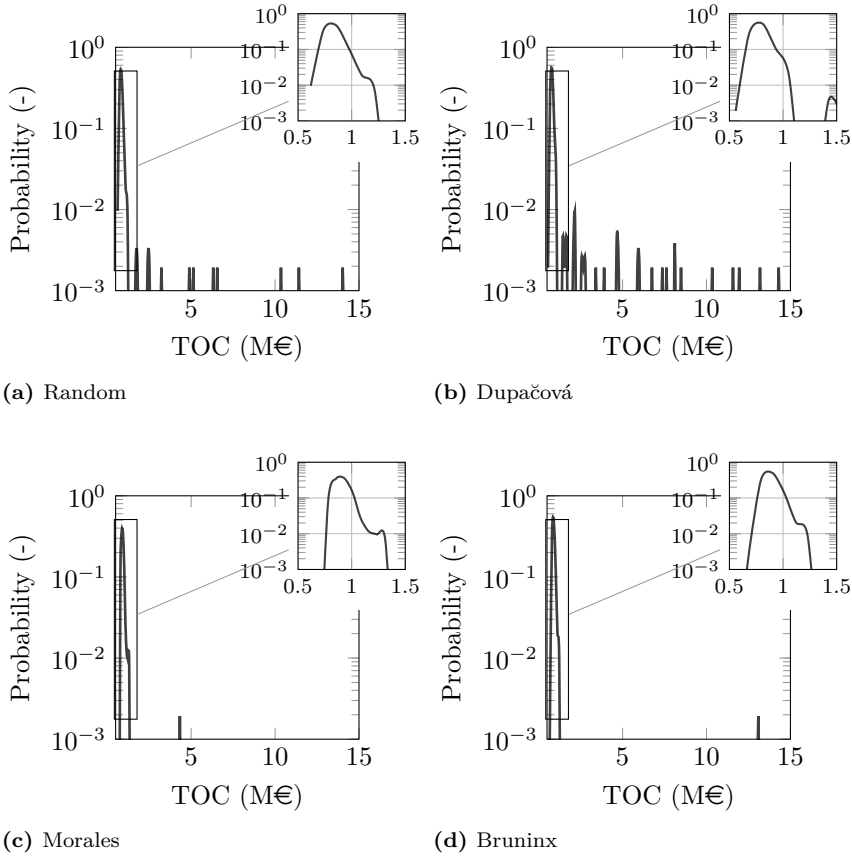

(a) Random **(b)** Dupačová

(c) Morales **(d)** Bruninx

Figure 4.21: The probability density function of the total operational cost (TOC) after MC ED evaluation of the UC schedules calculated via the SUC model considering reduced scenario sets containing 30 scenarios, selected with the four studied SRTs.

Solution stability, bias & non-spinning reserves

If non-spinning reserves are to be scheduled by the SUC model, similar trends are to be observed (Fig. 4.22). The overemphasis of negative forecast error scenarios in the method proposed by Morales et al. [122] leads to an overestimation of the expected total operational cost of 1.2% to 6.4% (bias). The solution obtained on the reduced scenario set obtained via the method of Morales et al. heavily

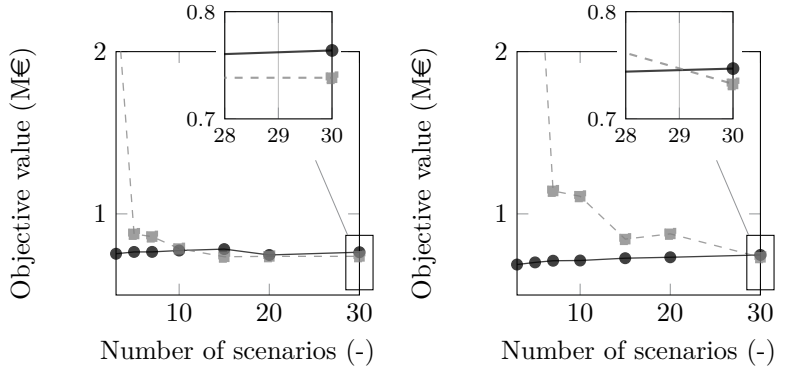

(a) Morales **(b)** Bruninx

Figure 4.22: Actively scheduling non-spinning reserves lowers the expected operational cost significantly. With the proposed SRT, stability is reached considering 30 scenarios. The solid line with circle markers corresponds to the first-stage objective (UC), the dashed line with square markers corresponds to the second-stage objective (ED).

relies on non-spinning flexibility providers. Their probability of activation is over-estimated during UC scheduling, which leads to over-estimations of the associated operational cost. During dispatch however, not dispatching scheduled non-spinning reserves does not lead to operational costs. The resulting schedule is thus overly conservative, but this conservatism is not penalized during dispatch (Fig. 4.22). As a result, the operational cost differences between the UC and ED stage increase compared to the situation without non-spinning reserves. The 'Morales' SRT thus yields a relatively stable, but biased solution. Stability is again reached when considering 30 scenarios, selected with the method proposed in Section 4.4.3. The difference in first and second-stage objective amounts to 1.9% (bias). Load shedding volumes are similar (approximately 0.5 MWh).

Solution stability, bias & PHES-based flexibility

Introducing PHES-based reserve providers, modeled by allowing scenario-specific output profiles for each PHES unit, leads to new challenges in reaching a stable solution. So far, we studied the ability of SRTs to capture the tails of the forecast error distribution and the impact thereof on the solution stability. The *duration* of a forecast error did not yet receive our attention. However, in the

case of scenario-specific PHES-output profiles, the ability of a SRT to identify scenarios that contain prolonged positive or negative forecast errors will prove to be detrimental to its performance. As PHES-based flexibility is only bound by strict constraints on the energy content in the upper reservoir in each scenario *individually*, deviations from the specific wind power scenarios considered during UC may lead to the unavailability of scheduled PHES-based flexibility during real-time dispatch. For the reader's convenience, we clarify these observations with the example provided in Chapter 2. Consider e.g. two scenarios, with an identical negative forecast error at time step t (scenario A) and t+1 (scenario B). In both scenarios, the PHES unit may be scheduled to discharge at those time steps to meet the demand, effectively providing upward reserves. If during dispatch a scenario C would be considered with an identical, negative forecast error on time step t *and* t+1, insufficient energy may be stored in the upper basin to cover the demand in those two subsequent time steps. The minimum energy content constraint was respected in scenario A and B, but the occurrence of scenario C was not considered during the optimization of the UC schedule. Similar reasoning does not apply to the scheduling of spinning and non-spinning capacity, as the supply of fuel (i.e. the equivalent of the stored water or energy in the PHES system) is unlimited on the short term. In addition, the PHES system allows matching the demand more closely in each of the wind power forecast scenarios. The resulting UC schedule is likely to be less robust to (relatively small) differences between the scenarios considered during UC and those used to perform the MC dispatch simulations.

To investigate the ability of a SRT to detect the importance of these prolonged forecast errors, we revisit the event-based verification framework introduced by Pinson and Girard [185] (Section 4.2). A new functional is proposed

$$g_3(\epsilon_{j,s}, k, h, \xi) = \prod_{j=k}^{j=k+h} \mathbf{1}\{\epsilon_{j,s} \leq \xi\}, \tag{4.36}$$

in which $\mathbf{1}\{\}$ is an indicator variable, which equals one if the expression between brackets is true and zero otherwise. $\epsilon_{j,s}$ is the wind power forecast error scenario to which this functional is applied, while k is an auxiliary variable to select the moment of interest in this scenario. Functional $g_3(\epsilon_{j,s}, k, h, \xi)$ allows detecting the occurrence of forecast errors in scenario $\epsilon_{j,s}$ below ξ for at least h hours. The probability of occurrence of such an event at each time step, as predicted by scenario set $\mathbf{S}$ containing N scenarios, is calculated and averaged as follows:

$$P_{h,\xi} = \frac{1}{T-h} \sum_{j=1}^{T-h} \left[\frac{1}{N} \sum_{s=1}^{N} g_3(\epsilon_{j,s}, k, h, \xi) \right] \tag{4.37}$$

with N the number of scenarios in the set $\mathbf{S}$. We apply functional $g_3(\epsilon_{j,s}, k, h, \xi)$ to the full scenario set and the reduced scenario set and calculate $P_{h,\xi}$ for the full

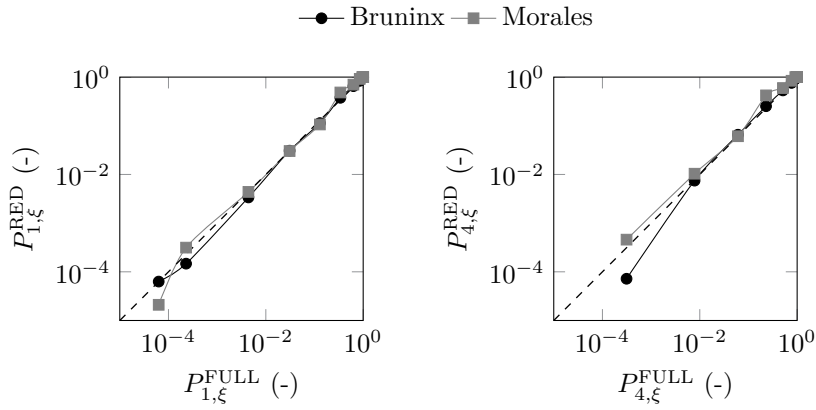

(a) $P_{1,\xi}$ **(b)** $P_{4,\xi}$

Figure 4.23: The probability of occurance of prolonged, negative forecast errors is underestimated in the reduced scenario sets obtained with the SRT proposed by Morales and in Section 4.4.3. $P_{h,\xi}$ is the probability of occurrence of a forecast error below ξ for at least h hours, as predicted by a scenario set. The superscript FULL refers to the full, original scenario set, the superscript RED to the reduced scenario set. Similar trends are observed for other h-values.

($P^{\text{FULL}}_{h,\xi}$) and the reduced scenario set ($P^{\text{RED}}_{h,\xi}$). In Fig. 4.23 these metrics are summarized in so-called pp-plots for h equal to one and four hours respectively. Large, negative forecast errors are characterized by a low $P_{h,\xi}$-value. As the forecast error increases, the $P_{h,\xi}$-value increases. If prolonged forecast errors, as described by functional $g_3(s_{j,s}, k, h, \xi)$, would occur with the same probability in the full and reduced scenario set, the $P^{\text{RED}}_{h,\xi}$-values would coincide with the straight, dashed line in Fig. 4.23. The deviation from this trend shows that both the SRT proposed by Morales et al. [122] and the SRT suggested in this dissertation (Section 4.4.3) underestimate the probability of prolonged negative forecast errors. This effect is more pronounced in the SRT proposed in this dissertation, as illustrated e.g. in Fig. 4.23b.

The impact of these observations on the solution stability is visualized in Fig. 4.24. Not considering non-spinning reserves, stable solutions are difficult to obtain. The risk-averse approach as proposed by Morales et al. [122] no longer leads to over-estimations of the total operational cost, breaking the trend observed in the solutions of the SUC problems in which PHES-based flexibility was not actively scheduled. The expected total operational cost is underestimated by 2% during UC optimization considering 30 scenarios (bias).

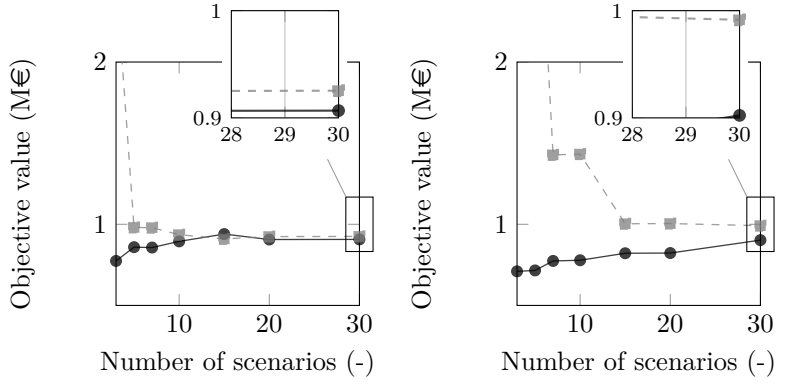

(a) Morales-SR & PHES **(b)** Bruninx-SR & PHES

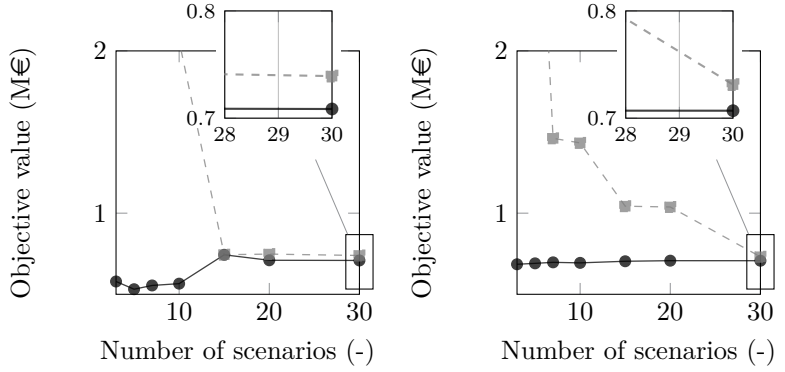

(c) Morales-SR, NSR & PHES **(d)** Bruninx-SR, NSR & PHES

Figure 4.24: Obtaining a stable solution is significantly more complex if PHES-based flexibility is actively scheduled as a reserve provider. The solid line with circle markers corresponds to the first-stage objective (UC), the dashed line with square markers corresponds to the second-stage objective (ED).

The approach discussed in Section 4.4.3 no longer yields a stable solution, with a difference in operational cost between the first-stage and second-stage problem of 9.8%.

With the introduction of non-spinning reserves, the difference in performance subsides. For both SRTs, the evolution to the stable solution is considerably slower (Fig. 4.22 and Fig. 4.24). The SRT as proposed by Morales et al. results

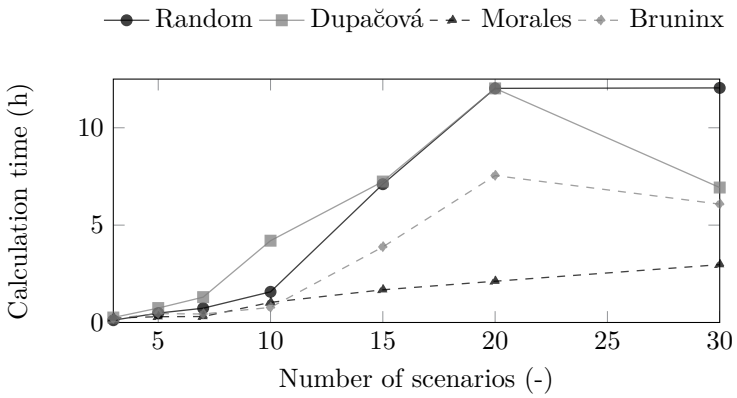

Figure 4.25: The calculation time per run of the SUC model as a function of the number of scenarios considered, obtained with four different SRTs.

in a stable solution considering 30 scenarios. The difference between the UC and ED objective functions amounts to 4.2% (bias). The technique proposed in Section 4.4.3 outperforms this solution by 1.1%. During UC optimization, the expected total operational cost is underestimated by 3.4% (bias).

4.5.3 Computational performance: reducing the computational cost of scenario reduction

The computational performance of a SUC model is highly dependent on the number of scenarios considered. Increasing the number of scenarios increases the dimensions of the problem, which results in high calculation times, even when using the most performant solvers. Figure 4.25 shows a comparison of the calculation time of the SUC problem on this particular day, solved considering scenario sets obtained with the four selected SRTs[29]. In all cases, the calculation time – i.e. the time required by the solver to yield a solution within the optimality gap – quickly rises from several hundreds seconds (3 scenarios) to several thousands seconds when considering 20 scenarios and more. However, some differences are evident. The calculation time rises significantly quicker when scenarios are selected randomly or via the method proposed by

[29]Note that we here report calculation times for the solving the full, explicit formulation of the stochastic problem. Although the solver uses parallel computing techniques, decomposition techniques enabling further parallelization and the associated reductions in computational cost have not been explored in this dissertation (Chapter 2).

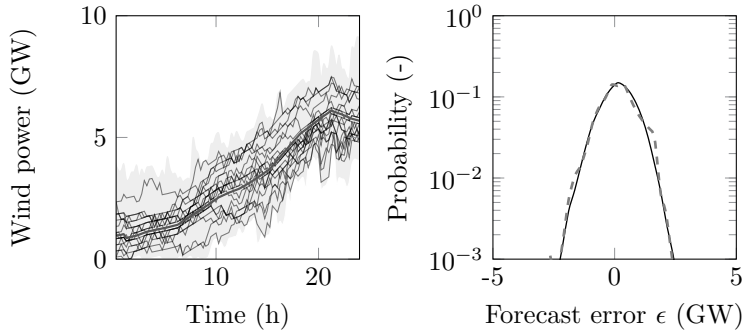

(a) Selected scenarios **(b)** Probability density function

Figure 4.26: Twenty selected wind power scenarios (solid lines, left) and the resulting probability density function represented by this reduced scenario set (dashed line, right), obtained with the method proposed in Section 4.4.3, based on the merit-order solution of the single-scenario equivalent problem. The grey area (left) indicates the range of forecast errors in the original scenario set. The solid line (right) shows the corresponding probability density function.

Dupačová et al. [38]. This may partially be explained by the consideration of a large number of similar scenarios, with a similar probability of occurrence, selected randomly or via the method proposed by Dupačová et al. [38], which leads to a relatively 'flat' objective function of the associated SUC problem. The slowest increase in calculation time is observed when scenarios are selected via the method of Morales et al. [122].

The computational burden of the fast-forward SRT is negligible compared to that of the SUC problem. Regardless of the metric chosen to characterize the scenarios and the number of scenarios to select, the fast-forward algorithm terminates within seconds. However, obtaining the metrics to characterize the scenarios is computationally intensive for the cost functions proposed by Morales et al. [122] and in this chapter. If one uses the cost function as proposed by Morales et al. [122], this requires solving one DUC problem and the economic dispatch problem for all scenarios in the initial scenario set. The DUC problem requires a MILP formulation and takes, on average, approximately 60 seconds to solve. The ED problem becomes a LP problem (if no non-spinning reserves are scheduled) or an easy-to-solve MILP problem (if non-spinning reserves are scheduled) problem. Moreover, this dispatch problem can be parallelized to a high degree: in the most extreme case, one can solve each economic dispatch problem on a separate thread. In this particular case, employing a moderate degree of parallelization, solving the dispatch for each of the 500 scenarios in the

initial set takes approximately 800 seconds. Although the computational effort involved is considerable, it is outweighed by the decrease in number of scenarios needed, and thus computational effort, to reach a stable solution of the SUC problem. If one uses the SRT as proposed in this chapter, this requires solving a DUC problem for each scenario considered. With an average solution time of 60 seconds per instance of the DUC problem, this leads to approximately 30,000 seconds of calculation time – the same order of magnitude as the calculation time required to solve a SUC problem. Although this may seem daunting, there are some possibilities to reduce this computational burden. First, this process can be highly parallelized. In the most extreme case, solving each DUC problem on a seperate thread (or machine), one can reduce the calculation time to approximately 60 seconds. Second, one can substitute the MILP formulation of the DUC problem with an easier-to-solve LP approximation or move to heuristic solutions of the UC problem, as exact values of the operational cost of the one-scenario equivalent problem are not needed during scenario reduction. This remark holds as well for the cost function proposed by Morales et al. [122].

In what follows, we will approximate the operational cost associated with each scenario via a simple MILP merit-order model. This model only considers the power balance, the minimum and maximum stable operating point of each power plant, the hydraulic constraints of the PHES system, the fuel and carbon emission costs. All other constraints are removed from the model. As a result, calculation times drop significantly. For this particular case, solving such a merit order model for all scenarios in the initial scenario set requires approximately 200 seconds. Note that this value is the same order of magnitude as the computational cost of the SRT as proposed by Morales et al. [122].

As shown in Fig. 4.26, the impact of exchanging the DUC-based operational cost of a scenario for a proxy based on a simpler merit-order model is limited. The fast-forward method succeeds in selecting a balanced mix of scenarios, containing positive and negative forecast errors. For this particular instance, the reduced set of scenarios slightly overestimates the probability of large negative forecast errors. However, the correspondence between the probability density function represented by the reduced set of scenarios and the original scenario set is still far superior to that obtained with other methods (Fig. 4.17).

In Fig. 4.27 we revisit the solution stability analysis. For sake of simplicity, only the results obtained considering scenario sets selected via the SRT proposed in Section 4.4.3, using the solution of a simplified merit order formulation of the single-scenario equivalent problem to characterize each scenario, are shown. These results should be compared with those shown in Fig. 4.19, 4.22 and 4.24 respectively. Regardless of the (un)availability of non-spinning and PHES-based reserves, the proposed metric allows selecting those scenarios that are relevant to obtain a stable solution. If PHES-based flexibility is not actively

scheduled, the expected total operational cost is slightly overestimated: the bias amounts to 2.7% (no non-spinning reserves) and 3.6% (non-spinning reserves). If scenario-specific PHES output profiles are allowed during UC scheduling, the resulting solutions are more cost-effective compared to those shown in Fig. 4.24. Especially if only spinning and PHES-based reserves are allowed, the improvement is considerable, as we previously did not find a stable solution.

4.5.4 Conclusion: scenario reduction

In this section, we provided an in-depth analysis of the stability and bias of the solutions of the SUC problem considering reduced scenario sets, representing the wind power forecast error on the first day of week 39. Four SRTs ('Random', 'Dupačová', 'Morales', 'Bruninx') and four UC strategies based on the availability of non-spinning and PHES-based flexibility providers were studied.

Only the SRT proposed by Morales et. al [122] and the SRT developed in this chapter allowed obtaining stable solutions. Actively scheduling PHES-based flexibility increases the difficulty of reaching these stable solutions considerably. For the first day of week 39, the analysis above showed that the bias introduced by the SRT is limited. For the SRTs proposed by Morales et al. and in Section 4.4.3, the bias varies between -3.4% and +4.2% ('Morales') and -1.7% and +2.2% ('Bruninx'), with a negative bias indicating an overestimation of the operational cost during the first-stage optimization. Such overestimations typically occur if PHES-based flexibility is not actively scheduled during the SUC optimization. The bias is, for the four SUC strategies, smaller if the reduced scenario set was obtained with the 'Bruninx' SRT.

However, these estimates of the bias may be too optimistic, as we assume that (i) the SGT does not introduce any approximation error or bias and (ii) the system operator has perfect foresight on some of the realizations of the uncertain wind power while solving the SUC problem, i.e. those contained in the reduced scenario tree $\bar{\epsilon}$. In the following section, we drop these assumptions and evaluate the solution of the SUC problem on a new set of scenarios, to ensure that the scenarios considered during UC optimization are not contained within the scenario tree during MC ED evaluation.

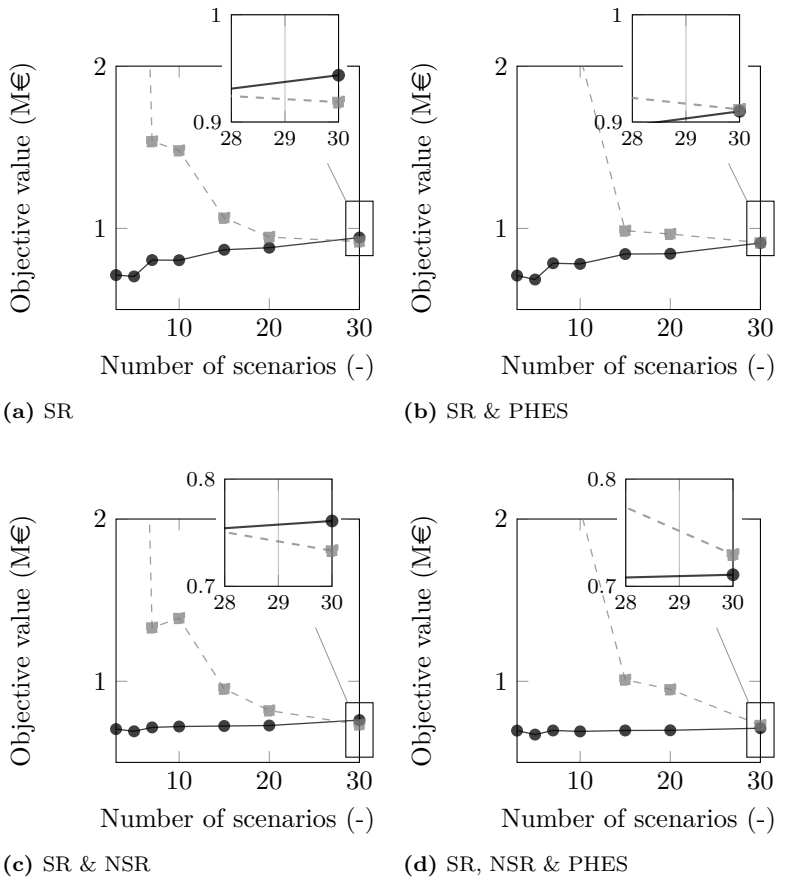

(a) SR **(b)** SR & PHES

(c) SR & NSR **(d)** SR, NSR & PHES

Figure 4.27: Stability is reached considering 30 scenarios selected with the SRT proposed in Section 4.4.3, using the solution of a simplified merit order formulation of the single-scenario equivalent problem to characterize each scenario. The solid line with circle markers corresponds to the first-stage objective (UC), the dashed line with square markers corresponds to the second-stage objective (ED).

4.6 Cross-comparision of selected scenario generation & reduction techniques

Table 4.6 summarizes the results of the Monte-Carlo evaluations of the UC schedules obtained considering 30 scenarios, selected from an initial set of 500 scenarios for each day using four different scenario reduction techniques. For the Monte-Carlo ED evaluations, we generate a new set of scenarios, using the SGT proposed in Section 4.2.3. Again, we consider four UC strategies, based on the available flexibility providers (spinning reserves 'SR', non-spinning reserves 'NSR', pumped hydro energy storage-based reserves 'PHES') to meet the demand. Four representative weeks were selected based on the residual demand, i.e. the demand minus the expected wind power generation. The week with the residual demand closest to the average weekly demand for electrical energy (week 30), the week with the lowest residual demand (week 52), the week with the highest residual energy demand (week 9) and the week with the highest variability in the residual demand profile (week 39) were selected. We will use the same weeks to test the performance of other UC models in Chapter 5.

Before we proceed to the numerical analysis (Section 4.6.2), we briefly discuss the influence of the SGT on and statistical relevance of the obtained results (Section 4.6.1).

4.6.1 Bias & confidence intervals

As outlined in Section 4.1, Kaut and Wallace [111] argue that the bias of the stable solution should be small (Section 4.1). The bias (Eq. 4.1) is the difference between the value of the true objective function at the optimal solution of the original problem (with a continuous, full description of the stochastic variable) and the approximation of the problem (with a discrete representation of the stochastic variable – i.e. the scenario tree). A stochastic upper bound on the bias on the stable solution $\overline{x}$ of the stochastic problem $\min_{x \in \mathbf{X}} G(x, \tilde{\epsilon})$ introduced by the SGT and the SRT is given by (Section 4.1)

$$\beta(\overline{x}) \lessapprox G(\overline{x}, \tilde{\epsilon}) - G(\overline{x}, \overline{\epsilon}) \approx G(\overline{x}, \breve{\epsilon}_{\mathrm{ED}}) - G(\overline{x}, \overline{\epsilon}) \tag{4.38}$$

We evaluate the solution $\overline{x}$ on a new, large set of scenarios $\breve{\epsilon}_{\mathrm{ED}}$, as such that the scenarios considered during UC optimization are not contained within the scenario tree during MC ED evaluation ($\overline{\epsilon} \not\subseteq \breve{\epsilon}_{\mathrm{ED}}$). $G(\overline{x}, \overline{\epsilon})$ is the first-stage objective, i.e. the objective of the SUC problem, solved on a reduced scenario tree $\overline{\epsilon}$.

However, determining the bias (Eq. (4.38)) may not be straightforward, as the results entail statistical fluctuations due to Monte-Carlo ED simulations on a finite scenario tree $\check{\epsilon}_{\text{ED}}$ rather than the 'real' stochastic process $\tilde{\epsilon}$. In other words, $G(\overline{x}, \check{\epsilon}_{\text{ED}})$ might not be a good estimator of $G(\overline{x}, \tilde{\epsilon})$. The stochastic character of the SGT at hand further increases the complexity of this bias estimation: as each run of the SGT yields a different scenario tree, the approximation error caused by $\check{\epsilon}_{\text{ED}}$ will be different from that introduced by $\check{\epsilon}_{\text{UC}}$, even if both trees have the same cardinality.

Based on the Central Limit Theorem, $G(\overline{x}, \check{\epsilon}_{\text{ED}})$ is assumed to follow normal distribution. This allows calculating a confidence interval around $G(\overline{x}, \check{\epsilon}_{\text{ED}})$ as an estimator of $G(\overline{x}, \tilde{\epsilon})$, characterized by a confidence level of $1 - \alpha$ and a width Δ ($[G(\overline{x}, \check{\epsilon}_{\text{ED}}) - \Delta, G(\overline{x}, \check{\epsilon}_{\text{ED}}) + \Delta]$) [191]:

$$\Delta = \frac{z_{1-\alpha/2} \cdot \sigma}{\sqrt{N}} \tag{4.39}$$

In this equation, σ is an estimator of the standard deviation and $z_{1-\alpha/2}$ the inverse of the standard normal cumulative probability density function evaluated at $1 - \alpha/2$. As recommended in [86], we will typically set α to 0.05. Note that the width of the confidence interval is directly dependent on the standard deviation. Unstable SUC solutions will trigger load shedding in some scenarios, which will result in large σ-values and thus wide confidence intervals.

In what follows, we will perform the second-stage dispatch evaluation on a new set of 500 scenarios $\check{\epsilon}_{\text{ED}}$. To ensure the comparability of the performance metrics calculated for the different UC schedules, the same sets of scenarios – i.e., different per day, but identical across the different SUC schedules obtained on scenarios sets selected with the different SRTs – are considered in the MC ED simulations. The objective value of the MC ED simulations may thus be considered a reliable metric for the performance of the SUC schedule, but should be interpreted with caution, the analysis above in mind.

4.6.2 A four-week analysis

Several trends can be identified in Table 4.6. First, the introduction of more flexibility providers (non-spinning reserves, PHES systems) results in more cost-effective UC schedules for all weeks and all scenario reduction techniques. These highly flexible units and energy storage systems allow following the demand more closely, i.e. with less online capacity. However, this increases the importance of identifying critical scenarios. Failing to select critical scenarios effectively leads to scheduling too little capacity, which results in ENS (energy not served), thus high expected TOCs and wide confidence intervals, during

dispatch, as illustrated in Table 4.6. Especially in weeks with high wind shares (WS), such as week 39 and 52, this may drastically increase the expected TOC (ED). The underlying causes of these increases in load shedding volumes were discussed at length above.

Second, large differences are apparent between the results obtained with different SRTs. As expected, the 'random' SRT performs worst: high volumes of load shedding in the Monte Carlo ED simulation results indicate that the randomly selected scenarios triggered an inadequate UC schedule, over all weeks and UC strategies. Although employing the SRT proposed by Dupačová et al. results in less ENS, the expected TOC (ED) still strongly exceeds that of the UC problem, indicating unstable, biased solutions.

The results obtained on scenario sets selected with the method of Morales et al. and the method proposed in this dissertation are, in general, similar. Both allow selecting a scenario set that triggers an adequate UC schedule, resulting in low ENS volumes and low expected TOC during dispatch. However, more subtle differences between the 'Morales' and 'Bruninx'-based results are found in Table 4.6. The risk-averse character of the SRT proposed by Morales et al. results in more scheduled capacity, effectively increasing the expected TOC during the UC phase. The difference in expected TOC (UC vs. ED) can be as high as 2.2 M€/week or 8%. This risk-averseness does lead to low ENS volumes, which results in low expected TOC (ED) and narrow confidence intervals. Note however that in our case study, one does not incur any cost for not-dispatched, scheduled non-spinning reserves or curtailment of RES-based generation, which favors risk-averse UC schedules. Using the SRT proposed in this dissertation, the resulting expected TOC obtained from the UC phase is, in twelve out of sixteen cases, closer to the expected TOC of the dispatch phase. The risk-neutral scenario set allows correctly evaluating the expected cost of load shedding and the expected cost of scheduling additional capacity. Due to the limited number of scenarios, the probability of load shedding during ED on some particular days may however be underestimated. In eight cases, this leads to an expected TOC during dispatch that exceeds that obtained with the UC schedule corresponding to the 'Morales' SRT (see Table 4.6). This is typically the result of high ENS volumes on one day in these weeks. Note that this typically increases the width of the confidence intervals w.r.t. the 'Morales'-based solutions. Especially when PHES-based flexibility is considered, the risk-averse character of the 'Morales' SRT leads to better results (see discussion above). This issue can however be resolved by considering more scenarios in the UC phase, as the expected TOC without the cost of ENS in Table 4.6 illustrates. Selecting more scenarios will likely increase the expected TOC of the UC phase and lower the expected volume of ENS and expected TOC of the ED phase, as we will illustrate in Chapter 5. This effect is expected to be stronger for the solutions based on

Table 4.6: Comparison of the performance of four SRTs during four representative weeks, considering four UC strategies: units scheduled in all scenarios may be used to meet demand ('SR'), PHES-based flexibility may be scheduled ('PHES') and fast-starting units may be scheduled with a scenario-dependent UC status ('NSR').

SRT			**Random**		**Dupačová**		**Morales**		**Bruninx**	
Flexibility providers			SR	SR NSR	SR	SR NSR	SR	SR NSR	SR	SR NSR
W30 (WS 10.6%)	**E[TOC UC]**	[M€]	**13.80**	**13.48**	**13.97**	**13.46**	**14.22**	**13.86**	**14.01**	**13.48**
	without ENS		13.77	13.39	13.91	13.36	14.21	13.83	13.86	13.46
	E[ENS UC]	[MWh]	2.21	8.69	6.16	9.78	1.47	2.7	15.52	2.07
	E[TOC ED]	[M€]	**13.72**	**13.26**	**13.71**	**13.20**	**13.69**	**13.09**	**13.65**	**13.16**
	without ENS		13.51	13.00	13.60	12.98	13.67	13.03	13.59	13.04
	Δ	[M€]	0.20	0.17	0.13	0.14	0.08	0.11	0.10	0.13
	E[ENS ED]	[MWh]	20.31	26.1	11.35	21.72	1.64	6.23	5.46	12.31
	E[WUF ED]	[%]	100.0	100.0	100.0	100.0	100.0	100.0	100.0	100.0
W9 (WS 13.5%)	**E[TOC UC]**	[M€]	**28.79**	**27.84**	**28.36**	**27.56**	**30.61**	**29.62**	**28.70**	**27.80**
	without ENS		28.77	27.84	28.25	27.55	30.36	29.21	28.69	27.76
	E[ENS UC]	[MWh]	1.92	0.46	11.17	0.7	24.55	41.02	1.82	3.63
	E[TOC ED]	[M€]	**28.43**	**28.52**	**28.49**	**27.63**	**28.43**	**27.43**	**28.26**	**27.30**
	without ENS		28.20	27.10	27.88	27.08	28.43	27.25	28.23	27.21
	Δ	[M€]	0.32	0.92	0.53	0.41	0.16	0.23	0.17	0.22
	E[ENS ED]	[MWh]	22.66	141.97	61.18	54.51	0.95	17.64	2.77	9.13
	E[WUF ED]	[%]	100.0	100.0	100.0	100.0	100.0	100.0	100.0	100.0
W39 (WS 52.3%)	**E[TOC UC]**	[M€]	**7.60**	**6.37**	**7.33**	**6.30**	**8.60**	**7.17**	**8.17**	**6.71**
	without ENS		7.55	6.24	7.31	6.26	8.42	7.15	8.05	6.64
	E[ENS UC]	[MWh]	5.18	12.6	1.94	3.98	18.67	1.38	12.15	7.09
	E[TOC ED]	[M€]	**10.06**	**10.47**	**9.90**	**9.32**	**8.12**	**6.65**	**8.10**	**6.57**
	without ENS		7.41	6.09	7.21	6.12	7.95	6.47	7.86	6.35
	Δ	[M€]	1.55	2.11	1.53	1.67	0.21	0.20	0.31	0.25
	E[ENS ED]	[MWh]	265.71	437.7	269.66	320.8	17.67	18.14	24.19	21.84
	E[WUF ED]	[%]	96.8	97.5	97.4	98.0	96.0	97.2	96.6	97.3
W52 (WS 86.3%)	**E[TOC UC]**	[M€]	**2.49**	**-**	**2.56**	**2.24**	**3.10**	**3.72**	**2.82**	**2.41**
	without ENS		2.49	-	2.55	2.23	2.95	2.98	2.80	2.41
	E[ENS UC]	[MWh]	0.06	-	0.67	0.74	14.26	75.29	1.63	0.07
	E[TOC ED]	[M€]	**5.63**	**-**	**3.92**	**4.12**	**2.95**	**2.51**	**3.23**	**2.88**
	without ENS		2.47	-	2.53	2.22	2.72	2.31	2.75	2.29
	Δ	[M€]	1.29	-	0.85	1.14	0.18	0.17	0.36	0.38
	E[ENS ED]	[MWh]	316.02	-	138.71	189.46	23.06	20.0	47.79	58.71
	E[WUF ED]	[%]	92.6	-	93.0	94.6	93.3	93.3	93.9	94.9

Table 4.6: All values are given per week. TOC is the total operational cost and ENS the Energy Not Supplied volume. WS is the Share of Wind energy in the total demand for electrical energy. WUF is the Wind Utilization Factor. Δ is the width of the 95% confidence interval on E[TOC ED].

SRT			**Random**		**Dupačová**		**Morales**		**Bruninx**	
Flexibility providers			SR PHES	SR PHES NSR	SR PHES	SR PHES NSR	SR PHES	SR PHES NSR	SR PHES	SR PHES NSR
W30 (WS 10.6%)	**E[TOC UC]**	[M€]	**13.53**	**13.26**	**13.64**	**13.18**	**14.04**	**13.51**	**13.61**	**13.10**
	without ENS		13.50	13.07	13.61	13.15	14.03	13.49	13.59	13.09
	E[ENS UC]	[MWh]	3.21	19.09	2.95	3.69	1.32	1.71	2.26	0.81
	E[TOC ED]	[M€]	**15.38**	**15.01**	**14.42**	**13.60**	**13.57**	**13.01**	**13.95**	**13.32**
	without ENS		13.33	12.96	13.38	12.96	13.53	12.96	13.39	12.96
	Δ	[M€]	1.00	0.92	0.62	0.35	0.12	0.13	0.38	0.25
	E[ENS ED]	[MWh]	204.46	205.27	103.73	63.68	4.69	5.44	55.92	36.01
	E[WUF ED]	[%]	100.0	100.0	100.0	100.0	100.0	100.0	100.0	100.0
W9 (WS 13.5%)	**E[TOC UC]**	[M€]	**28.47**	**27.72**	**28.04**	**27.29**	**28.73**	**29.17**	**28.81**	**27.47**
	without ENS		28.07	27.33	28.03	27.15	28.65	28.94	28.25	27.41
	E[ENS UC]	[MWh]	40.20	39.10	1.14	14.12	8.02	22.90	56.13	6.05
	E[TOC ED]	[M€]	**33.55**	**31.08**	**30.06**	**28.21**	**28.11**	**27.23**	**28.95**	**27.42**
	without ENS		27.58	26.94	27.66	26.99	27.94	27.10	27.85	27.10
	Δ	[M€]	2.66	2.11	1.41	0.96	0.28	0.25	0.84	0.37
	E[ENS ED]	[MWh]	596.58	414.03	240.15	122.12	16.56	12.77	109.51	31.48
	E[WUF ED]	[%]	100.0	100.0	100.0	100.0	100.0	100.0	100.0	100.0
W39 (WS 52.3%)	**E[TOC UC]**	[M€]	**6.93**	**6.06**	**7.05**	**6.01**	**8.10**	**6.74**	**7.75**	**6.44**
	without ENS		6.92	6.01	7.03	5.96	7.99	6.73	7.50	6.35
	E[ENS UC]	[MWh]	1.56	5.42	1.71	5.82	10.89	1.06	24.92	8.85
	E[TOC ED]	[M€]	**17.93**	**17.57**	**11.90**	**12.21**	**8.12**	**6.73**	**8.52**	**6.33**
	without ENS		6.83	6.00	6.96	5.74	7.58	6.25	7.36	5.60
	Δ	[M€]	4.22	4.30	2.53	2.96	0.5	0.49	0.99	0.68
	E[ENS ED]	[MWh]	1110	1156	493	646	54.03	48.32	115.5	73.16
	E[WUF ED]	[%]	97.2	98.1	97.4	98.3	96.7	98.0	96.4	97.9
W52 (WS 86.3%)	**E[TOC UC]**	[M€]	**4.47**	**2.20**	**2.46**	**2.12**	**2.82**	**-**	**2.75**	**2.31**
	without ENS		4.47	2.19	2.43	2.10	2.76	-	2.72	2.31
	E[ENS UC]	[MWh]	0.13	0.70	3.74	2.07	6.14	-	2.50	0.30
	E[TOC ED]	[M€]	**10.29**	**10.51**	**6.85**	**7.07**	**3.00**	**-**	**4.18**	**3.11**
	without ENS		4.49	2.24	2.45	2.19	2.68	-	2.71	2.28
	Δ	[M€]	2.12	2.86	2.10	2.17	0.27	-	0.83	0.55
	E[ENS ED]	[MWh]	579	827	440	488	31.62	-	146.6	82.58
	E[WUF ED]	[%]	94.7	94.7	94.1	95.5	95.2	-	92.4	94.8

scenario sets obtained with the SRT proposed in this chapter (Section 4.4.3) than for those obtained with the technique proposed by Morales et al. Indeed, the difference in expected ENS volumes is much smaller for these solutions, indicating a much smaller potential for improvement.

The calculation time required to solve a SUC model is $O(10^4 s)$. Considering all SRTs and UC strategies, the median calculation time is approximately 22,000 seconds. In 75% of all cases an optimal solution is reached in 51,000 seconds. In approximately 20% of all cases, the optimality gap is not reached and the optimization was stopped due to the imposed time limit (96,000 seconds). In two cases, no solution was found (week 52, 'Morales', 'SR, NSR & PHES' and week 52, 'Random', 'SR & NSR'). In all other cases, the optimality gap was below 3.8%. SUC problems with scenario sets obtained via the SRT proposed by Morales et al. and Dupačová et al. were typically more difficult to solve, but no clear trends could be identified.

4.6.3 Conclusion

Probability distance-based SRTs are by far the most used. Various cost functions, i.e. metrics to distinguish between two scenarios, are in use. In an extensive numerical case study, we show that different cost functions may have a significant impact on the scenarios selected and the resulting total operational cost of the associated UC schedule. The cost function proposed by Dupačová et al. is generic, thus readily applicable in a wide range of problems, but leads to poor results in a SUC setting. The risk-averse character of the cost function proposed by Morales et al. leads to low ENS volumes and low expected operational costs, but may be over-conservative. We proposed a risk-neutral cost function, which allows reaching a stable solution with a scenario set of reasonable size. However, our numerical case study revealed that when PHES-based flexibility is actively scheduled, the proposed risk-neutral SRT may not select sufficient scenarios that contain prolonged, negative forecast errors. As a result, a stable solution may not always be reached and the SRT proposed in this dissertation may be outperformed by the SRT proposed by Morales et al. [122].

4.7 Conclusion

Uncertainty in power systems can be adequately incorporated in short-term electricity generation system models by using stochastic programming. The resulting SUC models employ a direct representation of the uncertainty under the form of discrete scenarios to optimally trade-off (i) the socio-economic cost

of load shedding and curtailment of excess RES-based generation and (ii) the cost of reserve provision and deployment. However, the quality of this trade-off is fully dependent on the quality of the considered scenarios. We recognized that the SGTs and SRTs employed to obtain the relevant scenarios are a critical part of the operational model. Therefore, SGTs and SRTs need to be adapted to the optimization problem at hand – no method will fit all purposes.

Several SGTs were discussed and evaluated in the context of wind power forecast uncertainty in SUC models. A SGT, proposed by Pinson et al. [36] and refined by Ma et al. [193], was selected and improved. In a case study, we showed that this SGT allows generating scenario sets of reasonable size that form an adequate representation of the uncertainty on wind power forecasts.

To be able to solve the resulting SUC problem in reasonable time, the scenario set needs to be sufficiently small. It is therefore critical to ex-ante select those scenarios that will trigger an optimal UC schedule, which is the goal of SRTs. A multitude of SRTs is in use, as shown in the overview provided in Section 4.4, but probability distance-based SRTs remain by far the most-used. However, in a methodological and real-life case study we showed that the cost function employed in these methods to characterize the scenarios at hand, may not be adequate to identify critical (wind power forecast error) scenarios. Morales et al. [122] suggest a correction, but their approach is by definition risk-averse. We therefore proposed an alternative risk-neutral cost function, which allows obtaining stable solutions to the SUC problem with scenario sets of limited size. An extensive numerical case study showed that this risk-neutral approach may not select sufficient scenarios that contain prolonged negative forecast errors. In presence of PHES-based flexibility, this may lead to load shedding in real time, hence solution stability may be lost.

This work can be strengthened in the following ways. First, the proposed SGT may be improved by optimally redistributing the probability of occurrence of the retained scenarios – after removal of those that contain improbable events – to minimize the distortion of the underlying probability density functions. In addition, more optimal SGTs – e.g. with improved sampling procedures – may reduce the width of the confidence interval around the expected operational cost after Monte-Carlo economic dispatch evaluation. Second, the numerical analysis presented above, especially w.r.t. the solution stability analysis, may be extended. For example, the impact of other power system characteristics, longer time periods, large scenario sets and other sources of uncertainty – e.g. demand forecast errors or component outage – may be tested. Third, studying the performance of proposed SRT in transmission-constrained power systems may lead to interesting insights. Note that the proposed cost function in theory should capture the impact of transmission constraints, in contrast to the original cost function [38], which is unaffected by the introduction of

transmission constraints. Fourth, the presented research would greatly benefit from further positioning w.r.t. recently published SRTs, such as the importance sampling-inspired techniques proposed by Papavasiliou et al. [109, 110], the moment matching-technique introduced by Li et al. [221] or novel clustering techniques, developed by, a.o., Feng and Ryan [225, 223, 224]. Fifth, scheduling energy storage-based flexibility on a reduced set of scenarios is challenging. Further research may focus on specialized SRTs. Last, we only focused on the 'classical' SUC model. Hybrid models (Chapter 2) may allow the use of dedicated SRTs to enhance their computational performance. We will return to this issue in Chapter 5.

Chapter 5

Cross-comparision of selected unit commitment models: cost-efficiency, reliability and computational effort

Armed with the tools developed in Chapter 3 and 4, we are ready to compare the performance of the five UC models proposed in Chapter 2. In a case study, inspired by the Belgian power system, we analyze the ability of the UC models to account for uncertain wind power forecasts. To characterize the *performance* of a UC model, we will study, as outlined in Section 1.3,

- the operational *cost-efficiency* of the UC schedule, i.e. the operational cost associated with meeting the demand in a range of wind power realizations;
- the *computational effort* required to obtain the UC schedule;
- the *reliability* of the resulting UC schedule.

Ideally, one develops a UC model that is easy-to-solve, cost-efficient and reliable. The analysis in this chapter shows that these qualities are difficult to combine, but that the HUC and PUC formulations developed in this dissertation are attempts to reach this ambitious goal.

We subsequently study the DUC model (Section 5.2), the SUC model (Section 5.3), the IIUC model (Section 5.4), the HUC formulation (Section 5.5) and the PUC formulation (Section 5.6). Last, we formulate a conclusion (Section 5.7).

This chapter is based on the following papers:

- K. Bruninx, Y. Dvorkin, E. Delarue, H. Pandžić, W. D'haeseleer, and D. S. Kirschen, *Coupling Pumped Hydro Energy Storage with Unit Commitment,* IEEE Trans. Sustain. Energy, vol. 7, no. 2, pp. 786–796, 2016.
- K. Bruninx and E. Delarue, *A probabilistic unit commitment model: cost-effective, reliable and fast,* Submitted to IEEE Trans. Power Syst., 2015.
- K. Bruninx, K. Van den Bergh, E. Delarue, and W. D'haeseleer, *Optimization and Allocation of Spinning Reserves in a Low-Carbon Framework,* IEEE Trans. Power Syst., vol. 31, no. 2, pp. 872–882, 2016.
- K. Bruninx and E. Delarue, *Scenario Reduction Techniques and Solution Stability for Stochastic Unit Commitment Problems,* ENERGYCON, April 4–8, 2016, Leuven, Belgium.

5.1 Introduction

In this chapter, we present a quantitative analysis of the performance of the five UC models discussed in Chapter 2. We study the cost-effectiveness of the UC schedules obtained with these operational models, analyze the resulting reliability via the amount of load shedding and compare the calculation time between models. We will quantify the impact of the availability of different types of flexibility providers, such as non-spinning and PHES-based reserves, and the consideration or negligence of the expected operational cost associated with reserve procurement and activation. We sub-sequentially study

1. The deterministic UC model (Section 5.2), which will yield a lower bound on the calculation time and an upper bound on the expected total operational cost – a measure for the cost-effectiveness of the UC schedule. We will improve the cost-efficiency of the DUC model by explicitly considering PHES-based reserves with minimal impact on the calculation time;
2. The stochastic UC model (Section 5.3), of which stable solutions provide a lower bound on the expected total operational cost, but are characterized by a high computational cost;

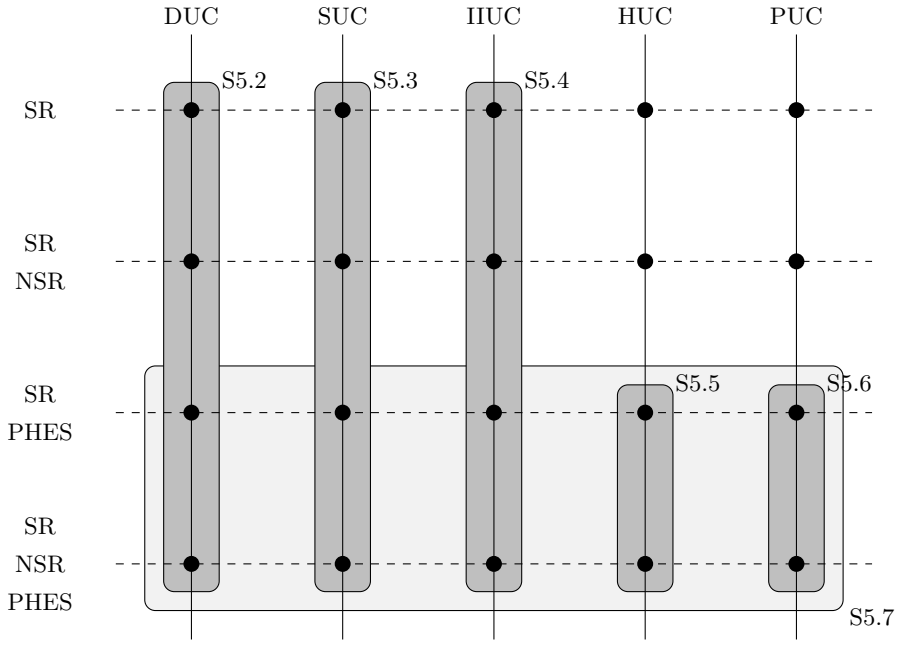

Figure 5.1: Graphical representation of the topics covered in each section in this chapter. Each dot represents a combination of a set of assumptions on the availability of flexibility providers (spinning (SR), non-spinning (NSR) and PHES-based reserves) and a UC formulation.

3. The improved interval UC model (Section 5.4), of which we improve the performance by explicitly considering non-spinning and PHES-based reserves at the expense of a minimal increase in calculation time;

4. The hybrid deterministic-stochastic UC model (Section 5.5), which approximates the stable solution of a SUC model at significantly lower computational effort. Special attention is paid to the required design exercise to quantify an optimal combination of reserve requirements and scenarios and the interaction with the scenario reduction technique employed;

5. The probabilistic UC model (Section 5.6), which contains a refined representation of the reserve requirements and the associated expected deployment costs in a deterministic model.

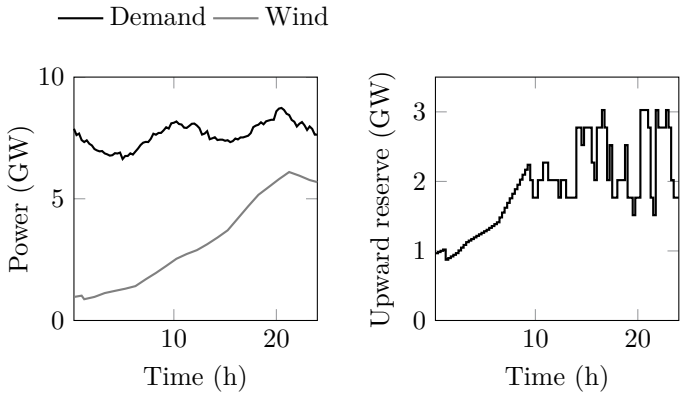

(a) Forecasted wind power and demand

(b) Upward reserve requirement

Figure 5.2: The demand, forecasted wind power and upward reserve requirement to cover 100% of the possible negative forecast errors on the first day of week 39. The upward reserve requirement is based on a large set of discrete wind power forecast scenarios, which is reflected in the changing reserve requirement per time step. On this day, the forecasted wind output ramps up from 1 GW to 6 GW, capable of covering 47% of the demand.

For the first three models, we present results for four settings of each UC model: a case in which only spinning reserves are available; a case with spinning and non-spinning flexibility, a setting in which PHES-based and spinning reserves are available and a situation in which spinning, non-spinning and PHES-based reserves can be used to satisfy the implicit or explicit reserve requirements (Fig. 5.1). For the two remaining models, the HUC and PUC, which were developed within this PhD dissertation, we only discuss the cases in which PHES-based flexibility is available, as it will prove to be a cost-efficient flexibility provider. Finally, we conclude this chapter with a cross-comparison of these UC formulations (Fig. 5.1 and Section 5.7).

This analysis is performed on a case study inspired by the Belgian power system assuming a 30% wind energy penetration on an annual, energy basis. Wind power is assumed to be the only source of uncertainty. Our perspective is that of an independent system operator, of whom we assume that he is responsible for all scheduling decisions and transactions (Chapter 1). The specifics of the case study are presented below (Section 5.1.1) and in Appendix B. To illustrate the various effects at play, we isolate the first day of week 39 of the calendar year, which is characterized by the system-wide demand and wind generation profiles shown in Fig. 5.2. Throughout this discussion we focus on the way the various

models procure and deploy upward reserves, due to the high operational cost impact of an inefficient or insufficient procurement of upward reserves, possibly triggering load shedding. To evaluate the performance of the UC formulations quantitatively, four representative weeks were selected based on the residual demand[1]. The week with the residual demand closest to the average weekly demand for electrical energy (week 30), the week with the lowest residual energy demand (week 52), the week with the highest residual energy demand (week 9) and the week with the residual demand profile with the highest variability (week 39) were selected, as in Chapter 4. During the 'average residual demand' week, wind energy covers approximately 11% of demand. The residual demand varies between 4,300 and 8,900 MW. Negative residual loads are experienced on a regular basis during the week with the lowest residual demand. The residual demand fluctuates between -2,500 and 7,400 MW. In week 9 (highest residual demand), the residual demand varies between 5,250 and 11,500 MW. To test the effect of variability, simulations were performed for week 39 (most variable residual demand), in which the residual demand exhibits ramps up to 1,650 MW/15 minutes.

5.1.1 The case study: data & common assumptions

The computational and cost performance of the UC formulations are compared on a model of the Belgian power system. The 14 GW peak demand at transmission level occurs in winter, while the lowest demand – around 6 GW – occurs during daytime in summer. The annual consumption, measured at the transmission level, is 83 TWh. Electrical energy generated from RES other than wind (7% annually) is treated as a demand correction and cannot be curtailed. The demand profile and wind power data were obtained from Elia, the Belgian TSO. The conventional generation fleet consists of 71 power plants and combined-heat-and-power plants, with a total of 13,920 MW of dispatchable capacity [87]. The nominal efficiency of each power plant is based on its type, fuel and age. The other technical characteristics of the power plants are based on ENTSO-E data [240] and summarized in Appendix B. One PHES system has been included, with a maximum capacity of 1,308 MW, a round trip efficiency of 75% and a storage capacity of 3,924 MWh. The minimum energy content of the storage facility is set to 10% of its capacity. Since we take a system perspective, the energy storage facility is operated at no explicit cost to the system operator. However, charging/discharging of the energy storage facility results in energy losses due to round-trip efficiencies $\epsilon_r < 1$. These losses are taken into account when the least-cost day-ahead UC schedule is determined.

[1]This residual demand is calculated as the difference between the historical demand time series and the rescaled historical wind power time series.

The maintenance costs of all generation and transmission assets, including the energy storage facility, are neglected. The CO_2-price is assumed to be 10 €/ton CO_2. The value of lost load $VOLL$ is 10,000 €/MWh. Curtailment of RES-based electricity generation is not penalized ($VOC = 0$ €/MWh). If reserve constraints containing slack variables are enforced, the value of shed reserves VOR equals 5,000 €/MW. These high $VOLL$ and VOR values ensure that load shedding and/or reserve curtailment are 'emergency measures' to satisfy the balance between demand and supply. In the presented case study, reserve shedding was never observed. Load shedding, scheduled during UC optimization, was only observed in the SUC, HUC and PUC solutions, but never under forecast conditions.

In all the UC models implemented in this work the network constraints are omitted. This assumption may lead to transmission congestion, especially under high wind penetration levels [241]. However, the Belgian power system that provides the basis for our simulations has sufficient (internal) transmission capacity to make the effect of congestion essentially negligible [242]. The Belgian day-ahead market is cleared as one zonal market (with a single price). Transmission constraints are checked in a second stage by the TSO, with potential redispatching to alleviate congestion [242]. Currently, this redispatching affects 0.08% of the yearly electricity production and increases the annual operating cost by approximately 0.3% (2.9 M€/year) [242]. Since the impact of transmission congestion on the operating cost is marginal, omitting these constraints does not significantly affect the conclusions of this case study. The omission of transmission constraints significantly reduces the computational burden of the UC models. For example, Papavasiliou et al. [110] report that a transmission-constrained SUC model for a relatively small system with 375 transmission lines requires from several to tens of hours to achieve a reasonably small duality gap, even for a relatively small number of scenarios.

The planning horizon considered in the optimization is 24 hours and the time step is 15 minutes. To ensure continuity, each optimization takes into account the values of the optimization variables over the previous 24 hours, based on the dispatch taking into account the scenario that represents the scaled measured wind power output of the previous day. Similarly, the next day is taken into account to ensure logical UC decisions and a correct evaluation of the value of stored energy in the PHES system at the end of the planning horizon (24 hours)[2].

To ensure a fair comparison between the different UC models, each model starts

[2]Note that as such, the models consider the value of stored energy in the energy storage system beyond the planning horizon. For short-term energy storage, one can assume that an extension of the planning horizon by a factor two is sufficient. For long-term energy storage however, other techniques will be needed [243].

from the same set of 500 scenarios that describes the uncertain wind power forecast. These scenarios are generated as discussed in Chapter 4, based on the continuous description of the forecast error developed in Chapter 3. For the DUC and PUC model, we will calculate an empirical probability density function for each time step in the optimization from this set of scenarios, used in a probabilistic reserve sizing technique (Chapter 3). From the same scenario set, the ramping scenarios for the IIUC model are constructed, as described in [86] and briefly discussed in Chapter 2. Using a modified probability distance-based scenario reduction technique (Chapter 4), a limited set of 30 to 50 scenarios is selected from the same set for consideration in the SUC model. As such, all UC models use the same information about the uncertain wind power forecast. Differences in performance (operational system cost, wind power curtailment and reliability) are thus solely due to differences between the UC formulations.

The resulting UC schedule is evaluated in terms of operational cost, curtailment of the uncertain wind power production and load shedding, by running Monte-Carlo-dispatch simulations for a new, large set of 500 scenarios, as in Chapter 4. The dispatch model is set up as a DUC model and is executed for each scenario individually, without any reserve requirements, with the unit commitment status set to that obtained from the respective UC model and the wind power forecast replaced by the wind power scenario at hand[3]. Only fast-starting units scheduled as non-spinning reserve are allowed to start-up or shut-down during dispatch if needed. Although this is a restrictive approach, which may not be representative of the corrective actions a system operator has at his disposal in real time, it is the only correct method to evaluate the quality of the UC schedule. Indeed, by limiting the available flexibility to the *scheduled* flexibility during dispatch, we can evaluate the adequacy of the UC schedule. Allowing other units to start-up or shut-down during dispatch would distort our results.

The UC models are implemented in GAMS 24.4 and MATLAB 2011b, using the MATLAB - GAMS coupling developed by Ferris et al. [244]. CPLEX 12.6 is used as solver. Calculations are run on the ThinKing HPC cluster of the KU Leuven, part of the Flemish Supercomputer Center (Dutch: *VSC, Vlaams Supercomputer Centrum*), using a 2.8GHz machine with 20 cores and 64GB of RAM. The optimality gap was set to 0.5% for all cases.

[3]This approach does not fully represent the structure of the decision problem a system operator is faced with. First, within the dispatch problem, there is no uncertainty. In reality, information is released as time progresses. As such, the dispatch of reserves is optimized and the flexibility of the power system might be overestimated. Second, adaptations of the UC status, except of fast-starting units, during the dispatch are not considered.

5.2 The baseline: improving the performance of deterministic UC formulations

In our first setting, we study the simplest of UC models: a deterministic variant of the problem, which only allows scheduling of spinning reserves to meet the reserve requirements. PHES systems are only used for energy arbitrage purposes, and are thus not allowed to offer regulation services. Similarly, fast-starting units may only provide reserves if they are online (no non-spinning reserves). The impact of the inclusion of the aforementioned reserve providers is studied in Section 5.2.2 (non-spinning reserves) and Section 5.2.3 (PHES-based reserves).

Deterministic UC models require ex-ante reserve sizing. As wind energy is the only source of uncertainty in the power system at hand, one can easily come up with a wide range of heuristics to determine the reserve requirements. For example, one can calculate the reserve requirement as a percentage of the installed wind power capacity, a percentage of the possible forecast error or via a probabilistic method, as proposed in Chapter 3[4]. We will illustrate, based on our four-week analysis, that even with a detailed, probabilistic description of the forecast error and a state-of-the-art probabilistic reserve sizing technique, a consistent, optimal reserve sizing rule is difficult to identify. We will not attempt to optimize the reserve sizing procedure – we merely want to illustrate the dependence of the quality of the UC schedule on the reserve sizing rule. A reserve sizing procedure that results in cost-optimal UC schedules during one week may trigger sub-optimal UC schedules during other weeks or in the same week when other flexibility providers are available.

5.2.1 Enhancing the performance of DUC formulations via advanced reserve calculation methods

Figure 5.3 shows the upward reserves, as procured in a DUC model, considering a dynamic reserve requirement obtained via the proposed probabilistic reserve sizing technique assuming various levels of design reliability (DR) on the first day of week 39. Throughout this chapter, the scheduled upward flexibility is calculated as the possible maximum increase in output of scheduled capacity

[4]In the proposed probabilistic method, the required reserves are calculated based on the cumulative probability a forecast error is contained in the interval formed by the downward and upward reserves for that forecast. This cumulative probability is referred to as the design reliability. For example, a reserve requirement calculated assuming a design reliability of 95% is the smallest interval formed by the downward and upward reserves at each time step that covers 95% of the forecast errors. The demand for reserves is calculated per time step and may thus change from time step to time step. The demand for reserves is furthermore constrained to the range of possible forecast errors and the demand for electricity.

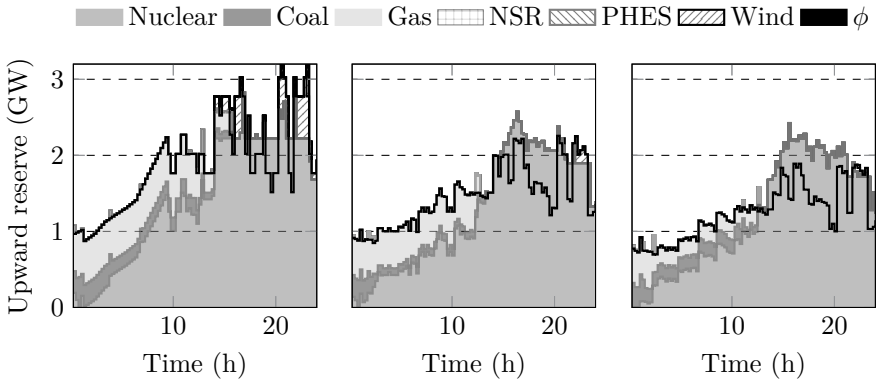

(a) DR: 100% **(b)** DR: 98% **(c)** DR: 95%.

Figure 5.3: The available upward flexibility (GW) on the first day of week 39, obtained with a DUC model considering a reserve requirement (black solid line) assuming design reliabilities (DR) equal to 95, 98 and 100% and only considering spinning reserves. The dynamic reserve requirement is based on a discrete set of scenarios, which is reflected in a different reserve requirement per time step.

with respect to their output under forecast conditions, accounting for their maximum stable operating point and ramping limits.

As the reserve requirement decreases, indicated by the solid black line in Fig. 5.3, the amount of scheduled reserve capacity decreases. The amount of coal- and gas-fired reserve capacity decreases considerably. Curtailment of forecasted wind power, 'recycled' as upward reserves, only occurs in the case of a 100% design reliability. However, note the significant 'overshoot' of scheduled reserve capacity, an effect which is especially visible in Fig. 5.3b and 5.3c. Nuclear capacity is the perceived lowest-cost flexibility provider in this particular instance, and these units are typically (1) large and (2) characterized by long minimum up and down times. Scheduling these units allows meeting the reserve requirements, but in fact triggers the availability of an upward reserve capacity that considerably exceeds the reserve requirement. Recall furthermore that curtailment of RES-based generation is free, and that the DUC model does not have any incentive to schedule downward flexibility.

With the reserve requirement corresponding to a design reliability of 98%, an expected operational cost of 0.94 M€/day is attained. Increasing the design reliability to 100% eliminates load shedding (5 MWh at a design reliability of

98%), increases curtailment by 36% and increases the expected operational cost up to 1.01 M€/day. Further reducing the design reliability to 95% leads to a significant increase in load shedding (18.4 MWh), which increases the expected operational cost to 1.01 M€/day, while the expected volume of curtailed RES-based generation decreases by 14%.

Based on these results, the existence of an optimal design reliability seems likely. Such an optimal reserve sizing rule should balance (1) the socio-economic cost of load shedding and curtailment of wind power and (2) the operational cost associated with procuring and deploying reserves. This is the subject of the four week analysis, of which the results are summarized in Table 5.1. This table contains the results of the DUC simulations, after MC ED evaluation, for six different levels of 'design reliability' in the probabilistic reserve sizing technique.

For weeks with a low wind share (WS), i.e. week 30 and week 9, decreasing the design reliability in the reserve sizing problem does not lead to a significant increase of the amount of load shedding. Indeed, load shedding volumes remain below 0.7 MWh (week 30) and 16.9 MWh (week 9) respectively. Due to less stringent reserve requirements, which require less capacity to be committed, operational costs decrease up to 0.4 M€/week in week 9. Note furthermore that the width of the corresponding confidence interval increases with increasing ENS-volumes. In week 30, the scheduled reserve capacity is nearly unaffected, despite less stringent reserve requirements. Some sub-optimal reserve procurement occurs at a design reliability of 99%. Curtailment does not occur in week 9 and week 30.

Similarly, decreasing the design reliability in week 52 and week 39, weeks with wind shares up to 50.3% and 78.5% respectively, leads to decreases in operational cost. In both weeks, the lowest operational cost occurs at a design reliability of 98%, which are characterized by a limited increase in the amount of load shedding (17.5 and 20.4 MWh respectively) and a moderate increase in the wind utilization factor (2.1 and 1.7 percentage points respectively). Further decreasing the design reliability leads to increases in the load shedding volume, hence high operational costs and wide confidence intervals. The simultaneous increase in the wind utilization and the associated fuel savings is insufficient to prevent the resulting total operational cost from increasing. Higher degrees of design reliability lead to excessive reserve scheduling, higher expected operational costs and lower wind utilization factors. The last effect is due to the scheduling of more capacity, which leads to a less 'compressible' power system.

So far, it seems that we are able to identify an optimal design reliability level (here: 98% in week 52 and 39, 96% in week 9 and 30). However, as mentioned above, we are not considering PHES-based reserves, nor non-spinning reserves. We will therefore typically have *more* flexibility available during dispatch than

accounted for in the reserve requirements. This is due to (1) the real-time availability of flexibility providers which we did not allow to satisfy the reserve requirement, such as PHES-based regulation services and (2) the 'overshoot' effect discussed above. In the subsequent sections we will illustrate that the inclusion of other flexibility providers, such as non-spinning and PHES-based reserves, allows meeting the reserve requirement more closely. In real time, we will have approximately the flexibility available that was accounted for in the reserve requirement, leading to less 'overshoot'. This will increase the importance of correctly setting the reserve requirement, and will show that it may be difficult to identify a consistent, optimal reserve requirement or design reliability.

Table 5.1: Performance of the DUC model only considering spinning reserves for design reliability levels between 95% and 100%. TOC is the total operational cost and ϕ the Energy Not Supplied volume. WUF is the Wind Utilization Factor, the percentage of available wind energy that is absorbed in the power system. WS is the Share of Wind energy in the total demand for electrical energy. Δ is the width of the 95% confidence interval on E[TOC].

(a) Week 30 (average residual demand)

Design reliability	[%]	95	96	97	98	99	100
E[TOC]	[M€]	13.7	13.7	13.7	13.8	13.9	13.8
Δ	[M€]	0.1	0.1	0.1	0.1	0.1	0.1
E[ϕ]	[MWh]	0.7	0.5	0.1	0.1	0	0
E[WUF]	[%]	100	100	100	100	100	100
E[WS]	[%]	10.6	10.6	10.6	10.6	10.6	10.6

(b) Week 9 (highest residual demand)

Design reliability	[%]	95	96	97	98	99	100
E[TOC]	[M€]	28.4	28.3	28.4	28.4	28.5	28.7
Δ	[M€]	0.4	0.3	0.3	0.2	0.2	0.1
E[ϕ]	[MWh]	27.1	16.9	8.8	0	0	0
E[WUF]	[%]	100	100	100	100	100	100
E[WS]	[%]	13.5	13.5	13.5	13.5	13.5	13.5

(c) Week 52 (lowest residual demand)

Design reliability	[%]	95	96	97	98	99	100
E[TOC]	[M€]	3.3	3.0	2.9	2.8	2.8	3.3
Δ	[M€]	0.6	0.5	0.4	0.2	0.1	0.01
E[ϕ]	[MWh]	80.0	54.7	36.8	17.5	3.4	0
E[WUF]	[%]	91.0	90.3	89.9	89.0	87.6	85.8
E[WS]	[%]	78.5	77.9	77.6	76.7	75.6	74.0

(d) Week 39 (most variable residual demand)

Design reliability	[%]	95	96	97	98	99	100
E[TOC]	[M€]	8.7	8.3	8.0	8.0	8.1	9.0
Δ	[M€]	1.1	0.8	0.5	0.3	0.1	0.05
E[ϕ]	[MWh]	134.9	89.1	38.3	20.4	2.1	0
E[WUF]	[%]	96.1	95.9	95.5	95.2	94.4	93.5
E[WS]	[%]	50.3	50.2	50.0	49.8	49.4	48.9

5.2.2 Cost-effective flexibility provision via non-spinning reserves

Non-spinning reserves may provide cost-effective upward flexibility. Unlikely, large negative forecast errors may be absorbed by dispatching fast-starting units in real time, avoiding the need for spinning reserves, which reduce the cost-efficiency of the UC schedule in close-to-forecast conditions. In this section, we discover how the DUC formulation addresses the scheduling of non-spinning reserves and how the availability of these flexibility providers interacts with the optimal reserve sizing rule. To analyze this effect, we allow highly flexible power plants to be scheduled as non-spinning reserve. In total, 35 fast-starting units, typically open cycle gas turbines or oil-fired power plants, with a total capacity of 1,118 MW are considered. These units can be scheduled at zero cost to meet the reserve requirements.

First, we again isolate the first day of week 39. The scheduled upward reserves are shown in Fig. 5.4, for instances of the same DUC model as above, each considering a reserve requirement that corresponds to a design reliability of 95%, 98% and 100% respectively. As the cost of procuring non-spinning reserves is set to zero ($NSRC_i = 0$) and the expected deployment cost of non-spinning reserves is not considered in the DUC formulation, these units are the perceived most cost-efficient upward flexibility providers. As a result, the DUC model will schedule non-spinning reserves to meet the reserve requirement. The upward reserves scheduled to meet the 100% design reliability reserve requirement no longer exceed the reserve requirement.

Notably, even when sufficient spinning capacity is available in the system, non-spinning reserves are procured (Fig. 5.4b and Fig. 5.4c). Recall that we show the *effectively available* upward flexibility, not the *scheduled* flexibility. The DUC model has sufficient upward flexibility from spinning units available, but, in this particular instance, chooses to schedule non-spinning reserves. As these last units do not result in additional operational costs, both solutions are equivalent. In some cases, we will therefore have more flexibility at our disposal during dispatch than required to meet the reserve requirement. In addition, recall that in this DUC model we so far have not accounted for the flexibility that the PHES system may offer. Scheduling PHES-based reserves is not yet allowed, but the PHES system may be used to balance the load during dispatch.

The resulting UC schedules are typically overly conservative, but highly flexible. Compared to the solutions of the DUC model only considering spinning reserves, the expected operational cost decreases considerably (up to 26% at a DR of 100%), the amount of curtailed RES-based generation decreases (approximately 49% at a DR of 100%) and the volume of load shedding remains approximately

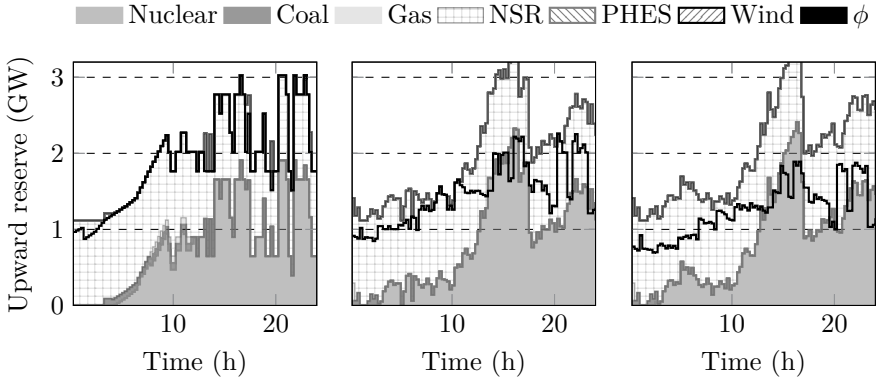

(a) DR: 100% **(b)** DR: 98% **(c)** DR: 95%.

Figure 5.4: The available upward flexibility (GW) on the first day of week 39 as obtained using the DUC model considering a reserve requirement (solid, black line) obtained with a probabilistic reserve sizing technique, assuming various design reliabilities (DR - 95%, 98% and 100%). Non-spinning ('NSR') and spinning reserves are considered.

the same. As the design reliability decreases, the expected operational cost rapidly increases in this particular instance. The UC schedule obtained with a reserve requirement with a design reliability of 98% is 4.5% more costly compared to the solution of the same instance with a reserve requirement with a design reliability of 100%. Although the volume of curtailed wind energy halves, an increase of the load shedding volume with 5.5 MWh suffices to offset the associated fuel cost savings. Regardless of the availability of a substantial amount of non-spinning reserves, insufficient reserve capacity is available between hour eight and ten. During these hours, the scheduled reserves do not exceed the reserve requirement, which proved to be insufficient to avoid load shedding during these hours. Further decreasing the design reliability to 95% magnifies these effects. The expected operational cost increases to 0.99 M€/day, an increase with 30% compared to the 100% design reliability solution, mainly due to an increased load shedding volume (23 MWh).

Again, a consistent, optimal reserve rule may exist when considering spinning and non-spinning reserves. To this end, we perform a four week analysis of the performance of the DUC model, now actively scheduling non-spinning reserves, considering reserve requirements corresponding to design reliabilities ranging from 95% to 100%. The results are summarized in Table 5.2.

Table 5.2: Performance of the DUC model with non-spinning reserves for design reliability levels between 95% and 100%. TOC is the total operational cost and ϕ the Energy Not Supplied volume. WUF is the Wind Utilization Factor, the percentage of available wind energy that is absorbed in the power system. WS is the Share of Wind energy in the total demand for electrical energy. Δ is the width of the 95% confidence interval on E[TOC].

(a) Week 30 (average residual demand)

Design reliability	[%]	95	96	97	98	99	100
E[TOC]	[M€]	13.2	13.3	13.3	13.2	13.2	13.2
Δ	[M€]	0.1	0.1	0.1	0.1	0.1	0.1
E[ϕ]	[MWh]	3.5	3.0	2.0	1.3	1.1	1.3
E[WUF]	[%]	100	100	100	100	100	100
E[WS]	[%]	10.6	10.6	10.6	10.6	10.6	10.6

(b) Week 9 (highest residual demand)

Design reliability	[%]	95	96	97	98	99	100
E[TOC]	[M€]	27.5	27.4	27.3	27.3	27.4	27.5
Δ	[M€]	0.4	0.4	0.2	0.2	0.2	0.2
E[ϕ]	[MWh]	29.2	19.8	7.3	2.7	2.1	2.0
E[WUF]	[%]	100	100	100	100	100	100
E[WS]	[%]	13.5	13.5	13.5	13.5	13.5	13.5

(c) Week 52 (lowest residual demand)

Design reliability	[%]	95	96	97	98	99	100
E[TOC]	[M€]	5.1	4.6	3.2	2.4	2.3	2.4
Δ	[M€]	0.8	0.6	0.4	0.2	0.1	0.02
E[ϕ]	[MWh]	101.1	65.5	35.6	16.1	4.0	0.2
E[WUF]	[%]	94.8	94.7	94.9	95.0	93.8	91.5
E[WS]	[%]	81.8	81.7	81.8	81.9	80.9	79.0

(d) Week 39 (most variable residual demand)

Design reliability	[%]	95	96	97	98	99	100
E[TOC]	[M€]	7.5	7.0	6.7	6.6	6.7	7.1
Δ	[M€]	1.0	0.7	0.5	0.3	0.2	0.1
E[ϕ]	[MWh]	118.4	70.2	44.0	16.5	6.1	0.6
E[WUF]	[%]	98.2	98.2	97.7	97.5	97.4	95.8
E[WS]	[%]	51.4	51.4	51.1	51.0	51.0	50.1

First, compared to the results in Table 5.1, the introduction of non-spinning reserves triggers significant cost reductions. For the results obtained assuming a 100% design reliability, expected operational cost decreases are between 0.7 M€/week and 1.9 M€/week. These reductions are especially noticeable during the weeks with high share of RES-based electricity generation, i.e. weeks 39 and 52. This is the result of an increased wind power utilization (up to 5.7 percentage points), which replaces conventional generation and, thus, allows meeting the balancing needs at a lower expected activation cost of non-spinning reserve. The amount of load shedding slightly increases compared to the results obtained considering only spinning reserves. This is an indication that the reserve requirement is more closely met. Small differences in the scenario set used to calculate the empirical distribution of the error, used in the reserve sizing technique, and the scenario set used during the Monte Carlo ED simulations trigger low volumes of load shedding. As the reserve requirement is more closely met, a less stringent reserve requirement leads to stronger increases in load shedding volumes.

Moderately decreasing the design reliability decreases the operational cost in three out of four weeks. The cost decrease is however less pronounced than in the results obtained with a DUC model only considering spinning reserves. Without non-spinning reserves, operational cost savings between 0.2 M€/week and 1.0 M€/week were observed (Table 5.1). With non-spinning reserves, the same operational cost savings amount to at most 0.5 M€/week. A too stringent reserve requirement is less severely penalized in the presence of non-spinning reserves, as scheduling and *not* dispatching these units will not result in any operational cost during dispatch. Without these non-spinning reserves, spinning capacity must be scheduled to meet the reserve requirements, which inherently results in operational inefficiencies if the reserve requirement is too strict or not strict enough. With the availability of non-spinning reserves, the possible operational cost savings associated with lowering the design reliability decrease, while the penalty for inadequate reserve procurement, i.e. the cost of load shedding, remains the same. In week 9 and 39, a design reliability of 98% can still be considered cost-optimal. At the expense of a moderate increase in load shedding, operational cost savings of 0.2 M€/week and 0.5 M€/week are realized. In week 52, a reserve requirement with a 99% design reliability is cost-optimal, triggering 3.8 MWh/week of additional load shedding, whilst lowering the total expected operational cost by 0.1 M€/week. In week 30, the model is indifferent to reserve requirements with a design reliability between 98 and 100%.

In what remains of this section, we will analyze whether these improvements in the performance of the DUC model are the result of correctly relaxing a too stringent reserve requirement, or that it is the result of not accounting for

available PHES-based flexibility to meet this requirement. Up to this point, the PHES system has been used solely for energy arbitrage purposes. This unit may however also provide cost-efficient regulation services during dispatch. Not considering this flexibility during the UC optimization may render the resulting schedule too conservative, but does not imply that the reserve requirement itself was too conservative.

5.2.3 Operational benefits of PHES-based regulation services[5]

In this section, we will quantify the attainable operational cost savings that arise from leveraging the regulation services that may be offered by a PHES system during the optimization of the UC decisions. To this end, we developed a novel set of constraints (Eq. (2.47)-(2.48), Chapter 2) to ensure the feasibility of dispatching the scheduled reserves. First, we discuss the behavior of the DUC model with and without PHES-based reserves in detail, based on the simulations for the first day of week 39 of the calendar year, which is characterized by the system-wide demand and wind generation profiles illustrated in Fig. 5.2. Throughout this discussion we focus on the provision of the upward reserves and illustrate the importance of constraints (2.47)-(2.48). Second, we demonstrate the operational benefits of the PHES system in providing regulation services throughout the calendar year. Before discussing the computational performance of the DUC formulation (Section 5.2.4), we also analyze the impact of the availability of non-spinning reserves on the value of PHES-based reserves and the interaction of PHES-based reserves with optimal reserve sizing.

The need for additional constraints on regulation services offered by PHES systems

Figure 5.5 shows the scheduled upward reserves as obtained with the DUC model considering a reserve requirement with a 100% design reliability. During the first hours of the day, conventional power plants and curtailment of RES-based generation are scheduled as upward reserve if the PHES system is not allowed to offer regulation services ($r_{r,j}^{\mathrm{P},+}, r_{r,j}^{\mathrm{P},-}, r_{r,j}^{\mathrm{T},-}, r_{r,j}^{\mathrm{T},+} = 0$), as shown in Fig. 5.5a. As the forecasted RES-based generation increases during the day, the high expected wind power output results in high reserve requirements provided mainly by cheap nuclear units. The availability of the PHES system to provide regulation

[5]This section is based on K. Bruninx, Y. Dvorkin, E. Delarue, H. Pandžić, W. D'haeseleer, and D. S. Kirschen, *Coupling Pumped Hydro Energy Storage with Unit Commitment,* IEEE Trans. Sustain. Energy, vol. 7, no. 2, pp. 786–796, 2016.

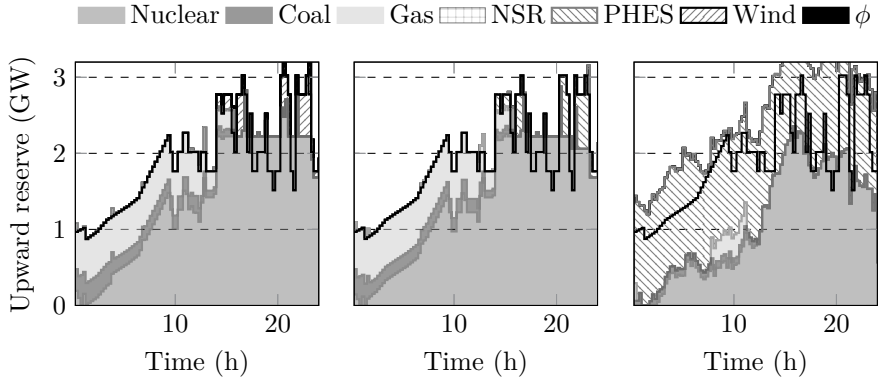

(a) No PHES-based reserves

(b) PHES-based reserves, incl. Eq. (2.47)-(2.48).

(c) PHES-based reserves, excl. Eq. (2.47)-(2.48).

Figure 5.5: The available upward flexibility (GW) as obtained on the first day of week 39, using a DUC model (a) not considering PHES-based flexibility, (b) considering PHES-based flexibility, constrained by Eq. (2.47)-(2.48) and (c) considering PHES-based flexibility, but excluding Eq. (2.47)-(2.48) from the model. The design reliability of the reserve requirement (black, solid line) is set to 100%.

services, constrained by Eq. (2.47)-(2.48), allows replacing mainly RES-based reserves (curtailment) by PHES-based reserves (Fig. 5.5b). The offered reserve power is based on the option to reduce the scheduled pumping power of the PHES system. This leads to a decrease of 40 MW in committed capacity on average, with peaks up to 433 MW. As a result, the expected operational cost decreases by 1%. The expected curtailment decreases by 1422 MWh or 42%. The reliability of the resulting UC schedule is unaffected if constraints Eq. (2.47)-(2.48) are enforced. If one omits constraints (2.47)-(2.48), the DUC formulation schedules upward reserves as shown in Fig. 5.5c: the PHES system is continuously scheduled as upward reserve. The operational cost under forecast conditions (i.e. the operational cost as obtained from the DUC model, before Monte-Carlo dispatch simulations) decreases by 13%, as less capacity needs to be committed to meet the demand and the reserve requirements. However, the limited energy storage capacity of the PHES system does not allow the activation of these reserves, resulting in load shedding during dispatch. For this specific day, the expected ENS volume reaches 354 MWh, which is to be compared with no ENS when the constraints (2.47)-(2.48) are included in the model. The expected operational costs, including the cost of ENS, quadruple.

In conclusion, the analysis above shows that the inclusion of the additional

constraints (2.47)-(2.48) is necessary to exploit the cost-effective regulation services that may be offered by PHES systems in DUC formulations. Neglecting these constraints may lead a modeler to believe the system is scheduled in a cost-effective manner, while insufficient availability of flexibility will trigger load shedding during real-time operation.

Quantifying the operational benefits of PHES-based regulation services & interaction with optimal reserve sizing

Table 5.3 compares the results of the Monte-Carlo simulations for the DUC formulation applied to the Belgian power system for four representative weeks. These simulations include two dispatch strategies: (1) the PHES system provides energy arbitrage only ('SR'), i.e. it is used to accommodate temporary surpluses or deficits in energy under forecast conditions, and (2) the PHES system provides both energy arbitrage and regulation services ('SR & PHES'). In the last case, the worst-case energy content constraints (Eq. (2.47) - (2.48)) are enforced to ensure the feasibility of the real-time dispatch of the scheduled reserves. For now, we focus on the performance of the DUC formulation only considering spinning reserves.

A number of trends can be identified in the results summarized in Table 5.3. First, allowing scheduling of regulation services offered by the PHES system reduces the expected operational cost. Indeed, for all weeks, the operational cost decreases if one considers the results obtained with a design reliability of 100%. In two out of four weeks, the decrease in operational cost is considerable. Especially at high shares of wind energy (week 39, high upward reserve requirements and flexible, expensive units needed to meet this requirement) and in weeks characterized by a high residual demand (week 9, low reserve requirements, but only expensive units available due to a high demand) the decrease in operational cost is significant. Operational cost savings vary between 0 and 0.2 M€/week. This cost reduction is the result of (i) an improved utilization of the available wind power and (ii) a more cost-efficient UC schedule. The first effect is illustrated by the Wind Utilization Factor (WUF) in Table 5.3, and the second was discussed in Section 5.4.1. By enforcing Eq. (2.47)-(2.48), the reliability of the UC schedules is unaffected by the presence of PHES-based reserves.

Second, reducing the design reliability of the reserve requirement reduces the operational cost in all considered weeks. The attainable operational cost savings vary between 0.2 M€/week (week 30) and 0.8 M€/week (week 39). Less stringent reserve requirements, combined with PHES-based reserves that allow the reserve requirement to be met more closely, lead to significant increases

Table 5.3: Performance of the DUC model considering spinnig reserves (SR) and PHES-based regulation services for design reliability levels between 95% and 100%. TOC is the total operational cost and ϕ the Energy Not Supplied volume. WUF is the Wind Utilization Factor, the percentage of available wind energy that is absorbed in the power system. WS is the Share of Wind energy in the total demand for electrical energy. Δ is the width of the 95% confidence interval on E[TOC].

(a) Week 30 (average residual demand)

		SR & PHES						SR
Design reliability	[%]	95	96	97	98	99	100	100
E[TOC]	[M€]	13.7	13.6	13.7	13.6	13.7	13.8	13.8
Δ	[M€]	0.1	0.1	0.1	0.1	0.1	0.1	0.1
E[ϕ]	[MWh]	1.3	0	0	0	0	0	0
E[WUF]	[%]	100	100	100	100	100	100	100
E[WS]	[%]	10.6	10.6	10.6	10.6	10.6	10.6	10.6

(b) Week 9 (highest residual demand)

		SR & PHES						SR
Design reliability	[%]	95	96	97	98	99	100	100
E[TOC]	[M€]	28.7	28.5	28.2	28.2	28.3	28.5	28.7
Δ	[M€]	0.8	0.6	0.3	0.2	0.2	0.1	0.1
E[ϕ]	[MWh]	81.4	56.5	16.9	1.9	0	0	0
E[WUF]	[%]	100	100	100	100	100	100	100
E[WS]	[%]	13.5	13.5	13.5	13.5	13.5	13.5	13.5

(c) Week 52 (lowest residual demand)

		SR & PHES						SR
Design reliability	[%]	95	96	97	98	99	100	100
E[TOC]	[M€]	3.5	3.0	2.9	2.8	2.8	3.3	3.3
Δ	[M€]	0.7	0.4	0.3	0.2	0.1	0.01	0.01
E[ϕ]	[MWh]	103.7	53.0	35.6	13.9	5.4	0	0
E[WUF]	[%]	91.6	90.9	90.7	89.8	88.1	86.7	85.8
E[WS]	[%]	79.0	78.4	78.3	77.5	76.0	74.8	74.0

(d) Week 39 (most variable residual demand)

		SR & PHES						SR
Design reliability	[%]	95	96	97	98	99	100	100
E[TOC]	[M€]	8.4	8.1	8.0	8.0	8.1	8.8	9.0
Δ	[M€]	1.0	0.8	0.5	0.3	0.1	0.1	0.05
E[ϕ]	[MWh]	111.9	69.4	44.2	17.2	1.5	0	0
E[WUF]	[%]	96.1	95.4	95.4	95.5	94.3	93.5	93.5
E[WS]	[%]	50.3	49.9	49.9	49.9	49.3	48.9	48.9

in wind utilization (week 39 and 52) and moderate decreases in reliability. Remarkably, in all weeks an optimal trade-off between reliability and operational cost is found at a design reliability of 98%. In part, this can be explained by the conservatism of the PHES constraints and the overshoot effect that persists, resulting in more available flexibility in real time than strictly required to meet the reserve requirements. Reducing the reserve requirement also affects the value of PHES-based reserves (compare Table 5.1 and Table 5.3). In week 30 and week 9, PHES-based reserves result in operational cost savings of 0.2 M€/week at the optimal design reliability level. In week 52 and 39, PHES-based reserves are no longer needed to meet the reserve requirement, and the associated cost savings are reduced to zero.

The impact of non-spinning reserves on the value of PHES-based regulation services

As non-spinning reserves can reduce the cost of regulation services, their presence will affect the value of the PHES-based regulation services. Scheduling non-spinning reserve reduces the operating cost by 0.6 M€/week to 1.9 M€/week (4.5% to 26.7%, respectively – see Table 5.4). Non-spinning reserves tend to reduce the value of regulation services provided by the PHES unit. PHES-based regulation services result in cost savings up to 0.2 M€/week (week 39) in the absence of non-spinning reserves. If non-spinning reserves are available, these units can provide the same regulation services more cost-effectively, which leads to an overall operational cost reduction, but no longer results in cost savings associated with PHES-based regulation services. Only in week 39, the week with the highest variability in the wind power output, PHES-based regulation services yield operational cost savings. Note furthermore that the reliability decreases slightly with the inclusion of PHES-based and non-spinning reserves.

Lowering the reserve constraints leads to operational cost savings in week 9 and week 39. A more cost-efficient UC schedule and an increased wind utilization (week 39) yield operational cost savings up to 0.4 M€/week at the expense of a moderate increase in load shedding volumes. The optimal design reliability equals 98% in week 9 and 99 % in week 39. In week 30, no significant changes were observed in the operational cost as the reserve requirement decreased. Over-procurement of non-spinning reserves still leads to UC schedules with high reliability levels and curtailment does not occur. Remarkably, in week 52, the operational cost drastically increases with decreasing reserve requirements. Although load shedding volumes increase, this increase alone does not explain the evolution of the operational cost. In this particular week, lowering the reserve requirements triggers scheduling other technologies to meet the demand and the reserve requirements. This switch to more flexible, more expensive-

Table 5.4: Performance of the DUC model considering spinnig reserves (SR), non-spinning reserves (NSR) and PHES-based regulation services for design reliability levels between 95% and 100%. TOC is the total operational cost and ϕ the Energy Not Supplied volume. WUF is the Wind Utilization Factor, the percentage of available wind energy that is absorbed in the power system. WS is the Share of Wind energy in the total demand for electrical energy. Δ is the width of the 95% confidence interval on E[TOC].

(a) Week 30 (average residual demand)

		SR, NSR & PHES						SR & NSR
Design reliability	[%]	95	96	97	98	99	100	100
E[TOC]	[M€]	13.3	13.3	13.3	13.2	13.3	13.2	13.2
Δ	[M€]	0.1	0.1	0.1	0.1	0.1	0.1	0.1
E[ϕ]	[MWh]	4.4	3.1	3.0	1.1	1.5	0.5	0.7
E[WUF]	[%]	100	100	100	100	100	100	100
E[WS]	[%]	10.6	10.6	10.6	10.6	10.6	10.6	10.6

(b) Week 9 (highest residual demand)

		SR, NSR & PHES						SR & NSR
Design reliability	[%]	95	96	97	98	99	100	100
E[TOC]	[M€]	27.7	27.6	27.3	27.3	27.4	27.5	27.5
Δ	[M€]	0.6	0.5	0.3	0.2	0.2	0.2	0.1
E[ϕ]	[MWh]	50.9	40.7	12.05	3.6	2.0	1.8	2.0
E[WUF]	[%]	100	100	100	100	100	100	100
E[WS]	[%]	13.5	13.5	13.5	13.5	13.5	13.5	13.5

(c) Week 52 (lowest residual demand)

		SR, NSR & PHES						SR & NSR
Design reliability	[%]	95	96	97	98	99	100	100
E[TOC]	[M€]	5.6	5.5	3.7	4.6	4.4	2.4	2.4
Δ	[M€]	0.8	0.5	0.4	0.2	0.1	0.03	0.1
E[ϕ]	[MWh]	108.7	63.5	37.1	19.7	3.4	0.1	0.2
E[WUF]	[%]	95.1	94.4	94.9	94.2	94.2	92.4	91.5
E[WS]	[%]	82.0	81.5	81.9	81.2	80.1	79.7	79.0

(d) Week 39 (most variable residual demand)

		SR, NSR & PHES						SR & NSR
Design reliability	[%]	95	96	97	98	99	100	100
E[TOC]	[M€]	7.7	7.4	6.8	6.8	6.7	6.9	7.1
Δ	[M€]	1.1	0.8	0.5	0.3	0.2	0.1	0.05
E[ϕ]	[MWh]	126.6	76.88	36.4	16.2	5.8	0.2	0.6
E[WUF]	[%]	98.2	98.0	97.5	97.7	97.3	96.0	95.8
E[WS]	[%]	51.4	51.3	51.0	51.1	50.3	79.7	50.1

Table 5.5: Comparison of the CPU time (s) per run of the DUC model, with and without non-spinning reserves, with and without PHES-based reserves. P(75) is the 75$^{\text{th}}$ percentile, P(90) is the 90$^{\text{th}}$ percentile.

	SR	SR & PHES	SR & NSR	SR, NSR & PHES
Median [s]	67	138	61	125
P(75) [s]	93	191	91	213
P(90) [s]	241	342	188	335

to-activate capacity is the result of not accounting for the expected cost of activating the scheduled reserves in real time.

5.2.4 Computational Performance

The resulting execution times (median and percentiles) for all DUC models are listed in Table 5.5. All solutions satisfy the optimality gap of 0.5%. If the PHES system is not allowed to offer regulation services in the DUC formulation, the median calculation time is approximately one minute. In general, the DUC problem takes more time to solve if the PHES system is allowed to offer regulation services. Median calculation times rise to approximately two minutes. The spread on the calculation times is furthermore limited: in 90% of the cases, an instance of the DUC problem solves within 4 minutes (no PHES-based reserves) to 6 minutes (with PHES-based reserves).

Introducing non-spinning reserves does not affect the calculation time considerably. On average, the calculation time decreases slightly. As the DUC formulation does not consider any operational costs w.r.t. the scheduling of non-spinning reserves, we are effectively 'relaxing' the reserve requirement. Some instances of the DUC problem, in which the reserve requirements were binding in absence of non-spinning reserves, may now be governed by other constraints. In absence of PHES-based reserves, the spread on the calculation times drops considerably. In 90% of all cases, a solution is found in just over three minutes, compared to four minutes without non-spinning reserves. If the PHES system is allowed to offer regulation services, the DUC model considers the complex trade-off between the provision of regulation services, which possibly requires forfeiting some arbitrage opportunities, and operational efficiency gains as the result of energy arbitrage. The spread on the calculation time again rises: 90% of the instances are solved within 5.5 minutes.

5.2.5 Concluding remarks

Traditionally, all UC models were deterministic models. Their deterministic character was a reflection of the power systems they were designed to study and of the computational limits of their time. However, when dealing with uncertainty, they require ex-ante reserve sizing. Before the introduction of intermittent RES-based generation in the system, limited uncertainty in the system allowed near-cost-optimal power system operation and planning with static reserve requirements. Large-scale intermittent RES-based generation however results in fluctuating levels of uncertainty, which requires dynamic (i.e. time-dependent) reserve requirements. In this section, we extensively studied the way a probabilistic reserve requirement interacts with scheduled upward reserves and how this affects reliability, curtailed wind energy and, ultimately, the expected operational cost. Relaxing the reserve constraints, i.e. not requiring that the scheduled reserves can absorb every possible forecast error, may trigger significant cost savings. Especially if the procured reserves are predominantly spinning reserves, which tend to be large in size, the gains associated with a less stringent reserve requirement can be large. Non-spinning reserves, provided by fast-starting units, are proven to be cost-effective reserve providers. These units allow following the reserve requirement more closely, which results in a more cost-efficient dispatch in close-to-forecast conditions, higher wind utilization factors and consequently, lower operational costs. We highlighted that scheduling non-spinning reserves in a DUC model may however be problematic, as the expected deployment cost of reserves is typically unknown in DUC formulations. Without the consideration of the expected deployment cost of these fast-starting flexibility providers, the risk of over-procuring upward reserves remains.

Deterministic UC models are sufficient to study energy arbitrage with PHES systems, but fail to account for the hydraulic constraints of the PHES system when offering regulation services. We here studied the impact of novel constraints on the PHES system, presented in Chapter 2, that allow co-optimizing the PHES dispatch and reserve provision decisions with the UC schedule of the conventional power plants. The proposed constraints are necessary to exploit the cost-effective regulation services that a PHES system may offer in a DUC formulation. The proposed DUC formulation achieves significant cost savings and increased wind power utilization rates at the expense of small CPU time increases compared to DUC models with sub-optimal reserve requirements or formulations in which PHES-based regulation is not considered. Although they are bound by conservative constraints, the introduction of PHES-based reserves allows following the reserve requirement more closely at a lower expected operational cost.

A consistent optimal reserve rule proved to be difficult to quantify ex-ante, as the cost of reserve procurement and activation is dependent on the state of the power system at each instance, the availability of flexibility providers, the probability of activation of the procured reserves and the expected socio-economic cost of curtailment and load shedding. In what follows, we will therefore use the results obtained from the DUC formulation considering the minimum reserve requirements covering 100% of the forecast errors. Although this approach is, in some case, somewhat conservative, it will provide an upper bound to the expected operational costs with near-zero load shedding volumes. Moreover, as these reserve requirements represent the limits of the domain of the distribution of wind power forecast error, obtained from the same, large set of scenarios used in the SUC, IIUC, HUC and PUC models, the implicit or explicit reserve requirements in each of these UC formulations are comparable. We will explicitly return to this point where relevant.

5.3 The benchmark: stable solutions of the stochastic unit commitment problem[6]

In this section, we analyze the results obtained with the SUC formulation. We will consider, as illustrated in Fig 5.1, four sets of assumptions on the availability of flexibility providers. In a first case, we only allow units that are online in all scenarios to cover the demand. In other words, only spinning reserves are considered. In a second set of simulations, we additionally allow fast-starting units to provide non-spinning reserves, modeled via a scenario-specific UC status for these units. In the first two cases, the output of the PHES unit is forced to be common to all scenarios, simplifying the SUC problem. Note that this is an 'artificial' constraint imposed on the SUC formulation. Allowing a scenario-specific output of the PHES unit reflects the fast-cycling nature of these units. However, this artificial constraint ensures the comparability of the obtained results with those of the DUC model that does not consider PHES-based reserves. In other words, we isolate the effect of a scenario-based representation of the uncertainty from distortions caused by the inability of the DUC formulation to account for the full regulation potential of the PHES system. During dispatch, the output of the PHES unit can however be adapted, which is consistent with the approach taken in the DUC simulations. In the third setting, spinning reserves and PHES-based reserves are allowed. By allowing a scenario-specific output profile for the PHES unit, the regulation services that

[6]Some elements in this section are based on K. Bruninx, K. Van den Bergh, E. Delarue, and W. D'haeseleer, *Optimization and Allocation of Spinning Reserves in a Low-Carbon Framework,* IEEE Trans. Power Syst., vol. 31, no. 2, pp. 872–882, 2016.

may be offered by the PHES unit can be exploited. Last, the combination of spinning, non-spinning and PHES-based reserves is studied.

As discussed in Chapter 4, solving a SUC problem considering 500 scenarios is computationally impossible without e.g. dedicated decomposition techniques and/or parallel computing [110]. The sheer size of the problem may render the SUC instance intractable. Therefore, more commonly, researchers consider a reduced set of scenarios when solving a SUC problem. In this section, we will employ the SRT as proposed in Chapter 4. Based on the solution stability analysis presented in that chapter and an extensive numerical analysis, we will consider 30 scenarios if only spinning or spinning and non-spinning flexibility is considered, which was shown to yield stable results in Chapter 4. With the availability of PHES-based flexibility, the stability of the SUC solutions was no longer guaranteed. Therefore, we will, for these cases, solve the SUC problem considering 50 (spinning and PHES-based reserves) and 40 (spinning, non-spinning and PHES-based reserves) scenarios. At these scenario set sizes, the problem becomes extremely computationally intensive. Solutions within the optimality gap could not always be obtained and solution stability remains an issue. We will return to this issue where relevant.

Before moving to the numerical analysis (Section 5.3.2), we first illustrate how the representation of the uncertainty via scenarios affects the resulting upward flexibility in Section 5.3.1. Third, we shed some light on the computational effort involved in solving a SUC instance (Section 5.3.3). Last, we formulate a conclusion.

5.3.1 Upward reserves, load shedding and wind power scenarios

In this section, we again isolate results of the SUC model on the first day of week 39 (Fig. 5.2) to illustrate the difference between the DUC and SUC formulations w.r.t. the representation of the uncertainty and how this impacts the scheduling of upward flexibility. Figure 5.6 shows the scheduled flexibility, as obtained from a DUC or SUC formulation under the four sets of assumptions on the availability of flexibility providers mentioned above. In the DUC model, we impose a reserve requirement equal to the maximum forecast error observed in a large set of scenarios, i.e. with a probabilistic reserve requirement with a design reliability of 100%. From the same set, we select 30 to 50 scenarios to represent the uncertainty in the SUC model. Both models start from the same scenario set, and thus have the same information on the uncertain wind power forecast. The number of scenarios differs depending on the flexibility providers available to avoid solution stability problems, an issue we alluded to in the

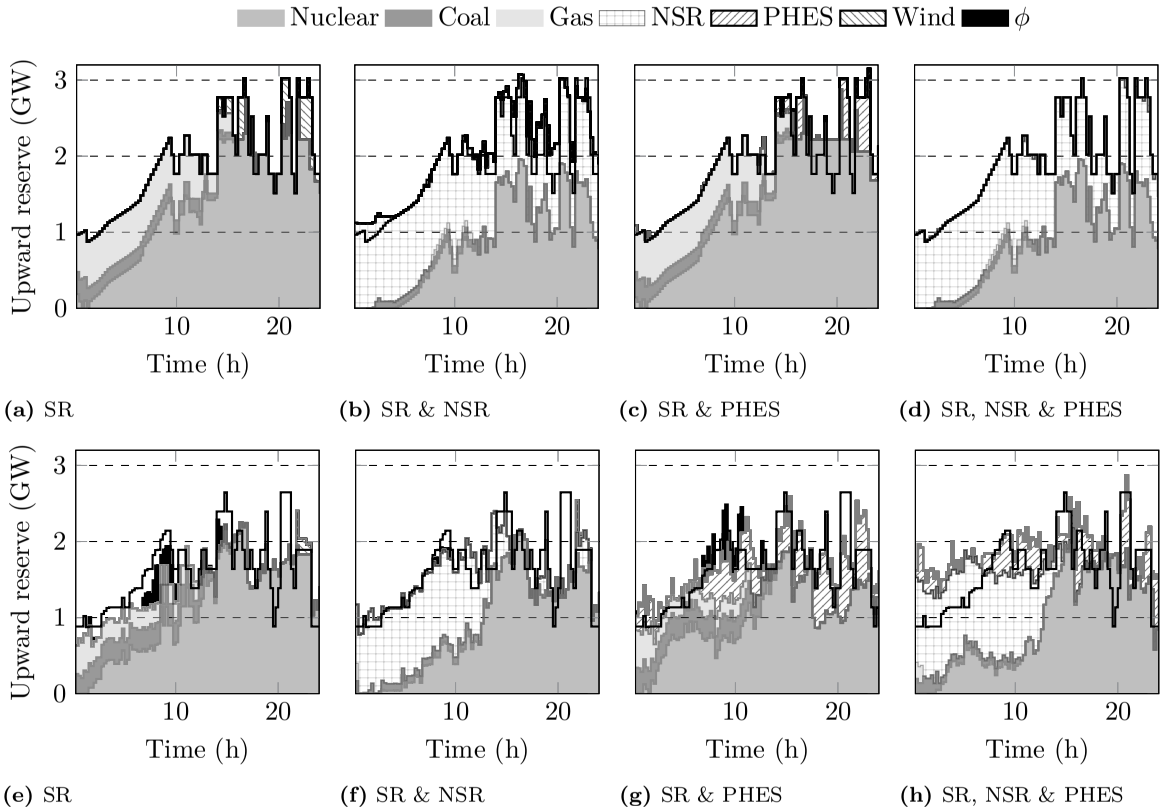

Figure 5.6: The available upward reserve capacity per UC formulation (top row: DUC, bottom row: SUC) on the first day of week 39. The solid black line indicates the total upward reserve requirement (DUC) or the equivalent upward reserve requirement (SUC), calculated as the highest negative forecast error at each time step in the reduced set of scenarios. The SUC model considers 30 to 50 scenarios.

introduction of this section and to which we will return in Section 5.3.2. Again, a similar analysis can be made for the scheduling of downward flexibility, but we will focus on upward flexibility due to the high cost of load shedding. The effect of procuring downward reserves - recall that the DUC formulation does not provide any incentive to schedule downward reserves - will be evident from the increase in wind utilization in the SUC solutions compared to their deterministic counterparts, which we will discuss in Section 5.3.2.

If only spinning reserves are available, the SUC formulation will result in significantly less scheduled upward flexibility compared to the equivalent deterministic model. The underlying cause of this observation is threefold. First, the SUC model has the possibility of scheduling load shedding[7] as 'flexibility provider', i.e. effectively shedding reserves (ϕ in Fig. 5.6). In the proposed formulation of the SUC model one obtains a UC schedule that reflects an optimal trade-off between reliability and the cost of ensuring that reliability. Load shedding is scheduled in extreme scenarios when the expected cost of load shedding is dominated by the cost reduction from committing less reserves, thus capacity[8]. In essence, the SUC model allows *internally* relaxing the implicit reserve requirements, represented via the considered scenarios to obtain an optimal trade-off between the expected cost of upward flexibility provision and load shedding. For this particular instance, this optimum lies around 4.5 MWh/day of expected load shedding. Second, the SUC formulation allows a more effective use of the PHES unit. Although the PHES output profile is common to all scenarios, it is optimized taking into account the full cost of flexibility procurement and deployment in all considered scenarios. The PHES unit can provide reserves indirectly by freeing up conventional capacity at certain time steps, avoiding the need to start-up an additional unit. This is also possible in the DUC formulation. However, as the DUC model does not consider the activation or deployment cost of reserves, this trade-off is ill-informed. Third, the implicit reserve requirement enforced by the selected scenarios is less stringent compared to the upward reserve requirement in the DUC problem. This last point can be illustrated by comparing the upward reserve requirement imposed on the DUC model, calculated as the maximal negative forecast error on each time step observed in a large set of scenarios (solid black line, Fig. 5.6a), and the equivalent upward reserve requirement imposed on the SUC problem, calculated as the maximal negative forecast error on each time step observed in the reduced set of scenarios (solid black line, Fig. 5.6e). The reduced scenario set is especially less strict during the last hours of the day, when the wind power forecast is particularly high and consequently, the

[7]The visualized load shedding 'volume' is the maximal observed load shedding in any scenario on each time step. It should not be related to an expected load shedding volume.

[8]Note that the resulting level of load shedding is thus sensitive to the value of lost load ($VOLL$). A sensitivity analysis towards this value is however out of the scope of this text.

residual demand is low and conventional flexibility is likely to be available, even without the consideration of scenarios with large negative forecast errors. Note that these are exactly those hours in which the results obtained with the DUC formulation resulted in over-procurement of upward reserves, even if the reserve requirement was lowered (Fig. 5.6a). During the first hours of the day, when the expected residual demand is high and hence only expensive-to-run power plants are available to meet the demand for upward flexibility, the equivalent reserve requirement is nearly identical to the reserve requirement imposed on the DUC problem.

Note furthermore that the equivalent reserve requirement is seemingly not always exactly met in the SUC solution. This is due to (1) the way we calculate the scheduled flexibility and (2) the way the PHES unit is scheduled, taking into account all scenarios. First, we calculate the scheduled upward flexibility as the headroom in the online power plants and correct this capacity according to the maximal ramp rate *assuming these units are running at their output level scheduled under forecast conditions*. Although this approach is consistent with the approach taken in the evaluation of the results of the DUC model, it is a conservative one. Indeed, in the SUC model, less stringent ramping requirements may be imposed by the scenarios. Typically, a unit will start to ramp up before a severe negative forecast error materializes, respecting its ramp rate. The required capacity to deliver the upward reserves to meet the demand in all scenarios may thus be lower than anticipated, assuming that the ramping requirements imposed on these reserves are equal to the difference between the maximal negative forecast error and the forecasted wind power output at each time step. Second, the common PHES output profile is optimized taking into account information of all considered scenarios. Seemingly excessive upward flexibility may be scheduled during periods of low residual demand to allow discharging of the PHES unit, freeing up capacity in these time steps. This effect is not explicitly visualized in Fig. 5.6e. During the Monte Carlo evaluation, load shedding occurs during the first part of the day, with a peak in the expected load shedding volume between hour 8 and 10, in which the SUC model shedded some load in demanding, but unlikely scenarios. The total expected load shedding volume amounts to approximately 2 MWh or less than 0.001% of the demand. The operational cost on this particular day, in which approximately 47% of the demand is covered by RES-based generation, decreases by approximately 9% compared to the DUC solution.

The availability of non-spinning reserves strongly reduces the need for spinning reserves. Especially during the first hours of the day, gas-fired, coal-fired and nuclear capacity is replaced by non-spinning, fast-starting units (Fig. 5.6f), which reduces the total expected operational cost with approximately 20% on this particular day. This is the result of a more flexible UC schedule, which

allows the absorption of more RES-based generation, and thus fuel cost savings. In this particular case, the amount of curtailed wind energy decreases by 37%. Note furthermore that the availability of these dynamic and cost-effective flexibility providers abolishes the need for reserve shedding in hours 7 to 10. Compared to the DUC solution, the SUC schedule relies much more on spinning capacity to provide upward flexibility in the second half of the day. During these hours, upward spinning flexibility can be procured and deployed cheaply, as the low forecasted residual demand allows running the nuclear plants below their maximal stable operating point. Compared to the DUC formulation, the SUC model yields a similar operational cost, a decrease in curtailment by 55% at the expense of an expected 3.9 MWh of load shedding.

Allowing scenario-specific PHES output profiles may further increase the cost-effectiveness of the SUC model, but also increases the complexity of the SUC problem. Figures 5.6c – 5.6h illustrate that the SUC model relies more on the PHES unit to meet the demand in all considered scenarios[9]. As PHES-based flexibility is only bound by strict constraints on its energy content in each scenario *individually*, deviations from the specific wind power scenarios considered during UC optimization may lead to the unavailability of scheduled PHES-based flexibility during real-time dispatch. This effect was discussed as well in Chapter 4, in which we showed that this contributes to the challenges in attaining a stable solution to a SUC problem considering a scenario-specific PHES output. Therefore, we here use 50 (spinning and PHES-based reserves) or 40 (spinning, non-spinning and PHES-based reserves) scenarios in the SUC model. Note that the equivalent upward reserve requirement obtained from a set of 30 or 50 scenarios is nearly identical, as illustrated in Fig. 5.6e and Fig. 5.6g. The reason for considering more scenarios is not to capture more extreme, individual forecast errors, but to include more extreme *sequences* of forecast errors, in which the regulation potential of the PHES unit is limited by its energy storage capacity. In this particular case, moving from 30 to 50 scenarios reduces operational costs by 7%, which is mostly due to a reduced expected load shedding volume (15 MWh is reduced to 4.2 MWh) and a strong increase in wind power utilization (curtailment is reduced by 55%). Compared to the DUC solution, the expected operational cost is reduced by approximately 10%. Despite the lower expected load shedding volume (0 MWh), the conservative DUC schedule requires much more curtailment (+100% compared to the SUC schedule).

Figure 5.6h illustrates the possible over-procurement of non-spinning reserves in the SUC model, an issue to which we alluded in the discussion of the SUC

[9]The PHES-based upward reserves at each time step scheduled by the SUC model are calculated as (1) the maximal reduction in pumping power and/or (2) the maximal increase in turbining power in any considered scenario compared to its output in the forecast scenario.

model in Chapter 2. Recall that the SUC formulation does not impose any so-called bundle constraints on the scheduling of non-spinning reserves. Imagine two scenarios, which contain an identical negative forecast error on the same time step j. The SUC model may schedule two different, identical fast-cycling units to meet the demand at time step j. However, the demand might be met by dispatching the same unit in the two scenarios. As for identical units both solutions present the same operational cost, the SUC formulation is indifferent to which of the solutions is retained. This may lead to the procurement of more non-spinning capacity than strictly necessary to meet the load in all scenarios, and thus a more 'robust' UC schedule, as illustrated in Fig. 5.6h. Compared to the DUC solution, which relies more on non-spinning reserves, the operational cost of the resulting SUC schedule is 4% lower, mainly due to a 40% decrease in curtailment.

5.3.2 Operational cost savings as the result of a scenario-based uncertainty representation

The results of the numerical analysis are summarized in Table 5.6. For each of the four weeks and each of the four combinations of flexibility providers, we show the expected total operational cost (E[TOC]), the wind utilization factor (E[WUF]), the expected energy not served or load shedding volume (E[ϕ]) and the expected share of wind energy, corrected for the expected curtailment, in the total demand for electrical energy (E[WS]). First, we focus on those instances that only consider spinning and non-spinning reserves. The output profile of the PHES system is common to all scenarios during UC scheduling, but may be adapted freely during the MC ED simulations.

Procuring spinning & non-spinning reserves

We solved the SUC model considering 30 scenarios, selected with the scenario reduction technique proposed in Section 4.4.3, and imposed a time limit of 96,000 seconds on the solver. The presented solutions are identical to those presented in Chapter 4. All instances yielded a solution that satisfies the optimality gap (0.5%). In the simplest of SUC formulations, which only allows a scenario-specific output for spinning units, thus spinning reserves (SR), the SUC formulation outperforms its deterministic counterpart in all considered weeks. Differences in operational cost vary between 0.1 M€/week and 0.9 M€/week or 1.4% and 11.1% in relative terms. Especially in weeks with a high wind share and a variable residual demand (week 39), the operational cost savings are considerable. This increase in operational efficiency is mostly due to an

Table 5.6: Performance of the DUC and SUC model with and without non-spinning reserves (NSR), with and without PHES-based flexibility (PHES). SR indicates the availability of spinning reserves. TOC is the total operational cost and ϕ the Energy Not Supplied volume. WUF is the Wind Utilization Factor, the percentage of available wind energy that is absorbed in the power system. WS is the Share of Wind power in the total demand for electrical energy. Δ is the width of the 95% confidence interval on E[TOC].

(a) Average residual demand (week 30).

		SR		SR & NSR		SR & PHES		SR, NSR & PHES	
		SUC	DUC	SUC	DUC	SUC	DUC	SUC	DUC
E[TOC]	[M€]	13.6	13.8	13.2	13.2	13.9	13.8	13.3	13.2
Δ	[M€]	0.1	0.1	0.1	0.1	0.4	0.1	0.2	0.1
E[ϕ]	[MWh]	5.5	0	12.3	1.3	46.0	0	36.0	0.7
E[WUF]	[%]	100	100	100	100	100	100	100	100
E[WS]	[%]	10.6	10.6	10.6	10.6	10.6	10.6	10.6	10.6

(b) Max. residual demand (week 9).

		SR		SR & NSR		SR & PHES		SR, NSR & PHES	
		SUC	DUC	SUC	DUC	SUC	DUC	SUC	DUC
E[TOC]	[M€]	28.3	28.7	27.3	27.5	28.1	28.5	27.2	27.5
Δ	[M€]	0.2	0.1	0.2	0.2	0.3	0.1	0.2	0.2
E[ϕ]	[MWh]	2.8	0	9.1	2.0	16.0	0	8.1	1.8
E[WUF]	[%]	100	100	100	100	100	100	100	100
E[WS]	[%]	13.5	13.5	13.5	13.5	13.5	13.5	13.5	13.5

(c) Min. residual demand (week 52).

		SR		SR & NSR		SR & PHES		SR, NSR & PHES	
		SUC	DUC	SUC	DUC	SUC	DUC	SUC	DUC
E[TOC]	[M€]	3.2	3.3	2.9	2.4	3.5	3.3	2.9	2.4
Δ	[M€]	0.3	0.01	0.2	0.02	0.4	0.01	0.4	0.03
E[ϕ]	[MWh]	47.7	0	58.7	0.2	85.0	0	65.5	0.1
E[WUF]	[%]	93.9	85.8	93.9	91.5	91.0	86.7	94.1	92.4
E[WS]	[%]	81.3	74.0	81.3	79.0	79.0	74.8	81.1	79.7

(d) Max. var. residual demand (week 39).

		SR		SR & NSR		SR & PHES		SR, NSR & PHES	
		SUC	DUC	SUC	DUC	SUC	DUC	SUC	DUC
E[TOC]	[M€]	8.1	9.0	6.6	7.1	8.4	8.8	6.3	6.9
Δ	[M€]	0.4	0.05	0.4	0.1	0.4	0.1	0.2	0.1
E[ϕ]	[MWh]	24.2	0	21.8	0.6	94.3	0	10.7	0.2
E[WUF]	[%]	96.6	93.5	97.3	95.8	96.0	93.5	97.2	96.0
E[WS]	[%]	50.5	48.9	50.9	50.1	50.2	48.9	51.2	50.3

increase in wind utilization (3.1 percentage points in week 39, 8.1 percentage points in week 52) as the result of the scheduling of more flexible units and the procurement of less upward reserve. This however does lead to higher load shedding volumes in all weeks: expected ENS volumes rise from 0 MWh (DUC, all weeks) to at most 47.7 MWh (SUC, week 52). The increased variance in the operational cost results in wider confidence intervals. The reported load shedding volumes however represent less than 0.003% of the load in all cases. Due to the high cost of load shedding ($VOLL = 10,000$ €/MWh), the expected operational cost savings of the SUC model are almost fully offset in some weeks. For example, in week 52, the difference in operational cost between the DUC solution and the SUC solution excluding the cost of load shedding would amount to 0.6 M€/week or 21%. However, due to the large load shedding volume, and the low total operational cost due to the high share of wind energy in the total demand, the operational cost savings are reduced to 0.1 M€/week or 3.1%.

With the inclusion of non-spinning reserves, which provide upward flexibility more cost-effectively, the expected operational cost decreases drastically in both the DUC and SUC solutions. Operational cost savings due to the introduction of non-spinning reserves vary between 0.3 and 1.5 M€/week for the SUC formulation, which is to be compared with savings between 0.6 and 1.9 M€/week for the DUC formulation. However, recall that the DUC formulation does not account for any operational costs associated with non-spinning reserves, which may lead to sub-optimal over-procurement of these flexibility providers. Indeed, in two weeks (week 9 and 39), the SUC formulation realizes operational cost savings w.r.t. the solutions of the DUC problem of 0.2 to 0.5 M€/week (0.7% and 7.5% respectively). In week 39, these differences in operational cost are mostly due to an increase in wind utilization. In week 9 however, the operational cost savings are due to the procurement of a more cost-effective mix of flexibility providers and a moderate amount of load shedding.

Note that the inclusion of non-spinning reserves allows following the residual load more closely in the scenarios. Less excess capacity needs to be contracted, which allows for operational cost savings, but also makes the solution more sensitive to not including certain events in the considered scenarios or the reserve requirements. Especially if the considered scenario set does not contain all large negative forecast errors, load shedding may occur. Indeed, in all weeks an increase in ENS volumes is to be expected in the SUC solutions considering non-spinning reserves. This may lead to an unstable solution, as is the case for some SUC solutions in week 52. The cost of load shedding, which represents 0.6 M€/week in this particular week, drives the expected operational cost of the SUC solutions above the TOC of the equivalent DUC solutions. If one excludes the cost of load shedding, the performance of the SUC and DUC formulation in week 52 is similar, with a slight cost-advantage for the SUC model.

PHES-based flexibility & solution stability

The aforementioned effect is also present if one considers a scenario-specific PHES output and spinning reserves. As illustrated in Chapter 4, considering 30 scenarios is insufficient to obtain stable solutions to the SUC problem in these cases. We therefore considered 50 scenarios and imposed a time limit of 50,000 seconds on the optimization[10]. In some cases, this was insufficient to find a solution of the SUC problem that satisfies the optimality gap. For week 30, 3 out of 7 SUC optimization problems did not yield a solution that satisfies the 0.5% optimality gap within the considered time limit. The median value of the resulting optimality gaps is 0.95%. In week 39, 3 sub-optimal solutions yielded a median optimality gap of 0.49%. One UC problem was not solved to optimality in week 9, which resulted in a median optimality gap of 0.31%. Two UC schedules did not satisfy the 0.5% optimality gap in week 52, which results in a median optimality gap of 0.95%[11]. For week 30, the presence of the nearly converged solutions deteriorates the cost-optimality of the SUC solution compared to the solution obtained by considering 30 scenarios. Therefore, for this particular week, we will consider the solutions based on a SUC considering 30 scenarios, as presented in Chapter 4[12]. Nevertheless, the SUC formulation is still outperformed by the DUC model in weeks 30 and 52. The SUC solutions are 0.1 M€/week to 0.2 M€/week more expensive. High volumes of load shedding are to be expected in both weeks, which correspond to less than 0.01% of the total load, but account for up to 0.8 M€/week in expected operational cost and trigger wide confidence intervals. Especially in weeks with high shares of wind energy, which drives down the absolute expected total operational cost, this increase in expected load shedding may deteriorate the performance of a SUC formulation. Indeed, for these particular cases, the operational cost even exceeds the expected operational cost of the case not considering PHES-based flexibility (compare the cases 'SR' and 'SR & PHES' in Table 5.6). In week 9 and 39, the SUC solution is 0.4 M€/week less expensive than the DUC solution. Although solution stability is not guaranteed, especially in week 39, the scenario-based representation of the uncertainty leads to a more cost-effective UC schedule and a higher WUF. If one excludes the cost of load

[10]This reduced time limit is the result of a trade-off between the computational cost of these simulations and the gain in numerical accuracy. Empirical testing showed that if a problem did not converge in the first 50,000 seconds, chances of finding a solution within the optimality gap after the first 50,000 seconds were very slim.

[11]Note that these values should not be interpreted as a relative cost reduction that may still be possible, as they might be the result of a lack of convergence of the lower bound.

[12]Note that only the number of scenarios considered in the SUC model differs. Scenarios were selected from the same initial scenario set, using the same scenario reduction method. The Monte Carlo dispatch evaluation was executed using the same, new set of at least 500 scenarios as in the other UC strategies for week 30.

shedding, the SUC formulation outperforms the equivalent DUC model in all weeks.

If one considers all flexibility providers ('SR, NSR & PHES'), the size of the resulting SUC problem drastically increases with the number of scenarios. However, in Chapter 4 we illustrated that considering 30 scenarios was insufficient to reach solution stability. We therefore here consider 40 scenarios and impose a time limit of 50,000 seconds on the optimization. Unfortunately, the problem size of a SUC model considering non-spinning reserves and 50 wind power forecast scenarios becomes so large that some instances of the SUC problem become intractable. The results shown are an updated version of those published in [45]. All instances yielded a solution that satisfies the optimality gap.

Only in week 9 and week 39, the SUC model succeeds in exploiting the flexibility provided by the PHES system in the presence of non-spinning reserves (Table 5.6). Expected operational cost levels drop by 0.1 to 0.3 M€/week compared to the equivalent solutions in which only spinning and non-spinning reserves are considered. Compared to the DUC solutions, operational cost reductions of 0.3 to 0.6 M€/week are realized. In week 9, these operational cost savings are solely to be attributed to a more cost-effective scheduling of spinning and non-spinning reserves. Curtailment does not occur and the amount of load shedding slightly decreases (1 MWh). In week 39, a more cost-optimal UC schedule is combined with the internalization of the reserve sizing problem, an increase in wind utilization and the associated operational fuel cost savings. In week 30 and week 52, the SUC solutions are less cost-effective than the DUC solutions. Especially in week 52, which is characterized by a low absolute expected operational cost due to a high wind share (see above), the high load shedding volumes trigger high operational costs. This results in an expected operational cost that exceeds that of the DUC solutions by 0.5 M€/week. Note that without the cost of load shedding, the SUC model outperforms the DUC formulation in all cases.

Remarkably, load shedding volumes decrease compared to the case considering only spinning and PHES-based reserves. The reason behind this effect is threefold. First, not all instances were solved to optimality when considering only spinning and PHES-based flexibility. These solutions were characterized by high load shedding volumes. Second, the SUC formulation does not impose any bundle constraints on the scheduling of non-spinning reserves (Section 5.3.1). Two identical units may both be scheduled in two different scenarios as non-spinning reserves at the same time step. As for identical units both solutions present the same operational cost, the SUC formulation is indifferent to which of the solutions is retained. This may lead to the procurement of more non-spinning capacity than strictly necessary to meet the load in all

Table 5.7: Comparison of the CPU time (s) per run of the DUC and SUC model, with and without non-spinning reserves (NSR), with and without PHES-based reserves. P(75) is the 75$^{\text{th}}$ percentile, P(90) is the 90$^{\text{th}}$ percentile. For the SUC model, we list the number of scenarios considered in the UC model between brackets.

	SR		SR & NSR		SR & PHES		SR, NSR & PHES	
	SUC(30)	DUC	SUC(30)	DUC	SUC(50)	DUC	SUC(40)	DUC
Median [s]	19,300	67	21,822	61	+50,000	138	28,921	125
P(75) [s]	+96,000	93	79,779	91	+50,000	191	36,296	213
P(90) [s]	+96,000	241	+96,000	188	+50,000	342	+50,000	335

scenarios, and thus a more 'robust' UC schedule, as discussed above. Last, in absence of non-spinning reserves, the SUC formulation tends to exploit the PHES system more aggressively. This PHES-based flexibility is however only bound by strict constraints on the energy content in the upper reservoir within each individual scenario. Deviations from the specific wind power scenarios considered during UC optimization may lead to the unavailability of scheduled PHES-based flexibility in real time (Section 5.3.1).

5.3.3 Computational performance

The computational effort involved in solving a SUC problem is high, as illustrated in Table 5.7. As discussed in the previous section, the first two sets of simulations, considering spinning and non-spinning reserves, but a scenario-independent PHES output profile, were executed considering 30 scenarios. For these cases, we imposed a time limit of 96,000 seconds on the solver. Median calculation times are between 5.4 and 6.1 hours. Solving a SUC problem considering non-spinning reserves typically takes somewhat longer in the median case, but these instances yield a solution within the optimality gap quicker for computationally more challenging instances. 75% of cases solve to optimality within 22.1 hours, whereas the SUC problems not considering non-spinning reserves require at least 26.6 hours[13].

Similar trends are to be observed in the calculation times of the cases considering PHES-based flexibility. Recall that we obtained these results from a SUC

[13]When we report a calculation time of the form '+96,000', this indicates that these instances (1) did not yield a solution in the optimality gap within the imposed time limit (here: 96,000 seconds) or (2) were obtained by so-called 'warm-starting' the problem with solutions obtained from a run of the same instance which initially did not yield a solution in the optimality gap within the imposed time limit.

formulation considering 50 (spinning reserves and PHES-based flexbility) and 40 scenarios (spinning, non-spinning and PHES-based reserves) respectively and imposed a time limit of 50,000 seconds on the optimization. Solving an instance of the SUC model considering spinning and PHES-based reserves takes at least 13.9 hours (median values). Including non-spinning reserves does not only yield more cost-efficient UC schedules, but also reduces the computational effort. Median calculation times are approximately 8 hours. In 75% of cases, a solution that satisfies the optimality gap is found within 10.1 hours.

Compared to the computational effort involved in solving a DUC problem, which is in the order of minutes, solving a SUC problem is a horrendous task. Moreover, the spread on the calculation times associated with solving a SUC problem is large compared to that observed in the calculation times of the equivalent DUC problems. 95% of the considered DUC instances yielded a solution within at most 3.6 times the associated median calculation time. For the SUC problems, the same factor equals at least five.

5.3.4 Concluding remarks

A scenario-based representation of the uncertainty in a UC model has a number of advantages. The scenario-specific output of the flexibility providers ensures the feasibility of dispatching the scheduled reserves in real time and allows accounting for the expected operational cost associated with the activation of reserves. The constraint of a common UC status, except for fast-cycling units providing non-spinning reserves, allows internalizing the reserve sizing and procurement problem. This may lead to more cost-efficient UC schedules, high wind utilization factors and moderate load shedding volumes.

However, capturing the uncertainty in a limited set of scenarios, or better, capturing all events relevant to the UC problem, to avoid excessive load shedding or curtailment of RES-based generation during dispatch, turns out to be a challenging task, as extensively discussed in Chapter 4 and illustrated by the results in Table 5.6. Especially when considering a scenario-specific PHES output profile, the limited number of scenarios that can be considered may limit the usability of SUC formulations. Moreover, even with scenario sets of limited size, solving an instance of the proposed SUC model may take hours and computational tractability may be an issue.

As a result, the total expected cost savings may be lower than expected, due to relatively high load shedding volumes. Nevertheless, we observed operational cost savings up to 0.9 M€/week or 11% w.r.t. the equivalent DUC solutions. Operational cost savings were especially high in weeks with a highly variable residual demand. In some cases the SUC formulation may be outperformed

by the DUC formulation, especially when energy storage systems are allowed to provide regulation services and the residual demand is low. Nevertheless, if the SUC problem is computationally tractable and its solution stable, it will provide a lower bound to the attainable operational cost.

5.4 Increasing the cost-efficiency of the improved interval unit commitment model[14]

In this section, we analyze the performance of the IIUC formulation and compare these results to those obtained with its stochastic and deterministic equivalents. Compared to the formulation proposed in [86], we added the possibility of flexibility provision via non-spinning, fast-starting units and PHES systems (Chapter 2). In Section 5.4.1 we discuss the behavior of the IIUC models in detail, based on the simulations for a specific day (the first day of week 39 of the calendar year, as in the discussion on the performance of the DUC and SUC formulation). The operational cost savings that result from the explicit inclusion of non-spinning reserves are discussed in Section 5.4.2. In Section 5.4.3 we demonstrate the operational benefits of PHES-based reserves in a four week analysis. We focus on the provision of upward reserves and illustrate the importance of constraints (2.114)-(2.115) in the IIUC formulation to exploit the cost-effective regulation services that PHES systems may offer, illustrating our observations with an example considering the first day of week 39. In addition, we analyze the impact of the availability of non-spinning reserves. Last, we discuss the computational performance of the IIUC formulation (Section 5.4.4).

5.4.1 Upward reserves scheduling based on ramping scenarios

Before illustrating the importance of the specific constraints on the PHES-based flexibility, as for the DUC model (Section 5.2), we focus on the interaction between the ramping scenarios and the resulting upward flexibility. We will analyze the scheduled capacity based on the first day of week 39, for which the ramping scenarios are visualized in Fig. 5.7. The ramping scenarios were calculated from the same scenario set that was used to obtain the reserve requirements for the DUC model and the reduced scenarios set for the SUC formulation. As explained in [86], these ramping scenarios reduce the conservatism of the IUC formulation by relaxing unnecessarily conservative

[14]This section contains elements from K. Bruninx, Y. Dvorkin, E. Delarue, H. Pandžić, W. D'haeseleer, and D. S. Kirschen, *Coupling Pumped Hydro Energy Storage with Unit Commitment,* IEEE Trans. Sustain. Energy, vol. 7, no. 2, pp. 786–796, 2016.

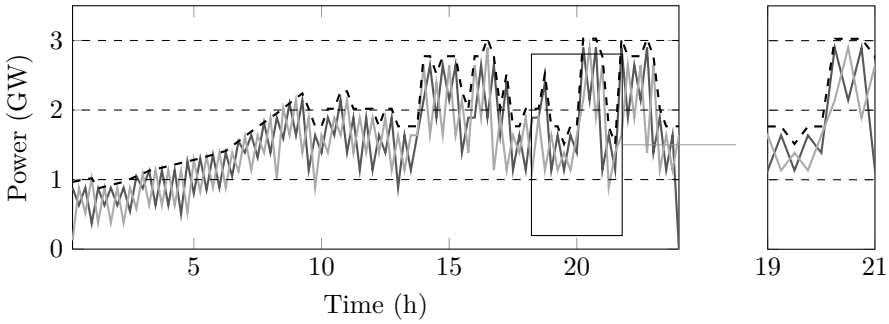

Figure 5.7: The downward ramping scenarios, containing the maximal negative forecast errors and their maximal downward ramp rate, which trigger upward reserves in the IIUC model, for the first day of week 39. Note that we have changed the sign of the wind power forecast errors in the figure, to facilitate the comparision with the upward reserve requirements imposed on the DUC problem (Fig. 5.2), here visualized by the dashed line. For details on the calculation of these ramping scenarios, see [86] and Chapter 2.

inter-hour ramping requirements, as illustrated in Fig. 5.7. In line with [86], which argues that the required inter-hour 'rampable capacity should be no more than the maximum up and down ramps observed over all scenarios' considered in an equivalent SUC model, in this work the ramping scenarios are obtained by calculating the maximum and minimum difference between the wind power output in two adjacent time steps over all scenarios. Although the slope of these ramping scenarios is lower than in the original IUC formulation, these scenarios ensure the same reserve capacity requirements by placing the end-points of each ramp at the upper and lower bounds of the domain of the forecast error at each time step. In Fig. 5.7 we show the two downward ramping scenarios, which represent the maximal downward ramp of a forecast error at each time step. A feasible dispatch enforced in each of these scenarios replaces the reserve requirements. These ramping scenarios are however assigned a zero probability and the operational cost is calculated only for the central forecast scenario. Load shedding is not allowed in the central forecast scenario, nor in the ramping scenarios.

As is to be expected, the scheduled flexibility as obtained from a IIUC model is very similar to that obtained from an equivalent deterministic model (Fig. 5.8). Indeed, as discussed in Chapter 2 and illustrated in Fig. 5.7, the upward reserves requirement imposed by the ramping scenarios in a IIUC formulation is equivalent to that in a DUC model. During the first hours of the day, gas-

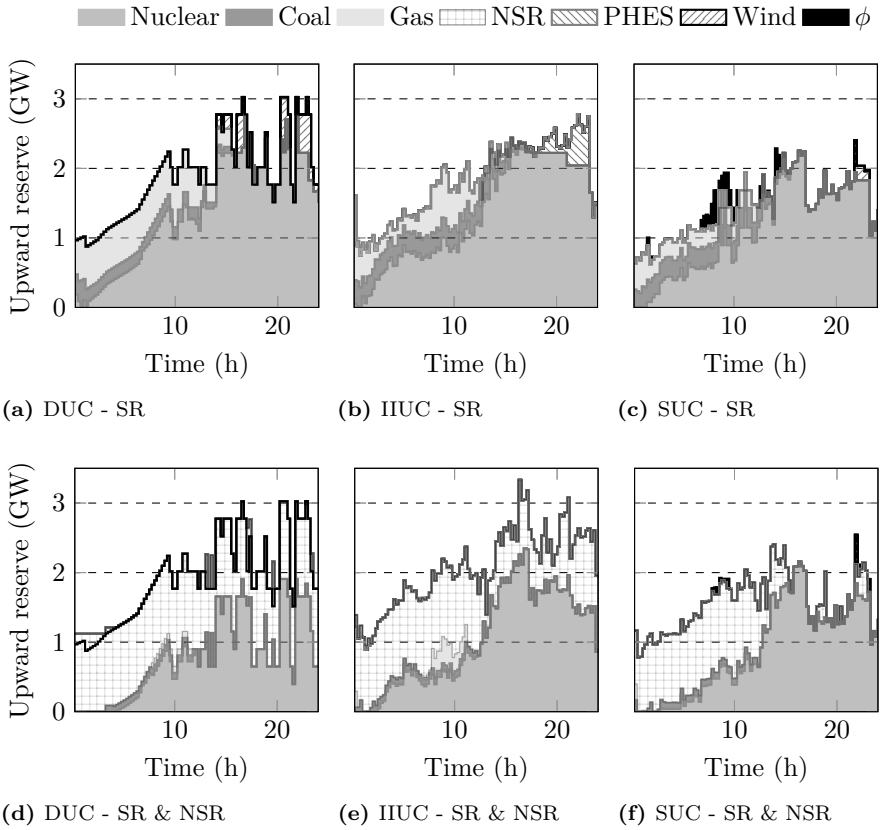

Figure 5.8: The available upward reserve capacity per technology and per UC formulation, considering spinning (SR) and non-spinning (NSR) flexibility. The solid black line indicates the total upward reserve requirement (DUC). The SUC considers 30 scenarios. The IIUC considers four ramping scenarios.

fired, coal-fired and nuclear power plants are scheduled as upward reserves (Fig. 5.8). As the forecasted RES-based generation increases during the day, the high expected wind power output results in high reserve requirements provided mainly by cheap nuclear units, which are available for regulation purposes due to the low residual demand. Two major differences are apparent in Fig. 5.8b. First, the scheduled upward flexibility in the IIUC solution is at some moments somewhat lower than that scheduled by the DUC model. This is the result of the ramping requirements imposed on the scheduled flexibility in the IIUC formulation, which are in this particular case less strict than those imposed

on the reserve capacity in the DUC model, as illustrated in Fig. 5.7. Recall that the headroom of scheduled, conventional power plants shown in Fig. 5.8b is limited to their ramping rate, assuming they are running at the scheduled output under forecast conditions. In the IIUC solution, they will however ramp-up according to the ramp rates imposed via the ramping scenarios, which are less strict than the aforementioned condition, imposed on upward reserves scheduled in a DUC model. Second, although we did not allow PHES-based flexibility to be scheduled to meet the demand in the ramping scenarios, some PHES-based flexibility is shown in Fig. 5.8b. As PHES-based reserves are not explicitly scheduled in the IIUC formulation, we here show the difference in output of the PHES system in the downward ramping scenarios ($s_{\mathrm{e}}^{\mathrm{R}-}$ and $s_{\mathrm{o}}^{\mathrm{R}-}$) compared to their output under forecast conditions (scenario s^{F}). As the forecasted RES-based generation increases, this frees up some capacity to store energy in the PHES. Therefore, the PHES implicitly 'offers' some upward reserve at the end of the day. This is in fact scheduled pumping in the central forecast scenario, which is forced to zero in the ramping scenarios[15]. The total load in the system thus decreases in the ramping scenarios compared to the forecast scenario, which is equivalent to the activation of upward reserves.

Unfortunately, the IIUC model suffers from the same drawbacks as the DUC formulation compared to the SUC formulation. Not accounting for the probability and operational cost of deploying the procured reserves does not allow (1) shedding of reserves, i.e. internalizing the reserve sizing problem, nor (2) scheduling an optimal mix of technologies providing upward reserves (Fig. 5.8c). In terms of operational cost, the IIUC solution is outperformed by both the DUC and SUC schedules on this particular day, by 6.4% and 15.9% respectively. Although the IIUC schedule allows for a higher uptake of RES-based generation (curtailment of wind power drops by 24.4%), the resulting fuel cost savings do not compensate for the higher operational cost associated with a shift to more flexible power plant technologies.

Introducing non-spinning reserves yields similar operational costs in the three considered UC formulations. Nevertheless, the operational cost compared to the case without non-spinning reserves decreases by 37%. In the DUC and IIUC models, these fast-starting units can be scheduled at zero cost to meet the reserve requirements and the demand in the ramping scenarios respectively ($NSRC_i = 0$). In the SUC formulation, non-spinning reserves are explicitly scheduled by allowing a scenario-specific UC status for fast-starting units. The

[15] As discussed in Chapter 2, when a PHES system is not allowed to actively participate in the implicit reserve requirements imposed by the ramping scenarios, the output of the PHES system is forced to zero in the ramping scenarios ($\forall r, \forall j, \forall s \in S^{\mathrm{R}} : g_{r,j,s}^{\mathrm{P}}, g_{r,j,s}^{\mathrm{T}} = 0$). This is in line with the approach taken in [86]. Although conservative, it will provide a benchmark solution to analyze the impact of the introduction of PHES-based reserves.

cost of activating non-spinning reserves is accounted for in the objective function of the SUC model (Section 5.3 and Chapter 2). As illustrated in Fig. 5.8, both the DUC and IIUC models over-procure non-spinning capacity to provide upward reserves due to their inability to account for the probability and cost of activation, especially towards the end of the day. Gas- and coal-fired generation are no longer providing upward flexibility.

5.4.2 Cost-effective flexibility provision via non-spinning reserves

Table 5.8 summarizes the results obtained from a four week analysis, using a DUC, SUC and IIUC model not considering PHES-based reserve provision. For the DUC model this means no PHES-based reserves may be scheduled, in the IIUC formulation the output of the PHES system is forced to zero in the ramping scenarios and in the SUC model the PHES output profile is identical in all scenarios. These results allow quantifying the performance of the IIUC w.r.t. the other formulations, excluding the impact of PHES-based reserves.

Only considering spinning reserves, it is obvious from Table 5.8 that the IIUC solutions are outperformed in terms of operational cost in all weeks by both the DUC and SUC schedules. Compared to the DUC solutions, operational costs rise by 0.2 M€/week to 0.8 M€/week. The reliability of the UC schedule is the same - no load shedding occurs - but the wind utilization is typically lower in the IIUC solutions. In week 39 the WUF drops by 1.2 percentage points, in week 52 the decrease amounts to 2 percentage points. Nevertheless, large differences in performance are to be noted in weeks in which curtailment does not occur (week 30 and week 9). The underlying cause of this effect is twofold. First, forcing the PHES-based output in the ramping scenarios considered in the IIUC model to zero is a very conservative approach. The demand in the ramping scenarios must be met by conventional capacity only, not accounting for the output of the PHES system under forecast conditions. In contrast, in the DUC and SUC formulation, the PHES system may be used to free up conventional capacity to provide upward reserves. The PHES system will not actively provide upward flexibility, but it will affect the available capacity to provide upward reserves. Second, the IIUC model will favor flexible, typically more expensive-to-run technologies, compared to the SUC solution. As the IIUC model, like the DUC formulation, does not account for the (expected) deployment cost, the model has no preference towards low-cost units to meet the demand in the ramping scenarios.

Both the IIUC and DUC solutions are outperformed by the SUC schedules. In terms of operational cost, differences between 0.3 M€/week (week 52) and

1.7 M€/week (week 39) are observed. The IIUC formulation suffers from the same drawbacks as the DUC model: the exclusion of an expected deployment cost in the objective function does not allow for internalization of the reserve sizing procedure, nor the procurement of an optimal technology mix providing upward reserves. In addition, the SUC formulation employs information from all scenarios and an estimate of the expected deployment cost of scheduled reserves to obtain an optimal, common PHES output profile. The result is a significantly lower expected operational cost, a modest increase in load shedding volumes and an increase in wind utilization.

Introducing non-spinning reserves leads to significant cost savings in all models. For the IIUC formulation, the expected operational cost drops by 0.8 M€/week to 2.1 M€/week. In weeks with relatively low shares of wind energy (week 30 and week 9), this reduces the difference in operational cost with the DUC solutions to zero (week 30) and 0.2 M€/week (week 9). The availability of non-spinning reserves allows for optimal scheduling under forecast conditions, as the demand in the ramping scenarios can be met by dispatching non-spinning reserves at zero cost. Recall that the operational cost in the IIUC model during UC scheduling is calculated under forecast conditions, without regard for the expected deployment cost of scheduled reserves. In weeks with high shares of wind energy (week 52 and 39), the wind utilization factor increases significantly compared to the case without non-spinning reserves (2.5 percentage points in week 39, 4.9 percentage points in week 52). Nevertheless, the WUF remains low compared to the WUF in the DUC and SUC solutions, resulting in operational costs that are significantly higher than in the DUC or SUC solutions. In week 52, the expected operational cost of the IIUC schedules is 0.3 M€/week higher than the DUC schedules. Due to a high volume of load shedding, the SUC schedule is 0.2 M€/week more expensive than the IIUC schedule. The results for week 39, characterized by a highly variable residual demand and a high wind share, show a large spread, even with the availability of non-spinning reserves. Compared to the DUC solution, the IIUC schedule is 0.6 M€/week more expensive, despite a higher reliability. The WUF is however 1 percentage point lower. The SUC schedule shows more load shedding (21.8 MWh versus 0.2 MWh in the IIUC solution), but outperforms the IIUC solution by 1.1 M€/week - an improvement of 16.6%. The WUF in the SUC solution is 2.5 percentage points higher.

Table 5.8: Performance of the DUC, IIUC and SUC models considering spinning reserves (SR) and non-spinning reserves (NSR). TOC is the total operational cost and ϕ the Energy Not Supplied volume. WUF is the Wind Utilization Factor, the percentage of available wind energy that is absorbed in the power system. WS is the Share of Wind energy in the total demand for electrical energy. Δ is the width of the 95% confidence interval on E[TOC].

(a) Week 30 (average residual demand)

		DUC		IIUC		SUC	
		SR	NSR	SR	NSR	SR	NSR
E[TOC]	[M€]	13.8	13.2	14.2	13.2	13.6	13.2
Δ	[M€]	0.1	0.1	0.1	0.1	0.1	0.1
E[ϕ]	[MWh]	0	0.5	0	0.8	5.5	12.3
E[WUF]	[%]	100	100	100	100	100	100
E[WS]	[%]	10.6	10.6	10.6	10.6	10.6	10.6

(b) Week 9 (highest residual demand)

		DUC		IIUC		SUC	
		SR	NSR	SR	NSR	SR	NSR
E[TOC]	[M€]	28.7	27.5	29.2	27.7	28.3	27.3
Δ	[M€]	0.1	0.2	0.1	0.1	0.2	0.2
E[ϕ]	[MWh]	0	2.0	0	1.7	2.8	9.1
E[WUF]	[%]	100	100	100	100	100	100
E[WS]	[%]	13.5	13.5	13.5	13.5	13.5	13.5

(c) Week 52 (lowest residual demand)

		DUC		IIUC		SUC	
		SR	NSR	SR	NSR	SR	NSR
E[TOC]	[M€]	3.3	2.4	3.5	2.7	3.2	2.9
Δ	[M€]	0.01	0.02	0.01	0.01	0.3	0.2
E[ϕ]	[MWh]	0	0.2	0	0	47.7	58.7
E[WUF]	[%]	85.8	91.5	83.8	88.7	93.9	93.9
E[WS]	[%]	74.0	79.0	72.2	76.5	81.3	81.3

(d) Week 39 (most variable residual demand)

		DUC		IIUC		SUC	
		SR	NSR	SR	NSR	SR	NSR
E[TOC]	[M€]	9.0	7.1	9.8	7.7	8.1	6.6
Δ	[M€]	0.05	0.1	0.05	0.1	0.4	0.4
E[ϕ]	[MWh]	0	0	0	0.2	24.2	21.8
E[WUF]	[%]	93.5	95.8	92.3	94.8	96.6	97.3
E[WS]	[%]	48.9	50.1	48.3	49.6	50.5	50.9

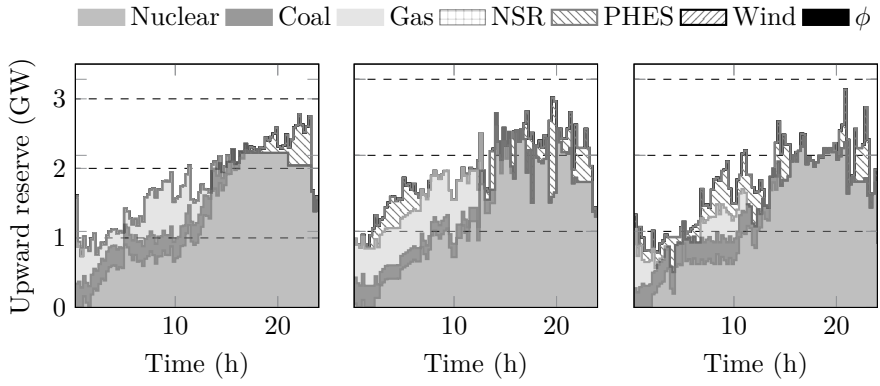

(a) No PHES-based reserves

(b) PHES-based reserves, incl. Eq. (2.114)-(2.115).

(c) PHES-based reserves, excl. Eq. (2.114)-(2.115).

Figure 5.9: The available upward flexibility on the first day of week 39, obtained with a IIUC model (a) not considering PHES-based flexibility, (b) considering PHES-based flexibility, constrained by Eq. (2.114)-(2.115) and (c) considering PHES-based flexibility, but excluding Eq. (2.114)-(2.115).

5.4.3 Operational benefits of PHES-based regulation services

So far, scheduling PHES-based flexibility to meet the demand in the so-called ramping scenarios was not considered. We forced the output of the PHES-systems to zero in these scenarios, which is a conservative approach, but ensured the feasibility of the scheduled reserves. To allow actively scheduling PHES-based reserves, simultaneously ensuring the feasibility of the real-time dispatch of scheduled PHES-based flexibility, we proposed constraints (2.114)-(2.115) in Chapter 2. We will illustrate their importance below.

The need for additional constraints on regulation services offered by PHES systems

Figure 5.9 shows the scheduled upward reserves as obtained with the IIUC model for three particular cases on the first day of week 39. First, the PHES system is not allowed to offer regulation services (Fig. 5.9a, identical to the results shown in Fig. 5.8). Second, the PHES system is allowed a scenario-specific, non-zero output in the ramping scenarios, constrained by Eq. (2.114)-(2.115) (Fig. 5.9b). Third, the results of the same model, excluding Eq. (2.114)-(2.115), are shown in Fig. 5.9c.

If the PHES system can be used to meet the demand in the ramping scenarios, constrained by Eq. (2.114)-(2.115), the PHES-based reserve capacity displaces some nuclear, coal- and gas-fired reserve capacity (Fig. 5.9b). The offered reserve capacity is based on the option to reduce the scheduled pumping power of the PHES system. The expected operational costs decreases by 12%. Expected curtailment drops by 37% or 1013 MWh, while the expected ENS volume is unaffected if Eq. (2.114)-(2.115) are enforced. If the constraints (2.114)-(2.115) are excluded from the model, the PHES system is scheduled to provide upward reserve throughout the day (Fig. 5.9c). The effect is less dramatic than in the DUC model (Section 5.2), as the output of the PHES system is still constrained by the energy balance constraint in the ramping scenarios (Eq. (2.66)). The resulting schedule is however sub-optimal, as the energy content of the PHES system is insufficient to allow dispatching all scheduled reserves in real time. As a result, an increase in expected load shedding volume (14 MWh) fully offsets the expected operational cost reduction by actively scheduling the PHES system as cost-effective upward flexibility.

In conclusion, the analysis above shows that the inclusion of the additional constraints (2.114)-(2.115) on the PHES system is necessary to exploit its cost-effective regulation services in IIUC formulations. Although less critical than in the DUC formulation, neglecting to include constraints (2.114)-(2.115) may lead to the unavailability of scheduled PHES-based regulation services during dispatch and, consequently, load shedding or excessive curtailment of RES-based generation.

The interaction between conventional & PHES-based reserves

With the additional constraints (2.114)-(2.115), the IIUC model can meet the demand for upward reserves more cost-effectively. On the first day of week 39, the scheduled upward flexibility, illustrated in Fig. 5.10, reduces the expected operational cost by 5.5% compared to the equivalent DUC solution and 12% compared to the IIUC solution not considering PHES-based regulation services. This is the result of a reduction in curtailment by 14% and a more extensive use of the PHES-based flexibility to meet the demand for upward flexibility. Note that compared to the upward flexibility scheduled by the SUC formulation, the use of the PHES unit as reserve provider is still limited. Nevertheless, the performance of the SUC and IIUC model is comparable on this particular day.

Non-spinning reserves are shown to reduce the cost of regulation services, thus their presence will affect the value of the PHES-based reserves. As illustrated in Fig. 5.10, both the DUC and IIUC solutions exhibit over-procurement of non-spinning capacity to provide upward reserves due to the inability of the

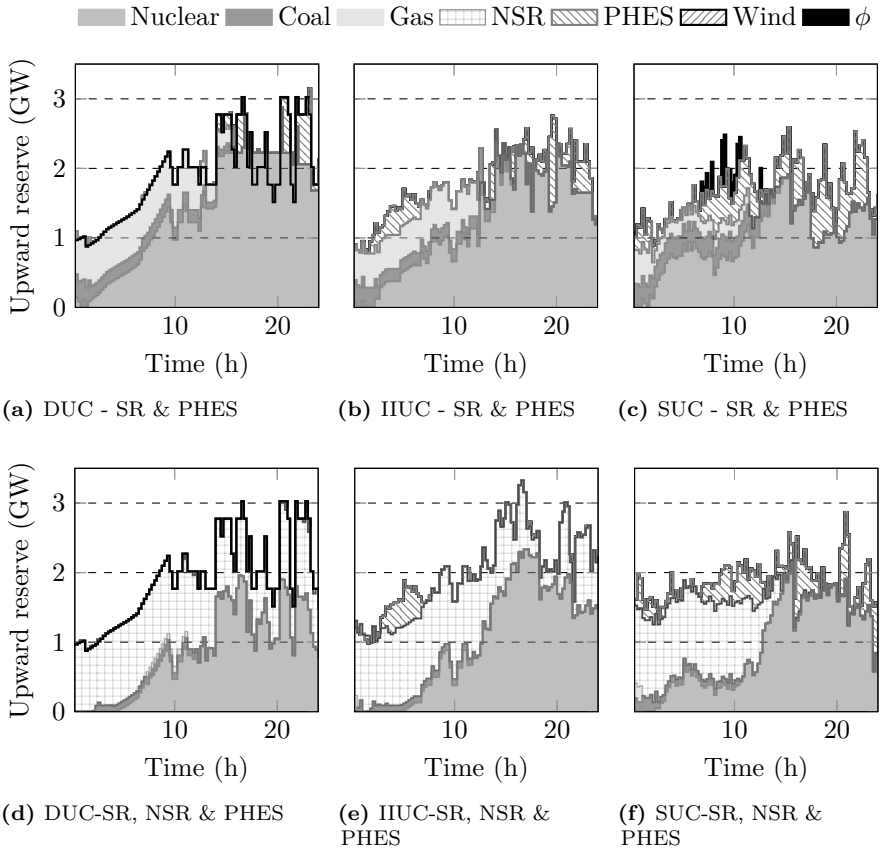

(a) DUC - SR & PHES **(b)** IIUC - SR & PHES **(c)** SUC - SR & PHES

(d) DUC-SR, NSR & PHES **(e)** IIUC-SR, NSR & PHES **(f)** SUC-SR, NSR & PHES

Figure 5.10: The available upward reserve capacity per technology and per UC formulation, considering spinning (SR), non-spinning (NSR) & PHES-based flexibility. The solid black line indicates the total upward reserve requirement (DUC). The SUC model considers 40 (with non-spinning reserves) or 50 scenarios (without non-spinning reserves). The IIUC formulation considers four ramping scenarios.

DUC and IIUC formulations to account for the associated probability and operational cost of activation. Gas- and coal-fired generation are no longer providing upward flexibility. PHES-based flexibility has a limited impact in the IIUC and DUC solutions considering non-spinning reserves, especially compared to the extensive use of the PHES unit to cover the demand in the SUC solution. Despite the sub-optimal procurement of flexibility, the expected operational

cost of the IIUC schedule drastically reduces, by approximately 30%, and is comparable to that of the SUC solution. The IIUC schedule is 2.2% more cost-effective than the equivalent DUC solution on this particular day. This effect is solely due to a switch of technologies providing upward reserves: the amount of curtailed RES-based generation remains the same.

The value of PHES-based regulation services

Table 5.9 compares the results of the Monte-Carlo ED simulations for the IIUC, DUC (Section 5.2) and SUC formulations (Section 5.3) applied to the Belgian power system for four representative weeks. These simulations include two dispatch strategies for the IIUC formulation: (1) the PHES system provides energy arbitrage only and (2) the PHES system provides both energy arbitrage and regulation services (indicated by 'PHES' in Table 5.9). The first set of results is identical to those reported in Table 5.8. In the DUC and SUC model, the PHES system was allowed to provide arbitrage and regulation services. In the DUC formulation, the worst-case energy balance feasibility constraints Eq. (2.47)-(2.48) were enforced to ensure the technical feasibility of the real-time activation of the scheduled reserves. Similarly, constraints (2.114)-(2.115) are enforced in those IIUC instances which consider PHES-based regulation services.

A number of trends can be identified in the results summarized in Table 5.9. First, considering only spinning (SR) and PHES-based reserves, allowing scheduling of regulation services offered by the PHES system reduces the expected operational cost at the expense of a negligible decrease in reliability. Indeed, for all weeks, the expected total operational cost of the IIUC schedules decreases significantly. Especially in weeks with high shares of wind energy (week 39, high upward reserve requirements and flexible, expensive units needed) and in weeks characterized by a high residual demand (week 9, low reserve requirements, but only expensive units available due to a high demand) the decrease in operational cost is significant. Operational cost savings up to 1.2 M€/week are observed. This cost reduction is the result of (1) an improved utilization of the available wind power and (2) a more cost-efficient UC schedule, made possible by the availability of the PHES system in the ramping scenarios. The first effect is illustrated by the Wind Utilization Factor (WUF) in Table 5.9, and the second was discussed in Section 5.4.1. By enforcing Eq. (2.114)-(2.115), the reliability of the UC schedules is nearly unaffected by the presence of PHES-based reserves. The cost associated with ENS accounts at most for 0.004 M€/week of the total operational cost. The expected ENS volumes represent less than 0.0001% of the load in all IIUC solutions.

Second, the operational costs considering PHES-based regulation services are

similar for both the DUC and IIUC solutions, with lower expected operational costs for the IIUC schedules in week 39 and 52. PHES-based regulation services allow meeting the reserve requirements with less committed capacity, which leads to a higher WUF for the DUC and IIUC solutions, and finally lower operational costs for the IIUC in week 39 and 52. Third, one can compare these results to those obtained with the SUC model. For the days in which we found SUC solutions that (almost) satisfy the optimality gap[16], the SUC formulation outperforms the IIUC and DUC model. In week 9, the SUC model outperforms the DUC and IIUC formulation by 2.1% and 3.9%, respectively, if the PHES system is only used for arbitrage, and 1.4% if the PHES system offers regulation services as well. However, due to the presence of some sub-optimal solutions in weeks 30 and 52, the SUC solution is outperformed by the IIUC and DUC schedules. For example, in week 52, the SUC model yields operational cost reductions up to 69% per day in three out of seven days compared to the IIUC formulation (30% overall). Due to the presence of four sub-optimal solutions, the global performance of the SUC model is 5.7% to 11.4% worse than that of the IIUC formulation. Furthermore, the SUC formulation typically results in more load shedding. This is partly the result of the presence of sub-optimal solutions, but also a consequence of actively scheduling load shedding in unlikely, extreme scenarios, which is not possible in the IIUC and DUC model. This load shedding volume represents a significant part of the total operational cost, but the curtailed load represents at most 0.006% of the total demand in the SUC solutions.

Scheduling of non-spinning reserve reduces the operational cost of the IIUC solutions by 0.6 M€/week to 2.1 M€/week (3.7% to 37.5%, respectively – see Table 5.9), comparable to the impact the availability of non-spinning reserves on the cost-effectiveness of the DUC formulation (see Table 5.3, Table 5.4 and the discussion in Section 5.2). These reductions are especially noticeable during the weeks with high shares of RES-based electricity generation, e.g. weeks 39 and 52, in which the inclusion of PHES-based reserves results in cost savings of 25% to 27% and 24% to 30%, respectively, dependent on the availability of non-spinning reserves. This is the result of an increased wind power utilization (up to 5.4 percentage points), which replaces conventional generation and, thus yields a lower expected operational cost. On the other hand, non-spinning reserves reduce the value of regulation services provided by the PHES unit. At most, the PHES unit results in cost savings of 0.8 M€/week (week 39), if non-spinning reserves can be scheduled, which is to be compared to an operational cost saving up to 1.2 M€/week (week 39), if non-spinning reserves are not considered. Furthermore, in some cases, such as week 30 and

[16] As mentioned before, we imposed a time limit of 50,000 seconds on the SUC optimization. In some cases, this was insufficient to find a solution of the SUC problem that satisfies the optimality gap, as discussed in Section 5.3.

Table 5.9: Performance of the DUC, IIUC and SUC models considering spinning reserves (SR), non-spinning reserves (NSR) and PHES-based reserves. TOC is the total operational cost and ϕ the Energy Not Supplied volume. WUF is the Wind Utilization Factor, the percentage of available wind energy that is absorbed in the power system. WS is the Share of Wind energy in the total demand for electrical energy. Δ is the width of the 95% confidence interval on E[TOC].

(a) Week 30 (average residual demand)

		DUC		IIUC				SUC	
			PHES			PHES		PHES	
		SR	NSR	SR	NSR	SR	NSR	SR	NSR
E[TOC]	[M€]	13.8	13.2	14.2	13.2	13.8	13.2	13.9	13.3
Δ	[M€]	0.1	0.1	0.1	0.1	0.1	0.1	0.4	0.2
E[ϕ]	[MWh]	0	0.7	0	0.8	0.4	0.5	46.0	36.0
E[WUF]	[%]	100	100	100	100	100	100	100	100
E[WS]	[%]	10.6	10.6	10.6	10.6	10.6	10.6	10.6	10.6

(b) Week 9 (highest residual demand)

		DUC		IIUC				SUC	
			PHES			PHES		PHES	
		SR	NSR	SR	NSR	SR	NSR	SR	NSR
E[TOC]	[M€]	28.5	27.5	29.2	27.7	28.5	27.5	28.1	27.2
Δ	[M€]	0.1	0.2	0.1	0.1	0.1	0.2	0.3	0.2
E[ϕ]	[MWh]	0	1.8	0	1.7	0	4.5	16.0	8.1
E[WUF]	[%]	100	100	100	100	100	100	100	100
E[WS]	[%]	13.5	13.5	13.5	13.5	13.5	13.5	13.5	13.5

(c) Week 52 (lowest residual demand)

		DUC		IIUC				SUC	
			PHES			PHES		PHES	
		SR	NSR	SR	NSR	SR	NSR	SR	NSR
E[TOC]	[M€]	3.3	2.4	3.5	2.7	3.1	2.5	3.5	2.9
Δ	[M€]	0.01	0.03	0.01	0.01	0.01	0.02	0.4	0.4
E[ϕ]	[MWh]	0	0.1	0	0	0	0.5	85.0	65.5
E[WUF]	[%]	86.7	92.4	83.8	88.7	86.5	91.9	91.0	94.1
E[WS]	[%]	74.8	79.7	72.2	76.5	74.6	79.2	79.0	81.1

(d) Week 39 (most variable residual demand)

		DUC		IIUC				SUC	
			PHES			PHES		PHES	
		SR	NSR	SR	NSR	SR	NSR	SR	NSR
E[TOC]	[M€]	8.8	6.9	9.8	7.7	8.6	6.9	8.4	6.3
Δ	[M€]	0.1	0.1	0.05	0.1	0.1	0.1	0.4	0.2
E[ϕ]	[MWh]	0	0.2	0	0.2	0	0.7	94.3	10.7
E[WUF]	[%]	93.5	96.0	92.3	94.8	93.2	95.6	96.0	97.2
E[WS]	[%]	48.9	50.3	48.3	49.6	48.8	50.0	50.2	50.9

9, the availability of PHES-based regulation services does not result in any cost savings, because non-spinning reserves can provide the required regulation services more cost-effectively.

Compared to the solutions of an equivalent SUC model considering non-spinning reserves, the operational cost obtained with a DUC or IIUC formulation remains high in week 9 and 39. Expected operational cost differences amount to 0.3 M€/week (week 9) and 0.6 M€/week (week 39) respectively. Although the SUC formulation tolerates higher load shedding volumes, the associated load shedding cost is outweighed by operational benefits resulting from the increase in wind utilization and the reduced procurement of upward reserves. In weeks 30 and 52, the differences between the results of the considered UC models are less pronounced. In both weeks, the limited scenario set considered during SUC scheduling does not contain sufficient information to avoid significant amounts of load shedding during dispatch. As a result, the operational cost of the UC schedule obtained with the SUC model exceeds that of the equivalent IIUC solution. If the cost of load shedding is excluded, the SUC model yields an expected operational cost of 2.3 M€ (week 52) and 12.9 M€ (week 30) respectively, which is comparable to the operational cost associated with the DUC and IIUC schedules.

5.4.4 Computational Performance

The resulting execution times (median and percentiles) for the DUC, IIUC and SUC models are shown in Table 5.10. We report calculation times with and without the consideration of non-spinning reserves ('NSR'), and with and without the availability of PHES-based regulation services (indicated by 'PHES' in Table 5.10).

Only considering spinning reserves, the DUC model typically solves the quickest, followed by the IIUC formulation. If the PHES system is not allowed to offer regulation services in the IIUC model, the median calculation time is approximately 3.8 minutes, compared to approximately 1 minute for the equivalent DUC formulation. If the PHES system provides regulation services, calculation times rise to 4.1 minutes (median). An equivalent DUC model solves in 2.3 minutes. Furthermore, note that the CPU times of the IIUC model show a larger spread than those of the DUC model. For 90% of all IIUC instances, a solution was found within 7.4 minutes (10.9 minutes if the PHES system only provides arbitrage). Compared to the SUC model, the IIUC formulation is still considerably less computationally challenging. The difference in calculation times is still two orders of magnitude. We also noted that the SUC model fails

Table 5.10: Comparison of the CPU time (s) per run of the DUC, IIUC and SUC model. P(75) is the 75$^{\text{th}}$ percentile, P(90) is the 90$^{\text{th}}$ percentile.

	DUC		IIUC				SUC	
	PHES				PHES		PHES	
	SR	NSR	SR	NSR	SR	NSR	SR	NSR
Median [s]	138	125	228	244	217	177	+50,000	28,921
P(75) [s]	191	213	507	328	400	289	+50,000	36,296
P(90) [s]	342	335	657	445	1,225	399	+50,000	+50,000

to yield a solution that satisfies the optimality gap of 0.5% in 50,000 seconds in over 50% of the cases (Section 5.3).

The computational cost of the IIUC model decreases considerably if non-spinning and PHES-based reserves are available (median values). In the presence of non-spinning reserves and without PHES-based regulation services, the spread on the calculation time of the IIUC model however drastically increases. The 90$^{\text{th}}$ percentile of the calculation time equals 20.5 minutes. The (spread on the) computational performance of the DUC model is unchanged. The DUC model remains approximately two times as fast as the IIUC formulation (median values). The presence of non-spinning reserves lowers the computational cost of the SUC formulation considerably, despite the presence of more binary variables. Nevertheless, the computational effort compared to that associated with a IIUC and DUC problem remains high.

5.4.5 Concluding remarks

The improved interval unit commitment (IIUC) model reduces a large set of scenarios to four ramping scenarios. These scenarios form an equivalent representation of the reserve requirements in a DUC model, but can be less strict as they are more reflective of real ramping requirements imposed on the UC schedule by uncertain wind power forecasts. The IIUC model however suffers from the same drawbacks as the DUC formulation, as it does not account for the expected deployment or activation cost of scheduled reserves. As a result, the model is unable to internalize the reserve sizing problem, nor can it procure an optimal mix of technologies to provide upward reserves. The ramping scenario-based representation of the uncertainty was shown to favor flexible, but typically more expensive-to-run units, which may further increase the expected operational cost of the resulting UC schedule.

Moreover, not considering PHES-based flexibility or non-spinning reserves in an IIUC model was shown to lead to very conservative UC schedules. (I)IUC models fail to account for the hydraulic constraints of the PHES system when offering regulation services, as illustrated in Section 5.4.1. Constraints (2.114)-(2.115), as proposed in Chapter 2, are shown to be necessary to exploit the cost-effective regulation services that a PHES system may offer in an IIUC model. We analyzed the impact of co-optimizing of the PHES dispatch decisions with the UC decisions of the conventional power plants in an IIUC model. Allowing PHES-based regulation services allows a system operator to achieve significant cost savings and increased wind power utilization rates with minimal impact on the system's reliability. The CPU time increase is minimal (median values), while the spread on the calculation times drastically reduces. The IIUC formulation attains lower operational costs than the DUC model at high wind energy penetration levels in absence of non-spinning reserves. Compared to solutions obtained from a SUC model, the operational cost remains high, as the IIUC formulation does not allow exploiting the full regulation potential of the PHES system and fails to account for the expected operational cost of deploying reserves during UC scheduling.

5.5 Combining speed & optimality: hybrid determistic-stochastic unit commitment[17]

In this section, we examine the performance of a novel UC formulation, combining a probabilistic reserve rule with a small set of scenarios in a hybrid deterministic-stochastic UC model. The ideas and parts of the text in this section were taken from our paper [45]. A number of modifications to the original publication [45] were made for sake of consistency with previous and following sections, in order to allow comparison between the results of different UC models. For example, we allow the PHES system to participate in the reserve requirements, which was not considered in [45]. We have updated all numerical results and text in this section accordingly. Where necessary or relevant, we have provided a reference to the original results.

In Section 5.5.1, we present the design of the proposed hybrid reserve rule. Based on simulations for the first day of week 39, we will show that the addition of a probabilistic reserve requirement to a SUC model with a relatively small set of scenarios allows approximating the expected costs (optimality) and expected loss of load (reliability) of the stable solution of the equivalent

[17]This section in based on K. Bruninx, K. Van den Bergh, E. Delarue, and W. D'haeseleer, *Optimization and Allocation of Spinning Reserves in a Low-Carbon Framework,* IEEE Trans. Power Syst., vol. 31, no. 2, pp. 872–882, 2016.

SUC problem. Calculation times are, however, significantly lower. A detailed analysis of the scheduled reserves shows that the scheduled flexibility is similar. To gain statistical significance, the performance of the proposed HUC model is investigated for four representative weeks of the year (Section 5.5.3). Results confirm that the proposed HUC model (7 scenarios, probabilistic reserve requirement with a design reliability of 85%) approximates the stable solution of the corresponding SUC model, at roughly one fifteenth (spinning and PHES-based reserves) to one fifth (spinning, non-spinning and PHES-based reserves) of the computational cost.

5.5.1 Design of a hybrid unit commitment policy

As a first step in the design of the hybrid reserve sizing and allocation model, we analyze the performance of various probabilistic reserve rules in combination with small scenario sets for the first day of week 39[18]. We consider a setting in which only spinning and PHES-based reserves may be scheduled and one in which spinning, non-spinning and PHES-based reserves are allowed. To allow focusing on the performance of the scheduling models, the dispatch is performed on the same scenario set used to determine the empirical probability distributions and to selected critical scenarios. Performance differences due to small differences in the scenario sets are hereby avoided[19]. As the solutions however may be biased towards the considered distribution or scenarios, we will evaluate the performance of the DUC, HUC and SUC models on a new, large set of scenarios in Section 5.5.3, as we did before.

The benchmark will be the stable solution of the corresponding SUC problem. As explained in Chapter 4, the stable solution is the best available proxy for the solution of the 'true' SUC problem, here approximated by the solution of the SUC problem considering 30 scenarios[20]. This solution is indicated by the intersection of the two dotted lines in Fig. 5.11a-5.11b, which summarize the results of our analysis of the performance of various hybrid UC strategies on the first day of week 39. The true solution of the full stochastic program –

[18]In our original publication, we performed the design of the HUC strategy on the day characterized by a residual demand closest to the yearly average. To allow comparing results of the various UC models, we here re-analyze the design on the first day of week 39.

[19]Note the similarity with the solution stability analysis in Chapter 4. In essence, we attempt to isolate the impact of a reduced representation of the uncertain wind power forecasts in the UC model.

[20]Although one can never definitely prove that this solution is stable – as this would require solving the 'true' SUC problem with a continuous description of the stochastic variable – the results show that the addition of more scenarios does not further improve the quality of the solution. The first and second-stage objective no longer change and are nearly identical. Hence, one can assume that this solution is stable and unbiased.

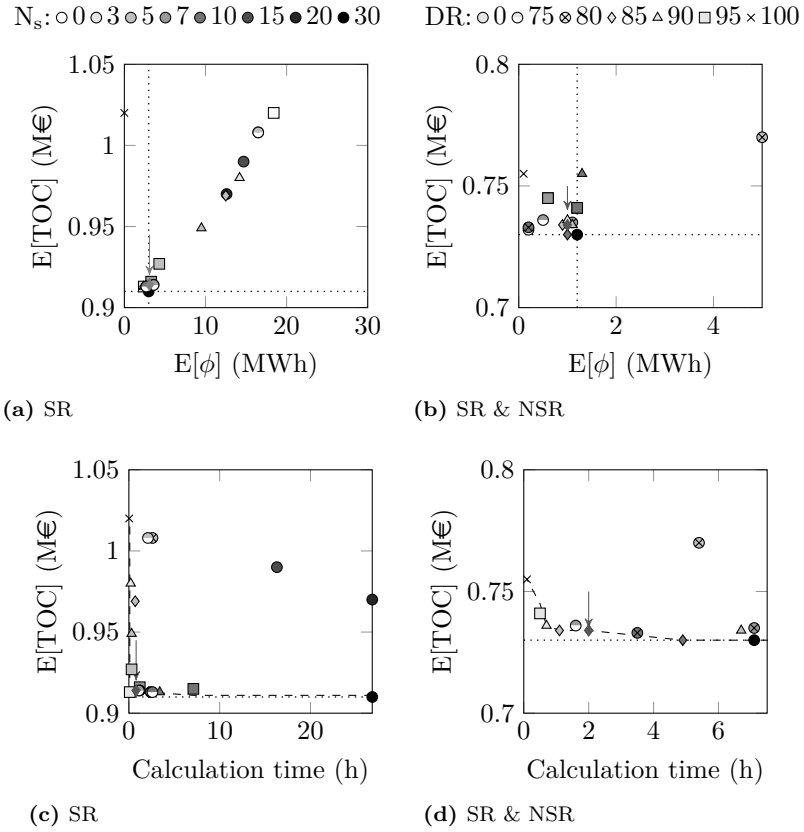

(a) SR **(b)** SR & NSR

(c) SR **(d)** SR & NSR

Figure 5.11: The proposed HUC strategy (reserves sized to capture 85% of the wind power forecast errors, complemented with 7 scenarios and indicated with an arrow) results in expected total operational costs (E[TOC]) and loss of load volumes (E[ϕ]) comparable to those associated with the stable solution of the SUC problem, while the required calculation time to obtain this solution is reduced drastically. The shape of the markers indicates the design reliability (DR) imposed on the probabilistic reserve sizing technique. The shading of the marker indicates the number of scenarios (N_s) in the optimization. The dashed lines in Fig. 5.11c and 5.11d represent an efficiency front: they connect the cost-optimal solutions as a function of the calculation time.

if it could be obtained – would be characterized by approximately the same expected cost (indicated by the horizontal dotted line in Fig. 5.11a-5.11b).

Without non-spinning reserves, the expected operational cost associated with the DUC solution – considering a reserve requirement with a design reliability of 100% – is about 10% higher than the stable solution of the SUC problem. Allowing scheduling non-spinning reserve, reduces the expected operational cost of both solutions considerably, as studied extensively in the previous sections. The resulting difference in operational cost decreases to about 4%[21]. However, the computational cost of obtaining these SUC solutions is extremely high: over 26 hours for the SUC instance not considering non-spinning reserves and approximately 7 hours if non-spinning reserves may be scheduled (Fig. 5.11c - 5.11d).

Reducing the number of scenarios in the SUC model leads to inferior results: expected costs increase due to less robust planning, which increases the amount of expected load shedding and thus the expected costs. This explains the near-linear trend right of the dotted vertical line in Fig. 5.11a. The slope of this trend line is directly related to the value of lost load (10,000 €/MWh). As more scenarios are added to the optimization, costs in general decrease. As shown in Fig. 5.11a, this process of convergence can be accelerated by adding a reserve requirement to the optimization. For example, considering only spinning reserves, a HUC model considering 5 scenarios and a reserve requirement with a design reliability of 90% outperforms the SUC solution considering 15 scenarios in this particular instance. The reserve requirements will ensure the availability of sufficient reserve capacity in the system in certain, not too extreme scenarios, while the scenarios ensure that this capacity is sufficiently flexible. Furthermore, these scenarios (1) cover certain extreme events or scenarios, which require more reserves than covered by the reserve constraint, and (2) ensure the expected deployment cost of the reserves required to cover these extreme events is accounted for in the objective function. The first effect is illustrated by the steady improvement of the solutions of the HUC models considering the same reserve requirement and more scenarios.

[21]In both cases, the difference in operational cost between the SUC and DUC solutions is significantly smaller than the cost differences reported in [45]. Recall however that we here employ an empirical distribution obtained from a large set of scenarios, rather than the continuous description developed in Chapter 3, which was used in [45] for reserve sizing. The latter only accounts for the dependency of the forecast error on the forecast, but neglects the inter-temporal dependency of the forecast error (i.e. auto-correlation effects). This is taken into account in the SGT (Chapter 4). As a result, the probability of extreme errors is likely to be overestimated based on the continuous description of the error. The empirical distribution does not suffer from this drawback, which is reflected in more optimal probabilistic reserve rules. In addition, PHES-based and non-spinning reserves are allowed in the DUC solution, which improve the cost-efficiency of the DUC solutions. These flexibility providers were not considered in the original DUC results reported in [45].

Alternatively, one could increase the design reliability of the reserve requirements in the HUC model in order to further accelerate the 'convergence' of the solution or to completely eliminate the need to consider scenarios in the optimization. However, as indicated in Fig. 5.11b, from a certain level of reserves, this triggers too much online capacity. As a result, the expected loss of load decreases, even below the level of the stable solution of the SUC problem, but operational costs may rise. In this particular case, this occurs e.g. when considering non-spinning reserves and a reserve requirement corresponding to a 95% design reliability. This 'overshoot' in reserve capacity also means that the difference between adding a small number of scenarios or considering a large scenario set does not affect the solution as much as for a SUC model (Fig. 5.11b). However, the presence of these scenarios does impact the type and amount of reserves scheduled, thus the reliability and expected operational cost of the obtained UC schedule (not shown in the Fig. 5.11a, see [45]).

With the proposed formulation of the HUC problem one obtains a UC schedule that reflects an optimal trade-off between reliability and the operational cost of ensuring that reliability, as in the SUC solution. Indeed, load shedding is scheduled in extreme scenarios when the expected cost of load shedding is dominated by the cost reduction from committing less reserves, thus capacity[22]. As shown in Fig. 5.11a, this optimum lies around 3.0 MWh/day of expected load shedding in the absence of non-spinning reserves. With non-spinning reserves, more cost-efficient reserve capacity is available, which allows near-zero load shedding volumes in the SUC, DUC and HUC solutions. The stable SUC solution is characterized by an expected load shedding volume of 1.2 MWh/day (Fig. 5.11b).

In general, as more scenarios are added to the optimization problem, calculation times increase (Fig. 5.11c - 5.11d). In the most extreme case, when only the forecast is considered (no scenarios, design reliability 100%), calculation times drop to approximately two minutes (Section 5.2). Adding scenarios steadily increases the calculation time. However, differences in calculation time are apparent between different hybrid strategies with the same number of scenarios. For this particular case, stringent reserve requirement, combined with a relatively high number of scenarios, yield high calculation times. In contrast, if one considers few scenarios, a more stringent reserve requirement is likely to result in lower calculation times. The results connected by the dashed lines in Fig. 5.11c and Fig. 5.11d can be seen as a Pareto front: for a specific calculation time, the dashed line indicates the lowest achievable expected operational cost. From that perspective, an efficient HUC setting – weighing optimality, calculation time and reliability, with and without non-spinning reserves available – is the

[22]Note that the resulting level of load shedding is thus sensitive to the value of lost load ($VOLL$). A sensitivity analysis towards this value is however out of the scope of this text.

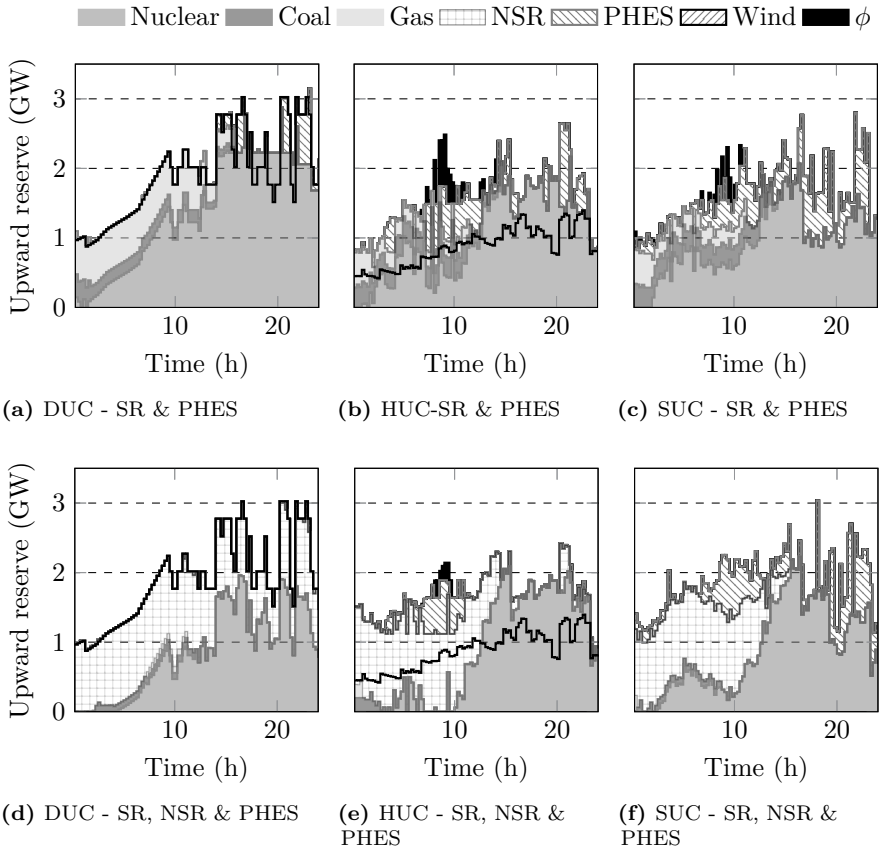

(a) DUC - SR & PHES **(b)** HUC-SR & PHES **(c)** SUC - SR & PHES

(d) DUC - SR, NSR & PHES **(e)** HUC - SR, NSR & PHES **(f)** SUC - SR, NSR & PHES

Figure 5.12: The available upward reserves as calculated with (1) the SUC model, considering 40 or 50 scenarios, (2) the HUC model, considering 7 scenarios and a probabilistic reserve constraint with a design reliability of 85% and (3) a DUC model considering a reserve requirement with a 100% design reliability on the first day of week 39. Spinning (SR), non-spinning (NSR) and PHES-based reserves are considered. The solid black line indicates the reserve requirement.

combination of seven scenarios and a probabilistic reserve rule that is designed to cover 85% of the forecast errors. The solutions corresponding to this hybrid strategy are indicated with an arrow in Fig. 5.11a-5.11d.

In terms of the scheduled upward reserves (Fig. 5.12), differences are more evident. The scheduled upward reserves as obtained from the SUC model (Fig. 5.12c and 5.12f) and the HUC formulation considering 7 scenarios and

a reserve requirement obtained with a design reliability of 85% (Fig. 5.12b and 5.12e)[23] are similar. Only considering spinning reserves, one observes that the schedule of the PHES system is still conservative compared to the SUC solution, but less conservative compared to the DUC schedule. The worst-case constraints on the PHES system's energy content (Chapter 2) do not allow fully relaxing the conservative scheduling of PHES-based reserves. The HUC schedule relies more on reserves provided by nuclear power plants than the SUC solution, but less than the DUC schedule. Compared to the DUC solution, significantly less gas-fired reserve capacity is scheduled by the HUC and SUC models. The HUC model sheds somewhat more load (as an upward reserve provider) compared to the SUC model, albeit at the same hours of the day. This last observation is an indication that the HUC formulation is able to identify those moments in which reserve provision is the most expensive, and possibly exceeds the associated benefits, i.e. avoiding load shedding. As illustrated in Fig. 5.11a, the HUC solution yields approximately the same expected load shedding volume as the SUC schedule after MC ED evaluation. Note that the reserve requirement imposed on the HUC model is insufficient to trigger sufficient reserve capacity to avoid load shedding in real time. The equivalent DUC formulation considering a reserve requirement with a design reliability of 85% would result in an expected load shedding volume of approximately 118 MWh on this particular day, compared to 3.8 MWh for the HUC solution. In terms of expected total operational cost, this DUC solution is approximately two times as expensive as the HUC schedule. Similarly, a SUC formulation only considering seven scenarios has insufficient information to schedule sufficient reserves. These observations were extensively discussed in Chapter 4 during the solution stability analysis. For this particular instance, a SUC model considering 7 scenarios results in approximately 123 MWh of load shedding and an expected operational cost that is almost two times as high as the expected operational cost of the HUC solution.

With the introduction of non-spinning reserves, the differences between the procured reserves in the three different UC solutions increase. As extensively discussed in Section 5.2, the DUC formulation considers the scheduling of non-spinning reserves as a no-regret option, as it does not consider any operational costs associated with procuring or dispatching non-spinning reserves. The SUC

[23]The upward flexibility scheduled by the HUC model is calculated as follows. For the conventional capacity, we calculate the upward flexibility as the maximal possible upward change in output w.r.t. the output of each of the units under forecast conditions and their technical restrictions. Non-spinning reserves are reported if they are scheduled as non-spinning reserves in the forecast scenario and dispatched in at least one of the other scenarios. Wind power is accounted for as upward reserve if it is curtailed in the forecast scenario. For the PHES-based reserves, we take the maximum of (1) the scheduled PHES-based reserves under forecast conditions and (2) their increase in discharging, augmented with their decrease in charging in one of the considered scenarios w.r.t. their output profile under forecast conditions.

and HUC model do consider the operational cost of activating non-spinning reserves via their activation or deployment in the considered scenarios. The low number of scenarios in the HUC formulation may however lead to an under- or overestimation of the expected operational cost associated with scheduling non-spinning reserves. In this particular instance, this results in more non-spinning reserves scheduled by the HUC model towards the end of the day. The HUC schedule relies more on nuclear capacity to provide regulation services, especially towards the end of the day. Note that compared to the DUC model, both the SUC and HUC formulation schedule more online capacity during the first hours of the day, when the demand is low, which allows the PHES system offering upward reserves in later hours. In terms of operational cost and load shedding volumes, the HUC and SUC solutions are comparable, with a slight cost advantage for the SUC solution. The observations made above on the equivalent DUC solutions, considering the reserve requirement of the HUC strategy, or the equivalent SUC problem considering seven scenarios, still hold. The equivalent DUC schedule results in 2.5 MWh of load shedding, but the associated total operational cost is 5% higher than that of the HUC solution. The load shedding volume is limited due to excessive non-spinning reserve procurement, which increase the expected operational cost. The equivalent SUC solution is approximately 3 times as costly as the HUC solution, which is the result of an expected load shedding volume of approximately 146 MWh.

In conclusion, we have shown that there exists a combination of a probabilistic reserve requirement with a certain design reliability and a reduced set of scenarios that, when combined in a HUC model, allows approximating the stable solution of the SUC model. Not only the operational cost, but also the scheduled spinning and non-spinning reserves and resulting reliability are similar. Solving such a hybrid model however takes significantly less time than the full stochastic problem. In what follows, we will analyze the performance of a HUC formulation considering 7 scenarios and a probabilistic reserve requirement corresponding to a design reliability of 85%. Before turning to a quantitative four week analysis, we want to focus the reader's attention on the interaction between the scenario reduction problem and the design of the HUC strategy.

5.5.2 Scenario reduction & hybrid deterministic-stochastic unit commitment strategies

So far, we have focused on the cost-efficiency of the HUC model as a result of the combination of a small number of scenarios, which allow approximating the expected cost of reserve provision and activation, which in turn allows optimal reserve scheduling and shedding, and a probabilistic reserve requirement. However, we did not yet focus on the way we identify those scenarios needed to

solve the HUC problem. We will employ the fast-forward probability distance-based SRT and we will use *the operational cost obtained from a deterministic equivalent problem* to characterize the scenarios during scenario reduction, as proposed in Chapter 4. This operational cost metric is a reflection of the impact of the inclusion of the associated scenario in the stochastic problem at hand. In the SRT developed for the SUC problem, this cost metric is calculated via a (simplified) single-scenario equivalent DUC problem. In the HUC formulation however, the deterministic equivalent problem, i.e. a DUC problem, already contains a reserve requirement. We will therefore calculate the cost metric, used to characterize each scenario, as the operational cost of the dispatch associated with each scenario, based on a UC schedule obtained from a DUC model constrained by the reserve requirement of the HUC model. Extreme scenarios, which are not captured by the reserve requirement of the HUC strategy, will be characterized by load shedding, and hence by a high expected operational cost. These scenarios, which determine the amount of flexibility needed, will therefore be more easily identified and selected via our modified fast-forward scenario reduction technique (Chapter 4).

As an example, we consider the HUC strategy constrained by a reserve requirement with a design reliability of 85%. To characterize each scenario in an initial, large set, we perform an ED optimization per scenario, considering a UC schedule obtained from a DUC problem, constrained by the reserve requirement above and considering the expected value over the wind power forecast scenarios. If one selects seven scenarios, using the aforementioned scenario characterization and the modified fast-forward scenario reduction method as proposed in Chapter 4, one obtains a discrete representation of the distribution of the wind power forecast error shown in Fig. 5.13. For reference, the original distribution (dashed, black line) of the forecast errors, as represented by the full set of scenarios, and the distribution as calculated from the reduced set of 50 scenarios used in the SUC problem (solid black line with diamond markers) are shown as well. The scenario set considered in the HUC problem captures the left tail of the distribution, which corresponds to negative forecast errors and possible load shedding, with reasonable accuracy. However, the probability of large negative forecast errors is not contained in the reduced scenario set. Nevertheless, load shedding volumes are limited, and the expected operational cost is low (see Fig. 5.13b and below). The right tail of the distribution, which corresponds to positive forecast errors and possible excess RES-based generation, is represented less accurately. The cost function used to characterize the forecast error does not allow differentiating between scenarios with various volumes of curtailment of RES-based generation, as curtailment is not penalized in the objective of the ED model. The positive forecast error events are somewhat 'lumped together', which results in a small peak in the distribution at the $\epsilon = 0$.

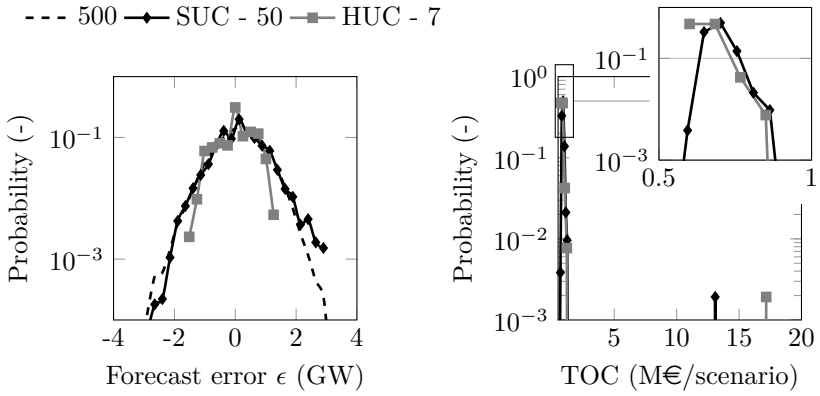

(a) Distribution of the error

(b) Distribution of the operational cost (MC ED simulations)

Figure 5.13: The empirical distribution of the forecast error, as obtained from the reduced scenario set considered in the SUC model (50 scenarios) and the HUC formulation (7 scenarios, reserve requirement with a design reliability of 85%). The reduced scenario set in the HUC model captures the left tail with reasonable accuracy, but the probability of extreme negative forecast errors is not accounted for (Fig. 5.13a), resulting in some load shedding, hence a high operational cost, in a few scenarios (Fig. 5.13b).

Due to the relatively small set of scenarios, some load shedding still occurs in a few scenarios during MC ED evaluation, which results in the high operational cost in those scenarios (Fig. 5.13b). Nevertheless, the expected operational cost of the HUC schedule is just slightly above that of the SUC solution, and significantly better than that of the DUC solution (see above).

Note that the development of such a scenario reduction technique, which considers the description of the uncertainty at hand enclosed in the reserve requirement during scenario reduction, has not yet been attempted in the scientific literature. Typically, researchers employ the well-known fast-forward scenario reduction technique [38] to select scenarios for consideration in a HUC problem. Examples include the work of Tuohy et al. [39] and Abrell and Kunz [132].

5.5.3 Performance of the hybrid unit commitment model

To evaluate the performance of the hybrid reserve sizing and allocation methodology, we turn to the four representative weeks, selected based on the residual demand. For these weeks, expected costs, curtailed wind energy and expected ENS volumes were calculated based on the SUC model considering 40 and 50 scenarios (Section 5.3) as well as with the proposed HUC model (seven scenarios, probabilistic reserve constraint designed to capture 85% of all forecast errors). We also report the solutions of the DUC model, considering a reserve requirement obtained from our probabilistic reserve sizing technique, assuming a design reliability of 100%. A comparison with a SUC model considering seven scenarios or a DUC model considering the same reserve requirement as in the HUC formulation is omitted. Our analysis in Chapter 4 and Section 5.3 showed that SUC solutions with such a low number of scenarios are characterized by extreme expected volumes of ENS, hence high operational costs. Similarly, UC schedules obtained from a DUC model constrained by a reserve requirement with a relatively low design probability will yield high ENS volumes, as we illustrated in Section 5.2. We furthermore differentiate between two cases, based on the availability of fast-starting units to provide non-spinning reserves. PHES systems offer regulation services in both situations. The results are summarized in Table 5.11.

Only considering spinning and PHES-based reserves, the HUC model yields significant cost savings w.r.t. the equivalent DUC solutions. The expected operational cost reductions vary between 0.2 M€/week and 0.6 M€/week. This is the result of a more efficient UC schedule, procuring less reserves and a higher absorption of available wind energy. The reduction in procured reserves however triggers increases in load shedding, tempering the operational cost decrease and increasing the width of the corresponding confidence intervals. At most, 0.004% of the total load is shed (week 39 and week 52). The wind utilization factor increases by 4.7 (week 52) and 2.1 percentage points (week 39) respectively. In three out of four weeks, the HUC solution outperforms the SUC solution. Operational cost differences between 0.2 M€/week (week 39) and 0.3 M€/week (week 30 and week 52) are observed. These differences in operational cost can partly be attributed to the higher expected ENS volumes in the SUC solutions. Only in week 9, the SUC solution outperforms the HUC solution (0.1 M€/week). Note that the HUC schedules achieve similar wind utilization factors as the SUC solutions.

The introduction of non-spinning reserves decreases the differences in operational cost between the SUC, HUC and DUC solutions. Compared to the DUC solutions, the HUC schedules are up to 0.3 M€/week less expensive (week 39). Only in week 52, the week with the highest wind share, the DUC model

Table 5.11: Performance of the proposed HUC model (7 scenarios, a reserve requirement with a design reliability of 85%), the SUC formulation considering 40 or 50 scenarios and a DUC formulation considering reserve requirements with a design reliability of 100%. TOC is the total operational cost. WUF is the wind utilization factor, the percentage of available wind energy that is absorbed in the system. WS is the Share of Wind energy in the total demand for electrical energy. Δ is the width of the 95% confidence interval on E[TOC].

(a) Average residual demand (week 30).

		SR & PHES			SR, NSR & PHES		
		SUC	HUC	DUC	SUC	HUC	DUC
E[TOC]	[M€]	13.9	13.6	13.8	13.3	13.2	13.2
Δ	[M€]	0.4	0.2	0.1	0.2	0.2	0.1
E[ϕ]	[MWh]	46.0	23.4	0	36.0	24.1	0.7
E[WUF]	[%]	100	100	100	100	100	100
E[WS]	[%]	10.6	10.6	10.6	10.6	10.6	10.6

(b) Max. residual demand (week 9).

		SR & PHES			SR, NSR & PHES		
		SUC	HUC	DUC	SUC	HUC	DUC
E[TOC]	[M€]	28.1	28.2	28.5	27.2	27.3	27.5
Δ	[M€]	0.3	0.4	0.1	0.2	0.3	0.2
E[ϕ]	[MWh]	16.0	28.5	0	8.1	11.5	1.8
E[WUF]	[%]	100	100	100	100	100	100
E[WS]	[%]	13.5	13.5	13.5	13.5	13.5	13.5

(c) Min. residual demand (week 52).

		SR & PHES			SR, NSR & PHES		
		SUC	HUC	DUC	SUC	HUC	DUC
E[TOC]	[M€]	3.5	3.0	3.3	2.9	2.6	2.4
Δ	[M€]	0.4	0.4	0.01	0.4	0.3	0.03
E[ϕ]	[MWh]	85.0	48.4	0	65.5	34.2	0.1
E[WUF]	[%]	91.0	91.4	86.7	94.1	94.2	92.4
E[WS]	[%]	79.0	78.8	74.8	81.1	81.3	79.7

(d) Max. var. residual demand (week 39).

		SR & PHES			SR, NSR & PHES		
		SUC	HUC	DUC	SUC	HUC	DUC
E[TOC]	[M€]	8.4	8.2	8.8	6.3	6.6	6.9
Δ	[M€]	0.4	0.6	0.1	0.2	0.5	0.1
E[ϕ]	[MWh]	94.3	61.81	0	10.7	40.8	0.2
E[WUF]	[%]	96.0	95.6	93.5	97.2	97.2	96.0
E[WS]	[%]	50.4	50.0	48.9	51.2	50.9	50.3

Table 5.12: Comparison of the CPU time (s) per run of the DUC, HUC and SUC model. P(75) is the 75$^{\text{th}}$ percentile, P(90) is the 90$^{\text{th}}$ percentile.

	SR & PHES			SR, NSR & PHES		
	SUC	HUC	DUC	SUC	HUC	DUC
Median [s]	+50,000	3,083	138	28,921	5,896	125
P_{75} [s]	+50,000	4,335	191	36,296	11,379	213
P_{90} [s]	+50,000	7,397	342	+50,000	16,068	395

outperforms the HUC and SUC model by 0.2 M€/week and 0.5 M€/week respectively. Again, increases in load shedding volumes dampen the attainable operational cost savings. The SUC solutions now outperform the HUC schedules in two out of four weeks. Operational cost differences between the HUC and SUC solutions vary from 0.1 M€/week (week 9) to 0.3 M€/week (week 39). The HUC schedules yield lower operational costs than the equivalent SUC solutions in week 30 (0.1 M€/week) and week 52 (0.3 M€/week). The differences in operational cost can mostly be attributed to the differences in ENS volumes. The SUC and HUC schedules allow for similar wind utilization factors, which are 1.2 to 1.8 percentage points higher than those observed in the DUC solutions.

5.5.4 Computational performance

If one considers spinning and PHES-based reserves, the proposed HUC model solves in approximately 3,000 seconds (median values). This is to be compared with 140 seconds for an equivalent DUC model and at least 50,000 seconds for an instance of the SUC problem (median values). The HUC model thus solves approximately 22 times slower than a DUC model, but 16 times faster than a SUC model. The spread on the calculation times of the HUC problems is limited. In 90% of cases, a solution within the optimality gap was found within 7,400 seconds or just over 2 hours.

The addition of non-spinning reserves strongly increases the complexity of the HUC problem at hand. The HUC model faces the complex trade-off between non-spinning, spinning and PHES-based flexibility. Recall that we require each scheduled non-spinning reserve provider to be dispatched in at least one scenario, which makes that the scheduling of fast-starting units as non-spinning reserve providers no longer is a 'no-regret' option as in the DUC formulation. As a result, calculation times approximately double (median values). A HUC model requires approximately 5,900 seconds or just under 100 minutes to solve. For 90% of the instances, a solution was found in approximately 16,000 seconds

or 4.5 hours. Remarkably, this trend of increasing calculation times with the introduction of non-spinning reserves is opposite to that found in the SUC problem. Considering median values, solving a SUC problem requires five times longer than solving the equivalent HUC problem. The calculation time of a DUC model is nearly unaffected by the introduction of non-spinnig reserves. Solving a HUC problem requires approximately 47 times more computational effort than solving the corresponding DUC problem (median values).

5.5.5 Concluding remarks

Stochastic UC models, with a direct representation of the uncertainty via a set of scenarios in the UC model, lead to an optimal trade-off between reliability and operational system cost, but are computationally intensive to solve. Furthermore, the literature and own research have shown that their performance can be improved by adding reserve requirements to the stochastic formulation and that probabilistic reserve requirements outperform any other reserve requirement in a deterministic UC model [45]. However, the addition of such a probabilistic reserve requirement to a SUC formulation has not yet been attempted.

We designed a hybrid deterministic-stochastic UC strategy, combining a state-of-the-art probabilistic reserve rule and a limited number of scenarios, selected via a dedicated scenario reduction technique. We analyzed the procurement of spinning, non-spinning and PHES-based reserves. As shown above, the addition of probabilistic reserve constraints to a SUC model can speed up the 'convergence' of the stochastic problem to its stable solution – i.e. the benchmark in our analysis. For the presented case study, we propose a HUC strategy considering seven scenarios and a probabilistic reserve requirement with a design reliability of 85%. The proposed HUC model was thoroughly tested for four representative weeks of the year. Especially without non-spinning reserves, the HUC model yields lower expected operational costs. Operational cost savings up to 0.5 M€/week and 0.6 M€/week w.r.t. the SUC and DUC solutions respectively are observed. Compared to the SUC problem, calculation times reduce by a factor 15. The introduction of non-spinning reserves results in a complex trade-off between non-spinning, spinning and PHES-based flexibility in the HUC formulation. Nevertheless, solving a HUC problem requires five times less time than the equivalent SUC problem and yields operational cost savings up to 0.3 M€/week.

5.6 Cost-effective, reliable & fast: a probabilistic unit commitment model[24]

In a probabilistic UC model, we will represent the reserve requirement as a set of intervals, each of which is coupled to a specific activation probability. With this information, we can include an approximation of the deployment cost of scheduled flexibility providers. In this section, we quantify the operational cost savings that are possible by employing a PUC formulation and compare the performance of PUC schedule with solutions of equivalent DUC and SUC formulations. These reductions in operational cost are the result of including the expected activation costs associated with reserves, which allows (1) the internalization of the reserve sizing problem; (2) scheduling an optimal technology mix to provide reserves and (3) the correct evaluation the operational benefits and costs associated with the procurement of downward flexibility (Chapter 2).

The starting point for the SUC, DUC and PUC models will be the same set of 500 scenarios to isolate the impact of the different approaches to represent uncertainty in a UC model. For the DUC and PUC model, we will calculate an empirical probability density function for each time step in the optimization from this set of scenarios. With the design reliability in the DUC equal to 100%, the total reserve requirement is identical to the reserve requirements enforced in the PUC model. In the SUC model, a limited number of critical scenarios will be selected via a modified probability-distance based fast forward scenario reduction method from the same set of scenarios (Chapter 4). We will distinguish two cases based on the available flexibility providers (Fig. 5.1). In the first setting, only spinning units may provide reserves. This allows focusing on (1) the trade-off between different technologies providing reserves and (2) the trade-off between the cost of providing reserves and the expected socio-economic cost of reserve shedding. In the second case, fast-starting units may provide non-spinning reserves. In both cases, PHES systems may provide arbitrage and regulation services. The feasibility of the real-time activation of the PHES-based flexibility is guaranteed via the same constraints as in the DUC formulation (Section 5.2 and Chapter 2).

The remainder of this section is organized as follows. First, we explore the impact of the number of reserve intervals or levels employed, which is an important design parameter of the PUC formulation, comparable with the (number of) scenarios considered in a SUC formulation (Section 5.6.1). We furthermore compare the scheduled flexibility to that obtained with an equivalent SUC and

[24]This section is based on K. Bruninx and E. Delarue, *A probabilistic unit commitment model: cost-effective , reliable and fast,* Submitted to IEEE Trans. Power Syst., 2015.

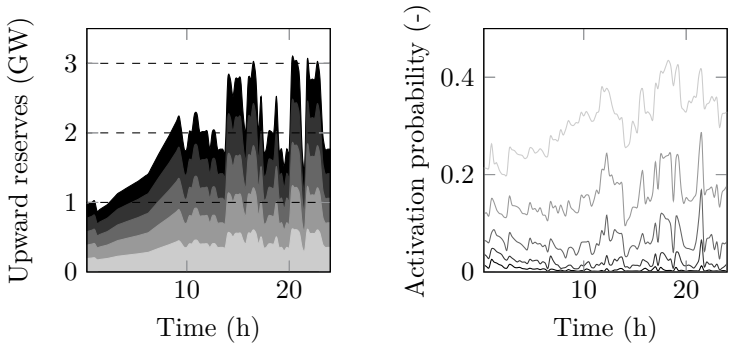

(a) Upward reserve levels

(b) Activation probability upward reserve levels

Figure 5.14: Assuming five reserve levels and given the distribution of the wind power forecast error, one can calculate (a) the reserve levels and (b) the asocciated activation probability at each time step, for each reserve level, which characterize the uncertain wind power forecast in the PUC formulation. The illustration above corresponds to the situation on the first day of week 39. The colors relate the reserve levels (left) to their activation probabilities (right).

DUC model for the first day of week 39. Second, the resulting operational cost and computational performance of the PUC model is compared to that of a SUC and DUC model in a four week analysis (Section 5.6.2 and Section 5.6.3 respectively).

5.6.1 Reserve levels & scheduled flexibilty

In this section, we study the behavior of the PUC model in detail based on simulations performed for the first day of week 39. Using the methodology described in Chapter 2, one can obtain a discrete number of reserve levels, each with their associated deployment probability, given the (empirical) distribution of the forecast error. Figure 5.14 shows the resulting reserve levels, indicated by the different colors, and their associated activation probability. In this particular example, the number of reserve levels for both upward and downward reserves was set to five. However, as shown below, the number of reserve levels may have a significant impact on the performance of the PUC formulation.

Figure 5.15 visualizes the effect of the number of reserve levels L on the expected operational cost, the reliability and the calculation time required to solve the

PUC problem. The expected operational cost (Fig. 5.15, top) is normalized with respect to the operational cost as obtained from the corresponding DUC model. In the same figure, the performance of the SUC model as a function of the number of scenarios considered during the UC optimization is visualized (cf. the solution stability analysis in Chapter 4). To allow focusing on the performance of the scheduling models, the dispatch is performed on the scenario set used to determine the empirical probability distributions (PUC) and to select critical scenarios (SUC), as we did to determine a HUC strategy (Section 5.5) and to analyze the solution stability and bias of SUC solutions in Chapter 4. Performance differences due to small differences in the scenario sets are hereby avoided. As the solutions however may be biased towards the considered distribution or scenarios, we will evaluate the performance of the DUC, PUC and SUC models on a *new* set of scenarios in Section 5.6.2, as we did before.

Discretizing the reserve requirement and accounting for the activation costs of the scheduled reserves results in a significant drop in operational costs if one considers sufficient reserve levels (Fig. 5.15). Two effects are at play. First, the PUC will 'relax' reserve constraints by scheduling load shedding during the UC phase (Fig. 5.16b and 5.16e), effectively internalizing the reserve sizing problem. Although this results in some load shedding during dispatch (Fig. 5.15, center), the expected operational cost is significantly lower (Fig. 5.15, top). This effect is the strongest when one does not consider non-spinning reserves. Spinning reserves are typically provided by larger units, which makes it more difficult to follow the upward reserve requirement exactly. To provide the last few MW's of upward reserve capacity, one might have to commit a new unit, which may result in a higher expected operational cost than curtailing some load.

In other words, the allocation and expected activation cost of the last MW's of reserves is too high. Non-spinning reserves are smaller in size and have lower allocation and expected activation costs at low activation probabilities, so this effect is less pronounced. Second, the consideration of the activation costs allows the model to schedule an optimal mix of technologies to provide upward and downward flexibility, further reducing the expected operational cost. For example, when non-spinning and spinning reserves are available, the operational cost keeps decreasing (Fig. 5.15, top) while the load shedding volume remains constant (Fig. 5.15, center). For this particular day, the second effect has a less pronounced impact on the operational cost (Fig. 5.15, top), but does impact the scheduled flexibility (Fig. 5.16). Note that the decrease in operational costs levels off above a certain number of reserve levels L. As of that point, more detailed representations of the distribution of the reserve requirement or forecast error do not lead to further improvements in the UC schedule, but do increase the complexity of the problem, as illustrated by the moderate increase in calculation time (Fig. 5.15, bottom).

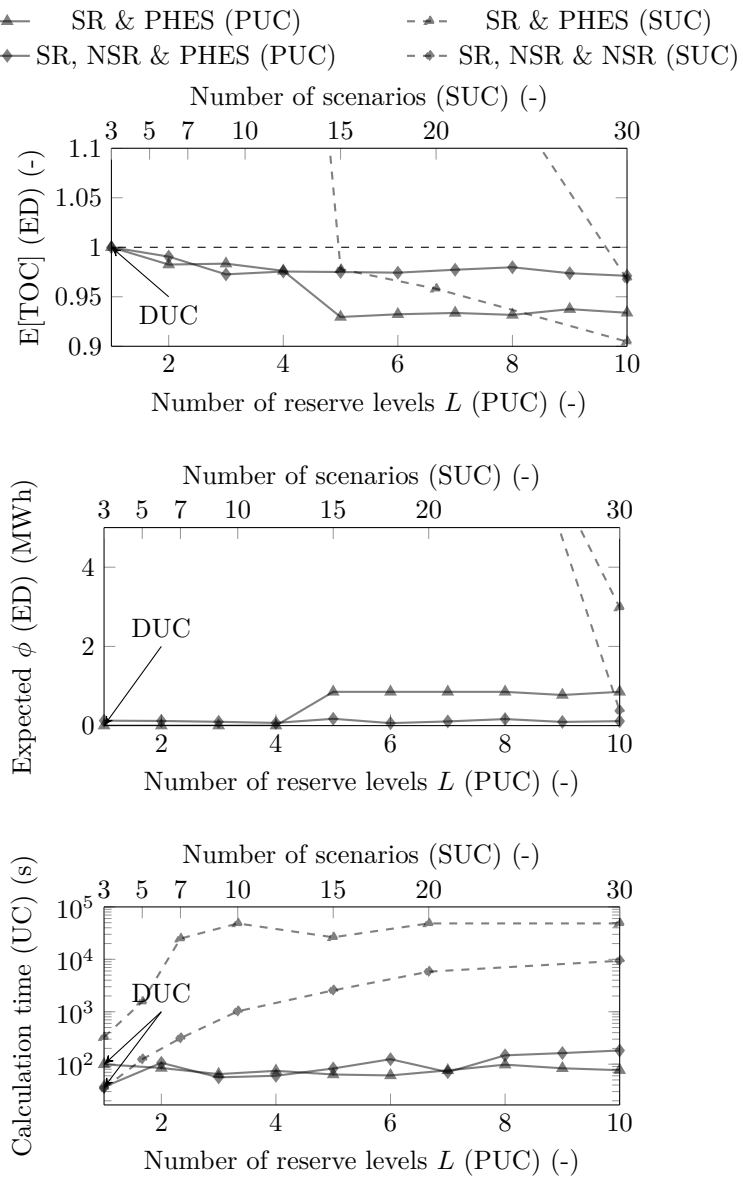

Figure 5.15: Increasing the number of reserve levels in a PUC formulation leads to reduced operational costs, but increases the calculation time. The operational cost (TOC) is shown relative to the operational cost as obtained from the equivalent DUC model. The markers indicate the (un)availability of non-spinning reserves, the solid lines correspond to the results obtained with a PUC model as a function of the number of reserve levels L (bottom axis). The dashed lines visualize the SUC results as a function of the number of scenarios considered (top axis).

Solving a DUC model takes 30 to 90 seconds. With the proposed formulation, this calculation time increases to 80-190 seconds (PUC, $L = 10$). When non-spinning reserves are available, the complexity of the problem and the calculation time typically increase. Note however that the increase in calculation time is moderate when compared to the evolution of the calculation time associated with solving a SUC problem with the number of scenarios considered (Fig. 5.15, bottom).

The presented analysis is analogous to a solution stability study in stochastic programming (Chapter 4). If one takes too few scenarios into account, the SUC model will underestimate the required reserves, which results in high load shedding volumes (Fig. 5.15, center) and high operational costs (Fig. 5.15, top). In this particular case, 30 scenarios are required to obtain a so-called stable solution [111, 45, 116]. Note that the evolution of the expected load-shedding volumes as a function of the number of scenarios considered in the SUC problem is opposite to that in the PUC solution as a function of the number of reserve levels. Starting from a UC schedule in which load shedding is not expected to occur, load shedding is gradually scheduled as a flexibility option with increasing granularity in the reserve levels in the PUC model. On the contrary, the SUC model starts from a UC schedule with high volumes of expected load shedding, reducing this volume as more detailed representations of the uncertain wind power forecast are considered (i.e. a higher number of scenarios). The quality of the resulting UC schedule is hence heavily dependent on the number of scenarios. Considering 30 scenarios, the SUC schedule outperforms the PUC solution (Fig. 5.15, left). The calculation time to solve a SUC problem however also strongly increases with the number of scenarios considered and rises from approximately 750 seconds to 5,800 seconds (5 scenarios) to at least 96,000 seconds (30 scenarios) (Fig. 5.15, bottom). If non-spinning reserves are to be scheduled in a SUC formulation, the size of the problem increases, but the calculation time decreases drastically (Section 5.3).

Figure 5.16 illustrates the scheduled upward flexibility as obtained from a DUC, PUC and SUC model for this particular day. The PUC model contains five reserve levels. We will focus on the scheduled upward flexibility because of the large impact of possible load shedding. However, a similar analysis could be conducted for downward flexibility. Several effects are visualized in Fig. 5.16. First, the PUC model actively schedules 'load shedding' (ϕ) as upward flexibility in reserve levels with a very low activation probability. This is the result of the internalization of the reserve sizing problem: the PUC model endogenously considers the trade-off between the expected cost of load shedding in less likely, extreme wind power conditions and the expected operational procurement and deployment costs of reserves. If 'load shedding' is scheduled, the expected deployment and procurement cost of the associated reserves exceeds the expected

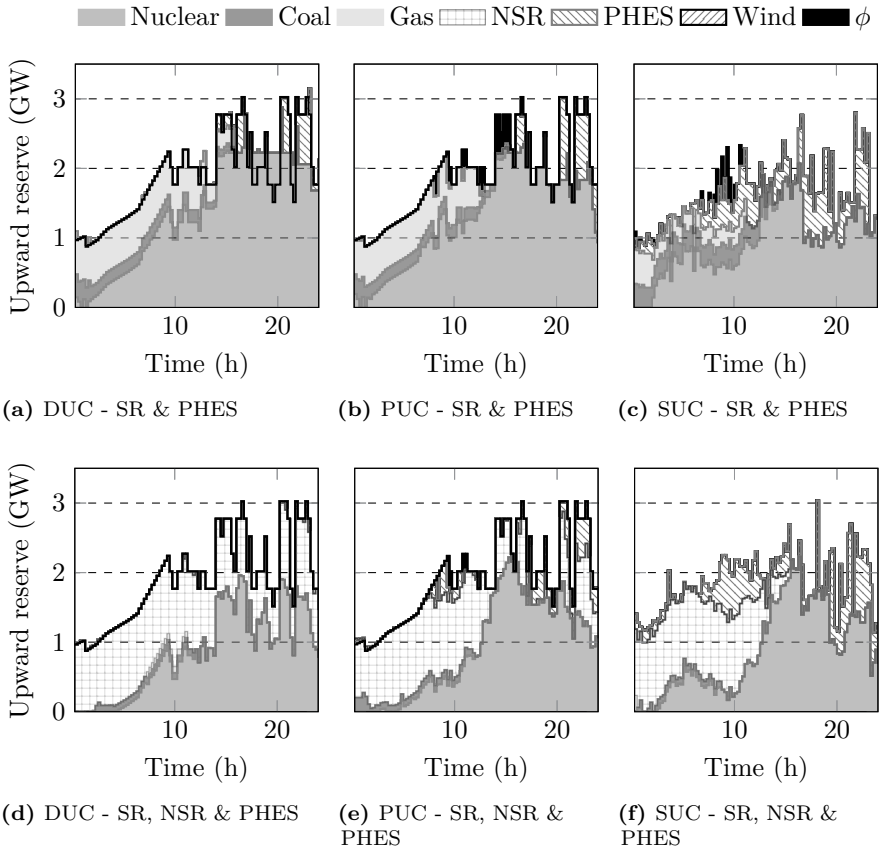

(a) DUC - SR & PHES **(b)** PUC - SR & PHES **(c)** SUC - SR & PHES

(d) DUC - SR, NSR & PHES **(e)** PUC - SR, NSR & PHES **(f)** SUC - SR, NSR & PHES

Figure 5.16: The available upward reserve capacity per technology and per UC formulation. The solid black line indicates the total upward reserve requirement in the PUC and DUC problem. The PUC model employs five reserve levels ($L = 5$). The SUC formulation considers 30 scenarios.

cost of load shedding. Consequently, fewer units have to be committed (Fig. 5.16a-5.16b and Fig. 5.16d-5.16e). When non-spinning reserves are available, more cost-effective low-activation-probability flexibility is available to meet the reserve requirement. Significantly less load shedding is scheduled (Fig. 5.16d-5.16e). Second, as non-spinning reserves do not present any allocation costs and activation costs are not considered in the DUC formulation, all units that can provide non-spinning reserves are scheduled by the DUC model (Fig. 5.16d). The PUC model typically schedules less non-spinning reserves and

more spinning reserves (nuclear) due to the high expected activation cost of the fast-starting units that may provide non-spinning reserves (Fig. 5.16e). Third, less RES-based upward reserve (curtailment under forecast conditions) is scheduled when non-spinning reserves are available. Fourth, both the DUC and PUC solution remain conservative compared to the SUC schedule. Less capacity is scheduled by the SUC model, while similar load shedding volumes are attained during dispatch (Fig. 5.15, center). Especially the potential regulation services of the PHES system remain underestimated in the PUC schedule due to the necessary, but conservative worst-case feasibility constraints. For a detailed discussion on the coupling between PHES-based reserves and UC models, the reader is referred to Section 5.2 and Chapter 2.

5.6.2 Performance of the PUC formulation

To evaluate the performance of the PUC formulation quantitatively, four representative weeks were selected based on the residual demand (Section 5.1). With the solutions of the SUC (Section 5.3) and DUC models (Section 5.2) as a benchmark, we are able to judge the performance of the PUC model.

During week 30 (average residual demand), the performance of the PUC and DUC models is comparable. Curtailment does not occur. The SUC model is outperformed by the DUC and PUC formulations. The UC schedule obtained with the SUC model is inadequate to meet the demand without load shedding in some scenarios, resulting in moderate expected load shedding volumes and, consequently, increased expected operational costs. The PUC model does result in more load shedding when non-spining reserves are considered, of which the associated cost in this particular case is of the same order of magnitude as the operational cost differences between the models.

Similar effects are observed in week 9 (max. residual demand). The PUC formulation however realizes operational cost savings of approximately 0.1 M€/ week or 0.4% (compared to the DUC solution). Load shedding volumes are similar in the DUC and PUC solutions. Curtailment does not occur. However, the SUC formulation allows scheduling some load shedding and exploiting the PHES system more effectively, which leads to a more cost-optimal procurement of upward reserves. The result is an operational cost saving of approximately 0.3 M€/week or approximately 1% compared to the PUC schedule. When considering non-spinning reserves, the performance of the DUC and PUC models is similar and 0.3 M€/week worse than that of the SUC formulation.

Table 5.13: Performance of the DUC, PUC and SUC models considering spinning (SR), non-spinning (NSR) and PHES-based reserves. TOC is the total operational cost. WUF is the wind utilization factor, defined as the percentage of available wind energy that is absorbed in the system. WS is the Share of Wind energy in the total demand for electrical energy. Δ is the width of the 95% confidence interval on E[TOC].

(a) Average residual demand (week 30).

		SR & PHES			SR, NSR & PHES		
		SUC	PUC	DUC	SUC	PUC	DUC
E[TOC]	[M€]	13.9	13.7	13.8	13.3	13.3	13.2
Δ	[M€]	0.4	0.1	0.1	0.2	0.1	0.1
E[ϕ]	[MWh]	46.0	0	0	36.0	1.8	0.7
E[WUF]	[%]	100	100	100	100	100	100
E[WS]	[%]	10.6	10.6	10.6	10.6	10.6	10.6

(b) Max. residual demand (week 9).

		SR & PHES			SR, NSR & PHES		
		SUC	PUC	DUC	SUC	PUC	DUC
E[TOC]	[M€]	28.1	28.4	28.5	27.2	27.5	27.5
Δ	[M€]	0.3	0.1	0.1	0.2	0.2	0.2
E[ϕ]	[MWh]	16.0	0	0	8.1	3.0	1.8
E[WUF]	[%]	100	100	100	100	100	100
E[WS]	[%]	13.5	13.5	13.5	13.5	13.5	13.5

(c) Min. residual demand (week 52).

		SR & PHES			SR, NSR & PHES		
		SUC	PUC	DUC	SUC	PUC	DUC
E[TOC]	[M€]	3.5	2.9	3.3	2.9	2.3	2.4
Δ	[M€]	0.4	0.03	0.01	0.4	0.04	0.03
E[ϕ]	[MWh]	85.0	3.0	0	65.5	4.0	0.1
E[WUF]	[%]	91.0	87.5	86.7	94.1	91.6	92.4
E[WS]	[%]	79.0	75.4	74.8	81.1	79.0	79.7

(d) Max. var. residual demand (week 39).

		SR & PHES			SR, NSR & PHES		
		SUC	PUC	DUC	SUC	PUC	DUC
E[TOC]	[M€]	8.4	8.4	8.8	6.3	6.7	6.9
Δ	[M€]	0.4	0.1	0.1	0.2	0.1	0.1
E[ϕ]	[MWh]	94.3	0.2	0	10.7	0.7	0.2
E[WUF]	[%]	96.0	93.8	93.5	97.2	96.0	96.0
E[WS]	[%]	50.4	49.1	48.9	51.2	50.2	50.3

During periods of low residual demand (week 52), curtailment of RES-based generation and the procurement of downward flexibility become decisive for the performance of the UC models. The PUC model explicitly considers the possible operational cost savings associated with downward flexibility, which results in operational cost savings of 0.4 M€/week (14%) to 0.1 M€/week (4.2%) compared to the DUC solutions. The difference in operational cost and curtailment is typically smaller when non-spinning reserves may be scheduled. As the DUC model does not consider the cost of activation of these fast-starting units, all of them are scheduled throughout the week. Although this is sub-optimal, the resulting UC schedule is highly flexible, resulting in an expected operational cost that approximates that of the PUC schedule. Convergence and solution stability issues result in high load shedding volumes, thus high expected operational costs, in the SUC solutions (Section 5.3). The PUC solutions are 0.6 M€/week less expensive. Note however that the expected operational cost associated with load shedding in the SUC solutions is of the same order of magnitude.

If the residual demand is strongly variable (week 39), the PUC formulation outperforms the DUC formulation by 0.2 to 0.4 M€/week (3.0% to 4.7% respectively). This is the result of scheduling load shedding as upward reserves, which allows covering the upward reserve requirement with less online capacity and to a lesser extent, scheduling of a more cost-efficient mix of technologies to meet the reserve requirement. The SUC model outperforms the PUC formulation, despite a higher volume of load shedding in the SUC solutions. The difference in operational cost is negligible when only considering spinning reserves, but amounts to 0.4 M€/week or 6.3 % when non-spinning reserves are available. In both cases, the resulting WUF is significantly higher in the SUC solutions.

5.6.3 Computational performance

Table 5.14 compares the calculation times (median, 75^{th} and 90^{th} percentile) of the DUC, PUC and SUC models. Solving a PUC model takes 3.3 to 4.8 minutes (median values). Considering non-spinning reserves considerably increases the calculation time. 90% of all simulations terminate within 5.8 minutes (without non-spinning reserves) and 7.6 minutes (with non-spinning reserves) respectively. This trend can be contrasted with the evolution of the calculation time of the DUC model, which is not significantly impacted by the introduction of non-spinning reserves. As discussed above, the DUC formulation does not face the complex trade-off between activation and allocation costs of spinning and non-spinning reserves, resulting in fast models, but sub-optimal UC schedules. Solving a DUC model takes approximately two minutes (median values). The

Table 5.14: Comparison of the CPU time (s) per run of the DUC, PUC and SUC model. P(75) is the 75$^{\text{th}}$ percentile, P(90) is the 90$^{\text{th}}$ percentile.

	SR & PHES			SR, NSR & PHES		
	SUC	PUC	DUC	SUC	PUC	DUC
Median [s]	+50,000	201	138	28,921	281	125
P_{75} [s]	+50,000	267	191	36,296	365	213
P_{90} [s]	+50,000	348	342	+50,000	455	395

spread on the calculation time of the DUC problem is limited: 95% of all simulations yield a solution in less than 6 minutes. Although solving a PUC model thus requires more time than an equivalent DUC model, this represents a significant improvement in calculation time compared to the SUC model, which takes approximately 8 hours (with non-spinning reserves) to in excess of 13.9 hours (without non-spinning reserves) to solve (median values)[25].

5.6.4 Concluding remarks

By defining distinct reserve levels, each with a probability of activation, one can account for the allocation and expected activation costs in a DUC model, abolishing the need for a scenario-based representation of the uncertain RES-based generation. This improves the performance of the resulting UC model considerably, as shown in Section 5.6.2, without the computational burden of a scenario-based SUC formulation (Table 5.14). The reason behind this is twofold. First, the model is able to account for possible operational cost savings resulting from the activation of downward reserves. Although excess RES-based generation can be curtailed, not absorbing unexpected increases in RES-based generation may be sub-optimal. Second, considering activation probabilities allows upward reserves to be provided cost-effectively by a mix of (1) cheap, frequently activated running power plants (spinning reserves), (2) expensive, but rarely activated offline power plants (non-spinning reserves), (3) PHES-based flexibility, (4) load shedding and (5) scheduled curtailment of RES-based electricity generation. Without the inclusion of activation probabilities and distinct reserve levels, this trade-off was not possible in a DUC formulation.

[25]When we report a calculation time of the form '+50,000', this indicates that these instances (1) did not yield a solution in the optimality gap within the imposed time limit (here: 50,000 seconds) or (2) were obtained by so-called 'warm-starting' the problem with solutions obtained from a run of the same instance which initially did not yield a solution in the optimality gap within the imposed time limit.

The resulting PUC formulation allows approximating the stable solution of a SUC model in calculation times similar to that of a deterministic formulation.

5.7 Conclusion: cross-comparison of the studied unit commitment formulations

With the detailed analysis of each of the five selected UC models in place, we are ready to perform a cross-comparison of their performance. We focused on three metrics: the expected operational cost of the UC schedule, the expected volume of load shedding or energy not-served and the computational effort involved in solving the UC problem. We summarize two of these metrics, the operational cost and the CPU time, in the visualization below (Fig. 5.17 and 5.18). As the cost of load shedding is accounted for in the total operational cost and the observed load shedding volumes are low, we will not revisit this metric.

For each model, we distinguish between two cases, based on the availability of fast-starting units as non-spinning reserve providers. We select the best available results for each week and each model. For the SUC formulation, this means that we will report results obtained from simulations in which PHES-based flexibility was not allowed during the optimization of the UC schedule for some particular weeks (see Section 5.3). For all others, we will use the results that were obtained by accounting for PHES-based regulation services in the UC problem, which has been shown to significantly improve the performance the UC schedules. To allow a fair comparison, we report DUC results that were obtained with a reserve requirement with a design reliability of 100%. Recall however that these DUC solutions may be somewhat too conservative, as the considered reserve requirements may be too strict and the DUC may overprocure reserves. These solutions will however provide an upper bound to the expected operational cost and a lower bound to the calculation time. Any model that consistently requires more time to solve than this DUC model and does not result in a more cost-efficient solution, should be discarded.

If one only considers spinning reserves, the SUC model yields the most cost-optimal UC schedules in three out of four studied weeks. Only in week 52, the week in which the residual demand is the lowest, the PUC schedules are most cost-optimal. With respect to the solutions of an equivalent DUC formulation, total expected cost differences are between 0.1 M€/week and 0.7 M€/week. In relative terms, the expected operational cost savings of a SUC formulation compared to a DUC formulation are between 1.4% and 8.0 % per week.

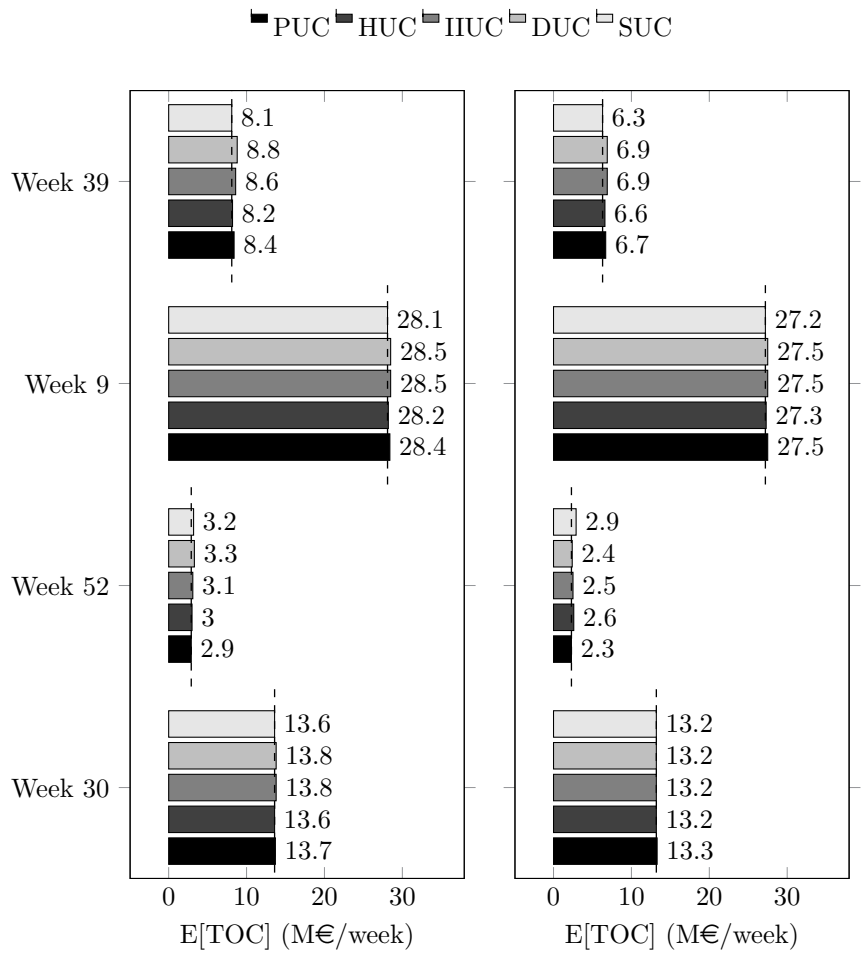

(a) Spinning & PHES-based reserves

(b) Spinning, non-spinning & PHES-based reserves

Figure 5.17: Cross-comparison of the five selected unit commitment models in terms of expected total operational cost. If the scenarios are an adequate representation of the uncertain wind power realization, the SUC model yields an optimal UC decision under uncertainty. The IIUC and DUC solutions are typically overly conservative. The PUC and HUC formulations approach the expected operational cost of the SUC solutions.

The performance of the IIUC formulation is similar to that of the DUC model. Only in week 39 and week 52, weeks with a high wind energy share, the IIUC solutions are 0.2 M€/week and 0.1 M€/week cheaper than the DUC solutions (2.3% and 6.1% respectively). The HUC formulation, developed in this dissertation, results in nearly as cost-efficient UC schedules as the SUC model[26].

The differences in expected operational cost between the HUC and SUC solutions are below 0.1 M€/week (week 39 and week 9). In week 52, the HUC schedule outperforms the SUC solution by 0.2 M€/week. The solutions of the PUC model are, in terms of operational cost, better than the DUC and IIUC solutions in all weeks. Compared to the DUC solutions, the operational cost differences are as high as 0.4 M€/week (4.5% in week 39 or 12.1% in week 52). The PUC formulation performs especially well in weeks with high wind shares. With respect to the solutions of the IIUC model, cost differences up to 0.2 M€/week are noted (6.9% in week 52, 2.3% in week 39). Nevertheless, the PUC formulation remains conservative compared to the SUC and HUC models, o.a. in scheduling PHES-based reserves and reserve shedding, which results in lower expected operational costs for the SUC and HUC solutions in three out of four weeks. Operational cost savings up to 0.3 M€/week are found, which represent at most 3.7% of the total operational cost. In week 52, the PUC solution outperforms the SUC schedule by 10.3% (0.3 M€/week). The SUC model heavily relies on PHES- and RES-based reserves, but has insufficient information, due to a limited scenario set, to ensure feasibility of activating these reserves during the real-time dispatch. In combination with the low residual demand, which triggers little scheduled capacity, this leads to load shedding in real time.

The differences between the solutions of the selected models in terms of the expected total operational costs fade with the introduction of non-spinning reserves. The SUC model still outperforms all other UC formulations in three out of four weeks, but the difference in expected operational cost decreases to at most 0.6 M€/week or 9.5% (week 39). The solutions of the DUC and IIUC problems are almost identical and perform significantly worse than those obtained with the SUC formulation in three out of four weeks. Only in week 52, the week with the lowest residual demand, the DUC and IIUC models perform well, with operational cost differences w.r.t. the SUC solution of up to 0.5 M€/week or 17.2%. The poor performance of the SUC model in this

[26]The operational cost differences reported in this section must be interpreted with caution, as they are dependent on the expected volume of load shedding and the value of lost load $VOLL$. In some cases, the volume of load shedding may be high, triggered by restrictive assumptions on a.o. the availability of fast-starting units during dispatch (Section 5.1), which may result in high relative operational cost differences compared to typical values found in the scientific literature.

particular week was discussed above. The DUC and IIUC model typically over-procure non-spinning reserves, as the associated expected operational cost of dispatching these units is not accounted for in the objective. In addition, the worst-case constraints on the PHES-based reserves to ensure the availability of these reserves in real time lead to underestimations of the regulation potential of the PHES systems. Although the schedule is typically too conservative, this allows avoiding load shedding, which results in a more cost-optimal solution than the SUC schedule in week 52. The HUC model considers some worst-case constraints on the scheduled PHES-based reserves, but these are insufficient to avoid load shedding during week 52. The expected operational cost of the HUC solution exceeds that of the DUC solution by 0.2 M€/week. In all other weeks, the HUC formulation performs well. Operational cost differences between the HUC and SUC solutions are limited to 0.1 M€/week (week 9) and 0.3 M€/week (week 39). The PUC model outperforms the IIUC and DUC formulation in three out of four considered weeks, with cost differences up to 0.2 M€/week or 4.3% (week 39). The SUC solutions are however still superior in three out of four cases, with expected operational cost differences up to 0.3 M€/week (4.5%, week 39). Only in week 52, the PUC model outperforms all other models. Cost differences are between 0.1 M€/week (w.r.t. the DUC solution) and 0.6 M€/week (w.r.t. the SUC solution).

The cost of these improvements in expected operational cost is typically a drastic increase in calculation time. Regardless of the presence of non-spinning reserves, the calculation times involved in solving a SUC problem are two orders of magnitude higher than those associated with the DUC, IIUC and PUC models. The introduction of PHES-based flexibility, modeled via a scenario-specific PHES output profile, proved to further increase the difficulty of finding a stable solution to the SUC problem. Introducing scenario-specific unit commitment decision variables for fast-starting power plants to mimic the scheduling of non-spinning reserves typically decreases the calculation time required to solve a SUC problem. As discussed in Chapter 4, the solution quality and calculation time both depend strongly on the number of scenarios considered. Combining a limited scenario set and reserve requirements in a HUC formulation strongly reduces the computational effort involved, with minimal loss in solution quality. Especially if one does not consider non-spinning reserves, the HUC formulation is significantly easier to solve than the SUC model. Calculation times decrease with a factor 15. Introducing non-spinning reserves doubles the calculation time of the HUC formulation, whereas the opposite effect is observed in the calculation times associated with solving a SUC problem. Nevertheless, a HUC problem considering non-spinning reserves typically still solves five times faster than the equivalent SUC problem. The DUC, IIUC and PUC models are comparable in computational effort, with solution times that are in the order of a few minutes.

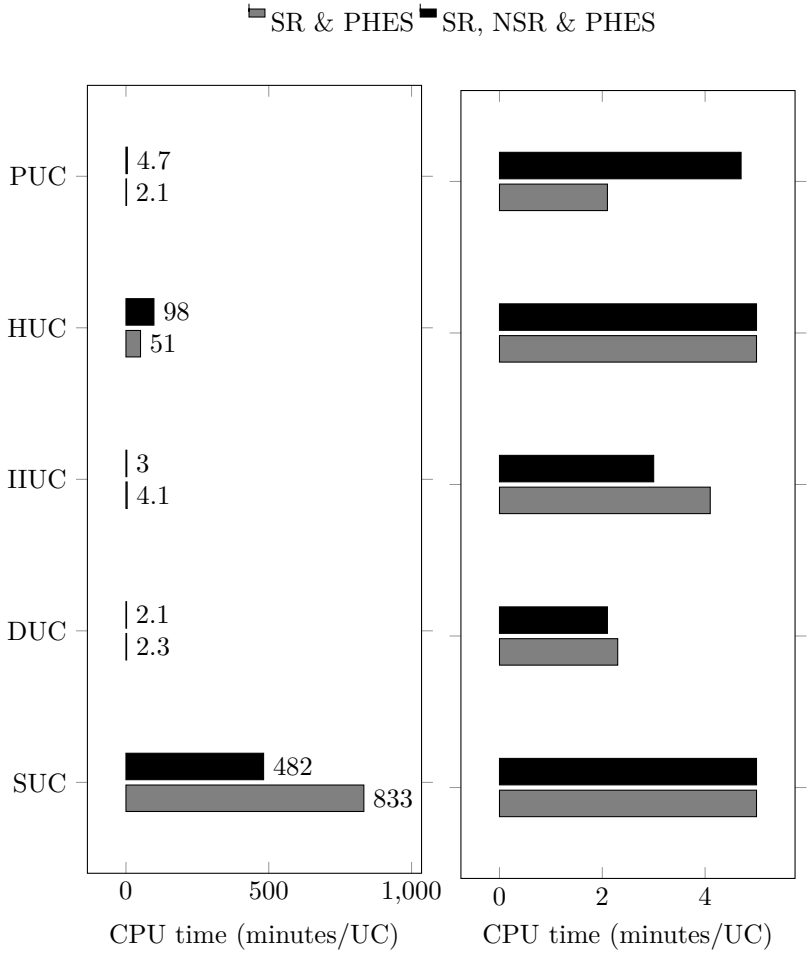

Figure 5.18: Cross-comparison of the five selected unit commitment models in terms of calculation time, with a detail of the lefthandside figure on the right. The reported calculation times are median values. Scenario-based UC models are typically more computationally expensive to solve. The calculation times reported for the SUC model were obtained from the corresponding SUC instances considering 30 scenarios (Chapter 4).

Adding non-spinning reserves typically decreases the calculation time, except for the PUC formulation. The PUC model in this case faces the complex trade-off between the expected operational cost of scheduling and activating non-spinning, spinning and PHES-based reserve capacity, whereas in the DUC and IIUC formulations the deployment costs associated with non-spinning reserves are not considered. Non-spinning reserves are considered to be 'free' and their availability effectively reduces the reserve requirements in the DUC or IIUC problem, decreasing the computational cost of solving these problems.

In conclusion, we showed the SUC formulation to yield the most cost-optimal UC schedules under uncertainty. The scenario-based representation of the uncertainty allows accounting for the full expected cost of reserve procurement and deployment, which enables internalizing the reserve sizing problem and the procurement of a cost-optimal mix of flexibility providers. Furthermore, it allows exploiting the full regulation potential of the available energy storage systems. However, the high computational burden and the sensitivity towards the considered scenarios may limit its practical applicability. In contrast, the DUC and IIUC models are easy to solve, but yield conservative UC schedules. Load shedding volumes will be low, but their failure to account for the expected deployment cost of procured reserves does not allow internalizing the reserve sizing problem or procuring a cost-optimal mix of reserve providers. This may cause excessive reserve procurement and high operational costs. In contrast, the HUC and PUC formulations, developed in this dissertation, combine a low computational effort with low load shedding volumes and low expected operational costs. Both formulations include, albeit in different ways, a coarse approximation of the expected deployment cost of procured reserves, effectively internalizing the reserve sizing problem. Nevertheless, the SUC schedules remain, in most cases, most cost-optimal, in part due to the conservative estimates of the regulation potential of the PHES system in the HUC and PUC formulation.

The presented HUC and PUC formulation can be used to assess the impact of uncertainty on reasonably large low-carbon electric power systems where SUC models would become computationally intractable. Likewise, independent system operators could use these models to optimize their UC decisions taking into account the uncertainty in their system. The PUC formulation has the additional advantage that it does not require scenario generation and reduction techniques. Moreover, many system operators are moving from point forecasts (i.e. a single forecast value at each time step) to interval or ensemble forecasts (i.e. intervals in which the realization of wind power will be contained with a certain probability). These last types of wind or solar power forecasts can be directly integrated in a PUC framework.

The presented analysis may be strengthened in the following ways. First, considering multiple sources of uncertainty and studying their interaction may

increase the added value of this work. Second, employing the presented models on multiple interconnected areas allows studying e.g. how these models allow pooling of reserves across areas, as well as the interaction of uncertainty in different areas. Moreover, the inclusion of transmission constraints, during the optimization of the UC schedule and real-time dispatch, will reveal which models ensure the feasibility of dispatching the scheduled reserves w.r.t. these grid constraints and how the computational burden associated with solving the resulting transmission-constrained UC problems evolves. Third, the dependency of the obtained results on the assumed underlying distribution could be studied, as e.g. the PUC model requires detailed knowledge of the probability of activation of each power plant offering reserves, at each time step. Fourth, the operation and planning of energy storage systems in scenario-based UC formulations merits further research. Ensuring the real-time availability of PHES-based regulation services scheduled via a UC model considering a scenario-based representation of the uncertainty proved to be challenging, and detrimental for the performance of the SUC and, to a lesser extent, the HUC formulation. A possible fix to this issue might be the inclusion of a larger set of scenarios, in which a feasible dispatch of the PHES system would be required, but of which the operational cost would not be accounted for in the objective function. Likewise, the performance of the DUC, IIUC and PUC models could be improved by reducing the conservatism of the constraints imposed on the PHES-based reserves. Fifth, dedicated decomposition methods and parallelization may significantly reduce the computational effort in solving e.g. SUC problems. Sixth, considering more scenarios in the MC ED evaluation and/or improved scenario generation techniques may reduce the width of the confidence intervals around the reported expected operational costs. Last, we have only focused on flexibility provision at the supply side. Although efficient scheduling of the flexibility available at the supply side may mitigate the impact of intermittent RES-based generation to some extent, its impact is undeniable. Exploiting flexibility available at the demand side may, in addition to a number of other advantages such an activation of the demand side could hold, further reduce the impact of the limited predictability of RES-based generation. This is the subject of the next chapter.

Chapter 6

Limitedly controllable demand response as flexibility provider

In light of the challenges that RES-based generation poses to power system operators, we have so far sought operational flexibility at the supply side. In this chapter, our focus turns to demand side management (DSM) as an arbitrage and regulation service provider. Demand side management, in the broad sense, entails all those actions aimed at modifying the electricity demand to increase customer's satisfaction and coincidentally produce the desired changes in the electric utilities load in magnitude and shape [245]. If applied correctly, DSM could come with a variety of benefits, such as, but not limited to, (1) a reduced electric power generation margin commonly used to deal with peak demands; (2) a higher operational efficiency in the generation, transmission and distribution of electric power; (3) more effective investments; (4) lower price volatility; (5) lower electricity costs and (6) a more cost-effective integration of intermittent RES-based generation [8, 246, 247]. In the scientific literature, three broad categories of DSM are identified: energy efficiency and conservation, on-site back up through local generation or storage and demand response [246]. Active demand response (ADR) is defined as 'changes in electric usage implemented directly or indirectly by end-use customers/prosumers from their current/normal consumption/injection patterns in response to certain signals' [248]. In contrast to ADR, passive demand response relates to changes in the normal consumption/injection patterns without interacting with the consumers (e.g. rolling black-outs).

In this chapter, the focus is on active demand response, for sake of brevity referred to as demand response (DR), and particularly on short-term load

shifting, with electric heating systems, leveraging the available thermal energy storage in the building structure and the domestic hot water storage tank. Such thermal energy storage facilitates modifying the electric load profile of electric heating systems by decoupling the demand for electrical and thermal power in time, which may yield substantial operational benefits on a power system level (cf. supra) [24]. The focus is on the methodology needed to adequately study the interaction between the demand side and the electricity generation system under demand response programs. A novel integrated model is presented and applied to evaluate the system value of DR-based arbitrage and regulation services. Moreover, we introduce a novel approach to account for the possibly limited controllability of demand response-based arbitrage and regulation services based on chance-constrained programming. We apply similar integrated models in [44, 43]. We briefly summarize the results of these papers in Chapter 7.

This chapter is based on the following papers:

- K. Bruninx, D. Patteeuw, E. Delarue, L. Helsen, and W. D'haeseleer, *Short-term demand response of flexible electric heating systems : the need for integrated simulations,* in EEM13, 10$^{\text{th}}$ International conference on the European Energy Market, May 27-31, 2013. Stockholm, Sweden.
- D. Patteeuw, K. Bruninx, A. Arteconi, E. Delarue, W. D'haeseleer, and L. Helsen, *Integrated modeling of active demand response with electric heating systems coupled to thermal energy storage systems,* Applied Energy, vol. 151, pp. 306–319, 2015.

The work presented in this chapter and in the publications listed above are the result of a close collaboration with D. Patteeuw, A. Arteconi and L. Helsen (Applied Mechanics and Energy Conversion, Dep. of Mechanical Engineering, KU Leuven) and G. Reynders, C. Protopapadaki and D. Saelens (Building Physics, Dep. of Civil Engineering, KU Leuven), especially with respect to the heating system, user behavior and building models and control strategies.

The numerical results (Section 6.4) and the presented model (Section 6.3) are an improved version of the results and models published in the papers above. These results and models were prepared in collaboration with Y. Dvorkin and D. S. Kirschen during a research stay at the University of Washington (Seattle, WA, USA) in the fall of 2015.

6.1 Introduction

System operators are seeking novel sources of operational flexibility to cost-effectively and reliably integrate variable and limitedly predictable electricity generation from renewable energy sources (RES). Demand response (DR) allows load to follow the RES-based generation, limiting the variability in the net load perceived by the power system [8, 249, 250]. As forecast errors are made, regulation services, i.e. controllable generation, energy storage or demand, must be procured ahead of time to ensure the system operator's ability to maintain the power system balance in real time. Demand response could provide cost-effective regulation services [8, 249, 251]. Residential consumers are however generally not willing to forfeit the foreseen end-use of the electrical energy as the benefits they perceive (e.g., a lower electricity bill) do not outweigh the drawbacks (e.g. thermal discomfort). Fortunately, a significant number of residential appliances contain some form of inherent 'energy storage'[1], which allows these loads to simultaneously be fully responsive and non-disruptive in terms of the perceived energy service, which makes them excellent candidates for DR [9]. Typical residential examples are thermostatically controlled loads (such as boilers, heat pumps, refrigerators and air conditioners), plug-in electric vehicles and deferrable loads, such as laundry machines and dish washers [9]. In this setting, thermal energy storage as a DR-enabling technology is often investigated. Arteconi et al. [24] note that a large range of thermal energy storage (TES) technologies exists and is in use for DR purposes. The built environment can even allow for thermal storage without installing specific TES [23]. Gils has identified a large potential for DR of flexible loads in Europe, mainly in countries with significant amounts of electric heating and air conditioning [252]. Although industrial DR is currently implemented in many power systems [10] and demand-side technologies are sufficiently mature to enable real-time DR control [253][2], the potential of residential DR remains to a large extent untapped [10, 11]. The adoption of residential DR is however actively pursued, as illustrated by the successful deployment of residential DR programs in e.g. the PJM system [12] and demonstration projects such as e.g. LINEAR [13, 11].

In part, this lack of adoption of residential DR programs stems from an inability to quantify the benefits for consumers and producers under DR programs [8].

[1] In the strict sense, no energy is stored. One can only shift the electrical load of these appliances in time, decoupling the energy service (e.g. heating) and the electric load of the appliance in time.

[2] Some authors contradict these statements, claiming that there are significant technical obstacles to be overcome, e.g. to transfer price signals to the consumer [254]. Most authors argue that control access to these loads could be or become very inexpensive with the advent of communication platforms [9, 25].

Model-based assessments of DR programs fail to take into account o.a. the impact of variability in the response of DR-adherent loads (see below) and in field tests it remains challenging to quantify the degree of response [255]. Often, power system models employ a simplified representation of the demand-side technology and thereby fail to capture the complex interaction between the supply and demand side, especially when storage-type customers are involved [21]. A number of so-called integrated models, with a detailed representation of the supply and demand side, have been proposed recently. However, these models (i) are typically deterministic in nature, i.e. they neglect the limited predictability of RES-based generation and the associated reserve procurement [250] and/or (ii) assume that the DR-adherent demand side technology responds deterministically to a control or price signal [249, 250]. Mathieu et al. [22] however show that DR-adherent loads can exhibit significant variability in their response to a control signal, which could have a profound effect on the value of DR for a system operator. This variability may stem from *forecast errors*, such as uncertainty on the behavior of the occupants, errors in weather forecasts and *model mismatch*, such as limited information on the state, constraints and dynamics of the DR-adherent load [256, 22, 255, 257].

In this chapter, the focus is on short-term load shifting (arbitrage) and the provision of regulation services via DR with electric heating systems, leveraging the inherent thermal storage in the building stock. The presented methodology is however more widely applicable. First, we discuss the available models in the scientific literature, and provide arguments for the use of integrated models. Second, we propose an integrated, probabilistic unit commitment (PUC, Chapter 2) and demand response model. We simultaneously consider the unit commitment (UC) scheduling problem under uncertain RES-based electricity generation, the associated reserve procurement problem and a physical model of the demand side technology. This model allows examining the operational cost savings that could result from DR-based arbitrage (i.e. load shifting) and DR-based regulation services (i.e. reserve provision). The presented model mimics power system operations assuming so-called 'direct load control' of the DR-adherent load. Although DR can be facilitated by various forms of incentive-based programs (direct load control, curtailable load) and/or price-based programs (real-time pricing, time-of-use pricing, peak pricing), each with its own opportunities and drawbacks [258], the direct load control approach allows studying the (theoretical) maximum system value that DR could hold for a system operator by avoiding all forms of market inefficiency [259]. Our approach goes beyond the state-of-the-art, combining a detailed physical demand side model [21] and a PUC model which considers the full cost of reserve procurement and deployment [41]. This PUC model significantly reduces the balancing costs associated with limitedly predictable RES-based generation compared to a DUC model, at the expense of a limited increase

in computational cost (Chapter 5). Third, we introduce chance constraints to assess the impact of variability in the response of DR-adherent loads on the attainable operational cost savings [128, 221]. Chance constraints have been used to study the impact of uncertain wind power production [260, 128, 63] and reserve procurement with uncertain demand response of thermostatically controlled loads [261, 260]. In the presented integrated model, the chance constraints are analytically reformulated as second-order conic constraints (SOCC) [128], which holds significant advantages, including scalability, accuracy and reduced computational requirements [128], over the scenario-based approach [62]. Although the reformulation used in this chapter requires the assumption that the variability in the response of the DR-adherent loads can be characterized by a normal distribution, distributionally robust chance constraints can be employed to capture other distributions [63].

Our results show that the presented integrated model adequately represents the interaction between the supply and demand side. In a case study, we show the operational cost savings that result from DR to be significant. Regardless of the availability of other flexibility providers, DR-based arbitrage reduces the total operational cost by 6% on average, across four representative weeks. The provision of reserves based on DR-adherent loads results in an additional 1 percentage point decrease in expected operational cost in this particular case study, without violating the thermal comfort constraints of the consumers providing these services or diminishing the reliability of the system. An additional analysis shows that allowing some thermal discomfort for the DR-adherent consumers may hold significant value at the system level. However, these operational cost savings, redistributed across the participating consumers, may be insufficient to compensate these consumers for the resulting thermal discomfort. Accounting for the limited controllability of DR-based arbitrage and regulation services in the day-ahead UC model shows that the attainable cost savings strongly decrease as power system operators become risk-averse. Even with near-perfect controllability of the DR-adherent load, a risk-averse system operator may see no added value in DR.

The remainder of this chapter is organized as follows. First, we review the current scientific literature w.r.t. the available modeling approaches, highlighting the need for integrated system models (Section 6.2). Second, an integrated model and a case study are introduced (Section 6.3), focusing on the modeling of DR with electric heating systems, its interactions with the electricity generation system and the chance constraints. To allow DR-adherent loads to provide regulation services, we develop a novel set of 'worst-case comfort constraints', in an approach similar to the one we have taken w.r.t. PHES-based regulation services in Chapter 2. Third, the results are discussed in Section 6.4. We focus on the attainable operational cost reductions associated with DR-based

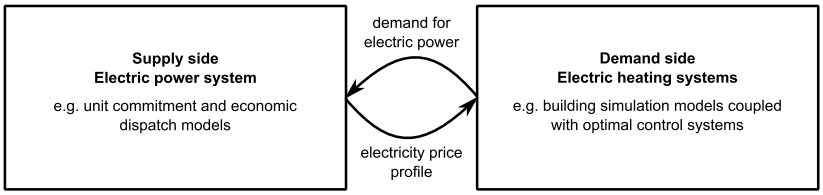

Figure 6.1: Conceptual schematic of the interaction between the supply side (i.e., the electric power system, typically represented via unit commitment and economic dispatch models) and the demand side (here electric heating systems, typically studied via building simulation models with optimal control systems).

arbitrage and regulation services. The robustness of these results is tested against the assumptions w.r.t. (1) the worst-case thermal comfort constraints and (2) the perfect controllability of DR-adherent loads. Finally, a conclusion is formulated.

6.2 The modeling challenge: a literature review[3]

In order to quantify the effects of introducing DR programs, the assessment of the interaction between supply and demand side is of paramount importance. Many models however still fail to incorporate the interactions between demand and supply in DR programs. In Fig. 6.1 a conceptual schematic of the interdependence of the demand side and the supply side (models) is shown. The electricity price profile, typically the result of a supply side model or market data, is a necessary input to the demand side model. Similarly, the demand for electric power, an output of the demand side model, is a necessary input of the supply side model. Nevertheless, even though many studies deal with, or even focus on, DR, often the supply side or the demand side are represented simplistically. When the focus is on electric power generation, most researchers employ typical UC and ED models, extended with an aggregated representation of the DR-adherent demand. Two typical representations of the flexible demand side are considered in this section: price-elasticity models [262, 19, 263, 264, 265] and so-called virtual generator models (VGMs) [266, 267, 20, 268] (Section 6.2.1). In contrast, in studies which are focused on the energy cost for the building owner,

[3]This section is based on the following paper: D. Patteeuw, K. Bruninx, A. Arteconi, E. Delarue, W. D'haeseleer, and L. Helsen, *Integrated modeling of active demand response with electric heating systems coupled to thermal energy storage systems,* Applied Energy, vol. 151, pp. 306–319, 2015. We expand the literature review presented in this publication and illustrate our findings with numerical results from this paper.

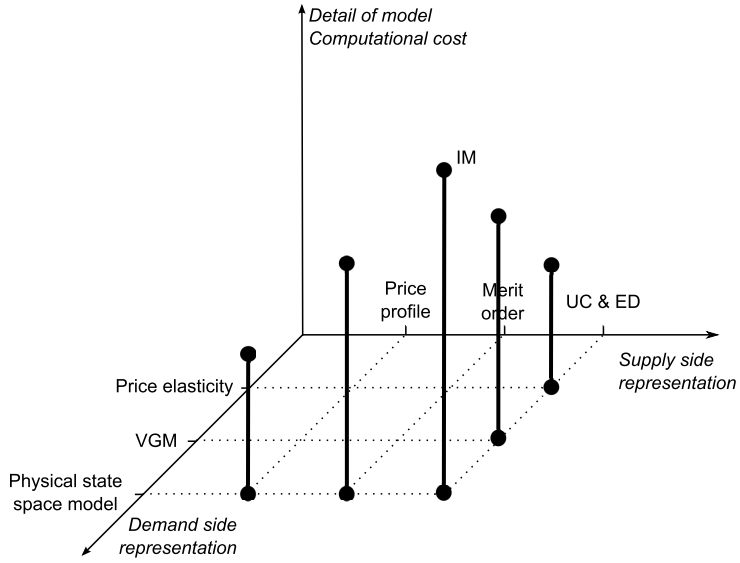

Figure 6.2: Schematic representation of selected modeling options, in order of ascending complexity and detail, in demand and supply side representations.

researchers often take the supply side of electric power system into account by considering a (fluctuating) electricity price [269, 270, 271, 272, 273, 274]. Although all of these modeling techniques have proven their merits, they are inadequate to study the true interaction between the demand side and the supply side under DR, especially when storage-type customers are involved. Recently, some authors [275, 276, 277, 278, 279, 280, 249, 25, 281] proposed integrated models of both the supply of, and demand for, electric power. We will discuss these integrated models in Section 6.2.3. The model presented in Section 6.3 falls in this last category.

Figure 6.2 shows schematically how the model detail and computational cost depend on the complexity of the supply side model and the demand side model. The integrated model, representing in detail both the supply side and the demand side, e.g. via a unit commitment and economic dispatch model and a physical state space model of the building and its heating system, is the most accurate representation, but is typically difficult to solve. Moving along the axis 'demand side representation', the latter can be represented by a VGM or by a price elasticity-based model, while the supply side is still represented via the unit commitment and economic dispatch model. Vice versa simplifying the supply side model, one can consider a so-called merit order model or an electricity price profile to simulate the supply side of the electric power system, keeping the

physical state space model for the flexible demand. In every case the resulting model is used in an optimization problem, with the purpose of minimizing the overall operational cost, at power system or building level. The models mentioned above were selected because they are often used in the scientifc literature. Note however that other models and combinations of models may exist.

In the remainder of this section, we illustrate the relevance of using such an integrated model to study DR, focusing on the interaction between the supply side and the demand side. To this end, a review of the modeling approaches found in the scientific literature is presented. We will qualitatively discuss the shortcomings of some of the approaches found in the scientific literature, and illustrate these observations with results from a methodological example considering flexible electric heating systems (heat pumps and auxiliary resistance heaters) coupled to thermal energy storage systems (the thermal mass of the building and hot water storage tanks), published in [21][4]. In the methodological example provided in this section, we will assume that the DR-adherent electric heating systems are perfectly controllable. Furthermore, no uncertainty is present in the power system at hand. In Section 6.3 and Section 6.4.1, we will gradually drop these assumptions.

6.2.1 Models with a focus on the supply side

To study electric power system-wide effects of flexible consumers, most researchers employ typical unit commitment and economic dispatch models, extended with an aggregated representation of the flexibility at the demand side. As indicated above, two main representations of the flexible demand side can be identified: price-elasticities and so-called virtual generator models (VGMs).

A price-elasticity is a measure of the change in demand in response to a change in the price of electricity. The assumed range of elasticities used in these models typically stem from analyses of historical data [19, 282], sometimes combined with a simulation model [283]. Among others, De Jonghe et al. [262, 19] develop an elasticity-based operational and investment model to determine the optimal generation mix. Sioshansi and Short [263] employ an elasticity-based model, comparable to that proposed in [19], to study the effect of real-time pricing on the usage of wind power. Kirschen and Strbac [264] propose a general scheme to incorporate a short-term price elasticity in generation scheduling and wholesale

[4]For sake of brevity, we will not repeat the specifics of this particular example, as the reported results are merely illustrative. It is however important to note that the assumptions differ from those in the case study reported in Section 6.4. For a thorough discussion of the results reported in this section, the reader is referred to [21].

electricity price setting models. Bompard et al. [265] study the effect of demand elasticity on congestion and market clearing prices via a linear price-elasticity model combined with an optimal power flow formulation.

Virtual generator models are typically used when a modeler wants to include the technical limitations of the demand side technology. The demand is modeled as an electricity generation or energy storage unit with a negative output. Demand reductions and shifts can be constrained in e.g. amount, time and ramping rate. Energy storage and possible losses can be incorporated. The constraints can be based on observations or detailed physical models. The VGM is scheduled and dispatched as a conventional power plant and therefore often used in the setting of direct load control [19]. These VGMs are used in various studies, e.g. to investigate the impact of DR on the marginal benefit for consumers [266], the effect of DR on reserve markets [267], the impact of DR in electric power systems with large wind power penetrations [20] and the benefits of demand side participation in the provision of ancillary services [268].

However, in both cases a modeler cannot assess the benefit of the studied DR scheme for the consumer based on these aggregated DR-representations. The feasibility of the resulting demand profile can be questioned, as one has no guarantee that the resulting electric power demand profile will be sufficient to ensure the required thermal comfort for each end-consumer. In addition, estimating the parameters of these demand side models may not be straightforward, as we illustrate below.

Price-elasticity models

Many studies on demand side flexibility use a price elasticity model to describe the price responsiveness of flexible customers. This elasticity is defined as

$$\epsilon_{\mathrm{u,k}} = \frac{\partial d_{\mathrm{u}}}{\partial p_{\mathrm{k}}} \cdot \frac{p_{0,\mathrm{k}}}{d_{0,\mathrm{u}}} \tag{6.1}$$

with p_{k} the price of electrical energy in hour k, and d_{u} the demand for electrical energy in hour u [266]. The index 0 indicates the initial or anchor electricity demand and price levels, i.e. the reference demand and price levels to which the elasticity will be related. If k equals u, the elasticity is referred to as the own-elasticity of the demand. Cross-elasticities ($k \neq u$) indicate the change in demand for electricity in hour u in response to a change in the price of electricity in hour k. Cross-elasticities are needed as consumers are generally not willing to solely reduce their demand, but are more likely to redistribute some of their demand, shifting it away from peak price to low price periods. For example, the redistribution of demand may yield a higher overall electricity consumption,

which cannot be captured by own-elasticities alone. Price elasticities are a powerful tool to capture the price responsiveness of many customers. However, these elasticities may not be suited to describe the responsiveness of storage-type customers when this energy storage is accompanied by losses not linearly dependent on the energy stored or on the power supplied, such as thermal systems.

When a modeler seeks to use price-elasticities to model the behavior of price-responsive consumers, he or she needs to estimate these elasticities ex-ante. This may not be a trivial task for new types of consumers, such as electric heating systems, as one might observe behavior that cannot be captured via a linear relationship between price and demand. To illustrate this, we use an integrated model, similar to the one presented in Section 6.3, to assess the mutual change of price and demand induced by the modification of the RES-based generation profile. This is equivalent to shifting the supply curve along the demand axis (Fig. 6.3). 180 RES-based generation profiles are considered (wind power profiles, obtained from the Belgian TSO, Elia, for the year 2013). Each of these profiles is scaled to represent 20% of the daily electrical energy demand. Due to a change in the RES-based generation profile, the consumers will see different electricity price levels as the supply curve changes. The thermal heating demand (i.e. the thermal comfort) remains unchanged in these simulations. The electricity reference price, as perceived by the electric heating systems, is here calculated as the marginal value of the power balance (Eq. (6.4), see below) in the integrated model.

From these simulations, one can obtain the price-demand couples for each hour in the optimization horizon. Fig. 6.3 shows the resulting price-demand couples in a particular hour in which the demand for thermal services is significant. If a price-elasticity could describe the change in demand in response to changes in the cost or price of electricity, the price-demand couples would form a straight, downward sloping line. However, as shown in Fig. 6.3, this is not the case. First, one can observe some atypical increases in demand in response to an increase in the marginal cost of electricity generation. This would correspond to a positive own-elasticity, which is uncommon in the electricity sector [19]. Second, different demand levels appear optimal for the same price level. A(n) (own) price-elasticity does not allow capturing these effects. These results show the difficulty of correctly predicting the elasticity ex-ante, needed to study DR via an elasticity-based model, when storage-type customers are involved.

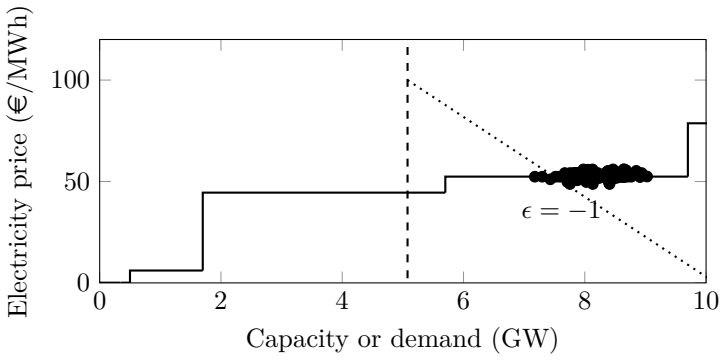

Figure 6.3: The resulting electricity price-demand couples in a particular hour, indicated by the black dots in the figure above, indicate that the price-responsiveness of thermal systems cannot be captured via an own-price elasticity. The supply curve (solid line) shown above is a simplified merit order-representation of the supply side of the electric power system. The dotted line shows a demand curve characterized by an own elasticity of -1. The dashed line indicates the inelastic part of the demand. The RES-based generation in this particular hour varied between 346 and 4,099 MW.

Virtual generator models

Alternatively, a flexible demand can be modeled through a virtual generator model. In essence, the demand is described as a generation or energy storage unit with a negative output and a set of constraints on this output. A generic representation of any energy storage unit can be formulated as follows:

$$E_j = E_{j-1} + \left(\dot{I}_j + \dot{G}_j - \dot{L}_j - \dot{D}_j\right) \cdot TP \tag{6.2}$$

The state of charge of any storage system at a certain time step j is typically modeled based on the energy content at the previous time step $j-1$ (E_{j-1}) and the withdrawal and the addition of energy during that time step j. In this equation, E_j stands for the energy content of the virtual storage unit, TP for the length of the considered time interval, $\dot{L}_j$ for the (thermal) losses of this unit, $\dot{D}_j \cdot TP$ for the energy demand (i.e. the amount of energy one extracts from the storage, the output), $\dot{I}_j$ for the power supplied to the storage and $\dot{G}_j$ for any other gains. Constraints can be imposed on each term in Eq. (6.2) to ensure that the technical constraints of the demand side technology and the comfort constraints of the consumers are respected. Again, the constraints and interaction terms, such as the loss term $\dot{L}_j$, must be quantified by the modeler ex-ante.

When this modeling approach is used to simulate a group of flexible storage-type consumers with electric heating systems, the limits on the output of the virtual generator, i.e. the electricity demand of the electric heating systems, can easily be deducted from the nameplate capacity of the electric heating systems. Other technical limitations, such as ramping limits and minimum on and off-times can be retrieved from the technical specifications of the heating systems. Constraints are also required on the size of the 'energy storage' unit, which typically consist of minimum and maximum energy limits for the storage capacity combined with a loss term or efficiency. The thermal losses, $\dot{L}_j$, and the gains, $\dot{G}_j$, in Eq. (6.2) capture the interaction of such a thermal system with its surroundings. Estimating these parameters becomes rapidly complex for thermal energy storage systems, as illustrated in [40]. Indeed, the thermal losses and gains are not only temperature and time dependent, but they are also dependent on user behavior (consumption of hot water, occupancy profiles, internal gains), weather conditions (ambient air temperature, solar heat gains) and the building structure (wall thickness, ventilation rate) [23]. For example, neglecting to model the internal and solar gains would yield a significantly lower state of charge, which in turn may result in an overestimation of the electricity demand via a VGM. Thus, in reality, this may lead to a violation of the comfort constraints on the consumers side. Time-dependent limits on the state of charge of the storage system could be used to represent the thermal comfort requirements of the occupants. Similar to the thermal losses and gains, these limits are highly dependent on the user behavior and weather conditions. In conclusion, the representation of a demand side thermal energy storage system and its interaction with the electric power system requires detailed knowledge of the state of charge, i.e. the temperatures, and disturbances imposed on that storage system. In a VGM it is necessary to estimate these interactions ex-ante, which can affect the reliability of the obtained results.

6.2.2 Models with a focus on the demand side

Thermal energy storage as a DR-enabler is often investigated as a 'pure' demand side technology. For example, Hewitt [284] studies the use of the built environment – i.e., its thermal inertia – as a TES, in the case of a heat pump delivering space heating and domestic hot water (DHW). Hewitt finds that both the building and the hot water tank are possible candidates for DR and, in order to assess the benefits for the consumers and generators under DR, he highlights the necessity of taking into account the dynamics of both the demand and supply side. However, when assessing the potential of a thermal system for DR, most authors start from a fixed electricity price profile as representation of the wholesale electricity market [269, 270, 271, 272, 273, 274] to determine the

modification of the electrical load pattern. A detailed physical model is used to represent the demand side in order to determine the electricity demand profile that yields the minimum energy cost for the customer. The authors typically conclude how much the electricity cost can be reduced for the owner of the building, but do not consider the possible feedback of the shifted electrical load pattern on the electricity price.

Based on such models, one can only draw conclusions for a single or small group of consumers. As of a certain number of consumers participating in the studied DR program, their modified behavior would start affecting the electricity price. This feedback of user behavior on the price of electricity is not taken into account in these models. Effectively, one assumes that a single consumer or a small group of consumers is exposed and reacts to e.g. a time-variant control or price signal. In this case, the resulting change in the overall demand profile is small enough to justify the assumption of a fixed price profile. The realism of this assumption may be questioned. Neglecting the feedback of the changed demand profile on the electricity price may however have a significant impact on the quality of the obtained results, as we illustrate in the following example.

State-space models with a price profile at the supply side

We use a state-space demand side model and a deterministic UC model separately in an iterative approach, as illustrated in Fig. 6.1, to study the effect of DR on a particular day. We use the UC model to obtain electricity price profiles, as a proxy of the wholesale electricity price profiles often employed in demand side-focused DR-studies. In the suggested iterative approach (see below), the UC model allows illustrating the effect of a changed demand profile on the electricity price profile and ultimately, the expected operational cost savings – an effect typically not considered in demand side-focused DR-research.

In a first iteration, the demand side model starts from a flat electricity price profile and determines the electricity demand resulting in a minimal total energy cost for the owners. This corresponds to minimizing the energy use on the demand side. The UC model considers a fixed electricity demand profile, including the demand profile of the electric heating systems determined by the demand side model in the previous iteration. Heating represents approximately 25% of the total electricity demand on this particular day. With this model, we determine the UC and ED schedule that minimizes the total operational cost for the system. The resulting price profile is then passed on to the demand side model. Iteratively, the demand side model is used to calculate a new electricity demand profile in response to this new electricity price profile, which is used as an input for the supply side model in the next iteration.

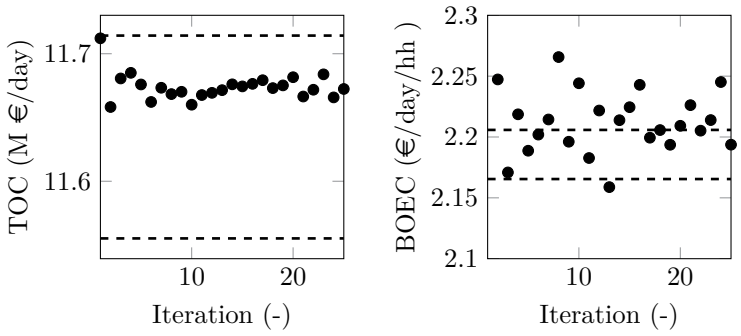

(a) Total Operational Cost (TOC)

(b) Average Building Owner Energy Cost (BOEC)

Figure 6.4: Evaluation of the total electricity production cost (TOC) and building owner energy cost (BOEC) in an interative demand-supply scheduling procedure. The supply side UC model considers a fixed demand profile, which is updated in every iteration according to a physical demand side model. The demand side model minimizes the BOEC, considering the time-variant electricity price profile that results from solving the UC model in the previous iteration. Each dot represents the TOC and BOEC respectively after an iteration. The dashed lines correspond to the TOC and BOEC obtained with an integrated model (lower limit) and a UC model in which the heating demand is not DR-adherent (upper limit).

When this iterative process was executed, it soon diverged. The demand side model tends to overreact to differences in the electricity price. This results in large peak demands, which can be higher than the available electricity generation capacity, when the electricity price is low. To avoid divergence, the changes in the electricity demand in each hour were limited to 10% of the electricity demand in the previous iteration. Note that more optimal iteration procedures may exist. Figure 6.4a shows the trajectory of the total operational cost of the electric power system. The operational costs shown in Fig. 6.4a are the total operational costs (TOC) obtained with the UC model. In the first iteration, the model yields the same result as if the electric heating systems would not adhere to any DR program. The following iterations show the reaction of the demand side model to a changing electricity price profile. The resulting decrease in operational costs is about one third of the total possible operational cost reduction due to DR as calculated with the IM (about 1.8%, to be compared with the 0.1% optimality gap imposed on the optimization). Further iterations allow attaining approximately two thirds of the total possible operational savings

(not shown in Fig. 6.4). Similarly, when looking at the costs for the building owners (BOEC or Building Owner Energy Cost - Fig. 6.4b), we note an erratic oscillation of the solution compared to the corresponding solution of the IM (dashed lines). The energy costs for the building owner (BOEC) are calculated as the demand profile of the electric heating systems times the electricity price profile used in the demand side optimization, i.e. the objective function of the demand side model. Note that, based on the demand side model results alone (Fig. 6.4b), a modeler might be led to believe that the optimal demand profile is reached. However, the total operational cost (Fig. 6.4a) obtained from the integrated UC model demonstrates that this is not the case.

In conclusion, this numerical example shows that conclusions based on models in which the supply side is represented via a (fixed) price profile are biased if changes in demand affect those electricity price profiles. This interaction can be integrated in such a modeling approach to some extent by moving to an iterative approach (see above) or by solving the demand side model and a simplified UC and ED model simultaneously. In [21], we illustrate the effectiveness of the last approach, i.e. the combination of a merit order model, a mere ranking of the different power plants in an ascending order of (average) operational production costs, and a physical model of the demand side[5]. Such a model (1) allows taking into account the effect of a change in the demand profile on the electricity price profile directly, abolishing the need for iterative procedures, (2) requires far less detail in the supply side model and (3) is less computationally intensive compared to an integrated approach. The simplifications in the supply side representation may however lead to unrealistic scheduling and dispatching of the considered power plants. Results obtained with such a simplified supply side model should thus always be interpreted with caution, e.g. via a re-evaluation of the resulting demand profile with a 'full' UC and ED model, to ensure the feasibility and cost-effectiveness of the obtained demand profile and UC schedule.

6.2.3 Integrated operational models

The literature review and the provided numerical examples show that neither a price-elasticity, nor a virtual generator model can fully describe the interaction between flexible electric heating systems and the electric power system. Furthermore, results based on a demand side model considering a fixed price profile cannot be extrapolated to calculate system-wide effects as they fail to describe the effect of changes in the demand profile on the supply side. In light

[5]One could categorize this approach as an integrated model (Section 6.2.3). However, in this dissertation we will reserve the term 'integrated model' for combinations of a physical demand side model and a UC model.

of these challenges, a number of authors have recently developed integrated models. Both the demand side and the supply side are represented by physical models and jointly optimized. A number of researchers have recently published on integrated models [275, 276, 277, 278, 279, 280], inspired by the model of Callaway [249]. They study comfort-constrained distributed heat pump management and intelligent charging of electric vehicles (1) as balancing service providers, with a particular focus on balancing wind power, (2) as a spinning reserve resource and (3) as a voltage stabilizing measure. The physical models of the heat pumps and electric vehicles are integrated in a linear programming representation of the electric power system. Hedegaard et al. [25, 281] developed an integrated model, including different types of TES and emission systems, to assess the potential of DR to balance wind power. However, some aspects of the thermal system are represented too simplistically in the model. For example, the heat pump's COP (coefficient of performance) is not temperature dependent and the solar gains are not taken into account. Dallinger and Wietschel [285] assess the potential of a fleet of electric vehicles for balancing intermittent RES-based electricity generation, representing the supply side by a simplified merit-order model.

Those integrated models incorporate in some way both the dynamic behavior of the supply side of the electric power system and the flexible electricity demand (represented by electric heating systems for the purposes of this study)[6]. Such an approach offers a number of advantages if the representation of the overall energy system is sufficiently detailed. First, the electricity demand from the thermal systems is closer to reality, as the occupants behavior is taken into account, as well as the weather conditions and the thermal behavior of the considered heating systems and dwellings. Second, all feedback effects of the redistribution of the electrical load — on demand and supply side — are represented correctly. For example, the losses (electrical and thermal) associated with load shifting can be precisely determined. Last, it ensures the end-use functionality of the demand side technology, while simultaneously guaranteeing the availability of the arbitrage and balancing services provided by DR on the supply side. However, those models are not devoid of disadvantages. First, the representation of e.g. a realistic building stock and the stochastic behavior of the occupants requires a detailed demand side model, which is difficult to set up and calibrate. Second, these models are typically difficult to solve numerically, with a high computational cost as a consequence.

The model presented in this chapter falls in this category of integrated optimization models. In terms of modeling, it improves the current state-

[6]Note that the difference between e.g. a VGM-like model and an integrated model is not strictly defined, but depends on the level of detail of the demand side representation required by the demand side technology at hand.

of-the-art by incorporating a more detailed representation of the demand side (occupant behavior, demand side technologies and thermal behavior of the dwellings) and by expanding the linear programming model of the power system to a more realistic mixed integer linear programming model. For example, Wang et al. [277] employ a three-state, one-zone state-space model to account for the thermal behavior of the buildings. In this dissertation, we represent the thermal behavior of the considered dwellings and the emissions systems via a nine-state, two-zone state-space model [286]. The two-zone structure of the model allows accounting for different comfort requirements in the day and night-zone of each dwelling [286]. The day- and night-zone are represented by five and four states respectively, which allows capturing the different thermal dynamics and time constants associated with e.g. the indoor air and the structural elements of the building. The importance of such a refinement is not to be underestimated, as, according to Wang et al. [277], '... the response (of the DR-adherent electric heating systems) directly depends on the thermal properties, the thermal time constant of the buildings in particular'. In addition, the inclusion of a physical model representing the demand side allows incorporating solar and internal gains, which form a non-negligible part of the thermal power supplied to the dwellings [21]. The more accurate representation of the supply side allows including start-up and shut-down costs and certain technical constraints with regard to the on- and off-times of the power plants. In addition, reserve procurement and deployment is considered explicitly through a state-of-the-art probabilistic UC model (Chapter 2 and 5) and demand response-adherent loads may offer regulation services. A novel set of constraints is developed to ensure the thermal comfort of the building owners providing these services. Last, the limited controllability of distributed flexibility providers such as DR-adherent load is explicitly considered via chance-constrained programming, an effect which has – to the best of our knowledge – not yet been studied in the scientific literature.

6.3 Methodology

In this section, we revisit the PUC model [41] (Chapter 2), which is extended with a physical demand side model [21]. The PUC formulation allows calculating an optimal UC schedule given an uncertain wind power forecast, the only source of uncertainty in this chapter (Chapter 1), by optimally scheduling conventional generation, energy storage and DR-adherent load. The demand-side model, representing the considered buildings and their heating systems, ensures that the thermal comfort of the occupants and the availability of hot water is guaranteed, regardless of the actual wind power production. The PUC model explicitly considers the reserve procurement and deployment cost and as such, it allows a cost-optimal trade-off between flexibility providers, including DR-adherent load.

By introducing chance constraints (Section 6.3.2), this model allows accounting for the impact of possible variability in the response of the DR-adherent demand.

The resulting UC schedule is evaluated in terms of operational cost, curtailment of the uncertain wind power production and load shedding, by running Monte-Carlo economic dispatch (ED) simulations for a set of 500 wind power scenarios per day[7]. In the dispatch simulations, a deterministic UC model is executed for each scenario individually, without any reserve requirements, with the unit commitment status set to that obtained from the PUC model and the wind power forecast replaced by the wind power scenario at hand. Fast-starting units are allowed to start-up or shut-down during dispatch if this results in a more cost-optimal dispatch[8]. The DR-adherent load is optimized given the realization of the wind power scenario, assuming perfect foresight and perfect controllability during dispatch. Scenarios are generated as described in Chapter 4, using a statistical description of the wind power forecast (error) taken from Chapter 3.

The UC and ED models are implemented in GAMS 24.2 using Mixed Integer Linear and Quadratically Constrained Programming (MILP and MIQCP). CPLEX 12.6 is used as solver. Calculations are run on the ThinKing HPC cluster of the KU Leuven, using a 2.8GHz machine with 20 cores and 64GB of RAM. The optimality gap was set to 0.5%.

6.3.1 Comfort-constrained PUC formulation

In a PUC model, the power plants are scheduled and dispatched in such a way that the overall expected operational cost over the simulated time period is minimized. The PUC model was introduced in Chapter 2. For the reader's convenience, it is briefly summarized below[9]. The total operational cost consists of fuel costs $fc_{i,j}$, start-up costs $sc_{i,j}$, ramping costs $rc_{i,j}$, CO_2-emission costs $co_2t_{i,j}$, the cost of load shedding ($TP \cdot VOLL \cdot \phi_j$, with ϕ_j the load shed and $VOLL$ the value of lost load) and the activation or deployment cost of reserves ($acsr^{+}_{i,j,l}$, $acnsr^{+}_{i,j,l}$, $acsr^{-}_{i,j,l}$, $TP \cdot VOLL \cdot \phi^{+,\mathrm{L}}_{j,l}$, see below). The objective

[7]This ensures that the width of the 95% confidence interval Δ (Chapter 4) around the expected operational cost is below 1.5% of that expected operational cost in all studied cases.

[8]Note that in the previous chapters, we did not allow fast-starting units to start-up during dispatch. In the previous chapters, our goal was to compare the quality of the different models. Here, we are investigating the system value that demand response may have. We therefore employ a model that reflects day-to-day power system operations as close as possible. This implies intra-day adaptations of the unit commitment schedule of flexible units.

[9]In this chapter, we simplify the formulation found in Chapter 2 on two fronts. First, the transmission grid and all associated constraints are not considered. Second, as we will typically set the value of curtailed RES-based generation to zero, we have excluded the associated terms in the objective function.

function reads

$$\min \sum_i \sum_j (sc_{i,j} + fc_{i,j} + co_2t_{i,j} + rc_{i,j}) \tag{6.3}$$

$$+ \sum_j TP \cdot VOLL \cdot \phi_j + \sum_j \sum_l P_l^+ \cdot TP \cdot VOLL \cdot \phi_{j,l}^{+,\mathrm{L}}$$

$$+ \sum_i \sum_j \sum_l (P_{j,l}^+ \cdot (acsr_{i,j,l}^+ + acnsr_{i,j,l}^+) + P_{j,l}^- \cdot acsr_{i,j,l}^-)$$

The start-up cost ($sc_{i,j}$), fuel cost ($fc_{i,j}$) and the CO_2-emission cost ($co_2t_{i,j}$) are dependent on the output of the power plant i (set I) on time step j (set J), the fuel used and the technology. Ramping costs are triggered by changes in output of the power plant. The operational cost under forecast conditions (first and second term in Eq. (2.160)) is complemented with the reserve activation costs (third and fourth term in Eq. (2.160)). These activation costs are dependent on the probability of activation of the reserve level l (set L) (upward: $P_{j,l}^+$, downward: $P_{j,l}^-$) and the operational costs associated with each flexibility option (spinning reserves $acsr_{i,j,l}^+$ and $acsr_{i,j,l}^-$, non-spinning reserves $acnsr_{i,j,l}^+$ or load-shedding $TP \cdot VOLL \cdot \phi_{j,l}^{+,\mathrm{L}}$) scheduled to provide the reserves in this level. Spinning reserves result in fuel and CO_2-emission costs. The activation cost of non-spinning reserves ($acnsr_{i,j,l}^+$) additionally contains start-up costs. Activating upward reserves will always result in an operational cost increase ($acsr_{i,j,l}^+, acnsr_{i,j,l}^+ \geq 0$). Downward reserves may however trigger cost reductions ($acsr_{i,j,l}^-$), as fuel is saved if conventional generation is replaced by an unexpected increase in RES-based generation. The activation cost of curtailment (downward flexibility) is assumed to be zero, while load shedding (upward flexibility) is penalized at the value of lost load $VOLL$ (third term in Eq. (2.160)). Activating PHES- and DR-based reserves do not result in explicit costs, but ensuring their availability increases the cost under forecast conditions. For example, for a PHES system to provide upward reserves, the state of charge should be sufficient to allow the deployment of these reserves, effectively increasing the amount of charging and/or decreasing the amount of discharging under forecast conditions (Chapter 2).

This optimization is subjected to a number of constraints. First, the supply and demand for electricity must be equal at all time steps j. The power balance condition reads:

$$\forall j: \quad D_j + d_j^{\mathrm{H}} - \phi_j = \sum_i g_{i,j} + G_j^{\mathrm{MR}} + G_j^{\mathrm{F}} - \chi_j + \sum_r \left(g_{r,j}^{\mathrm{T}} - g_{r,j}^{\mathrm{P}}\right) \tag{6.4}$$

The demand for electric power $D_j + d_j^{\mathrm{H}}$ must be met by (1) electricity generated from dispatchable power plants $g_{i,j}$; (2) must-run generation G_j^{MR}; (3) the

uncertain wind power forecast G_j^{F}, which can be curtailed (χ_j); (4) the net injection of power from PHES systems $\sum_r \left(g_{r,j}^{\mathrm{T}} - g_{r,j}^{\mathrm{P}}\right)$ and (5) the shedding of load ϕ_j.

The first part of the demand D_j, i.e. the total demand for electric power except the electricity demand associated with DR-adherent residential electric heating systems, on each time step j is assumed to be known and fixed. The second part of the demand, i.e. the DR-adherent demand of the heating systems d_j^{H}, is determined via an explicit, integrated demand-side model. NB_h buildings of type h (set H) are considered, each of which is equipped with a heat pump (HP) and auxiliary heater (A) to provide space heating (SH) and hot water (HW):

$$\forall j: \quad d_{\mathrm{j}}^{\mathrm{H}} = \sum_{\mathrm{h}} NB_h \cdot \left(p_{\mathrm{h,j}}^{\mathrm{HP}} + p_{\mathrm{h,j}}^{\mathrm{A}}\right) \tag{6.5}$$

$$\forall h, \forall j: \quad 0 \leq p_{\mathrm{h,j}}^{\mathrm{HP}} = p_{\mathrm{h,j}}^{\mathrm{HP,SH}} + p_{\mathrm{h,j}}^{\mathrm{HP,HW}} \leq \overline{P_{\mathrm{h}}^{\mathrm{HP}}} \tag{6.6}$$

$$\forall h, \forall j: \quad 0 \leq p_{\mathrm{h,j}}^{\mathrm{A}} = p_{\mathrm{h,j}}^{\mathrm{A,SH}} + p_{\mathrm{h,j}}^{\mathrm{A,HW}} \leq \overline{P_{\mathrm{h}}^{\mathrm{A}}} \tag{6.7}$$

$$\forall h, \forall j: \quad p_{\mathrm{h,j}}^{\mathrm{HP,SH}},\ p_{\mathrm{h,j}}^{\mathrm{HP,HW}},\ p_{\mathrm{h,j}}^{\mathrm{A,SH}},\ p_{\mathrm{h,j}}^{\mathrm{A,HW}} \geq 0 \tag{6.8}$$

The electric power consumption of each heat pump h ($p_{\mathrm{h,j}}^{\mathrm{HP}}$) and the auxiliary heater h ($p_{\mathrm{h,j}}^{\mathrm{A}}$) is restricted to the capacity of the heat pump ($\overline{P_{\mathrm{h}}^{\mathrm{HP}}}$) or auxiliary heater ($\overline{P_{\mathrm{h}}^{\mathrm{A}}}$) respectively and is split in the consumption for space heating ($p_{\mathrm{h,j}}^{\mathrm{A,SH}}$, $p_{\mathrm{h,j}}^{\mathrm{HP,SH}}$) and hot water production ($p_{\mathrm{h,j}}^{\mathrm{A,HW}}$, $p_{\mathrm{h,j}}^{\mathrm{HP,HW}}$). Electric power is converted to thermal power via the so-called coefficient of performance (COP) of the heat pump ($COP_{\mathrm{h}}^{\mathrm{SH}}$)[10] and is split in thermal power supplied to the day ($\dot{q}_{\mathrm{h,j}}^{\mathrm{DZ,SH}}$) or night zone ($\dot{q}_{\mathrm{h,j}}^{\mathrm{NZ,SH}}$) of building h:

$$\forall h, \forall j: \quad \dot{q}_{\mathrm{h,j}}^{\mathrm{DZ,SH}} + \dot{q}_{\mathrm{h,j}}^{\mathrm{NZ,SH}} = COP_{\mathrm{h}}^{\mathrm{SH}} \cdot p_{\mathrm{h,j}}^{\mathrm{HP,SH}} + p_{\mathrm{h,j}}^{\mathrm{A,SH}} \tag{6.9}$$

$$\forall h, \forall j: \quad \dot{q}_{\mathrm{h,j}}^{\mathrm{DZ,SH}},\ \dot{q}_{\mathrm{h,j}}^{\mathrm{NZ,SH}} \geq 0 \tag{6.10}$$

Note that we assume a one-to-one conversion of electric power to thermal power in the auxiliary heater. The thermal behavior of the building is described by a linear state-space model ($A_{h,p}$, $B_{h,p}^{\mathrm{DZ}}$, $B_{h,p}^{\mathrm{NZ}}$) (for details, see [287, 286]):

$$\forall h, \forall p, \forall j: \quad t_{h,p,j}^{\mathrm{SH}} = A_{h,p} \cdot t_{h,p,j-1}^{\mathrm{SH}} + B_{\mathrm{h,p}}^{\mathrm{DZ}} \cdot \dot{q}_{\mathrm{h,j}}^{\mathrm{DZ,SH}} + B_{\mathrm{h,p}}^{\mathrm{NZ}} \cdot \dot{q}_{\mathrm{h,j}}^{\mathrm{NZ,SH}} + E_{h,p,j}^{\mathrm{SH}} \tag{6.11}$$

[10] The procedure to determine the COP of the heat pumps is discussed in Section 6.3.3.

$$\forall h, \forall p, \forall j: \quad \underline{T^{\mathrm{SH}}_{h,p,j}} \leq t^{\mathrm{SH}}_{\mathrm{h,p,j}} \leq \overline{T^{\mathrm{SH}}_{h,p,j}} \tag{6.12}$$

This set of linear equations describes the evolution of the temperature in each state p (set P) over time ($t^{\mathrm{SH}}_{h,p,j}$) as a function of the supplied thermal power ($\dot{q}^{\mathrm{DZ,SH}}_{\mathrm{h,j}}$, $\dot{q}^{\mathrm{NZ,SH}}_{\mathrm{h,j}}$) and external disturbances $E^{\mathrm{SH}}_{h,p,j}$, such as solar gains or the thermal losses to the surroundings. The state space matrices $A_{h,p}$, $B^{\mathrm{DZ}}_{\mathrm{h,p}}$ and $B^{\mathrm{NZ}}_{\mathrm{h,p}}$ make up a linear model describing the thermal conductances and capacities in the heating system and the building, along with linear approximations of the convective and radiative heat transfer coefficients. Constraint (6.12) ensures that the temperature remains within predefined bounds, i.e. that the thermal comfort of the occupants w.r.t. space heating is guaranteed.

Similarly, the temperature of the water in the hot water storage tank $t^{\mathrm{HW}}_{\mathrm{h,j}}$ is determined as follows [287]:

$$\begin{aligned} \forall h, \forall j: \quad t^{\mathrm{HW}}_{\mathrm{h,j}} &= t^{\mathrm{HW}}_{\mathrm{h,j-1}} - G_h \cdot \left(t^{\mathrm{HW}}_{\mathrm{h,j}} - T^{\mathrm{E}}\right) \\ &\quad + C_h \cdot \left(COP^{\mathrm{HW}}_{\mathrm{h}} \cdot p^{\mathrm{HP,HW}}_{\mathrm{h,j}} + p^{\mathrm{A,HW}}_{\mathrm{h,j}} - \dot{Q}^{\mathrm{D}}_{\mathrm{h,j}}\right) \end{aligned} \tag{6.13}$$

$$\forall h, \forall j: \quad \underline{T^{\mathrm{HW}}_{\mathrm{h,j}}} \leq t^{\mathrm{HW}}_{\mathrm{h,j}} \leq \overline{T^{\mathrm{HP}}_{\mathrm{h}}} \tag{6.14}$$

The evolution of the water temperature in the storage tank $t^{\mathrm{HW}}_{\mathrm{h,j}}$ is dependent on (1) the losses to the surroundings, governed by G_{h}, the thermal resistance of the storage tank and the temperature of the surroundings T^{E}, and (2) the thermal power supplied to the hot water storage tank. C_h is the thermal capacity of the storage tank. $\dot{Q}^{\mathrm{D}}_{\mathrm{h,j}}$ represents the withdrawal of thermal power due to hot water consumption and follows a predefined profile. Constraint (6.14) ensures the availability of hot water at a minimum temperature $\underline{T^{\mathrm{HW}}_{\mathrm{h,j}}}$ and limits the hot water temperature to the maximum supply temperature of the heat pump $\overline{T^{\mathrm{HP}}_{\mathrm{h}}}$. By controlling temperature set-points $t^{\mathrm{HW}}_{\mathrm{h,j}}$ and $t^{\mathrm{SH}}_{h,p,j}$, load shifting can be realized without violating the thermal comfort requirements of the consumers w.r.t. space heating and the availability of hot water (Eq. (6.12) and Eq. (6.14)).

Second, the power plants have several technical constraints, such as a minimum and maximum output level, minimum up and down times and ramping rates, different per fuel and technology. Third, the PHES systems are included in the model via the energy balance of the PHES. The net output of the PHES system ($g^{\mathrm{T}}_{r,j} - g^{\mathrm{P}}_{r,j}$) can be positive (discharging, $g^{\mathrm{T}}_{r,j}$) or negative (charging, $g^{\mathrm{P}}_{r,j}$) and is constrained to the capacity of the PHES system. The energy content of the PHES unit is limited to a minimum and maximum level. The corresponding constraints, describing the technical limits of the power plants

and PHES systems, are identical to those enforced in the original PUC model (Chapter 2). For sake of brevity, they are not repeated here.

Last, reserve requirements are introduced. The upward and downward reserve requirements are split in L levels, each of which correspond to a specific activation probability (upward $P^{+}_{j,l}$ or downward $P^{-}_{j,l}$):

$$\forall j, \forall l: \; D^{+}_{j,l} = \sum_{i} \left(r^{+,\mathrm{L}}_{i,j,l} + nsr^{+,\mathrm{L}}_{i,j,l} \right) + r^{\mathrm{P},+,\mathrm{L}}_{j,l} + r^{\mathrm{T},+,\mathrm{L}}_{j,l} + \chi^{+,\mathrm{L}}_{j,l} + \phi^{+,\mathrm{L}}_{j,l} + \sum_{h} NB_h \cdot r^{\mathrm{H},+}_{h,j,l} \tag{6.15}$$

$$\forall j, \forall l: \; D^{-}_{j,l} = \sum_{i} r^{-,\mathrm{L}}_{i,j,l} + \chi^{-,\mathrm{L}}_{j,l} + r^{\mathrm{P},-,\mathrm{L}}_{j,l} + r^{\mathrm{T},-,\mathrm{L}}_{j,l} + \sum_{h} NB_h \cdot r^{\mathrm{H},-}_{h,j,l} \tag{6.16}$$

Additional load shedding ($\phi^{+,\mathrm{L}}_{j,l}$) and curtailment of RES-based generation ($\chi^{-,\mathrm{L}}_{j,l}$ and $\chi^{+,\mathrm{L}}_{j,l}$) are explicitly considered as flexibility options. Upward RES-based reserves are constrained to the 'scheduled' curtailment, i.e. curtailment of the forecasted wind power, while downward RES-based reserves correspond to the additional curtailment of positive forecast errors (Chapter 2). Conventional spinning ($r^{+,\mathrm{L}}_{i,j,l}$, $r^{-,\mathrm{L}}_{i,j,l}$) and non-spinning reserves ($nsr^{+,\mathrm{L}}_{i,j,l}$) are constrained to the available ramping capacity and minimum/maximum stable operating point of generator i. Similarly, we assign the PHES-based reserves ($r^{\mathrm{P},+,\mathrm{L}}_{j,l}$, $r^{\mathrm{T},+,\mathrm{L}}_{j,l}$, $r^{\mathrm{P},-,\mathrm{L}}_{j,l}$, $r^{\mathrm{T},-,\mathrm{L}}_{j,l}$), restricted to the capacity and scheduled output of the PHES system, to one or more reserve levels l (Chapter 2). The feasibility of the activation of the PHES-based reserves is guaranteed by including a 'worst-case reserve activation evaluation'. In such a worst-case evaluation, all scheduled upward or downward PHES-based reserves are deployed. By enforcing constraints on the energy storage level under these worst-case conditions, the feasibility of the deployment of the scheduled reserves in real time is guaranteed (Chapter 2). Recall that PHES-based reserves may be scheduled at no explicit cost, but that the worst-case feasibility conditions must always be satisfied. Similarly, DR-based reserves ($r^{\mathrm{H},+}_{h,j,l}$, $r^{\mathrm{H},-}_{h,j,l}$) are bound by technical and 'worst-case' comfort constraints. First, the DR-based reserves are limited to the scheduled consumption of the electric heating systems and the capacity of the

heating systems:

$$\forall h, \forall j: \quad \sum_{l} r_{h,j,l}^{\mathrm{H},+} = r_{h,j}^{\mathrm{HP,SH},+} + r_{h,j}^{\mathrm{HP,HW},+} + r_{h,j}^{\mathrm{A,SH},+} + r_{h,j}^{\mathrm{A,HW},+} \tag{6.17}$$

$$\forall h, \forall j: \quad \sum_{l} r_{h,j,l}^{\mathrm{H},-} = r_{h,j}^{\mathrm{HP,SH},-} + r_{h,j}^{\mathrm{HP,HW},-} + r_{h,j}^{\mathrm{A,SH},-} + r_{h,j}^{\mathrm{A,HW},-} \tag{6.18}$$

$$\forall h, \forall j: \quad 0 \leq p_{\mathrm{h,j}}^{\mathrm{HP}} + r_{\mathrm{h,j}}^{\mathrm{HP,SH},-} + r_{\mathrm{h,j}}^{\mathrm{HP,HW},-} \leq \overline{P_{\mathrm{h}}^{\mathrm{HP}}} \tag{6.19}$$

$$\forall h, \forall j: \quad 0 \leq p_{\mathrm{h,j}}^{\mathrm{A}} + r_{\mathrm{h,j}}^{\mathrm{A,SH},-} + r_{\mathrm{h,j}}^{\mathrm{A,HW},-} \leq \overline{P_{\mathrm{h}}^{\mathrm{A}}} \tag{6.20}$$

$$\forall h, \forall j: \quad 0 \leq r_{\mathrm{h,j}}^{\mathrm{HP,SH},+} \leq p_{\mathrm{h,j}}^{\mathrm{HP,SH}} \tag{6.21}$$

$$\forall h, \forall j: \quad 0 \leq r_{\mathrm{h,j}}^{\mathrm{A,SH},+} \leq p_{\mathrm{h,j}}^{\mathrm{A,SH}} \tag{6.22}$$

$$\forall h, \forall j: \quad 0 \leq r_{\mathrm{h,j}}^{\mathrm{HP,HW},+} \leq p_{\mathrm{h,j}}^{\mathrm{HP,HW}} \tag{6.23}$$

$$\forall h, \forall j: \quad 0 \leq r_{\mathrm{h,j}}^{\mathrm{A,HW},+} \leq p_{\mathrm{h,j}}^{\mathrm{A,HW}} \tag{6.24}$$

$$\forall h, \forall j: \quad r_{h,j}^{\mathrm{HP,SH},-},\ r_{h,j}^{\mathrm{HP,HW},-},\ r_{h,j}^{\mathrm{A,SH},-},\ r_{h,j}^{\mathrm{A,HW},-} \geq 0 \tag{6.25}$$

Second, reserves offered by the DR-adherent load should only be scheduled if their deployment would not result in the violation of the comfort constraints (Eq. (6.12) and (6.14)). To ensure thermal comfort upon activation of these reserves, we calculate the thermal power supplied to the day and night zone ($\dot{q}_{\mathrm{h,j}}^{\mathrm{DZ,SH},+}$, $\dot{q}_{\mathrm{h,j}}^{\mathrm{NZ,SH},+}$, $\dot{q}_{\mathrm{h,j}}^{\mathrm{DZ,SH},-}$, $\dot{q}_{\mathrm{h,j}}^{\mathrm{NZ,SH},-}$) if these reserves would be activated in one direction:

$$\begin{aligned} \forall h, \forall j: \quad \dot{q}_{\mathrm{h,j}}^{\mathrm{DZ,SH},+} + \dot{q}_{\mathrm{h,j}}^{\mathrm{NZ,SH},+} &= p_{\mathrm{h,j}}^{\mathrm{A,SH}} - r_{\mathrm{h,j}}^{\mathrm{A,SH},+} \\ &\quad + COP_{\mathrm{h}}^{\mathrm{HP,SH}} \cdot \left(p_{\mathrm{h,j}}^{\mathrm{HP,SH}} - r_{\mathrm{h,j}}^{\mathrm{HP,SH},+} \right) \end{aligned} \tag{6.26}$$

$$\begin{aligned} \forall h, \forall j: \quad \dot{q}_{\mathrm{h,j}}^{\mathrm{DZ,SH},-} + \dot{q}_{\mathrm{h,j}}^{\mathrm{NZ,SH},-} &= p_{\mathrm{h,j}}^{\mathrm{A,SH}} + r_{\mathrm{h,j}}^{\mathrm{A,SH},-} \\ &\quad + COP_{\mathrm{h}}^{\mathrm{HP,SH}} \cdot \left(p_{\mathrm{h,j}}^{\mathrm{HP,SH}} + r_{\mathrm{h,j}}^{\mathrm{HP,SH},-} \right) \end{aligned} \tag{6.27}$$

$$\forall h, \forall j: \quad \dot{q}_{\mathrm{h,j}}^{\mathrm{DZ,SH},+},\ \dot{q}_{\mathrm{h,j}}^{\mathrm{NZ,SH},+},\ \dot{q}_{\mathrm{h,j}}^{\mathrm{DZ,SH},-},\ \dot{q}_{\mathrm{h,j}}^{\mathrm{NZ,SH},-} \geq 0 \tag{6.28}$$

This allows calculating the impact of sequentially deploying all upward or downward DR-based reserves on the temperature in each building via Eq.

(6.11), similar to the worst-case feasibility evaluation of the PHES-based reserves. By constraining the resulting 'worst-case' temperatures to the interval $[\underline{T^{\mathrm{SH}}_{h,p,j}}, \overline{T^{\mathrm{SH}}_{h,p,j}}]$ (Eq. (6.12)), thermal comfort is ensured even if all scheduled upward or downward reserves would be deployed in real time. For example, for the worst-case scenario in which all DR-based upward reserves were to be deployed:

$$\forall h, \forall p, \forall j: \quad t^{\mathrm{SH},+}_{h,p,j} = A_{h,p} \cdot t^{\mathrm{SH},+}_{h,p,j-1} + B^{DZ}_{h,p} \cdot \dot{q}^{\mathrm{DZ,SH},+}_{\mathrm{h,j}} + B^{NZ}_{h,p} \cdot \dot{q}^{\mathrm{NZ,SH},+}_{\mathrm{h,j}} + E^{\mathrm{SH}}_{h,p,j} \tag{6.29}$$

$$\forall h, \forall p, \forall j: \quad \underline{T^{\mathrm{SH}}_{\mathrm{h,p,j}}} - \underline{\Delta T^{\mathrm{SH}}_{\mathrm{h,p,j}}} \leq t^{\mathrm{SH},+}_{\mathrm{h,p,j}} \tag{6.30}$$

in which $t^{\mathrm{SH},+}_{\mathrm{h,p,j}}$ is the temperature under worst-case upward activation conditions, constrained by the lower temperature bound $\underline{T^{\mathrm{SH}}_{h,p,j}}$. The parameter $\underline{\Delta T^{\mathrm{SH}}_{\mathrm{h,p,j}}}$ may be used to relax the conservatism of the constraints above (see further). Similarly, upon activation of all downward reserves, the maximum temperature limit should be respected:

$$\forall h, \forall p, \forall j: \quad t^{\mathrm{SH},-}_{h,p,j} = A_{h,p} \cdot t^{\mathrm{SH},-}_{h,p,j-1} + B^{DZ}_{h,p} \cdot \dot{q}^{\mathrm{DZ,SH},-}_{\mathrm{h,j}} + B^{NZ}_{h,p} \cdot \dot{q}^{\mathrm{NZ,SH},-}_{\mathrm{h,j}} + E^{\mathrm{SH}}_{h,p,j} \tag{6.31}$$

$$\forall h, \forall p, \forall j: \quad t^{\mathrm{SH},-}_{\mathrm{h,p,j}} \leq \overline{T^{\mathrm{SH}}_{\mathrm{h,p,j}}} + \overline{\Delta T^{\mathrm{SH}}_{\mathrm{h,p,j}}} \tag{6.32}$$

Additionally, one needs to enforce worst-case comfort constraints on the temperature of the water in the hot water storage tank by duplicating Eq. (6.13)-(6.14) in a worst-case reserve deployment scenario. If one neglects the impact of a change in the temperature of the water in the storage vessel on the thermal losses to the surroundings, these worst-case evaluations simplify to the following two constraints:

$$\forall h, \forall j: \quad t^{\mathrm{HW}}_{\mathrm{h,j}} - \sum_{j^*=1}^{j} C_h \cdot \left(COP^{\mathrm{HP,HW}}_{\mathrm{h,j^*}} \cdot r^{\mathrm{HP,HW},+}_{\mathrm{h,j^*}} + r^{\mathrm{A,HW},+}_{\mathrm{h,j^*}} \right) \geq \underline{T^{\mathrm{HW}}_{\mathrm{h,j}}} \tag{6.33}$$

$$\forall h, \forall j: \quad t^{\mathrm{HW}}_{\mathrm{h,j}} + \sum_{j^*=1}^{j} C_h \cdot \left(COP^{\mathrm{HP,HW}}_{\mathrm{h}} \cdot r^{\mathrm{HP,HW},-}_{\mathrm{h,j^*}} + r^{\mathrm{A,HW},-}_{\mathrm{h,j^*}} \right) \leq \overline{T^{\mathrm{HP}}_{\mathrm{h}}} \tag{6.34}$$

This approximation is sufficient, as G_{h} is a small number. Moreover, as the thermal losses to the surroundings are proportional to the temperature difference

$t_{\mathrm{h,j}}^{\mathrm{HW}} - T^{\mathrm{E}}$, we will (1) overestimate the impact of deploying upward reserves and (2) underestimate the impact of deploying downward reserves on the temperature. The lower temperature bound $\underline{T_{\mathrm{h,j}}^{\mathrm{HW}}}$ will thus in all cases be respected and all scheduled upward reserves may be deployed in real time without loss of comfort. The deployment of downward reserves may be limited due to supply temperature limits of the heat pump ($\overline{T_{\mathrm{h}}^{\mathrm{HP}}}$), which may result in a small increase in curtailment of RES-based generation in real time.

Demand response-based reserves, like PHES-based reserves, may be scheduled at no explicit cost to the system operator. However, through the worst-case comfort constraints above, the demand of the electric heating systems will have to be increased or decreased under forecast conditions to ensure feasibility upon activation. These changes in demand will trigger different operational costs, and hence impact the objective of the integrated PUC model.

Although constraints Eq. (6.26)-(6.34) result in a conservative scheduling of the DR-based regulation services, they do ensure that the scheduled reserves can be deployed without loss of comfort. To exploit additional regulation services provided the heating systems at hand, one could (1) loosen the temperature bounds imposed in the worst-case evaluations, as illustrated above via the parameters $\overline{\Delta T_{\mathrm{h,p,j}}^{\mathrm{SH}}}$ and $\underline{\Delta T_{\mathrm{h,p,j}}^{\mathrm{SH}}}$ and/or (2) allow some discomfort, i.e. violations of the temperature band $[\underline{T_{h,p,j}^{\mathrm{SH}}}, \overline{T_{h,p,j}^{\mathrm{SH}}}]$ under 'worst-case' conditions, penalized in the objective function at a so-called price or cost of discomfort [288, 289]. In Section 6.4 we explore the impact of relaxing the temperature bounds in the worst-case evaluation during UC scheduling, but we do not consider a discomfort cost to avoid unwanted interactions with the cost of load shedding. We will study the impact of relaxing the worst-case constraint in the UC scheduling problem via the parameters $\overline{\Delta T_{\mathrm{h,p,j}}^{\mathrm{SH}}}$ and $\underline{\Delta T_{\mathrm{h,p,j}}^{\mathrm{SH}}}$ (see Eq. (6.30)). In our case study, we set $\overline{\Delta T_{\mathrm{h,p,j}}^{\mathrm{SH}}}$ and $\underline{\Delta T_{\mathrm{h,p,j}}^{\mathrm{SH}}}$ equal for all time steps, all states and all building types equal to a single value ΔT. In essence, this parameter allows the thermal comfort boundaries under worst-case conditions to be violated by ΔT degrees Kelvin at each time step. Note that the comfort constraints under forecast conditions (Eq. (6.12)) are unchanged. Thermal discomfort caused by extreme forms of DR-based arbitrage is thus not allowed. During the MC ED simulations, the original temperature bounds are imposed on the optimization and the thermal discomfort is minimized by penalizing the thermal discomfort at a high cost in the objective function (Section 6.4.3). Load shedding is not allowed in these dispatch simulations. As such, all reserve inadequacies need to be solved by violating the thermal comfort requirements. For example, if insufficient upward reserves are available, reducing the load (reducing the temperature below the comfort constraint) is the 'last-resort' flexibility option

to maintain the power system balance. In the results reported in Section 6.4.3, we will however not include the cost of thermal discomfort. By comparing these expected operational cost-estimates with the expected operational cost obtained from simulations in which thermal discomfort was not allowed during UC scheduling ($\Delta T = 0$), we obtain estimates for the system value of thermal discomfort (see Section 6.4.3). Note that we only allow thermal discomfort w.r.t. to space heating, not in the hot water production, as the perceived discomfort cost would be extremely high.

6.3.2 Accounting for variability in the response of DR-adherent loads via chance-constrained programming

The model above allows optimizing conventional generation, energy storage systems and DR-adherent demand, but assumes that all components of the system are equally controllable. Although generators and large-scale energy storage systems show some variability in their response to a control signal of e.g. a system operator [290], this variability may be expected to be significantly lower than that of DR-adherent demand or regulation services [22]. Therefore, we introduce chance constraints to account for the possible variability in the response of DR-adherent loads to a control or price signal. We will focus on the aggregated effect of limited controllability of DR-adherent loads and will not attempt to pinpoint the different sources or the degree of variability in the response.

The deterministic decision variables d_j^{H}, $\sum_h NB_h \cdot r_{h,j,l}^{\mathrm{H},+}$ and $\sum_h NB_h \cdot r_{h,j,l}^{\mathrm{H},-}$ become stochastic decision variables, indicated with a tilde (e.g. $\widetilde{d_j^{\mathrm{H}}}$) below. Separating the variability in their response in a proportional δ^{P} and non-proportional component δ^{NP}, the limitedly controllable DR-adherent demand and regulation services can be expressed as

$$\forall j: \quad \widetilde{d_j^{\mathrm{H}}} = (1 + \delta^{\mathrm{P}}) \cdot d_j^{\mathrm{H}} + \delta^{\mathrm{NP}} \tag{6.35}$$

$$\forall j, \forall l: \quad \sum_h \widetilde{NB_h \cdot r_{h,j,l}^{\mathrm{H},+}} = (1 - \delta^{\mathrm{P}}) \cdot \sum_h NB_h \cdot r_{h,j,l}^{\mathrm{H},+} - \delta^{\mathrm{NP}} \tag{6.36}$$

$$\forall j, \forall l: \quad \sum_h \widetilde{NB_h \cdot r_{h,j,l}^{\mathrm{H},-}} = (1 - \delta^{\mathrm{P}}) \cdot \sum_h NB_h \cdot r_{h,j,l}^{\mathrm{H},-} - \delta^{\mathrm{NP}} \tag{6.37}$$

with δ^{NP} and δ^{P} stochastic parameters that follow a certain distribution. The power balance (6.4) and reserve requirements (6.15)-(6.16) are reformulated as

chance constraints:

$$Pr\Bigg(\forall j:\ D_j + \widetilde{d_j^{\mathrm{H}}} - \phi_j \leq \sum_i g_{i,j} + G_j^{\mathrm{F}} - \chi_j + \sum_r \left(g_{r,j}^{\mathrm{T}} - g_{r,j}^{\mathrm{P}}\right)\Bigg) \geq 1-\epsilon \tag{6.38}$$

$$Pr\Bigg(\forall j,\forall l:\ D_{j,l}^{+} \leq \sum_i \left(r_{i,j,l}^{+,\mathrm{L}} + nsr_{i,j,l}^{+,\mathrm{L}}\right) + r_{j,l}^{\mathrm{P},+,\mathrm{L}} + r_{j,l}^{\mathrm{T},+,\mathrm{L}} + \chi_{j,l}^{+,\mathrm{L}} + \phi_{j,l}^{+,\mathrm{L}} + \sum_h \widetilde{nb_h \cdot r_{h,j,l}^{\mathrm{H},+}}\Bigg) \geq 1-\epsilon \tag{6.39}$$

$$Pr\Bigg(\forall j,\forall l:\ D_{j,l}^{-} \leq \sum_i r_{i,j,l}^{-,\mathrm{L}} + \chi_{j,l}^{-,\mathrm{L}} + r_{j,l}^{\mathrm{P},-,\mathrm{L}} + r_{j,l}^{\mathrm{T},-,\mathrm{L}} + \sum_h \widetilde{nb_h \cdot r_{h,j,l}^{\mathrm{H},-}}\Bigg) \geq 1-\epsilon \tag{6.40}$$

Constraint (6.38) ensures that the scheduled generation exceeds the demand with a probability (operator Pr) of $1-\epsilon$. Similarly, Eq. (6.39)-(6.40) ensure that the reserve requirements are satisfied with a probability of 1-ϵ. ϵ is a small number, i.e. the probability that the constraints above are violated.

For any distribution, these constraints can be enforced in a scenario-based approach [62]. In this particular case however, the variability in the demand response has many, assumed independent contributions. Via the Central Limit Theorem, the assumption that δ^P and δ^{NP} follow a normal distribution can be justified. This allows analytically reformulating the problem as a MIQCP or MILP, which can be solved directly with the off-the-shelf commercial solvers, such as CPLEX or Gurobi [63]. The reformulated problem is identical to the original problem, instead of an approximation of the original problem as in the scenario-based approach. For more information on the reformulation, see Appendix E.

6.3.3 Case study

The simulations are run for a power system inspired by the Belgian power system, assuming a 50% wind power penetration (annually, energy basis). The demand

profile at transmission level D_j (2011) and wind power data (2012–2013) are obtained from Elia, the Belgian TSO [87]. The Belgian conventional generation system, consisting of 71 power plants and combined-heat-and-power plants, in total 13,920 MW of dispatchable capacity, has been taken from Elia [87]. The conventional generation system is identical to the power system studied in the previous chapters (Appendix B), with the following exceptions: (1) eight state-of-the-art 450 MW combined cycle gas turbines were added to the system to meet the increased demand for electricity due to the electrification of heating; (2) nuclear power plants are assumed to be inflexible, with a minimum power output of 95% of their nominal capacity. Open cycle gas turbines and oil-fired units with a size of less than 100 MW, a minimum up- and down time of 1 time step and the capability to ramp from zero output to full capacity within a time step are considered as 'fast-starting units'. In total 35 fast-starting units (in total 1,118 MW) are considered in this case study. One PHES system has been included, with a maximum capacity of 1,308 MW, a round-trip efficiency of 75% and a storage capacity of 3,924 MWh. The CO_2-price is set to 10 €/tCO_2. The value of lost load is set to 10,000 €/MWh. Curtailment of RES-based generation is assumed to be free.

The user behavior, heating system and building models are based on [286, 291, 292, 287]. The total number of buildings ($\sum_h NB_h$) is assumed to be approximately one million, which is the expected number of detached buildings for Belgium in 2030 [291]. For sake of simplicity, the detached buildings are represented by an 'average' building, in which the day zone and night zone have a surface area of 132 m^2 and 138 m^2 respectively [293]. All these buildings are assumed to have undergone a renovation of windows, air tightness, walls, floor and roof resulting in low energy buildings with an average U-value of 0.3 W/K and a ventilation rate of 0.4 ACH (air changes per hour). As shown by Patteeuw et al. [43], the DR potential of buildings is very similar once these are thoroughly insulated. The dynamic building model is a linear state space model based on Reynders et al. [286]. The building model is a two-zone (day/night), nine-state model. The heating system in each building is an air-coupled heat pump and a back-up electric resistance heater which supplies heat to the floor heating system in the day and night zones, as well as to the storage tank for domestic hot water [287, 44]. The heat pump is sized to meet 80% of the peak heat demand, the rest of the peak demand is covered by a back-up electric resistance heater. The COP of the heat pump is determined according to Bettgenhäuser et al. [294], assuming a nominal supply water temperature of the floor heating of 35 °C [271]. The hot water storage storage tanks are either 200 l or 300 l, depending on the maximum daily hot water demand at 50 °C. The maximum supply temperature of the heat pump is 60 °C. When occupants are present, the lower bounds for the indoor temperature set points are 20 °C and 18 °C for the day zone and night zone respectively, while the

upper bounds are $22\,^{\circ}C$ and $20\,^{\circ}C$ respectively [295]. When occupants are not present in the dwelling, the lower bound is set to $16\,^{\circ}C$. The upper bound is unchanged. Cooling is not considered. 52 stochastic user behavior profiles were generated using the method of Baetens and Saelens [292], linked to the comfort constraints above. The resulting set of demand side models were aggregated by averaging the effective lower temperature bounds [287]. Weather data is based on measurement data for Uccle (Brussels, Belgium – 2013). Solar gains are calculated using the model proposed by Baetens et al. [296]. The structure of the demand side model is very similar to that proposed by Širokỳ et al. [297], Oldewurtel et al. [298] and Henze et al. [299]. The accuracy of the heating system model is validated against a detailed physical simulation model using the IDEAS library [300] in Modelica, as described in [287].

To calculate the probability of activation and the size of the reserve levels, we approximate the wind power forecast error distribution by five upward and five downward reserve levels ($L = 5$), as we did in Chapter 5. The probability that the scheduled reserves are activated, depends on the forecast of intermittent generation, changing from time step to time step. Details on the calculation of the activation probability and size of the reserve levels are given in Chapter 2.

The planning horizon considered in the optimization is 24 hours. The time step is 15 minutes. To ensure continuity, each optimization takes into account the values of the optimization variables over the previous 24 hours, based on the dispatch on the scenario that represents the scaled measured wind power output of the previous day, and the demand, wind power forecast and reserve requirements on the 24 hours following the day of interest, as in Chapter 5.

6.4 Results & Discussion

For the numerical analysis below, four representative weeks were selected based on an estimate of the operational cost savings attainable via DR as a form of energy arbitrage. To obtain these estimates of the attainable weekly operational cost savings, we solve the model above for a full year, but treat the wind power forecast as perfect. No reserve constraints are imposed, reducing the integrated PUC model to an integrated DUC model, and the resulting schedule is not re-evaluated in a dispatch simulation. Following the methodology of Arteconi et al. [44], we calculate the weekly value of DR-based arbitrage as the difference between (1) the total operational cost of the system when the DR-adherent demand is fully and perfectly controllable and (2) the total operational cost of the system when the DR-capable heating systems are non-responsive and minimize their own energy use. The week in which DR yields the highest (week

7, representing 12% of the year), lowest (week 15, representing 32% of the year) and closest-to-the-average operational cost savings (week 9, representing 30% of the year) are selected in the heating season. Additionally, one week outside the heating season is selected (week 25, representing 26% of the year).

Before moving to the discussion of the four-week analysis, we first present a detailed analysis on a particular day (the sixth day of week 7), illustrating the impact of DR-based arbitrage and regulation services. In our analysis of this particular day, we will assume that the DR-adherent load is perfectly controllable. Second, the benefits of perfectly controllable DR are quantified in a four-week analysis (Section 6.4.2). Third, the system value of thermal discomfort, i.e. allowing thermal discomfort during UC scheduling under 'worst-case conditions', is investigated (Section 6.4.3). Again, we assume the DR-adherent load to be perfectly controllable, an assumption we will drop in Section 6.4.4. In Section 6.4.4, the impact of variability in the response of DR-adherent loads is analyzed for the week in which DR yields the highest operational cost savings, i.e. week 7.

6.4.1 Demand response, arbitrage and reserve scheduling

On the sixth day of week 7, wind energy is capable of covering approximately 42% of the total electricity demand, of which 15% is related to space heating and domestic hot water production. As the demand[11] and wind power are poorly correlated, the residual demand[12] exhibits a significant variability (Fig. 6.5a). This variability does not only affect the scheduling of units to meet the demand under forecast conditions, but also the availability of conventional capacity to meet the upward reserve requirements (Fig. 6.5c).

Introducing perfectly controllable DR-based arbitrage strongly reduces the variability in the residual demand (Fig. 6.5a). The heating demand is shifted to the hours of lower consumption, hence lower electricity costs, and so-called 'valley filling' occurs. This allows not only for a more cost-effective UC schedule, but also for a more efficient use of the available resources to meet the reserve requirements. Less spinning reserves (SR), more non-spinning reserves (NSR) and less reserve shedding (ϕ^+) are scheduled ('DR-arbitrage' - Fig. 6.5d). Although the amount of curtailed wind power, used to meet the reserve requirements, increases, the

[11] The demand of the electric heating systems, if they are not responsive to DR-signals ('No DR'), is fixed to the demand profile that results from the minimization of the energy use to meet the thermal comfort constraints for each building, without regard for the constraints or operational costs on the supply side. To determine these 'minimum energy use' demand profiles, we employ the same demand side model as in the integrated model.

[12] The residual demand is calculated as the total demand corrected for the wind power forecast. This is the load profile perceived by the conventional power plants in the system.

expected operational cost (i.e., after MC ED simulations) reduces by 16% and the expected curtailment drops by 40%. The expected ENS-volume decreases from 1.5 MWh to 0 MWh.

Leveraging the DR-adherent heating demand to provide cost-effective regulation services, still assumed to be perfectly controllable, may further decrease the expected operational cost ('DR-regulation' - Fig. 6.5e). If no thermal discomfort under 'worst-case conditions' is allowed during UC scheduling ($\Delta T = 0$), the resulting residual demand is visualized in Fig. 6.5a. By increasing the heating demand during periods in which curtailment of available RES-based electricity generation would occur, the temperature in certain buildings is increased above the lower temperature bound (dotted line with square markers, Fig. 6.5b). This allows the DR-adherent demand to provide upward regulation services (Fig. 6.5e) without violating the comfort constraints if all upward reserves are activated (dashed grey line, Fig. 6.5b). The amount of spinning reserves (SR) is slightly reduced, curtailment is no longer needed to meet the reserve requirements and no reserve shedding is scheduled (ϕ^+). On this particular day, the expected operational cost decreases by approximately 3% compared to the 'DR-arbitrage only'-case and 19% compared to the 'no DR'-case. Curtailment volumes drop by 33% compared to the 'DR-arbitrage only'-case and 60% compared to the 'no DR'-case. The reliability is unaffected compared to the 'DR-arbitrage only'-case.

By reducing the worst-case comfort constraints with ΔT (Eq. (6.30) and Fig. 6.5b, dotted black line with circle markers), one can further increase the amount of reserves provided by DR-adherent heating systems (Fig. 6.5f). This reduces the amount of spinning reserves needed to meet the reserve requirement, but upon activation of these reserves the thermal comfort will no longer be guaranteed (Fig. 6.5b, solid grey line). If one does not account for the monetary compensation for this thermal discomfort, payable to the consumers, operational cost savings on this particular day are approximately 0.2 M€ or 0.2 €/household. This benefit is however to be weighted against the thermal discomfort[13] experienced by the DR-adherent consumers, which here amounts to – on average – 0.1 Kh/hh. Recall that load shedding was not allowed during this dispatch simulation (Section 6.3).

[13]Thermal discomfort is here defined as the equivalent number of hours, averaged over all households, that the thermal comfort constraints are violated by 1 K, expressed in Kh/hh (Kelvin hour per house hold).

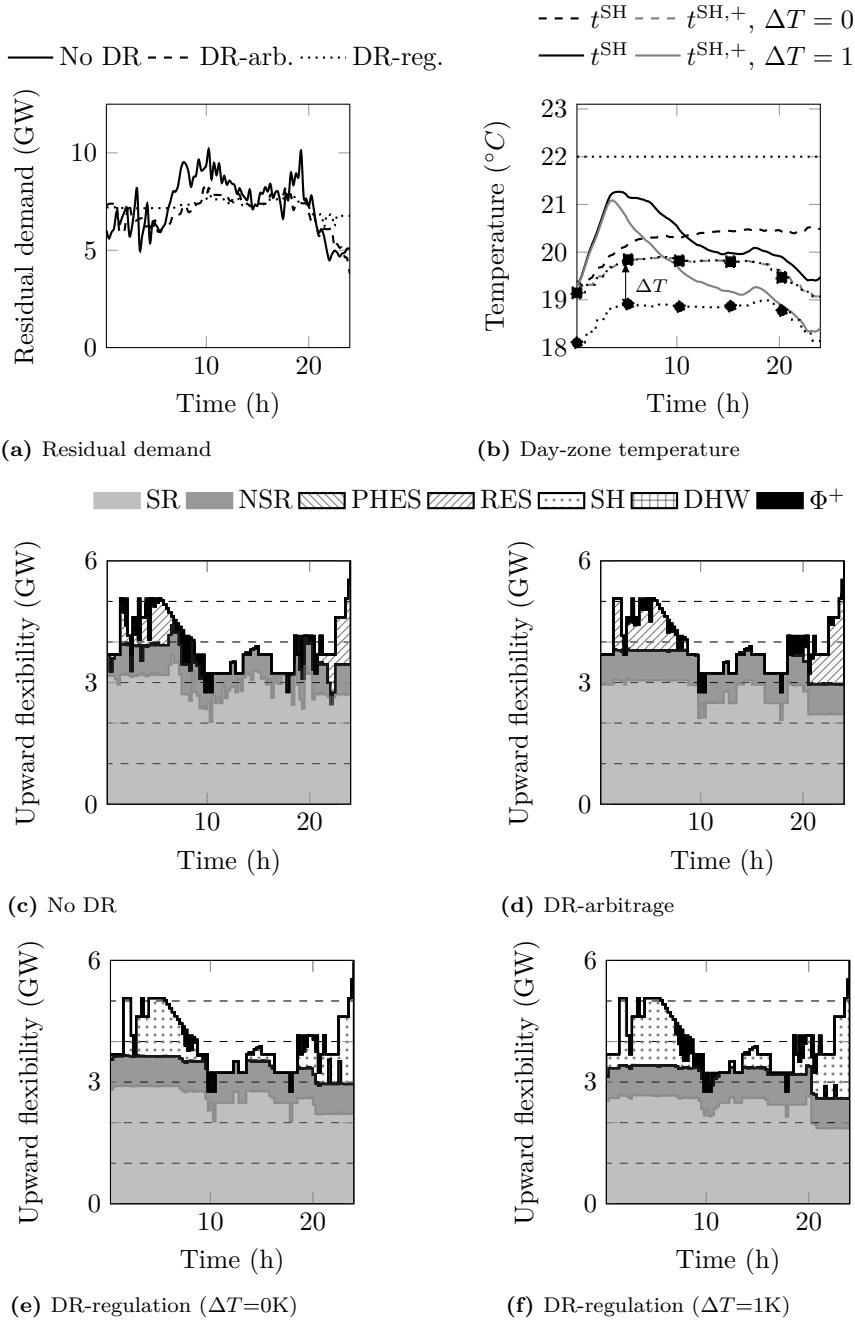

(a) Residual demand

(b) Day-zone temperature

(c) No DR

(d) DR-arbitrage

(e) DR-regulation (ΔT=0K)

(f) DR-regulation (ΔT=1K)

Figure 6.5: Introducing perfectly controllable DR reduces the variability in the residual demand (Fig. 6.5a), which allows for a more cost-effective UC schedule and reserve procurement (6.5d). DR-based reserves further increase the cost-effectiveness of the UC schedule (Fig. 6.5e), without violating the thermal comfort constraints of the reserve providers (Fig. 6.5b) unless the worst-case comfort constraints are relaxed (Fig. 6.5f).

6.4.2 The system value of DR-based arbitrage and regulation services

In our four-week analysis of the system value of DR-based arbitrage and regulation services, we consider three UC strategies. In the case 'SR' only spinning reserves may be scheduled. In the 'SR & NSR' case additionally non-spinning reserves are available to meet the reserve requirements. In the case 'SR, NSR & PHES', spinning, non-spinning and PHES-based reserves are available. For each of these UC strategies, we calculate the expected total operational cost (E[TOC]), the expected wind utilization factor (E[WUF]), the resulting total demand (E[Load]) and the share of electrical energy generated from non-renewable resources (1-E[WS]) in three DR-settings. In the reference case ('Ref.'), the DR-capable load is not responsive. The electricity demand of the electric heating systems is fixed to a 'minimum energy use' profile. Second, the DR-capable heating systems are only used for arbitrage purposes ('Arb.'). Last, both arbitrage and regulation services may be procured from the DR-adherent load ('Reg.'). We will assume that (1) the DR-adherent load is perfectly controllable and (2) thermal comfort must be guaranteed if DR-based regulation services are scheduled ($\Delta T = 0$).

Assuming the DR-adherent demand does not exhibit any variability in its response to a control signal, significant cost savings are to be expected from DR-based arbitrage and regulation services (Fig. 6.6). On average[14], the operational cost decreases by 6 pp (percentage points) when considering DR-based arbitrage ('Arb.', Fig. 6.6a). An additional one percentage point decrease can be realized when the DR-adherent loads are also allowed to provide regulation services ('Reg.', Fig. 6.6a). The reliability of the resulting UC schedules is unaffected: at most 0.0004% of the load is shed. Remarkably, the value of DR-based arbitrage and regulation services remains unaffected when other flexibility providers, here non-spinning reserves ('NSR') and PHES-based reserves are available to meet the reserve requirements. Note that the presence of these flexibility providers, in particular non-spinning reserves, does decrease the operational cost (on average 4 pp), but does not affect the value of DR-based arbitrage and regulation services. During the heating season, the operational cost decrease as a result of DR-arbitrage varies between 5 pp (week 15) and 10 pp (week 7). The additional operational cost decrease due to DR-regulation services varies between 1 pp (week 7 and 9) and 2 pp (week 15). Outside the heating season, the demand of the electric heating systems, thus the available DR-flexibility, is significantly lower. The operational cost decrease resulting from DR-based arbitrage and regulation is limited (max. 2 pp). Allowing non-spinning reserves and PHES-

[14]The average is calculated as a weighted average of the four weeks, using the weights listed in the introduction of this section.

based reserves results in an expected operational cost decrease of 11% outside the heating season (week 25).

The main driver of these cost reductions is an increased utilization of the available wind power (Fig. 6.6b) and a more efficient scheduling and dispatching of the conventional power plants. On average, the Wind Utilization Factor (WUF) increases from 74.9%-77.5% ('No DR') to 82.1%-84.2% ('Arb.') to 83.4%-85.3% ('Reg.'). This increase of WUF is the result of (i) shifting demand to periods of excess wind power generation and (ii) increasing the demand to increase the indoor temperature in order to allow the DR-adherent heating systems to provide upward reserves (see Section 6.4.1). This does however increase the total demand as a result of increased thermal losses and a higher average indoor temperature (Fig. 6.6c). The average increase in total demand amounts to 2.5% ('PHES-based reserves', 'Arb.') to 3.2% ('Spin. reserves', 'Arb. & Reg.'). The availability of non-spinning and PHES-based reserves limits the increase in demand, as less excess wind power is available to be absorbed by the DR-adherent heating systems (Fig. 6.6b). On the contrary, the consideration of DR-based reserves typically increases the total demand due to the higher indoor temperatures required to provide (upward) reserves. As a result, the share of non-renewable energy sources in the fuel mix (Fig. 6.6d) does not decrease as fast as the WUF increases. On average, 67.7% to 66.2% of the demand would be satisfied with electricity generated from non-renewable energy sources in the absence of DR. This drops to 65.6%–64.4% and 65.1%–63.9% when considering DR-based arbitrage and regulation respectively.

6.4.3 The system value of thermal discomfort

The results summarized in Fig. 6.6a show that there is limited value in DR-regulation services. The value of these regulation services may however be impaired by the conservatism of the scheduling process: by imposing worst-case constraint (6.30), thermal comfort is guaranteed even under the most averse conditions, i.e. a wind power realization that requires the activation of all DR-based reserves. The likelihood of such an event might however be limited. In such cases, Eq. (6.30) may be too conservative, which would inhibit the exploitation of cost-effective DR-based regulation services, thus lead to sub-optimal solutions. We will study the impact of relaxing the worst-case constraint in the UC scheduling problem via the parameter ΔT. In essence, this parameter allows the thermal comfort boundaries under worst-case conditions to be violated by ΔT degrees Kelvin at each time step. During dispatch, the original comfort constraints will be imposed. These boundaries may however be violated at a high cost (10,000 €/Kh). Load shedding is not allowed during these dispatch simulations, effectively minimizing thermal discomfort while

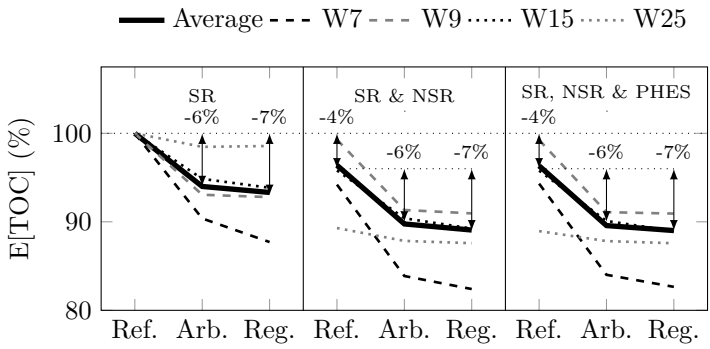

(a) Expected total operational cost, normalized w.r.t. the expected operational cost obtained under the assumption of only spinning reserves and no DR.

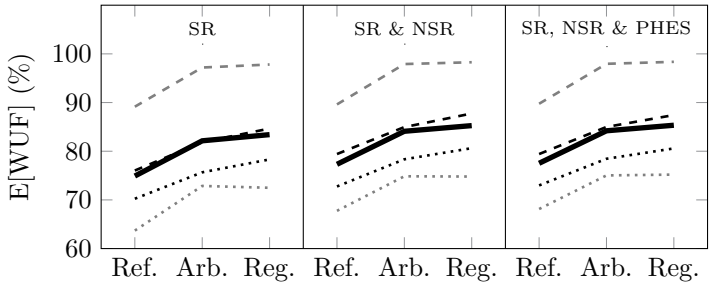

(b) Wind Utilization Factor (WUF), expressed as a percentage of the available wind energy.

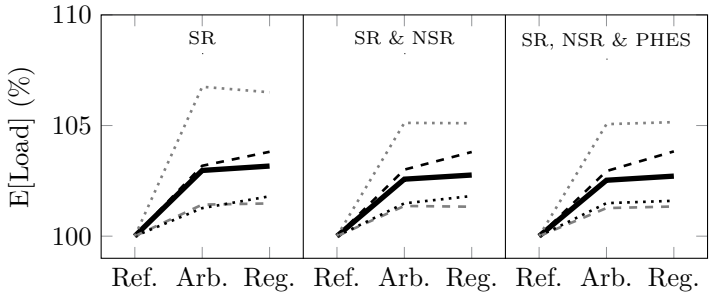

(c) Total demand for electrical energy, normalized w.r.t to the demand if the heating systems are not DR-adherent.

Figure 6.6: Demand response leads to significant operational cost savings (Fig. 6.6a), even in the presence of other cost-effective flexibility providers. This is predominantly caused by an increased wind utilization (Fig. 6.6b), predominantly triggered by DR-based arbitrage. The resulting thermal losses lead to an increase in demand (Fig. 6.6c).

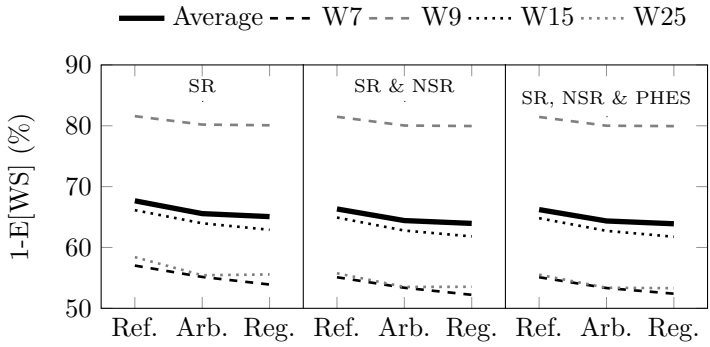

(d) The share of the demand covered by non-renewables sources.

Figure 6.6: *(Cont'd)* The resulting thermal losses lead to an increase in demand (Fig. 6.6c), which limits the decrease of the share of electricity generated from non-renewable energy sources (1-E[WS], with WS the share of wind energy in the total demand) (Fig. 6.6d).

maintaining the power system balance (Section 6.3). Throughout this analysis, we assume that the DR-adherent loads are perfectly controllable.

Figure 6.7 shows the expected total operational cost after dispatch for ΔT values equal to 0 (reference case), 1 and 2 K. The cost of thermal discomfort, i.e. the equivalent number of hours that the thermal comfort bounds are violated by 1 K times the penalty proposed above (10,000 €/Kh), is not included. The visualized operational cost reductions, attainable by allowing thermal discomfort, must thus be interpreted as upper bounds to the system value of thermal discomfort, not corrected for the monetary compensation that occupants who experience thermal discomfort would require. If only spinning and DR-based reserves may be procured, violating the thermal comfort constraints under 'worst-case conditions' during UC scheduling reduces the expected total operational cost by 2% to 3% on average. The inclusion of non-spinning and PHES-based reserves decreases the expected operational cost by 3% to 4% (average values) w.r.t. the situation in which only spinning and DR-based reserves ($\Delta T = 0$ K) may be scheduled. Allowing thermal discomfort under 'worst-case conditions' during UC scheduling yields a total expected operational cost reduction of 5% ($\Delta T = 1$ K) to 6% ($\Delta T = 2$ K). Note however that the differences between the three considered weeks increase. In week 9, non-spinning reserves result in an expected operational cost decrease of 2%. ΔT-values of 1 K and 2 K yield an additional 1 percentage point, respectively 2 percentage point decrease. In contrast, the inclusion of non-spinning reserves in week 7 allows for a 7% decrease

in expected operational cost ($\Delta T = 0$ K). If thermal discomfort under 'worst-case conditions' is allowed during UC scheduling, this results in an additional decrease in operational cost up to 7 percentage points ($\Delta T = 2$ K). Note that week 7 is also the week in which the introduction of DR-based arbitrage and regulation services had the largest impact (Fig. 6.6a).

The resulting operational cost decrease (Fig. 6.7a) should be weighted against the expected thermal discomfort experienced by the DR-adherent heating system owners (Fig. 6.7b). Figure 6.7b shows the average, equivalent number of hours that the thermal comfort constraints of the DR-adherent consumers are violated by 1 K, i.e. the thermal discomfort, as a function of the ΔT-value considered during UC scheduling. On average, thermal discomfort ranges between 1.3 and 3 Kh/hh/week ($\Delta T = 1$ K) and 2.9 and 4.8 Kh/hh/week ($\Delta T = 2$ K). In week 7, in which we observed significant operational cost reductions as a result of allowing thermal discomfort under 'worst-case conditions' during UC scheduling (Fig. 6.7a), the associated thermal discomfort varies between 2.3 and 12 Kh/hh/week (spinning and DR-based reserves), 11.3 and 15.6 Kh/hh/week (spinning, non-spinning and DR-based reserves) and 11.4 and 19.3 Kh/hh/week (spinning, non-spinning, PHES-based and DR-based reserves). Note that in this particular week, thermal discomfort is also observed in the results corresponding to a UC schedule obtained with ΔT equal to zero, as load shedding was not allowed in these simulations and insufficient reserves were procured to meet the demand.

If a DR-adherent consumer experiences thermal discomfort, he or she will have to be compensated. The available budget for this compensation may be estimated as the operational cost decrease shown in Fig. 6.7a. Redistributing these operational cost savings across all DR-consumers would result in an average compensation of 0.13 to 0.42 € per Kh of thermal discomfort. The highest compensation is observed in results that show little thermal discomfort ($\Delta T = 1$ K) and were obtained only considering spinning and DR-based reserves. In week 7, in which relaxing the worst-case comfort constraint on the DR-based reserves results in the largest operational cost savings, this value would vary between 0.06 to 0.42 €/Kh.

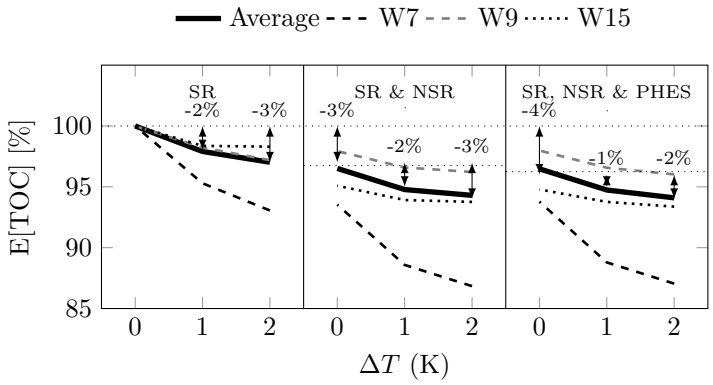

(a) Expected total operational cost (TOC), normalized w.r.t. expected total operational cost obtained if only spinning and DR-based reserves are available, but thermal discomfort is not allowed ($\Delta T = 0$ K).

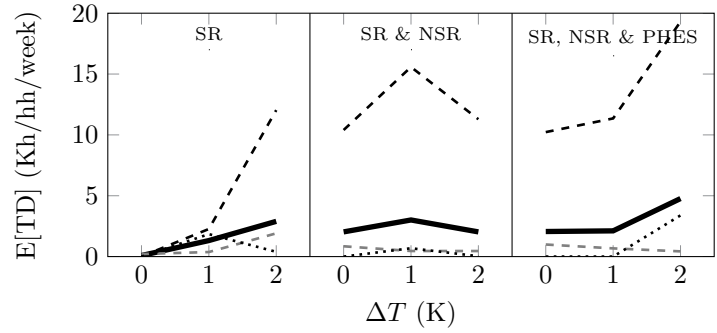

(b) Exepected thermal discomfort (TD) per household per week, based on a dedicated MC ED evaluation of the UC schedules obtained with the corresponding ΔT-value.

Figure 6.7: Allowing thermal discomfort under 'worst-case conditions', limited by parameter ΔT, during UC scheduling yields significant reductions in expected operational cost (Fig. 6.7a), but triggers thermal discomfort during real-time dispatch (Fig. 6.7b).

6.4.4 The impact of limited controllability on the system value of DR

To illustrate the impact that a limited controllability may have on the system value of DR with electric heating systems, we focus on a particular setting for week 7, in which DR achieved the highest operational cost savings. Only DR-based arbitrage and spinning reserves may be scheduled. Demand response is not scheduled to provide reserves, thus thermal comfort must be guaranteed under all conditions. Through the chance-constrained programming framework proposed in Section 6.3.2, we will determine a lower bound to the impact of limited controllability on the attainable operational cost savings associated with DR as follows. We will assume that a system operator plans the power plants and energy storage systems day-ahead, considering the limited controllability on the DR-based arbitrage through chance constraint (6.38). In real time however, i.e. during the MC ED evaluation, the DR-adherent loads are assumed to be perfectly controllable. By comparing the resulting expected operational cost with the case in which DR-based arbitrage was assumed to be perfectly controllable during UC scheduling, we obtain an estimate of the operational cost increase a system operator would incur by *scheduling* the electricity generation system accounting for the limitedly controllability of DR-adherent loads. The impact of real-time limited controllability is not included, which makes the obtained values a lower bound on the operational cost impact of limitedly controllable DR-adherent loads.

Focusing on the non-proportional component of the controllability ($\delta^{\mathrm{NP}} \sim N(\mu^{\mathrm{NP}}, (\sigma^{\mathrm{NP}})^2)$) and assuming a zero mean ($\mu^{\mathrm{NP}} = 0$ MW), we obtain the results summarized in Fig. 6.8. We study three values of the standard deviation σ^{NP}, a metric for the controllability of the DR-adherent loads, namely 5 MW, 25 MW and 50 MW. These values are to be compared with the average electric heating demand during week 7, which equals approximately 2,000 MW. The system operator has to decide upon a value of ϵ, which corresponds to the probability that the obtained UC schedule will be inadequate to meet the load. It is a reflection of the system operator's risk-averseness. If ϵ equals 0.5, the system operator does not account for the limited controllability of the DR-adherent loads, given the symmetry of the Gaussian distribution and the zero mean (μ^{NP}). Hence, the total operational cost will – by definition, given our approach to the MC ED evaluation – be equal to that obtained assuming perfect controllability during UC scheduling (Fig. 6.8a). In contrast, if ϵ equals 0.01, the corresponding UC schedule is capable of meeting the load in 99% (1-ϵ) of all realizations of the DR-adherent load. This will require scheduling more units, which may increase the expected operational cost. Figure 6.8a shows the expected operational cost after MC ED dispatch, assuming that

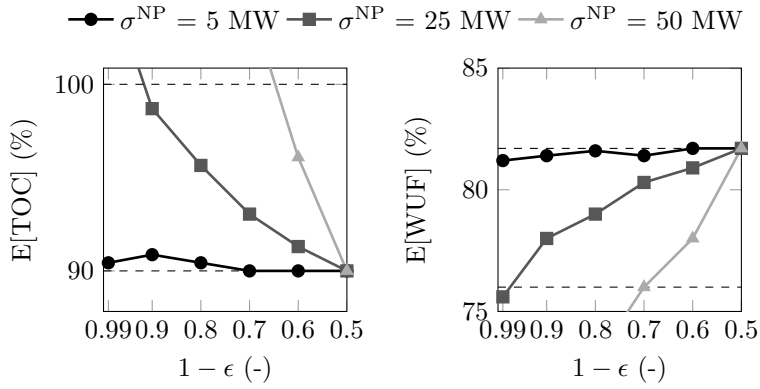

(a) Total operational cost (TOC) **(b)** Wind utilization factor (WUF)

Figure 6.8: Limited controllability of DR-adherent loads may significantly reduce the attainable operational cost savings, especially if the system operator is risk-averse. This is the result of a less efficient UC schedule, which allows lower wind utilization factors.

the DR-adherent loads are perfectly controllable in real time, executed for UC schedules that were obtained with the integrated UC model considering chance constraint (6.38) for various values of ϵ. The expected operational cost is normalized to the expected operational cost one obtains if the electric heating systems are not DR-adherent. The dashed line at 90% indicates the operational cost attainable with perfectly controllable DR-adherent loads (arbitrage only).

Considering low standard deviations σ^{NP}, the possible variability in the response of DR-adherent loads does not diminish the attainable cost savings significantly. Only if a system operator is very risk-averse, the expected operational cost slightly increases. However, if σ^{NP} equals 25 MW - which amounts to 1.25% of the average, instantaneous electric heating demand in this particular week -, this strongly affects the attainable operational cost savings, even if the system operator is not too risk-averse. For example, if a system operator plans the power system at hand to be able to meet the demand in 70% of all realizations of the DR-adherent demand, the attainable operational cost savings drop from 10% to 7%. If a system operator is very risk-averse, limitedly controllable DR may result in higher operational costs than obtained in the corresponding setting without DR. Logically, this effect is even more pronounced if one considers higher σ^{NP}-values.

This increase in operational costs is the result of a less-efficient UC schedule, as

more units must be committed to maintain the power system balance in 1-ϵ of all realizations of the limitedly controllable DR-adherent load. This results in a less compressible power system, a lower wind utilization and hence, higher operational costs. In this particular week, perfectly controllable DR allows to increase the wind utilization factor (WUF) from approximately 76% (no DR) to 82% (Fig. 6.8b). The WUF is nearly unaffected for low σ^{NP}-values, but drastically reduces for σ^{NP} equal to 25 MW. If the UC schedule was calculated to be able to meet the demand in 99% of all realizations of the DR-adherent load, wind utilization factor drops to 75.6%.

6.5 Conclusion

Demand response, a particular form of demand side management, refers to all changes in electricity usage implemented directly by end-use consumers, thereby deviating from their normal consumption patterns, in response to certain signals, such as electricity prices. If these signals are timely and sufficiently strong, this could lead to, among other effects, a higher operational efficiency in the generation, transmission and distribution of electric power. Although there is a large potential for DR identified in the literature, especially for DR considering electric heating systems and thermal loads, there are still a number of obstacles to be overcome before a large scale roll-out of DR technologies can take place.

In order to quantify the operational effects associated with the introduction of these DR-programs, we have developed an integrated modeling approach in this chapter. This model allows capturing the effect of DR on the supply and demand side of the electric power system, as well as quantifying the attainable operational cost savings from a system perspective. Focusing on DR with electric heating systems, we have applied this integrated model in a case study inspired by the Belgian power system, assuming a high wind energy penetration and a large-scale roll-out of DR-capable electric heating systems. Our numerical analysis shows that arbitrage and regulation services, based on DR, could hold significant economic value. The observed operational cost savings amount to – on average – 6% for arbitrage and 7% for arbitrage and regulation combined. These operational cost savings may be attained without tampering with the thermal comfort of the home owners providing these services. If this thermal comfort may be violated, an additional operational cost decrease of 2% (arbitrage) to 3% (arbitrage and regulation) may be realized in this particular case study. However, the impact on the thermal comfort of the home owners would be significant and the available budget to compensate them for this thermal discomfort may be limited. Furthermore, we tested the robustness of our results to the assumption of perfect controllability of the DR-adherent loads. Via a chance-constrained

programming approach, we showed the controllability of DR-providers to be critical to the attainable operational cost savings. Even with a near perfect controllability, risk-averse system operators may see no value in DR.

The presented model may be used by other researchers to investigate the effect of DR on the electric power system and the presented results may guide others in the development of their own models. Demand aggregators may use this work to develop operational models to schedule and optimize their use of thermostatically controlled loads in DR programs.

The proposed methodology may be strengthened in the following ways. First, the numerical analysis was only executed for a system inspired by the Belgian power system and only considered electric heating systems as a DR-technology. Studying other power systems and/or DR-technologies may reveal other effects. Second, the inclusion of a thermal discomfort cost and a study of its interaction with the equivalent parameter on the electric power system side, the value of lost load, may hold interesting results. Third, in our analysis of the impact of limited controllability, we did not study the interaction with other flexibility providers, such as fast-starting units and PHES systems, or the impact of limitedly controllable DR-based reserves. In addition, we limited the influence of limited controllability to the day-ahead UC stage. Considering limitedly controllable DR in the MC ED simulations may provide interesting insights. Fourth, we assumed that the objectives of the owners of the electric heating systems and the system operator aligned perfectly. Studying conflicting objectives, for example through bi-level programming, may reveal interesting effects. Fifth, we reduced the diversity of the demand side flexibility providers to a number of representative households. Furthermore, we neglected the constraints transmission and distribution grids may impose on the optimization problem. Moving to more detailed representations of the distribution of building types, user behavior,... and the inclusion of transmission and distribution grid models may further increase the realism of the obtained results. Last, our analysis only focused on the operational cost savings attainable through DR-based arbitrage and regulation services. The required investments to enable real-time control of DR-adherent residential heating systems and the impact of a large-scale roll-out of DR on the investment in RES-based and conventional electricity generation capacity has not been studied.

Chapter 7

Applications

Up to this point, our focus has been on the methodology. However, a methodology is of course only as relevant as the research question it is designed to address. In this brief chapter, we will illustrate the scientific relevance of the presented methodological developments in two applications.

First, we will provide estimates of a lower bound on the balancing costs associated with wind power forecast errors (Section 7.1). These estimates are based on the results of the HUC model, studied in Chapter 2 and Chapter 5. A similar analysis for solar power forecast errors was performed in [135], not repeated here for sake of brevity.

Second, we revisit the integrated model developed to study demand response with electric heating systems. The results presented in Chapter 6, which were used to illustrate the working principles of the integrated model, are based on a number of assumptions. Below, we investigate the impact of two sets of critical assumptions on the system value of arbitrage opportunities offered by demand response with electric heating systems. First, the impact of different building types and heating systems is investigated. Estimates of the operational cost reductions, the reduced need for investment in peak power plant capacity and reductions in CO_2 emissions are combined with estimates of the investment costs at the demand side to obtain a so-called CO_2-abatement cost associated with demand response with electric heating systems (Section 7.2.1). Second, we investigate the impact of the market penetration, i.e. the number of building owners that participate in the DR program, on the attainable operational cost reductions and the reduced need for investment at the supply side (Section 7.2.2).

Section 7.1 is based on the following papers:

- K. Bruninx, E. Delarue, and W. D'haeseleer, *The cost of wind power forecast errors in the Belgian power system,* in 2nd BAEE research workshop, October 4, 2013 (Leuven, Belgium) and in 37th IAEE International Conference 2014, June 22–25, 2014 (New York City, NY, USA).
- K. Bruninx, E. Delarue, and W. D'haeseleer, *The impact of uncertainty on wind power forecasts on power system balancing: reserve sizing, allocation and activation,* in Windfarms, July 8–10, 2015 (Leuven, Belgium).

7.1 Estimates of the balancing cost associated with wind power forecast errors

In this section, we will focus on the balancing cost resulting from a specific source of uncertainty, namely the error on wind power forecasts, and the impact of this forecast error on the operational power system costs and CO_2 emissions. The focus will be on short-term balancing, but not on the shortest time scales (seconds to minutes). In a case study, inspired by the Belgian power system, we will provide an estimate of the technical lower bound on the balancing cost associated with wind power forecast errors by comparing results of a state-of-the-art hybrid deterministic-stochastic UC model and a perfect foresight DUC model (Section 7.1.2). Our results show that, even with state-of-the art generation system scheduling models, significant balancing costs persist.

The remainder of this section is organized as follows. First, a brief literature review is presented. Our focus is on the range of balancing cost-estimates found in the scientific literature and on the methodologies employed to obtain those values (Section 7.1.1). Second, the methodology used in this section, and its added value compared to those found in the literature, is discussed (Section 7.1.2). Last, numerical results are presented for a case study considering a power system inspired by the Belgian power system, assuming a wind power penetration of 30% (annual, energy basis) in Section 7.1.3.

7.1.1 Literature review[1]

Numerous academic articles, reports and meta-studies on the integration costs of renewables – and wind power in particular – have appeared over the last decade [4, 5, 6, 7]. Some researches have tried to summarize the results of these studies by calculating the balancing cost associated with wind power. The most recent overviews have been composed by Holtinnen et al. [304, 305] and Hirth et al. [306, 6]. Although the regions studied and the methodologies used are quite different, most studies - based on power system models - conclude that balancing costs for wind energy vary between 1 and 4 €/MWh of wind energy for thermal-dominated systems and are less than 1 €/MWh of wind energy for hydro-dominated systems (Fig. 7.1). In these hydro-dominated power systems, balancing costs drop considerably as hydro units can provide balancing services at almost zero-cost, although exceptions are found in the literature. For example, the recent NEA report 'Nuclear Energy and Renewables' lists balancing costs up to 5.3 €/MWh wind energy in Finland [307]. Balancing costs in most cases slightly increase with the wind power penetration. Hirth et al. [306, 6] report, based on an extensive literature review, balancing costs up to 6 €/MWh (model-based studies) and some outliers up to 13 €/MWh (market data analysis). Model-based studies show a moderate increase of the balancing cost with the wind power penetration. Imbalance price analyses show erratic balancing costs as a function of the wind power penetration and are, in most cases, considerably higher than model-based estimates. However, such high balancing costs were only reported for low wind power penetrations. Moreover, the market design may contain punitive mark-ups on imbalance prices and imbalance prices may show large variations in time and across markets [6]. The estimates of balancing cost, obtained from market data analysis, may thus not be representative for the 'true' balancing cost [6].

In general, one can thus distinguish between two types of studies that estimate the cost of additional balancing services to overcome wind power forecast errors. A first group of studies uses *market data*, i.e. observed imbalances, imbalance prices and activated reserve volumes. Such evaluations are limited to the historical conditions (e.g. low penetrations, market design) and imbalance prices may not reflect the real cost of providing those balancing services [308]. Moreover, market failures are not uncommon and forecasts may be biased due to the market design or the forecast methodology. Alternatively, researchers use *unit commitment and dispatch models* to investigate the impact

[1]This literature review is an updated version of the literature review in the following publication: K. Bruninx, E. Delarue, and W. D'haeseleer, *The cost of wind power forecast errors in the Belgian power system,* in 37$^{\text{th}}$ IAEE International Conference 2014, June 22–25, 2014. New York City, NY, USA. We do not aim to be exhaustive in the presented literature review. A more elaborate literature review can be found in, among others [135, 301, 302, 303].

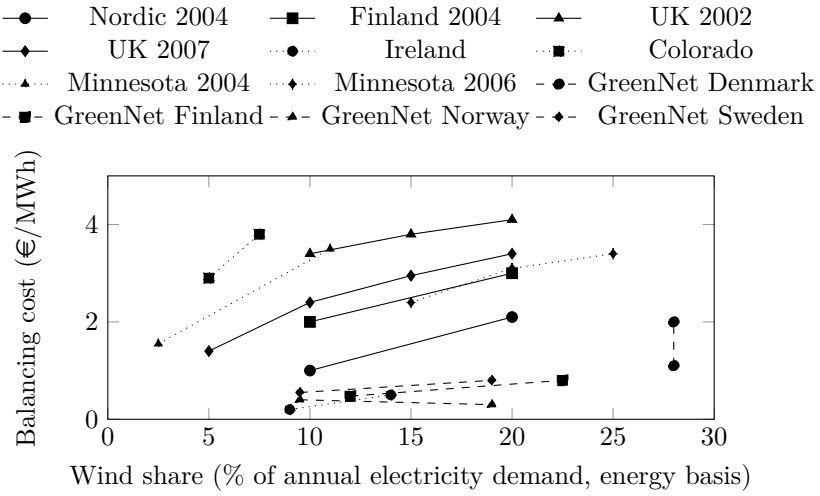

Figure 7.1: Estimated balancing costs, expressed in €/MWh of wind energy, are between 1 and 4 €/MWh of wind energy for systems dominated by thermal units and less than 1 €/MWh wind energy for hydro-dominated systems. The balancing cost weakly increases with the wind share. Selected data from Holtinnen et al. [304, 305].

of imperfect forecast on power system operations, reliability and system costs. These models have their obvious shortcomings, such as the accuracy of the model in representing a real-life power system, sensitivity to data, ... and some more subtle features that drive the obtained results. First, most models are deterministic in nature (e.g. Delarue et al. [144], Ortega-Vazquez and Kirschen [46], Sioshansi [309], Andrianesis and Liberopoulos [310], NREL [311] and the 'implications of intermittency' study by Pöyry [312]). As we extensively illustrated in this disseration (Chapter 2 and Chapter 5), the solutions of these deterministic models may be significantly sub-optimal and highly dependent on the assumed reserve requirements, which may lead to over-estimations of the balancing cost. The balancing cost is typically calculated by comparing the total operational cost of this solution (including the reserves) to a solution of the same model in which no reserves were required and/or a dispatch of the resulting UC schedule over a (large) number of possible realizations of wind power. Note that few authors execute multiple dispatches – considering different wind power scenarios – for each UC schedule to evaluate the cost of activating the reserves. If this step is omitted, one only obtains an estimate for the so-called *allocation or procurement cost* of the reserves. By evaluating the UC schedule for a large

set of wind power scenarios, a statistically relevant estimate of the full *balancing cost*, including the expected *deployment cost* of the operational reserves, can be obtained. Second, these models typically only consider the direct operational costs associated with imperfect forecasts. Indirect costs, such as cycling costs [313], are not taken into account [311]. These indirect costs can however be significant [314][2].

As a solution to the first shortcoming of UC models, stochastic variants are proposed. The uncertainty is represented via a set of scenarios, which allows accounting for the full expected cost of reserve allocation and activation, internalizing the reserve sizing problem (Chapter 2). In theory, this leads to an optimal UC schedule under uncertainty, weighing operational reliability and cost (Chapter 4 and 5). By comparing the obtained results after a Monte Carlo ED evaluation with the solutions of a Monte-Carlo deterministic UC model in which no uncertainty exists, one can determine a lower bound on the balancing (and cycling costs) due to forecast errors. Of course, a statistically relevant estimate of the balancing cost requires sufficient scenarios to capture the stochastic behavior of wind power (forecast errors) during Monte Carlo ED evaluation and during the UC optimization, in order to reach a stable, unbiased solution of the stochastic problem (Chapter 4).

Due to the computational burden and complexity of SUC models (Chapter 5), few researchers have attempted to estimate the (lower bound on the) balancing cost as a result of wind power forecast errors via a SUC model. Tuohy et al. [39] study the Irish system with an assumed wind power penetration of 34.2% of the gross energy demand. They use an improved version of the well-known WILMAR model. Although not explicitly mentioned, an additional balancing cost of approximately 3 €/MWh wind can be calculated from the reported results. However, the calculated balancing cost excludes the cost of load shedding and cycling costs are not taken into account. Sturt and Strbac [205] investigate the British power system with a wind penetration of 35%. The balancing cost varies between 4.7 and 6.8 £/MWh of available wind energy. Although the reported number of start-ups of the considered fleet of power plants changes drastically under uncertainty, this is not reflected in increased cycling costs.

Compared to the current scientific literature, we go beyond the state-of-the-art on two fronts. First, cycling costs are considered, in addition to fuel, CO_2-emission and start-up costs, in the analysis. Second, we will employ a detailed and verified hybrid deterministic-stochastic UC framework, which allows us to

[2]In [314], the focus is on the increase in cycling costs due the increased variability in the residual demand profile with rising shares of RES-based generation. Imperfect RES-based generation forecasts and their impact on cycling costs are however not considered.

determine a statistically relevant lower bound on the balancing cost associated with limitedly predictable wind power.

7.1.2 Methodology

We will employ a stochastic modeling framework that allows us to study and evaluate the impact of intermittent wind power on this balancing cost, based on our work presented at the 37$^{\text{th}}$ IAEE Int. Conf. [42] and the Windfarms 2015 Colloquium [315]. For each day, we solve two (sets of) UC problems:

(1) A hybrid stochastic-deterministic UC (HUC) model, considering reserve requirements and a limited set of scenarios representing the uncertain wind power forecast. The resulting UC schedule is analyzed via Monte-Carlo ED simulations. For a large set of scenarios, generated via the method presented in Chapter 4, an ED optimization is executed in order to obtain a proxy for the expected performance of the model. These dispatch simulations are set up as a DUC model in which the UC schedule is fixed to that obtained from the HUC problem;

(2) In parallel, we solve a DUC model without any reserve requirements or uncertainty for each of the scenarios in the aforementioned set individually. This will yield the *perfect foresight* solution – no uncertainty on the wind power forecast exists in these results.

Based on these simulations, estimates of the balancing cost can be determined. The resulting expected cost of problem (1) is compared with an expected cost obtained from simulations in which perfect foresight on the wind power forecast error is assumed (problem (2)). As such, we obtain a proxy for the *balancing cost*, including the expected operational cost associated with the activation of the scheduled reserves. This balancing cost can be split in the activation and allocation costs. By comparing the resulting operational cost of the HUC schedule under forecast conditions (a scenario in the Monte-Carlo ED evaluation of the UC schedule obtained in (1)) to the cost obtained from a deterministic model in which no reserves are maintained, considering the forecasted wind power (a scenario in the Monte-Carlo DUC perfect foresight analysis in (2)), one obtains a proxy for *reserve allocation cost*. These are costs incurred by the system operator to keep capacity available for up- and downward regulation. Subtracting this reserve allocation cost from the balancing cost yields a proxy of the *deployment or activation cost*.

Throughout the analysis, we will take the perspective of a system operator, i.e. we assume that we have control and knowledge of all elements in the power

system. We will solve the reserve allocation problem one day before the actual realization of the uncertain variable reveals itself (Chapter 1). Although the chosen perspective is distinctly different from the way markets currently deal with uncertainty, it allows us to focus on the impact of uncertainty on the power system. Indeed, by assuming perfect foresight (except on the uncertain variables) and control on all assets of the power system at hand, distorting influences, such as e.g. market inefficiencies, are removed from the equation. What is left, is the impact of intermittent RES-based electricity generation.

Case study

We will study the cost of wind power forecast errors in a system inspired by the Belgian electric power system. The power system, demand and wind power data is identical to that in Chapter 5. We assume a wind power penetration of 30% (annual, energy basis)[3]. Interconnections with other power systems and the internal transmission network are not considered. A full description of the case study can be found in Appendix B. The HUC model is identical to that in Chapter 5. We assume that all flexibility providers may be scheduled (spinning, non-spinning and PHES-based reserves), but fast-starting units may not be dispatched in real time if they are not scheduled as non-spinning reserve. The resulting UC schedule is evaluated on at least 500 wind power scenarios per day (Chapter 4). The perfect foresight DUC simulations are performed on the same sets of scenarios.

7.1.3 Results & discussion

First, we illustrate the methodology described above with an example, based on simulations for the first day of week 39. Second, we calculate estimates of the balancing cost of wind power for the same four weeks used to analyze the performance of the studied UC models (Chapter 5).

Figure 7.2 shows the distribution of the operational cost of (1) the Monte Carlo ED evaluations of the HUC schedule and (2) the perfect foresight DUC solutions for this particular day. The dashed lines correspond to the expected value of the distributions. The difference between the two is referred to as the balancing cost, i.e. the total expected increase in operational cost as the result of reserve procurement and deployment, which here amounts to approximately 56

[3]In [42], we provide estimates of the balancing cost for wind power penetrations between 5% and 30%. In this section, we study the balancing cost for a single annual wind power penetration level, but report results for four different weeks. These weeks are characterized by wind power penetration levels between 10.6% and 77.1%.

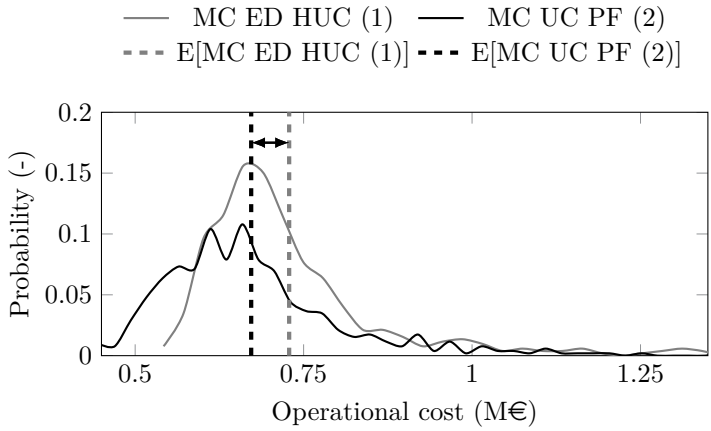

Figure 7.2: The distribution of the operational cost of (1) the Monte Carlo ED evaluations of the HUC schedule and (2) the perfect foresight (PF) DUC solutions, obtained on 500 wind power forecast scenarios for the first day of week 39. The dashed lines indicate the expected value of the distributions at hand. The arrow indicates the balancing cost.

k€/day or 0.7 €/MWh of available wind energy. To separate the activation or deployment and the allocation or procurement cost, we compare the operational cost under forecast conditions with and without reserve requirements imposed on the UC schedule. Although this separation in activation and allocation costs is somewhat arbitrary, it allows estimating the impact of uncertain wind power forecasts on day-ahead scheduling and real-time operation of the conventional power plants. Note that, given the definition above, activation 'costs' can also be negative: the HUC model may anticipate situations in which the wind power production exceeds the forecast by scheduling flexible generation. In real time, fuel and carbon costs can be avoided by ramping down or shutting down these units.

Four representative weeks were selected, assuming a wind energy penetration level of 30% (annually, energy basis), using (scaled) wind and demand data for the year 2013, as we did in Chapter 5. These weeks were selected based on the residual demand, i.e. the total electricity demand corrected for the wind energy generated in each week. The week with the residual demand closest to the average weekly demand for electrical energy (week 30), the week with the lowest residual energy demand (week 52), the week with the highest residual energy demand (week 9) and the week with the residual demand profile with the highest variability (week 39) were selected.

Based on the Monte Carlo ED evaluation of the HUC schedule and the Monte-Carlo perfect foresight DUC simulations we have estimated a lower bound for the additional operational balancing costs that appear with the integration of limitedly predictable wind power. The observed balancing cost varies between 34 k€/day and 429 k€/day, with an average of 134 k€/day. In relative terms, the balancing cost represents 1.3% to 55.1% of the total expected operational cost per day, with an average of 16%. The highest balancing costs are observed in week 9 (high residual demand, only expensive units available to provide balancing services) and week 39 (high wind energy penetration, variable residual demand, which requires flexible, expensive units), the lowest balancing costs are observed in week 30. The balancing cost represents the largest relative share in the total expected operational cost in week 52.

The driver of the balancing cost is an increase in fuel (and, to a lesser extent carbon emission) costs, attributed to the two following effects. First, the uncertainty on wind power forecast requires the commitment of some additional reserve capacity, triggered by the reserve constraints and the scenarios imposed on the HUC optimization. During dispatch under near-forecast conditions, more units will be running in part-load and thus at a lower efficiency as compared to the perfect foresight situation. As such, the average fuel cost per MWh increases. Second, this increase in committed capacity leads to a less compressible power system. Power plants cannot operate below their minimum stable operating point. If the sum of the minimum stable operating points of all committed units and the available wind power exceeds the demand, this leads to curtailment of RES-based generation, increasing the average fuel cost per MWh of demand. Start-up costs are increased due to the uncertainty, but no clear trend can be distilled from the data. On average, ramping costs are nearly unaffected and are in general low compared to the fuel costs.

The results of the described case study are summarized in Table 7.1. We report the following system characteristics for the four selected weeks: (1) the balancing cost, separated in allocation and activation costs and normalized w.r.t. the available RES-based generation; (2) the change in wind utilization factor in percentage points; (3) change in the volume of load that is not met due to imperfect wind power forecasts (ENS, energy not served); (4) the share of wind power in the demand during each week, corrected for curtailment; (5) the increase in CO_2 emissions in each week. Balancing costs between 0.6 €/MWh wind energy (week 52) and 5.4 €/MWh wind energy (week 9) are observed. Allocation costs vary between 0.4 €/MWh and 6.0 €/MWh. At higher wind energy penetration levels (week 39 and 52), capacity with low variable costs can be used as reserve capacity. Note that this capacity is typically less flexible, which leads to high volumes of curtailment (which is assumed to be free). In addition, wind power can participate in the reserve requirements, lowering the

		Week 30	Week 9	Week 52	Week 39
Balancing cost	(€/MWh)	**4.8**	**5.4**	**0.6**	**1.6**
Allocation cost	(€/MWh)	6.0	4.6	0.4	1.9
Activation cost	(€/MWh)	-1.2	0.8	0.2	-0.3
ΔE[WUF]	(pp)	0	0	-7.32	-2.95
E[WS]	(%)	10.6	13.5	77.7	50.2
ΔE[ENS]	(MWh/week)	1.8	18.5	5.5	17.3
$\Delta E[CO_2]$	(ton/week)	7285.8	3952.2	443.1	6902.5

Table 7.1: The balacing cost (the sum of the activation and allocation cost) expressed in €/MWh available wind energy, the change in the wind utilization factor (WUF) in percentage points (pp), the increase in ENS (energy not served) volumes, the increase in CO_2 emissions and the expected share of wind energy (WS) corrected for curtailment of RES-based generation in each of the selected weeks.

average allocation cost. Activation costs are between -1.2 €/MWh and 0.8 €/MWh and are highly dependent on the availability of regulation capacity with low variable costs (e.g. scheduled curtailment or storage). Recall that activation 'costs' can also be negative: when the wind power production exceeds the forecast, fuel and carbon costs can be avoided in other conventional units. Energy not served-volumes are low and only limitedly affect the balancing cost. In each instance, they represent less than 0.0001% of the load. CO_2 emissions rise significantly compared to the perfect foresight simulations. Emissions increase by 443 ton CO_2/week to 7285.8 CO_2/week or 1.9% to 34.8%[4].

7.1.4 Conclusion

Imperfect wind power forecasts require adequate reserve scheduling procedures in order to minimize the balancing cost. However, even with state-of-the-art electricity generation system scheduling models, significant allocation and activation costs may persist. The balancing costs are strongly dependent on the variable cost of the available reserve capacity. In this particular case study of the Belgian power system on four representative weeks, balancing costs between 0.6 €/MWh wind energy and 5.4 €/MWh wind energy are observed. These

[4]The increased emission costs are accounted for in the balancing cost, but the low CO_2-emission penalty, here set to 10 €/ton CO_2, dampens the impact of these increased CO_2-emission costs on the balancing cost. Emission costs make up 1% to 11% of the balancing cost.

values are in line with values found in the literature. Balancing costs make up 1.3% to 55.1% of the total expected operational cost per day, with an average of 16%, driven by an increase in fuel costs. Likewise, CO_2 emissions are shown to rise up to 34.8% compared to the case where no uncertainty exists on the wind power forecast.

The non-negligible balancing costs highlight the importance of adequate and cost-effective reserve requirements. Power system operators, utilities and policy makers jointly should strive to

- improve, or give incentives to improve, forecasts of RES-based electricity generation, even at low penetrations;
- ensure that sufficient capacity is available to provide these balancing services, as wind power pushes the much-needed flexible units out of the fuel mix [42];
- employ state-of-the-art operational modeling techniques to estimate and/or schedule the required reserves needed to cover the remaining uncertainty, in order to minimize the resulting balancing costs.

This work may be strengthened in the following ways. First, the profitability of the dispatchable units under these high wind power penetrations should be investigated. If operators are unable to recover fixed costs, power plants may be decommissioned. Balancing costs and reliability will be affected. Ideally, one accounts for investments and disinvestments. Second, the inclusion of uncertainty during the dispatch and the adaptation of the UC schedule during the dispatch (e.g. activating fast-starting units not scheduled as non-spinning reserves) is currently not included. This would further increase the realism of the model, as in reality information becomes available as time progresses. In addition, multiple sources of uncertainty could be integrated in the model. Third, the obtained balancing costs could be compared to and validated against market data, such as imbalance volumes and prices, as well as (activated) reserve volumes. Last, the inclusion of other sources of flexibility, such as demand response and interconnections with other power systems, could reduce the balancing cost, as illustrated in Chapter 6.

Section 7.2 is based on the following papers:

- A. Arteconi, D. Patteeuw, K. Bruninx, E. Delarue, W. D'haeseleer, and L. Helsen, *Active demand response with electric heating systems: impact of market penetration,* submitted to Applied Energy, 2016.
- D. Patteeuw, G. Reynders, K. Bruninx, C. Protopapadaki, E. Delarue, W. D'haeseleer, D. Saelens, and L. Helsen, CO_2*-abatement cost of residential heat pumps with Active Demand Response : demand- and supply-side effects,* Applied Energy, vol. 156, 2015, pp. 490–501.

The work on demand response presented in this section is the result of a close collaboration with D. Patteeuw, A. Arteconi and L. Helsen (Applied Mechanics and Energy Conversion, Mechanical Engineering, KU Leuven) and G. Reynders, C. Protopapadaki and D. Saelens (Building Physics, Civil Engineering, KU Leuven), especially with respect to the heating system, user behavior and building models and control strategies. The author of this dissertation actively participated in the research that led to the publications above, but did not take a leading role. D. Patteeuw and A. Arteconi were the principal investigators.

7.2 Demand response with electric heating systems

In this section, we present a summary of two case studies on demand response with electric heating systems, in which we used an integrated model closely related to the one presented in Chapter 6. In both cases, the focus is on perfectly controllable DR-based arbitrage. First, we calculate a so-called CO_2-abatement cost associated with demand response with electric heating systems for different building types and heating systems [43] (Section 7.2.1). Second, the impact of the number of DR-adherent consumers on the value of DR-based arbitrage is investigated [44] (Section 7.2.2).

We present a brief summary of the methodology and results discussed in the aforementioned publications. We do not intend to provide a full discussion of the results, but to illustrate the possible applications of the developed integrated modeling approach (Chapter 6). For a thorough discussion of the results, the interested reader is referred to [43] (CO_2-abatement cost) and [44] (market penetration) respectively.

7.2.1 CO_2-abatement cost associated with demand response with electric heating systems

Heat pumps are often suggested as a key technology for decreasing the CO_2 emissions associated with space heating in the residential building sector [316]. According to a study for the European Heat Pump Association [294], a large-scale introduction of heat pumps could reduce CO_2 emissions by 34% to 46% in the building sector of certain European countries by 2030. Bayer et al. [317] report a reduction up to 80% in CO_2 emissions associated with space heating for multiple European countries, depending mainly on the heat pump efficiency, the replaced fuel (gas or heating oil) and the CO_2 intensity of the electricity generation system. However, these estimates are typically obtained based on a number of questionable assumptions. First, the CO_2 emissions associated with the electricity consumption of the heat pumps is typically assessed by considering an average CO_2 intensity of the electricity-generation system. These emissions are however dependent on the *instantaneous* CO_2 intensity of the electricity generation system, which may significantly deviate from the average CO_2 intensity. Second, the electricity demand associated with a massive heat pump introduction may correlate with the peak electricity demand, increasing the need for peak power capacity [318]. Third, if heat pumps would be installed in large numbers in the future, the question arises whether all building types show equal benefits and thus should be given the same priority for deployment. Typically, few building topologies are considered. Finally, the impact of DR programs is typically not included.

In [43], we present a thorough assessment of the CO_2-emission savings potential of DR-adherent residential heat pumps, which we summarize below. The CO_2-emission savings are determined by applying an integrated demand-supply model, similar to the one presented in Chapter 6. In order to compare the suitability of different building types, heating systems and heating emission systems, a CO_2-abatement cost is calculated as a measure for the cost of reducing CO_2 emissions by switching from a conventional condensing gas boiler to a heat pump.

A few studies report a CO_2-abatement cost for heat pumps w.r.t. other heating systems. Joelsson [319] reports an abatement cost of 100 €/ton CO_2 for a heat pump compared to a condensing gas boiler, -120 €/ton CO_2 compared to an oil-fired boiler and -190 €/ton CO_2 compared to direct electric heating. These values are obtained by considering yearly average values for the energy use, the heat pump performance and the efficiency of the electricity-generation system. Kesicki [320] employs a long-term energy planning model, UK MARKAL, which considers system-wide interactions, and finds that heat pumps would become widely implemented in the UK if the CO_2 price exceeds 137 £/ton

CO_2. However, Kesicki reports that his study lacks the inclusion of more than two building types, heat pump peak demand, demand side management and occupant behavior. Our work [43] goes beyond the state-of-the-art by thoroughly taking into account all important factors for determining the CO_2-abatement cost, specifically: the operational cost and CO_2-emission reductions, the investment in heat pumps and the investment in extra peak power plant capacity needed to cover the possible increase in peak electricity demand.

Methodology

In many West-European countries, like Belgium, a commonly installed heating system is the condensing gas boiler (CGB) [321], which is assumed to be the baseline heating system in this study. Installing a heat pump (HP) instead of a CGB entails a higher investment cost, but may lower CO_2 emissions and operational costs. The operational and investment cost, along with the expected CO_2-emissions reduction, can be summarized in a system-wide CO_2-abatement cost (AC):

$$AC = \frac{a_{\mathrm{i}}^{\mathrm{n}}(I^{\mathrm{HP}} - I^{\mathrm{CGB}} + I^{\mathrm{PP}}) - (OPEX^{\mathrm{CGB}} - OPEX^{\mathrm{HP}})}{(CO_2^{\mathrm{CGB}} - CO_2^{\mathrm{HP}})} \tag{7.1}$$

$$a_i^n = \frac{1-(1+i)^{-n}}{i} \tag{7.2}$$

I^{HP} and I^{CGB} represent the investment cost of the heat pump and condensing gas boiler, respectively. I^{PP} is the investment cost associated with extra peak electricity generation capacity. $OPEX$ are the annual operational costs and CO_2 stands for the annual CO_2 emissions. The annual operational costs are to be compared with the annuity a_i^n of the investment cost, in which the number of years, n, is considered to be the life time of the heat pump (20 years, as in [322]) and i the discount rate (3.5% in this study).

The cost of generating the additional electricity demand of the heat pumps, $OPEX^{\mathrm{HP}}$, is determined through the application of an integrated model, similar to the one presented in Chapter 6. Some simplifications are made to allow year-long simulations: (1) the electricity generation system is represented via a so-called merit-order model [21] and (2) the limited predictability of RES-based electricity generation is not considered. $OPEX^{\mathrm{CGB}}$ is the cost of the natural gas for the CGB, assumed to be available at the wholesale-market price (here 25 €/$\mathrm{MWh_{th}}$). Other operational costs, such as costs for transmission and distribution, and taxes are ignored.

Assuming a CO_2 intensity of 205 kg CO_2/$\mathrm{MWh_{th}}$ [323] for natural gas and zero CO_2 intensity for RES-based electricity generation, the CO_2-abatement

cost can be determined via the difference in CO_2 emissions between the case in which the building is heated with a CGB, CO_2^{CGB}, and with a heat pump, CO_2^{HP}. The emissions due to the heat pump arise from an increase in electricity consumption and are determined via the integrated model.

The investment costs include both the investment in the heat pump, I^{HP}, the deferred investment in a condensing gas boiler, I^{CGB}, and the investment in extra electric peak power capacity I^{PP}, valued at 750 €/kW [324]. This investment in additional peak capacity to meet the increased electricity demand is determined ex-ante. Using the integrated model for the critical week with the highest residual electricity demand, we minimize the installed capacity of the power plants. By comparing this result with the installed capacity prior to the integration of electric heating, we determine the required additional power plant capacity.

Case study

The electricity system, as well as the building types, are based on a possible future Belgian setting with a high RES penetration at the electricity-generation side and increased insulation of the buildings. For sake of consistency, all input profiles to the model, such as weather data, RES-based electricity generation and electricity demand, are based on data for the same year (2013) and for the same country (Belgium). The RES-based electricity generation is scaled up in order to represent a high-RES system with 30% and 10% of the annual electrical energy demand covered by wind and PV respectively. The electricity-generation system is assumed to consist solely of combined-cycle gas turbines and open-cycle gas turbines.

Only single-family residential buildings are considered. The building descriptions for the dynamic models originate from a bottom-up stock model based on the TABULA [293] building stock, as presented by Protopapadaki et al. [291], to which additions for new and renovated buildings are made. A total of 36 different building types is considered, representing the Belgian residential building stock. The latter is divided in three typologies, six age classes and two renovation levels. The three different building typologies are typical for single-family buildings (i.e., detached, semi-detached and terraced houses). Each of these typologies is subdivided in six age classes (i.e., before 1945, 1945-1970, 1971-1990, 1991-2005, 2006-2012, after 2012), of which the most recent class corresponds to low-energy houses. For each age class before 2005, two renovation scenarios are considered. First, a 'mild' renovation scenario includes roof insulation, replacement of the windows and an improvement of the air tightness. In the second, 'thorough', renovation scenario the outer walls and

floor are also insulated [291]. The thermal behavior and heat demand of the dwellings are modeled using a two-zone reduced-order building model consisting of a 9 states lumped capacity model [286]. This thermal network model is translated to a linear state-space model, as in Chapter 6. It is assumed that for each case, i.e. for each combination of a building case and heating system case, which we will study separately, the electricity demand of the building at hand is scaled up to the equivalent of 250,000 buildings.

Three main cases for the heating and domestic hot water production system are considered: (1) an air-coupled heat pump (ACHP) with radiators, (2) an ACHP combined with floor heating and (3) a ground-coupled heat pump (GCHP) with floor heating. Floor heating is only considered in the buildings built after 1990, for which the nominal heating power allows applying low temperature heat emission systems, such as floor heating [325]. For each renovation case with radiators, it was chosen to keep the original heat-emission system for low-temperature heating after renovation. For the 'mildly' renovated buildings, depending on the age category, this leads to a nominal supply water temperature for zone heating that can be higher than $60\,^{\circ}C$. This is too high to be supplied by a standard heat pump, in which case a double-compression, high-temperature air-coupled heat pump is considered [326]. The heat pump's efficiency is typically expressed by the coefficient of performance (COP) which is assumed constant during the course of each week [271], is predetermined considering the average outside temperature and an average supply water temperature of the heat emission system according to Bettgenhäuser et al. [294]. The heat pump is sized to cover 80% of the nominal heat demand, with the peak heat demand delivered by a back-up electric heater.

The cost of a CGB is assumed to be $3,200$ € and independent of the size. The heat pump investment cost is based on Van der Veken et al. [327]. Depending on the nominal heating capacity, $\dot{Q}_{\text{nom}}$ in kW, of the heat pump, Van der Veken et al. pose a cost for a ground-coupled heat pump of $(1,000 \cdot \dot{Q}_{\text{nom}} + 10,000)$ €. The cost of a low-temperature air-coupled heat pump depends on whether it is connected to radiators $(675 \cdot \dot{Q}_{\text{nom}} + 7,150)$ € or to floor heating $(410 \cdot \dot{Q}_{\text{nom}} + 7,650)$ €. For a high temperature air-coupled heat pump, a cost of $(385 \cdot \dot{Q}_{\text{nom}} + 9,450)$ € is assumed, based on Heylen et al. [326].

In order to represent the user behavior regarding temperature set points and domestic hot water demand, 52 stochastic user behavior profiles were generated using the method of Baetens and Saelens [292]. In order to reduce calculation time, this user behavior is aggregated by averaging the predetermined, effective lower temperature bounds [287]. The upper bounds for the indoor temperature setpoint equal $22\,^{\circ}C$ and $20\,^{\circ}C$ for the day zone and night zone respectively [295].

Results

Figure 7.3 visualizes the resulting CO_2-abatement cost as a function of the seasonal performance factor (SPF) of the heating system in each building. The SPF is defined as the ratio of the thermal energy delivered throughout the year and the yearly electrical energy consumption of the heat pump[5]. It is a measure of the efficiency of the heating system. There is a clear 'clustering' of the results based on the four heat pump cases. The 'mildly' renovated buildings (SPF 1.8 to 2.1) exhibit the highest abatement costs. Applying DR for these buildings does bring the abatement cost closer to that of the 'thoroughly' renovated buildings. For 'thoroughly' renovated buildings, coupling the heat pump to the radiators leads to somewhat higher seasonal performance factors (SPF 2.3 to 2.6) and lower abatement costs. The lowest abatement costs are obtained with the air-coupled heat pumps coupled to floor heating (SPF 2.5 to 3). In the best case, an abatement cost of 110 €/ton CO_2 is obtained. Ground-coupled heat pumps (SPF 3.3 to 4) lead to the highest CO_2-emission savings, but this is not enough to counteract the higher investment cost; hence the abatement cost is on average 15 €/ton CO_2 higher than for the air-coupled heat pump with floor heating. Note that for the same SPF, little differences are observed between the considered building types. If the buildings are well insulated, i.e. the 'thoroughly' renovated buildings and buildings built after 2005, the associated CO_2-abatement cost depends mainly on the type and SPF of the heating system. The SPF is directly affected by the supply-water temperature, which depends on the heat emission system (thus building type). Throughout all cases, the application of DR is beneficial and lowers the abatement cost with 287 €/ton CO_2 on average.

In [43], we provide a detailed discussion of the drivers of the abatement cost. We summarize our findings below. For more details, the interested reader is referred to [43]. First, the relative **change in CO_2 emissions** associated with replacing a condensing gas boiler with a heat pump is highly dependent on the SPF of the heat pump. The mildly renovated buildings, all equipped with a high temperature ACHP (SPF 1.8 to 2.1), show CO_2-emissions reductions of 15% to 25%. For the thoroughly renovated buildings with an ACHP and radiators (SPF 2.3 to 2.6), the CO_2-emission reduction is higher: 25% to 35%. The buildings with floor heating combined with an ACHP (SPF 2.5 to 3) or a GCHP (SPF 3.3 to 4) allow a decrease in CO_2 emissions of 30% to 40% and 40% to 55%, respectively. Applying DR leads to an additional reduction in CO_2 emissions of approximately 15% on average, as demand is shifted from inefficient OCGT units to efficient CCGT units and moments of excess RES-

[5]The electricity consumption of auxiliary systems, such as the circulation pump of the heat emission system and the source pump of the ground-coupled heat pump, is not included.

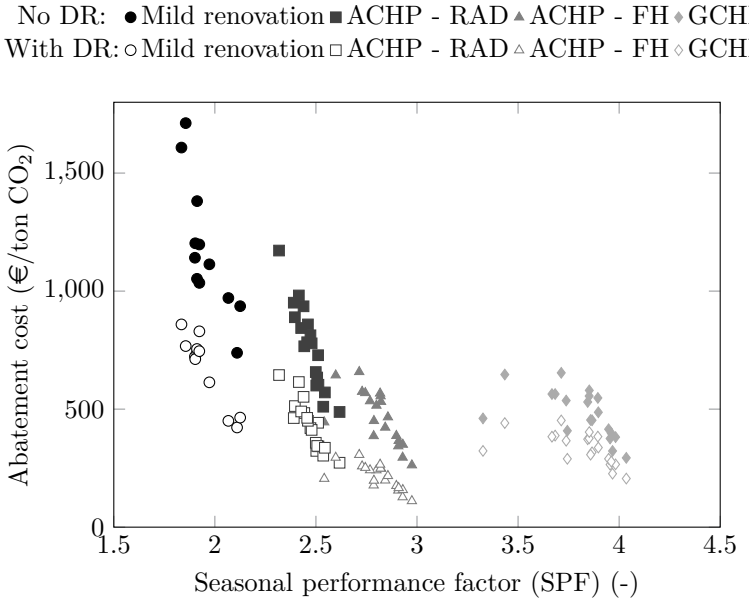

Figure 7.3: The CO_2-abatement cost as a function of the heat pump's seasonal performance factor (SPF) for a discount rate of 3.5%. 'ACHP' stands for air-coupled heat pump, 'GCHP' for ground-coupled heat pump, 'RAD' for radiators and 'FH' for floor heating.

based generation. For the cases with floor heating, applying DR seems to cancel out the differences between the building types, leading to a CO_2-emission reduction of approximately 45% or 60% for an ACHP or GCHP, respectively. Note that these are all relative reductions in CO_2 emissions. As the building is better insulated and the annual heat demand lowers, the absolute CO_2 emissions reduce significantly. Similar trends are to be observed w.r.t. the operational cost reductions triggered by switching to electric heating.

Second, the **investment in additional peak power plant capacity**, here valued at 750 €/kW [324] and fully allocated to the heat pumps in the calculation of the abatement cost, can be an important term in the CO_2-abatement cost. The need for additional peak power plant capacity depends highly on the simultaneity of the heat pumps' demand and the other electricity demand, assumed to be fixed, at peak periods. For the considered climate and demand profile, i.e. Belgium, the highest demand of the heat pumps will occur at cold and dark days which typically coincides with the peak electricity demand.

We use the integrated model in the critical week (i.e. with the highest peak electricity demand) and minimize the installed power plant capacity to determine the required additional peak power plant capacity investment (Section 7.2.1). Without DR-programs, the additional peak demand per building is strongly correlated with the nominal electric capacity of the heat pump. The nominal capacity of the heat pump is in turn closely related to the heat demand (and thus the renovation level) and the efficiency of the heat pump. Considering buildings with the same heat demand, a ground-coupled heat pump would hence perform best, as this system has the highest COP and therefore the lowest nominal capacity. Demand response-based peak shifting can drastically reduce the required additional peak power plant capacity, but becomes less effective at higher nominal electric heat pump capacities. The reason for this effect is twofold. First, the buildings with a higher electricity demand under design conditions are also the less insulated buildings for which preheating is less efficient. Second, the load can only be shifted a limited number of hours. If a significant number of heat pumps perform this shift, the hours before the peak might become 'saturated'. Hence, buildings with floor heating are generally better suited for peak shifting than the same building with radiators due to their larger thermal capacity and higher insulation levels.

Third, the **investment cost of the heating system** has a significant impact on the abatement cost. This investment cost is dependent on the type of heat pump, the nominal heating capacity and the emission system (floor heating or radiators and water-supply temperature). Ground-coupled heat pumps are the most expensive. The investment cost of a heat pump decreases if the nominal capacity decreases (lower heat demand of the building) and the water-supply temperature decreases (floor heating). Note that the investment costs of the building renovation are not considered.

The lower values of the CO_2-abatement cost found in this study are in the same order of magnitude as in the work of Joellson [319] and Kesicki [320]. However, those studies do not highlight the large spread in abatement cost associated with the building renovation level, the type of heat pump installed and the application of DR. As shown above, these factors cause the abatement cost to vary between 110 and 1,700 €/ton CO_2. Furthermore, this study takes into account operational and investment costs at both demand and generation side, in contrast to the aforementioned studies.

Conclusion

In [43], we employed an integrated model similar to the one presented in Chapter 6 to calculate a so-called CO_2-abatement cost for DR-adherent electric heating systems in different building types. We summarized our findings above, and showed that the abatement cost varies between 110 and 1,700€/ton CO_2 in this particular case study. This large spread on the obtained results is driven by the seasonal performance factor of the heat pump, which in turn depends on the building and heating system characteristics. We identified two key characteristics that determine the abatement cost. The first key characteristic is the renovation level of the considered dwellings. Installing a heat pump in 'mildly' renovated buildings causes a low relative reduction in CO_2 emissions, but the required investments in the heating system and peak power plant capacity are high. Buildings which have undergone a 'thorough' renovation, as well as new buildings, show a substantially lower CO_2-abatement cost and CO_2 emissions. The second factor is the heating system. For the new buildings and the 'thoroughly' renovated buildings, an air-coupled heat pump combined with floor heating is the most competitive heating system in terms of CO_2-abatement cost. The ground-coupled heat pump leads to higher CO_2-emission savings, but results in a higher abatement cost due to a higher investment cost. Introducing DR-adherent heat pumps leads to a higher operational efficiency and a higher utilization of the available RES-based generation, reducing CO_2 emissions. By shifting heating demand away from moments of peak demand, the need for additional investments in peak power capacity is decreased. As a result the abatement cost decreases, on average, by 287 €/ton CO_2 across all considered cases.

7.2.2 The impact of the market penetration on the value of demand response with electric heating systems

In [44], we study the impact of a changing market penetration of, i.e. the number of consumers with, DR-adherent electric heating systems on its system value. The main contribution is the attempt to quantify the economic benefits of DR programs both from a customer's and an overall system's perspective. In the literature, other estimates of the economic benefit of DR-adherent electric heating can be found. In Mathieu et al. [328], in which DR-adherent loads are modeled as a virtual energy storage, the amount of energy storage and revenues provided by DR-adherent thermostatically controlled loads is assessed: e.g., for heat pumps these amount to 22 - 56 USD/year/household for participating in ancillary service markets. Papaefthymiou et al. [329] show that the cost savings due to demand side management (DSM) with heat pumps in the

German electricity market are in a range between 25 €/year/household and 40 €/year/household considering a large population of buildings. Hedegaard and Munster [330] state that the flexible operation of individual heat pumps provides a socio-economic cost reduction of about 60 - 200 €/year/household in the context of wind power integration, mainly driven by deferred investments in the power system.

The analysis in [44], summarized below, goes beyond the state-of-the-art on two fronts. First, the employed integrated model adequately represents the technical and comfort constraints, both on the demand and supply side, which allows for a realistic estimate of the value of DR. Second, in the aforementioned publications, the amount of DR-adherent load is typically fixed. Below, we explicitly study the effect of changing the number of DR-adherent consumers with electric heating systems. This allows evaluating to what extent a deployment of these residential DR resources is desirable and profitable.

Methodology

The integrated model used in this case study is identical to that presented in Chapter 6, with the exception of two simplifications. First, the supply side model is reduced to a merit-order model [21]. Only fuel costs are considered. Second, the RES-based generation is assumed to be forecasted perfectly. The model hence does not carry any reserve requirements.

In each simulation, the number of buildings is identical. However, only a certain percentage of those buildings may be DR-adherent. Building owners that do not participate in the DR program, are assumed to minimize their own energy use. The associated electricity demand profiles are predetermined by solving the demand side model separately and minimizing the energy cost for each building owner, assuming they face a flat electricity tariff. The resulting profiles are imposed on the integrated model, in order to ensure comparability between the results obtained with different DR penetration rates. The DR-adherent loads are assumed to be perfectly controllable.

Case study

The electricity system is based on a possible future Belgian setting. For the sake of consistency, all input profiles to the model, such as weather data, RES-based electricity generation and electricity demand, are obtained from data for the same year (2013) and for the same country (Belgium). The RES-based electricity generation is scaled up in order to represent a high-RES system with 15% of

the electric energy consumption covered by wind and 15% by PV respectively. The electricity generation system is assumed to consist solely of combined-cycle gas turbines and open-cycle gas turbines.

The demand side model is identical to the one considered in the case study of Chapter 6. The number of buildings is assumed to be about one million, which is the expected number of detached buildings for Belgium in 2030 [291]. These detached buildings are represented by an 'average' building as suggested in the TABULA [293] project. All these buildings are assumed to have undergone a renovation of windows, air tightness, walls, floor and roof resulting in low energy buildings with an average U-value of 0.3 W/m^2K and a ventilation rate of 0.4 ACH (air changes per hour). The dynamic building model is a linear state space model based on Reynders et al. [286]. The user behavior is based on the model by Baetens and Saelens [292], which was used to generate 52 stochastic user behavior profiles. When the occupants are present, the lower bounds for the indoor temperature set points are $20\,^{\circ}C$ and $18\,^{\circ}C$ for the day zone and night zone respectively, while the upper bounds are $22\,^{\circ}C$ and $20\,^{\circ}C$ respectively [295]. The heating system consists of an air coupled heat pump (ACHP) which supplies heat to the floor heating system in the day and night zones, as well as to the storage tank for domestic hot water (HW). The heat pump is sized to meet 80% of the peak heat demand, the rest of the peak demand is covered by a back up electric resistance heater. The coefficient of performance (COP) of the heat pump is assumed to be constant throughout each optimization period (168 hours) [271] and is predetermined according to Bettgenhäuser et al. [294] considering the average outside temperature during that week and a nominal supply water temperature of the floor heating system of $35\,^{\circ}C$. The hot water storage tanks are either 200 l or 300 l, depending on the maximum daily hot water demand. The upper temperature bound for the hot water in the storage tank is $60\,^{\circ}C$, which is the maximum temperature up to which the heat pump can deliver heat.

Results

One of the main purposes of our investigation [44] is to illustrate the effect of a variable DR participation of customers with electric heating on the electricity generation system. The controllable demand from the electric heating systems is assumed to be controllable at a certain 'DR penetration rate', namely 5%, 25%, 50% and 100%. A penetration rate of 100% means all heat pumps participate in the DR program. Likewise, a penetration rate of 5% means 5% of the heating demand is controllable and 95% of the building owners minimize their own energy use. Figure 7.4 visualizes the main results of our study. Below, we present the highlights of this analysis. For details, the reader is referred to [44].

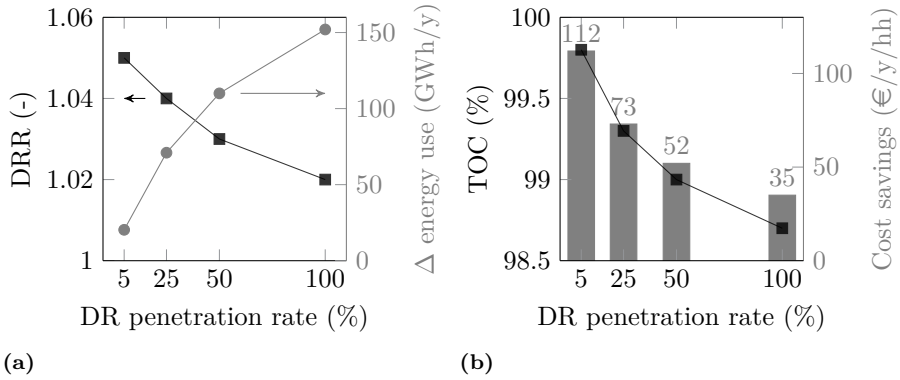

Figure 7.4: The rate of DR participation influences the demand recovery ratio (DRR) (squares, left axis in Figure 7.4a) as well as the total increase in electricity demand (circles, right axis in Figure 7.4a). Increasing the DR participation rate also has an effect on the operational cost savings, both in total (squares, left axis in Figure 7.4b) and per household (hh) (bars, right axis in Figure 7.4b).

Demand response allows for a more efficient operation of conventional power plants and a reduction in curtailment of RES-based electricity generation, reducing the operational cost of the system. Figure 7.4b shows the trend of the total operational cost (TOC), normalized w.r.t. the total operational cost in the case of no DR participation. The total operational cost, determined at power system level, includes only fuel costs and hence no investment costs, ramping costs, CO_2-emission costs nor start-up costs. The maximum cost reduction for the considered configuration of the system is about 1.3% or approximately 35.5 M€/year. CO_2 emissions are at most reduced by 0.29 Mton/year. Demand response allows a more cost-effective scheduling of the power plants and a higher absorption of RES-based generation, but at the expense of an increase in demand (Fig. 7.4a, 'Δ energy use'). This increase varies between 20 GWh to 150 GWh annually, which is a small amount compared to the total electricity demand of approximately 90 TWh. The demand increases with increasing DR penetration rates in a sub-linear fashion. This sub-linear trend is due to a 'saturation' of the usefulness of flexibility in the power system. Additional DR-based flexibility is not used as intensively, because the need for load shifting has already been fulfilled. During moments of load shifting, the burden of load shifting is however carried by more buildings, resulting in smaller deviations from the minimum energy use demand profile, i.e. the electricity consumption profile

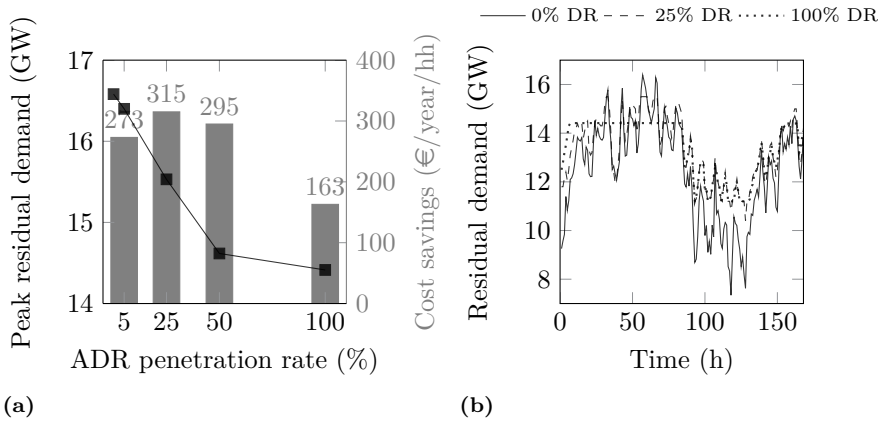

Figure 7.5: Peak residual power production trend and corresponding avoided investment cost divided among participants (Fig. 7.5a). The lines correspond to the peak residual electricity demand (left axis), the bars indicate the associated cost saving per household (hh) (right axis). Figure 7.5b illustrates the effect of load shifting during the most critical week of the year for three DR penetration rates (0%, 25% and 100%).

that minimizes the energy use for space heating, for each building individually. The ratio of the observed electric energy use by the flexible electric heating systems and the minimum electric energy use of those heating systems is defined as the demand recovery ratio (DRR) [19, 40]. This ratio allows quantifying the increase in energy use due to thermal losses. Figure 7.4a illustrates the average DRR for the buildings participating in the DR-program. If 5% of the buildings are participating, the relative increase in energy use per dwelling is the highest, as these consumers face the highest incentive to shift their demand. Additional DR consumers face lower opportunities for load shifting, because of the aforementioned saturation effect. Assuming that the operational savings can be entirely divided among the participants of the DR scheme, the annual operational cost saving per building owner ranges between 35 and 112 €/year/household and decreases with the DR penetration rate (Fig. 7.4b (bars, right axis)). A lower effort is required (i.e. load shifting) and lower benefits (i.e. operational cost savings) per participant are attainable if more consumers are involved. The relative operational cost and the cost savings per household exhibit a sub-linear trend in accordance with the trend observed in the energy use (Fig. 7.4a).

In addition to the operational cost savings, DR also allows reducing investments in peak power plant capacity. In order to quantify the potential for peak shifting, a new simulation is performed, in which the peak demand is minimized in two critical winter weeks with the highest peak residual electricity demand, namely the second and third week of January. Figure 7.5a (solid line) shows how the residual peak demand decreases almost linearly with the DR penetration, until a 50% DR penetration is reached. From this point onwards, a certain saturation of the peak shifting potential is observed. The economic benefit of peak shifting (see Figure 7.5a) can be estimated by assuming an investment cost of 1,250 €/kW for the peak power plants [331]. Hence, a capacity decrease of 2,000 MW corresponds to a deferred investment worth approximately 2,500 M€. Assuming that the avoided investment costs are shared among the participants annually, with a plant life time of 25 years and a discount rate of 3.5 %, the cost saving per participant fluctuates around 300 €/year/household, until a 50% DR penetration is reached (Figure 7.5a, bars). This behavior depends on the nearly linear relationship between number of buildings involved in the DR-program and peak demand reduction for DR penetration rates between 5 and 50%. The aforementioned saturation effect however lowers the attainable cost savings per participant at 100% DR penetration. Note that the exact value of these cost savings is highly dependent on the assumed investment cost, discount rate and power plant life time.

In conclusion, the total cost saving ranges between about 400 €/year/household (5% DR-penetration) and about 200 €/year/household (100% DR-penetration) and is largely attributed to deferred investments in the electricity generation system. Hedegaart and Munster [330] obtained similar values for the socio-economic benefits associated with DR, considering the investment costs of a wide diffusion of heat pumps systems.

To test the robustness of the obtained results, we performed a sensitivity analysis towards some critical assumptions in this case study. First, the role of the demand-side comfort constraints and technology was investigated. Simulations for a full year, focusing on the operational impact of demand response, showed that (i) further increasing the upper temperature limits from $22\,^{\circ}C$ to $24\,^{\circ}C$ holds no economic value; (ii) the operational cost savings are mostly the result of shifting heating demand in time, and to a lesser extent the result of shifting electricity demand associated with hot water production; (iii) increasing the temperature bound on the hot water tank or its size increases the thermal losses, but with limited additional economic value for the system. A similar analysis was conducted with respect to the peak shifting potential, which revealed that (i) only space heating allows reducing the peak electricity demand, regardless of the domestic hot water tank size or temperature limits; and (ii) increasing the upper temperature bound to $24\,^{\circ}C$ does not further reduce this peak electricity

demand. Third, the interaction between demand response and the share and type of RES-based generation was studied.

Conclusion

As summarized above, in [44] we attempt to evaluate the system value of the flexibility enclosed in the thermal inertia of buildings and thermal energy storage in domestic hot water tanks, in terms of energy use and operational costs, if it is exploited through DR programs. The main conclusions are the following. First, higher DR penetration rates increase the attainable operational costs savings, but decrease the savings per household as less load shifting per dwelling is necessary. Smaller deviations from the minimum energy use electricity demand profile per dwelling are required to achieve the same load shifting, leading to lower thermal losses per dwelling. Second, DR can be put into practice with the considered demand side technologies without changing the particular constraints or design configurations from current practice. Space heating is more attractive for DR purposes, even if it is only present during the heating season. Additionally, this demand contributes the most to the winter peak electricity demand and is thus also the most attractive for peak shifting. The total annual cost saving ranges between about 400 €/year/household and about 200 €/year/household and is predominately caused by deferred investments in the electricity generation system.

Note however that the analysis above is not quantitatively exhaustive with respect to all possible DR benefits and costs. For example, we did not consider the provision of DR-based reserves. In addition, to evaluate the economic viability of a DR program, the operational cost savings (Figure 7.4b) should be compared to the investments required to implement the necessary DR technology in every dwelling [25], which was out of the scope of our work [44].

7.3 Conclusion

In this chapter, we demonstrated the scientific relevance of the methodological contributions from previous chapters in three more policy-oriented case studies. First, we demonstrated that the unit commitment framework (Chapters 2-5) may be used to calculate estimates of the balancing cost associated with e.g. wind power forecast errors. These estimates are relevant to researchers, utilities and policy makers as (partial) measures of the integration costs of intermittent RES-based electricity generation. Second, the value of demand response as a means of CO_2-emission reduction was studied. The obtained CO_2-abatement cost has its obvious short-comings, but provides a metric to compare the cost-effectiveness of different technologies in reducing CO_2 emissions. Third, we demonstrated the decrease in the additional value of DR as more and more consumers participate in DR-programs. The proposed methodology, here applied to DR-adherent electric heating systems, allows estimating the deployment level of DR resources that is desirable and profitable.

Chapter 8

Concluding remarks & suggestions for future research

The unprecedented deployment of variable and limitedly predictable electricity generation from renewable energy sources (RES) forces power system operators to radically rethink the way power systems are studied, designed and operated. To minimize the balancing costs associated with the limited predictability of, o.a., wind power, system operators are seeking novel sources of flexibility, such as energy storage or demand response, and improved methods to size, procure and deploy the required operational reserves. In light of these challenges, we proposed a modeling framework to analyze the impact of stochastic RES-based electricity generation, novel operational flexibility providers and an activated demand side on day-to-day power system operation.

In this final chapter, we look back on the developments presented in this dissertation. We focus on our contributions and the conclusions drawn. In addition, we formulate some suggestions for future research, in particular w.r.t. further methodological improvements of the presented models and techniques.

8.1 Concluding remarks

At the core of this dissertation we find five unit commitment models. Each of these operational models was specifically designed or adapted to solve the same operational problem: the scheduling of a number of power plants, energy storage systems and controllable load to meet a certain demand for electricity at the lowest operational cost, considering stochastic RES-based electricity generation. Nevertheless, significant differences in the formulation (Chapter 2) and performance of these models – i.e. the operational cost, reliability and calculation time associated with their solutions – have been observed in a case study inspired by the Belgian power system, in which we have assumed wind power to be the only source of uncertainty (Chapter 5).

The most-common unit commitment model, a deterministic model considering reserve requirements or DUC model, is easy to solve and yields reliable unit commitment schedules. However, these unit commitment schedules were shown to be sub-optimal and overly conservative, which we mostly attributed to the inability of a deterministic model to account for the expected deployment cost of the scheduled reserves. Not considering this expected deployment cost leads to the need for ex-ante reserve sizing, sub-optimal procurement of reserve providers and over-procurement of non-spinning reserves. The performance of these DUC models can however be improved by (1) the inclusion of energy storage-based reserve providers (Chapter 2 and Chapter 5) and (2) adequate reserve sizing techniques (Chapter 3 and 5). To allow for energy storage-based reserve provision, we have developed a novel set of constraints to ensure their real-time availability (Chapter 2), which has proved to reduce the resulting operational cost, despite their overly conservative nature (Chapter 5). To improve the reserve sizing procedure, we have introduced a probabilistic technique, based on a novel distributional description of the wind power forecast error (Chapter 3). Despite its obvious shortcomings (Chapter 2 and Chapter 5), the deterministic model provides a benchmark for the analysis of existing and the development of new unit commitment models: its calculation time should be regarded as a lower bound, while the total operational cost associated with a DUC schedule can be interpreted as an upper bound. If a UC model consistently takes more time to yield a solution than a DUC model, it should result in a lower operational cost.

At the other end of the spectrum, we find the stochastic unit commitment (SUC) model. In theory, the direct scenario-based representation of the uncertainty in the UC model allows accounting for the full expected cost of reserve procurement and deployment, which enables the internalization of the reserve sizing problem and the procurement of a cost-optimal mix of flexibility providers. In addition, the potential regulation services provided by energy storage systems may optimally be exploited (Chapter 2). The numerical results presented in this

dissertation (Chapter 5) support these claims, but have also shown that a SUC model is computationally expensive to solve, which may limit its practical applicability. Moreover, the quality of the UC schedule is fully dependent on the considered scenarios (Chapter 5). In this regard, we have highlighted that the scenario generation and reduction techniques employed in the context of SUC models cannot be decoupled from the SUC problem itself (Chapter 4). More specifically, we have shown that the fast forward heuristic, an often-used probability distance-based scenario reduction technique, may lead to unstable and biased results. We have proposed a novel metric to characterize the scenarios at hand during scenario reduction, which is designed to reflect the impact of a scenario on the objective function and the decision variables of the SUC problem. With this improved characterization of the impact of a scenario, stable and unbiased solutions to the SUC problem may be obtained, but the computational cost of solving a SUC problem remains extremely high.

In pursuit of a UC model that combines the cost-effectiveness of the SUC model and the low calculation times of the DUC model, researchers have proposed a myriad of alternative formulations, with varying degrees of success. One of these alternative UC models is the improved interval unit commitment (IIUC) model, which we have studied in Chapter 2 and Chapter 5. The IIUC model reduces the representation of the uncertain variable to four so-called ramping scenarios, which allow enforcing ramping requirements on the scheduled reserves that are more reflective of the ramps these reserves will need to absorb in real time. However, the IIUC model fails to incorporate the expected deployment cost of the scheduled reserves and hence suffers from the same drawbacks as the DUC formulation. In this dissertation, we have improved the cost-effectiveness of the IIUC schedules by explicitly accounting for the regulation services that non-spinning and energy storage-based flexibility providers may offer (Chapter 2 and Chapter 5). Despite these improvements, the easy-to-solve IIUC model leads to UC schedules that are characterized by approximately the same operational cost as the DUC solutions.

In contrast, the hybrid and probabilistic UC formulations, developed in this dissertation, allow for the combination of a low computational effort, high reliability and low expected operational costs (Chapter 2 and Chapter 5). Both formulations include, albeit in different ways, a coarse approximation of the expected deployment cost of procured reserves, effectively internalizing the reserve sizing problem. Accounting for the expected deployment cost furthermore allows monetizing the operational benefits associated with downward flexibility and procuring a cost-optimal mix of reserve providers. In the hybrid deterministic-stochastic unit commitment (HUC) model we combine a probabilistic reserve requirement and a limited set of scenarios, selected via a dedicated scenario reduction technique. The stable solution of the equivalent

SUC problem can be approximated via this formulation, but at a strongly reduced computational cost. Alternatively, the probabilistic unit commitment (PUC) model characterizes the need for operational flexibility via a set of reserve intervals or levels, each with a corresponding deployment or activation probability. Although the calculation time required to solve an instance of the PUC problem is similar to that of a DUC problem, we observe significant decreases in the expected operational cost. Nevertheless, the SUC formulation remains, in most cases, more cost-optimal, in part due to the conservative estimates of the regulation services that an energy storage system may offer in the HUC and PUC formulation.

The low computational burden of the PUC model furthermore allows integrating physical demand side models, which has enabled us to study the value of demand response (DR) as an arbitrage and regulation service provider (Chapter 6). We illustrated this approach with the development of an integrated PUC model considering DR with electric heating systems, leveraging the thermal inertia of residential buildings, heat emission systems and hot water tanks to decouple the instantaneous electricity demand and the end-energy use. Such an integrated model allows capturing the effect of DR on the supply and demand side, in contrast to many approaches found in the scientific literature, as well as quantifying the attainable operational cost savings from a system perspective. Our numerical analysis revealed that DR-based arbitrage and regulation services could hold significant economic value, which may be obtained without tampering with the thermal comfort of the home owners providing these services. Thermal discomfort may be allowed to reduce the operational system cost, but the resulting operational costs savings at system level may be small and insufficient to compensate home owners for the experienced discomfort. However, these results were obtained under the assumption of perfectly controllable DR-adherent loads. Via a state-of-the-art chance-constrained programming approach, we have shown the effective degree of controllability of DR-providers to be critical to the attainable operational cost savings. Even with a near perfect controllability, risk-averse system operators may see no value in DR.

Regardless of the unit commitment model chosen, adequately capturing the RES-based generation in a statistical distribution (DUC, PUC, IIUC, HUC) or a discrete set of scenarios (SUC, HUC) has been shown to be of critical importance for the performance of the model and for the evaluation of the resulting UC schedules. In this dissertation, we have proposed a novel statistical, distribution-based description of the wind power forecast error, based on the Lévy α–stable distribution (Chapter 3). These distributions allow modeling the skewness and kurtosis observed in the wind power forecast error data – in contrast to the Gaussian and β-distributions currently proposed in the literature. Especially capturing the kurtosis, i.e. a measure for the amount of probability

contained in the tails of the distribution, is of critical importance if one aims to employ such distributional descriptions in e.g. probabilistic reserve sizing procedures. The same distribution provides the necessary information for the generation of scenario sets of a reasonable size that form an adequate discrete representation of the uncertainty on wind power forecasts (Chapter 4).

In summary, to study uncertainty in electricity generation systems and the way (novel) flexibility providers are deployed to mitigate the impact of this uncertainty, a system's approach is required. To obtain statistically relevant results, one should start from a thorough characterization of the uncertainty at hand (Chapter 3). This statistical description of the uncertainty must be employed in state-of-the-art operational models (Chapter 2), which adequately capture the costs and technical limits of the flexibility providers in the power system and the interaction between them (Chapter 6), in order not to over- or underestimate the impact of the uncertainty (Chapter 5). The PUC and HUC model, developed in this dissertation, are in this regard a good trade-off between computational complexity and cost-effectiveness. If computational cost is the main concern, e.g. due to the size of the power system at hand, the PUC model allows to obtain near-cost-optimal UC schedules in minutes. If cost-effectiveness is the priority, the HUC model may be a suitable alternative for the SUC model, which may become intractable for real-life power systems. Moreover, the resulting solutions must be carefully evaluated (Chapter 5), preferably over a wide, but realistic range of realizations of the uncertainty at hand (Chapter 4).

The presented HUC and PUC formulation can be used to assess the impact of uncertainty on reasonably large low-carbon electric power systems for which SUC models would become computationally intractable. Likewise, independent system operators could use these models to optimize their UC decisions taking into account the uncertainty in their system. The PUC formulation has the additional advantage that it does not require scenario generation and reduction techniques. Moreover, many system operators are moving from point forecasts (i.e. a single forecast value at each time step) to interval or ensemble forecasts (i.e. intervals in which the realization of wind power will be contained with a certain probability). This last type of wind or solar power forecasts can be directly integrated in a PUC framework. The integrated model may be used by other researchers to investigate the effect of DR on the electric power system and the presented results may guide others in the development of their own models. Demand aggregators may use the presented approach to develop operational models to optimize the scheduling and operation of DR-adherent loads.

8.2 Suggestions for future research

With respect to the **statistical characterization of the stochastic variable**, the following suggestions can be made to strengthen the presented research. First, the procedure for the estimation and optimization of the parameters of the distributions may be improved, e.g. by employing a maximum likelihood estimation method. The objective function (min. squared residuals) utilized in this dissertation has merely been chosen to demonstrate the superiority of the stable distributions in capturing the shape of the wind power forecast error. If one aims to characterize specific shape characteristics of the stochastic variable at hand (e.g. the tails or peaks), this criterion might not be suitable. Further developing the proposed methodology and applying it to other data sets, e.g. obtained from larger geographical areas, may lead to interesting insights.

The **probabilistic reserve sizing procedure** proposed in this dissertation requires the modeler to postulate a so-called design reliability. The associated operational cost to reach that reliability level – i.e. to meet the resulting reserve requirements – and the expected operational benefits – i.e. avoiding load shedding and excessive curtailment of RES-based generation – were not accounted for in the reserve sizing procedure. Further research may focus on more cost-effective ex-ante reserve sizing methods, balancing the (expected) cost of load shedding, curtailment of RES-based electricity generation and the procurement and deployment cost of operational reserves, in line with the approach proposed by Ortega-Vazquez and Kirschen [98, 93, 46].

The presented **scenario generation technique** may be improved in the following ways. First, better sampling procedures may exist. For example, employing a conditional sampling technique may reduce the number of samples or scenarios needed to capture the distribution at hand. Second, the proposed scenario generation technique requires an estimate of the covariance matrix, here obtained via an exponential covariance function. More optimal estimation procedures may exist and may further improve the match between the generated set of scenarios and the stochastic variable they are designed to represent. Third, the removal of scenarios that contain improbable events results in a small distortion of the distribution represented by the set of scenarios. This distortion may be minimized by optimally redistributing the probability of the removed scenarios over the retained scenarios, an improvement not pursued in this dissertation. Last, applying the presented technique to other stochastic variables will further illustrate its versatility.

Although the modified **scenario reduction technique**, developed in Chapter 4, yields small enough scenario sets to keep the resulting SUC problem tractable, while maintaining the solution quality, this line of research may be strengthened

in the following ways. First, the numerical analysis presented in Chapter 4, especially w.r.t. the solution stability analysis, may be extended. For example, the impact of other power system characteristics, longer time periods, larger scenario sets and other sources of uncertainty may be tested. Second, the interaction between the reduced scenario set and the scheduling of energy storage-based flexibility has been proven to be critical for the performance of the SUC model. Further research may focus on novel approaches to identify those scenarios that are particularly challenging in scheduling an electricity generation system which includes energy storage systems. Last, the presented research would greatly benefit from further positioning w.r.t. recently published scenario reduction techniques. For example, importance sampling-inspired techniques, such as those proposed by Papavasiliou et al. [109, 110], novel moment-matching techniques, as introduced by Li et al. [221], and novel clustering techniques, developed by, a.o., Feng and Ryan [225, 223, 224], were only qualitatively discussed in this dissertation.

The presented **unit commitment models** may also be improved. First, the operation and scheduling of energy storage systems in scenario-based UC formulations merits further research. Ensuring the feasibility of energy storage-based regulation services with a scenario-based representation of the uncertainty proved to be challenging, and detrimental for the performance of the SUC formulation. A possible fix for the observed issues might be the inclusion of a larger set of scenarios, in which a feasible dispatch of the energy storage system would be required, but of which the operational cost would not be accounted for in the objective function. Likewise, the performance of the DUC, IIUC and PUC models could be improved by reducing the conservatism of the constraints imposed on the energy storage-based reserves. The performance of the DUC and PUC formulation may further be improved by increasing the realism of the ramping constraints imposed on the scheduled reserves. Second, dedicated decomposition methods and parallelization may significantly reduce the computational effort associated with solving SUC problems [110]. Likewise, more efficient formulations – so-called tight and compact formulations – of the resulting operational optimization problems may reduce their computational cost [28]. Third, other, more cost-optimal hybrid UC formulations may exist. For example, a combination of a SUC and an IIUC model, as proposed by Dvorkin et al. [130], may improve the cost-efficiency of the IIUC formulation and reduce the computational burden of the SUC problem. Furthermore, the inclusion of an approximation of the expected deployment cost of scheduled reserves may enable scheduling a cost-optimal mix of flexibility providers (e.g. spinning vs. non-spinning capacity) and monetizing the benefits associated with scheduling downward flexibility. Fourth, the relation between the presented PUC model and chance-constrained UC models may be investigated. Employing chance-constrained programming techniques, such as the presented analytical

reformulation of the chance constraints, in the PUC model may lead to interesting results. Last, further positioning the presented formulations w.r.t. other UC formulations, such as robust or chance-constrained UC models, and expanding the numerical analysis, e.g. by considering other power systems, other sources of uncertainty, ..., may lead to interesting insights.

With respect to the presented integrated model and **demand response**-research, the following improvements can be made. First, the numerical analysis was only executed for a system inspired by the Belgian power system and only considered electric heating systems as a DR-technology. Studying other power systems or DR-technologies may reveal other effects. Second, the inclusion of a thermal discomfort cost and a study of its interaction with the equivalent parameter on the electric power system side, the value of lost load, may hold interesting results. Third, in our analysis of the impact of limited controllability, we did not study the interaction with other flexibility providers, such as non-spinning reserves and energy storage systems, or the impact of limitedly controllable DR-based reserves. Furthermore, we limited the variability in the response of DR-adherent loads to a control signal to the day-ahead planning stage. Fourth, we assumed that the objectives of the owners of the electric heating systems and the system operator are perfectly aligned. Studying conflicting objectives, for example by employing bi-level programming techniques, may reveal interesting insights. Last, we have reduced the diversity of the demand side flexibility providers to a number of representative households. Moving to more detailed representations of the heterogeneity in building types, user behavior, ... may further increase the realism of the obtained results.

In addition to the possible methodological advancements described above, the presented models and tools allow for a wide range in applications, which we only limitedly pursued in this dissertation (Chapter 7). For example, considering multiple, statistically dependent sources of uncertainty and studying their interaction may lead to interesting insights and increase the added value of this work. Additionally, one could use the presented models to study the benefits and challenges associated with pooling of reserves across multiple interconnected areas, as well as the interaction of uncertainty in different areas. The inclusion of transmission constraints, during the optimization of the UC schedule and the real-time dispatch, will reveal which models ensure the feasibility of dispatching the scheduled reserves w.r.t. these grid constraints and how the calculation times are impacted by the associated increase in problem size. Last, a comparison of the results from the aforementioned UC models and the outcome of real, liberalized electricity markets, e.g. w.r.t. the historical fuel shares in the electricity generation mix, may reveal the (in)applicability of the presented UC models in such a liberalized context.

Appendix A

Publications not included in this dissertation

In addition to the research presented in the main body of this dissertation, we also studied related issues that arise with the integration of RES-based electricity generation and in the wake of some policy decisions. As this research does not strictly align with the objectives of this dissertation (Section 1.3), these publications were not included in the body of this dissertation. We summarize our findings below and refer the interested reader to the related publications.

A.1 Impact of the German nuclear phase-out on Europe's electricity generation

After the events in Fukushima on March 11 2011, the German government decided to revise its nuclear policy. The seven oldest and the Krümmel nuclear power plants (NPPs), in total about 8.8 GW in capacity, were shut down mid March 2011. The remaining nine NPPs (12.7 GW in total) will be shut down before the end of 2022. At the same time, the German government has confirmed its ambitious goal, announced in the fall of 2010, to reduce overall greenhouse gas emissions by 40% in 2020 compared to 1990 levels. By 2050, the aim is to reduce this further to 5 to 20% of the 1990 levels, leading to a virtually carbon-free electricity sector. Renewables (RES) are projected to contribute 35% in 2020 and 80% in 2050 in electricity generation. The combination of these climate goals and the nuclear phase-out raises questions concerning the

impact of these decisions on the operational security of the electricity system — on a German and on a European scale, on the short and the long term.

In [332, 333], we focus on the technical feasibility (electricity generation and transmission) and the impact on the CO_2 emissions of the German nuclear phase-out on the short term (2012-2022). We employ a detailed electricity generation simulation model, including the German transmission grid and its international connections. A range of different conventional and renewable energy sources (RES) scenarios is considered. Results are presented for the changes in electricity generation, on the flows in the electric network, on operational reliability issues (i.e. whether the system is able to guarantee a safe operation in all scenarios), curtailment of available electricity generated from RES, the CO_2 intensity of the German electricity generation and congestion on the transmission grid.

The scenario analysis shows that nuclear generation will be replaced mainly by coal- and lignite-based generation. This increases the CO_2 intensity of the German electricity sector on the short term. Furthermore, the results indicate that the German electricity export will decrease and under certain circumstances, the power system may be unable to meet the demand. Keeping some nuclear power plants online, would mitigate these effects. The amount of electricity generated from RES is shown to be the main driver for grid congestion.

We published our findings in

- K. Bruninx, D. Madzharov, E. Delarue, and W. D'haeseleer, *Impact of the German nuclear phase-out on Europe's electricity generation — A comprehensive study*, Energy Policy, vol. 60, pp. 251–261, 2013.
- K. Bruninx, D. Madzharov, E. Delarue, and W. D'haeseleer, *Impact Of The German Nuclear Phase-Out On Europe's Electricity Generation*, in EEM12, 9th International Conference on the European Energy Market, May 10–12, 2012. Florence, Italy.

A.2 Bidding strategies for Virtual Power Plants considering CHPs and intermittent renewables

Energy efficiency and renewable-energy sources (RES) are fundamental parts of the European energy policy. For this reason, efficient distributed generation technologies such as combined heat and power coupled to district heating (CHP–DH) and RES-based electricity are promoted. Additionally, those CHP–DH systems may offer a source of flexibility to the power system to balance the intermittent output of RES-based electricity generation. From a

market perspective, this could be achieved by aggregating RES-based electricity generation and CHP-DH in a virtual power plant (VPP).

In this context, we present a methodology to evaluate the optimal bidding strategy of a VPP composed of a CHP–DH system and RES-based electricity generation in [334, 335]. The objective is to investigate the optimal bidding strategy for a VPP that uses the flexibility of a CHP-DH system to compensate for the uncertainties regarding RES-based electricity generation and market prices. The VPP operator nominates its energy production profile to the day ahead market the day before the actual delivery. In real time, any deviation from the day-ahead schedule is settled in the imbalance market. The uncertainties on the RES-based generation and market prices are modeled using a two-stage stochastic programming approach.

Three different bidding strategies are studied: 'static', 'flexible DA' and 'flexible RT'. The major difference between the studied strategies lies in the dispatch decisions. The 'static' strategy does not allow adjustments of the scheduled output of the CHP unit after closure of the day-ahead market. The 'flexible DA' and 'flexible RT' strategies differ from each other in terms of the information available at the moment of deciding on possible the redispatch actions. The 'flexible DA' redispatches the CHP for the whole day assuming full knowledge of the RES-based electricity generation, but under uncertainty regarding the imbalance price. The 'flexible RT' strategy allows the VPP to adjust its position at each time step depending on the RES generation and imbalance price scenarios.

The results show that in comparison with the 'static' strategy, the 'flexible DA' operation results in a profit increase during summer (5900 €/week), the intermediate season (2800 €/week) and winter (2700 €/week). This increase is moderate compared to the total fuel cost in these seasons. Larger profits are achieved for all seasons when the 'flexible RT' strategy is applied. For instance, during winter the difference between the 'flexible RT' operation and the 'static' case amounts to 22,600 €/week, approximately 5% of the fuel cost.

These observations resulted in the following publications:

- J. Zapata Riveros, K. Bruninx, K. Poncelet, and W. D'haeseleer, *Bidding strategies for virtual power plants considering CHPs and intermittent renewables*, Energy Convers. Manag., vol. 103, pp. 408—418, 2015.
- J. Zapata Riveros, K. Bruninx, K. Poncelet, and W. D'haeseleer, *Bidding of a VPP in the day-ahead market under uncertainty: profit optimization & risk aversion*, in Young Energy Engineers & Economists Seminar 2014, Dresden, Germany, April 9–10, 2014.

A.3 Effects of large-scale power to gas conversion on the power, gas and carbon sectors and their interactions

Storage will be needed, among other options, to ensure an efficient and reliable operation of the electric power system. The power to gas (PtG) concept provides a possibility to store excess RES-based electricity power and as such it can increase the utilization of RES-based electricity generation. The renewable methane, produced via PtG, can be stored in the gas system and used e.g. for electricity generation. The gas system has a much larger storage capacity compared to current electricity storage technologies. However, PtG introduces additional, unidentified interactions between the gas, electricity and carbon (CO_2) sector. Therefore, we developed an operational model in [336, 243] that includes the gas, electricity and CO_2 sector to analyze the effects of PtG on these sectors and on the interactions between them.

Based on a case study, it is found that PtG partially transfers capacity and flexibility problems, triggered by the introduction of intermittent RES-based electricity generation, from the electricity to the gas sector. Moreover, a downward pressure on the gas prices is observed. The effects of PtG are generally smaller than those of the large-scale introduction of intermittent renewable electricity generation. Complex inter-sector dependencies are introduced through the CO_2 that is required in the PtG process. If PtG is to be deployed at large scale, this study of these effects is relevant for policy makers, regulators, energy market participants and system operators.

These observations led to the following publications:

- J. Vandewalle, K. Bruninx, and W. D'haeseleer, *Effects of large-scale power to gas conversion on the power, gas and carbon sectors and their interactions*, Energy Convers. Manag., vol. 94, pp. 28–39, 2014.
- J. Vandewalle, K. Bruninx, and W. D'haeseleer, *The interaction of a high renewable energy/low carbon power system with the gas system through power to gas*, in 14th IAEE European Energy Conference, October 28–31, 2014. Rome, Italy.

Appendix B

Case study: data & assumptions

In the Belgian power system, the peak demand in this system typically occurs in winter time and equals about 14 GW, while the lowest demand – around 6 GW – typically occurs during daytime in the summer. The annual Belgian demand amounts to about 82 TWh [182]. Note that Elia reports the transmission system load, which does not account for decentralized generation and accounts for the import-export balance. Unless specified otherwise, we have used this demand without any corrections[1]. In other words, we assume that the distributed generation profile and import-export balance is fixed – only the remaining grid load has to be met. Electrical energy from RES other than wind and waste incineration (7% of annual electric energy demand, approximately 1,000 MW in installed capacity) connected to the transmission grid is treated as a demand correction and cannot be curtailed. The demand profile (2012–2014) and wind power data (2012–2014) are obtained from Elia, the Belgian TSO [87]. The Belgian conventional generation system anno 2013, consisting of 71 conventional power plants and combined-heat-and-power plants, in total 13,920 MW of dispatchable capacity, has been taken from Elia [87]. Nuclear

[1]To be precise, the reported demand is the sum of the measured injections on all voltage levels above 30 kV, corrected for the energy needed to pump water to the upper basin of the pumped hydro energy storage plant in Coo. As little information is available on the generation that occurs at voltage levels below 30 kV, we have chosen not to correct the load profiles provided to avoid distortion of the data. E.g. solar power generation could be added to the load profile to account for own-consumption. However, during sunny days, the generated power may not be fully consumed in locally and fed in the 30 kV grid, and as such it will be accounted for in the Elia grid load. Moreover, some solar power installations are connected to the Elia grid [337].

power plants represent 5,925 MW, coal-fired generation 760 MW and gas-fired generation approximately 5,975 MW. Peaking units (small gas turbines or internal combustion engines) amounts to 1,260 MW. In the case studies presented throughout the text, the installed capacity of intermittent RES-based generation, in particular wind and solar power, will be varied. The assumptions on these installed capacities will be mentioned where relevant. The demand profile and the available dispatchable capacity remain unchanged throughout the text, except in Chapter 6, where we will add eight state-of-the-art CCGT units to the system.

The nominal efficiency of the power plants is based on the type, the fuel and the age of the power plant. The other technical characteristics of the power plants are based on Schröder et al. [338] and ENTSO-E [240]. They are summarized in Table B.1. Ramp-up and ramp-down constraints are assumed equal. The start-up costs depend on the fuel and size of the power plant. The relative efficiency A_i allows to calculate the efficiency η_i of the power plant in partial loading (output g_i) conditions via the following equation:

$$\eta_i(g_i) = \eta_i(\overline{P_i}) \cdot \left[1 + A_i \cdot \ln\left(\frac{g_i}{\overline{P_i}}\right)\right] \tag{B.1}$$

Open cycle gas turbines and oil-fired units with a size of less than 100 MW, a minimum up- and down time of 1 time step and the capability to ramp from zero output to full capacity within a time step are considered as 'fast-starting units'. In total 35 fast-starting units (1,118 MW) are considered in this case study. One pumped hydro storage power plant has been included, with a maximum capacity of 1,308 MW, a round trip efficiency of 75% and a storage capacity of 3,924 MWh. The minimum energy content of the storage facility is set to 10% of the maximal capacity. Other hydro-power generation, about 250 MW in installed capacity, is not accounted for. The CO_2-price is set to 10 €/ton CO_2. The value of lost load is set to 10,000 €/MWh, while the value of reserve shedding VOR equals 5,000 €/MWh. Curtailment is assumed to be free. The costs of the various fuels and their carbon content are based on [240]. Direct start-up costs are augmented with indirect start-up costs. Cycling and indirect start-up costs are taken from [314].

Table B.1: Technical characteristics of the power plants in the considered power system, based on Elia [87], Schröder et al. [338], ENTSO-E [240] and own calculations. PWR stands for pressurized water reactor, a type of nuclear reactor. A SPP is a conventional steam power plants, CCGT a combined-cycle gas turbine. The gas turbines are indicated by GT.

Technology	Fuel	Costs				Efficiency		Dynamics			
	Fuel	Fuel cost (€/MWh_{prim})	Start-up costs (€/MW)	Raming cost (€/MW)	CO_2-content (ton CO_2/MWh_{prim})	Max. efficiency $\eta_i(\overline{P_i})$ (%)	Relative efficiency A_i (-)	$\underline{P_i}$ (% $\overline{P_i}$)	Ramp-up (% $\overline{P_i}$/min)	Min. up-time (h)	Min. down-time (h)
PWR	UO_2	2	35	-	0	33	-	50	3	8	8
SPP	Coal	12	80	1.8	0.338	35–46	0.08	43	3	6	3
SPP	Gas	25	73	1.4	0.205	40–48	0.08	40	2	4	2
CCGT	Gas	25	45	0.5	0.205	40–58	0.20	35	2	2	1
GT	Gas	25	42.4	0.8	0.205	35–42	0.30	30	6	0.5	0.5
Peaker	Oil	35	42.4	0.8	0.281	32–48	0.30	35	10	0.25	0.25

Appendix C

Tight & compact UC formulations

C.1 Deterministic unit commitment model

The presented formulation, developed by Van den Bergh et al. [15], is shown to be more tight and compact than that as proposed by Carrion and Arroyo [88], based on the formulations proposed by Morales et al. [77] and Ostrowski et al. [78]. For a detailed discussion on the DUC model, see [15]. The minimum up- and down-times have been included in the model as in Rajan and Takriti [79]. The constraints on the minimum and maximum stable operating point of each power plant are tightened according to Morales et al. [77]. The ramping constraints are based on Ostrowski et al. [78].

Objective function

$$
\begin{aligned}
min \quad c(g,z) = & \sum_i \sum_j \left(sc_{i,j} + fc_{i,j} + co_2 t_{i,j} + rc_{i,j}\right) \\
& + \sum_j \sum_m TP \cdot \left(VOLL \cdot \phi_{j,m} + VOC \cdot \chi_{j,m}\right) \\
& + \sum_i \sum_j NSRC_i \cdot y_{i,j} + \sum_j VOR \cdot \left(s_j^+ + s_j^-\right)
\end{aligned}
\tag{C.1}
$$

$$\forall i, \forall j: \quad fc_{i,j} = TP \cdot \left(C_i \cdot z_{i,j} + MA_i \cdot \left(g_{i,j} - \underline{P_i} \cdot z_{i,j}\right)\right) \tag{C.2}$$

$$\forall i, \forall j: \quad co_2t_{i,j} = CO_2P \cdot TP \cdot \left(B_i \cdot z_{i,j} + MB_i \cdot \left(g_{i,j} - \underline{P_i} \cdot z_{i,j}\right)\right) \tag{C.3}$$

$$\forall i, \forall j: \quad sc_{i,j} = STC_i \cdot v_{i,j} \tag{C.4}$$

$$\forall i, \forall j: \quad rc_{i,j} \geq RCP_i \cdot \left(g_{i,j} - g_{i,j-1} - \underline{P_i} \cdot v_{i,j}\right) \tag{C.5}$$

$$\forall i, \forall j: \quad rc_{i,j} \geq RCP_i \cdot \left(g_{i,j-1} - g_{i,j} - \underline{P_i} \cdot w_{i,j}\right) \tag{C.6}$$

$$\forall i, \forall j: \quad rc_{i,j} \geq 0 \tag{C.7}$$

Power balance

$$\forall j, \forall m: \quad D_{j,m} - \phi_{j,m} = \sum_i I^{\mathrm{G}}_{m,i} \cdot g_{i,j} + inj_{j,m} + G^{\mathrm{MR}}_{j,m} + G^{\mathrm{F}}_{j,m} - \chi_{j,m} \tag{C.8}$$

$$+ \sum_r I^{\mathrm{PHES}}_{m,r} \cdot \left(g^{\mathrm{T}}_{r,j} - g^{\mathrm{P}}_{r,j}\right)$$

$$\forall j, \forall m: \quad 0 \leq \chi_{j,m} \leq G^{\mathrm{F}}_{j,m} \tag{C.9}$$

$$\forall j, \forall m: \quad 0 \leq \phi_{j,m} \leq D_{j,m} \tag{C.10}$$

Reserve constraints

$$\forall j: \quad D^+_j = \sum_i \left(r^+_{i,j} + nsr^+_{i,j}\right) + \sum_m \chi_{j,m} + \sum_r \left(r^{\mathrm{P},+}_{r,j} + r^{\mathrm{T},+}_{r,j}\right) + s^+_j \tag{C.11}$$

$$\forall j | \sum_m \chi_{j,m} = 0: \quad D^-_j = \sum_i r^-_{i,j} + \sum_r \left(r^{\mathrm{P},-}_{r,j} + r^{\mathrm{T},-}_{r,j}\right) + s^-_j \tag{C.12}$$

Minimum and maximum stable operating point power plants

$$\forall i, \forall j: \quad g_{i,j} + r^+_{i,j} \leq \overline{P_i} \cdot z_{i,j} \tag{C.13}$$

$$\forall i, \forall j: \quad g_{i,j} - r^-_{i,j} \geq \underline{P_i} \cdot z_{i,j} \tag{C.14}$$

$$\forall i, \forall j: \quad g_{i,j},\ r^+_{i,j},\ r^-_{i,j} \geq 0 \tag{C.15}$$

$$\forall i | \{MUT_i \geq 2\}, \forall j: \quad g_{i,j} + r^+_{i,j} \leq \overline{P_i} \cdot z_{i,j} - \left(\overline{P_i} - \underline{P_i}\right) \cdot \left(v_{i,j} + w_{i,j+1}\right) \tag{C.16}$$

$$\forall i|\{K_{i,j} \geq 2\}, \forall j|\{j \leq T - K_{i,j}\} : g_{i,j} + r^{+}_{i,j} \leq \overline{P_i} \cdot z_{i,j+K_{i,j}} - \sum_{k=1}^{K_{i,j}} \overline{P_i} \cdot v_{i,j+k} + \sum_{k=1}^{K_{i,j}} \left(\underline{P_i} + (k-1) \cdot \overline{\Delta P^{-}_i} \cdot w_{i,j+k} \right) \quad \text{(C.17)}$$

$$\forall i, \forall j : K_{i,j} = \min\{MUT_i,\ \frac{\overline{P_i} - \underline{P_i}}{\overline{\Delta P^{-}_i}} + 1,\ T - j\} \quad \text{(C.18)}$$

Ramping constraints power plants

$$\forall i \notin I^{\text{FAST}}, \forall j : \quad g_{i,j} + r^{+}_{i,j} \leq g_{i,j-1} + \overline{\Delta P^{+}_i} \cdot (z_{i,j} - v_{i,j}) + \underline{P_i} \cdot v_{i,j} \quad \text{(C.19)}$$

$$\forall i \notin I^{\text{FAST}}, \forall j : \quad g_{i,j} - r^{-}_{i,j} \geq g_{i,j-1} - \overline{\Delta P^{-}_i} \cdot z_{i,j} - \underline{P_i} \cdot w_{i,j} \quad \text{(C.20)}$$

$$\forall i \in I^{\text{FAST}}, \forall j : \quad g_{i,j} + r^{+}_{i,j} \leq g_{i,j-1} + \overline{\Delta P^{+}_i} \cdot z_{i,j} \quad \text{(C.21)}$$

$$\forall i \in I^{\text{FAST}}, \forall j : \quad g_{i,j} - r^{-}_{i,j} \geq g_{i,j-1} - \overline{\Delta P^{-}_i} \cdot (z_{i,j} + w_{i,j}) \quad \text{(C.22)}$$

$$\forall i|\{MUT_i \geq 2\}, \forall j : \quad g_{i,j} + r^{+}_{i,j} \leq g_{i,j-1} + \underline{P_i} \cdot v_{i,j} + \overline{\Delta P^{+}_i} \cdot (z_{i,j} - v_{i,j} - w_{i,j+1}) \quad \text{(C.23)}$$

$$\forall i|\{MUT_i \geq 2\}, \forall j : \quad g_{i,j} - r^{-}_{i,j} \geq g_{i,j-1} - \underline{P_i} \cdot w_{i,j} - \overline{\Delta P^{-}_i} \cdot (z_{i,j} - v_{i,j} - v_{i,j-1}) \quad \text{(C.24)}$$

$$\forall i|\{MUT_i \geq 2\}, \forall j : \ g_{i,j} + r^{+}_{i,j} \leq g_{i,j-2} + \underline{P_i} \cdot (v_{i,j} + v_{i,j-1} + w_{i,j-1}) + \overline{\Delta P^{+}_i} \cdot (2 \cdot z_{i,j} - 2 \cdot v_{i,j} - v_{i,j-1}) \quad \text{(C.25)}$$

$$\forall i|\{MUT_i \geq 2\}, \forall j : \ g_{i,j} - r^{-}_{i,j} \geq g_{i,j-2} - \underline{P_i} \cdot (w_{i,j} + w_{i,j-1}) - \overline{\Delta P^{-}_i} \cdot (2 \cdot z_{i,j} + w_{i,j} - 2 \cdot v_{i,j-1} - 2 \cdot v_{i,j}) \quad \text{(C.26)}$$

Minimum up- and downtime power plants

$$\forall i \notin I^{\text{FAST}}, \forall j: \quad \sum_{k=1}^{MUT-1} v_{i,j-k} \leq z_{i,j} \tag{C.27}$$

$$\forall i \notin I^{\text{FAST}}, \forall j: \quad \sum_{k=1}^{MDT-1} w_{i,j-k} \leq 1 - z_{i,j} \tag{C.28}$$

$$\forall i, \forall j: \quad z_{i,j} - z_{i,j-1} - v_{i,j} + w_{i,j} = 0 \tag{C.29}$$

$$\forall i, \forall j: \quad v_{i,j} + w_{i,j} \leq 1 \tag{C.30}$$

$$\forall i, \forall j: \quad z_{i,j},\ v_{i,j},\ w_{i,j} \in \{0,1\} \tag{C.31}$$

Non-spinning reserves

$$\forall i \in I^{\text{FAST}}, \forall j: \quad \underline{P_i} \cdot y_{i,j} \leq nsr^{+}_{i,j} \leq \overline{P_i} \cdot y_{i,j} \tag{C.32}$$

$$\forall i \in I^{\text{FAST}}, \forall j: \quad y_{i,j} + z_{i,j} \leq 1 \tag{C.33}$$

$$\forall i \in I^{\text{FAST}}, \forall j: \quad y_{i,j} \in \{0,1\} \tag{C.34}$$

$$\forall i \notin I^{\text{FAST}}, \forall j: \quad y_{i,j},\ nsr^{+}_{i,j} = 0 \tag{C.35}$$

DC load flow

$$\forall j, \forall n: \quad f_{j,n} = \sum_{m} PTDF_{n,m} \cdot inj_{j,m} \tag{C.36}$$

$$\forall j, \forall n: \quad -CAP_n \leq f_{j,n} \leq CAP_n \tag{C.37}$$

$$\forall j: \quad \sum_{m} inj_{j,m} = 0 \tag{C.38}$$

Pumped hydro energy storage

$$\forall r, \forall j: \quad e_{r,j} = TP \cdot \left(g^{\mathrm{P}}_{r,j} \cdot \sqrt{\epsilon_r} - \frac{g^{\mathrm{T}}_{r,j}}{\sqrt{\epsilon_r}} \right) + e_{r,j-1} \tag{C.39}$$

$$\forall r, \forall j: \quad \underline{E_r} \leq e_{r,j} \leq \overline{E_r} \tag{C.40}$$

$$\forall r, \forall j: \quad 0 \leq g^{\mathrm{P}}_{r,j} + r^{\mathrm{P},-}_{r,j} \leq \overline{P_r} \cdot p_{r,j} \tag{C.41}$$

$$\forall r, \forall j: \quad 0 \leq g^{\mathrm{T}}_{r,j} + r^{\mathrm{T},+}_{r,j} \leq \overline{P_r} \cdot t_{r,j} \tag{C.42}$$

$$\forall r, \forall j: \quad r^{\mathrm{T},-}_{r,j} \leq g^{\mathrm{T}}_{r,j} \tag{C.43}$$

$$\forall r, \forall j: \quad r^{\mathrm{P},+}_{r,j} \leq g^{\mathrm{P}}_{r,j} \tag{C.44}$$

$$\forall r, \forall j: \quad p_{r,j} + t_{r,j} \leq 1 \tag{C.45}$$

$$\forall r, \forall j: \quad e_{r,j} + TP \cdot \sum_{1}^{j} \left(\frac{r^{\mathrm{T},-}_{r,j}}{\sqrt{\epsilon_r}} + r^{\mathrm{P},-}_{r,j} \cdot \sqrt{\epsilon_r} \right) \leq \overline{E_r} \tag{C.46}$$

$$\forall r, \forall j: \quad e_{r,j} - TP \cdot \sum_{1}^{j} \left(\frac{r^{\mathrm{T},+}_{r,j}}{\sqrt{\epsilon_r}} + r^{\mathrm{P},+}_{r,j} \cdot \sqrt{\epsilon_r} \right) \geq \underline{E_r} \tag{C.47}$$

$$\forall r, \forall j: \quad g^{\mathrm{P}}_{r,j}, g^{\mathrm{T}}_{r,j}, r^{\mathrm{P},+}_{r,j}, r^{\mathrm{P},-}_{r,j}, r^{\mathrm{T},+}_{r,j}, r^{\mathrm{T},-}_{r,j} \geq 0 \tag{C.48}$$

$$\forall r, \forall j: \quad p_{r,j},\ t_{r,j} \in \{0, 1\} \tag{C.49}$$

C.2 Stochastic unit commitment model

Objective function

$$\min c(g,z) = \sum_i \sum_j \left(sc_{i,j} + \sum_s \pi_s \cdot (fc_{i,j,s} + co_2t_{i,j,s} + rc_{i,j,s}) \right) \tag{C.50}$$
$$+ \sum_j \sum_m \sum_s \pi_s \cdot TP \cdot (VOLL \cdot \phi_{j,m,s} + VOC \cdot \chi_{j,m,s})$$
$$+ \sum_i \sum_j NSRC_i \cdot y_{i,j}$$

$$\forall i, \forall j, \forall s: \; fc_{i,j,s} \geq TP \cdot \left(C_i \cdot z_{i,j} + MA_i \cdot \left(g_{i,j,s} - \underline{P_i} \cdot z_{i,j} \right) \right) \tag{C.51}$$

$$\forall i, \forall j, \forall s: \; co_2t_{i,j,s} \geq CO_2P \cdot TP \cdot \left(B_i \cdot z_{i,j} + MB_i \cdot \left(g_{i,j,s} - \underline{P_i} \cdot z_{i,j} \right) \right) \tag{C.52}$$

$$\forall i, \forall j: \quad sc_{i,j} \geq STC_i \cdot v_{i,j} + \sum_s \pi_s \cdot STC_i \cdot v^*_{i,j,s} \tag{C.53}$$

$$\forall i, \forall j, \forall s: \; rc_{i,j,s} \geq RCP_i \cdot \left(g_{i,j,s} - g_{i,j-1,s} - \underline{P_i} \cdot v_{i,j} \right) \tag{C.54}$$

$$\forall i, \forall j, \forall s: \; rc_{i,j,s} \geq RCP_i \cdot \left(g_{i,j-1,s} - g_{i,j,s} - \underline{P_i} \cdot w_{i,j} \right) \tag{C.55}$$

$$\forall i, \forall j, \forall s: \; fc_{i,j,s} \geq TP \cdot \left(C_i \cdot z^*_{i,j,s} + MA_i \cdot \left(nsr^+_{i,j,s} - \underline{P_i} \cdot z^*_{i,j,s} \right) \right)$$

$$\forall i, \forall j, \forall s: \; co_2t_{i,j,s} \geq CO_2P \cdot TP \cdot \left(B_i \cdot z^*_{i,j,s} \right. \tag{C.56}$$
$$\left. + MB_i \cdot \left(nsr^+_{i,j,s} - \underline{P_i} \cdot z^*_{i,j,s} \right) \right)$$

$$\forall i, \forall j, \forall s: \; rc_{i,j,s} \geq RCP_i \cdot \left(nsr^+_{i,j,s} - nsr^+_{i,j-1,s} - \overline{\Delta P_i^+} \cdot v^*_{i,j,s} \right) \tag{C.57}$$

$$\forall i, \forall j, \forall s: \; rc_{i,j,s} \geq RCP_i \cdot \left(nsr^+_{i,j-1,s} - nsr^+_{i,j,s} - \overline{\Delta P_i^-} \cdot w^*_{i,j,s} \right) \tag{C.58}$$

$$\forall i, \forall j, \forall s: \; rc_{i,j,s} \geq 0 \tag{C.59}$$

Power balance

$$\forall j, \forall m, \forall s: \quad D_{j,m} - \phi_{j,m,s} = \sum_i I^{\mathrm{G}}_{m,i} \cdot \left(g_{i,j,s} + nsr^{+}_{i,j,s}\right) + G^{\mathrm{MR}}_{j,m} + G^{\mathrm{F}}_{j,m,s} - \chi_{j,m,s} + inj_{j,m,s} + \sum_r I^{\mathrm{PHES}}_{m,r} \cdot \left(g^{\mathrm{T}}_{r,j,s} - g^{\mathrm{P}}_{r,j,s}\right) \tag{C.60}$$

$$\forall j, \forall m, \forall s: \quad 0 \leq \chi_{j,m,s} \leq G^{\mathrm{F}}_{j,m,s} \tag{C.61}$$

$$\forall j, \forall m, \forall s: \quad 0 \leq \phi_{j,m,s} \leq D_{j,m} \tag{C.62}$$

$$\sum_j \sum_m \sum_s \pi_s \cdot TP \cdot \phi_{j,m,s} \leq \overline{\Phi} \quad \text{(optional)} \tag{C.63}$$

Minimum and maximum operating point power plants

$$\forall i, \forall j, \forall s: \quad \underline{P_i} \cdot z_{i,j} \leq g_{i,j,s} \leq \overline{P_i} \cdot z_{i,j} \tag{C.64}$$

$$\forall i | \{MUT_i \geq 2\}, \forall j, \forall s: \quad g_{i,j,s} \leq \overline{P_i} \cdot z_{i,j} - \left(\overline{P_i} - \underline{P_i}\right) \cdot (v_{i,j} + w_{i,j+1}) \tag{C.65}$$

$$\forall i | \{K_{i,j} \geq 2\}, \forall j | \{j \leq T - K_{i,j}\}, \forall s: \quad g_{i,j,s} \leq \overline{P_i} \cdot z_{i,j+K_{i,j}} - \sum_{k=1}^{K_{i,j}} \overline{P_i} \cdot v_{i,j+k} + \sum_{k=1}^{K_{i,j}} \left(\underline{P_i} + (k-1) \cdot \overline{\Delta P^{-}_i} \cdot w_{i,j+k}\right) \tag{C.66}$$

$$\forall i, \forall j: K_{i,j} = \min\{MUT_i, \ \frac{\overline{P_i} - \underline{P_i}}{\overline{\Delta P^{-}_i}} + 1, \ T - j\} \tag{C.67}$$

Ramping constraints power plants

$$\forall i \notin I^{\mathrm{FAST}}, \forall j, \forall s: \ g_{i,j,s} \leq g_{i,j-1,s} + \overline{\Delta P^{+}_i} \cdot (z_{i,j} - v_{i,j}) + \underline{P_i} \cdot v_{i,j} \tag{C.68}$$

$$\forall i \notin I^{\mathrm{FAST}}, \forall j, \forall s: \ g_{i,j,s} \geq g_{i,j-1,s} - \overline{\Delta P^{-}_i} \cdot z_{i,j} - \underline{P_i} \cdot w_{i,j} \tag{C.69}$$

$$\forall i \in I^{\mathrm{FAST}}, \forall j, \forall s: \ g_{i,j,s} \leq g_{i,j-1,s} + \overline{\Delta P^{+}_i} \cdot z_{i,j} \tag{C.70}$$

$$\forall i \in I^{\mathrm{FAST}}, \forall j, \forall s: \ g_{i,j,s} \geq g_{i,j-1,s} - \overline{\Delta P^{-}_i} \cdot (z_{i,j} + w_{i,j}) \tag{C.71}$$

$$\forall i|\{MUT_i \geq 2\}, \forall j, \forall s: \; g_{i,j,s} \leq g_{i,j-1,s} + \underline{P_i} \cdot v_{i,j} + \overline{\Delta P_i^+} \cdot (z_{i,j} - v_{i,j} - w_{i,j+1}) \tag{C.72}$$

$$\forall i|\{MUT_i \geq 2\}, \forall j, \forall s: \; g_{i,j,s} \geq g_{i,j-1,s} - \underline{P_i} \cdot w_{i,j} - \overline{\Delta P_i^-} \cdot (z_{i,j} - v_{i,j} - v_{i,j-1}) \tag{C.73}$$

$$\forall i|\{MUT_i \geq 2\}, \forall j, \forall s: \; g_{i,j,s} \leq g_{i,j-2,s} + \underline{P_i} \cdot (v_{i,j} + v_{i,j-1} + w_{i,j-1}) + \overline{\Delta P_i^+} \cdot (2 \cdot z_{i,j} - 2 \cdot v_{i,j} - v_{i,j-1}) \tag{C.74}$$

$$\forall i|\{MUT_i \geq 2\}, \forall j, \forall s: \; g_{i,j,s} \geq g_{i,j-2,s} - \underline{P_i} \cdot (w_{i,j} + w_{i,j-1}) - \overline{\Delta P_i^-} \cdot (2 \cdot z_{i,j} + w_{i,j} - 2 \cdot v_{i,j-1} - 2 \cdot v_{i,j}) \tag{C.75}$$

Minimum up- and downtime power plants

$$\forall i \notin I^{\text{FAST}}, \forall j: \quad \sum_{k=1}^{MUT-1} v_{i,j-k} \leq z_{i,j} \tag{C.76}$$

$$\forall i \notin I^{\text{FAST}}, \forall j: \quad \sum_{k=1}^{MDT-1} w_{i,j-k} \leq 1 - z_{i,j} \tag{C.77}$$

$$\forall i, \forall j: \quad z_{i,j} - z_{i,j-1} - v_{i,j} + w_{i,j} = 0 \tag{C.78}$$

$$\forall i, \forall j: \quad v_{i,j} + w_{i,j} \leq 1 \tag{C.79}$$

$$\forall i, \forall j: \quad z_{i,j},\ v_{i,j},\ w_{i,j} \in \{0,1\} \tag{C.80}$$

$$\forall i \in I^{\text{FAST}}, \forall j, \forall s: \quad z_{i,j} + z^*_{i,j,s} \leq 1 \tag{C.81}$$

$$\forall i \in I^{\text{FAST}}, \forall j, \forall s: \quad z^*_{i,j,s} - z^*_{i,j-1,s} - v^*_{i,j,s} + w^*_{i,j,s} = 0; \tag{C.82}$$

$$\forall i \in I^{\text{FAST}}, \forall j, \forall s: \quad v^*_{i,j,s} + w^*_{i,j,s} \leq 1 \tag{C.83}$$

$$\forall i \in I^{\text{FAST}}, \forall j, \forall s: \quad z^*_{i,j,s},\ v^*_{i,j,s},\ w^*_{i,j,s} \in \{0,1\} \tag{C.84}$$

$$\forall i \notin I^{\text{FAST}}, \forall j, \forall s: \quad z^*_{i,j,s},\ v^*_{i,j,s},\ w^*_{i,j,s} = 0 \tag{C.85}$$

DC load flow

$$\forall j, \forall n, \forall s: \quad f_{j,n,s} = \sum_{m} PTDF_{n,m} \cdot inj_{j,m,s} \tag{C.86}$$

$$\forall j, \forall n, \forall s: \quad -CAP_n \leq f_{j,n,s} \leq CAP_n \tag{C.87}$$

$$\forall j, \forall s: \quad \sum_{m} inj_{j,m,s} = 0 \tag{C.88}$$

Pumped hydro energy storage

$$\forall r, \forall j, \forall s: \quad e_{r,j,s} = TP \cdot \left(g^{\mathrm{P}}_{r,j,s} \cdot \sqrt{\epsilon_r} - \frac{g^{\mathrm{T}}_{r,j,s}}{\sqrt{\epsilon_r}} \right) + e_{r,j-1,s} \tag{C.89}$$

$$\forall r, \forall j, \forall s: \quad \underline{E_r} \leq e_{r,j,s} \leq \overline{E_r} \tag{C.90}$$

$$\forall r, \forall j, \forall s: \quad 0 \leq g^{\mathrm{T}}_{r,j,s} \leq \overline{P_r} \cdot t_{r,j,s} \tag{C.91}$$

$$\forall r, \forall j, \forall s: \quad 0 \leq g^{\mathrm{P}}_{r,j,s} \leq \overline{P_r} \cdot p_{r,j,s} \tag{C.92}$$

$$\forall r, \forall j, \forall s: \quad p_{r,j,s} + t_{r,j,s} \leq 1 \tag{C.93}$$

Non-spinning reserves

$$\forall i \in I^{\mathrm{FAST}}, \forall j, \forall s: \quad \underline{P_i} \cdot z^*_{i,j,s} \leq nsr^+_{i,j,s} \leq \overline{P_i} \cdot z^*_{i,j,s} \tag{C.94}$$

$$\forall i \in I^{\mathrm{FAST}}, \forall j, \forall s: \quad nsr^+_{i,j,s} \leq nsr^+_{i,j-1,s} + \overline{\Delta P^+_i} \cdot z^*_{i,j,s} \tag{C.95}$$

$$\forall i \in I^{\mathrm{FAST}}, \forall j, \forall s: \quad nsr^+_{i,j,s} \geq nsr^+_{i,j-1,s} - \overline{\Delta P^-_i} \cdot (z^*_{i,j,s} + w^*_{i,j,s}) \tag{C.96}$$

$$\forall i, \forall j, \forall s: \; y_{i,j} \geq z^*_{i,j,s} \tag{C.97}$$

$$\forall i, \forall j: \; y_{i,j} \in \{0, 1\} \tag{C.98}$$

$$\forall i \notin I^{\mathrm{FAST}}, \forall j, \forall s: \quad y_{i,j}, nsr^+_{i,j,s} = 0 \tag{C.99}$$

C.3 Improved interval unit commitment model

Objective function

$$\min c(g,z) = \sum_i \sum_j \left(sc_{i,j} + fc_{i,j} + co_2t_{i,j} + rc_{i,j}\right) \tag{C.100}$$
$$+ \sum_j \sum_m TP \cdot \left(VOLL \cdot \phi_{j,m,s} + VOC \cdot \chi_{j,m,s^{\mathrm{F}}}\right)$$
$$+ \sum_i \sum_j NSRC_i \cdot y_{i,j}$$

$$\forall i, \forall j: \; fc_{i,j} \geq TP \cdot \left(C_i \cdot z_{i,j} + MA_i \cdot \left(g_{i,j,s^{\mathrm{F}}} - \underline{P_i} \cdot z_{i,j}\right)\right) \tag{C.101}$$

$$\forall i, \forall j: \; co_2t_{i,j} \geq CO_2P \cdot TP \cdot \left(B_i \cdot z_{i,j} + MB_i \cdot \left(g_{i,j,s^{\mathrm{F}}} - \underline{P_i} \cdot z_{i,j}\right)\right) \tag{C.102}$$

$$\forall i, \forall j: \; sc_{i,j} \geq STC_i \cdot v_{i,j} \tag{C.103}$$

$$\forall i, \forall j: \; rc_{i,j} \geq RCP_i \cdot \left(g_{i,j,s^{\mathrm{F}}} - g_{i,j-1,s^{\mathrm{F}}} - \underline{P_i} \cdot v_{i,j}\right) \tag{C.104}$$

$$\forall i, \forall j: \; rc_{i,j} \geq RCP_i \cdot \left(g_{i,j-1,s^{\mathrm{F}}} - g_{i,j,s^{\mathrm{F}}} - \underline{P_i} \cdot w_{i,j}\right) \tag{C.105}$$

$$\forall i, \forall j: \; rc_{i,j} \geq 0 \tag{C.106}$$

Power balance

$$\forall j, \forall m, \forall s: \; D_{j,m} - \phi_{j,m,s} = \sum_i I^{\mathrm{G}}_{m,i} \cdot \left(g_{i,j,s} + nsr^{+}_{i,j,s}\right) + G^{\mathrm{MR}}_{j,m} \tag{C.107}$$
$$+ G^{\mathrm{F}}_{j,m,s} - \chi_{j,m,s} + inj_{j,m,s}$$
$$+ \sum_r I^{\mathrm{PHES}}_{m,r} \cdot \left(g^{\mathrm{T}}_{r,j,s} - g^{\mathrm{P}}_{r,j,s}\right)$$

$$\forall j, \forall m, \forall s: \quad 0 \leq \chi_{j,m,s} \leq G^{\mathrm{F}}_{j,m,s} \tag{C.108}$$

$$\forall j, \forall m, \forall s: \quad \phi_{j,m,s} = 0 \quad \text{(ommitted if no feasible solution is found)} \tag{C.109}$$

Minimum and maximum operating point power plants

$$\forall i, \forall j, \forall s: \quad \underline{P_i} \cdot z_{i,j} \leq g_{i,j,s} \leq \overline{P_i} \cdot z_{i,j} \tag{C.110}$$

$$\forall i | \{MUT_i \geq 2\}, \forall j, \forall s: \quad g_{i,j,s} \leq \overline{P_i} \cdot z_{i,j} - \left(\overline{P_i} - \underline{P_i}\right) \cdot (v_{i,j} + w_{i,j+1}) \tag{C.111}$$

$$\forall i | \{K_{i,j} \geq 2\}, \forall j | \{j \leq T - K_{i,j}\}, \forall s: \quad g_{i,j,s} \leq \overline{P_i} \cdot z_{i,j+K_{i,j}} - \sum_{k=1}^{K_{i,j}} \overline{P_i} \cdot v_{i,j+k} + \sum_{k=1}^{K_{i,j}} \left(\underline{P_i} + (k-1) \cdot \overline{\Delta P_i^-} \cdot w_{i,j+k}\right) \tag{C.112}$$

$$\forall i, \forall j: K_{i,j} = \min\{MUT_i, \ \frac{\overline{P_i} - \underline{P_i}}{\overline{\Delta P_i^-}} + 1, \ T - j\} \tag{C.113}$$

Ramping constraints power plants

$$\forall i \notin I^{\text{FAST}}, \forall j: \ g_{i,j,s^{\text{F}}} \leq g_{i,j-1,s^{\text{F}}} + \overline{\Delta P_i^+} \cdot (z_{i,j} - v_{i,j}) + \underline{P_i} \cdot v_{i,j} \tag{C.114}$$

$$\forall i \notin I^{\text{FAST}}, \forall j: \ g_{i,j,s^{\text{F}}} \geq g_{i,j-1,s^{\text{F}}} - \overline{\Delta P_i^-} \cdot z_{i,j} - \underline{P_i} \cdot w_{i,j} \tag{C.115}$$

$$\forall i \in I^{\text{FAST}}, \forall j: \ g_{i,j,s^{\text{F}}} \leq g_{i,j-1,s^{\text{F}}} + \overline{\Delta P_i^+} \cdot z_{i,j} \tag{C.116}$$

$$\forall i \in I^{\text{FAST}}, \forall j: \ g_{i,j,s^{\text{F}}} \geq g_{i,j-1,s^{\text{F}}} - \overline{\Delta P_i^-} \cdot (z_{i,j} + w_{i,j}) \tag{C.117}$$

$$\forall i | \{MUT_i \geq 2\}, \forall j: \ g_{i,j,s^{\text{F}}} \leq g_{i,j-1,s^{\text{F}}} + \underline{P_i} \cdot v_{i,j} + \overline{\Delta P_i^+} \cdot (z_{i,j} - v_{i,j} - w_{i,j+1}) \tag{C.118}$$

$$\forall i | \{MUT_i \geq 2\}, \forall j: \ g_{i,j,s^{\text{F}}} \geq g_{i,j-1,s^{\text{F}}} - \underline{P_i} \cdot w_{i,j} - \overline{\Delta P_i^-} \cdot (z_{i,j} - v_{i,j} - v_{i,j-1}) \tag{C.119}$$

$$\forall i | \{MUT_i \geq 2\}, \forall j: \ g_{i,j,s^{\text{F}}} \leq g_{i,j-2,s^{\text{F}}} + \underline{P_i} \cdot (v_{i,j} + v_{i,j-1} + w_{i,j-1}) + \overline{\Delta P_i^+} \cdot (2 \cdot z_{i,j} - 2 \cdot v_{i,j} - v_{i,j-1}) \tag{C.120}$$

$$\forall i | \{MUT_i \geq 2\}, \forall j: \ g_{i,j,s^{\text{F}}} \geq g_{i,j-2,s^{\text{F}}} - \underline{P_i} \cdot (w_{i,j} + w_{i,j-1}) - \overline{\Delta P_i^-} \cdot (2 \cdot z_{i,j} + w_{i,j} - 2 \cdot v_{i,j-1} - 2 \cdot v_{i,j}) \tag{C.121}$$

$$\forall i \notin I^{\text{FAST}}, \forall j \in J^{\text{E}}: \; g_{i,j,s_e^{\text{R}+}} \leq g_{i,j-1,s_e^{\text{R}+}} + \overline{\Delta P_i^+} \cdot (z_{i,j} - v_{i,j}) + \underline{P_i} \cdot v_{i,j} \tag{C.122}$$

$$\forall i \in I^{\text{FAST}}, \forall j \in J^{\text{E}}: \; g_{i,j,s_e^{\text{R}+}} \leq g_{i,j-1,s_e^{\text{R}+}} + \overline{\Delta P_i^+} \cdot z_{i,j} \tag{C.123}$$

$$\forall i \notin I^{\text{FAST}}, \forall j \in J^{\text{O}}: \; g_{i,j,s_o^{\text{R}+}} \leq g_{i,j-1,s_o^{\text{R}+}} + \overline{\Delta P_i^+} \cdot (z_{i,j} - v_{i,j}) + \underline{P_i} \cdot v_{i,j} \tag{C.124}$$

$$\forall i \in I^{\text{FAST}}, \forall j \in J^{\text{O}}: \; g_{i,j,s_o^{\text{R}+}} \leq g_{i,j-1,s_o^{\text{R}+}} + \overline{\Delta P_i^+} \cdot z_{i,j} \tag{C.125}$$

$$\forall i \notin I^{\text{FAST}}, \forall j \in J^{\text{E}}: \; g_{i,j,s_e^{\text{R}-}} \geq g_{i,j-1,s_e^{\text{R}-}} - \overline{\Delta P_i^-} \cdot z_{i,j} - \underline{P_i} \cdot w_{i,j} \tag{C.126}$$

$$\forall i \in I^{\text{FAST}}, \forall j \in J^{\text{E}}: \; g_{i,j,s_e^{\text{R}-}} \geq g_{i,j-1,s_e^{\text{R}-}} - \overline{\Delta P_i^-} \cdot (z_{i,j} + w_{i,j}) \tag{C.127}$$

$$\forall i \notin I^{\text{FAST}}, \forall j \in J^{\text{O}}: \; g_{i,j,s_o^{\text{R}-}} \geq g_{i,j-1,s_o^{\text{R}-}} - \overline{\Delta P_i^-} \cdot z_{i,j} - \underline{P_i} \cdot w_{i,j} \tag{C.128}$$

$$\forall i \in I^{\text{FAST}}, \forall j \in J^{\text{O}}: \; g_{i,j,s_o^{\text{R}-}} \geq g_{i,j-1,s_o^{\text{R}-}} - \overline{\Delta P_i^-} \cdot (z_{i,j} + w_{i,j}) \tag{C.129}$$

Minimum up- and downtime power plants

$$\forall i \notin I^{\text{FAST}}, \forall j: \quad \sum_{k=1}^{MUT-1} v_{i,j-k} \leq z_{i,j} \tag{C.130}$$

$$\forall i \notin I^{\text{FAST}}, \forall j: \quad \sum_{k=1}^{MDT-1} w_{i,j-k} \leq 1 - z_{i,j} \tag{C.131}$$

$$\forall i, \forall j: \quad z_{i,j} - z_{i,j-1} - v_{i,j} + w_{i,j} = 0 \tag{C.132}$$

$$\forall i, \forall j: \quad v_{i,j} + w_{i,j} \leq 1 \tag{C.133}$$

$$\forall i, \forall j: \quad z_{i,j}, \; v_{i,j}, \; w_{i,j} \in \{0,1\} \tag{C.134}$$

$$\forall i \in I^{\text{FAST}}, \forall j, \forall s: \quad z^*_{i,j,s} - z^*_{i,j-1,s} - v^*_{i,j,s} + w^*_{i,j,s} = 0; \tag{C.135}$$

$$\forall i \in I^{\text{FAST}}, \forall j, \forall s: \quad v^*_{i,j,s} + w^*_{i,j,s} \leq 1 \tag{C.136}$$

$$\forall i \in I^{\text{FAST}}, \forall j, \forall s: \quad z_{i,j} + z^*_{i,j,s} \leq 1 \tag{C.137}$$

$$\forall i \in I^{\text{FAST}}, \forall j, \forall s: \quad z^*_{i,j,s}, \; v^*_{i,j,s}, \; w^*_{i,j,s} \in \{0,1\} \tag{C.138}$$

$$\forall i \notin I^{\mathrm{FAST}}, \forall j, \forall s: \quad z^*_{i,j,s},\ v^*_{i,j,s},\ w^*_{i,j,s} = 0 \tag{C.139}$$

DC load flow

$$\forall j, \forall n, \forall s: \quad f_{j,n,s} = \sum_m PTDF_{n,m} \cdot inj_{j,m,s} \tag{C.140}$$

$$\forall j, \forall n, \forall s: \quad -CAP_n \leq f_{j,n,s} \leq CAP_n \tag{C.141}$$

$$\forall j, \forall s: \quad \sum_m inj_{j,m,s} = 0 \tag{C.142}$$

Pumped hydro energy storage

$$\forall r, \forall j: \quad e_{r,j,s^{\mathrm{F}}} = TP \cdot \left(g^{\mathrm{P}}_{r,j,s^{\mathrm{F}}} \cdot \sqrt{\epsilon_r} - \frac{g^{\mathrm{T}}_{r,j,s^{\mathrm{F}}}}{\sqrt{\epsilon_r}} \right) + e_{r,j-1,s^{\mathrm{F}}} \tag{C.143}$$

$$\forall r, \forall j, \forall s \in S^{\mathrm{R}}: \ e_{r,j,s} = e_{r,j-1,s^{\mathrm{F}}} + TP \cdot \left(g^{\mathrm{P}}_{r,j,s} \cdot \sqrt{\epsilon_r} - \frac{g^{\mathrm{T}}_{r,j,s}}{\sqrt{\epsilon_r}} \right) \tag{C.144}$$

$$\forall r, \forall j, \forall s: \quad \underline{E_r} \leq e_{r,j,s} \leq \overline{E_r} \tag{C.145}$$

$$\forall r, \forall j, \forall s: \quad 0 \leq g^{\mathrm{T}}_{r,j,s} \leq \overline{P_r} \cdot t_{r,j,s} \tag{C.146}$$

$$\forall r, \forall j, \forall s: \quad 0 \leq g^{\mathrm{P}}_{r,j,s} \leq \overline{P_r} \cdot p_{r,j,s} \tag{C.147}$$

$$\forall r, \forall j, \forall s: \quad p_{r,j,s} + t_{r,j,s} \leq 1 \tag{C.148}$$

$$\forall r, \forall j \in J^{\mathrm{O}}, \forall s \in \{s^{\mathrm{R}+}_{\mathrm{e}}, s^{\mathrm{R}-}_{\mathrm{e}}\}: \ g^{\mathrm{P}}_{r,j,s},\ g^{\mathrm{T}}_{r,j,s} = 0 \tag{C.149}$$

$$\forall r, \forall j \in J^{\mathrm{E}}, \forall s \in \{s^{\mathrm{R}+}_{\mathrm{o}}, s^{\mathrm{R}-}_{\mathrm{o}}\}: \ g^{\mathrm{P}}_{r,j,s},\ g^{\mathrm{T}}_{r,j,s} = 0 \tag{C.150}$$

$$\begin{aligned} \forall r, \forall j, \forall s \in \{s^{\mathrm{R}-}_{\mathrm{e}}, s^{\mathrm{R}-}_{\mathrm{o}}\}: e_{r,j,s^{\mathrm{F}}} &- \sum_{j^*=1}^{j} \sum_s TP \cdot \frac{\Delta^- g^{\mathrm{T}}_{r,j,s}}{\sqrt{\epsilon_r}} \\ &- \sum_{j^*=1}^{j} \sum_s TP \cdot \Delta^- g^{\mathrm{P}}_{r,j,s} \cdot \sqrt{\epsilon_r} \geq \underline{E_r} \end{aligned} \tag{C.151}$$

$$\forall r, \forall j, \forall s \in \{s_{\mathrm{e}}^{\mathrm{R}+}, s_{\mathrm{o}}^{\mathrm{R}+}\} : e_{r,j,s^{\mathrm{F}}} + \sum_{j^*=1}^{j} \sum_{s} TP \cdot \frac{\Delta^+ g_{r,j,s}^{\mathrm{T}}}{\sqrt{\epsilon_r}} + \sum_{j^*=1}^{j} \sum_{s} TP \cdot \Delta^+ g_{r,j,s}^{\mathrm{P}} \cdot \sqrt{\epsilon_r} \leq \overline{E_r} \tag{C.152}$$

$$\forall r, \forall j : \quad \Delta^+ g_{r,j}^{\mathrm{P}} \geq g_{r,j,s_o^{\mathrm{R}+}}^{\mathrm{P}} + g_{r,j,s_e^{\mathrm{R}+}}^{\mathrm{P}} - g_{r,j,s^{\mathrm{F}}}^{\mathrm{P}} \tag{C.153}$$

$$\forall r, \forall j : \quad \Delta^+ g_{r,j}^{\mathrm{T}} \geq g_{r,j,s^{\mathrm{F}}}^{\mathrm{T}} - g_{r,j,s_o^{\mathrm{R}+}}^{\mathrm{T}} - g_{r,j,s_e^{\mathrm{R}+}}^{\mathrm{T}} \tag{C.154}$$

$$\forall r, \forall j : \quad \Delta^- g_{r,j}^{\mathrm{P}} \geq g_{r,j,s^{\mathrm{F}}}^{\mathrm{P}} - g_{r,j,s_o^{\mathrm{R}-}}^{\mathrm{P}} - g_{r,j,s_e^{\mathrm{R}-}}^{\mathrm{P}} \tag{C.155}$$

$$\forall r, \forall j : \quad \Delta^- g_{r,j}^{\mathrm{T}} \geq g_{r,j,s_o^{\mathrm{R}-}}^{\mathrm{T}} + g_{r,j,s_e^{\mathrm{R}-}}^{\mathrm{T}} - g_{r,j,s^{\mathrm{F}}}^{\mathrm{T}} \tag{C.156}$$

$$\forall r, \forall j : \quad \Delta^+ g_{r,j}^{\mathrm{P}},\ \Delta^+ g_{r,j}^{\mathrm{T}},\ \Delta^- g_{r,j}^{\mathrm{T}},\ \Delta^- g_{r,j}^{\mathrm{P}} \geq 0 \tag{C.157}$$

Non-spinning reserves

$$\forall i \in I^{\mathrm{FAST}}, \forall j, \forall s \in S^{\mathrm{R}} : \quad \underline{P_i} \cdot z_{i,j,s}^* \leq nsr_{i,j,s}^+ \leq \overline{P_i} \cdot z_{i,j,s}^* \tag{C.158}$$

$$\forall i \in I^{\mathrm{FAST}}, \forall j \in J^{\mathrm{E}} : \ nsr_{i,j,s_e^{\mathrm{R}+}}^+ \leq nsr_{i,j-1,s_e^{\mathrm{R}+}}^+ + \overline{\Delta P_i^+} \cdot z_{i,j}^* \tag{C.159}$$

$$\forall i \in I^{\mathrm{FAST}}, \forall j \in J^{\mathrm{O}} : \ nsr_{i,j,s_o^{\mathrm{R}+}}^+ \leq nsr_{i,j-1,s_o^{\mathrm{R}+}}^+ + \overline{\Delta P_i^+} \cdot z_{i,j}^* \tag{C.160}$$

$$\forall i \in I^{\mathrm{FAST}}, \forall j \in J^{\mathrm{E}} : \ nsr_{i,j,s_e^{\mathrm{R}-}}^+ \geq nsr_{i,j-1,s_e^{\mathrm{R}-}}^+ - \overline{\Delta P_i^-} \cdot \left(z_{i,j}^* + w_{i,j}^*\right) \tag{C.161}$$

$$\forall i \in I^{\mathrm{FAST}}, \forall j \in J^{\mathrm{O}} : \ nsr_{i,j,s_o^{\mathrm{R}-}}^+ \geq nsr_{i,j-1,s_o^{\mathrm{R}-}}^+ - \overline{\Delta P_i^-} \cdot \left(z_{i,j}^* + w_{i,j}^*\right) \tag{C.162}$$

$$\forall i \in I^{\mathrm{FAST}}, \forall j, \forall s \in S^{\mathrm{R}} : \ y_{i,j} \geq z_{i,j,s}^* \tag{C.163}$$

$$\forall i \notin I^{\mathrm{FAST}}, \forall j, \forall s : \quad y_{i,j}, nsr_{i,j,s}^+ = 0 \tag{C.164}$$

$$\forall i, \forall j : \quad nsr_{i,j,s^{\mathrm{F}}}^+, z_{i,j,s^{\mathrm{F}}}^*, v_{i,j,s^{\mathrm{F}}}^*, w_{i,j,s^{\mathrm{F}}}^* = 0 \tag{C.165}$$

C.4 Hybrid unit commitment model

Objective function

$$\min c(g,z) = \sum_i \sum_j \left[sc_{i,j} + \sum_s \pi_s \cdot (fc_{i,j,s} + co_2t_{i,j,s} + rc_{i,j,s}) \right] \tag{C.166}$$
$$+ \sum_j \sum_m \sum_s \pi_s \cdot TP \cdot (VOLL \cdot \phi_{j,m,s} + VOC \cdot \chi_{j,m,s})$$
$$+ \sum_i \sum_j NSRC_i \cdot y_{i,j} + \sum_j VOR \cdot \left(s_j^+ + s_j^-\right)$$

$$\forall i, \forall j, \forall s: \; fc_{i,j,s} \geq TP \cdot \left(C_i \cdot z_{i,j} + MA_i \cdot \left(g_{i,j,s} - \underline{P_i} \cdot z_{i,j}\right)\right) \tag{C.167}$$

$$\forall i, \forall j, \forall s: \; co_2t_{i,j,s} \geq CO_2P \cdot TP \cdot \left(B_i \cdot z_{i,j} \right. \tag{C.168}$$
$$\left. + MB_i \cdot \left(g_{i,j,s} - \underline{P_i} \cdot z_{i,j}\right)\right)$$

$$\forall i, \forall j: \quad sc_{i,j} \geq STC_i \cdot v_{i,j} \tag{C.169}$$

$$\forall i, \forall j, \forall s: \; rc_{i,j,s} \geq RCP_i \cdot \left(g_{i,j,s} - g_{i,j-1,s} - \underline{P_i} \cdot v_{i,j}\right) \tag{C.170}$$

$$\forall i, \forall j, \forall s: \; rc_{i,j,s} \geq RCP_i \cdot \left(g_{i,j-1,s} - g_{i,j,s} - \underline{P_i} \cdot w_{i,j}\right) \tag{C.171}$$

$$\forall i, \forall j, \forall s \in \{S/s^{\mathrm{F}}\}: \; fc_{i,j,s} \geq TP \cdot \left(C_i \cdot z^*_{i,j,s} \right. \tag{C.172}$$
$$\left. + MA_i \cdot \left(nsr^+_{i,j,s} - \underline{P_i} \cdot z^*_{i,j,s}\right)\right)$$

$$\forall i, \forall j, \forall s \in \{S/s^{\mathrm{F}}\}: \; co_2t_{i,j,s} \geq CO_2P \cdot TP \cdot \left(B_i \cdot z^*_{i,j,s} \right. \tag{C.173}$$
$$\left. + MB_i \cdot \left(nsr^+_{i,j,s} - \underline{P_i} \cdot z^*_{i,j,s}\right)\right)$$

$$\forall i, \forall j: \; sc_{i,j} \geq \sum_{s \in \{S/s^{\mathrm{F}}\}} \pi_s \cdot STC_i \cdot v^*_{i,j,s} \tag{C.174}$$

$$\forall i, \forall j, \forall s \in \{S/s^{\mathrm{F}}\}: \; rc_{i,j,s} \geq RCP_i \cdot \left(nsr^+_{i,j,s} - nsr^+_{i,j-1,s} \right. \tag{C.175}$$
$$\left. - \overline{\Delta P_i^+} \cdot v^*_{i,j,s}\right)$$

$$\forall i, \forall j, \forall s \in \{S/s^{\mathrm{F}}\}: \; rc_{i,j,s} \geq RCP_i \cdot \left(nsr^{+}_{i,j-1,s} - nsr^{+}_{i,j,s} - \overline{\Delta P_i^{-}} \cdot w^{*}_{i,j,s}\right) \tag{C.176}$$

$$\forall i, \forall j, \forall s: \; rc_{i,j,s} \geq 0 \tag{C.177}$$

Power balance

$$\forall j, \forall m: \; D_{j,m} - \phi_{j,m,s^{\mathrm{F}}} = \sum_i I^{\mathrm{G}}_{m,i} \cdot \left(g_{i,j,s^{\mathrm{F}}}\right) + G^{\mathrm{MR}}_{j,m} + G^{\mathrm{F}}_{j,m,s^{\mathrm{F}}} - \chi_{j,m,s^{\mathrm{F}}} + inj_{j,m,s^{\mathrm{F}}} + \sum_r I^{\mathrm{PHES}}_{m,r} \cdot \left(g^{\mathrm{T}}_{r,j,s^{\mathrm{F}}} - g^{\mathrm{P}}_{r,j,s^{\mathrm{F}}}\right) \tag{C.178}$$

$$\forall j, \forall m, \forall s \in \{S/s^{\mathrm{F}}\}: \; D_{j,m} - \phi_{j,m,s} = \sum_i I^{\mathrm{G}}_{m,i} \cdot \left(g_{i,j,s} + nsr^{+}_{i,j,s}\right) + G^{\mathrm{MR}}_{j,m} + G^{\mathrm{F}}_{j,m,s} - \chi_{j,m,s} + inj_{j,m,s} + \sum_r I^{\mathrm{PHES}}_{m,r} \cdot \left(g^{\mathrm{T}}_{r,j,s} - g^{\mathrm{P}}_{r,j,s}\right) \tag{C.179}$$

$$\forall j, \forall m, \forall s: \quad 0 \leq \chi_{j,m,s} \leq G^{\mathrm{F}}_{j,m,s} \tag{C.180}$$

$$\forall j, \forall m, \forall s: \quad 0 \leq \phi_{j,m,s} \leq D_{j,m} \tag{C.181}$$

$$\sum_j \sum_m \sum_s \pi_s \cdot TP \cdot \phi_{j,m,s} \leq \overline{\Phi} \quad \text{(Optional)} \tag{C.182}$$

Reserve constraints

$$\forall j: \; D^{+}_j = \sum_i \left(r^{+}_{i,j} + nsr^{+}_{i,j,s^{\mathrm{F}}}\right) + \sum_m \chi_{j,m,s^{\mathrm{F}}} + \sum_r \left(r^{\mathrm{P},+}_{r,j} + r^{\mathrm{T},+}_{r,j}\right) + s^{+}_j \tag{C.183}$$

$$\forall j | \sum_m \chi_{j,m,s^{\mathrm{F}}} = 0: \; D^{-}_j = \sum_i r^{-}_{i,j} + \sum_r \left(r^{\mathrm{P},-}_{r,j} + r^{\mathrm{T},-}_{r,j}\right) + s^{-}_j \tag{C.184}$$

$$\forall j: s^{-}_j, \; s^{+}_j \geq 0 \tag{C.185}$$

Minimum and maximum operating point

$$\forall i, \forall j, \forall s: \quad \underline{P_i} \cdot z_{i,j} \leq g_{i,j,s} \leq \overline{P_i} \cdot z_{i,j} \tag{C.186}$$

$$\forall i, \forall j: \; g_{i,j,s^{\mathrm{F}}} + r^{+}_{i,j} \leq \overline{P_i} \cdot z_{i,j} \tag{C.187}$$

$$\forall i, \forall j: \; g_{i,j,s^{\mathrm{F}}} - r^{-}_{i,j} \geq \underline{P_i} \cdot z_{i,j} \tag{C.188}$$

$$\forall i | \{MUT_i \geq 2\}, \forall j, \forall s: \quad g_{i,j,s} \leq \overline{P_i} \cdot z_{i,j} - \left(\overline{P_i} - \underline{P_i}\right) \cdot (v_{i,j} + w_{i,j+1}) \tag{C.189}$$

$$\forall i | \{MUT_i \geq 2\}, \forall j: \; g_{i,j,s^{\mathrm{F}}} + r^{+}_{i,j} \leq \overline{P_i} \cdot z_{i,j} - \left(\overline{P_i} - \underline{P_i}\right) \cdot (v_{i,j} + w_{i,j+1}) \tag{C.190}$$

$$\forall i | \{K_{i,j} \geq 2\}, \forall j | \{j \leq T - K_{i,j}\}, \forall s: \quad g_{i,j,s} \leq \overline{P_i} \cdot z_{i,j+K_{i,j}} - \sum_{k=1}^{K_{i,j}} \overline{P_i} \cdot v_{i,j+k} + \sum_{k=1}^{K_{i,j}} \left(\underline{P_i} + (k-1) \cdot \overline{\Delta P_i^{-}} \cdot w_{i,j+k}\right) \tag{C.191}$$

$$\forall i | \{K_{i,j} \geq 2\}, \forall j | \{j \leq T - K_{i,j}\}: \quad g_{i,j,s^{\mathrm{F}}} + r^{+}_{i,j} \leq \overline{P_i} \cdot z_{i,j+K_{i,j}} - \sum_{k=1}^{K_{i,j}} \overline{P_i} \cdot v_{i,j+k} + \sum_{k=1}^{K_{i,j}} \left(\underline{P_i} + (k-1) \cdot \overline{\Delta P_i^{-}} \cdot w_{i,j+k}\right) \tag{C.192}$$

$$\forall i, \forall j: K_{i,j} = \min\{MUT_i, \; \frac{\overline{P_i} - \underline{P_i}}{\overline{\Delta P_i^{-}}} + 1, \; T - j\} \tag{C.193}$$

Ramping constraints power plants

$$\forall i \notin I^{\mathrm{FAST}}, \forall j, \forall s: \; g_{i,j,s} \leq g_{i,j-1,s} + \overline{\Delta P_i^{+}} \cdot (z_{i,j} - v_{i,j}) + \underline{P_i} \cdot v_{i,j} \tag{C.194}$$

$$\forall i \notin I^{\mathrm{FAST}}, \forall j, \forall s: \; g_{i,j,s} \geq g_{i,j-1,s} - \overline{\Delta P_i^{-}} \cdot z_{i,j} - \underline{P_i} \cdot w_{i,j} \tag{C.195}$$

$$\forall i \in I^{\mathrm{FAST}}, \forall j, \forall s: \; g_{i,j,s} \leq g_{i,j-1,s} + \overline{\Delta P_i^{+}} \cdot z_{i,j} \tag{C.196}$$

$$\forall i \in I^{\mathrm{FAST}}, \forall j, \forall s: \; g_{i,j,s} \geq g_{i,j-1,s} - \overline{\Delta P_i^{-}} \cdot (z_{i,j} + w_{i,j}) \tag{C.197}$$

$$\forall i \notin I^{\text{FAST}}, \forall j: \; g_{i,j,s^{\text{F}}} + r^{+}_{i,j} \leq g_{i,j-1,s^{\text{F}}} + \overline{\Delta P^{+}_{i}} \cdot (z_{i,j} - v_{i,j}) + \underline{P_i} \cdot v_{i,j} \tag{C.198}$$

$$\forall i \notin I^{\text{FAST}}, \forall j: \; g_{i,j,s^{\text{F}}} - r^{-}_{i,j} \geq g_{i,j-1,s^{\text{F}}} - \overline{\Delta P^{-}_{i}} \cdot z_{i,j} - \underline{P_i} \cdot w_{i,j} \tag{C.199}$$

$$\forall i \in I^{\text{FAST}}, \forall j: \; g_{i,j,s^{\text{F}}} + r^{+}_{i,j} \leq g_{i,j-1,s^{\text{F}}} + \overline{\Delta P^{+}_{i}} \cdot z_{i,j} \tag{C.200}$$

$$\forall i \in I^{\text{FAST}}, \forall j: \; g_{i,j,s^{\text{F}}} - r^{-}_{i,j} \geq g_{i,j-1,s^{\text{F}}} - \overline{\Delta P^{-}_{i}} \cdot (z_{i,j} + w_{i,j}) \tag{C.201}$$

$$\forall i | \{MUT_i \geq 2\}, \forall j, \forall s: \; g_{i,j,s} \leq g_{i,j-1,s} + \underline{P_i} \cdot v_{i,j} + \overline{\Delta P^{+}_{i}} \cdot (z_{i,j} - v_{i,j} - w_{i,j+1}) \tag{C.202}$$

$$\forall i | \{MUT_i \geq 2\}, \forall j, \forall s: \; g_{i,j,s} \geq g_{i,j-1,s} - \underline{P_i} \cdot w_{i,j} - \overline{\Delta P^{-}_{i}} \cdot (z_{i,j} - v_{i,j} - v_{i,j-1}) \tag{C.203}$$

$$\forall i | \{MUT_i \geq 2\}, \forall j, \forall s: \; g_{i,j,s} \leq g_{i,j-2,s} + \underline{P_i} \cdot (v_{i,j} + v_{i,j-1} + w_{i,j-1}) + \overline{\Delta P^{+}_{i}} \cdot (2 \cdot z_{i,j} - 2 \cdot v_{i,j} - v_{i,j-1}) \tag{C.204}$$

$$\forall i | \{MUT_i \geq 2\}, \forall j, \forall s: \; g_{i,j,s} \geq g_{i,j-2,s} - \underline{P_i} \cdot (w_{i,j} + w_{i,j-1}) - \overline{\Delta P^{-}_{i}} \cdot (2 \cdot z_{i,j} + w_{i,j} - 2 \cdot v_{i,j-1} - 2 \cdot v_{i,j}) \tag{C.205}$$

$$\forall i | \{MUT_i \geq 2\}, \forall j: \; g_{i,j,s^{\text{F}}} + r^{+}_{i,j} \leq g_{i,j-1,s^{\text{F}}} + \underline{P_i} \cdot v_{i,j} + \overline{\Delta P^{+}_{i}} \cdot (z_{i,j} - v_{i,j} - w_{i,j+1}) \tag{C.206}$$

$$\forall i | \{MUT_i \geq 2\}, \forall j: \; g_{i,j,s^{\text{F}}} - r^{-}_{i,j} \geq g_{i,j-1,s^{\text{F}}} - \underline{P_i} \cdot w_{i,j} - \overline{\Delta P^{-}_{i}} \cdot (z_{i,j} - v_{i,j} - v_{i,j-1}) \tag{C.207}$$

$$\forall i | \{MUT_i \geq 2\}, \forall j: \; g_{i,j,s^{\text{F}}} + r^{+}_{i,j} \leq g_{i,j-2,s^{\text{F}}} + \overline{\Delta P^{+}_{i}} \cdot (2 \cdot z_{i,j} - 2 \cdot v_{i,j} - v_{i,j-1}) + \underline{P_i} \cdot (v_{i,j} + v_{i,j-1} + w_{i,j-1}) \tag{C.208}$$

$$\forall i | \{MUT_i \geq 2\}, \forall j: \; g_{i,j,s^{\text{F}}} - r^{-}_{i,j} \geq g_{i,j-2,s^{\text{F}}} - \underline{P_i} \cdot (w_{i,j} + w_{i,j-1}) - \overline{\Delta P^{-}_{i}} \cdot (2 \cdot z_{i,j} + w_{i,j} - 2 \cdot v_{i,j-1} - 2 \cdot v_{i,j}) \tag{C.209}$$

Minimum up- and downtime power plants

$$\forall i \notin I^{\text{FAST}}, \forall j: \quad \sum_{k=1}^{MUT-1} v_{i,j-k} \leq z_{i,j} \tag{C.210}$$

$$\forall i \notin I^{\text{FAST}}, \forall j: \quad \sum_{k=1}^{MDT-1} w_{i,j-k} \leq 1 - z_{i,j} \tag{C.211}$$

$$\forall i, \forall j: \quad z_{i,j} - z_{i,j-1} - v_{i,j} + w_{i,j} = 0 \tag{C.212}$$

$$\forall i, \forall j: \quad v_{i,j} + w_{i,j} \leq 1 \tag{C.213}$$

$$\forall i, \forall j: \quad z_{i,j},\ v_{i,j},\ w_{i,j} \in \{0,1\} \tag{C.214}$$

$$\forall i \in I^{\text{FAST}}, \forall j, \forall s: \quad z^*_{i,j,s} - z^*_{i,j-1,s} - v^*_{i,j,s} + w^*_{i,j,s} = 0; \tag{C.215}$$

$$\forall i \in I^{\text{FAST}}, \forall j, \forall s: \quad v^*_{i,j,s} + w^*_{i,j,s} \leq 1 \tag{C.216}$$

$$\forall i \in I^{\text{FAST}}, \forall j, \forall s: \quad z_{i,j} + z^*_{i,j,s} \leq 1 \tag{C.217}$$

$$\forall i \in I^{\text{FAST}}, \forall j: \quad z^*_{i,j,s},\ v^*_{i,j,s},\ w^*_{i,j,s} \in \{0,1\} \tag{C.218}$$

$$\forall i \notin I^{\text{FAST}}, \forall j, \forall s: \quad z^*_{i,j,s},\ v^*_{i,j,s},\ w^*_{i,j,s} = 0 \tag{C.219}$$

DC load flow

$$\forall j, \forall n, \forall s: \quad f_{j,n,s} = \sum_m PTDF_{n,m} \cdot inj_{j,m,s} \tag{C.220}$$

$$\forall j, \forall n, \forall s: \quad -CAP_n \leq f_{j,n,s} \leq CAP_n \tag{C.221}$$

$$\forall j, \forall s: \quad \sum_m inj_{j,m,s} = 0 \tag{C.222}$$

Pumped hydro energy storage

$$\forall r, \forall j, \forall s: \quad e_{r,j,s} = TP \cdot \left(g^{\mathrm{P}}_{r,j,s} \cdot \sqrt{\epsilon_r} - \frac{g^{\mathrm{T}}_{r,j,s}}{\sqrt{\epsilon_r}} \right) + e_{r,j-1,s} \tag{C.223}$$

$$\forall r, \forall j, \forall s: \quad \underline{E_r} \leq e_{r,j,s} \leq \overline{E_r} \tag{C.224}$$

$$\forall r, \forall j, \forall s: \quad 0 \leq g^{\mathrm{T}}_{r,j,s} \leq \overline{P_r} \cdot t_{r,j,s} \tag{C.225}$$

$$\forall r, \forall j, \forall s: \quad 0 \leq g^{\mathrm{P}}_{r,j,s} \leq \overline{P_r} \cdot p_{r,j,s} \tag{C.226}$$

$$\forall r, \forall j: \quad 0 \leq r^{\mathrm{P},+}_{r,j} \leq g^{\mathrm{P}}_{r,j,s^{\mathrm{F}}} \tag{C.227}$$

$$\forall r, \forall j: \quad 0 \leq g^{\mathrm{P}}_{r,j,s^{\mathrm{F}}} + r^{\mathrm{P},-}_{r,j} \leq \overline{P_r} \cdot p_{r,j,s^{\mathrm{F}}} \tag{C.228}$$

$$\forall r, \forall j: \quad 0 \leq g^{\mathrm{T}}_{r,j,s^{\mathrm{F}}} + r^{\mathrm{T},+}_{r,j} \leq \overline{P_r} \cdot t_{r,j,s^{\mathrm{F}}} \tag{C.229}$$

$$\forall r, \forall j: \quad 0 \leq r^{\mathrm{T},-}_{r,j} \leq g^{\mathrm{T}}_{r,j,s^{\mathrm{F}}} \tag{C.230}$$

$$\forall r, \forall j, \forall s: \quad p_{r,j,s} + t_{r,j,s} \leq 1 \tag{C.231}$$

$$\forall r, \forall j, \forall s: \quad p_{r,j,s},\ t_{r,j,s} \in \{0,1\} \tag{C.232}$$

$$\forall r, \forall j: \quad e_{r,j,s^{\mathrm{F}}} + TP \cdot \sum_{1}^{j} \left(\Delta g^{\mathrm{P}}_{r,j} + \frac{r^{\mathrm{T},-}_{r,j}}{\sqrt{\epsilon_r}} + r^{\mathrm{P},-}_{r,j} \cdot \sqrt{\epsilon_r} \right) \leq \overline{E_r} \tag{C.233}$$

$$\forall r, \forall j: \quad e_{r,j,s^{\mathrm{F}}} - TP \cdot \sum_{1}^{j} \left(\Delta g^{\mathrm{T}}_{r,j} + \frac{r^{\mathrm{T},+}_{r,j}}{\sqrt{\epsilon_r}} + r^{\mathrm{P},+}_{r,j} \cdot \sqrt{\epsilon_r} \right) \geq \underline{E_r} \tag{C.234}$$

$$\forall r, \forall j, \forall s: \ \delta g^{\mathrm{T}}_{r,j,s} = \frac{g^{\mathrm{T}}_{r,j,s}}{\sqrt{\epsilon_r}} - \left(\frac{g^{\mathrm{T}}_{r,j,s^{\mathrm{F}}}}{\sqrt{\epsilon_r}} + \frac{r^{\mathrm{T},+}_{r,j}}{\sqrt{\epsilon_r}} + r^{\mathrm{P},+}_{r,j} \cdot \sqrt{\epsilon_r} \right) \tag{C.235}$$

$$\forall r, \forall j, \forall s: \ \Delta g^{\mathrm{T}}_{r,j} \geq \delta g^{\mathrm{T}}_{r,j,s} \tag{C.236}$$

$$\forall r, \forall j, \forall s: \ \delta g^{\mathrm{P}}_{r,j,s} = g^{\mathrm{P}}_{r,j,s} \cdot \sqrt{\epsilon_r} - \left(g^{\mathrm{P}}_{r,j,s^{\mathrm{F}}} \cdot \sqrt{\epsilon_r} + \frac{r^{\mathrm{T},-}_{r,j}}{\sqrt{\epsilon_r}} + r^{\mathrm{P},-}_{r,j} \cdot \sqrt{\epsilon_r} \right) \tag{C.237}$$

$$\forall r, \forall j, \forall s: \ \Delta g^{\mathrm{P}}_{r,j} \geq \delta g^{\mathrm{P}}_{r,j,s} \tag{C.238}$$

$$\forall r, \forall j, \forall s: \ \Delta g^{\mathrm{T}}_{r,j},\ \delta g^{\mathrm{T}}_{r,j,s},\ \Delta g^{\mathrm{P}}_{r,j},\ \delta g^{\mathrm{P}}_{r,j,s} \geq 0 \tag{C.239}$$

Non-spinning reserves

$$\forall i \in I^{\text{FAST}}, \forall j, \forall s: \quad \underline{P_i} \cdot z^*_{i,j,s} \leq nsr^+_{i,j,s} \leq \overline{P_i} \cdot z^*_{i,j,s} \tag{C.240}$$

$$\forall i \in I^{\text{FAST}}, \forall j, \forall s: \quad nsr^+_{i,j,s} \leq nsr^+_{i,j-1,s} + \overline{\Delta P^+_i} \cdot z^*_{i,j,s} \tag{C.241}$$

$$\forall i \in I^{\text{FAST}}, \forall j, \forall s: \quad nsr^+_{i,j,s} \geq nsr^+_{i,j-1,s} - \overline{\Delta P^-_i} \cdot (z^*_{i,j,s} + w^*_{i,j,s}) \tag{C.242}$$

$$\forall i \in I^{\text{FAST}}, \forall j, \forall s: \; y_{i,j} \geq z^*_{i,j,s} \tag{C.243}$$

$$\forall i \in I^{\text{FAST}}, \forall j: \; y_{i,j} \in \{0,1\} \tag{C.244}$$

$$\forall i \in I^{\text{FAST}}, \forall j: \; nsr^+_{i,j,s^{\text{F}}} \leq \overline{P_i} \cdot \sum_{s \in S/s^{\text{F}}} z^*_{i,j,s} \tag{C.245}$$

$$\forall i \notin I^{\text{FAST}}, \forall j, \forall s: \; nsr^+_{i,j,s} = 0 \tag{C.246}$$

C.5 Probabilistic unit commitment model

Objective function

$$min \quad c(g,z) = \sum_i \sum_j (fc_{i,j} + sc_{i,j} + co_2t_{i,j} + rc_{i,j}) \tag{C.247}$$
$$+ \sum_j TP \cdot VOC \cdot \chi_j + \sum_j TP \cdot VOLL \cdot \phi_j + \sum_i \sum_j NSRC_i \cdot y_{i,j}$$
$$+ \sum_i \sum_j \sum_l (P^+_{j,l} \cdot (acsr^+_{i,j,l} + acnsr^+_{i,j,l}) - P^-_{j,l} \cdot acsr^-_{i,j,l})$$
$$+ \sum_j \sum_l TP \cdot VOLL \cdot P^+_{j,l} \cdot \phi^{+,\mathrm{L}}_{j,l}$$
$$+ \sum_j \sum_l TP \cdot VOC \cdot (P^-_{j,l} \cdot \chi^{-,\mathrm{L}}_j - P^+_{j,l} \cdot \chi^{+,\mathrm{L}}_j)$$

$$\forall i, \forall j: \quad fc_{i,j} = TP \cdot \big(C_i \cdot z_{i,j} + MA_i \cdot \big(g_{i,j} - \underline{P_i} \cdot z_{i,j}\big)\big) \tag{C.248}$$

$$\forall i, \forall j: \quad co_2t_{i,j} = CO_2P \cdot TP \cdot \big(B_i \cdot z_{i,j} + MB_i \cdot \big(g_{i,j} - \underline{P_i} \cdot z_{i,j}\big)\big) \tag{C.249}$$

$$\forall i, \forall j: \quad sc_{i,j} = STC_i \cdot v_{i,j} \tag{C.250}$$

$$\forall i, \forall j: \quad rc_{i,j} \geq RCP_i \cdot \big(g_{i,j} - g_{i,j-1} - \underline{P_i} \cdot v_{i,j}\big) \tag{C.251}$$

$$\forall i, \forall j: \quad rc_{i,j} \geq RCP_i \cdot \big(g_{i,j-1} - g_{i,j} - \underline{P_i} \cdot w_{i,j}\big) \tag{C.252}$$

$$\forall i, \forall j: \quad rc_{i,j} \geq 0 \tag{C.253}$$

$$\forall i, \forall j, \forall l: \ acnsr^+_{i,j,l} = STC_i \cdot v^*_{i,j,l} + TP \cdot (C_{i,j} + CO_2P \cdot D_{i,j}) \cdot z^*_{i,j,l} \tag{C.254}$$
$$+ TP \cdot (MA_i + CO_2P \cdot MB_i) \cdot (nsr^{+,\mathrm{L}}_{i,j,l} - \underline{P_i} \cdot z^*_{i,j,l})$$

$$\forall i, \forall j, \forall l: acsr^+_{i,j,l} = r^{+,\mathrm{L}}_{i,j,l} \cdot TP \cdot (MA_i + CO_2P \cdot MB_i) \tag{C.255}$$

$$\forall i, \forall j, \forall l: acsr^-_{i,j,l} = r^{-,\mathrm{L}}_{i,j,l} \cdot TP \cdot (MA_i + CO_2P \cdot MB_i) \tag{C.256}$$

Power balance

$$\forall j, \forall m: \quad D_{j,m} - \phi_{j,m} = \sum_i I^{\mathrm{G}}_{m,i} \cdot g_{i,j} + inj_{j,m} + G^{\mathrm{MR}}_{j,m} + G^{\mathrm{F}}_{j,m} - \chi_{j,m} + \sum_r I^{\mathrm{PHES}}_{m,r} \cdot \left(g^{\mathrm{T}}_{r,j} - g^{\mathrm{P}}_{r,j}\right) \tag{C.257}$$

$$\forall j, \forall m: \quad 0 \leq \chi_{j,m} \leq G^{\mathrm{F}}_{j,m} \tag{C.258}$$

$$\forall j: \sum_l \chi^{+,\mathrm{L}}_{j,l} \leq \sum_m \chi_{j,m} \tag{C.259}$$

$$\forall j, \forall l: \chi^{+,\mathrm{L}}_{j,l},\ \chi^{-,\mathrm{L}}_{j,l} \geq 0 \tag{C.260}$$

$$\forall j, \forall m: \quad 0 \leq \phi_{j,m} \leq D_{j,m} \tag{C.261}$$

$$\forall j, \forall l: \quad 0 \leq \phi^{+,\mathrm{L}}_{j,l} \leq\ D^{+}_{j,l} \tag{C.262}$$

Reserve constraints

$$\forall j, \forall l:\ D^{+}_{j,l} = \sum_i \left(r^{+,\mathrm{L}}_{i,j,l} + nsr^{+,\mathrm{L}}_{i,j,l}\right) + r^{\mathrm{P},+,\mathrm{L}}_{j,l} + r^{\mathrm{T},+,\mathrm{L}}_{j,l} + \chi^{+,\mathrm{L}}_{j,l} + \phi^{+,\mathrm{L}}_{j,l} \tag{C.263}$$

$$\forall j, \forall l:\ D^{-}_{j,l} = \sum_i r^{-,\mathrm{L}}_{i,j,l} + \chi^{-,\mathrm{L}}_{j,l} + r^{\mathrm{P},-,\mathrm{L}}_{j,l} + r^{\mathrm{T},-,\mathrm{L}}_{j,l} \tag{C.264}$$

Minimum and maximum stable operating point power plants

$$\forall i, \forall j: \quad g_{i,j} + r^{+}_{i,j} \leq \overline{P_i} \cdot z_{i,j} \tag{C.265}$$

$$\forall i, \forall j: \quad g_{i,j} - r^{-}_{i,j} \geq \underline{P_i} \cdot z_{i,j} \tag{C.266}$$

$$\forall i, \forall j: \quad g_{i,j},\ r^{+}_{i,j},\ r^{-}_{i,j} \geq 0 \tag{C.267}$$

$$\forall i, \forall j: \quad \sum_l r^{+,\mathrm{L}}_{i,j,l} = r^{+}_{i,j} \tag{C.268}$$

$$\forall i, \forall j: \quad \sum_l r^{-,\mathrm{L}}_{i,j,l} = r^{-}_{i,j} \tag{C.269}$$

$$\forall i, \forall j, \forall l: \quad r^{+,\mathrm{L}}_{i,j,l},\ r^{-,\mathrm{L}}_{i,j,l} \geq 0 \tag{C.270}$$

$$\forall i | \{MUT_i \geq 2\}, \forall j:\ g_{i,j} + r^{+}_{i,j} \leq \overline{P_i} \cdot z_{i,j} - \left(\overline{P_i} - \underline{P_i}\right) \cdot (v_{i,j} + w_{i,j+1}) \tag{C.271}$$

$$\forall i|\{K_{i,j} \geq 2\}, \forall j|\{j \leq T - K_{i,j}\} : g_{i,j} + r^{+}_{i,j} \leq \overline{P_i} \cdot z_{i,j+K_{i,j}} - \sum_{k=1}^{K_{i,j}} \overline{P_i} \cdot v_{i,j+k} + \sum_{k=1}^{K_{i,j}} \left(\underline{P_i} + (k-1) \cdot \overline{\Delta P^{-}_{i}} \cdot w_{i,j+k} \right) \quad \text{(C.272)}$$

$$\forall i, \forall j : K_{i,j} = \min\{MUT_i,\ \frac{\overline{P_i} - \underline{P_i}}{\overline{\Delta P^{-}_{i}}} + 1,\ T - j\} \quad \text{(C.273)}$$

Ramping constraints power plants

$$\forall i \notin I^{\text{FAST}}, \forall j : \quad g_{i,j} + r^{+}_{i,j} \leq g_{i,j-1} + \overline{\Delta P^{+}_{i}} \cdot (z_{i,j} - v_{i,j}) + \underline{P_i} \cdot v_{i,j} \quad \text{(C.274)}$$

$$\forall i \notin I^{\text{FAST}}, \forall j : \quad g_{i,j} - r^{-}_{i,j} \geq g_{i,j-1} - \overline{\Delta P^{-}_{i}} \cdot z_{i,j} - \underline{P_i} \cdot w_{i,j} \quad \text{(C.275)}$$

$$\forall i \in I^{\text{FAST}}, \forall j : \quad g_{i,j} + r^{+}_{i,j} \leq g_{i,j-1} + \overline{\Delta P^{+}_{i}} \cdot z_{i,j} \quad \text{(C.276)}$$

$$\forall i \in I^{\text{FAST}}, \forall j : \quad g_{i,j} - r^{-}_{i,j} \geq g_{i,j-1} - \overline{\Delta P^{-}_{i}} \cdot (z_{i,j} + w_{i,j}) \quad \text{(C.277)}$$

$$\forall i|\{MUT_i \geq 2\}, \forall j : \quad g_{i,j} + r^{+}_{i,j} \leq g_{i,j-1} + \underline{P_i} \cdot v_{i,j} + \overline{\Delta P^{+}_{i}} \cdot (z_{i,j} - v_{i,j} - w_{i,j+1}) \quad \text{(C.278)}$$

$$\forall i|\{MUT_i \geq 2\}, \forall j : \quad g_{i,j} - r^{-}_{i,j} \geq g_{i,j-1} - \underline{P_i} \cdot w_{i,j} - \overline{\Delta P^{-}_{i}} \cdot (z_{i,j} - v_{i,j} - v_{i,j-1}) \quad \text{(C.279)}$$

$$\forall i|\{MUT_i \geq 2\}, \forall j : \ g_{i,j} + r^{+}_{i,j} \leq g_{i,j-2} + \underline{P_i} \cdot (v_{i,j} + v_{i,j-1} + w_{i,j-1}) + \overline{\Delta P^{+}_{i}} \cdot (2 \cdot z_{i,j} - 2 \cdot v_{i,j} - v_{i,j-1}) \quad \text{(C.280)}$$

$$\forall i|\{MUT_i \geq 2\}, \forall j : \ g_{i,j} - r^{-}_{i,j} \geq g_{i,j-2} - \underline{P_i} \cdot (w_{i,j} + w_{i,j-1}) - \overline{\Delta P^{-}_{i}} \cdot (2 \cdot z_{i,j} + w_{i,j} - 2 \cdot v_{i,j-1} - 2 \cdot v_{i,j}) \quad \text{(C.281)}$$

Minimum up- and downtime power plants

$$\forall i \notin I^{\text{FAST}}, \forall j: \quad \sum_{k=1}^{MUT-1} v_{i,j-k} \leq z_{i,j} \tag{C.282}$$

$$\forall i \notin I^{\text{FAST}}, \forall j: \quad \sum_{k=1}^{MDT-1} w_{i,j-k} \leq 1 - z_{i,j} \tag{C.283}$$

$$\forall i, \forall j: \quad z_{i,j} - z_{i,j-1} - v_{i,j} + w_{i,j} = 0 \tag{C.284}$$

$$\forall i, \forall j: \quad v_{i,j} + w_{i,j} \leq 1 \tag{C.285}$$

$$\forall i, \forall j: \quad z_{i,j},\ v_{i,j},\ w_{i,j} \in \{0,1\} \tag{C.286}$$

DC load flow

$$\forall j, \forall n: \quad f_{j,n} = \sum_{m} PTDF_{n,m} \cdot inj_{j,m} \tag{C.287}$$

$$\forall j, \forall n: \quad -CAP_n \leq f_{j,n} \leq CAP_n \tag{C.288}$$

$$\forall j: \quad \sum_{m} inj_{j,m} = 0 \tag{C.289}$$

Pumped hydro energy storage

$$\forall r, \forall j: \quad e_{r,j} = TP \cdot \left(g^{\text{P}}_{r,j} \cdot \sqrt{\epsilon_r} - \frac{g^{\text{T}}_{r,j}}{\sqrt{\epsilon_r}} \right) + e_{r,j-1} \tag{C.290}$$

$$\forall r, \forall j: \quad \underline{E_r} \leq e_{r,j} \leq \overline{E_r} \tag{C.291}$$

$$\forall r, \forall j: \quad 0 \leq g^{\text{P}}_{r,j} + r^{\text{P},-}_{r,j} \leq \overline{P_r} \cdot p_{r,j} \tag{C.292}$$

$$\forall r, \forall j: \quad 0 \leq g^{\text{T}}_{r,j} + r^{\text{T},+}_{r,j} \leq \overline{P_r} \cdot t_{r,j} \tag{C.293}$$

$$\forall r, \forall j: \quad r^{\text{T},-}_{r,j} \leq g^{\text{T}}_{r,j} \tag{C.294}$$

$$\forall r, \forall j: \quad r^{\text{P},+}_{r,j} \leq g^{\text{P}}_{r,j} \tag{C.295}$$

$$\forall r, \forall j: \quad p_{r,j} + t_{r,j} \leq 1 \tag{C.296}$$

$$\forall r, \forall j: \quad g^{\text{P}}_{r,j}, g^{\text{T}}_{r,j}, r^{\text{P},+}_{r,j}, r^{\text{P},-}_{r,j}, r^{\text{T},+}_{r,j}, r^{\text{T},-}_{r,j} \geq 0 \tag{C.297}$$

$$\forall r, \forall j: \quad p_{r,j},\ t_{r,j} \in \{0,1\} \tag{C.298}$$

$$\forall r, \forall j: \quad e_{r,j} + TP \cdot \sum_{1}^{j} \left(\frac{r_{r,j}^{\mathrm{T},-}}{\sqrt{\epsilon_r}} + r_{r,j}^{\mathrm{P},-} \cdot \sqrt{\epsilon_r} \right) \leq \overline{E_r} \tag{C.299}$$

$$\forall r, \forall j: \quad e_{r,j} - TP \cdot \sum_{1}^{j} \left(\frac{r_{r,j}^{\mathrm{T},+}}{\sqrt{\epsilon_r}} + r_{r,j}^{\mathrm{P},+} \cdot \sqrt{\epsilon_r} \right) \geq \underline{E_r} \tag{C.300}$$

$$\forall j: \quad \sum_{l} r_{j,l}^{\mathrm{P},+,\mathrm{L}} = \sum_{r} r_{r,j}^{\mathrm{P},+} \tag{C.301}$$

$$\forall j: \quad \sum_{l} r_{j,l}^{\mathrm{P},-,\mathrm{L}} = \sum_{r} r_{r,j}^{\mathrm{P},-} \tag{C.302}$$

$$\forall j: \quad \sum_{l} r_{j,l}^{\mathrm{T},+,\mathrm{L}} = \sum_{r} r_{r,j}^{\mathrm{T},+} \tag{C.303}$$

$$\forall j: \quad \sum_{l} r_{j,l}^{\mathrm{T},-,\mathrm{L}} = \sum_{r} r_{r,j}^{\mathrm{T},-} \tag{C.304}$$

$$\forall j, \forall l: \quad r_{j,l}^{\mathrm{T},-,\mathrm{L}},\ r_{j,l}^{\mathrm{T},+,\mathrm{L}},\ r_{j,l}^{\mathrm{P},-,\mathrm{L}},\ r_{j,l}^{\mathrm{P},+,\mathrm{L}} \geq 0 \tag{C.305}$$

Non-spinning reserves

$$\forall i \in I^{\mathrm{FAST}}, \forall j: \quad \underline{P_i} \cdot y_{i,j} \leq nsr_{i,j}^{+} \leq \overline{P_i} \cdot y_{i,j} \tag{C.306}$$

$$\forall i \in I^{\mathrm{FAST}}, \forall j: \quad \sum_{l} nsr_{i,j,l}^{+,\mathrm{L}} = nsr_{i,j}^{+} \tag{C.307}$$

$$\forall i \in I^{\mathrm{FAST}}, \forall j, \forall l: \quad \underline{P_i} \cdot z_{i,j,l}^{*} \leq nsr_{i,j,l}^{+,\mathrm{L}} \leq \overline{P_i} \cdot z_{i,j,l}^{*} \tag{C.308}$$

$$\forall i \in I^{\mathrm{FAST}}, \forall j: \quad \sum_{l} z_{i,j,l}^{*} \leq 1 \tag{C.309}$$

$$\forall i \in I^{\mathrm{FAST}}, \forall j: \quad y_{i,j} + z_{i,j} \leq 1 \tag{C.310}$$

$$\forall i \in I^{\mathrm{FAST}}, \forall j, \forall l: \quad z_{i,j,l}^{*} \leq y_{i,j} \tag{C.311}$$

$$\forall i \in I^{\mathrm{FAST}}, \forall j, \forall l: \quad z_{i,j,l}^{*} - z_{i,j-1,l}^{*} + v_{i,j,l}^{*} - w_{i,j,l}^{*} = 0 \tag{C.312}$$

$$\forall i \in I^{\mathrm{FAST}}, \forall j, \forall l: \quad y_{i,j},\ z_{i,j,l}^{*},\ v_{i,j,l}^{*},\ w_{i,j,l}^{*} \in \{0,1\} \tag{C.313}$$

$$\forall i \notin I^{\mathrm{FAST}}, \forall j, \forall l: \quad y_{i,j},\ nsr_{i,j}^{+},\ nsr_{i,j,l}^{+,\mathrm{L}},\ z_{i,j,l}^{*},\ v_{i,j,l}^{*},\ w_{i,j,l}^{*} = 0 \tag{C.314}$$

Appendix D

The Lévy α-stable distribution

In this appendix[1], the stable distributions and two important properties (stability or invariance under addition and the Generalized Central Limit Theorem) are introduced. The goal is to give a brief overview for practical use, not to provide a full overview or proof of the properties of the stable distributions. For this, the reader is referred to the specialized literature, such as (amongst others) Nolan [167, 168, 169], Zolotarev [170, 171] and Smaorodnitsky and Taqqu [172]. For the implementation of the stable distribution probability density function in MATLAB®, see Nolan [167].

The Lévy α-stable distribution

The pdf and cumulative probability density function (cdf) of a Lévy α-stable distribution cannot be expressed in analytical form. The characteristic function[2] $\phi(u)$ of a random stable variable X can be parametrized and is most often written as in Samorodnitsky and Taqqu [172, 169] :

$$\phi(u) = \begin{cases} \exp\left(-\gamma^{\alpha}|u|^{\alpha}[1 - i\beta - \tan(\frac{\pi\alpha}{2}) \cdot \text{sign}(u)] + i\delta u\right) & \alpha \neq 1 \\ \exp\left(-\gamma|u|[1 + i\beta - \frac{2}{\pi} \cdot \text{sign}(u) \cdot \ln|u|] + i\delta u\right) & \alpha = 1 \end{cases} \tag{D.1}$$

[1]This appendix is based on K. Bruninx, E. Delarue, and W. D'haeseleer, *Statistical description of the error on wind power forecasts via a Lévy alpha-stable distribution,* in YEEES 2012, Young Energy Engineers & Economists Seminar 2012, December 7, 2012, Florence, Italy and EUI RSCAS Working Paper 2013/50, 2013, pp. 1–8.

[2]For a random variable X with cumulative distribution function F(x), the characteristic function $\phi(u)$ is defined as $\phi(u) = E\left[\exp(iuX)\right] = \int_{-\infty}^{\infty} \exp(iux) dF(x)$ with $u \in \Re$ and $i = \sqrt{-1}$.

The parameters of this family of distributions $\mathrm{S}(\alpha, \beta, \gamma, \delta)$ are

- α, an index of stability $(0 < \alpha \leq 2)$;
- β, a skewness parameter $(-1 \leq \beta \leq 1)$;
- γ, a scale parameter $(\gamma > 0)$;
- δ, a location parameter $(\delta \in \Re)$.

The index of stability α determines the total probability contained in the tails, thus the kurtosis, of the distribution. The probability in the tails is inversely proportional to α. A positive skewness parameter β yields a distribution skewed to the right. The degree of skewness is larger as β rises. Similar reasoning applies to negative β-values. The third parameter γ defines the scale of the distribution and is linked to the variance σ^2 for $\alpha = 2$. The location parameter δ coincides with the mean of the distribution for $\alpha \geq 1$. For $\alpha < 1$, the mean of the distribution is not defined and δ will be some other parameter which describes the location of the distribution[3].

The Lévy α-stable distributions is non-zero for (the *support* of the distribution) [169]

$$\text{support } \mathrm{S}(\alpha, \beta, \gamma, \delta) = \begin{cases} [\delta, \infty) & \alpha \leq 1 \ \ \& \ \ \beta = 1 \\ (-\infty, \delta] & \alpha \leq 1 \ \ \& \ \ \beta = -1 \\ [-\infty, \infty] & \text{otherwise} \end{cases}$$

However, in this dissertation, the domain of x is limited to $[-G_j^{\mathrm{F}}, 1 - G_j^{\mathrm{F}}]$, the domain of the forecast error at each time step. The pdf is normalized such that the integral of the pdf equals 1 on the supported domain.

The Gaussian $(\mathrm{N}(\mu, \sigma^2) \rightarrow \mathrm{S}(2, \beta, 2^{-0.5} \cdot \sigma, \mu))$, the Cauchy (scale γ and location δ: $\mathrm{C}(\delta, \gamma) \rightarrow \mathrm{S}(1, 0, \gamma, \delta)$) and Lévy distribution (scale γ and location δ: $\mathrm{L}(\delta, \gamma) \rightarrow \mathrm{S}(0.5, 1, \gamma, \delta)$) are all stable distributions that can be described via the parametrization above. Only in these cases, the probability density function can be expressed analytically.

[3]This can be generalized as follows: the p^{th} moment of a stable random variable is finite if and only if $p \leq \alpha$ [173]. Thus, for $\alpha < 1$, the first moment (mean) is not finite. For $1 \leq \alpha < 2$ the mean is finite, but the second moment (variance) is infinite. The variance is finite if and only if $\alpha = 2$.

Parameter estimation

This lack of closed form density functions complicates statistical inference for stable distributions, such as parameter estimation. Multiple methods have been developed. In general, one can distinguish the following methods [173]:

- **Sample Quantile Methods:** These methods are considered to be the fastest, but as well the least accurate methods. The best known method is that of McCulloch [174], a robust approach for $\alpha \geq 0.6$. This method has been used in this dissertation, see Chapter 3.
- **Sample Characteristic Function Methods:** Given n independent and identically distributed (iid) random samples, the sample characteristic function $\phi^*(u)$ is defined as $\frac{1}{n}\sum_{i=1}^{n}\exp(itx_i)$ and used as an approximation of the characteristic function $\phi(u)$. Based on that approximative characteristic function, the parameters can be estimated.
- **Maximum Likelihood Method:** In this group of techniques, the log-likelihood function is maximized for a set of parameters, given an iid random sample. These techniques provide the highest accuracy, but sometimes suffer from robustness issues and are slower.

Other methods, such as Monte Carlo-based schemes or indirect inference-methods and estimators of the tail index α (for example the Hill-estimator [339]), are not discussed here.

Stability or invariance under addition

Stability or invariance under addition can be defined as follows (see Nolan [169]):

Definition 1. *Non-degenerate X is **stable** if and only if for all $n > 1$, there exist constants $c_\mathrm{n} > 0$ and $d_\mathrm{n} \in \Re$ such that*

$$\sum_{\mathrm{i}=1}^{\mathrm{n}} X_\mathrm{i} = c_\mathrm{n} X + d_\mathrm{n} \tag{D.2}$$

*where X_i are n iid copies of X. X is **strictly stable** if and only if $d_\mathrm{n} = 0$ for all n.*

It can furthermore be shown that the only possible choice for the scaling constant is $c_\mathrm{n} = n^{\frac{1}{\alpha}}$ with some $\alpha \in (0, 2]$. This can be translated in a parametrization of

the characteristic function $\phi(u)$ for the stable distributions. It can be shown that this characteristic function has the same form as that of the Lévy α-stable distribution family (see Nolan [169]). Therefore, by definition (Eq. (D.1)), a Lévy α-stable distribution is any distribution that is stable. Based on this stability property, any linear weighted sum of iid stable distributions results in a stable distribution. With the same characteristic exponent α but different location, scale and skewness parameters (δ_i, γ_i, β_i) and weights p_i, this yields [160][4]:

$$\sum_{\mathrm{i}=1}^{\mathrm{n}} p_\mathrm{i} \cdot S(\alpha, \beta_\mathrm{i}, \gamma_\mathrm{i}, \delta_\mathrm{i}) = S(\alpha, \frac{\sum_{\mathrm{i}=1}^{\mathrm{n}} \gamma_\mathrm{i} |p_\mathrm{i}|^\alpha \beta_\mathrm{i}}{\sum_{\mathrm{i}=1}^{\mathrm{n}} \gamma_\mathrm{i} |p_\mathrm{i}|^\alpha}, \sum_{\mathrm{i}=1}^{\mathrm{n}} \gamma_\mathrm{i} |p_\mathrm{i}|^\alpha, \sum_{\mathrm{i}=1}^{\mathrm{n}} p_\mathrm{i} \delta_\mathrm{i}) \tag{D.3}$$

Generalized Central Limit Theorem (GCLT): stable distributions as limiting distributions

The classical central limit theorem states that the normalized sum of iid terms with a finite variance converges to a normal distribution. More precise (see [159]):

Theorem 1. *Let X_i be n iid random variables with a finite variance $\sigma^2 = E\left[X_\mathrm{i} - E(X)\right]^2$. The **Central Limit Theorem** then states that*

$$\lim_{\mathrm{n}\to\infty} n^{-0.5} \sigma^{-1} \sum_{\mathrm{i}=1}^{\mathrm{n}} \left(X_\mathrm{i} - E\left[X\right]\right) \tag{D.4}$$

is a reduced Gaussian variable.

This result is the basis for the presumed occurrence of the Gaussian distribution in many practical applications, such as the description of the WPFE. One argues that the sum of a large number of iid variables – such as the various sources of the WPFE – from a finite-variance distribution will be (asymptotically) normally distributed. However, this theoretical result has been contradicted by empirical findings in many fields. Often, this is caused by infinite-variance distributed variables. If however the assumption of a finite variance is dropped in the CLT, one can show via the Pareto-Doeblin-Gnedenko conditions[5] (power law behavior) and stability arguments (Section D) that the limit (D.4) exists in a real sense

[4] Eq. (D.3) only holds for the parametrization of Eq. (D.1). Other parametrizations will yield other expressions for the β, γ and δ-parameters. Furthermore, if $\alpha = 1$, the resulting δ-parameter has to be calculated as $\sum_{\mathrm{i}=1}^{n} p_\mathrm{i}\delta_\mathrm{i} - \frac{2}{\pi}\sum_{\mathrm{i}=1}^{\mathrm{n}} \beta_\mathrm{i} p_\mathrm{i} \gamma_\mathrm{i} \ln|p_\mathrm{i}|$ (see Nolan [169]).

[5] See Mandelbrot [159]. In the description of the WPFE, it is assumed that these requirements are met.

and that this is the stable law (Section D and [159, 160]). Therefore, if the variance of a large set of random variables tends to infinity, a GCLT-argument may be employed to justify a Lévy α-stable distribution as the description of the sum of these variables. This is summarized in the Generalized Central Limit Theorem (GCLT):

Theorem 2. *Let X_i be n iid random variables with a variance σ^2. The* ***Generalized Central Limit Theorem*** *then states that Eq. (D.4) is a reduced variable that satisfies the stability equation. If X has a finite variance, the limiting distribution is Gaussian (CLT). If X does not have a finite variance, the limit is stable non-Gaussian if and only if the conditions of Pareto-Doeblin-Gnedenko are satisfied for some stability index $\alpha \in (0, 2]$.*

Applications of stable distributions

Nolan [167] reports three reasons to employ a stable distribution. First, when there are solid (theoretical) reasons to expect a non-Gaussian stable model: for example the reflection of a rotating mirror, yielding a Cauchy distribution. The second reason is the Generalized Central Limit Theorem. Many observed quantities are the sum of many small terms, thus could be described via a stable distribution. The third reason according to Nolan is purely empirical: many data sets show heavy tails and skewness, properties that are well described by a stable distribution. The hypothesis of stability is however impossible to prove [167]. No standard, widely-accepted tests for assessing stability are available (see [167, 173] and references therein).

Stable, α-stable, stable Paretian or Lévy stable laws were first introduced by Lévy [340]. Despite of the lack of closed expressions for the pdf and the standard stability tests, they have been proposed to model several physical and economic processes [169][6]. For example: the price of a stock [159, 160, 161, 173], multivariate financial portfolios [341, 342], loss distribution models [343], network traffic [344], wave power [345] and other fields [167, 169, 161, 162, 163, 173, 346, 347]. For a comprehensive overview of applications of stable distributions, see Nolan [169].

[6]The first author to propose the stable distribution to describe heavy-tailed financial data was Mandelbrot [159, 160]. After initial support in the first years of his publication, Mandelbrots stable distribution hypothesis was questioned. In the 1990s the stable distribution has made a dramatic comeback in economics [173].

Appendix E

Chance constraints: analytical reformulation

An analytical reformulation of a chance constraint [128] holds two main advantages over a scenario-based approach. First, it is an accurate representation of the original problem [128]. Second, the computational burden of the resulting problem is lower than that of the scenario-based probem [221, 63]. Below we present the analytical reformulation for a random parameter that follows a normal distribution [128]. Chance constraints considering random parameters that follow other distributions can be reformulated using distributionally robust chance constraints [63].

Consider the following chance constraint:

$$Pr\left(a^T \cdot x \leq b\right) \geq 1 - \epsilon \tag{E.1}$$

with a a random parameter that follows a normal distribution $N(\mu, \Sigma)$. For $1-\epsilon \geq 0.5$, this constraint can be reformulated as the following convex constraint:

$$b - \mu^T \cdot x \geq \Phi^{-1}(1-\epsilon) \cdot \sqrt{x^T \cdot \Sigma \cdot x} \tag{E.2}$$

with $\Phi(\eta)$ the Normal cumulative probability distribution and Σ the variance. This can be represented as a second-order conic constraint, which can effectively be solved with off-the-shelve commercial solvers as CPLEX and Gurobi. Moving

b to the right-hand side, this constraint reads:

$$\mu^T \cdot x + \Phi^{-1}(1-\epsilon) \cdot t \leq b \tag{E.3}$$

$$t \geq ||\sqrt{\Sigma} \cdot x||_2 \tag{E.4}$$

By definition, Σ is positive, and in the case we will consider below, $x \geq 0$. This allows us to recast the last constraint as

$$t^2 \geq \sum_j \Sigma_j \cdot x_j^2 \tag{E.5}$$

In the particular case that the random parameter is additive (instead of proportional, as in Eq. (E.1)), the chance constraint can be recasted as a simple linear constraint. A chance constraint of the form of Eq. (E.6) below

$$Pr\left(a^T \cdot x + \delta \leq b\right) \geq 1 - \epsilon \tag{E.6}$$

can be reformulated as

$$a^T \cdot x + \mu + \Phi^{-1}(1-\epsilon) \cdot \sqrt{\Sigma} \leq b \tag{E.7}$$

Applying the theory above to the chance constraints (6.38)-(6.40) and assuming

$$\delta^{\mathrm{P}} \sim N(\mu^{\mathrm{P}}, (\sigma^{\mathrm{P}})^2) \tag{E.8}$$

$$\delta^{\mathrm{NP}} \sim N(\mu^{\mathrm{NP}}, (\sigma^{\mathrm{NP}})^2) \tag{E.9}$$

we can reformulate the power balance as follows:

$$\begin{aligned} \forall j: \; & D_j + (1+\mu_j^P) \cdot d_j^{\mathrm{H}} + \mu_j^{NP} + \Phi^{-1}(1-\epsilon) \cdot (t + \sigma^{NP}) \\ & = \sum_i g_{i,j} + G_j^{\mathrm{F}} - \chi_j + \sum_r \left(g_{r,j}^{\mathrm{T}} - g_{r,j}^{\mathrm{P}}\right) + \phi_j \end{aligned} \tag{E.10}$$

$$t^2 \geq \sum_j (\sigma_j^P \cdot d_{\mathrm{j}}^{\mathrm{H}})^2 \tag{E.11}$$

with t an auxiliary decision variable (no physical meaning). The reserve constraints can be recasted as

$$\begin{aligned} \forall j, \forall l: \; D_{j,l}^{+} = & \sum_i \left(r_{i,j,l}^{+,\mathrm{L}} + nsr_{i,j,l}^{+,\mathrm{L}}\right) + r_{j,l}^{\mathrm{P},+,\mathrm{L}} + r_{j,l}^{\mathrm{T},+,\mathrm{L}} + \chi_{j,l}^{+,\mathrm{L}} + \phi_{j,l}^{+,\mathrm{L}} \\ & + (1-\mu_j^P) \cdot \sum_h NB_h \cdot r_{h,j,l}^{\mathrm{H},+} - \mu_j^{NP} - \Phi^{-1}(1-\epsilon) \cdot (s + \sigma^{NP}) \end{aligned} \tag{E.12}$$

$$s^2 \geq \sum_j \sum_l \left(\sigma_j^P \cdot \sum_h NB_h \cdot r_{h,j,l}^{\mathrm{H},+} \right)^2 \tag{E.13}$$

$$\forall j, \forall l: \; D_{j,l}^- = \sum_i r_{i,j,l}^{-,\mathrm{L}} + \chi_{j,l}^{-,\mathrm{L}} + r_{j,l}^{\mathrm{P},-,\mathrm{L}} + r_{j,l}^{\mathrm{T},-,\mathrm{L}} \tag{E.14}$$

$$+ (1 - \mu_j^P) \cdot \sum_h NB_h \cdot r_{h,j,l}^{\mathrm{H},+} - \mu_j^{NP} - \Phi^{-1}(1-\epsilon) \cdot (u + \sigma^{NP})$$

$$u^2 \geq \sum_j \sum_l \left(\sigma_j^P \cdot \sum_h NB_h \cdot r_{h,j,l}^{\mathrm{H},-} \right)^2 \tag{E.15}$$

with s and u auxiliary decision variables.

Bibliography

[1] G. Corbetta, I. Pineda, and J. Wilkes, "Wind in Power: 2014 European Statistics," tech. rep., European Wind Energy Association, Brussels, Belgium, 2015.

[2] European Photovoltaic Industry Association, "Market Report 2013," tech. rep., Brussels, Belgium, 2014.

[3] IEA, *World Energy Outlook 2015*. Paris, France: OECD Publishing, 2015.

[4] OECD/IEA, *The Power of Transformation - Wind, Sun and the Economics of Flexible Power Systems*. Paris, France: OECD Publishing, 2014.

[5] OECD/NEA, *Nuclear Energy and Renewables - System Effects in Low-carbon Electricity Systems*. Paris, France: OECD Publishing, 2012.

[6] L. Hirth and I. Ziegenhagen, "Balancing power and variable renewables: Three links," *Renewable and Sustainable Energy Reviews*, vol. 50, pp. 1035–1051, 2015.

[7] L. Hirth, "The market value of variable renewables," *Energy Economics*, vol. 38, pp. 218–236, 2013.

[8] G. Strbac, "Demand side management: Benefits and challenges," *Energy Policy*, vol. 36, no. 12, pp. 4419–4426, 2008.

[9] D. S. Callaway and I. A. Hiskens, "Achieving Controllability of Electric Loads," *Proceedings of the IEEE*, vol. 99, no. 1, pp. 184–199, 2011.

[10] J. Torriti, M. G. Hassan, and M. Leach, "Demand response experience in Europe: Policies, programmes and implementation," *Energy*, vol. 35, no. 4, pp. 1575–1583, 2010.

[11] B. Dupont, *Residential Demand Response Based on Dynamic Electricity Pricing : Theory and Practice*. PhD thesis, KU Leuven, 2015.

[12] PJM, "Demand response," tech. rep., PJM, Audubon, PA, USA, 2015.

[13] L. consortium, "LINEAR - Demand Response for Families," tech. rep., Energyville, Genk, Belgium, 2014.

[14] E. Delarue, *Modelling electricity generation systems - development and application of electricity generation optimization and simulation models, with particular focus on CO2 emissions*. PhD thesis, KU Leuven, 2009.

[15] K. Van Den Bergh, K. Bruninx, E. Delarue, and W. D'haeseleer, "LUSYM: a Unit Commitment Model formulated as a Mixed-Integer Linear Program." KU Leuven Energy Institute Working Paper WP EN2014-07. Available online: `http://www.mech.kuleuven.be/en/tme/research/energy_environment/PublicationsEnergyandenvironment/Journalpapers`, 2015.

[16] D. Couckuyt, D. Orlic, K. Bruninx, A. Zani, A.-C. Leger, N. Grisey, T. Anderski, N. Grisey, and G. Sanchis, "E-highway2050 - D2.3 System simulations analysis and overlay-grid development," tech. rep., European Commission (EC), 2015.

[17] A. Papavasiliou and S. Oren, "Reserve requirements for wind power integration: A scenario-based stochastic programming framework," *IEEE Transactions on Power Systems*, vol. 26, no. 4, pp. 2197–2206, 2011.

[18] E. M. Constantinescu, V. M. Zavala, M. Rocklin, S. Lee, and M. Anitescu, "A computational framework for uncertainty quantification and stochastic optimization in unit commitment with wind power generation," *IEEE Transactions on Power Systems*, vol. 26, no. 1, pp. 431–441, 2011.

[19] C. De Jonghe, *Short-term demand response in electricity generation planning and scheduling*. PhD thesis, KU Leuven, 2011.

[20] K. Dietrich, J. M. Latorre, L. Olmos, and A. Ramos, "Demand response in an isolated system with high wind integration," *IEEE Transactions on Power Systems*, vol. 27, no. 1, pp. 20–29, 2012.

[21] D. Patteeuw, K. Bruninx, A. Arteconi, E. Delarue, D. William, and L. Helsen, "Integrated modeling of active demand response with electric heating systems coupled to thermal energy storage systems," *Applied Energy*, vol. 151, pp. 306–319, 2014.

[22] J. L. Mathieu, D. S. Callaway, and S. Kiliccote, "Variability in automated responses of commercial buildings and industrial facilities to dynamic electricity prices," *Energy and Buildings*, vol. 43, no. 12, pp. 3322–3330, 2011.

[23] G. Reynders, T. Nuytten, and D. Saelens, "Potential of structural thermal mass for demand-side management in dwellings," *Building and Environment*, vol. 64, pp. 187–199, 2013.

[24] A. Arteconi, N. Hewitt, and F. Polonara, "State of the art of thermal storage for demand-side management," *Applied Energy*, vol. 93, pp. 371–389, 2012.

[25] K. Hedegaard, B. V. Mathiesen, H. Lund, and P. Heiselberg, "Wind power integration using individual heat pumps–analysis of different heat storage options," *Energy*, vol. 47, no. 1, pp. 284–293, 2012.

[26] K. De Vos, *Sizing and allocation of operating reserves - Following wind power integration.* PhD thesis, KU Leuven, 2012.

[27] P. Luickx, *The backup of wind power - Analysis of the parameters influencing the wind power integration in electricity generation systems.* PhD thesis, KU Leuven, 2009.

[28] G. Morales-Espana, *Unit commitment: computational performance, system representation and wind uncertainty management.* PhD thesis, Universidad Pontificia Comillas, Madrid, Spain, 2014.

[29] E. Karangelos and F. Bouffard, "Towards Full Integration of Demand-Side Resources in Joint Forward Energy/Reserve Electricity Markets," *IEEE Transactions on Power Systems*, vol. 27, no. 1, pp. 280–289, 2012.

[30] G. Morales-Espana, A. Ramos, and J. Garcia-Gonzalez, "An MIP Formulation for Joint Market-Clearing of Energy and Reserves Based on Ramp Scheduling," *IEEE Transactions on Power Systems*, vol. 29, no. 1, pp. 476–488, 2014.

[31] B. F. Hobbs, M. H. Rothkopf, R. P. O'Neill, and H.-P. Chao, eds., *The Next Generation of Electric Power Unit Commitment Models.* International Series in Operations Research & Management Science, Boston: Kluwer Academic Publishers, 2002.

[32] R. Baldick, U. Helman, B. Hobbs, and R. O'Neill, "Design of Efficient Generation Markets," *Proceedings of the IEEE*, vol. 93, no. 11, pp. 1998–2012, 2005.

[33] P. González, J. Villar, C. A. Díaz, and F. A. Campos, "Joint energy and reserve markets: Current implementations and modeling trends," *Electric Power Systems Research*, vol. 109, pp. 101–111, 2014.

[34] S. S. Oren and R. Sioshansi, "Joint Energy and Reserves Auction with Opportunity Cost Payment for Reserves." Energy Policy and Economics Working Paper Series. Available online: `http://www.ieor.berkeley.edu/~oren/pubs/oppcost_ieee.pdf`, 2003.

[35] A. J. Conejo, M. Carrión, and J. M. Morales, *Decision Making Under Uncertainty in Electricity Markets*. International Series in Operations Research & Management Science, Boston, MA, USA: Springer US, 2010.

[36] P. Pinson, H. Madsen, H. A. Nielsen, G. Papaefthymiou, and B. Klöckl, "From probabilistic forecasts to statistical scenarios of short-term wind power production," *Wind Energy*, vol. 12, no. 1, pp. 51–62, 2009.

[37] N. Gröwe-Kuska, H. Heitsch, and W. Römisch, "Scenario reduction and scenario tree construction for power management problems," in *2003 IEEE Bologna PowerTech - Conference Proceedings*, vol. 3, (Bologna, Italy), pp. 152–158, IEEE, June 23-26, 2003.

[38] J. Dupačová, N. Gröwe-Kuska, and W. Römisch, "Scenario reduction in stochastic programming," *Mathematical Programming*, vol. 95, no. 3, pp. 493–511, 2003.

[39] A. Tuohy, P. Meibom, E. Denny, and M. O'Malley, "Unit Commitment for Systems With Significant Wind Penetration," *IEEE Transactions on Power Systems*, vol. 24, no. 2, pp. 592–601, 2009.

[40] K. Bruninx, D. Patteeuw, E. Delarue, L. Helsen, and W. D'haeseleer, "Short-term demand response of flexible electric heating systems : the need for integrated simulations," in *EEM13, 10th International conference on the European Energy Market*, (Sweden, Stockholm), May 27-31, 2013.

[41] K. Bruninx and E. Delarue, "A probabilistic unit commitment model: cost-effective , reliable and fast." KU Leuven Energy Institute Working Paper WP EN2015-15. Available online: `http://www.mech.kuleuven.be/en/tme/research/energy_environment/PublicationsEnergyandenvironment/Journalpapers`, 2015.

[42] K. Bruninx, E. Delarue, and W. D'haeseleer, "The cost of wind power forecast errors in the Belgian power system," in *IAEE Int. Conf. 2014*, (NYC, NY, USA), June 15-18, 2014.

[43] D. Patteeuw, G. Reynders, K. Bruninx, C. Protopapadaki, E. Delarue, W. D'haeseleer, D. Saelens, and L. Helsen, "CO2-abatement cost of residential heat pumps with active demand response: demand- and supply-side effects," *Applied Energy*, vol. 156, pp. 490–501, 2015.

[44] A. Arteconi, D. Patteeuw, K. Bruninx, E. Delarue, W. D'haeseleer, and L. Helsen, "Active demand response with electric heating systems : impact of market penetration." KU Leuven Energy Institute Working Paper WP EN2015-15. Available online: `http://www.mech.kuleuven.be/en/tme/research/energy_environment/PublicationsEnergyandenvironment/Journalpapers`, 2016.

[45] K. Bruninx, K. V. D. Bergh, E. Delarue, and W. D'haeseleer, "Optimization and allocation of spinning reserves in a low carbon framework," *IEEE Transactions on Power Systems*, vol. 31, no. 2, pp. 872–882, 2016.

[46] M. A. Ortega-Vazquez and D. S. Kirschen, "Assessing the Impact of Wind Power Generation on Operating Costs," *IEEE Transactions on Smart Grid*, vol. 1, no. 3, pp. 295–301, 2010.

[47] Q. P. Zheng, J. Wang, and A. L. Liu, "Stochastic Optimization for Unit Commitment - A Review," *IEEE Transactions on Power Systems*, vol. 30, no. 4, pp. 1913–1924, 2015.

[48] C. Cardozo, "Unit Commitment with uncertainties - State of the art," in *Journées JCGE'2014 - SEEDS*, (Saint-Louis, France), June 4-5, 2014.

[49] H. Dai, N. Zhang, and W. Su, "A Literature Review of Stochastic Programming and Unit Commitment," *Journal of Power and Energy Engineering*, vol. 03, no. 04, pp. 206–214, 2015.

[50] M. Tahanan, W. van Ackooij, A. Frangioni, and F. Lacalandra, "Large-scale Unit Commitment under uncertainty: a literature survey," tech. rep., Universita di Pisa, Pisa, Italy, 2014.

[51] A. Papavasiliou, *Coupling Renewable Energy Supply with Deferrable Demand*. PhD thesis, University of California, Berkeley, CA, USA, 2011.

[52] J. Kiviluoma, P. Meibom, and A. Tuohy, "Short-Term Energy Balancing With Increasing Levels of Wind Energy," *IEEE Transactions on Sustainable Energy*, vol. 3, no. 4, pp. 769–776, 2012.

[53] B. Saravanan, S. Das, S. Sikri, and D. P. Kothari, "A solution to the unit commitment problem—a review," *Frontiers in Energy*, vol. 7, no. 2, pp. 223–236, 2013.

[54] F. Galiana, F. Bouffard, J. Arroyo, and J. Restrepo, "Scheduling and Pricing of Coupled Energy and Primary, Secondary, and Tertiary Reserves," *Proceedings of the IEEE*, vol. 93, no. 11, pp. 1970–1983, 2005.

[55] G. Yongpei and J. Wang, "Uncertainty Sets for Robust Unit Commitment," *IEEE Transactions on Power Systems*, vol. 29, no. 3, pp. 1439–1440, 2014.

[56] D. Bertsimas, E. Litvinov, X. A. Sun, J. Zhao, and T. Zheng, "Adaptive Robust Optimization for the Security Constrained Unit Commitment Problem," *IEEE Transactions on Power Systems*, vol. 28, no. 1, pp. 52–63, 2013.

[57] D. Pozo and J. Contreras, "A Chance-Constrained Unit Commitment With an Security Criterion and Significant," *IEEE Transactions on Power Systems*, vol. 28, no. 3, pp. 2842–2851, 2013.

[58] P. Xiong and P. Jirutitijaroen, "A stochastic optimization formulation of unit commitment with reliability constraints," *IEEE Transactions on Smart Grid*, vol. 4, no. 4, pp. 2200–2208, 2013.

[59] U. A. Ozturk, M. Mazumdar, and B. Norman, "A solution to the stochastic unit commitment problem using chance constrained programming," vol. 19, no. 3, pp. 1589–1598, 2004.

[60] J. F. Restrepo and F. D. Galiana, "Assessing the yearly impact of wind power through a new hybrid deterministic/stochastic unit commitment," *IEEE Transactions on Power Systems*, vol. 26, no. 1, pp. 401–410, 2011.

[61] Q. Wang, Y. Guan, and J. Wang, "A chance-constrained two-stage stochastic program for unit commitment with uncertain wind power output," *IEEE Transactions on Power Systems*, vol. 27, no. 1, pp. 206–215, 2012.

[62] G. Calafiore and M. Campi, "The scenario approach to robust control design," *IEEE Transactions on Automatic Control*, vol. 51, no. 5, pp. 742–753, 2006.

[63] M. Lubin, Y. Dvorkin, and S. Backhaus, "A Robust Approach to Chance Constrained Optimal Power Flow with Renewable Generation," *IEEE Transactions on Power Systems*, vol. PP, no. 99, pp. 1–11, 2015.

[64] D. Pozo, J. Contreras, and E. E. Sauma, "Unit Commitment With Ideal and Generic Energy Storage Units," *IEEE Transactions on Power Systems*, vol. 29, no. 6, pp. 2974–2984, 2014.

[65] Y. V. Makarov, P. Du, M. C. W. Kintner-Meyer, C. Jin, and H. F. Illian, "Sizing Energy Storage to Accommodate High Penetration of Variable Energy Resources," *IEEE Transactions on Sustainable Energy*, vol. 3, no. 1, pp. 34–40, 2012.

[66] H. Pandžić, Y. Wang, T. Qiu, Y. Dvorkin, and D. S. Kirschen, "Near-Optimal Method for Siting and Sizing of Distributed Storage in a Transmission Network," *IEEE Transactions on Power Systems*, vol. PP, pp. 1–13, 2014.

[67] NHA's Pumped Storage Development Council, "Challenges and Opportunities For New Pumped Storage Development," tech. rep., 2012.

[68] A. Kalantari and F. D. Galiana, "On the significance of hydro storage in leveraging wind integration in thermal systems," in *2012 9th International Conference on the European Energy Market*, (Florence,Italy), pp. 1–8, IEEE, May 10-12, 2012.

[69] R. Aihara, A. Yokoyama, F. Nomiyama, and N. Kosugi, "Optimal operation scheduling of pumped storage hydro power plant in power system with a large penetration of photovoltaic generation using genetic algorithm," in *2011 IEEE Trondheim PowerTech*, (Trondheim, Norway), pp. 1–8, IEEE, June 13-19, 2011.

[70] S. J. Kazempour, M. Hosseinpour, and M. P. Moghaddam, "Self-scheduling of a joint hydro and pumped-storage plants in energy, spinning reserve and regulation markets," in *2009 IEEE Power & Energy Society General Meeting*, (Calgary, Canada), pp. 1–8, IEEE, July 26-30, 2009.

[71] R. Jiang, J. Wang, and Y. Guan, "Robust Unit Commitment With Wind Power and Pumped Storage Hydro," *IEEE Transactions on Power Systems*, vol. 27, no. 2, pp. 800–810, 2012.

[72] N. Padhy, "Unit Commitment—A Bibliographical Survey," *IEEE Transactions on Power Systems*, vol. 19, no. 2, pp. 1196–1205, 2004.

[73] I. Farhat and M. El-Hawary, "Optimization methods applied for solving the short-term hydrothermal coordination problem," *Electric Power Systems Research*, vol. 79, no. 9, pp. 1308–1320, 2009.

[74] H. Yamin, "Review on methods of generation scheduling in electric power systems," *Electric Power Systems Research*, vol. 69, no. 2-3, pp. 227–248, 2004.

[75] S. Sen and D. Kothari, "Optimal thermal generating unit commitment: a review," *International Journal of Electrical Power & Energy Systems*, vol. 20, no. 7, pp. 443–451, 1998.

[76] G. Morales-Espana, J. M. Latorre, and A. Ramos, "Tight and Compact MILP Formulation for the Thermal Unit Commitment Problem," *IEEE Transactions on Power Systems*, vol. 28, no. 4, pp. 4897–4908, 2013.

[77] G. Morales-Espana, J. M. Latorre, and A. Ramos, "Tight and Compact MILP Formulation of Start-Up and Shut-Down Ramping in Unit Commitment," *IEEE Transactions on Power Systems*, vol. 28, no. 2, pp. 1288–1296, 2013.

[78] J. Ostrowski, M. F. Anjos, and A. Vannelli, "Tight Mixed Integer Linear Programming Formulations for the Unit Commitment Problem," *IEEE Transactions on Power Systems*, vol. 27, no. 1, pp. 39–46, 2012.

[79] D. Rajan, S. Takriti, and Y. Heights, "IBM Research Report Minimum Up / Down Polytopes of the Unit Commitment Problem with Start-Up Costs," tech. rep., IBM Research Division, 2005.

[80] G. Morales-España, *Unit Commitment: computational performance, system representation and wind uncertainty management.* PhD thesis, Universidad Pontificia Comillas, TU Delft, KTH, 2014.

[81] R. Bixby and E. Rothberg, "Progress in computational mixed integer programming - A look back from the other side of the tipping point," *Annals of Operations Research*, vol. 149, no. 1, pp. 37–41, 2007.

[82] Energy Exemplar, "Plexos - Integrated Energy Model." Available online: `www.energyexemplar.com/software/plexos-desktop-edition`, year = 2016.

[83] WILMAR, "Wilmar Joint Market Model." Available online: `www.wilmar.risoe.dk`, 2016.

[84] A. Ott, "Evolution of computing requirements in the PJM market: Past and future," *IEEE PES General Meeting*, pp. 1–4, 2010.

[85] K. Bruninx, Y. Dvorkin, E. Delarue, H. Pandžić, W. D'haeseleer, and D. S. Kirschen, "Coupling Pumped Hydro Energy Storage with Unit Commitment," *IEEE Transactions on Sustainable Energy*, vol. 7, no. 2, pp. 786–796.

[86] H. Pandžić, Y. Dvorkin, T. Qiu, Y. Wang, and D. S. Kirschen, "Toward Cost-Efficient and Reliable Unit Commitment Under Uncertainty," *IEEE Transactions on Power Systems*, vol. PP, no. 99, pp. 1–13, 2015.

[87] Elia NV, "Elia - The Belgian transmission system operator." Available online: `www.elia.be`, 2016.

[88] M. Carrion and J. Arroyo, "A Computationally Efficient Mixed-Integer Linear Formulation for the Thermal Unit Commitment Problem," *IEEE Transactions on Power Systems*, vol. 21, no. 3, pp. 1371–1378, 2006.

[89] J. Arroyo and A. Conejo, "Optimal response of a thermal unit to an electricity spot market," *IEEE Transactions on Power Systems*, vol. 15, no. 3, pp. 1098–1104, 2000.

[90] A. Frangioni, C. Gentile, and F. Lacalandra, "Tighter approximated MILP formulations for unit commitment problems," *IEEE Transactions on Power Systems*, vol. 24, no. 1, pp. 105–113, 2009.

[91] K. Van Den Bergh, E. Delarue, and W. D'haeseleer, "DC power flow in unit commitment models." KU Leuven Energy Institute WP EN2014-12. Available online: `http://www.mech.kuleuven.be/en/tme/research/energy_environment/Pdf/wpen2014-12.pdf`, 2014.

[92] K. Purchala, *Modeling and analysis of techno-economic interactions in meshed high voltage grids exhibiting congestion.* Phd dissertation, KU Leuven, 2005.

[93] M. A. Ortega-Vazquez and D. S. Kirschen, "Estimating the Spinning Reserve Requirements in Systems With Significant Wind Power Generation Penetration," *IEEE Transactions on Power Systems*, vol. 24, no. 1, pp. 114–124, 2009.

[94] K. Van Den Bergh, R. Broder, K. Bruninx, E. Delarue, W. D'haeseleer, and B. Hobbs, "The benefits of coordinating the sizing , allocation and activation of flexibility between market zones." KU Leuven Energy Institue Working Paper 2015-14. Available online: `http://www.mech.kuleuven.be/en/tme/research/energy_environment/PublicationsEnergyandenvironment/Journalpapers`, 2015.

[95] R. Wiebking, "Stochastische modelle zur optimalen lastverteilung in einem kraftwerksverbund," *Zeitschrift für Operations Research*, vol. 21, no. 6, pp. B197–B217, 1977.

[96] S. Takriti, J. Birge, and E. Long, "A stochastic model for the unit commitment problem," *IEEE Transactions on Power Systems*, vol. 11, no. 3, pp. 1497–1508, 1996.

[97] P. Carpentier and G. Gohen, "Stochastic optimization of unit commitment: a new decomposition framework," *IEEE Transactions on Power Systems*, vol. 11, no. 2, pp. 1067–1073, 1996.

[98] M. A. Ortega-Vazquez and D. S. Kirschen, "Should the spinning reserve procurement in systems with wind power generation be deterministic or probabilistic?," in *2009 International Conference on Sustainable Power Generation and Supply*, (Nanjing, China), pp. 1–9, IEEE, April 6-7, 2009.

[99] K. Bruninx and E. Delarue, "A Statistical Description of the Error on Wind Power Forecasts for Probabilistic Reserve Sizing," *IEEE Transactions on Sustainable Energy*, vol. 5, no. 3, pp. 995–1002, 2014.

[100] Y. Dvorkin, D. S. Kirschen, and M. A. Ortega-Vazquez, "Assessing flexibility requirements in power systems," *IET Generation, Transmission & Distribution*, vol. 8, no. 11, pp. 1820–1830, 2014.

[101] Y. Wang, Q. Xia, and C. Kang, "Unit Commitment With Volatile Node Injections by Using Interval Optimization," *IEEE Transactions on Power Systems*, vol. 26, no. 3, pp. 1705–1713, 2011.

[102] A. Botterud, Z. Zhou, J. Wang, J. Valenzuela, J. Sumaili, R. J. Bessa, H. Keko, and V. Miranda, "Unit commitment and operating reserves with probabilistic wind power forecasts," in *2011 IEEE Trondheim PowerTech*, (Trondheim, Norway), pp. 1–7, IEEE, June 19-23, 2011.

[103] K. De Vos, J. Driesen, and R. Belmans, "Assessment of imbalance settlement exemptions for offshore wind power generation in Belgium," *Energy Policy*, vol. 39, no. 3, pp. 1486–1494, 2011.

[104] F. V. Louveaux and R. Schultz, "Chapter 4: Stochastic Integer Programming," in *Handbooks in Operations Research and Management Science Vol. 10 – Stochastic Programming* (A. Ruszczynski and A. Shapiro, eds.), vol. 10 of *Handbooks in Operations Research and Management Science*, pp. 213–266, Elsevier, 2003.

[105] F. Bouffard, F. Galiana, and A. Conejo, "Market-Clearing With Stochastic Security— Part I: Formulation," *IEEE Transactions on Power Systems*, vol. 20, no. 4, pp. 1818–1826, 2005.

[106] Y. Dvorkin, Y. Wang, H. Pandžić, and D. Kirschen, "Comparison of scenario reduction techniques for the stochastic unit commitment," in *IEEE PES General Meeting*, (New Harbor, MD, USA), pp. 1–5, IEEE, 27-31 July 2014.

[107] P. A. Ruiz, C. R. Philbrick, and P. W. Sauer, "Wind power day-ahead uncertainty management through stochastic unit commitment policies," in *2009 IEEE/PES Power Systems Conference and Exposition*, (Seattle, WA, USA), pp. 1–9, IEEE, March 15-18, 2009.

[108] D. Lew, G. Brinkman, E. Ibanez, B. Hodge, and J. King, "Western wind and solar integration study," tech. rep., National Renewable Energy Laboratory NREL/TP-5500, 2010.

[109] A. Papavasiliou and S. S. Oren, "Multiarea Stochastic Unit Commitment for High Wind Penetration in a Transmission Constrained Network," *Operations Research*, vol. 61, no. 3, pp. 578–592, 2013.

[110] A. Papavasiliou, S. S. Oren, and B. Rountree, "Applying High Performance Computing to Transmission-Constrained Stochastic Unit Commitment for Renewable Energy Integration," *IEEE Transactions on Power Systems*, vol. 30, no. 3, pp. 1109–1120, 2015.

[111] M. Kaut and S. W. Wallace, "Evaluation of scenario-generation methods for stochastic programming," *Pacific Journal of Optimization*, vol. 3, no. 2, pp. 257–271, 2007.

[112] P. Kundur, N. J. Balu, and M. G. Lauby, *Power system stability and control*, vol. 7. McGraw-hill New York, 1994.

[113] C. Lowery and M. O'Malley, "Impact of Wind Forecast Error Statistics Upon Unit Commitment," *IEEE Transactions on Sustainable Energy*, vol. 3, no. 4, pp. 760–768, 2012.

[114] K. Bruninx, E. Delarue, and W. D'haeseleer, "Statistical description of the error on wind power forecasts via a Lévy alpha-stable distribution," *EUI RSCAS Working Paper 2013/50*, pp. 1–8, 2012.

[115] P. Pinson and G. Kariniotakis, "Conditional Prediction Intervals of Wind Power Generation," *IEEE Transactions on Power Systems*, vol. 25, no. 4, pp. 1845–1856, 2010.

[116] K. Bruninx and E. Delarue, "Scenario Reduction Techniques and Solution Stability for Stochastic Unit Commitment Problems," in *ENERGYCON 2016*, (Leuven, Belgium), IEEE, 4-8 April 2016.

[117] S. Cerisola, A. Baíllo, J. M. Fernández-López, A. Ramos, and R. Gollmer, "Stochastic Power Generation Unit Commitment in Electricity Markets: A Novel Formulation and a Comparison of Solution Methods," *Operations Research*, vol. 57, no. 1, pp. 32–46, 2009.

[118] C. C. Carøe and J. Tind, "L-shaped decomposition of two-stage stochastic programs with integer recourse," *Mathematical Programming*, vol. 83, no. 1-3, pp. 451–464, 1998.

[119] S. M. Ryan, R. J.-B. Wets, D. L. Woodruff, C. Silva-Monroy, and J.-P. Watson, "Toward scalable, parallel progressive hedging for stochastic unit commitment," in *2013 IEEE Power & Energy Society General Meeting*, (Vancouver, Britisch Columbia, Canada), pp. 1–5, IEEE, July 21-25, 2013.

[120] K. Cheung, D. Gade, C. Silva-Monroy, S. M. Ryan, J.-P. Watson, R. J.-B. Wets, and D. L. Woodruff, "Toward scalable stochastic unit commitment," *Energy Systems*, vol. 6, no. 3, pp. 417–438, 2015.

[121] A. Ruszczyński, "Chapter 3: Decomposition Methods," in *Handbooks in Operations Research and Management Science Vol. 10 – Stochastic Programming* (A. Ruszczynski and A. Shapiro, eds.), pp. 141–211, Elsevier, 2003.

[122] J. Morales and S. Pineda, "Scenario reduction for futures market trading in electricity markets," *IEEE Transactions on Power Systems*, vol. 24, no. 2, pp. 878–888, 2009.

[123] P. Ruiz, C. Philbrick, and P. Sauer, "Modeling Approaches for Computational Cost Reduction in Stochastic Unit Commitment Formulations," *IEEE Transactions on Power Systems*, vol. 25, no. 1, pp. 588–589, 2010.

[124] C. Zhao and Y. Guan, "Unified Stochastic and Robust Unit Commitment," *IEEE Transactions on Power Systems*, vol. 28, no. 3, pp. 3353–3361, 2013.

[125] D. Bertsimas and M. Sim, "The price of robustness," *Operations research*, vol. 52, pp. 35–53, 2004.

[126] A. Lorca and A. Sun, "Adaptive Robust Optimization with Dynamic Uncertainty Sets for Multi-Period Economic Dispatch under Significant Wind," *IEEE Transactions on Power Systems*, pp. 1–16, 2014.

[127] D. Bertsimas and M. Sim, "Tractable Approximations to Robust Conic Optimization Problems," *Mathematical Programming*, vol. 107, no. 1, pp. 5–36, 2005.

[128] D. Bienstock, M. Chertkov, and S. Harnett, "Chance-Constrained Optimal Power Flow: Risk-Aware Network Control under Uncertainty," *SIAM Review*, vol. 56, no. 3, pp. 461–495, 2014.

[129] W. Lei, M. Shahidehpour, and Z. Li, "Comparison of Scenario-Based and Interval Optimization Approaches to Stochastic SCUC," *IEEE Transactions on Power Systems*, vol. 27, no. 2, pp. 913–921, 2012.

[130] Y. Dvorkin, H. Pandžić, M. A. Ortega-Vazquez, and D. S. Kirschen, "A Hybrid Stochastic/Interval Approach to Transmission-Constrained Unit Commitment," *IEEE Transactions on Power Systems*, vol. 30, no. 2, pp. 621–631, 2015.

[131] P. A. Ruiz, C. R. Philbrick, and P. W. Sauer, "Wind power day-ahead uncertainty management through stochastic unit commitment policies," in *2009 IEEE/PES Power Systems Conference and Exposition*, pp. 1–9, IEEE, March 15-18, 2009.

[132] J. Abrell and F. Kunz, "Integrating Intermittent Renewable Wind Generation – A Stochastic Multi-Market Electricity Model for the European Electricity Market." DIW Discussion papers. Available online `http://www.diw.de/discussionpapers`, 2013.

[133] G. Liu, S. Member, and K. Tomsovic, "Quantifying Spinning Reserve in Systems With Signi fi cant Wind Power Penetration," *IEEE Transactions on Power Systems*, vol. 27, no. 4, pp. 2385–2393, 2012.

[134] J. Xiao, B. M. S. Hodge, J. F. Pekny, and G. V. Reklaitis, "Operating reserve policies with high wind power penetration," *Comp. Chem. Eng.*, vol. 35, no. 9, pp. 1876–1885, 2011.

[135] J. Fissette, *The cost of solar power forecast errors in the Belgian power system.* Master thesis, KU Leuven, 2015.

[136] C. Monteiro, R. Bessa, V. Miranda, A. Botterud, J. Wang, G. Conzelmann, Decision and Information Sciences, and INESC Porto, "Wind Power Forecasting : State-of-the-Art 2009," Tech. Rep. ANL/DIS-10-1, Argonne National Laboratory, Lemont, Illinois, USA, 2009.

[137] P. Pinson, *Estimation of the uncertainty in wind power forecasting.* PhD thesis, Centre Energéticque et Procédés, Ecole des Mines de Paris, Paris, France, 2006.

[138] M. Lange, *Analysis of the Uncertainty of Wind Power Predictions.* PhD thesis, Fakultät Mathematik un Naturwissenschaften, Carl von Ossietzky Universität Oldenburg, Oldenburg, Germany, 2003.

[139] Y. Makarov, C. Loutan, and P. de Mello, "Operational Impacts of Wind Generation on California Power Systems," *IEEE Transactions on Power Systems*, vol. 24, no. 2, pp. 1039–1050, 2009.

[140] R. Doherty and M. O'Malley, "A New Approach to Quantify Reserve Demand in Systems With Significant Installed Wind Capacity," *IEEE Transactions on Power Systems*, vol. 20, no. 2, pp. 587–595, 2005.

[141] F. Bouffard and F. D. Galiana, "Stochastic security for operations planning with significant wind power generation," in *2008 IEEE Power and Energy Society General Meeting - Conversion and Delivery of Electrical Energy in the 21st Century*, (Pittsburgh, Pennsylvania, USA), pp. 1–11, IEEE, July 20-24, 2008.

[142] K. Methaprayoon, C. Yingvivatanapong, W.-J. Lee, and J. R. Liao, "An Integration of ANN Wind Power Estimation Into Unit Commitment Considering the Forecasting Uncertainty," *IEEE Transactions on Industry Applications*, vol. 43, no. 6, pp. 1441–1448, 2007.

[143] B. C. Ummels, M. Gibescu, E. Pelgrum, W. L. Kling, and A. J. Brand, "Impacts of Wind Power on Thermal Generation Unit Commitment and Dispatch," *IEEE Transactions on Energy Conversion*, vol. 22, no. 1, pp. 44–51, 2007.

[144] E. Delarue and W. D'haeseleer, "Adaptive mixed-integer programming unit commitment strategy for determining the value of forecasting," *Applied Energy*, vol. 85, no. 4, pp. 171–181, 2008.

[145] E. D. Delarue, P. J. Luickx, and W. D'haeseleer, "The actual effect of wind power on overall electricity generation costs and CO2 emissions," *Energy Conversion and Management*, vol. 50, no. 6, pp. 1450–1456, 2009.

[146] H. Bludszuweit, J. Dominguez-Navarro, and A. Llombart, "Statistical Analysis of Wind Power Forecast Error," *IEEE Transactions on Power Systems*, vol. 23, no. 3, pp. 983–991, 2008.

[147] H. Bludszuweit and J. Dominguez-Navarro, "A Probabilistic Method for Energy Storage Sizing Based on Wind Power Forecast Uncertainty," *IEEE Transactions on Power Systems*, vol. 26, no. 3, pp. 1651–1658, 2011.

[148] G. Bathurst, J. Weatherill, and G. Strbac, "Trading wind generation in short term energy markets," *IEEE Transactions on Power Systems*, vol. 17, no. 3, pp. 782–789, 2002.

[149] A. Fabbri, T. Gomez San Roman, J. Rivier Abbad, and V. Mendez Quezada, "Assessment of the Cost Associated With Wind Generation Prediction Errors in a Liberalized Electricity Market," *IEEE Transactions on Power Systems*, vol. 20, no. 3, pp. 1440–1446, 2005.

[150] B.-M. Hodge and M. Milligan, "Wind power forecasting error distributions over multiple timescales," in *Power and Energy Society General Meeting, IEEE*, pp. 1–8, July 24-28, 2011.

[151] N. Menemenlis, M. Huneault, and A. Robitaille, "Computation of Dynamic Operating Balancing Reserve for Wind Power Integration for the Time-Horizon 1–48 Hours," *IEEE Transactions on Sustainable Energy*, vol. 3, no. 4, pp. 692–702, 2012.

[152] K. Dietrich, J. M. Latorre, L. Olmos, A. Ramos, and J. P. Ignacio, "Stochastic Unit Commitment Considering Uncertain Wind Production in an Isolated System," in *4th Conference on Energy Economics and Technology*, (Dresden, Germany), pp. 1–6, April 3, 2009.

[153] M. Lange, "On the Uncertainty of Wind Power Predictions – Analysis of the Forecast Accuracy and Statistical Distribution of Errors," *Journal of Solar Energy Engineering*, vol. 127, no. 2, p. 177, 2005.

[154] P. Pinson, *Estimation of the uncertainty in wind power forecasting.* PhD thesis, Ecole des Mines de Paris, 2006.

[155] P. Pinson, H. A. Nielsen, and H. Madsen, "Methods for the Estimation of the Uncertainty of Wind Power Forecasts," tech. rep., 2007.

[156] P. Pinson, H. Nielsen, H. Madsen, and G. Kariniotakis, "Skill forecasting from ensemble predictions of wind power," *Applied Energy*, vol. 86, no. 7-8, pp. 1326–1334, 2009.

[157] P. Pinson, T. Ranchin, and G. Kariniotakis, "Short-term Wind Power Prediction for Offshore Wind Farms - Evaluation of Fuzzy-Neural Network Based Models," in *Global Wind Power Conference (GWPC'10)*, pp. 1–9, 2010.

[158] S. Tewari, C. J. Geyer, and N. Mohan, "A Statistical Model for Wind Power Forecast Error and its Application to the Estimation of Penalties in Liberalized Markets," *IEEE Transactions on Power Systems*, vol. 26, no. 4, pp. 2031–2039, 2011.

[159] B. Mandelbrot, "The Variation of Certain Speculative Prices," *The Journal of Business*, vol. 36, no. 4, pp. 349–419, 1963.

[160] E. F. Fama, "The behavior of Stock-Market Prices," *The Journal of Business*, vol. 38, no. 1, pp. 34–105, 1965.

[161] S. Borak, W. K. Härdle, and R. Weron, "Stable distributions." SFB 649 "Economic Risk" Discussion Papers No. 2005.008. Online: `http://hdl.handle.net/10419/25027`, 2005.

[162] J.-P. Bouchard and M. Potters, *Theory of financial risks - From statistical physics to risk management.* Cambridge University Press, 2000.

[163] J. H. McCulloch, "Financial applications of stable distributions," in *Statistical Methods in Finance* (G. Maddala and C. Rao, eds.), vol. 14 of *Handbook of Statistics*, pp. 393 – 425, Elsevier, 1996.

[164] B.-M. Hodge, D. Lew, M. Milligan, and H. Holttinen, "Wind Power Forecasting Error Distributions: An International Comparison," in *Transmission Networks for Offshore Wind Power Plants Conference*, (Lisbon, Portugal), November 13-15, 2012.

[165] H. Holttinen and M. Milligan, "Methodologies to determine operating reserves due to increased wind power," *IEEE Transactions on Sustainable Energy*, vol. 3, no. 4, pp. 713–723, 2012.

[166] U. Focken, M. Lange, K. Mönnich, H.-P. Waldl, H. G. Beyer, and A. Luig, "Short-term prediction of the aggregated power output of wind farms—a statistical analysis of the reduction of the prediction error by spatial smoothing effects," *Journal of Wind Engineering and Industrial Aerodynamics*, vol. 90, no. 3, pp. 231–246, 2002.

[167] J. P. Nolan, "Fitting Data and Assessing Goodness-of- fitt with Stable Distributions." Available online: `http://academic2.american.edu/~jpnolan/stable/DataAnalysis.pdf`, 1999.

[168] J. P. Nolan, "An overview of multivariate stable distributions." [Online]. Available: `http://academic2.american.edu/~jpnolan/stable/overview.pdf`, 2008.

[169] J. P. Nolan, *Stable Distributions - Models for Heavy Tailed Data*. Boston: Birkhauser, 2013. In progress, Chapter 1 online available at `http://academic2.american.edu/~jpnolan`.

[170] V. Zolotarev, *One-Dimensional Stable Distributions*. Translations of Mathematical Monographs, Providence, USA: American Mathematical Society, 1986.

[171] V. Uchaikin and V. Zolotarev, *CHANCE and STABILITY - Stable Distributions and their Applications*. Zeist, The Netherlands: VSP, 1999.

[172] G. Samoradnitsky and M. Taqqu, *Stable Non-Gaussian Random Processes: Stochastic Models With Infinite Variance*. Stochastic Modeling, Boca Raton, Florida, USA: Chapman & Hall, 1994.

[173] S. Borak, A. Misiorek, and R. Weron, "Models for Heavy-tailed Asset Returns." Available online: `http://mpra.ub.uni-muenchen.de/25494/1/MPRA_paper_25494.pdf`, 2010.

[174] J. McCulloch, "Simple consistent estimators of stable distribution parameters," *Communications in Statistics, Simulation and Computation*, vol. 15, pp. 1109–1136, 1986.

[175] R. Weron, "Levy-stable distributions revisited: tail index > 2 does not exclude the Levy-stable regime," *International Journal of Modern Physics*, vol. 12, no. 2, pp. 209–223, 2001.

[176] A. H. Murphy and R. L. Winkler, "A General Framework for Forecast Verification," *Monthly Weather Review*, vol. 115, no. 7, pp. 1330–1338, 1987.

[177] N. L. Johnson and S. Kotz, *Continuous univariate distributions - 2*. Hoboken, New Jersey, USA: John Wiley & Sons, Ltd, 1970.

[178] P.-J. Marsboom, "Voorspellingen en gerealiseerde productie windvermogen (dutch)," tech. rep., Elia NV., Brussels, Belgium, 2012.

[179] Elia Group, "Elia Grid Data." Online: `www.elia.be`, 2013.

[180] P. Englezos and N. Kalogerakis, *Applied Parameter Estimation for Chemical Engineers*. New York City, NY, USA: CRC Press, 2000.

[181] J. Wang, A. Botterud, R. Bessa, H. Keko, L. Carvalho, D. Issicaba, J. Sumaili, and V. Miranda, "Wind power forecasting uncertainty and unit commitment," *Applied Energy*, vol. 88, no. 11, pp. 4014–4023, 2011.

[182] Elia NV, "Evolution of ancillary services needs to balance the Belgian control area towards 2018," tech. rep., Elia NV, Brussels, Belgium, 2013.

[183] P.-J. Marsboom, "Forecast and actual solar-PV power generation," tech. rep., Elia N.V., Brussels, Belgium, 2013.

[184] A. Shapiro, "Chapter 6: Monte Carlo Sampling Methods," in *Handbooks in Operations Research and Management Science Vol. 10 – Stochastic Programming* (A. Ruszczynski and A. Shapiro, eds.), pp. 353–425, Elsevier, 2003.

[185] P. Pinson and R. Girard, "Evaluating the quality of scenarios of short-term wind power generation," *Applied Energy*, vol. 96, pp. 12–20, 2012.

[186] R. J. Bessa, V. Miranda, A. Botterud, J. Wang, and E. M. Constantinescu, "Time Adaptive Conditional Kernel Density Estimation for Wind Power Forecasting," *IEEE Transactions on Sustainable Energy*, no. 4, pp. 1–10, 2012.

[187] J. Dupačová, G. Consigli, and S. W. Wallace, "Scenarios for Multistage Stochastic Programs," *Annals of Operations Research*, vol. 100, no. 1, pp. 25–53, 2000.

[188] A. J. King, S. W. Wallace, and M. Kaut, "Chapter 4: Scenario-Tree Generation: With Michal Kaut," in *Modeling with Stochastic Programming* (T. Mikosch, S. I. Resnick, and S. M. Robinson, eds.), New York: Springer Series in ORFE, 2012.

[189] G. Pflug, "Scenario tree generation for multiperiod financial optimization by optimal discretization," *Mathematical Programming*, vol. 89, no. 2, pp. 251–271, 2001.

[190] W. Römisch, "Chapter 8: Stability of Stochastic Programming Problems," in *Handbooks in Operations Research and Management Science Vol. 10 – Stochastic Programming* (A. Ruszczynski and A. Shapiro, eds.), pp. 483–554, Elsevier, 2003.

[191] G. Hahn and S. Shapiro, *Statistical Models in Engineering.* New York, NY, USA: Wiley, 1967.

[192] J. Gomez-Martinez, M. Ortega-Vazquez, and L. F. Ochoa, "Scenario selection of wind forecast errors for stochastic unit commitment: A UK case study," in *IEEE PES Innovative Smart Grid Technologies (ISGT-Europe)*, (Istanbul, Turkey), pp. 1–6, October 12-15, 2014.

[193] X.-Y. Ma, Y.-Z. Sun, and H.-L. Fang, "Scenario Generation of Wind Power Based on Statistical Uncertainty and Variability," *IEEE Transactions on Sustainable Energy*, vol. 4, no. 4, pp. 894–904, 2013.

[194] M. Kaut and S. W. Wallace, "Evaluation of scenario-generation methods for stochastic programming." Available online: `www.math.ntnu.no/~hek/OptimeringVK/Wallace/EvaluationKautWallace.pdf`, 2003.

[195] T. Homem-de Mello, "On rates of convergence for stochastic optimization problems under non-iid sampling," *SIAM Journal on Optimization*, vol. 19, no. 2, pp. 524–551, 2006.

[196] H. Varian, "Bootstrap Tutorial," *The Mathematica Journal*, vol. 9, no. 4, pp. 768–775, 2005.

[197] J. R. Brige and F. Louveaux, *Introduction to stochastic programming.* New York: Springer US, 1997.

[198] J. Wang, M. Shahidehpour, and Z. Li, "Security-constrained unit commitment with volatile wind power generation," *IEEE Transactions on Power Systems*, vol. 23, no. 3, pp. 1319–1327, 2008.

[199] G. Papaefthymiou and P. Pinson, "Modeling of spatial dependence in wind power forecast uncertainty," in *Proceedings of the 10th International Conference on Probabilistic Methods Applied to Power Systems 2008 (PMAPS'08)*, (Rincon, Puerto Rico, USA), pp. 1–9, 25-29 May 2008.

[200] Y. Feng, I. Rios, S. M. Ryan, K. Spürkel, J.-P. Watson, R. J.-B. Wets, and D. L. Woodruff, "Toward scalable stochastic unit commitment. part 1: load scenario generation," *Energy Systems*, vol. 6, no. 3, pp. 309–329, 2015.

[201] I. Rios, R. J. B. Wets, and D. L. Woodruff, "Multi-period forecasting and scenario generation with limited data," tech. rep., University of California Davis, Davis, CA, USA, 2013.

[202] V. Pappala, I. Erlich, K. Rohrig, and J. Dobschinski, "A Stochastic Model for the Optimal Operation of a Wind-Thermal Power System," *IEEE Transactions on Power Systems*, vol. 24, no. 2, pp. 940–950, 2009.

[203] F. Bouffard and F. Galiana, "Stochastic Security for Operations Planning With Significant Wind Power Generation," *IEEE Transactions on Power Systems*, vol. 23, no. 2, pp. 306–316, 2008.

[204] K. C. Sharma, P. Jain, and R. Bhakar, "Wind Power Scenario Generation and Reduction in Stochastic Programming Framework," *Electric Power Components and Systems*, vol. 41, no. 3, pp. 271–285, 2013.

[205] A. Sturt and G. Strbac, "Efficient Stochastic Scheduling for Simulation of Wind-Integrated Power Systems," *IEEE Transactions on Power Systems*, vol. 27, no. 1, pp. 323–334, 2012.

[206] M. A. Plazas, A. J. Conejo, and F. J. Prieto, "Multimarket optimal bidding for a power producer," *IEEE Transactions on Power Systems*, vol. 20, no. 4, pp. 2041–2050, 2005.

[207] R. Nürnberg and W. Römisch, "A two-stage planning model for power scheduling in a hydro-thermal system under uncertainty," *Optimization and Engineering*, vol. 3, no. 4, pp. 355–378, 2002.

[208] R. Barth, S. Lennart, C. Weber, H. Brand, and D. J. Swider, "WILMAR Deliverable 6.2 (d) Methodology of the Scenario Tree Tool," tech. rep., 2006.

[209] J. Morales, R. Mínguez, and A. Conejo, "A methodology to generate statistically dependent wind speed scenarios," *Applied Energy*, vol. 87, no. 3, pp. 843–855, 2010.

[210] P. E. de Mello, N. Lu, and Y. Makarov, "An optimized autoregressive forecast error generator for wind and load uncertainty study," *Wind Energy*, vol. 14, no. 8, pp. 967–976, 2011.

[211] S. Sen, L. Yu, and T. Genc, "A Stochastic Programming Approach to Power Portfolio Optimization," *Operations Research*, vol. 54, no. 1, pp. 55–72, 2006.

[212] K. Høyland and S. W. Wallace, "Generating Scenario Trees for Multistage Decision Problems," *Management Science*, vol. 47, no. 2, pp. 295–307, 2001.

[213] K. Høyland, M. Kaut, and S. Wallace, "A heuristic for moment-matching scenario generation," *Computational Optimization and Applications*, vol. 24, no. 2, pp. 169–185, 2003.

[214] R. Hochreiter and G. C. Pflug, "Financial scenario generation for stochastic multi-stage decision processes as facility location problems," *Annals of Operations Research*, vol. 152, no. 1, pp. 257–272, 2006.

[215] G. C. Pflug, "Chapter 7: Stochastic Optimization and Statistical Inference," in *Handbooks in Operations Research and Management Science Vol. 10 – Stochastic Programming* (A. Ruszczynski and A. Shapiro, eds.), vol. 10, pp. 427–482, Elsevier, 2003.

[216] H. Heitsch and W. Römisch, "Scenario reduction algorithms in stochastic programming," *Computational optimization and applications*, vol. 24, no. 2, pp. 187–206, 2003.

[217] H. Heitsch and W. Römisch, "Generation of multivariate scenario trees to model stochasticity in power management," in *2005 IEEE Russia Power Tech (PowerTech)*, (Moscow, Russia), pp. 1–7, IEEE, 25-27 June 2005.

[218] G. B. Dantzig and G. Infanger, "Large-Scale Stochastic Linear Programs: Improtance sampling and Benders Decomposition," tech. rep., 1991.

[219] G. Infanger, "Monte Carlo (importance) sampling within a Benders Decomposition Algorithm fro Stochastic Linear Programs," *Annals of Operations Research*, vol. 28, pp. 69–95, 1992.

[220] R. Hochreiter and G. Pflug, "Scenario tree generation as a multidimensional facility location problem," tech. rep., AURORA TR2002-33, 2002.

[221] J. Li, F. Lan, and H. Wei, "A Scenario Optimal Reduction Method for Wind Power Time Series," *IEEE Transactions on Power Systems*, vol. 31, no. 2, pp. 1657–1658, 2016.

[222] Y. Feng and S. M. Ryan, "Scenario construction and reduction applied to stochastic power generation expansion planning," *Computers and Operations Research*, vol. 40, no. 1, pp. 9–23, 2013.

[223] Y. Feng, *Scenario generation and reduction for long-term and short-term power system generation planning under uncertainties*. PhD thesis, Iowa State University, 2014.

[224] Y. Feng and S. M. Ryan, "Scenario Reduction for Stochastic Unit Commitment with Wind Penetration," in *PES General Meeting | Conference & Exposition, 2014 IEEE*, (National Harbour, MD), pp. 1–5, July 27-31, 2014.

[225] Y. Feng and S. M. Ryan, "Solution sensitivity-based scenario reduction for stochastic unit commitment," *Computational Management Science*, vol. 13, no. 1, pp. 26–62, 2016.

[226] S. Lloyd, "Least squares quantization in PCM," *IEEE Transactions on Information Theory*, vol. 28, no. 2, pp. 129–137, 1982.

[227] D. Arthur and S. Vassilvitskii, "k-means++: The advantages of careful seeding," in *Proceedings of the eighteenth annual ACM-SIAM symposium on Discrete algorithms*, vol. 8, (New Orleans, Louisiana, USA), pp. 1027–1035, 7-9 January 2007.

[228] A. Greenhall, *Wind Scenarios for Stochastic Energy Scheduling*. PhD thesis, University of Washington, 2013.

[229] Y. Wang, *Scenario reduction heuristics for a rolling stochastic programming simulation of bulk energy flows with uncertain fuel costs*. PhD thesis, Iowa State University, 2010.

[230] H. Heitsch and W. Römisch, "Scenario tree reduction for multistage stochastic programs," in *Computational Management Science*, vol. 6, pp. 117–133, 2009.

[231] H. Heitsch and W. Römisch, "Scenario tree modeling for multistage stochastic programs," *Mathematical Programming*, vol. 118, no. 2, pp. 371–406, 2009.

[232] S. Pineda and A. Conejo, "Scenario reduction for risk-averse electricity trading," *IET Generation, Transmission & Distribution*, vol. 4, no. 6, pp. 694–705, 2010.

[233] C. Lowery and M. O'Malley, "Wind Power Scenario Tree Tool: Development and Methodology," in *Reliability and Risk Evaluation of*

Wind Integrated Power Systems (R. Billinton, R. Karki, and A. K. Verma, eds.), pp. 13–28, Springer, 2013.

[234] P. Meibom, H. V. Larsen, R. Barth, H. Brand, C. Weber, and O. Voll, "WILMAR Deliverable D6.2 (b) WILMAR Joint Market Model Documentation," tech. rep., 2006.

[235] L. Wu, M. Shahidehpour, and Z. Li, "Comparison of scenario-based and interval optimization approaches to stochastic SCUC," *IEEE Transactions on Power Systems*, vol. 27, no. 2, pp. 913–921, 2012.

[236] J. M. Latorre, S. Cerisola, and A. Ramos, "Clustering algorithms for scenario tree generation: Application to natural hydro inflows," *European Journal of Operational Research*, vol. 181, no. 3, pp. 1339–1353, 2007.

[237] W. L. de Oliveira, C. Sagastizábal, D. D. J. Penna, M. E. P. n. Maceira, and J. M. Damázio, "Optimal scenario tree reduction for stochastic streamflows in power generation planning problems," *Optimization Methods and Software*, vol. 25, no. 6, pp. 917–936, 2010.

[238] H. Pandžić, T. Qiu, and D. S. Kirschen, "Comparison of state-of-the-art transmission constrained unit commitment formulations," in *IEEE Power and Energy Society General Meeting*, (Vancouver, BC, Canada), pp. 1–5, 21-25 July 2013.

[239] S. Rachev, "The Monge-Kantorovich mass transference problem and its stochastic applications," *Theory of Probability & Its Applications*, vol. XXIX, no. 4, 1985.

[240] ENTSO-E, "ENTSO-E Data Portal." Online: `https://www.entsoe.eu/resources/data-portal/`, 2013.

[241] E. Lannoye, D. Flynn, and M. O'Mally, "Transmission, Variable Generation, and Power System Flexibility," *IEEE Transactions on Power Systems*, vol. 30, no. 1, pp. 1–10, 2015.

[242] K. Van den Bergh, D. Couckuyt, E. Delarue, and W. D'haeseleer, "Redispatching in an interconnected electricity system with high renewables penetration," *Electric Power System Research*, vol. 127, no. 10, pp. 64–72, 2015.

[243] J. Vandewalle, K. Bruninx, and W. D'Haeseleer, "Effects of large-scale power to gas conversion on the power, gas and carbon sectors and their interactions," *Energy Conversion and Management*, vol. 94, pp. 28–39, 2014.

[244] M. C. Ferris, R. Jain, and S. Dirkse, "GDXMRW : Interfacing GAMS and MATLAB." Available online: `http://www.gams.com/dd/docs/tools/gdxmrw.pdf`, 2011.

[245] C. Gellings, "The concept of demand-side management for electric utilities," *Proceedings of the IEEE*, vol. 73, no. 10, pp. 1468–1470, 1985.

[246] P. Warren, "A review of demand-side management policy in the uk," *Renewable and Sustainable Energy Reviews*, vol. 29, pp. 941–951, 2014.

[247] A. Pina, C. Silva, and P. Ferrão, "The impact of demand side management strategies in the penetration of renewable electricity," *Energy*, vol. 41, no. 1, pp. 128–137, 2012.

[248] X. He, L. Hancher, I. Azevedo, N. Keyaerts, L. Meeus, and J.-M. Glachant, "Shift, not drift: towards active demand response and beyond," tech. rep., 2013.

[249] D. S. Callaway, "Tapping the energy storage potential in electric loads to deliver load following and regulation, with application to wind energy," *Energy Conversion and Management*, vol. 50, no. 5, pp. 1389–1400, 2009.

[250] J. L. Mathieu, M. Kamgarpour, J. Lygeros, G. Andersson, and D. S. Callaway, "Arbitraging Intraday Wholesale Energy Market Prices With Aggregations of Thermostatic Loads," *IEEE Transactions on Power Systems*, vol. 30, no. 2, pp. 763–772, 2014.

[251] H. Hao, B. M. Sanandaji, K. Poolla, and T. L. Vincent, "Aggregate Flexibility of Thermostatically Controlled Loads," *IEEE Transactions on Power Systems*, vol. 30, no. 1, pp. 189–198, 2015.

[252] H. C. Gils, "Assessment of the theoretical demand response potential in europe," *Energy*, vol. 67, pp. 1–18, 2014.

[253] P. Palensky and D. Dietrich, "Demand side management: Demand response, intelligent energy systems, and smart loads," *IEEE Transactions on Industrial Informatics*, vol. 7, no. 3, pp. 381–388, 2011.

[254] C. Bergaentzlé, C. Clastres, and H. Khalfallah, "Demand-side management and European environmental and energy goals: an optimal complementary approach," *Energy Policy*, vol. 67, no. April, pp. 858–869, 2014.

[255] J. L. Mathieu, M. G. Vaya, and G. Andersson, "Uncertainty in the flexibility of aggregations of demand response resources," in *IECON 2013 - 39th Annual Conference of the IEEE Industrial Electronics Society*, (Vienna, Austria), pp. 8052–8057, IEEE, November 10-13, 2013.

[256] J. L. Mathieu, D. S. Callaway, and S. Kiliccote, "Examining uncertainty in demand response baseline models and variability in automated responses to dynamic pricing," *Proceedings of the IEEE Conference on Decision and Control*, pp. 4332–4339, December 12-15, 2011.

[257] N. Lu, D. P. Chassin, and S. E. Widergren, "Modeling uncertainties in aggregated thermostatically controlled loads using a state queueing model," *IEEE Transactions on Power Systems*, vol. 20, no. 2, pp. 725–733, 2005.

[258] B. Shen, G. Ghatikar, Z. Lei, J. Li, G. Wikler, and P. Martin, "The role of regulatory reforms, market changes, and technology development to make demand response a viable resource in meeting energy challenges," *Applied Energy*, vol. 130, pp. 814 – 823, 2014.

[259] A. Kosek, G. Costanzo, H. Bindner, and O. Gehrke, "An overview of demand side management control schemes for buildings in smart grids," in *IEEE International Conference on Smart Energy Grid Engineering (SEGE)*, (UOIT, Oshawa, Canada), pp. 1–9, August 28-30, 2013.

[260] M. Vrakopoulou, J. L. Mathieu, and G. Andersson, "Stochastic Optimal Power Flow with Uncertain Reserves from Demand Response," in *2014 47th Hawaii International Conference on System Sciences*, (Waikoloa, HI, USA), pp. 2353–2362, January 6-9, 2014.

[261] B. Li and J. L. Mathieu, "Analytical Reformulation of Chance-Constrained Optimal Power Flow with Uncertain Load Control," in *IEEE PowerTech*, (Eindhoven, The Netherlands), June 29 - July 2, 2015.

[262] C. De Jonghe, B. F. Hobbs, and R. Belmans, "Optimal Generation Mix With Short-Term Demand Response and Wind Penetration," *IEEE Transactions on Power Systems*, vol. 27, no. 2, pp. 830–839, 2012.

[263] R. Sioshansi and W. Short, "Evaluating the impacts of real-time pricing on the usage of wind generation," *IEEE Transactions on Power Systems*, no. 2007, pp. 1–14, 2009.

[264] D. S. Kirschen and G. Strbac, "Factoring the elasticity of demand in electricity prices," *IEEE Transactions on Power Systems*, vol. 15, no. 2, pp. 612–617, 2000.

[265] E. Bompard and E. Carpaneto, "The role of load demand elasticity in congestion management and pricing," *Power Engineering Society Summer Meeting, 2000, IEEE*, vol. 4, pp. 2229–2234, July 16-20, 2000.

[266] C. L. Su, *Optimal Demand-Side Participation in Day-Ahead Electricity Markets*. PhD thesis, University of Manchester, 2007.

[267] Y. Tan and D. Kirschen, "Co-optimization of Energy and Reserve in Electricity Markets with Demand-side Participation in Reserve Services," *2006 IEEE PES Power Systems Conference and Exposition*, pp. 1182–1189, October 29- November 1, 2006.

[268] E. Karangelos and F. Bouffard, "Towards Full Integration of Demand-Side Resources in Joint Forward Energy/Reserve Electricity Markets," *IEEE Transactions on Power Systems*, vol. 27, no. 1, pp. 280–289, 2012.

[269] G. P. Henze, C. Felsmann, and G. Knabe, "Evaluation of optimal control for active and passive building thermal storage," *International Journal of Thermal Sciences*, vol. 43, no. 2, pp. 173–183, 2004.

[270] W. A. Qureshi, N.-K. C. Nair, and M. M. Farid, "Impact of energy storage in buildings on electricity demand side management," *Energy Conversion and Management*, vol. 52, no. 5, pp. 2110 – 2120, 2011.

[271] C. Verhelst, F. Logist, J. V. Impe, and L. Helsen, "Study of the optimal control problem formulation for modulating air-to-water heat pumps connected to a residential floor heating system," *Energy and Buildings*, vol. 45, pp. 43 – 53, 2012.

[272] M. Ali, J. Jokisalo, K. Siren, and M. Lehtonen, "Combining the demand response of direct electric space heating and partial thermal storage using lp optimization," *Electric Power Systems Research*, vol. 106, pp. 160–167, 2014.

[273] M. Marwan, G. Ledwich, and A. Ghosh, "Demand-side response model to avoid spike of electricity price," *Journal of Process Control*, vol. 24, no. 6, pp. 782 – 789, 2014.

[274] R. Missaoui, H. Joumaa, S. Ploix, and S. Bacha, "Managing energy smart homes according to energy prices: Analysis of a building energy management system," *Energy and Buildings*, vol. 71, pp. 155–167, 2014.

[275] T. Williams, D. Wang, C. Crawford, and N. Djilali, "Integrating renewable energy using a smart distribution system: Potential of self-regulating demand response," *Renewable Energy*, vol. 52, pp. 46–56, 2013.

[276] D. Wang, S. Parkinson, W. Miao, H. Jia, C. Crawford, and N. Djilali, "Hierarchical market integration of responsive loads as spinning reserve," *Applied Energy*, vol. 104, pp. 229–238, 2013.

[277] D. Wang, S. Parkinson, W. Miao, H. Jia, C. Crawford, and N. Djilali, "Online voltage security assessment considering comfort-constrained demand response control of distributed heat pump systems," *Applied Energy*, vol. 96, pp. 104–114, 2012.

[278] S. Parkinson, D. Wang, C. Crawford, and N. Djilali, "Wind integration in self-regulating electric load distributions," *Energy Systems*, vol. 3, no. 4, pp. 341–377, 2012.

[279] S. Parkinson, D. Wang, and N. Djilali, "Toward low carbon energy systems: The convergence of wind power, demand response, and the electricity grid," in *Innovative Smart Grid Technologies - Asia (ISGT Asia), 2012 IEEE*, (Tianjin, China), pp. 1–8, May 21 - 24, 2012.

[280] S. Parkinson, D. Wang, C. Crawford, and N. Djilali, "Comfort-Constrained Distributed Heat Pump Management," *Energy Procedia*, vol. 12, pp. 849–855, 2011.

[281] K. Hedegaard and O. Balyk, "Energy system investment model incorporating heat pumps with thermal storage in buildings and buffer tanks," *Energy*, vol. 63, pp. 356–365, 2013.

[282] M. Filippini, "Short- and long-run time-of-use price elasticities in Swiss residential electricity demand," *Energy Policy*, vol. 39, no. 10, pp. 5811–5817, 2011.

[283] J. T. Bernard, D. Bolduc, and D. Belanger, "Quebec residential electricity demand: a microeconometric approach," *Canadian Journal of Economics*, vol. 29, no. 1, pp. 92–113, 1996.

[284] N. J. Hewitt, "Heat pumps and energy storage. the challenges of implementation," *Applied Energy*, vol. 89, no. 1, pp. 37–44, 2012.

[285] D. Dallinger and M. Wietschel, "Grid integration of intermittent renewable energy sources using price-responsive plug-in electric vehicles," *Renewable and Sustainable Energy Reviews*, vol. 16, no. 5, pp. 3370–3382, 2012.

[286] G. Reynders, J. Diriken, and D. Saelens, "Quality of grey-box models and identified parameters as function of the accuracy of input and observation signals," *Energy and Buildings*, vol. 82, pp. 263–274, 2014.

[287] D. Patteeuw and L. Helsen, "Residential buildings with heat pumps, a verified bottom-up model for demand side management studies," in *9th International Conference on System Simulation in Buildings*, no. 1, (Liège, Belgium), pp. 1–19, December 10-12, 2014.

[288] N. Good, E. Karangelos, A. Navarro-Espinosa, and P. Mancarella, "Optimization Under Uncertainty of Thermal Storage-Based Flexible Demand Response With Quantification of Residential User's Discomfort," *IEEE Transactions on Smart Grid*, vol. 6, no. 5, pp. 2333–2342, 2015.

[289] J. A. Wright, H. A. Loosemore, and R. Farmani, "Optimization of building thermal design and control by multi-criterion genetic algorithm," *Energy and Buildings*, vol. 34, no. 9, pp. 959–972, 2002.

[290] M. Ortega-Vazquez and D. Kirschen, "Optimising the spinning reserve requirements considering failures to synchronise," *IET Generation, Transmission & Distribution*, vol. 2, no. 5, p. 655, 2008.

[291] C. Protopapadaki, G. Reynders, and D. Saelens, "Bottom-up modelling of the Belgian residential building stock: impact of building stock descriptions," in *9th International Conference on System Simulation in Buildings*, vol. 2, (Liège, Belgium), December 10-12, 2014.

[292] R. Baetens and D. Saelens, "Modelling uncertainty in district energy simulations by stochastic residential occupant behaviour," *Journal of Building Performance Simulation*, vol. 1493, pp. 1–17, 2015.

[293] W. Cyx, N. Renders, M. Van Holm, and S. Verbeke, "fIEE TABULA typology approach for building stock energy assessment," tech. rep., VITO, Vlaamse instelling voor technologisch onderzoek, 2011.

[294] K. Bettgenhäuser, M. Offermann, T. Boermans, M. Bosquet, J. Grözinger, B. von Manteuffel, and N. Surmeli, "Heat pump implementation scenarios until 2030, appendix," tech. rep., Ecofys, 2013.

[295] L. Peeters, R. De Dear, J. Hensen, and W. D'haeseleer, "Thermal comfort in residential buildings: Comfort values and scales for building energy simulation," *Applied Energy*, vol. 86, no. 5, pp. 772–780, 2009.

[296] R. Baetens, R. De Coninck, J. Van Roy, B. Verbruggen, J. Driesen, L. Helsen, and D. Saelens, "Assessing electrical bottlenecks at feeder level for residential net zero-energy buildings by integrated system simulation," *Applied Energy*, vol. 96, pp. 74–83, 2012.

[297] J. Širokỳ, F. Oldewurtel, J. Cigler, and S. Prívara, "Experimental analysis of model predictive control for an energy efficient building heating system," *Applied Energy*, vol. 88, no. 9, pp. 3079–3087, 2011.

[298] F. Oldewurtel, A. Parisio, C. N. Jones, D. Gyalistras, M. Gwerder, V. Stauch, B. Lehmann, and M. Morari, "Use of model predictive control and weather forecasts for energy efficient building climate control," *Energy and Buildings*, vol. 45, pp. 15–27, 2012.

[299] G. P. Henze, D. E. Kalz, S. Liu, and C. Felsmann, "Experimental analysis of model-based predictive optimal control for active and passive building thermal storage inventory," *HVAC&R Research*, vol. 11, no. 2, pp. 189–213, 2005.

[300] R. De Coninck, R. Baetens, D. Saelens, A. Woyte, and L. Helsen, "Rule-based demand-side management of domestic hot water production with heat pumps in zero energy neighbourhoods," *Journal of Building Performance Simulation*, vol. 7, no. 4, pp. 271–288, 2014.

[301] J. C. Smith, M. R. Milligan, E. A. DeMeo, and B. Parsons, "Utility wind integration and operating impact state of the art," *IEEE Transactions on Power Systems*, vol. 22, no. 3, pp. 900–908, 2007.

[302] E. A. DeMeo, G. A. Jordan, C. Kalich, J. King, M. R. Milligan, C. Murley, B. Oakleaf, and M. J. Schuerger, "Accomodating wind's natural behavior," *IEEE Power and Energy Magazine*, vol. 5, no. 6, pp. 59–67, 2007.

[303] R. Gross, P. Heptonstall, D. Anderson, T. Green, M. Leach, and J. Skea, "The Costs and Impacts of Intermittency : An assessment of the evidence on the costs and impacts of intermittent generation on the British electricity network," tech. rep., UK ERC/Imperial College London, London, UK, 2006.

[304] H. Holttinen, P. Meibom, A. Orths, B. Lange, M. O'Malley, J. O. Tande, A. Estanqueiro, E. Gomez, L. Söder, G. Strbac, J. C. Smith, and F. van Hulle, "Impacts of large amounts of wind power on design and operation of power systems, results of IEA collaboration," *Wind Energy*, vol. 14, no. 2, pp. 179–192, 2011.

[305] E. C. Hnolog, H. Holttinen, J. Kiviluoma, N. A. Cutululis, A. Orths, I. Pineda, B. Lange, J. Dillon, J. Kondoh, M. Gibescu, J. O. Tande, A. Estanqueiro, E. Gomez, C. Smith, M. Milligan, and D. Lew, "Design and operation of power systems with large amount of wind power (IEA Wind Task 25)," tech. rep., IEA, 2011.

[306] L. Hirth, "Integration Costs and the Value of Wind Power." USAEE Working Paper No. 13-149. Available online: `http://dx.doi.org/10.2139/ssrn.2335386`, 2012.

[307] Nuclear Energy Agency, "Nuclear Energy and Renewables - System effects in low-carbon electricity systems," tech. rep., Paris, France, 2013.

[308] L. Hirth and I. Ziegenhagen, "Balancing Power and Variable Renewables A Glimpse at German Data." USAEE Working Paper No. 13-154. Available online: `http://dx.doi.org/10.2139/ssrn.2371752`, 2013.

[309] R. Sioshansi, "Evaluating the Impacts of Real-Time Pricing on the Cost and Value of Wind Generation," *IEEE Transactions on Power Systems*, vol. 25, no. 2, pp. 741–748, 2010.

[310] P. Andrianesis and G. Liberopoulos, "The "hidden cost" of renewable energy sources in electricity pool markets," in *2012 9th International Conference on the European Energy Market*, (Florence, Italy), pp. 1–8, IEEE, May 10-12, 2012.

[311] NREL, "Western wind and solar integration study," tech. rep., 2010.

[312] Pöyry, "Implications of intermittency: A multi-client study," tech. rep., 2009.

[313] K. Van den Bergh, E. Delarue, and W. D'haeseleer, "The impact of renewable injections on cycling of conventional power plants," in *10th International Conference on the European Energy Market (EEM10)*, (Stockholm, Sweden), pp. 1–8, IEEE, May 27-31, 2013.

[314] K. Van den Bergh and E. Delarue, "Cycling of conventional power plants: Technical limits and actual costs," *Energy Conversion and Management*, vol. 97, pp. 70–77, 2015.

[315] K. Bruninx, E. Delarue, and W. D'Haeseleer, "The impact of uncertainty on wind power forecasts on power system balancing : reserve sizing , allocation and activation," in *Windfarms 2015: Int. Colloquium on "Large wind-power plants: interaction, control and integration"*, (Leuven, Belgium), July 8-10, 2015.

[316] D. Johnston, R. Lowe, and M. Bell, "An exploration of the technical feasibility of achieving CO_2 emission reductions in excess of 60% within the UK housing stock by the year 2050," *Energy Policy*, vol. 33, no. 13, pp. 1643–1659, 2005.

[317] P. Bayer, D. Saner, S. Bolay, L. Rybach, and P. Blum, "Greenhouse gas emission savings of ground source heat pump systems in europe: A review," *Renewable and Sustainable Energy Reviews*, vol. 16, no. 2, pp. 1256–1267, 2012.

[318] P. Luickx, L. Peeters, L. Helsen, and W. D'haeseleer, "Influence of massive heat-pump introduction on the electricity-generation mix and the GHG effect, belgian case study," *International Journal of Energy Research*, vol. 32, no. 1, pp. 57–67, 2008.

[319] A. Joelsson, *Primary energy efficiency and* CO_2 *mitigation in residential buildings.* PhD thesis, Mid Sweden University, 2008.

[320] F. Kesicki, "Costs and potentials of reducing CO_2 emissions in the UK domestic stock from a systems perspective," *Energy and Buildings*, vol. 51, pp. 203–211, 2012.

[321] L. Peeters, J. Van der Veken, H. Hens, L. Helsen, and W. D'haeseleer, "Control of heating systems in residential buildings: Current practice," *Energy and Buildings*, vol. 40, no. 8, pp. 1446–1455, 2008.

[322] M. B. Blarke, "Towards an intermittency-friendly energy system: Comparing electric boilers and heat pumps in distributed cogeneration," *Applied Energy*, vol. 91, no. 1, pp. 349–365, 2012.

[323] D. Gómez, J. Watterson, B. Americano, C. Ha, G. Marland, E. Matsika, L. Namayanga, B. Osman-Elasha, J. Kalenga Saka, and K. Treanton, "Guidelines for national greenhouse gas inventories.," tech. rep., IPCC, 2006.

[324] IEA, "Projected costs of generating electricity, 2010 edition," tech. rep., IEA, Paris, France, 2010.

[325] J. Babiak, B. W. Olesen, and D. Petras, *Low temperature heating and high temperature cooling*. REHVA, 2009.

[326] E. Heylen, R. Jordens, D. Patteeuw, and L. Helsen, "The potential of air-water heat pumps in a Belgian residential retrofit context in relation to future electricity prices," in *9th International Conference on System Simulation in Buildings*, (Liège, Belgium), pp. 694–712, December 10-12, 2014.

[327] J. Van der Veken, J. Creylman, and T. Lenaerts, "Studie naar kostenoptimale niveaus van de minimumeisen inzake energieprestaties van nieuwe residentiële gebouwen.," tech. rep., Knowledge center Energy, Thomas More Kempen / KU Leuven, 2013.

[328] J. L. Mathieu, M. E. Dyson, and D. S. Callaway, "Resource and revenue potential of california residential load participation in ancillary services," *Energy Policy*, vol. 80, pp. 76 – 87, 2015.

[329] G. Papaefthymiou, B. Hasche, and C. Nabe, "Potential of heat pumps for demand side management and wind power integration in the german electricity market," *IEEE Transactions on Sustainable Energy*, vol. 3, no. 4, pp. 636–642, 2012.

[330] K. Hedegaard and M. Münster, "Influence of individual heat pumps on wind power integration – energy system investments and operation," *Energy Conversion and Management*, vol. 75, pp. 673 – 684, 2013.

[331] International Energy Agency and OECD Nuclear Energy Agency, "Projected Costs of Generating Electricity," tech. rep., International Energy Agency and OECD Nuclear Energy Agency, Paris, France, 2015.

[332] K. Bruninx, D. Madzharov, E. Delarue, and W. D'haeseleer, "Impact of the German nuclear phase-out on Europe's electricity generation—A comprehensive study," *Energy Policy*, vol. 60, pp. 251–261, 2013.

[333] K. Bruninx, D. Madzharov, E. Delarue, and W. D'haeseleer, "Impact Of The German Nuclear Phase-Out On Europe ' s Electricity Generation," in *EEM12, 9th International Conference on the European Energy Market*, (Florence, Italy), May 10-12, 2012.

[334] J. Zapata Riveros, K. Bruninx, K. Poncelet, and W. D'haeseleer, "Bidding strategies for virtual power plants considering CHPs and intermittent renewables," *Energy Conversion and Management*, vol. 103, pp. 408–418, 2015.

[335] J. Zapata Riveros, K. Bruninx, K. Poncelet, and W. D'haeseleer, "Bidding of a VPP in the day-ahead market under uncertainty: profit optimization & risk aversion," in *YEEES 2014*, (Dresden,Germany), pp. 1–21, April 9-10, 2014.

[336] J. Vandewalle, K. Bruninx, and W. D'haeseleer, "The interaction of a high renewable energy/low carbon power system with the gas system through power to gas," in *14th IAEE European Energy Conference*, (Rome, Italy), pp. 1–20, October 28-31, 2014.

[337] Elia NV, "Facts & Figures 2013," tech. rep., Brussels, Belgium, 2013.

[338] A. Schröder, F. Kunz, J. Meiss, R. Mendelevitch, and C. Von Hirschhausen, "Current and Prospective Costs of Electricity Generation until 2050," tech. rep., DIW Berlin, Berlin, Germany, 2013.

[339] B. M. Hill, "A Simple General Approach to Inference About the Tail of a Distribution," *The Annals of Statistics*, vol. 3, no. 5, pp. 1163–1174, 1975.

[340] P. Lévy, *Calcul des probabilités*. PCMI collection, Gauthier-Villars, 1925.

[341] T. Kozubowski, "Geometric stable laws: Estimation and applications," *Mathematical and Computer Modelling*, vol. 29, no. 10-12, pp. 241–253, 1999.

[342] T. Kozubowski and A. Panorska, "Multivariate geometric stable distributions in financial applications," *Mathematical and Computer Modelling*, vol. 29, no. 10-12, pp. 83–92, 1999.

[343] K. Dutta and J. Perry, "A Tale of Tails : An Empirical Analysis of Loss Distribution Models for Estimating Operational Risk Capital," Tech. Rep. 212, Federeal Reserve Bank of Boston, 2007.

[344] R. J. Adler, R. Feldman, and M. Taqqu, *A practical guide to heavy tails: statistical techniques and applications*. Birkhäuser, 1998.

[345] R. Pierce, "Application of the positive alpha-stable distribution," in *Proceedings of the IEEE Signal Processing Workshop on Higher-Order Statistics*, (Banff, Alberta, Canada), pp. 420–424, IEEE Comput. Soc, July 21-23, 1997.

[346] C. Nikias and M. Shao, *Signal processing with alpha-stable distributions and applications*. Adaptive and learning systems for signal processing, communications, and control, Wiley, 1995.

[347] C.-Y. Yang, K.-C. Hsu, and K.-C. Chen, "The use of the Levy-stable distribution for geophysical data analysis," *Hydrogeology Journal*, vol. 17, no. 5, pp. 1265–1273, 2008.

Curriculum Vitae

Kenneth Bruninx

° September 6, 1988 (Genk, Belgium)

Work experience:

2011 – 2016 Research assistant at the KU Leuven, Mechanical Engineering, Division of Applied Mechanics and Energy Conversion. Research at the doctoral level.

Education at the university level:

2013 – 2015 Master of Science in het Management, KU Leuven.
Magna cum laude.

2009 – 2011 Master of Science in de ingenieurswetenschappen: energie, KU Leuven.
Cum laude.

2006 – 2009 Bachelor in de ingenieurswetenschappen: werktuigkunde, KU Leuven.
Cum laude.

List of publications

Status on April 26, 2016

Articles in international journals with peer-review

Accepted manuscripts

- K. Bruninx, Y. Dvorkin, E. Delarue, H. Pandžić, W. D'haeseleer, and D. S. Kirschen, *Coupling Pumped Hydro Energy Storage with Unit Commitment,* IEEE Transactions on Sustainable Energy, vol. 7, no. 2, pp. 786–796, March 2016.
- K. Bruninx, K. Van den Bergh, E. Delarue, and W. D'haeseleer, *Optimization and Allocation of Spinning Reserves in a Low-Carbon Framework,* IEEE Transactions on Power Systems, vol. 31, no. 2, pp. 872–882, March 2016.
- D. Patteeuw, G. Reynders, K. Bruninx, C. Protopapadaki, E. Delarue, W. D'Haeseleer, D. Saelens, and L. Helsen, CO_2*-abatement cost of residential heat pumps with Active Demand Response: demand- and supply-side effects,* Applied Energy, vol. 156, pp. 490–501, October 2015.
- J. Zapata Riveros, K. Bruninx, K. Poncelet, and W. D'haeseleer, *Bidding strategies for Virtual Power Plants considering CHPs and intermittent renewables,* Energy Conversion Management, vol. 103, pp. 408–41, October 2015.
- D. Patteeuw, K. Bruninx, A. Arteconi, E. Delarue, W. D'haeseleer, and L. Helsen, *Integrated modeling of active demand response with electric heating systems coupled to thermal energy storage systems,* Applied Energy, vol. 151, pp. 306–319, August 2015.

- J. Vandewalle, K. Bruninx, and W. D'haeseleer, *Effects of large-scale power to gas conversion on the power, gas and carbon sectors and their interactions,* Energy Conversion Management, vol. 94, pp. 28-–39, April 2014.
- K. Bruninx and E. Delarue, *A Statistical Description of the Error on Wind Power Forecasts for Probabilistic Reserve Sizing,* IEEE Transactions on Sustainable Energy, vol. 5, no. 3, pp. 995—1002, July 2014.
- K. Bruninx, D. Madzharov, E. Delarue, and W. D'haeseleer, *Impact of the German nuclear phase-out on Europe's electricity generation — A comprehensive study,* Energy Policy, vol. 60, pp. 251—261, September 2013.

Submitted manuscripts

- K. Van Den Bergh, R. Broder, K. Bruninx, E. Delarue, W. D'haeseleer, and B. Hobbs, *The benefits of coordinating the sizing, allocation and activation of flexibility between market zones,* Submitted to Electric Power Systems Research, March 2016.
- Arteconi, D. Patteeuw, K. Bruninx, E. Delarue, W. D'haeseleer, and L. Helsen,*Active demand response with electric heating systems: impact of market penetration,* Submitted to Applied Energy, January 2016.
- K. Bruninx and E. Delarue, *A probabilistic unit commitment model: cost-effective, reliable and fast,* Submitted to IEEE Transactions on Power Systems, November 2015.

Symposia and conference contributions

Conference contributions, published in full in the conference proceedings

- K. Bruninx and E. Delarue, *Scenario Reduction Techniques and Solution Stability for Stochastic Unit Commitment Problems,* in IEEE ENERGYCON, Leuven, Belgium, April 4–8, 2016.
- J. Vandewalle, K. Bruninx, and W. D'haeseleer, *The interaction of a high renewable energy/low carbon power system with the gas system through power to gas,* in 14$^{\text{th}}$ IAEE European Energy Conference, Rome, Italy, October 28–31, 2014.

- K. Bruninx, E. Delarue, and W. D'haeseleer, *The cost of wind power forecast errors in the Belgian power system,* in 37$^{\text{th}}$ IAEE International Conference, New York City, NY, USA, June 15–18, 2014.
- J. Zapata Riveros, K. Bruninx, K. Poncelet, and W. D'haeseleer, *Bidding of a VPP in the day-ahead market under uncertainty: profit optimization & risk aversion,* in Young Energy Engineers & Economists Seminar 2014, Dresden, Germany, April 9–10, 2014.
- K. Bruninx, D. Patteeuw, E. Delarue, L. Helsen, and W. D'haeseleer, *Short-term demand response of flexible electric heating systems: the need for integrated simulations,* in EEM13, 10$^{\text{th}}$ International conference on the European Energy Market, Stockholm, Sweden, May 27–31, 2013.
- K. Bruninx, E. Delarue, and W. D'haeseleer, *Statistical description of the error on wind power forecasts via a Lévy alpha-stable distribution,* in YEEES 2012, Young Energy Engineers & Economists Seminar 2012, Florence, Italy, December 7, 2012.
- K. Bruninx, D. Madzharov, E. Delarue, and W. D'haeseleer, *Impact Of The German Nuclear Phase-Out On Europe's Electricity Generation,* in EEM12, 9$^{\text{th}}$ International Conference on the European Energy Market, Florence, Italy, May 10–12, 2012.

Meeting abstracts, presented at conferences and symposia, published or not published in proceedings

- K. Bruninx, Y. Dvorkin, E. Delarue, W. D'haeseleer, and D. S. Kirschen, *The System Value of Arbitrage and Balancing Services with Residential Demand Response*, in 39$^{\text{th}}$ IAEE International Conference, Bergen, Norway, June 19–22, 2016.
- K. Bruninx, E. Delarue, and W. D'haeseleer, *The impact of uncertainty on wind power forecasts on power system balancing: reserve sizing, allocation and activation,* in Windfarms 2015: Int. Colloquium on Large wind-power plants: interaction, control and integration, Leuven, Belgium, July 8–10, 2015.
- E. Delarue and Bruninx, K., *Facilitating Renewables Integration through Demand Response: a Modeling Approach*, in Chaire European Electricity Markets (CEEM) Conference on Elements of a New Target Model for European Electricity Markets, Paris, France, July 8–9, 2015.

- K. Bruninx, E. Delarue, and W. D'haeseleer, *The Cost of Wind Power Forecast Errors in the Belgian Power System,* in 2nd BAEE Research Workshop, Leuven, Belgium, October 4, 2013.
- D. Patteeuw, K. Bruninx, A. Arteconi, E. Delarue, W. D'haeseleer, and L. Helsen, *Integrated modeling of active demand response with electric heating systems: benefits and applications*, BERA Workshop on demand flexibility in Belgian electricity grids, Brussels, Belgium, January 26, 2012.
- K. Bruninx, E. Delarue, and W. D'haeseleer, *Need for integrated simulations: integration of electricity supply and demand,* in IBPSA NVL studiedag Intelligente gebouwen voor intelligente steden, Antwerp, Belgium, October 16, 2012.

Technical reports

- D. Couckuyt, D. Orlic, K. Bruninx, A. Zani, A.-C. Leger, T. Anderski, N. Grisey, and G. Sanchis, *E-highway2050 - D2.3 System simulations analysis and overlay-grid development,* European Commission (EC), Brussels, Belgium, 2015. Available online: `www.e-highway2050.eu/results`.
- K. Bruninx, D. Orlic, D. Couckuyt, N. Grisey, B. Betraoui, T. Anderski, Y. Surmann, N. T. Franck, G. Keane, B. Hickman, D. Huertas-Hernando, M. Wilk, and R. Jankowski, *E-highway2050 - D2.1: Data sets of scenarios for 2050,* European Commission (EC), Brussels, Belgium, 2013. Available online: Available online: `www.e-highway2050.eu/results`.

Working papers, published by an external party:

- K. Bruninx, E. Delarue, and W. D'haeseleer, *Statistical description of the error on wind power forecasts via a Lévy alpha-stable distribution,* EUI RSCAS Working Paper 2013/50, 2013. Available online: `http://cadmus.eui.eu/handle/1814/27520`.

Magazine articles:

- E. Delarue, K. Bruninx, and W. D'haeseleer, *Nood aan geïntegreerde simulaties: Integratie van elektriciteitsproductie en consumptie,* TVVL Magazine (Dutch), 2013.

FACULTY OF ENGINEERING SCIENCE
DEPARTMENT OF MECHANICAL ENGINEERING
ENERGY & ENVIRONMENT
Celestijnenlaan 300 box 2421
B-3001 Heverlee